BEILSTEIN JOURNAL OF ORGANIC CHEMISTRY

Chemistry in flow systems III

Edited by Andreas Kirschning

Imprint

Beilstein Journal of Organic Chemistry
www.bjoc.org
ISSN 1860-5397
Email: journals-support@beilstein-institut.de

The *Beilstein Journal of Organic Chemistry* is published by the Beilstein-Institut zur Förderung der Chemischen Wissenschaften.

Beilstein-Institut zur Förderung der Chemischen Wissenschaften
Trakehner Straße 7–9
60487 Frankfurt am Main
Germany
www.beilstein-institut.de

Beilstein Journal of Organic Chemistry

Chemistry in flow systems III

Andreas Kirschning

Editorial

Open Access

Address:
Leibniz University of Hannover, Schneiderberg 1B, 30167 Hannover, Germany

Email:
Andreas Kirschning - andreas.kirschning@oci.uni-hannover.de

Keywords:
flow chemistry

Beilstein J. Org. Chem. **2013,** *9,* 1696–1697.
doi:10.3762/bjoc.9.193

Received: 09 August 2013
Accepted: 12 August 2013
Published: 16 August 2013

This article is part of the Thematic Series "Chemistry in flow systems III".

Guest Editor: A. Kirschning

The third Thematic Series on flow chemistry published in the Beilstein Journal of Organic Chemistry demonstrates the emerging importance of transforming chemical synthesis in the laboratory from a classical batch approach to continuous processes by using micro- and miniaturized flow reactors. In the past two decades this technology has seen a dramatic increase of visibility. Considering an analyses of the accompanied developments in flow synthesis one has to acknowledge that the topic has shifted among different disciplines with a variety of intensities and focus.

In the late eighties and nineties, the idea of miniaturising continuous chemical processes was mainly pursued by chemical engineers. They were fully aware of the quest for an intensification of the process and the advantages associated with continuously operated chemical processes. The benefits of miniaturizing flow systems are evident when considering the excellent heat and mass transfer properties of these small technical devices. Chemical engineers developed beautifully designed reactors, mixers and interfaces for the online monitoring of continuous processes. The major inspiration came from the process and development units in the chemical industry, where continuously operated pilot plants already played a key role. Conceptually, highly modular microreaction systems developed by Ehrfeld Mikrosystem BTS and by CPC (Cellular Process Chemistry Systems) are marvelous examples of these engineered driven achievements.

In the late nineties, organic chemists from both industry and academia, which included our group, became involved in the use of microreactors and provided a myriad of synthetic examples. The combined work of experts from engineering and chemical synthesis was highly fruitful and is so until today. This combination of expertise has catalyzed the development of microreactor technology in the applied context of synthesis and production.

Chemical engineers depend on input from chemists and synthetic chemists will only advance the field of miniaturized flow synthesis if they are aware of the technical and engineering aspects. This includes the quest for developing analytical devices for online monitoring and feedback loops for optimising synthetic protocols.

Several of these aspects can be found in this third Thematic Series on flow chemistry. I am thankful to all my colleagues

who contributed with their excellent research to this issue. The Beilstein Team is acknowledged for the handling of the manuscripts and referee reports in a very pleasant and professional manner.

Andreas Kirschning

Hannover, August 2013

Beilstein Journal of Organic Chemistry

3D-printed devices for continuous-flow organic chemistry

Vincenza Dragone, Victor Sans, Mali H. Rosnes, Philip J. Kitson and Leroy Cronin*

Full Research Paper

Open Access

Address:
School of Chemistry, University of Glasgow, University Avenue, Glasgow G12 8QQ, UK. Web: http://www.croninlab.com

Email:
Leroy Cronin* - Lee.Cronin@glasgow.ac.uk

* Corresponding author

Keywords:
3D printing; flow chemistry; flow IR; in-line analysis; imine reduction; imine synthesis; millifluidics; reactionware

Beilstein J. Org. Chem. **2013,** *9,* 951–959.
doi:10.3762/bjoc.9.109

Received: 14 January 2013
Accepted: 25 April 2013
Published: 16 May 2013

This article is part of the Thematic Series "Chemistry in flow systems III".

Guest Editor: A. Kirschning

Abstract

We present a study in which the versatility of 3D-printing is combined with the processing advantages of flow chemistry for the synthesis of organic compounds. Robust and inexpensive 3D-printed reactionware devices are easily connected using standard fittings resulting in complex, custom-made flow systems, including multiple reactors in a series with in-line, real-time analysis using an ATR-IR flow cell. As a proof of concept, we utilized two types of organic reactions, imine syntheses and imine reductions, to show how different reactor configurations and substrates give different products.

Introduction

The use of flow chemistry and 3D-printing technology is expanding in the field of organic synthesis [1-5]. The application of continuous-flow systems is frequently found in chemistry, and is beginning to have a significant impact on the way molecules are made [1-3]; on the other hand the application of 3D-printing technology in synthetic chemistry still has many aspects that can be investigated. The benefits resulting from the utilization of 3D-printing techniques to create bespoke reactionware for synthetic chemistry have recently been reported [4,5].

3D printing consists of the fabrication of three-dimensional physical objects from a digital model [6]. The 3D printer takes the virtual design from computer-aided design (CAD) software and reproduces it layer-by-layer until the physical definition of the layers gives the designed object. The significant advantage of this technique is that the architecture can be concisely controlled. 3D printing allows chemists to build devices with high precision, including complex geometries and intricate internal structures such as channels with well-defined size dimensions. Furthermore, understanding the kinetics of the processes can allow the (re-)designing of the reactionware, allowing us to combine additional kinetic knowledge with reactor designs. Moreover, the additive manufacturing process of the devices takes a short time and results in a cheap procedure for the fabrication of fluidic devices [7]. All this is impor-

tant in chemistry, and in particular for the realization of micro- and millifluidic devices.

Microfluidic devices compatible with a wide range of organic solvents and reagents are usually made of silicon or glass, which requires specialized manufacturing techniques and are expensive to fabricate [8]. There is growing interest in the use of polymers that can be employed to fabricate devices in a rapid and inexpensive fashion [9]. One of the most commonly employed polymers is poly(dimethylsiloxane) (PMDS), due to its low cost and the possibility of rapid prototyping. Nevertheless, it is not suitable for carrying out organic reactions as it can absorb the reactants and will swell in most nonaqueous solvents [8]. 3D-printing technology offers the possibility of employing polypropylene (PP), a thermopolymer that is inert in a range of organic solvents and organic compounds, cheaper than PMDS, and compatible with the available 3D printers.

Herein, we demonstrate the versatility and convenience of using 3D-printed reactors for the synthesis of organic compounds, using flow techniques with an in-line ATR-IR flow cell to monitor the reactions in real time. There are several examples of different techniques used for real-time analyses in the literature, such as UV–vis [4,5,10,11], IR [5,10,12-14], and even NMR spectroscopy [15-17]. The use of in-line spectroscopy allows for the monitoring of reaction steps that include unstable compounds or hazardous species [18]. Further, the use of such techniques may also be used to obtain quantitative information about reaction progress and to rapidly optimize the reaction conditions "on the fly".

First, an in-house designed and 3D-printed reactionware device was employed for the synthesis of imines from the reaction of a range of aldehydes and primary amines. Secondly, two reactors were connected in series to first perform an imine synthesis and then subsequently an imine reduction, with this second setup showing the potential for using the 3D-printed devices as reliable tools in multistep synthesis. This showed that the simplicity of designing and building flow reactors employing 3D-printing techniques allows for an easy and convenient integration of devices in a flow setup. Therefore it represents a very attractive way to design and build new continuous-flow rigs for organic synthesis.

Results and Discussion

Experimental setup

The 3D-printed flow reactors used to carry out the organic syntheses were designed by using a 3D CAD software package (Autodesk123D®), which is freely distributed and produces files that can be converted to the correct format read by the 3DTouch™ printer. This 3D printer heats a thermopolymer through the extruder, depositing the material in a layer-by-layer fashion, converting the design into the desired 3D reactionware.

The thermoplastic employed to fabricate the devices presented herein is PP, selected to print robust, inexpensive and chemically inert devices. Comparing PP with other common and accessible thermoplastics, which have been used in 3D printing before, such as polylactic acid (PLA) and polyacrylates, in PP we can find the required characteristics to perform a chemical reaction: thermostability up to 150 °C, high chemical inertia, and low cost. PLA is widely used in medicinal chemistry because of its biocompatibility; however, from a chemical point of view its use is limited to a few solvents and organic compounds, and to preserve its integrity it can only be used up to temperatures of 60–66 °C [19]. Polyacrylates consist of a vast group of polymers with different physical and chemical properties; however their chemical compatibility is low. In fact they are not generally recommended for exposure to alcohol, glycols, alkalis, brake fluids, or to chlorinated or aromatic hydrocarbons [20]. Therefore, PP was the plastic of choice for the device fabrication.

The shape of the 3D-printed reactionware devices used herein (Figure 1) was chosen in order to combine a short design and print time with the robustness required for a flow system.

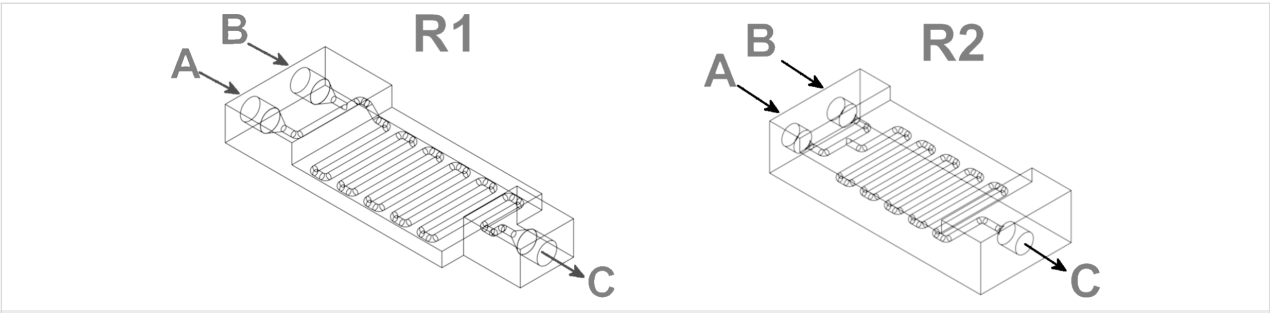

Figure 1: Schematic representation of the 3D-printed reactionware devices employed in this work showing the internal channels. Both have two inputs (A and B) and one output (C). The main difference consists in the length of the inlets/outlets: the dimension of the inlets/outlets in R1 is 3 mm and in R2 it is 6 mm where the latter is designed to match the size of standard check-valves.

Each device has two inlets, followed by a mixing point, a length of reactor to ensure a controlled residence time (which is given by dividing the reactor volume by the total flow rate), and one outlet. The approximate volume of the first reactor (R1, see Figure 1, left) is ca. 0.4 mL and was employed in the imine syntheses, while the second reactor (R2, see Figure 1, right) has a volume of ca. 0.35 mL and was employed connected to another R2 for the imine reduction processes. All the characteristics of the devices are summarized in Table 1.

The 3D-printed devices were integrated in the flow systems using 1.58 mm outer diameter (OD) polytetrafluoroethylene (PTFE) tubing, with an internal diameter of 0.5 mm and standard connectors made of polyfluoroelastomer (FPM) and polyether ether ketone (PEEK). PEEK is a harder plastic than PP and, thus, allowed the screwing of the standard connectors into the softer PP inlets/outlets of the devices, resulting in a tight seal to the device. The screw connectors increase the chemical tolerance of the 3D-printed reactor as well as its chemical compatibility, compared to our previous devices [5]. The connectors at the device inlets were equipped with check valves (made of PEEK with a Chemraz® O-ring, which is compatible with organic solvents and compounds) to prevent potential backflow issues. The reactor inlets were connected to the syringe pumps containing the starting material solutions, whilst the outlets were connected to the in-line ATR-IR flow cell (see Figure 2). These improvements are a considerable step forward compared to our previous report on 3D printing fluidics [5], as they facilitate the integration of the devices, increase the chemical compatibility, improve the range of pressure that can be handled by the system, and enable the easy configuration for the use of ancillary equipment.

Figure 2: Flow system setup, where a R1 is connected to the syringe pumps and the ATR-IR flow cell with standard connectors.

Device 1: Imine formation

Here we show the 3D-printed device as a millifluidic reactor for the synthesis of imines under flow conditions. We monitored the reaction progress with the help of an in-line ATR-IR flow cell, which is a very useful technique for the monitoring of organic reactions under flow conditions [10,21-26]. The flow setup used for these syntheses consists of two syringe pumps, each of them connected to one of the inlets of the 3D-printed reactionware device R1. The syringe pumps were filled with the starting materials with a carbonyl compound (**1a**–**c**) being

Table 1: 3D-printed reactionware device characteristics.

Entry	Characteristics	R1	R2
1	printing time (min)	248	367
2	PP mass (g)	24.01	33.74
3	dimensions (mm)	30 × 80.2 × 10	70 × 30 × 15
4	internal diameter (mm)	1.5	1.5
5	theoretical volume[a] (mL)	0.54	0.51
6	reactor volume	0.4	0.35

[a]The theoretical internal volumes of the devices are higher than the measured volumes. This is due to the printing process, where the internal channel diameter is always slightly smaller than the designed one.

placed in syringe pump no. 1 and with a primary amine (**2a**–**d**) being placed in syringe pump no. 2 (Figure 3).

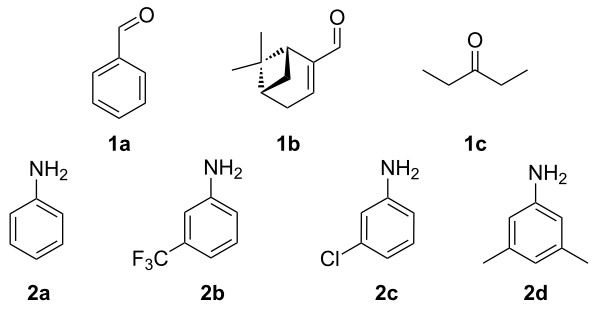

Figure 3: Carbonyl compounds and primary amines used in the syntheses reported in this work. Carbonyl compounds: benzaldehyde (**1a**); R-(−)-myrtenal (**1b**); 3-pentanone (**1c**). Aniline derivatives: aniline (**2a**); 3-(trifluoromethyl)aniline (**2b**); 3-chloroaniline (**2c**); 3,5-dimethylaniline (**2d**).

The experiments were conducted using 2 M methanolic solutions of the different substrates. This is convenient from a processing point of view, since high concentrations favor increased reaction kinetics [26] whilst minimizing the amount of waste generated during the downstream work-up [27]. The reactor output was connected with a length of tubing with a volume 0.1 mL to the IR flow cell. Hence, the total flow reactor volume (V_R) was 0.5 mL. The syntheses of the imines were monitored by an in-line ATR-IR flow cell and were conducted at a total flow rate of 0.25 mL min^{-1}, where two equimolar methanolic solutions of **1** and **2** were flowed into R1 at the same flow rate. The residence time was calculated as the time taken for the solutions to go from the mixing point inside the 3D-printed reactor to the analytical device, thus taking into account the subsequent pieces of tubing employed, and resulted to be 2 minutes. The choice of a short residence time is to allow for a more reliable comparison of the imines synthesized and also to avoid the formation of the Michael addition adduct [28] (the thermodynamic compound) in the reaction between compounds **1b** and **2a**.

For the first experiment, we studied the reaction of benzaldehyde (**1a**) with the aniline derivatives **2a**–**d** (Figure 3), to synthesize the *N*-benzylideneanilines **3a**–**d** (see Table 2). The different substituents on the amine compounds have an electronic effect on the reactive center, thus influencing the observed conversion, i.e., an electron-donating group (EDG) in the meta-position of the aniline ring gives a higher percentage conversion than does an electron-withdrawing group (EWG) [28]. In fact, Table 2 shows that the conversion of benzaldehyde (**1a**) to imine **3a** (Table 2, entry 1; obtained by reacting **1a** with **2a**), is higher than with the conversion of **1a** to imine **3b** (Table 2, entry 2; obtained by reacting **1a** with **2b**). The conversion of **1a** to imine **3c** (Table 2, entry 3; reaction of **1a** with **2c**), is the same as the formation of **3a**, whilst the formation of **3d** (reaction of **1a** with **2d**) has the highest conversion %.

Table 2: Conversion of benzaldehyde (**1a**) into imines **3a**–**d**.

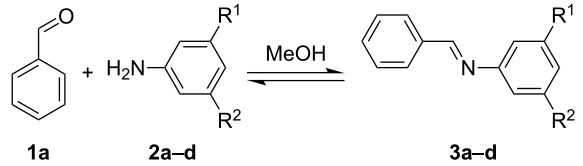

Entry	Product	Conversion (%)
1	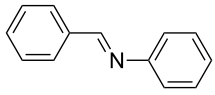 **3a**	96
2	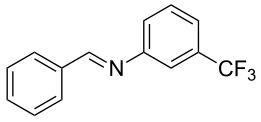 **3b**	85
3	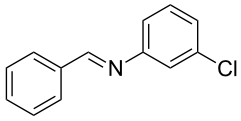 **3c**	96
4	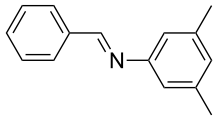 **3d**	99

Figure 4 shows the effect of the EWG and EDG substituents of a phenyl ring through the IR spectra of compounds **3b** (on the left) and **3d** (on the right). In both graphs the imine spectrum (in red) is compared with the spectrum of the starting materials (dash line): the aldehyde peak of benzaldehyde (**1a**) at 1704 cm^{-1} (in black) disappears when it reacts with compound **2d** (Figure 4, on the left), while it is still present when combined with compound **2b** (Figure 4, on the right). ^{1}H NMR spectroscopy was used to confirm the conversion rate of **1a** to the *N*-benzylideneaniline derivatives **3a**–**d**.

To calculate the conversion of the benzaldehyde (**1a**) into the imines **3a**–**d** when combined with the amines **2a**–**d**, a calibration of the IR spectra of benzaldehyde at known concentrations was obtained. The different concentrations of the substrates used for the IR analysis do not significantly affect the intensity

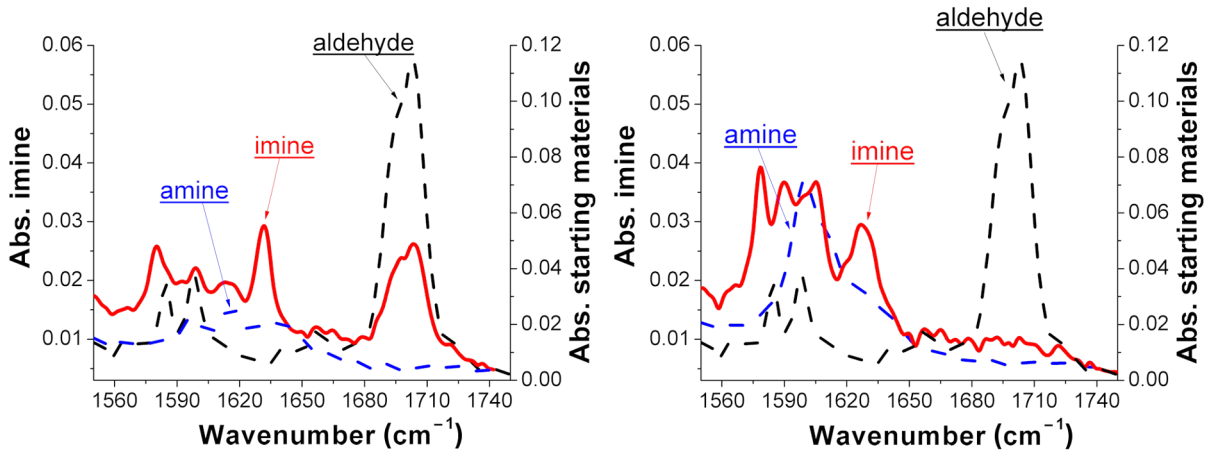

Figure 4: ATR-IR spectra of the synthesis of compounds **3b** (on the left) and **3d** (on the right). The spectrum on the left shows the reaction that does not go to completion due to the EWG substituent on the meta-position of the primary amine **2b** (see Supporting Information File 1).

of the area of the solvent band at 1022 cm^{-1} (A_{1022}). Hence, it is possible to use the solvent peaks to normalize the different spectra, allowing for comparison of the results. From this data a calibration curve can be obtained dividing the area of the benzaldehyde band at 1704 cm^{-1} (A_{1704}) by A_{1022}, calculated for five different molar concentrations of the methanolic solutions of benzaldehyde. We used 2 M, 1 M, 0.5 M, 0.25 M and 0.125 M methanolic solutions of benzaldehyde, and the relative areas were calculated using the corrected solvent-band area (A_s*) and adding A_{1704} to it, in order to minimize the slight change of A_{1022} with the concentration of the benzaldehyde (Figure 5).

Different flow rates were assayed to elucidate the effect of the reaction time. To synthesize imine **3a**, equimolar amounts of benzaldehyde (**1a**) and aniline (**2a**) were mixed in ratio 1:1 (v/v) at different flow rates in the range 0.25–1.5 mL min^{-1}. The reported spectra are focused in the region of the IR spectra where the conversion of aldehyde **1a** to imine **3a** can be followed (see Figure 6). Following the red spectra (synthesis of **3a** with the shortest residence time) it can be seen that the imine band at 1627 cm^{-1} is more intense compared to the one in black (synthesis of **3a** with the highest residence time). The observed conversion range found was between 94% and 97%. Under the studied conditions, very high conversions have been obtained with residence times as low as 20 seconds.

Further imine syntheses in-flow were conducted with the 3D-printed millifluidic reactor R1 and monitored with the in-line ATR-IR (Table 3).

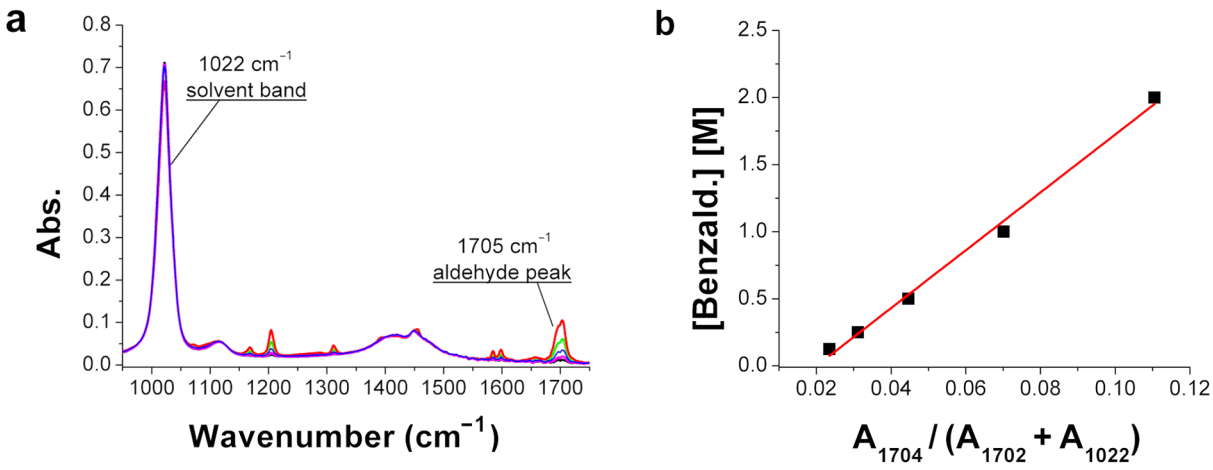

Figure 5: (a) IR spectra of benzaldehyde at different concentrations. The solvent peak at 1022 cm^{-1} remains constant while the aldehyde peak at 1704 cm^{-1} increases with the concentration of benzaldehyde. (b) Calibration curve of the different molar concentrations of benzaldehyde is shown. Equation 1: [benzaldehyde] = −0.432 + 21.56 × A_{1704} / (A_{1022} + A_{1704}) and the R^2 = 0.993.

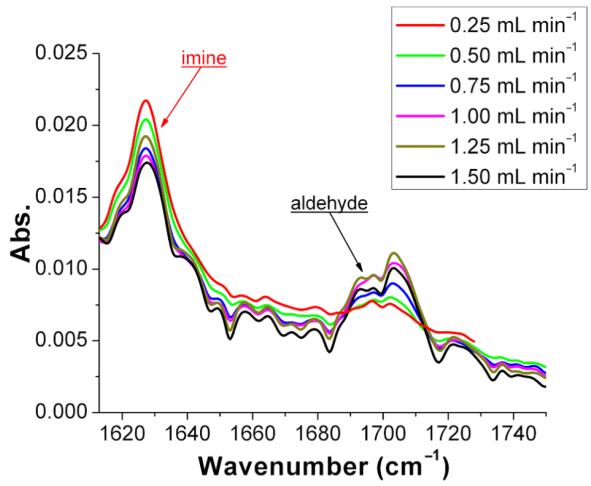

Figure 6: Comparison of the IR spectra of imine **3a**, derived from benzaldehyde (**1a**) and aniline (**2a**), synthesized at different flow rates. The conversion of **3a** at different flow rates was calculated using the equation of the calibration curve (see Figure 4), and for a flow rate of 0.25 mL min^{-1} was 97% and at a flow rate of 1.5 mL min^{-1}, 94%.

Table 3: Conversion of carbonyl compounds **1b** and **1c** with aniline (**2a**) into imines **3e** and **3f**.

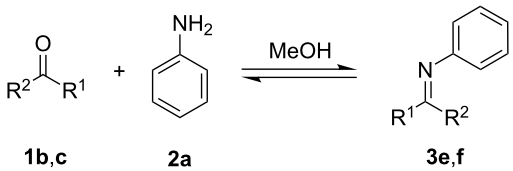

Entry	Product	Conversion (%)
1	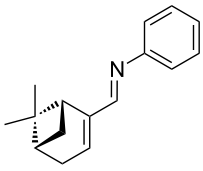 **3e**	94
2	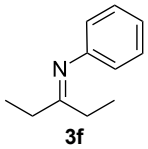 **3f**	–

The results of these reactions are summarized in Table 3 where it can be seen that the reaction between aniline (**2a**) and R-(−)-myrtenal (**1b**) readily takes place to give imine **3e** (Table 3, entry 1), whilst no product can be observed under these conditions for the reaction of **2a** with 3-pentanone (**1c**), due to the lower reactivity of the latter. For details, see the IR spectrum of compound **3f** in section 5 of Supporting Information File 1. ^{1}H NMR spectra were used to calculate the conversion rate of aldehyde **1b** into imine **3e**.

Device 2: Imine reduction

To further prove the reliability of the 3D-printed devices as flow reactors, we decided to connect one reactor to the other and perform a two steps flow reaction in an automated way. To this end, we employed two R2 reactionware devices connected in series (Figure 7), to monitor the formation of the final product using the in-line ATR-IR flow cell. We ran the imine synthesis in the first of the two reactors (R2'), and once formed we subsequently reduced it in the second reactor (R2"). R2' was connected to the syringe pumps containing the starting materials (compounds **1a** and **2a–d**) for the imine synthesis as previously described (but with a longer residence time than described above, to ensure a complete conversion of the substrates), before imines **3a–d** were directly introduced to R2" for the subsequent reduction.

The reduction of imines is a strategy to synthesize functionalized secondary amines [23,24], although only a few examples of reductions in microfluidic devices have been reported in the literature [5,23-25]. The condensation reactions were conducted using a 2 M solution of benzaldehyde (**1a**) in MeOH as before, which was pumped through inlet B' into reactor R2' at 0.0125 mL min^{-1} and mixed with a 2 M solution of the aniline

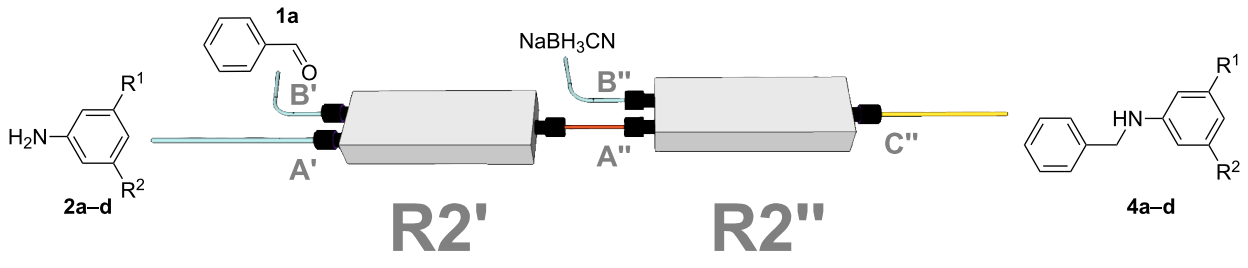

Figure 7: Representation of the setup for the two-step flow reaction employed in this work. The first reactor (R2') is used to synthesize the imines under previously optimized conditions. The product is then directly introduced into the next reactor (R2") and mixed with the reducing agent to produce the secondary amine.

derivatives **2a–d** in MeOH introduced through inlet A' at the same flow rate, keeping the aldehyde/amine ratio (1:1) (v/v) as described for the imine synthesis in R1. We selected this low flow rate to obtain a sufficient residence time (t_R = 14 min) for a full conversion of **1a** into imines **3a–d**. Reactor R2' was connected to the inlet A" of a second device (R2") where the freshly formed imine was mixed with the reducing agent, cyanoborohydride ($NaBH_3CN$) in MeOH (1 M), introduced through inlet B", and the two equimolar solutions were pumped through R2" at the same flow rate. The molar and volumetric ratios hydride/imine were kept constant (1:1) to produce the corresponding amines with a residence time of 7 min. The reducing agent was selected because it is mild but effective, and it prevents the undesired formation of bubbles or problems related to over-reduction, which could be expected in this range of concentrations when using conventional reducing agents, such as $NaBH_4$. Using this methodology, imines **3a–d** were reduced affording the corresponding secondary amines **4a–d** (Table 4).

Table 4: Table of the compounds used to study the imine reduction.

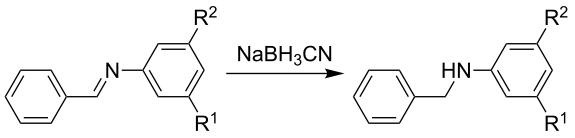

3a–d **4a–d**

Entry	Product **4**	Yield (%)
1	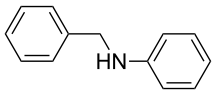 **4a**	78
2	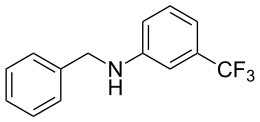 **4b**	99
3	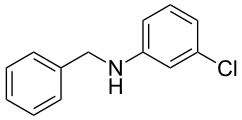 **4c**	96
4	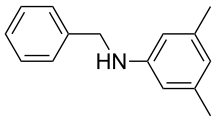 **4d**	97

^{1}H NMR spectroscopy and MS spectrometry confirmed the presence of the amines.
^{1}H NMR spectra were used to calculate the conversion rate of the amines **4a–d**.

The reactions were followed by monitoring the absence of the imine and aldehyde bands in the in-line ATR-IR flow cell, focusing the attention on the region of the IR spectrum between 1720 cm^{-1} and 1550 cm^{-1}, where the disappearance of the imine band (around 1630 cm^{-1}) can be observed. Figure 8 shows the spectra of imine **3b** (red) and its corresponding reduced product, compound **4b** (green) as an example; in the red spectrum a complete conversion of the aldehyde into imine **3b** can be observed (due to the absence of the aldehyde peak at 1704 cm^{-1}), and in the green spectrum the imine peak at 1632 cm^{-1} has completely disappeared.

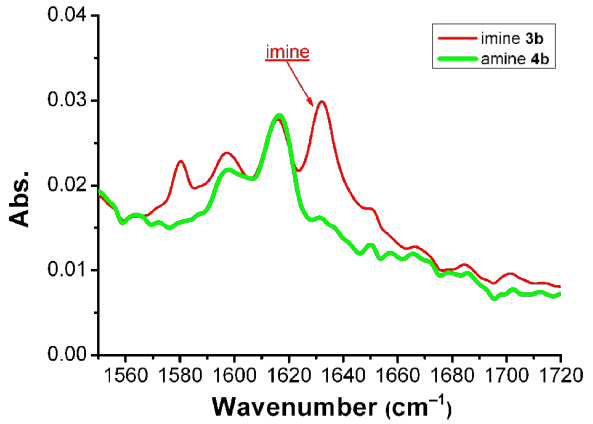

Figure 8: Example of an ATR-IR graph in which an imine spectrum is compared with the reduced imine spectrum.

In addition to the IR analysis, compounds **4a–d** were collected and analyzed by mass spectrometry (MS), HPLC and ^{1}H NMR spectroscopy. In all the studied cases, the analytical data confirmed full conversion of the substrates into the corresponding amines.

Conclusion

We have demonstrated that it is possible to integrate 3D-printed reactionware devices into a flow system, which highlights the great versatility and modularity of 3D-printed reaction devices. The possibility of connecting the reactors using standard fittings allows for better seals and facilitates the reuse of the devices, compared to our previously published procedures [5]. Further, the versatility of the 3D-printed reactionware has been demonstrated by studying and optimizing the residence time to synthesize a range of imines and secondary amines and to monitor the reactions in real time using in-line IR spectroscopy.

These robust, inexpensive and chemically inert 3D-printed reactors have proven suitable vessels for single-step as well as multistep reactions in flow. The chemical and thermal stability of PP makes this generation of custom built flow reactors suitable for the investigation of more complex chemistry. There-

fore the next step will be to design and print reactionware devices tailored to selected chemistry, such as by increasing the inlets/outlets numbers, adapting the channel size to the different stages of a reaction, and including reservoir chambers, etc.

We strongly believe that the ease of combining robust and cheap devices with other instruments in the laboratory can lead us to build new reactionware for the faster optimization of chemical processes as well as opening the potential for the discovery and implementation of array chemistry. We are currently investigating the effect of the device architecture on the reaction performed by using 3D-printed reactors made of PP, testing their robustness and chemical inertia in different environments, and designing new geometries to further develop the 3D printing technology and the 3D-printed reactionware, as well as the development of a range of universal chemical modules.

Supporting Information

Supporting Information File 1

3D printing materials and method, experimental and characterization of compounds.
[http://www.beilstein-journals.org/bjoc/content/supplementary/1860-5397-9-109-S1.pdf]

Acknowledgements

L.C. thanks the EPSRC and the EPSRC creativity@home scheme, the Royal Society/Wolfson Foundation, the Leverhulme Trust and the University of Glasgow, WestCHEM for financial support. Thanks to Saskia Buchwald for the technical support and Dr. Jennifer S. Mathieson for helpful discussion.

References

1. Wiles, C.; Watts, P. *Eur. J. Org. Chem.* **2008,** *10,* 1655–1671. doi:10.1002/ejoc.200701041
2. Wegner, J.; Ceylan, S.; Kirschning, A. *Chem. Commun.* **2011,** *47,* 4583–4592. doi:10.1039/c0cc05060a
3. Lange, H.; Carter, C. F.; Hopkin, M. D.; Burke, A.; Goode, J. G.; Baxendale, I. R.; Ley, S. V. *Chem. Sci.* **2011,** *2,* 765–769. doi:10.1039/c0sc00603c
4. Symes, M. D.; Kitson, P. J.; Yan, J.; Richmond, C. J.; Cooper, G. J. T.; Bowman, R. W.; Vilbrandt, T.; Cronin, L. *Nat. Chem.* **2012,** *4,* 349–354. doi:10.1038/nchem.1313
5. Kitson, P. J.; Rosnes, M. H.; Sans, V.; Dragone, V.; Cronin, L. *Lab Chip* **2012,** *12,* 3267–3271. doi:10.1039/c2lc40761b
6. Cooper, K. G. *Rapid Prototyping Technology: Selection and Application;* Marcel Dekker, Inc.: New York, 2001; p 1. doi:10.1201/9780203910795
7. Pereira, T. F.; Oliveira, M. F.; Maia, I. A.; Silva, J. V. L.; Costa, M. F.; Thiré, R. M. S. M. *Macromol. Symp.* **2012,** *319,* 64–73. doi:10.1002/masy.201100237
8. Zhang, X.; Haswell, S. J. *MRS Bull.* **2006,** *31,* 95–99. doi:10.1557/mrs2006.22
9. McCreedy, T. *Anal. Chim. Acta* **2001,** *427,* 39–43. doi:10.1016/S0003-2670(00)01174-0
10. Carter, C. F.; Lange, H.; Ley, S. V.; Baxendale, I. R.; Wittkamp, B.; Goode, J. G.; Gaunt, N. L. *Org. Process Res. Dev.* **2010,** *14,* 393–404. doi:10.1021/op900305v
11. Griffiths-Jones, C. M.; Hopkin, M. D.; Jönsson, D.; Ley, S. V.; Tapolczay, D. J.; Vickerstaffe, E.; Ladlow, M. *J. Comb. Chem.* **2007,** *9,* 422–430. doi:10.1021/cc060152b
12. Brodmann, T.; Koos, P.; Metzger, A.; Knochel, P.; Ley, S. V. *Org. Process Res. Dev.* **2012,** *16,* 1102–1113. doi:10.1021/op200275d
13. Moore, J. S.; Jensen, K. F. *Org. Process Res. Dev.* **2012,** *16,* 1409–1415. doi:10.1021/op300099x
14. Rueping, M.; Bootwicha, T.; Sugiono, E. *Beilstein J. Org. Chem.* **2012,** *8,* 300–307. doi:10.3762/bjoc.8.32
15. Shapira, B.; Karton, A.; Aronzon, D.; Frydman, L. *J. Am. Chem. Soc.* **2004,** *126,* 1262–1265. doi:10.1021/ja0389422
16. Bernstein, M. A.; Štefinović, M.; Sleigh, C. J. *Magn. Reson. Chem.* **2007,** *45,* 564–571. doi:10.1002/mrc.2007
17. Iggo, J. A.; Kawashima, Y.; Liu, J.; Hiyama, T.; Nozaki, K. *Organometallics* **2003,** *22,* 5418–5422. doi:10.1021/om0304917
18. van den Broek, S. A. M. W.; Leliveld, J. R.; Becker, R.; Delville, M. M. E.; Nieuwland, P. J.; Koch, K.; Rutjes, F. P. J. T. *Org. Process Res. Dev.* **2012,** *16,* 934–938. doi:10.1021/op2003437
19. Giordano, R. A.; Wu, B. M.; Borland, S. W.; Cima, L. G.; Sachs, E. M.; Cima, M. J. *J. Biomater. Sci., Polym. Ed.* **1996,** *8,* 63–75. doi:10.1163/156856297X00588
20. Novosel, E. C.; Meyer, W.; Klechowitz, N.; Krüger, H.; Wegener, M.; Walles, H.; Tovar, G. E. M.; Hirth, T.; Kluger, P. J. *Adv. Eng. Mater.* **2011,** *13,* B467–B475. doi:10.1002/adem.201180018
21. Qian, Z.; Baxendale, I. R.; Ley, S. V. *Chem.–Eur. J.* **2010,** *16,* 12342–12348. doi:10.1002/chem.201002147
22. Wensink, H.; Benito-Lopez, F.; Hermes, D. C.; Verboom, W.; Gardeniers, H. J. G. E.; Reinhoudt, D. N.; van den Berg, A. *Lab Chip* **2005,** *5,* 280–284. doi:10.1039/b414832k
23. Fan, X.; Sans, V.; Yaseneva, P.; Plaza, D. D.; Williams, J.; Lapkin, A. *Org. Process Res. Dev.* **2012,** *16,* 1039–1042. doi:10.1021/op200373m
24. Sedelmeier, J.; Ley, S. V.; Baxendale, I. R. *Green Chem.* **2009,** *11,* 683–685. doi:10.1039/b821752a
25. Kirschning, A.; Altwicker, C.; Dräger, G.; Harders, J.; Hoffmann, N.; Hoffmann, U.; Schönfeld, H.; Solodenko, W.; Kunz, U. *Angew. Chem., Int. Ed.* **2001,** *40,* 3995–3998. doi:10.1002/1521-3773(20011105)40:21<3995::AID-ANIE3995>3.0.CO;2-V
26. Anastas, P. T.; Warner, J. C. *Green Chemistry : Theory and Practice;* Oxford University Press: New York, 1998.
27. Wiles, C.; Watts, P. *Chem. Commun.* **2011,** *47,* 6512–6535. doi:10.1039/c1cc00089f
28. Bruice, P. Y. *Organic Chemistry,* 6th ed.; Prentice Hall: New Jersey, 2010.

Beilstein Journal of Organic Chemistry

Simple and rapid hydrogenation of *p*-nitrophenol with aqueous formic acid in catalytic flow reactors

Rahat Javaid*, Shin-ichiro Kawasaki, Akira Suzuki and Toshishige M. Suzuki*

Full Research Paper

Open Access

Address:
Research Center for Compact Chemical System, National Institute of Advanced Industrial Science and Technology, AIST, 4-2-1 Nigatake, Miyagino-ku, Sendai, Miyagi 983-8551, Japan

Email:
Rahat Javaid* - rahat-javaid@aist.go.jp; Toshishige M. Suzuki* - tm-suzuki@aist.go.jp

* Corresponding author

Keywords:
catalytic tubular reactor; flow chemistry; formic acid; hydrogenation; *p*-aminophenol; *p*-nitrophenol

Beilstein J. Org. Chem. **2013,** *9,* 1156–1163.
doi:10.3762/bjoc.9.129

Received: 22 February 2013
Accepted: 23 May 2013
Published: 14 June 2013

This article is part of the Thematic Series "Chemistry in flow systems III".

Guest Editor: A. Kirschning

Abstract

The inner surface of a metallic tube (i.d. 0.5 mm) was coated with a palladium (Pd)-based thin metallic layer by flow electroless plating. Simultaneous plating of Pd and silver (Ag) from their electroless-plating solution produced a mixed distributed bimetallic layer. Preferential acid leaching of Ag from the Pd–Ag layer produced a porous Pd surface. Hydrogenation of *p*-nitrophenol was examined in the presence of formic acid simply by passing the reaction solution through the catalytic tubular reactors. *p*-Aminophenol was the sole product of hydrogenation. No side reaction occurred. Reaction conversion with respect to *p*-nitrophenol was dependent on the catalyst layer type, the temperature, pH, amount of formic acid, and the residence time. A porous and oxidized Pd (PdO) surface gave the best reaction conversion among the catalytic reactors examined. *p*-Nitrophenol was converted quantitatively to *p*-aminophenol within 15 s of residence time in the porous PdO reactor at 40 °C. Evolution of carbon dioxide (CO_2) was observed during the reaction, although hydrogen (H_2) was not found in the gas phase. Dehydrogenation of formic acid did not occur to any practical degree in the absence of *p*-nitrophenol. Consequently, the nitro group was reduced via hydrogen transfer from formic acid to *p*-nitrophenol and not by hydrogen generated by dehydrogenation of formic acid.

Introduction

The flow reaction process enables continuous material production simply by feeding the reactants into one end of the reactor and obtaining the products from the other end [1-9]. Recently, we developed catalytic tubular reactors of less than 0.5 mm inner diameter, of which the interior surfaces were coated uniformly with thin (1–2 μm) palladium (Pd), platinum (Pt), and rhodium (Rh) layers by an electroless plating procedure [10,11]. These tubular reactors combined the merit of flow reaction

processing with the catalytic properties of various metals. Unlike packed-bed catalysts, hollow tubular reactors can minimize the mass transfer resistance and therefore ensure a smooth flow of reactants without causing an undesirable pressure drop or clogging of reactor tubes. In addition, the tubular reactor offers a large surface-to-volume ratio, good mixing and heat-transfer properties that enhance the reaction rate [5]. We have studied flow reactions, including the decomposition of hydrogen peroxide, oxidation of organic dyes, carbon–carbon coupling, and conversion of formic acid to hydrogen (H_2) and carbon dioxide (CO_2), using catalytic tubular reactors [10-13].

p-Aminophenol is an important intermediate produced in the syntheses of various chemicals including dyes, pharmaceuticals, and anticorrosive lubricants [14-16]. The catalytic hydrogenation of aromatic nitro compounds with H_2 has been studied extensively in the presence of Pd, Pt, Ni, and Rh metals [14,16-22]. In the light of the commercial importance of *p*-aminophenol, improvement of catalytic performance was attempted by using nanoparticles (NPs) of Au, Pd, and Ni immobilized on various solid supports. Apart from the use of gaseous H_2, the reduction of *p*-nitrophenol with sodium borohydride ($NaBH_4$) was studied catalyzed with core–shell Au–Pd NPs and Au NPs [23-26]. Formic acid is another attractive H_2 source because it is safe, easy to handle, and requires no high-pressure equipment. Formic acid and formate have been used as effective H_2 donors in the catalytic transfer hydrogenation of aromatic nitro compounds [27-31].

Here we attempted the hydrogenation of *p*-nitrophenol with formic acid in catalytic flow-through tubular reactors. Because Pd-based catalysts have usually been regarded as the most active catalysts [27,28,32], we modified the inner surface of tubular reactors with thin Pd, porous Pd, and their oxidized metal layers. Herein, we present a simple, rapid and convenient process for the reduction of *p*-nitrophenol, which is compatible with high reaction conversion under mild conditions.

Results and Discussion

Fabrication of the catalytic tubular reactors

Electroless plating is a simple and efficient methodology to coat the inner wall of a tubular reactor with various thin metal layers. Aside from the plating of a single Pd layer, we examined co-plating of Pd and Ag from their 9:1 (atomic ratio) mixed solution, as depicted in Figure 1a. Metal ions in the plating solution are stabilized against precipitation by complex forma-

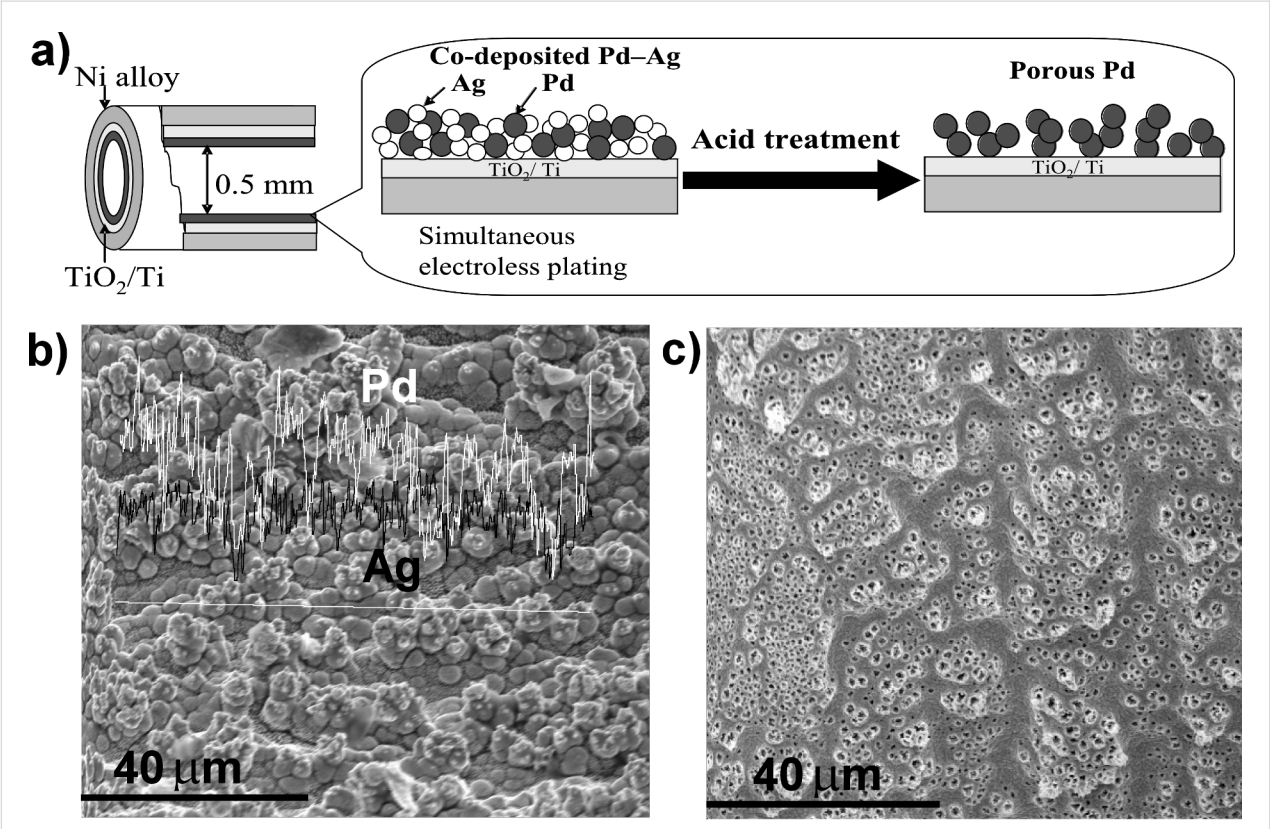

Figure 1: (a) Graphical presentation of Pd–Ag co-plating and sequential removal of Ag to give a porous Pd surface. (b) SEM image of Pd–Ag co-plated surface along with EDX presentation of Pd and Ag deposition. (c) Surface morphology of porous Pd.

tion with EDTA and NH_3, which also controls the deposition rate of the individual metal by modifying the redox potential [33]. SEM and EDX analysis of the plated layer indicated the mixed distribution of Pd and Ag over the inner surface (Figure 1b). It has been observed that Ag is preferentially plated. Therefore, a small excess of Ag (13%) was deposited over the atomic ratio present in the plating solution [33]. When the Ag content exceeds 15% in the Pd–Ag co-plating, the plating solution becomes considerably unstable and tends to give undesirable precipitation.

Selective dissolution of the less-noble element out of a bimetallic mixture or alloy results in the formation of a unique metallic sponge structure of the noble component [34,35]. We attempted to modify the reactor wall with a porous Pd layer. Continuous passage of 4 M HNO_3 into the reactor with a Pd–Ag co-plated layer preferentially dissolved Ag, leaving pores behind. Figure 1c shows an SEM image of the porous Pd surface after removal of Ag, where numerous pores are observed. Direct determination of the porosity of the porous metal layer was difficult because it firmly adhered and resisted removal from the inner surface of the narrow tube. Instead we conducted similar co-plating of Pd and Ag (9:1) on a glass surface. The plated Pd–Ag film was peeled from the glass surface. Then Ag leached out by acid treatment of the film. The BET specific surface area and average pore diameter were determined respectively as 8.8 $m^2\ g^{-1}$ (106 $m^2\ cm^{-3}$ as for volume base) and 9.4 nm.

The oxidized palladium (PdO) surface often gave high catalytic activity [11,13,36-41]. Air oxidation of Pd and the porous Pd layer in the tubular reactors was conducted at 750 °C under air flow for 2 h. The XPS analysis confirmed complete oxidation of the Pd surface to PdO, as presented in our previous study [13].

Hydrogenation of *p*-nitrophenol in the catalytic flow reactors

The experimental setup of our flow reaction system is simple, as depicted in Figure 2, where a reactor tube loop was immersed in a water bath maintained at constant temperature. An aqueous solution containing *p*-nitrophenol and formic acid was supplied continuously from one end and collected in fractions at the other open end. The reaction solution flow is smooth and stable because the catalytic reactors are hollow tubes, avoiding the pressure drop and plugging.

The evolution of gas bubbles was observed during the reaction forming an alternate gas–liquid slug flow. GC analysis of the gas phase evidenced the evolution of CO_2 as a sole product and H_2 was not found. The hydrogenation reaction of *p*-nitrophenol was followed by UV–vis spectroscopy. The analytical UV–vis

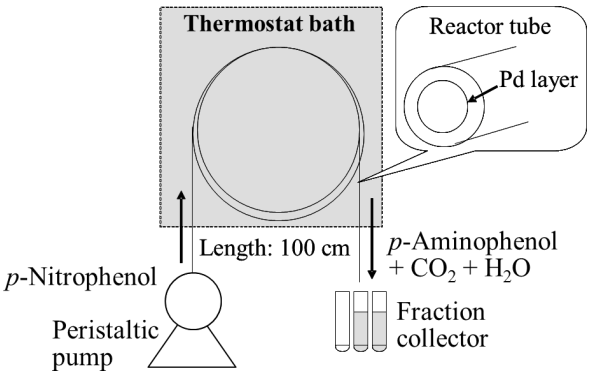

Figure 2: Schematic diagram of experimental setup used for the catalytic hydrogenation of *p*-nitrophenol.

peaks of *p*-nitrophenol and *p*-aminophenol are sufficiently separated both under acidic and basic conditions (Supporting Information File 1). The spectral difference between acidic and basic solutions is responsible for the association and dissociation of phenolic proton. The concentration of *p*-nitrophenol was determined by absorbance at 317 nm (acidic conditions) using the calibration curve. The presence of isosbestic points in the spectra (Supporting Information File 1) of the reaction mixture indicates that *p*-aminophenol is a sole product in the solution, and consequently no side reaction occurs as expressed in Scheme 1.

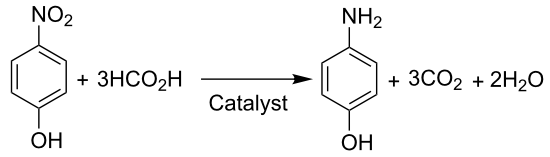

Scheme 1: Hydrogenation of *p*-nitrophenol with formic acid.

Catalytic activity of the reactors

Hydrogenation of 0.01 M *p*-nitrophenol with 0.1 M formic acid was conducted in aqueous solution at 30 °C and 40 °C by using tubular reactors coated with Pd, porous Pd, metallic Pd–Ag and porous PdO. The pH of the aqueous reaction solution as prepared was 2.2. The flow rate was fixed to 0.8 mL min^{-1}, which corresponds to 14.7 s of residence time in the tubular reactor. Figure 3 shows the reaction conversion of *p*-nitrophenol obtained by using the respective tubular reactors. The catalytic surface unquestionably contributed to facilitation of the reaction, because practically no reaction took place in the absence of the catalytic layer, even at 70 °C. It is noteworthy that oxidation of the Pd surface improved the catalytic activity

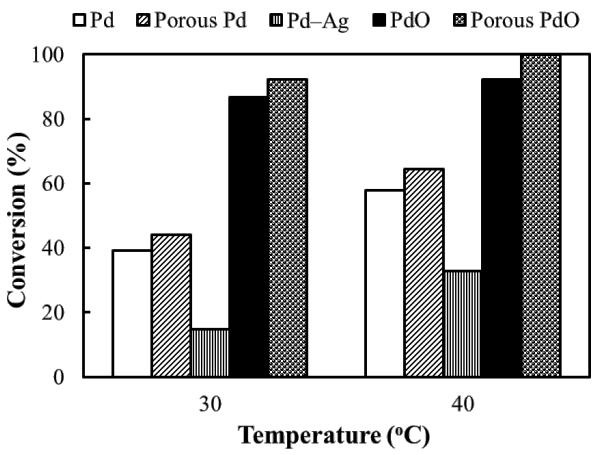

Figure 3: Influence of temperature on the conversion of 0.01 M *p*-nitrophenol with 0.1 M formic acid at 30 °C and 40 °C. Tubular reactors coated with Pd, PdO, Pd–Ag, porous Pd or porous PdO were applied for demonstration of the catalytic activity. All experiments were conducted with 14.7 s residence time.

remarkably. The number of surface hydroxy groups increases with the oxidation of Pd, allowing more intimate interaction with the reactants (see below). Addition of 13% Ag to Pd greatly decreased the catalytic activity, presumably because Ag suppresses and inhibits the active Pd site. In fact, when Ag was removed by acid, the catalytic activity was revived. Moreover, the reactor with a porous PdO surface gave markedly superior conversion (>99 %) compared to that of the corresponding nonporous counterparts.

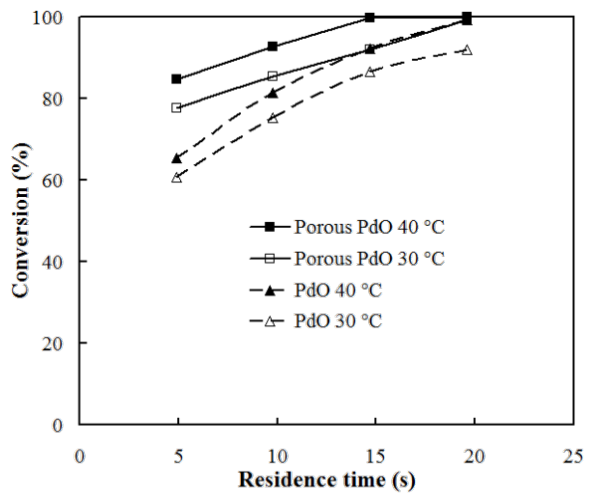

Figure 4: Effect of residence time on the conversion of 0.01 M *p*-nitrophenol with 0.1 M formic acid at 30 °C and 40 °C using PdO and porous-PdO-coated tubular reactors.

Superior catalytic activity of the porous surface was also confirmed by the effect of the residence time (flow rate) in the reactors. As presented in Figure 4, the reactor of porous PdO invariably attained higher conversion with shorter residence time than any other reactor. For example, 100% conversion was attained after 14.7 s residence time for porous PdO, whereas nonporous PdO required 19.6 s. The porous and rough reactor surface provided more contact opportunity with substrates, with which a much higher surface-area-to-volume ratio can be attained. The total amount of Pd present in the tube inner layer does not represent the concentration of active catalyst, since only surface metal atoms work as active sites. Therefore we estimated the number of surface Pd atoms using the observed surface area of porous Pd, the number of closely packed Pd atoms in a face centred cubic (fcc) crystal unit, and the atomic radius of Pd (0.137 nm) [32]. The catalytic activity expressed in terms of turnover frequency (TOF) was calculated to be around 320 h^{-1} (mol of substrate per mol of Pd site per hour) at 40 °C. This value is much higher than those reported for the catalytic transfer hydrogenation of *p*-nitrophenol and benzyl acetate in a flow system [30,32].

We conducted the reaction while changing the concentration of formic acid and maintaining the *p*-nitrophenol concentration to 0.01 M. According to the reaction stoichiometry expressed in Scheme 1, three times the molar concentration of formic acid is necessary for the reduction of one mole of *p*-nitrophenol. In the present flow reaction, at least 0.05 M formic acid was necessary to attain the maximum reaction conversion of 92.1% at 30 °C (Figure 5), which corresponds to a 1.7 times excess of the reducing agent to the *p*-nitrophenol. Further increases of concentration did not improve the reaction outcomes (Figure 5).

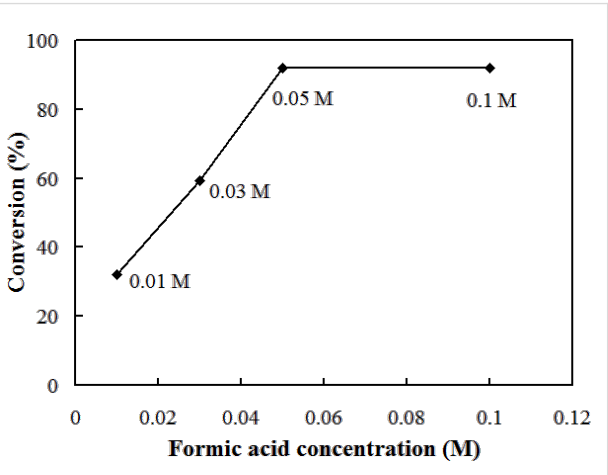

Figure 5: Effect of the concentration of formic acid on the conversion of 0.01 M *p*-nitrophenol. The formic acid concentration varied: 0.01 M, 0.03 M, 0.05 M and 0.1 M. Porous-PdO-coated reactor was used at 30 °C, with a residence time of 14.7 s.

Transfer hydrogen from formic acid to *p*-nitrophenol

Dehydrogenation of formic acid and its subsequent reduction of nitro group is a possible reaction pathway. However as mentioned, CO_2 was a sole product in the gas phase and H_2 was not found even at an increased temperature of 70 °C. To ensure that the nitro group is not reduced by H_2 generated by dehydrogenation of formic acid, we conducted a control test where *p*-nitrophenol was absent. Notably when *p*-nitrophenol was not present in the reaction solution formic acid was not consumed at all at the present reaction temperature. In our previous study, more than 250 °C was necessary for the dehydrogenation of formic acid in the Pd-coated tubular reactor [13]. Consequently, we concluded that the nitro group was reduced in a transfer hydrogenation process and not by molecular H_2 generated from the dehydrogenation of formic acid. In contrast to hydrogenation using gaseous H_2, the present system using formic acid as hydrogen donor has the advantages of convenience and safety.

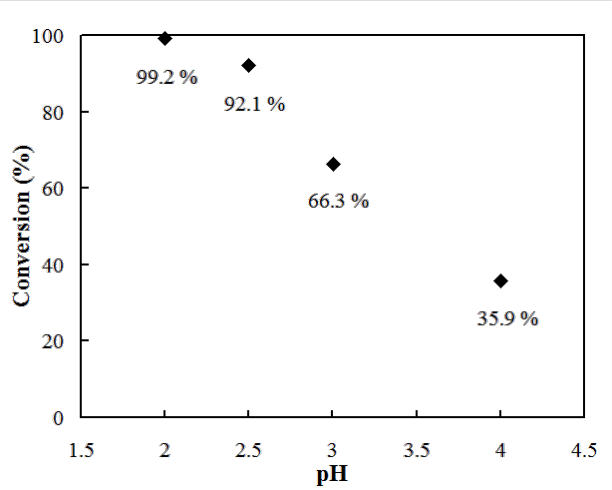

Figure 6: Effect of pH on the conversion of 0.01 M *p*-nitrophenol by using 0.05 M formic acid. The porous PdO coated reactor was used at 30 °C and a residence time of 14.7 s.

The PdO surface has a higher number of hydroxy groups than that of metallic Pd providing more opportunity for interaction sites with the substrates. This is in accordance with the higher reaction conversion attained by oxidized PdO reactor tube than that by the metallic Pd reactor tube. The reaction efficiency in a porous PdO reactor apparently depends on the pH of the reaction solution, as given in Figure 6. The decrease of pH produced markedly better conversion. By considering the pK_a of formic acid (3.5), the acid form (HCO_2H) contributes to the reaction conversion better than basic formate (HCO_2^-) does. H_2 transfer from formic acid to a nitro compound has often been facilitated in the presence of a base, such as triethylamine and NH_3 [28,32,42-44]. Therefore, the addition of such bases is usually necessary for transfer hydrogenation. As in the present case, base-free catalytic transfer hydrogenation of a nitro compound is a rather rare example [31,45]. One plausible explanation is a pH dependence of the electrostatic interaction between formic acid/formate and the catalytic surface. The oxidized Pd surface (PdO) is equilibrated with Pd–OH and Pd–O^- in aqueous solution depending on the pH [46]. Increase in the number of Pd–O^- at high-pH region makes the surface more negative and inhibits the access of formate (HCO_2^-) and phenolate (NO_2–Ph–O^-) anions, although at low pH, such repulsion of Pd–OH and the acidic reactants is suppressed.

Long-term stability

To evaluate the long-term stability and activity of the catalytic reactor, the reaction was run for 100 h at 30 °C and another 100 h at 40 °C. In these experiments, a solution of 0.01 M *p*-nitrophenol and 0.05 M formic acid was fed continuously to the reactor tube at a fixed residence time of 14.7 s. The solution was collected out of the reactor in fractions and the conversion was determined. As Figure 7 shows, the reaction was stable over this period. Palladium was not found in the reaction solution by the ICP–AES analysis, indicating that the leaching of Pd from the reactor tube was negligible during these experimental runs. Unlike other catalytic approaches for the reduction of *p*-nitrophenol [25,47-49], our catalytic flow system requires no product separation procedure. Moreover, we observed no decrease in the catalytic activity.

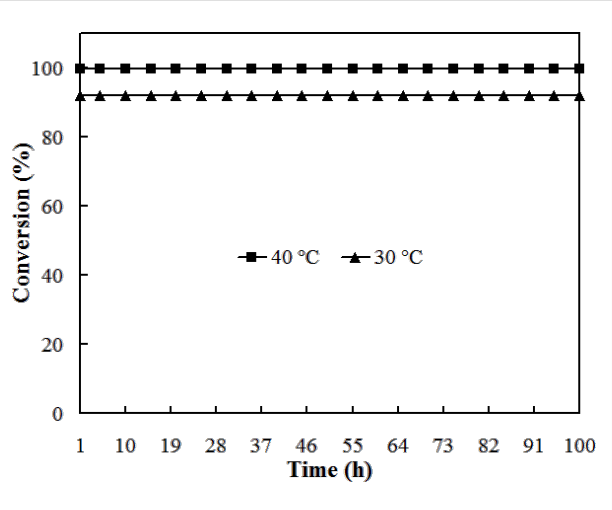

Figure 7: Long-term testing for continuous hydrogenation of 0.01 M *p*-nitrophenol with 0.05 M formic acid in the porous PdO-coated reactor. Residence time: 14.7 s.

Conclusion

A flow electroless plating procedure was employed to produce a thin metal-catalyst coating layer over the inner surface of a tubular reactor. Co-plating of Pd and Ag yielded mixed distrib-

uted Pd and Ag inner surfaces, which further gave a porous Pd surface by preferential dissolution of Ag by HNO_3. A hollow tubular reactor combined with the catalytic inner surface enabled rapid and continuous reaction under a smooth flow of reactants and products. The versatility of these catalytic tubular reactors was demonstrated through efficient and rapid reduction of *p*-nitrophenol by using formic acid. The nitro group is reduced in a transfer hydrogenation process and not by molecular H_2 generated from dehydrogenation of formic acid. The porous and oxidized Pd surface showed better catalytic activity because of the increased surface area and roughness. No significant sign of deactivation of the catalyst or leaching of Pd was observed through 100 h continuous reaction, which demonstrates the robustness of the present catalytic reactors.

Experimental

Materials and reagents

Reagent-grade formic acid (HCO_2H, 98%), *p*-nitrophenol, palladium acetate [$Pd(CH_3COO)_2$], silver nitrate ($AgNO_3$), disodium ethylenediamine tetraacetate (EDTA–Na_2), ammonia (NH_3, 28%), hydrazine monohydrate, nitric acid (HNO_3, 60%) and hydrogen peroxide (H_2O_2, 30%) were purchased from Wako Pure Chemical Industries Ltd. and were used without further purification.

Fabrication of tubular reactors

A double-layered tube (o.d. 1.6 mm, i.d. 0.5 mm, length 100 cm) composed of Inconel 625 and titanium (Ti) inner layer (thickness 120 μm) was fabricated by E.S.Q. Co., Japan, by elongation of the titanium inlaid Inconel 625 piece by stretch-draw process, and used as the reactor support [11]. The Ti inner surface was oxidized to TiO_2 with H_2O_2 under supercritical water conditions (450 °C, 30 MPa). The TiO_2 surface, which is suitable for Pd plating, also acts as a barrier to prevent intermetallic diffusion of Ti and the metal catalyst. The TiO_2 surface was activated with Pd seeds before electroless plating. Plating of Pd was then conducted according to the procedure described in previous reports [10-12]. By 5 h plating at 50 °C, 67.3 mg of Pd was deposited, which corresponds to a Pd inner wall thickness of 3.6 μm. The Pd surface was oxidized by calcination of the tubular reactor at 750 °C for 2 h under air flow.

Co-plating of Pd and silver (Ag) was typically performed by passing (0.5 mL min^{-1}) an aqueous solution containing 9 mM $Pd(CH_3COO)_2$, 1 mM $AgNO_3$, 0.15 M EDTA–Na_2, 4 M NH_3, and 10 mM hydrazine monohydrate through the reactor tube at 60 °C. After 3 h plating, 67.7 mg of Pd (87%) and 10.1 mg of Ag (13%) were deposited inside the tubular reactor. After plating, washing with water was conducted to remove the chemicals remaining inside the tube. The Pd–Ag mixed layer thickness was estimated as ca. 4.2 μm.

Subsequent removal of Ag by passing 4 M HNO_3 (840 mL) at 25 °C with a flow rate of 0.5 mL min^{-1} gave the porous Pd surface as observed by SEM imaging. The remaining amounts of Pd and Ag were 48.1 mg (94%) and 2.9 mg (5.7%), respectively. We separately co-plated Pd and Ag film on a glass surface with the same chemical composition. Then the thin film (3.5 μm) was peeled and treated with 4 M HNO_3 and provided to the BET specific surface area and pore diameter measurements at 77 K by nitrogen absorption isotherm.

Hydrogenation of *p*-nitrophenol

A typical reaction procedure is the following, using the experimental setup depicted in Figure 2. The reactor tube and container of reaction stock solution were immersed in a water bath to maintain a constant temperature. The reaction was conducted at ambient pressure. An aqueous solution containing *p*-nitrophenol (10 mM) and formic acid was fed into the tubular reactor (100 cm long with inner volume of 196 μL) at a constant flow rate controlled by a peristaltic pump. The solution out of the reactor tube was collected in fractions and the UV–vis absorption spectra were measured. The analytical UV–vis peaks of substrate and product are sufficiently separated and the concentration of *p*-nitrophenol was ascertained by the absorbance at 317 nm using the calibration curve. The residence time was estimated from the volume of reaction solution at a fixed time divided by the inner volume of the reactor tube. Leaching of Pd from the reactor tube during the reaction was checked by inductively coupled plasma–atomic emission spectroscopy (ICP–AES) analysis of the fractionated reaction solution.

Instruments

The metal concentration was analyzed using ICP– atomic emission spectroscopy (ICP–AES, Model SPS 3100; SII Nano Technology Inc.). The morphology of the inner surface of the catalytic tubular reactors was observed by scanning electron microscopy (SEM) equipped with an energy-dispersive X-ray spectrometer (EDX, XL30S; Philips Co.). UV–vis absorption spectra were recorded at room temperature by using a spectrophotometer (U–3310; Hitachi). The collected gaseous products were analyzed by using a gas chromatograph (GC–8A; Shimadzu Corp.) equipped with thermal conductivity detector (TCD). A molecular sieve (5 Å) column (3 mm × 6 m) was used for H_2 with argon as the carrier gas, whereas a Porapak–Q column (3 mm × 3 m) was used coupled with helium as the carrier gas for CO_2 analysis. The specific surface area and pore diameter of the porous Pd were determined volumetrically (N_2 adsorption) by using Belsorp MAX. Samples were degassed at 250 °C under vacuum prior to the measurement.

Supporting Information

The Supporting Information features the isosbestic points in the UV–vis spectra of the reaction mixture indicating that *p*-aminophenol is the sole product and no side reaction occurs.

Supporting Information File 1

Analytical and spectral data.
[http://www.beilstein-journals.org/bjoc/content/supplementary/1860-5397-9-129-S1.pdf]

References

1. Wiles, C.; Watts, P. *Green Chem.* **2012,** *14,* 38–54. doi:10.1039/c1gc16022b
2. Wegner, J.; Ceylan, S.; Kirschning, A. *Adv. Synth. Catal.* **2012,** *354,* 17–57. doi:10.1002/adsc.201100584
3. Wegner, J.; Ceylan, S.; Kirschning, A. *Chem. Commun.* **2011,** *47,* 4583–4592. doi:10.1039/c0cc05060a
4. Holladay, J. D.; Wang, Y.; Jones, E. *Chem. Rev.* **2004,** *104,* 4767–4790. doi:10.1021/cr020721b
5. Mason, B. P.; Price, K. E.; Steinbacher, J. L.; Bogdan, A. R.; McQuade, D. T. *Chem. Rev.* **2007,** *107,* 2300–2318. doi:10.1021/cr050944c
6. Garcia-Verdugo, E.; Liu, Z.; Ramirez, E.; Garcia-Serna, J.; Fraga-Dubreuil, J.; Hyde, J. R.; Hamley, P. A.; Polakoff, M. *Green Chem.* **2006,** *8,* 359–364. doi:10.1039/b515470g
7. Kirschning, A. *Beilstein J. Org. Chem.* **2011,** *7,* 1046–1047. doi:10.3762/bjoc.7.119
8. Oyamada, H.; Naito, T.; Kobayashi, S. *Beilstein J. Org. Chem.* **2011,** *7,* 735–739. doi:10.3762/bjoc.7.83
9. Bogdan, A. R.; Sach, N. W. *Adv. Synth. Catal.* **2009,** *351,* 849–854. doi:10.1002/adsc.200800758
10. Javaid, R.; Tanaka, D. A. P.; Kawanami, H.; Suzuki, T. M. *Chem. Lett.* **2009,** *38,* 146–147. doi:10.1246/cl.2009.146
11. Javaid, R.; Kawanami, H.; Chatterjee, M.; Ishizaka, T.; Suzuki, A.; Suzuki, T. M. *Catal. Commun.* **2010,** *11,* 1160–1164. doi:10.1016/j.catcom.2010.05.018
12. Javaid, R.; Kawanami, H.; Chatterjee, M.; Ishizaka, T.; Suzuki, A.; Suzuki, T. M. *Chem. Eng. J.* **2011,** *167,* 431–435. doi:10.1016/j.cej.2010.08.080
13. Javaid, R.; Kawasaki, S.; Ookawara, R.; Sato, K.; Nishioka, M.; Suzuki, A.; Suzuki, T. M. *Appl. Catal., A: Gen.* submitted.
14. Du, Y.; Chen, H.; Chen, R.; Xu, N. *Appl. Catal., A* **2004,** *277,* 259–264. doi:10.1016/j.apcata.2004.09.018
15. Corbett, J. F. *Dyes Pigm.* **1999,** *41,* 127–136. doi:10.1016/S0143-7208(98)00075-8
16. Rode, C. V.; Vaidya, M. J.; Chaudhari, R. V. *Org. Process Res. Dev.* **1999,** *3,* 465–470. doi:10.1021/op990040r
17. Vaidya, M. J.; Kulkarni, S. M.; Chaudhari, R. V. *Org. Process Res. Dev.* **2003,** *7,* 202–208. doi:10.1021/op025589w
18. Lu, H.; Yin, H.; Liu, Y.; Jiang, T.; Yu, L. *Catal. Commun.* **2008,** *10,* 313–316. doi:10.1016/j.catcom.2008.09.015
19. Wang, J.; Yuan, Z.; Nie, R.; Hou, Z.; Zheng, X. *Ind. Eng. Chem. Res.* **2010,** *49,* 4664–4669. doi:10.1021/ie1002069
20. Yao, H.; Emmett, P. H. *J. Am. Chem. Soc.* **1959,** *81,* 4125–4132. doi:10.1021/ja01525a001
21. Yao, H.-C.; Emmett, P. H. *J. Am. Chem. Soc.* **1961,** *83,* 796–799. doi:10.1021/ja01465a011
22. Yao, H.-C.; Emmett, P. H. *J. Am. Chem. Soc.* **1962,** *84,* 1086–1091. doi:10.1021/ja00866a003
23. Venkatesan, P.; Santhanalakshmi, J. *Nanosci. Nanotechnol.* **2011,** *1,* 43–47. doi:10.5923/j.nn.20110102.08
24. Panigrahi, S.; Basu, S.; Praharaj, S.; Pande, S.; Jana, S.; Pal, A.; Ghosh, S. K.; Pal, T. *J. Phys. Chem. C* **2007,** *111,* 4596–4605. doi:10.1021/jp067554u
25. Kuroda, K.; Ishida, T.; Haruta, M. *J. Mol. Catal. A: Chem.* **2009,** *298,* 7–11. doi:10.1016/j.molcata.2008.09.009
26. Du, D.-Y.; Qin, J.-S.; Wang, T.-T.; Li, S.-L.; Su, Z.-M.; Shao, K.-Z.; Lan, Y.-Q.; Wang, X.-L.; Wang, E.-B. *Chem. Sci.* **2012,** *3,* 705–710. doi:10.1039/c2sc00586g
27. Brieger, G.; Nestrick, T. J. *Chem. Rev.* **1974,** *74,* 567–580. doi:10.1021/cr60291a003
28. Prasad, K.; Jiang, X.; Slade, J. S.; Clemens, J.; Repič, O.; Blacklock, T. J. *Adv. Synth. Catal.* **2005,** *347,* 1769–1773. doi:10.1002/adsc.200505132
29. Yu, J.-Q.; Wu, H.-C.; Ramarao, C.; Spencer, J. B.; Ley, S. V. *Chem. Commun.* **2003,** 678–679. doi:10.1039/b300074p
30. Xiang, Y.; Li, X.; Lu, C.; Ma, L.; Zhang, Q. *Appl. Catal., A* **2010,** *375,* 289–294. doi:10.1016/j.apcata.2010.01.004
31. Wienhöfer, G.; Sorribes, I.; Boddien, A.; Westerhaus, F.; Junge, K.; Junge, H.; Llusar, R.; Beller, M. *J. Am. Chem. Soc.* **2011,** *133,* 12875–12879. doi:10.1021/ja2061038
32. Rajagopal, S.; Spatola, A. F. *Appl. Catal., A* **1997,** *152,* 69–81. doi:10.1016/S0926-860X(96)00342-0
33. Tanaka, D. A. P.; Tanco, M. A. L.; Niwa, S.-i.; Wakui, Y.; Mizukami, F.; Namba, T.; Suzuki, T. M. *J. Membr. Sci.* **2005,** *247,* 21–27. doi:10.1016/j.memsci.2004.06.002
34. Rugolo, J.; Erlebacher, J.; Sieradzki, K. *Nat. Mater.* **2006,** *5,* 946–949. doi:10.1038/nmat1780
35. Tominaka, S.; Hayashi, T.; Nakamura, Y.; Osaka, T. *J. Mater. Chem.* **2010,** *20,* 7175–7182. doi:10.1039/c0jm00973c
36. Simplício, L. M. T.; Brandão, S. T.; Sales, E. A.; Lietti, L.; Bozon-Verduraz, F. *Appl. Catal., B* **2006,** *63,* 9–14. doi:10.1016/j.apcatb.2005.08.009
37. Meng, L.; Jia, A.-P.; Lu, J.-Q.; Luo, L.-F.; Huang, W.-X.; Luo, M.-F. *J. Phys. Chem. C* **2011,** *115,* 19789–19796. doi:10.1021/jp2056688
38. Lin, R.; Luo, M.; Xin, Q.; Sun, G. *Catal. Lett.* **2004,** *93,* 139–144. doi:10.1023/B:CATL.0000017067.19873.32
39. Hadi, A.; Yaacob, I. I. *Catal. Today* **2004,** *96,* 165–170. doi:10.1016/j.cattod.2004.06.118
40. Liu, X.; Liu, J.; Geng, F.; Li, Z.; Li, P.; Gong, W. *Front. Chem. Sci. Eng.* **2012,** *6,* 34–37. doi:10.1007/s11705-011-1163-3
41. Euzen, P.; Le Gal, J.-H.; Rebours, B.; Martin, G. *Catal. Today* **1999,** *47,* 19–27. doi:10.1016/S0920-5861(98)00280-6
42. Gowda, D. C.; Mahesh, B. *Synth. Commun.* **2000,** *30,* 3639–3644. doi:10.1080/00397910008086990
43. Gowda, D. C.; Gowda, A. S. P.; Baba, A. R.; Gowda, S. *Synth. Commun.* **2000,** *30,* 2889–2895. doi:10.1080/00397910008087439
44. Cortese, N. A.; Heck, R. F. *J. Org. Chem.* **1977,** *42,* 3491–3494. doi:10.1021/jo00442a008
45. Soltani, O.; Ariger, M. A.; Vázquez-Villa, H.; Carreira, E. M. *Org. Lett.* **2010,** *12,* 2893–2895. doi:10.1021/ol1008894

46. Dougherty, G. M.; Rose, K. A.; Tok, J. B.-H.; Pannu, S. S.; Chuang, F. Y. S.; Sha, M. Y.; Chakarova, G.; Penn, S. G. *Electrophoresis* **2008,** *29,* 1131–1139. doi:10.1002/elps.200700448
47. Lu, X.; Bian, X.; Nie, G.; Zhang, C.; Wang, C.; Wei, Y. *J. Mater. Chem.* **2012,** *22,* 12723–12730. doi:10.1039/c2jm16559g
48. Rajesh, R.; Venkatesan, R. *J. Mol. Catal. A: Chem.* **2012,** *359,* 88–96. doi:10.1016/j.molcata.2012.04.001
49. Chi, Y.; Yuan, Q.; Li, Y.; Tu, J.; Zhao, L.; Li, N.; Li, X. *J. Colloid Interface Sci.* **2012,** *383,* 96–102. doi:10.1016/j.jcis.2012.06.027

License and Terms

Beilstein Journal of Organic Chemistry

Hypervalent iodine/TEMPO-mediated oxidation in flow systems: a fast and efficient protocol for alcohol oxidation

Nida Ambreen, Ravi Kumar and Thomas Wirth*

Full Research Paper

Open Access

Address:
Cardiff University, School of Chemistry, Park Place, Cardiff CF10 3AT, UK

Email:
Thomas Wirth* - wirth@cf.ac.uk

* Corresponding author

Keywords:
alcohols; carbonyl compounds; flow chemistry; microreactor; oxidation

Beilstein J. Org. Chem. **2013,** *9,* 1437–1442.
doi:10.3762/bjoc.9.162

Received: 17 May 2013
Accepted: 28 June 2013
Published: 17 July 2013

This article is part of the Thematic Series "Chemistry in flow systems III".

Guest Editor: A. Kirschning

Abstract

Hypervalent iodine(III)/TEMPO-mediated oxidation of various aliphatic, aromatic and allylic alcohols to their corresponding carbonyl compounds was successfully achieved by using microreactor technology. This method can be used as an alternative for the oxidation of various alcohols achieving excellent yields and selectivities in significantly shortened reaction times.

Introduction

Oxidation of alcohols to carbonyl compounds plays an important role in organic chemistry. The transformation is traditionally achieved by using chromium-based reagents such as the Collins reagent, activated manganese dioxide, or procedures known as the Swern [1], Pfitzner–Moffatt [2] or Parikh–Doering oxidation [3]. In synthetic chemistry, selective methods for the oxidation of alcohols are highly sought after, and methods with the ability to differentiate between various functional groups are desired. The use of hypervalent iodine reagents in organic chemistry has increased during recent years [4-6]. Hypervalent iodine compounds in general have emerged as versatile oxidizing agents with compounds such as DMP (Dess–Martin periodinane) and IBX finding regular utility as highly selective oxidizing agents [7-9]. The use of the nitroxyl radical TEMPO (2,2,6,6-tetramethylpiperidine-1-oxyl) as a catalyst in the oxidation of alcohols has gained much attention in recent years [10-12]. The redox cycle involves beside TEMPO also the corresponding hydroxylamine and the oxoammonium cation, which oxidizes the alcohol and is converted to TEMPO–H [13]. Hypervalent iodine(III) reagents in combination with a catalytic amount of TEMPO have already been reported in highly selective oxidations of alcohols to carbonyl compounds [14].

The development of efficient flow-reactor systems for molecular transformations is an important area in organic synthesis. The introduction of more general platforms to perform reactions under continuous flow rather than in batch mode has

led to improvements regarding safety and sustainability. Microreactor technology can be beneficial over classical approaches in a variety of chemical reactions. Many reactions can benefit from the properties of microreactors. Enhanced mass- and heat transfer and short diffusion distances can lead to better yields within shorter reaction times [15]. Herein, we describe the development of continuous-flow systems using hypervalent iodine reagents in the TEMPO-mediated oxidation of alcohols with the advantage of significantly shortened reaction times. Several other oxidative processes have already been reported in flow chemistry [16].

Results and Discussion

Benzyl alcohol was chosen as a substrate in order to examine the efficiency of the reaction and the microreactor flow system. In a batch reaction, the mixture of benzyl alcohol (**1a**) and (diacetoxyiodo)benzene (**2**) did not show any reaction after stirring for 12 h in dichloromethane at 35 °C. The addition of a catalytic amount TEMPO to the reaction mixture led to a rapid conversion to benzaldehyde (**3a**). For initial investigations of a flow system, a simple setup consisting of two syringes driven by a syringe pump, a T-connector and a tubing reactor (PTFE tubing, length: 4 m, internal diameter: 0.75 mm) was used for the oxidation of benzyl alcohol to benzaldehyde. The tubing reactor was inserted in a water bath at constant temperature as shown in Figure 1. In all flow experiments, the alcohol substrate **1** and oxidant **2** were mixed in one syringe, and the reaction started by combining this mixture with the solvent stream of a second syringe containing the catalyst TEMPO.

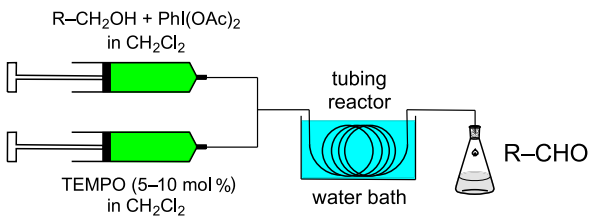

Figure 1: Flow setup for alcohol oxidations.

The reactions have been performed at 35 °C. With a residence time of 30 s the conversion to benzaldehyde was determined by GC to be 52%. Increasing the residence time to 1 min, 2 min and 4.5 min led to conversions of 65%, 79% and 95%, respectively. The reaction is incomplete if performed with amounts below 5 mol % of TEMPO (1 mol % TEMPO: 67% conversion, 2 mol % TEMPO: 81% conversion). Therefore all experiments were performed with at least 5 mol % TEMPO catalyst.

To extend the substrate scope, various benzylic, aliphatic and allylic alcohols were investigated. Good yields at short reaction times and a high selectivity towards the oxidized products were observed as shown in Table 1. Over-oxidation to the corres-

Table 1: Products and yields in the oxidation of alcohols performed in a tubing reactor at a total flow rate of 0.4 mL/min (residence time: 4.5 min) at 35 °C.

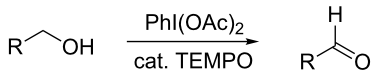

Entry	Alcohol	Product	Reference[a]	Conversion (%)[b]	Yield (%)[c]
1	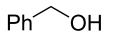	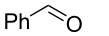	[17]	100	49
2	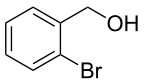	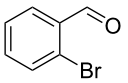	[18]	99	79
3	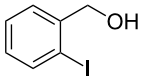	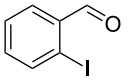	[19]	100	95
4	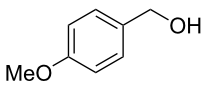	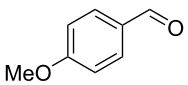	[17]	99	82
5	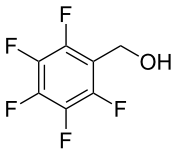	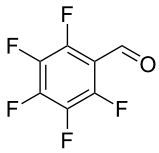	[20]	96	51

Table 1: Products and yields in the oxidation of alcohols performed in a tubing reactor at a total flow rate of 0.4 mL/min (residence time: 4.5 min) at 35 °C. (continued)

6	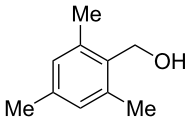	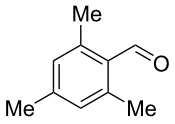	[21]	97	75
7	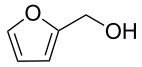	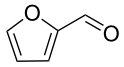	[17]	80	48
8	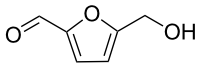	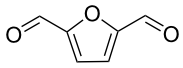	[22]	89	61
9	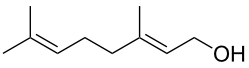	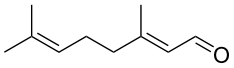	[17]	96	76
10	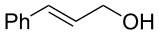	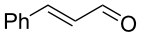	[17]	97	97
11	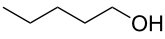	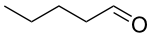	[23]	89	87
12	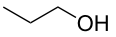		[24]	100	–
13	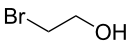	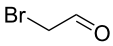	[25]	56	–
14	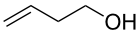	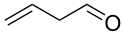	[26]	87	–
15	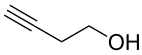	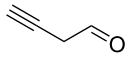	[27]	100	–
16	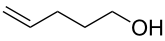	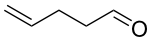	[28]	87	–
17	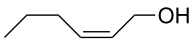	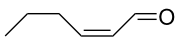	[19]	88	–
18	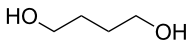	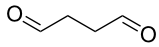	[29]	91	–
19	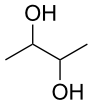	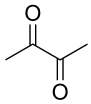	[30]	77	–
20	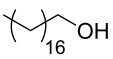		[31]	–	95
21	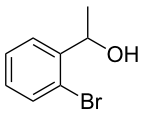	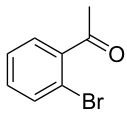	[32]	100	–
22	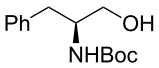	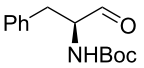	[33]	n.d.	52
23	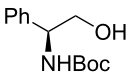	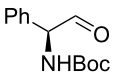	[33]	n.d.	40

[a]Spectral properties consistent with literature data. [b]Conversions determined by GC. n.d.: not determined. [c]Isolated yields.

ponding carboxylic acids was not detected and high selectivities were obtained.

In larger scale reactions (0.5 g), the conversion monitored by GC was nearly quantitative. Isolated yields were lower than those indicated by GC and largely reflect losses from isolation procedures for individual products. The optimized reaction time of 4.5 min was then used to convert also a larger amount of benzyl alcohol (15 mmol) to benzaldehyde, which was isolated as the reaction product in 49% yield. These results provide further evidence that this flow process is effective for oxidation methods initially discovered and developed under batch conditions. The substrate scope of the catalytic method in this flow process reflects that of the method originally developed in

batch. *N*-Boc protected (*S*)-phenylalaninol [34] (Table 1, entry 22) was oxidized to the corresponding aldehyde [35] without loss of optical purity as determined by the optical rotations of starting material and product [36]. *N*-Boc protected (*S*)-phenylglycinol [37] (Table 1, entry 23) suffered from some optical degradation probably during the work-up [38]. Aldehydes are rarely target molecules of pharmaceutical synthesis. These functional groups rather represent highly useful intermediates for subsequent reactions. The addition of 1,2-diaminobenzene to the crude oxidation product of 2,3-butanediol (Table 1, entry 19) allowed the direct and almost quantitative synthesis of 2,3-dimethylquinoxaline with *para*-toluenesulfonic acid as catalyst in the subsequent condensation reaction performed in a batch system (Scheme 1) [39] The oxidation–condensation sequence described here generates almost no byproducts except iodobenzene which can be removed very easily during the chromatographic purification of the product and should enable direct progression to the subsequent synthetic steps, without the need for isolation or purification of the intermediate aldehyde or ketone.

Conclusion

In conclusion, a highly efficient and selective continuous-flow reaction for the oxidation of different alcohols was developed. Apart from short reaction times, high conversions and excellent selectivities were obtained. These features, together with the low toxicity of the reagents, make the process attractive compared to the batch reaction. The economical and benign oxidation is broadly applicable to a wide range of alcohols.

Experimental

General: ^{1}H NMR and ^{13}C NMR spectra were recorded on a AV-400 Bruker spectrometer by using the solvents indicated with 400 and 100 MHz, respectively. All reactions were monitored by thin-layer chromatography that was performed on precoated sheets of silica gel 60. GC analyses were performed on a GC-FID (Varian 3900) chromatograph. All purchased chemicals were used without further purification.

General procedure for the alcohol oxidation in flow

Solutions of (diacetoxyiodo)benzene (1.1 equiv) and the alcohol (50 mg) in CH_2Cl_2 (1.5 mL) and 2,2,6,6-tetramethyl-1-piperidinyloxyl (TEMPO) (5–10 mg, 10–20 mol %) in CH_2Cl_2 (1.5 mL) were loaded in two syringes. Both syringes were placed in a syringe pump (Fusion 100) and connected via a T-piece to a tubing reactor (PTFE, length: 4 m, internal diameter: 0.75 mm). The tubing reactor was immersed in a thermocontrolled water bath at 35 °C. The total flow rate was adjusted to 0.4 mL min^{-1} resulting in a residence time of 4.5 min. The reaction mixture exiting the flow reactor was quenched with water and, after completion of the reaction, extracted with CH_2Cl_2. The combined organic layers were dried over magnesium sulfate and the solvents were removed in vacuo. Direct analysis with GC allowed the determination of the conversion by comparison of the product peak with the peak of the starting alcohol.

Large scale oxidation of benzyl alcohol in flow

The reaction was performed with the Vapourtec E-Series using a PFA tubing reactor. Benzyl alcohol (2 g, 18.5 mmol) and (diacetoxyiodo)benzene (6.3 g 19.5 mmol) were dissolved in CH_2Cl_2 (120 mL). 2,2,6,6-Tetramethyl-1-piperidinyloxyl (TEMPO) (160 mg, 1 mmol) was dissolved in CH_2Cl_2 (120 mL). Both solutions (flow rates: 2 mL min^{-1} each) were mixed in a T-piece before entering the tubing reactor (volume: 10 mL) resulting in a residence time of 5 min. After constant flow had been achieved, 200 mL of the reaction solution was collected in a flask containing water (20 mL) as a quenching agent. After completion of the reaction, the organic phase was removed and the aqueous phase was extracted with CH_2Cl_2 (3 × 20 mL). The combined organic layers were dried over magnesium sulfate, and the solvents were removed in vacuo. The crude reaction mixture was purified by flash chromatography on silica using hexane/ethyl acetate (9:1) as eluent. Some benzaldehyde was lost during the drying processes and 0.8 g (7.5 mmol, 49%) was isolated.

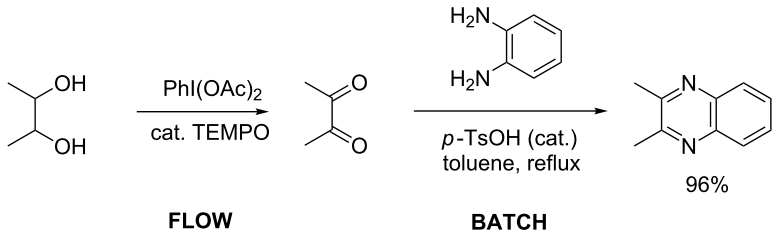

Scheme 1: Oxidation–condensation sequence in the synthesis of 2,3-dimethylquinoxaline.

Procedure for the aldehyde and diamine condensation

1,2-Phenylenediamine (0.59 mg 0.55 mmol) was added to the crude oxidized product of 2,3-butanediol (50 mg 0.55 mmol) and dissolved in toluene in a round-bottom flask, and *p*-toluenesulfonic acid was added as catalyst. The reaction mixture was heated under reflux for 2 hours and monitored by TLC. After the completion of the reaction the solvent was evaporated, and the reaction mixture was extracted with CH_2Cl_2 and water. The organic layers were dried over magnesium sulfate and the solvents were removed in vacuo. The ^{1}H NMR analysis showed a clean spectrum of the condensation product.

Acknowledgements

We thank the Schlumberger Foundation for support through a Faculty for the Future fellowship (N.A.) and the EPSRC National Mass Spectrometry Facility, Swansea, for mass spectrometric data.

References

1. Omura, K.; Swern, D. *Tetrahedron* **1978,** *34,* 1651–1660. doi:10.1016/0040-4020(78)80197-5
2. Pfitzner, K. E.; Moffatt, J. G. *J. Am. Chem. Soc.* **1963,** *85,* 3027–3028. doi:10.1021/ja00902a036
3. Parikh, J. R.; Doering, W. v. E. *J. Am. Chem. Soc.* **1967,** *89,* 5505–5507. doi:10.1021/ja00997a067
4. Hypervalent Iodine Chemistry. In *Modern Developments in Organic Synthesis;* Wirth, T., Ed.; *Topics in Current Chemistry*; 2003; p 224.
5. Zhdankin, V. V. *ARKIVOC* **2009,** *(i),* 1–62.
6. Wirth, T. *Angew. Chem., Int. Ed.* **2005,** *44,* 3656–3665. doi:10.1002/anie.200500115
7. Wirth, T. IBX – New Reactions with an Old Reagent. In *Organic Synthesis Highlights V;* Schmalz, H.-G.; Wirth, T., Eds.; Wiley-VCH: Weinheim, Germany, 2003; pp 144–150.
8. Richardson, R. D.; Zayed, J. M.; Altermann, S.; Smith, D.; Wirth, T. *Angew. Chem., Int. Ed.* **2007,** *46,* 6529–6532. doi:10.1002/anie.200702313
9. Tohma, H.; Kita, Y. *Adv. Synth. Catal.* **2004,** *346,* 111–124. doi:10.1002/adsc.200303203
10. Bobbit, J. M.; Brückner, C.; Merbouh, N. *Org. React.* **2009,** *74,* 106–424. doi:10.1002/0471264180.or074.02
11. Tebben, L.; Studer, A. *Angew. Chem., Int. Ed.* **2011,** *50,* 5034–5068. doi:10.1002/anie.201002547
12. Tilley, L. J.; Bobbitt, J. M.; Murray, S. A.; Camire, C. E.; Eddy, N. A. *Synthesis* **2013,** *45,* 326–329. doi:10.1055/s-0032-1317861
13. Ma, Y.; Loyns, C.; Price, P.; Chechik, V. *Org. Biomol. Chem.* **2011,** *9,* 5573–5578. doi:10.1039/c1ob05475a
14. De Mico, A.; Margarita, R.; Parlanti, L.; Vescovi, A.; Piancatelli, G. *J. Org. Chem.* **1997,** *62,* 6974–6977. doi:10.1021/jo971046m
15. Wirth, T., Ed. *Microreactors in Organic Synthesis and Catalysis;* Wiley-VCH: Weinheim, Germany, 2013.
16. Ye, X.; Johnson, M. D.; Diao, T.; Yates, M. H.; Stahl, S. S. *Green Chem.* **2010,** *12,* 1180–1186. doi:10.1039/c0gc00106f
17. Iinuma, N.; Moriyama, K.; Togo, H. *Tetrahedron* **2013,** *69,* 2961–2970. doi:10.1016/j.tet.2013.02.017
18. Lin, C.-K.; Lu, T.-J. *Tetrahedron* **2010,** *66,* 9688–9693. doi:10.1016/j.tet.2010.10.053
19. Hoover, J. M.; Stahl, S. S. *J. Am. Chem. Soc.* **2011,** *133,* 16901–16910. doi:10.1021/ja206230h
20. Claramunt, R. M.; López, C.; López, A.; Pérez-Medina, C.; Pérez-Torralba, M.; Alkorta, I.; Elguero, J.; Escames, G.; Acuña-Castroviejo, D. *Eur. J. Med. Chem.* **2011,** *46,* 1439–1447. doi:10.1016/j.ejmech.2011.01.027
21. Hu, Y. L.; Liu, Q. F.; Lu, T. T.; Lu, M. *Catal. Commun.* **2010,** *11,* 923–927. doi:10.1016/j.catcom.2010.03.017
22. Hanson, S. K.; Wu, R.; Silks, L. A. *Org. Lett.* **2011,** *13,* 1908–1911. doi:10.1021/ol103107v
23. The Aldrich Library of ^{13}C and ^{1}H FT NMR Spectra, Alrich Chemical Company Inc., 1993, *Vol. 1*, 729C.
24. Makulski, W.; Jackowski, K. *J. Mol. Struct.* **2003,** *651–653,* 265–269. doi:10.1016/S0022-2860(02)00638-5
25. Li, W.; Li, J.; Wu, Y.; Fuller, N.; Markus, M. A. *J. Org. Chem.* **2010,** *75,* 1077–1086. doi:10.1021/jo902014z
26. Airiau, E.; Spangenberg, T.; Girard, N.; Breit, B.; Mann, A. *Org. Lett.* **2010,** *12,* 528–531. doi:10.1021/ol902718q
27. Blankespoor, R. L.; Smart, R. P.; Batts, E. D.; Kiste, A. A.; Lew, R. E.; Van Vliet, M. E. *J. Org. Chem.* **1995,** *60,* 6852–6859. doi:10.1021/jo00126a040
28. Siebuma, A.; van Wijk, A.; Schoevaart, R.; Kieboom, T. *J. Mol. Catal. B* **2006,** *41,* 141–145. doi:10.1016/j.molcatb.2006.04.003
29. Hardy, P. M.; Nicholls, A. C.; Rydon, H. N. *J. Chem. Soc., Perkin Trans. 2* **1972,** 2270–2278. doi:10.1039/P29720002270
30. Hirasawa, S.; Watanabe, H.; Kizuka, T.; Nakagawa, Y.; Tomishige, K. *J. Catal.* **2013,** *300,* 205–216. doi:10.1016/j.jcat.2013.01.014
31. Biraboneye, A. C.; Madonna, S.; Maher, P.; Kraus, J.-L. *ChemMedChem* **2010,** *5,* 79–85. doi:10.1002/cmdc.200900418
32. Schröder, N.; Wencel-Delord, J.; Glorius, F. *J. Am. Chem. Soc.* **2012,** *134,* 8298–8301. doi:10.1021/ja302631j
33. Morita, T.; Nagasawa, Y.; Yahiro, S.; Matsunaga, H.; Kunieda, T. *Org. Lett.* **2001,** *3,* 897–899. doi:10.1021/ol015535r
34. Wu, Y.-C.; Zhu, J. *J. Org. Chem.* **2008,** *73,* 9522–9524. doi:10.1021/jo8021988
35. Alfaro, R.; Yuste, F.; Ortiz, B.; Sánchez-Obregón, R.; Ruano, J. L. G. *Tetrahedron* **2009,** *65,* 357–363. doi:10.1016/j.tet.2008.10.037
36. (*S*)-*N*-(*tert*-Butyloxycarbonyl)phenylalaninol: $[\alpha]_D^{27}$ = –24.0 (*c* = 0.83, $CHCl_3$); literature [34]: $[\alpha]_D^{25}$ = –27.0 (*c* = 1.7, $CHCl_3$ (*S*)-*N*-(*tert*-Butoxycarbonyl)-2-amino-3-phenylpropanal: $[\alpha]_D^{25}$ = –36.0 (*c* = 0.5, MeOH); literature [35] $[\alpha]_D$ = –37.9 (*c* = 1.0, MeOH).
37. Cox, G. G.; Harwood, L. M. *Tetrahedron: Asymmetry* **1994,** *5,* 1669–1672. doi:10.1016/0957-4166(94)80077-4
38. (*S*)-*N*-(*tert*-Butyloxycarbonyl)phenylglycinol: $[\alpha]_D^{27}$ = +37.0 (*c* = 0.97, $CHCl_3$); literature [37]: $[\alpha]_D^{23}$ = +38.7 (*c* = 1.06, $CHCl_3$). (*S*)-*N*-(*tert*-Butoxycarbonyl)-2-amino-2-phenylethanal: $[\alpha]_D^{25}$ = –0.5 (*c* = 0.06, MeOH); literature [33] $[\alpha]_D$ = –2.9 (*c* = 3.0, $CHCl_3$).
39. Morales-Castellanos, J. J.; Ramirez-Hernández, K.; Gómez-Flores, N. S.; Rodas-Suárez, O. R.; Peralta-Cruz, J. *Molecules* **2012,** *17,* 5164–5176. doi:10.3390/molecules17055164

Beilstein Journal of Organic Chemistry

Controlled synthesis of poly(3-hexylthiophene) in continuous flow

Helga Seyler, Jegadesan Subbiah, David J. Jones, Andrew B. Holmes and Wallace W. H. Wong*

Full Research Paper

Open Access

Address:
School of Chemistry, Bio21 Institute, University of Melbourne, 30 Flemington Road, Parkville, Victoria 3010, Australia

Email:
Wallace W. H. Wong* - wwhwong@unimelb.edu.au

* Corresponding author

Keywords:
conjugated polymers; continuous-flow synthesis; controlled polymerization; flow chemistry; organic solar cell materials

Beilstein J. Org. Chem. **2013,** *9,* 1492–1500.
doi:10.3762/bjoc.9.170

Received: 29 April 2013
Accepted: 02 July 2013
Published: 25 July 2013

This article is part of the Thematic Series "Chemistry in flow systems III".

Guest Editor: A. Kirschning

Abstract

There is an increasing demand for organic semiconducting materials with the emergence of organic electronic devices. In particular, large-area devices such as organic thin-film photovoltaics will require significant quantities of materials for device optimization, lifetime testing and commercialization. Sourcing large quantities of materials required for the optimization of large area devices is costly and often impossible to achieve. Continuous-flow synthesis enables straight-forward scale-up of materials compared to conventional batch reactions. In this study, poly(3-hexylthiophene), P3HT, was synthesized in a bench-top continuous-flow reactor. Precise control of the molecular weight was demonstrated for the first time in flow for conjugated polymers by accurate addition of catalyst to the monomer solution. The P3HT samples synthesized in flow showed comparable performance to commercial P3HT samples in bulk heterojunction solar cell devices.

Introduction

Poly(3-hexylthiophene), P3HT, is the most investigated material in bulk heterojunction (BHJ) organic solar cells (OSC) [1]. The reasons for its dominance in the field include its simple chemical structure, controlled synthetic method, reasonable spectral absorption, good semiconducting properties, high chemical stability, and wide commercial availability. Its emergence as a semiconducting material came with the development of synthetic methods that enable production of highly regioregular P3HT with good control of the molecular weight [2,3]. Currently, the preferred method for the synthesis of regioregular P3HT is the Kumada catalyst transfer polymerization (KCTP) or also referred to as Grignard metathesis polymerization (GRIM) [4,5]. This method is attractive because of readily available reagents, relatively mild reaction conditions, and short polymerization time. In the most basic reaction setup, 2,5-dibromo-3-hexylthiophene is treated with one equivalent of alkylmagnesium chloride to form a mixture of monosubstituted thiophene Grignard monomers (Scheme 1a). On addition of a desired amount of Ni(II) catalyst, the active catalyst species is formed in solution, and polymerization proceeds until all of the

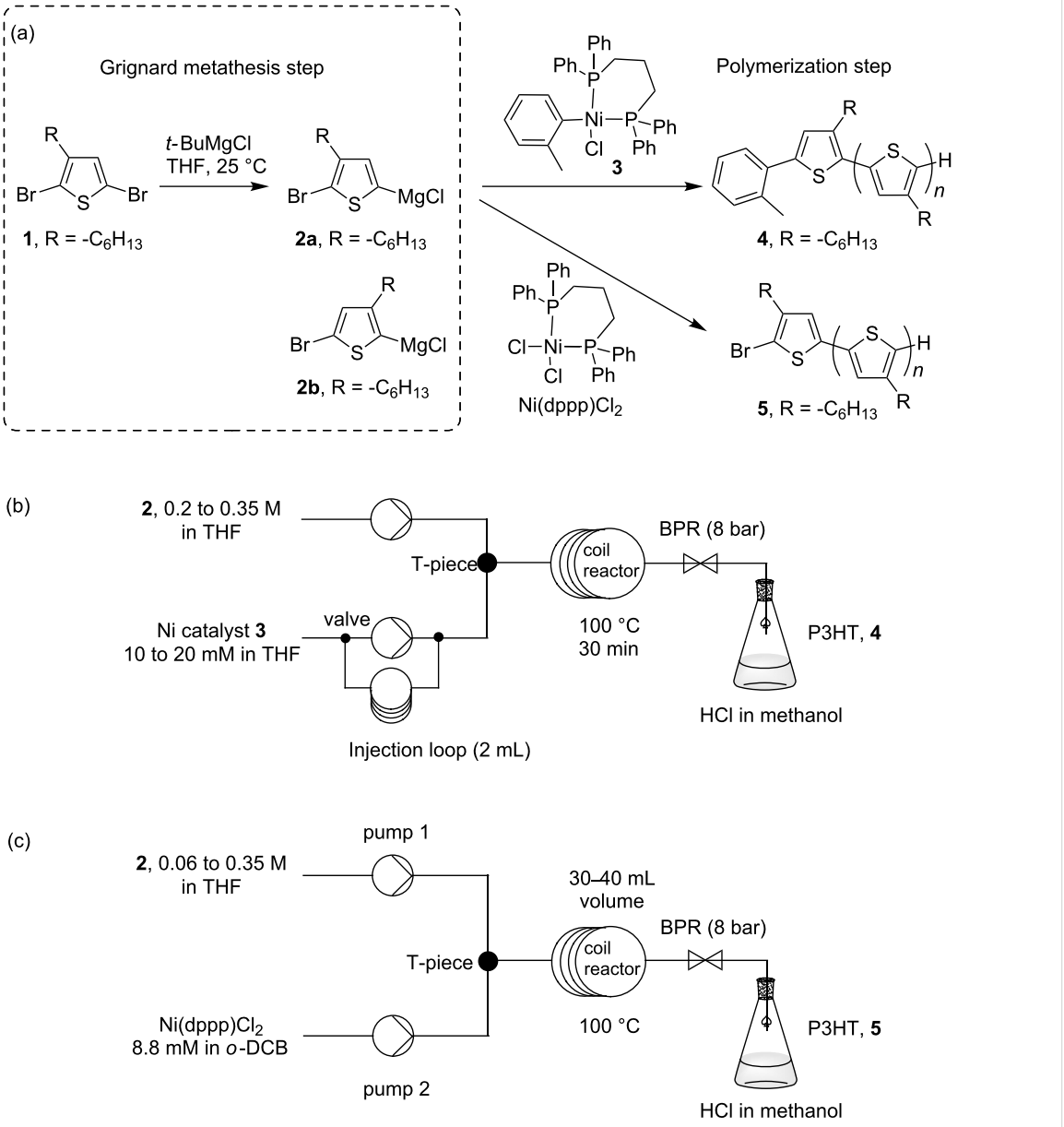

Scheme 1: (a) Preparation of thiophene Grignard monomer and synthesis of P3HT by Kumada catalyst transfer polymerization. (b) Schematic representation for the flow setup using nickel complex **3** and (c) Ni(dppp)Cl_2.

reactive Grignard monomer has been consumed. Controlled polymerization and high molecular weights have been demonstrated by many research groups with variations to this general method [6-9].

Significant quantities of materials are required for the optimization of large-area roll-to-roll printed organic solar cells [3,10]. While some of the organic semiconducting materials can be obtained commercially an a hundreds-of-grams scale, it is important to explore methods for scaled-up production in order to gain access to in-house materials at reasonable costs and lead times. In addition, batch-to-batch variations in the molecular weight distribution have been observed in commercial polymer samples, leading to differences in material deposition and film quality. This will almost certainly create problems with the performance consistency of large-area roll-to-roll printed devices. To this end, we have started to examine some key reactions in the synthesis of organic electronic materials using continuous-flow processing [11-13].

Continuous-flow synthesis methods offer several advantages over traditional batch methods [14-18]. The scale-up of reactions is not only straightforward in continuous processing, but there are also benefits in high reaction reproducibility through

accurate parameter control, superior heating and mixing of reagents, boosting reaction rates, and safe handling of reactive intermediates. Using a commercial continuous-flow tube reactor [19], we have already demonstrated multigram synthesis of fullerene derivatives by cycloaddition reactions [11] as well as rapid conjugated-polymer synthesis using Suzuki–Miyaura and Stille coupling [12]. In this study, the continuous-flow synthesis of P3HT is examined. Distinct from a recent report of P3HT synthesis in a droplet-based microreactor [20], development of the flow synthesis is described in detail and controlled polymerization of P3HT, both in terms of molecular weight and regioregularity, has been achieved in this work. In particular, the feed ratio of catalyst to monomer was accurately controlled giving polymers with molecular weights ranging from 5 to 40 kg/mol as desired. In addition, BHJ devices prepared using commercial, batch and flow-synthesized P3HT gave comparable performance.

Results and Discussion

The most widely used synthetic route to regioregular P3HT is the Kumada catalyst transfer polycondensation (KCTP) developed by the McCullough group [6] and the Yokozawa group [7]. In a representative experiment for the preparation of P3HT, the thiophene Grignard monomer **2** is prepared from the magnesium exchange reaction of an alkyl Grignard reagent and 2,5-dibromo-3-hexylthiophene (**1**, Scheme 1a). It should be noted here that a mixture of Grignard monomers **2a** and **2b** is produced in this step, typically in a ratio of 75:25. Only **2a** participates in the polymerization step on addition of the catalyst, Ni(dppp)Cl_2, as a solid (Scheme 1a) [6]. As KCTP is a quasi-living polymerization, the product molecular weight can be controlled by adjusting the monomer-to-catalyst ratio [21].

At the start of this study, the aim was to transfer conventional batch reaction conditions for P3HT synthesis to continuous-flow processing. The polymerization step in flow was examined first with the thiophene Grignard monomer prepared in batch. Good solubility and solvent compatibility in the polymerization are essential factors to be evaluated for the translation into flow methods. The accurate addition of Ni catalyst to the thiophene Grignard monomer results in the desired catalyst-to-monomer ratio and molecular-weight control. An initial attempt was made to prepare a solution of the commonly used Ni(dppp)Cl_2 catalyst in tetrahydrofuran (THF) which was then added to a solution of the thiophene Grignard monomer. Two problems immediately arose from this early experiment. The Ni(dppp)Cl_2 catalyst only has modest solubility in THF at room temperature. This limited the concentration of the polymerization reaction. The second more serious problem is the dissociation of the catalyst species in THF solution. There was a visible color change in the Ni(dppp)Cl_2/THF solution from orange to colorless over a period of several minutes. The dissociation of the catalyst species was accompanied by a decrease in catalyst activity leading to low polymer formation. To solve this problem, we were inspired by the work of a number of research groups, in which polymerization was externally initiated from an active tolyl-functionalized nickel complex **3** (Scheme 1a) [8,9,22]. The tolyl–nickel species **3** is soluble and shows good stability in THF in an inert environment. Further, polymers initiated with this complex showed lower defect levels [23,24]. After successfully experimenting with this catalyst in batch conditions, the reagent was applied in flow processing for the synthesis of P3HT (Scheme 1b).

The thiophene Grignard reagent **2** was prepared by traditional batch chemistry and the conversion and regioisomeric ratio were assessed in quenching experiments (Scheme 1a, ratio **2a** to **2b** 77:23; see Figure S2 in Supporting Information File 1 for ^{1}H NMR data). The Ni catalyst **3** was delivered to a T-piece via an injection loop and mixed with a stream of Grignard **2** (Scheme 1b) [25]. The mixture was directed to a preheated coil reactor (polyfluoroalkoxy, PFA) at 100 °C with a retention time of 30 min. The polymer solution was then quenched in methanolic HCl (2 M) and the precipitated product was collected. The monomer-to-initiator ratio was adjusted through the variation of flow rates and reagent concentrations (Table 1).

Table 1: Flow polymerizations initiated with *o*-tolyl–nickel complex **3**.[a]

Entry	[**2**] M	Flow rate, **2** mL/min	[Catalyst **3**] M	Flow rate, **3** mL/min	Catalyst mol %	Time min	M_n[b] kg/mol	M_w/M_n
1	0.2	1	0.02	0.3	3	23	6.2	1.5
2	0.2	1	0.01	0.3	1.5	23	9.6	1.8
3	0.2	0.9	0.01	0.3	0.9	23	21.3	1.6
4	0.35	1[c]	0.01	0.15[c]	0.43	53	37.7[d]	1.5

[a]Polyfluoroalkoxy (PFA) tube reactor volume = 30 mL and heated at 100 °C. [b]Molecular weight values obtained by GPC in toluene calibrated against polystyrene standards with refractive index detection. [c]Flow rates were readjusted after the injection of reagents to afford a residence time of 53 min. [d]Data obtained after Soxhlet extraction with methanol and petroleum spirits 40–60 °C.

Gel-permeation chromatography (GPC) analysis in toluene (against polystyrene standards) revealed the formation of polymer with number-average molecular weights (M_n) ranging from 5 to 40 kg/mol. The M_n values increased linearly with nickel catalyst content, providing evidence for the quasi-living nature [21] of the polymerization in flow processing (Table 1 and Figure 1). In fact, the molecular-weight data obtained in conventional batch reactions were very similar to those recorded in continuous-flow reactions (Figure 1). Matrix-assisted laser desorption ionization mass spectrometry (MALDIMS) and ^{1}H NMR experiments were used to determine the degree of end-group control in these polymerizations [8,26]. From the mass of the polymeric species and the distinctive proton resonance of the end-groups, it was possible to detect the presence of *o*-tolyl/H, H/H and Br/H end-groups (Figure 2 and Supporting Information File 1 for details). As Ni catalyst **3** was prepared from Ni(dppp)Cl_2 and used directly in the polymerization, the formation of different end-group species can be attributed to polymer initiation by residual Ni(dppp)Cl_2 species [24].

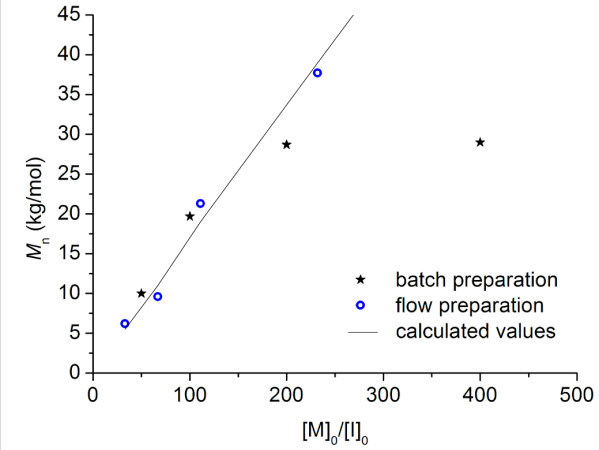

Figure 1: Plot of number-average molecular weight, M_n, versus monomer–catalyst ratio $[M]_0/[I]_0$ for batch and flow samples prepared by external initiation using Ni catalyst **3** (see Table 1 for experimental data).

While Ni catalyst **3** successfully initiated polymerizations in the time frame of this experiment, it lacked the long term stability in solution required for potential large-scale flow production of P3HT. An alternative approach was to dissolve Ni(dppp)Cl_2 in a solvent system that limited the ligand-dissociation phenomenon observed in THF. After the screening of a number of organic solvents, Ni(dppp)Cl_2 was found to be soluble in *o*-dichlorobenzene (*o*-DCB) and showed good stability with

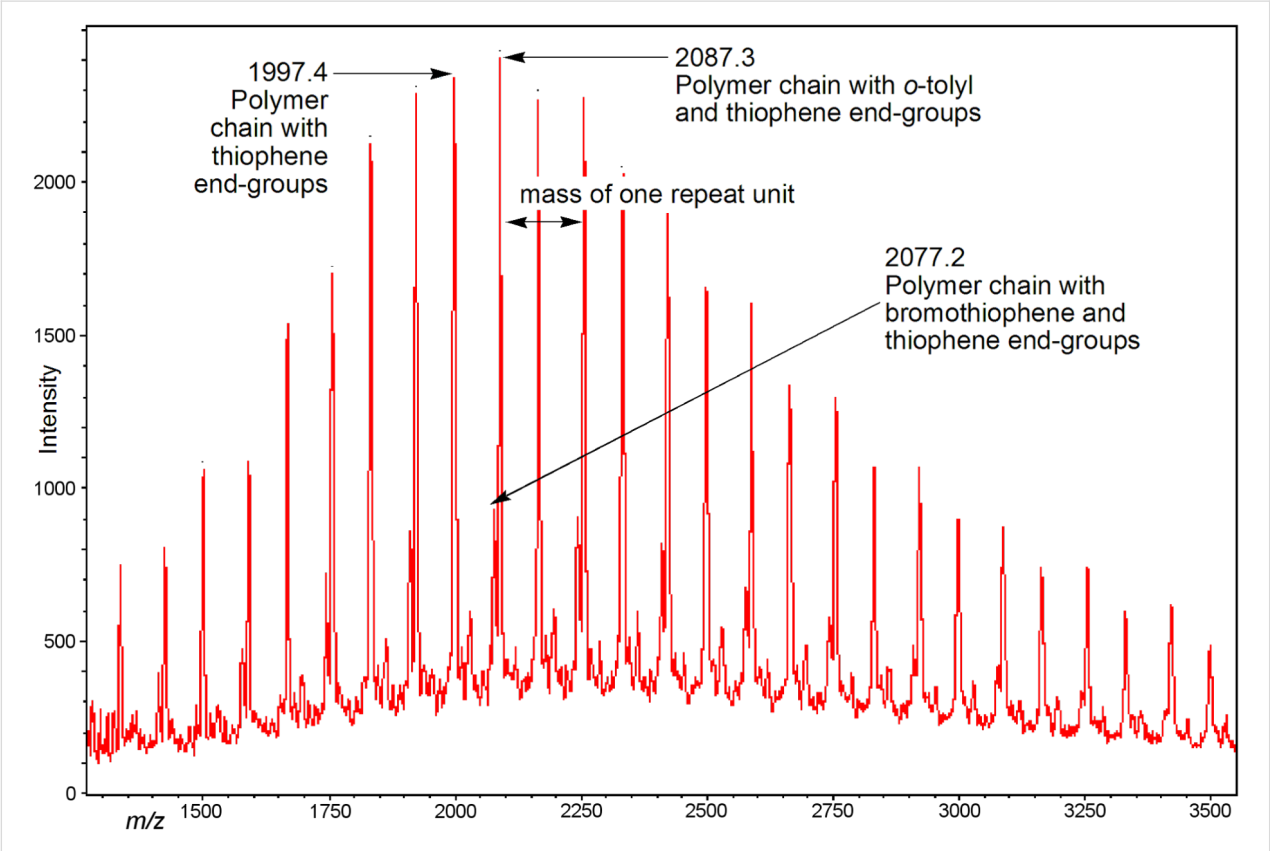

Figure 2: MALDI mass spectrum of low-molecular-weight preparation (GPC, M_n = 6.2 kg/mol) of P3HT in continuous flow. Signals corresponding to polymer chains with *o*-tolyl/H, H/H and Br/H end groups were observed.

catalytic activity maintained over several days under normal atmospheric conditions. It is interesting to note that *o*-DCB did not adversely affect the polymerization in batch reactions despite the possibility that the aryl chloride solvent might participate in the Kumada reaction. Apparently, the reactivity of aryl chloride is significantly lower than that of aryl bromide under these reaction conditions.

With the catalytic activity of Ni(dppp)Cl_2 in *o*-DCB confirmed in batch reactions, continuous-flow processing was investigated (Scheme 1c, see Supporting Information File 1 for batch synthesis procedures). The preparation of various molecular weights was achieved by fine-tuning of the monomer-to-catalyst ratio $[M]_0/[I]_0$, by varying the concentration of the Grignard reagent **2** and the flow rates of the monomer and catalyst. The results for the flow polymerizations are summarized in Table 2, and Figure 3 shows the correlation between $[M]_0/[I]_0$ and molecular weight and comparison with batch experiments. The polymerization in flow compared well with the theoretical molecular weights up to 20 kg/mol. High-molecular-weight P3HT (M_p 66.7 kg/mol) was obtained in continuous flow and this was achieved in shorter reaction time compared to the batch reaction (Table 2, entry 5). The deviation from the calculated values at high molecular weights in flow processing and in batch reactions with short reaction time (30 min) indicated that longer reaction times were required (Figure 3). In batch reaction with long polymerization times (1 h), the measured molecular-weight values matched with the calculated numbers from the $[M]_0/[I]_0$ ratio (Figure 3). As our current flow setup is limited by the size of the coil reactors, we anticipate that larger coil reactor volumes would ensure high-throughput production of high-molecular-weight P3HT in continuous flow.

In our studies, stainless-steel tube reactors were also examined for the synthesis of P3HT. In comparison to polyfluoroalkoxy (PFA) tube reactors, stainless-steel tube reactors offer the advantage of low gas permeability. Satisfactory results were

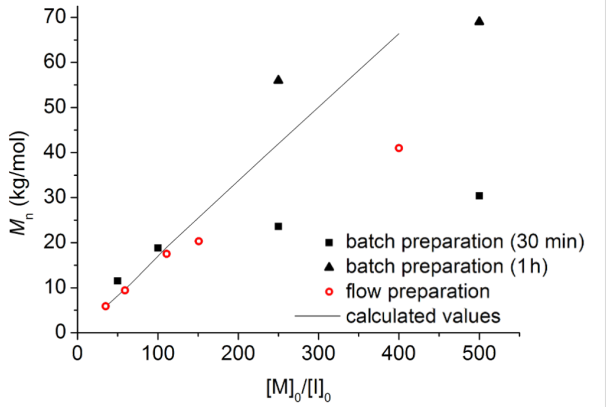

Figure 3: Plot of number-average molecular weight, M_n, versus monomer–catalyst ratio $[M]_0/[I]_0$ for batch and flow samples prepared with Ni(dppp)Cl_2 catalyst dissolved in *o*-DCB (see Table 2 for experimental data).

achieved for relatively low degrees of polymerization in the stainless-steel reactors (Table 2, entries 1 and 2). Interestingly, higher molecular weights could only be achieved in the PFA reactors (Table 2, entries 3–5). This suggests that the nickel-catalyzed polymerization is incompatible with the stainless-steel reactor and we speculate that the nickel content in stainless steel may be the cause of the incompatibility especially at the elevated reaction temperatures used.

To demonstrate the flow synthesis of P3HT from 2,5-dibromo-3-hexylthiophene (**1**), the Grignard metathesis step was performed in the tube reactor followed by the addition of the Ni(dppp)Cl_2 catalyst for the polymerization (Scheme 2). In this telescoped process, the thiophene Grignard compounds **2a** and **2b** were formed in the first coil and subsequently mixed with the catalyst stream and fed into the second reactor (Scheme 2). The two-step reaction was performed under superheated conditions (at 250 psi back pressure) and the reagent flow rates were adjusted to deliver reasonable reaction times for both reactors. For the Grignard metathesis step, a stock solution containing

Table 2: Data for flow polymerization using Ni(dppp)Cl_2 catalyst dissolved in *o*-DCB.[a]

Entry	[**2**] M	Flow rate, **2** mL/min	Flow rate, Ni(dppp)Cl_2 mL/min	Catalyst mol %	Time min	M_n (M_{calcd}) kg/mol	M_p kg/mol	M_w/M_n
1	0.06	1	0.2	2.9	33	5.9 (5.6)	13	2
2	0.2	1	0.4	1.7	30	9.6 (9.4)	22	1.9
3	0.2	0.9	0.18	0.9	27	17.5 (18)	31	1.6
4	0.35	0.7	0.18	0.7	34	20.3 (25.1)	33.5	1.5
5	0.35	1[b]	0.1[b]	0.25	50	41[c] (66)	66.7[c]	1.4

[a]Stainless-steel tube reactor volume = 40 mL for entries 1 and 2; PFA tube reactor volume = 30 mL for entries 3 to 5. Reactors heated to 100 °C. [b]Flow rate was readjusted after injection of reagents to afford 50 min residence time. [c]After Soxhlet extraction with methanol and petroleum spirits 40–60 °C.

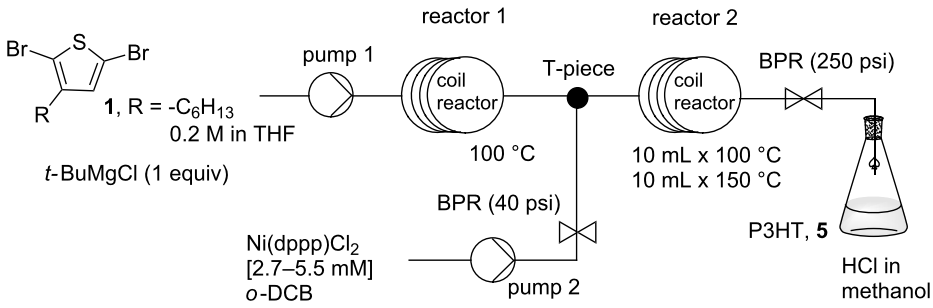

Scheme 2: Schematic representation of the telescoped preparation of P3HT in a flow reactor.

both 2,5-dibromo-3-hexylthiophene (**1**) and the *tert*-butylmagnesium chloride (0.2 M in THF) were allowed to react at 100 °C with a retention time of 20 min in reactor coil 1.

$Ni(dppp)Cl_2$ catalyst in *o*-DCB was added to this reaction stream and the polymerization was heated at 150 °C for 18 min. Under these conditions, we succeeded in obtaining P3HT with M_n of 31 kg/mol and polydispersity of 1.5 (Table 3, entry 1). The regioregularity was estimated to be 95% from the integration of the α-methylene protons in the ^1H NMR spectrum (Figure 4). The same degree of regioregularity was observed for a batch sample of similar molecular weight. Additionally, the variation of the molecular weight was investigated when the $[M]_0/[I]_0$ ratio was varied. As expected, increasing the concentration or the flow rate of the catalyst stock solution, afforded lower-molecular-weight polymers (Table 3, entries 2 and 3).

Table 3: Data for the telescoped synthesis of P3HT from 2,5-dibromo-3-hexylthiophene (**1**) in flow.[a]

Entry	Flow rate, monomer mL/min	[Catalyst] mM	Flow rate, $Ni(dppp)Cl_2$ mL/min	Catalyst mol %	Time[b] min	M_n kg/mol	M_p kg/mol	M_w/M_n
1	1	2.7	0.1	0.14	18	31[c]	49[c]	1.5[c]
2	1	5.5	0.1	0.28	18	20.5	47	1.9
3	1	5.5	0.18	0.5	28[d]	8	16	1.8

[a]Reactor 1 (PFA × 2) volume = 20 mL; reactor 2 (PFA and stainless steel) = 20 mL. [b]Residence time for the polymerization. [c]After Soxhlet extraction with methanol and petroleum spirits 40–60 °C. [d]Reaction time was adjusted by slowing down the flow rate after reactor 1.

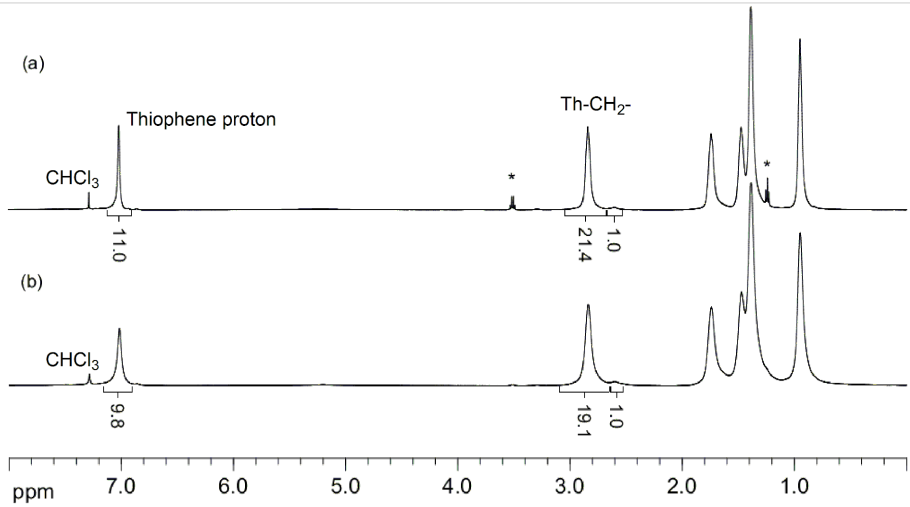

Figure 4: ^1H NMR ($CDCl_3$, 500 MHz) spectra of P3HT samples prepared in (a) flow and (b) batch show comparable regioregularity of approximately 95% for both processes. P3HT prepared in flow (M_n = 20 kg/mol) and in batch (M_n = 17 kg/mol) (* designates residual solvent).

In order to assess the device performance of P3HT synthesized using flow methods described in this study, bulk heterojunction (BHJ) solar cells were fabricated and tested. BHJ devices were fabricated with the following device geometry: ITO/PEDOT:PSS/P3HT:$PC_{61}BM$ (1:1)/ZnO nanoparticle/Al, where ITO = indium tin oxide, PEDOT:PSS = poly(3,4-ethylenedioxythiophene):poly(styrenesulfonate) and $PC_{61}BM$ = [6,6]-phenyl-C_{61}-butyric acid methyl ester (Figure 5a). The P3HT:$PC_{61}BM$ active layer was deposited by spin coating from chlorobenzene solution. Device fabrication and characterizations were performed in air (see Supporting Information File 1 for details).

The current-density–voltage (J–V) curves for the solar-cell devices prepared from various P3HT samples are shown in Figure 5b. The device performance parameters for the different P3HT samples were all rather similar with power conversion efficiency (PCE) ranging from 2.1 to 2.6% (Table 4). The short circuit current density (J_{sc}) parameter showed the largest variations and this directly correlated with the thickness of the device active layer (Table 4). Thinner active layers absorbed less of the incoming irradiation leading to decreased J_{sc}. It is pleasing to note that the performance of the commercial P3HT sample (Merck lisicon SP001) was comparable to that of P3HT from flow synthesis (Table 4). It should be noted that the lower PCE of these devices compared with some literature values [1] was attributed to the fact that all devices were fabricated and measured in air. Interestingly, P3HT samples with different end-group variations did not have significant effects on device performance. These results are extremely encouraging for the product of device-grade P3HT using continuous-flow methods with simple benchtop equipment.

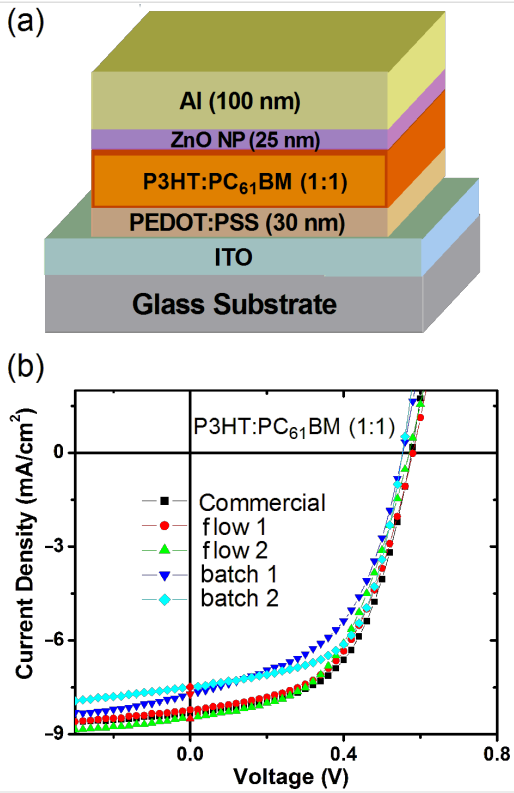

Figure 5: (a) Schematic diagram of the photovoltaic device geometry and (b) J–V curves of BHJ solar cells with P3HT:$PC_{61}BM$ active layer deposited by spin coating from chlorobenzene solution. Commercial = Merck P3HT (lisicon SP001); flow 1 = Table 1, entry 4; flow 2 = Table 2, entry 5; batch 1 = P3HT synthesized with catalyst **3**; batch 2 = P3HT synthesized with Ni(dppp)Cl_2.

Conclusion

P3HT has been successfully synthesized in continuous flow by using a commercially available benchtop flow reactor. After optimization of reaction conditions, good molecular-weight control was achieved by adjusting the monomer-to-catalyst ratio with variations in reagent concentration and flow rates. This methodology enables the controlled synthesis of conjugated polymers in flow exclusively by the adjustment of the feed of monomer and initiator into the tube reactor. The major challenge in this study was to find compatible nickel catalyst systems for the Kumada polymerization step in flow. Both *o*-tolyl–Ni catalyst **3** in THF and Ni(dppp)Cl_2 in *o*-DCB were highly active in continuous processing conditions, and high-molecular-weight P3HT was obtained for both catalysts. Apart from the molecular weight of the polymers, the P3HT samples

Table 4: Solar cell data for devices containing various P3HT samples.[a]

P3HT[b]	M_n kg/mol	Thickness[c] nm	J_{sc} mA/cm^2	V_{oc} V	FF %	PCE %
Merck	50	145	8.30	0.58	54	2.60
Flow 1	38	160	8.20	0.58	53	2.54
Flow 2	41	175	8.50	0.58	50	2.47
Batch 1	24	125	7.50	0.56	58	2.45
Batch 2	34	140	7.70	0.56	50	2.15

[a]J_{sc} = short circuit current density; V_{oc} = open circuit voltage; FF = fill factor; PCE = power conversion efficiency; performance shown was the average from 6 pixels with an area of 0.1 cm^2. [b]Merck = Merck lisicon SP001; flow 1 = Table 1, entry 4; flow 2 = Table 2, entry 5; batch 1 = P3HT synthesized with catalyst **3**; batch 2 = P3HT synthesized with Ni(dppp)Cl_2. [c]Thickness of active layer. Measurements were performed in air.

synthesized in flow showed comparable regioregularity to samples from batch synthesis. The telescoped flow synthesis of P3HT from 2,5-dibromo-3-hexylthiophene (**1**) was also achieved on the benchtop flow reactor. Finally, BHJ solar cells containing flow-synthesized P3HT showed comparable performance to both commercial and batch-synthesized samples. This study paves the way for the continuous-flow synthesis of other polymers using the KCTP method. With efficient synthesis of polymers possible in a benchtop flow reactor, scale-up of such materials will become straight forward leading to reduction in production costs and improvements in reproducibility.

Experimental

General: The continuous-flow experiments were conducted by using a Vapourtec R2/R4 unit with multiple perfluoroalkoxy PFA (10 mL internal volume) or stainless steel (10 mL internal volume) reactors connected in series. All solvents were degassed and reactions were performed under anaerobic conditions. The reactants were channelled into the tube reactor by pumping solvent from a reservoir. Residence times in the reactor coils were defined by the flow rate and the volume of the reactor. The system was thoroughly dried by first flushing with anhydrous methanol followed by dried acetone before refilling with anhydrous reaction solvent. Reported yields do not account for axial dispersion of the reaction mixture and the formation of the regioisomer **2b**. Gel permeation chromatography (GPC) data was obtained by using toluene as the eluent and calibrated against polystyrene reference standards.

Materials: 2,5-Dibromo-3-hexylthiophene [27], 2-bromo-5-chloromagnesium-3-hexylthiophene [28], and *cis*-chloro(2-tolyl)(dppp)nickel(II) complex [8] were prepared according to procedures described in the literature. Commercial reagents were used as purchased without further purification. Commercial P3HT (lisicon SP001, M_n 50 kg/mol, M_w 79 kg/mol) was acquired from Merck KGaA, Darmstadt, Germany.

Synthetic procedure for 2-bromo-5-chloromagnesium-3-hexylthiophene (**2**): *tert*-Butylmagnesium chloride (8 mL) was added dropwise to a solution of 2,5-dibromo-3-hexylthiophene (1.826 g, 5.6 mmol) in dry THF (20 mL) and the mixture was stirred overnight at room temperature. An aliquot was quenched in water and extracted with petroleum spirits 40–60 °C, and the conversion was monitored by ^{1}H NMR spectroscopy.

Flow synthesis of P3HT via external initiation with nickel catalyst **3**: Stock solutions containing 2-bromo-5-chloromagnesium-3-hexylthiophene (**2**) (0.35/0.2 M) and Ni(dppp)(*o*-tolyl)Cl **3** (20/10 mM) were pumped into the PFA coil reactor (3 × 10 mL, 100 °C) at specific flow rates (see Table 1). The variation of the respective concentrations and flow rates afforded four different monomer-to-initiator ratios (3, 1.5, 0.9, 0.43 mol %). The stream outlet was fitted with an 8 bar back-pressure regulator. The mixtures were quenched and precipitated from methanolic HCl (2 M), centrifugated and washed with the same solvent three times. The lower molecular weight sample was then washed with acetone, and the high-molecular-weight samples were washed with petroleum spirits 40–60 °C. Yield (M_n = 37.7 kg/mol): 37 mg, 43%. ^{1}H NMR ($CDCl_3$, 500 MHz) δ 0.92 (t, 3H, J = 7 Hz), 1.32–1.37 (m, 4H), 1.41–1.46 (m, 2H), 1.68–1.74 (m, 2H), 2.49 (s, 0.06), 2.81 (t, 2H, J = 7.7 Hz), 6.98 (s, 1H), 7.16 (d, 0.02H, J = 5.2 Hz), 7.22–7.25 (m, 0.03H), 7.43–7.45 (m, 0.02H); ^{13}C NMR ($CDCl_3$, 100 MHz) δ 139.87, 133.69, 130.47, 128.58, 31.69, 30.50, 29.46, 29.26, 22.65, 14.12.

Flow synthesis of P3HT by in situ initiation with Ni(dppp)Cl_2: Stock solutions (0.35 M/0.2 M/0.06 M) containing 2-bromo-5-chloromagnesium-3-hexylthiophene (**2**) and Ni(dppp)Cl_2 (8.8 mM) were pumped into the PFA coil reactor (3 × 10 mL, 100 °C, PFA) or into the stainless steel (SS) reactor (40 mL, 100 °C) at specific flow rates (see Table 2). The variation of the concentration of the thiophene monomer and adjusting of the flow rates afforded five different monomer-to-initiator ratios (2.9, 1.7, 0.9, 0.7, 0.25 catalyst mol %). The stream outlet was fitted with an 8 bar back-pressure regulator. The reaction mixtures were quenched by direct precipitation of the stream leaving the reactor, from methanolic HCl (2 M). The polymers were centrifugated and washed with the same solvent three times. The lower molecular weight sample was then washed with acetone, whereas the rest of the samples were washed with petroleum spirits 40–60 °C. Yield (M_n 5.9 kg/mol): 32 mg, 65%.^{1}H NMR ($CDCl_3$, 500 MHz) δ 0.91 (m, 3H), 1.25–1.44 (m, 6H), 1.70 (m, 2H), 2.82 (s, 2H), 6.98 (s, 1H); ^{13}C NMR ($CDCl_3$, 100 MHz) δ 139.88, 133.69, 130.47, 128.59, 31.69, 30.50, 29.46, 29.25, 22.65, 14.11.

Telescoped preparation of P3HT: A stock solution containing 2,5-dibromo-3-hexylthiophene (0.2 M, THF) and *tert*-butylmagnesium chloride (1 equiv) was pumped into the PFA coil reactor (2 × 10 mL, 100 °C) at 1 mL/min flow rate, resulting in 20 min residence time. The solution was then mixed with a second stream containing Ni(dppp)Cl_2 catalyst (2.7 mM) at 0.1 mL/min to give a 0.1 mol % catalyst content and directed into a series of two reactors (at 100 °C or/and 150 °C). The inner pressure of the system was adjusted to give a continuous steady flow using a 250 psi back-pressure regulator located at the outlet of the system. The mixture was quenched into methanol, centrifuged and washed with the same solvent three times. The concentrations of the catalyst and flow rates were varied to adjust the monomer-to-initiator ratio (see Table 3). The polymer was subjected to Soxhlet extraction with methanol and petroleum

spirits (40–60 °C). Yield (M_n = 31 kg/mol): 70 mg, 40%. ^{1}H NMR ($CDCl_3$, 500 MHz) δ 0.94 (s, 3H), 1.23–1.55 (m, 6H), 1.73 (m, 2H), 2.82 (s, 2H), 7.0 (s, 1H); ^{13}C NMR ($CDCl_3$, 100 MHz) δ 139.88, 133.71, 130.49, 128.59, 31.70, 30.51, 29.26, 22.65, 14.11.

Supporting Information

Supporting Information File 1

Synthetic procedures for batch reactions, characterization of P3HT samples including NMR and MALDI-TOF spectra, and procedures for device preparation.
[http://www.beilstein-journals.org/bjoc/content/supplementary/1860-5397-9-170-S1.pdf]

Acknowledgements

This work was made possible by support from the Australian Solar Institute (Fellowship for W. W. H. Wong and project grant), the Victorian Organic Solar Cell Consortium, the Victorian State Government Department of Business Innovation (Victorian Science Agenda), and the Department of Primary Industries (Energy Technology Innovation Strategy).

References

1. Brabec, C. J.; Gowrisanker, S.; Halls, J. J. M.; Laird, D.; Jia, S. J.; Williams, S. P. *Adv. Mater.* **2010,** *22,* 3839. doi:10.1002/adma.200903697
2. McCullough, R. D.; Lowe, R. D.; Jayaraman, M.; Anderson, D. L. *J. Org. Chem.* **1993,** *58,* 904. doi:10.1021/jo00056a024
3. Marrocchi, A.; Lanari, D.; Facchetti, A.; Vaccaro, L. *Energy Environ. Sci.* **2012,** *5,* 8457. doi:10.1039/c2ee22129b
4. McCullough, R. D. *Adv. Mater.* **1998,** *10,* 93. doi:10.1002/(SICI)1521-4095(199801)10:2<93::AID-ADMA93>3.0.CO;2-F
5. Kiriy, A.; Senkovskyy, V.; Sommer, M. *Macromol. Rapid Commun.* **2011,** *32,* 1503. doi:10.1002/marc.201100316
6. Loewe, R. S.; Ewbank, P. C.; Liu, J.; Zhai, L.; McCullough, R. D. *Macromolecules* **2001,** *34,* 4324. doi:10.1021/ma001677+
7. Yokoyama, A.; Miyakoshi, R.; Yokozawa, T. *Macromolecules* **2004,** *37,* 1169. doi:10.1021/ma035396o
8. Senkovskyy, V.; Sommer, M.; Tkachov, R.; Komber, H.; Huck, W. T. S.; Kiriy, A. *Macromolecules* **2010,** *43,* 10157. doi:10.1021/ma1024889
9. Bronstein, H. A.; Luscombe, C. K. *J. Am. Chem. Soc.* **2009,** *131,* 12894. doi:10.1021/ja9054977
10. Yang, J.; Vak, D.; Clark, N.; Subbiah, J.; Wong, W. W. H.; Jones, D. J.; Watkins, S. E.; Wilson, G. *Sol. Energy Mater. Sol. Cells* **2013,** *109,* 47. doi:10.1016/j.solmat.2012.10.018
11. Seyler, H.; Wong, W. W. H.; Jones, D. J.; Holmes, A. B. *J. Org. Chem.* **2011,** *76,* 3551. doi:10.1021/jo2001879
12. Seyler, H.; Jones, D. J.; Holmes, A. B.; Wong, W. W. H. *Chem. Commun.* **2012,** *48,* 1598. doi:10.1039/C1CC14315H
13. Seyler, H.; Haid, S.; Kwon, T.-H.; Jones, D. J.; Bäuerle, P.; Holmes, A. B.; Wong, W. W. H. *Aust. J. Chem.* **2013,** *66,* 151. doi:10.1071/CH12406
14. Jas, G.; Kirschning, A. *Chem.–Eur. J.* **2003,** *9,* 5708. doi:10.1002/chem.200305212
15. Mason, B. P.; Price, K. E.; Steinbacher, J. L.; Bogdan, A. R.; McQuade, D. T. *Chem. Rev.* **2007,** *107,* 2300. doi:10.1021/cr050944c
16. Razzaq, T.; Kappe, C. O. *Chem.–Asian J.* **2010,** *5,* 1274. doi:10.1002/asia.201000010
17. Geyer, K.; Codée, J. D. C.; Seeberger, P. H. *Chem.–Eur. J.* **2006,** *12,* 8434. doi:10.1002/chem.200600596
18. Hartman, R. L.; McMullen, J. P.; Jensen, K. F. *Angew. Chem., Int. Ed.* **2011,** *50,* 7502. doi:10.1002/anie.201004637
19. Continuous flow reactor Vapourtec R2/R4 unit. http://www.vapourtec.co.uk.
20. Bannock, J. H.; Krishnadasan, S. H.; Nightingale, A. M.; Yau, C. P.; Khaw, K.; Burkitt, D.; Halls, J. J. M.; Heeney, M.; de Mello, J. C. *Adv. Funct. Mater.* **2013,** *23,* 2123. doi:10.1002/adfm.201203014
21. Iovu, M. C.; Sheina, E. E.; Gil, R. R.; McCullough, R. D. *Macromolecules* **2005,** *38,* 8649. doi:10.1021/ma051122k
22. Smeets, A.; Van den Bergh, K.; De Winter, J.; Gerbaux, P.; Verbiest, T.; Koeckelberghs, G. *Macromolecules* **2009,** *42,* 7638. doi:10.1021/ma901888h
23. Kohn, P.; Huettner, S.; Komber, H.; Senkovskyy, V.; Tkachov, R.; Kiriy, A.; Friend, R. H.; Steiner, U.; Huck, W. T. S.; Sommer, J.-U.; Sommer, M. *J. Am. Chem. Soc.* **2012,** *134,* 4790. doi:10.1021/ja210871j
24. Doubina, N.; Ho, A.; Jen, A. K. Y.; Luscombe, C. K. *Macromolecules* **2009,** *42,* 7670. doi:10.1021/ma901410k
25. The use of reagent loops in flow chemistry can be advantageous for multiple reasons (e.g., chemical compatibility, minimization of reagent dead volumes). The use of the reagent loop in preliminary experiments was chosen to minimize reagent consumption and to evaluate the stability of the catalyst in the system. In this way, the stock solution was kept refrigerated in a Schlenk flask ensuring that the polymerization results are not influenced by potential catalyst decomposition.
26. Liu, J.; Loewe, R. S.; McCullough, R. D. *Macromolecules* **1999,** *32,* 5777. doi:10.1021/ma9905324
27. Chen, T.-A.; Wu, X.; Rieke, R. D. *J. Am. Chem. Soc.* **1995,** *117,* 233. doi:10.1021/ja00106a027
28. Lohwasser, R. H.; Thelakkat, M. *Macromolecules* **2011,** *44,* 3388. doi:10.1021/ma200119s

License and Terms

Beilstein Journal of Organic Chemistry

Efficient continuous-flow synthesis of novel 1,2,3-triazole-substituted β-aminocyclohexanecarboxylic acid derivatives with gram-scale production

Sándor B. Ötvös, Ádám Georgiádes, István M. Mándity, Lóránd Kiss and Ferenc Fülöp*

Full Research Paper

Open Access

Address:
Institute of Pharmaceutical Chemistry, University of Szeged, Eötvös u. 6, H-6720 Szeged, Hungary

Email:
Ferenc Fülöp* - fulop@pharm.u-szeged.hu

* Corresponding author

Keywords:
β-amino acids; click chemistry; continuous-flow; copper; flow chemistry; triazoles

Beilstein J. Org. Chem. **2013,** *9,* 1508–1516.
doi:10.3762/bjoc.9.172

Received: 16 May 2013
Accepted: 02 July 2013
Published: 29 July 2013

This article is part of the Thematic Series "Chemistry in flow systems III".

Guest Editor: A. Kirschning

Abstract

The preparation of novel multi-substituted 1,2,3-triazole-modified β-aminocyclohexanecarboxylic acid derivatives in a simple and efficient continuous-flow procedure is reported. The 1,3-dipolar cycloaddition reactions were performed with copper powder as a readily accessible Cu(I) source. Initially, high reaction rates were achieved under high-pressure/high-temperature conditions. Subsequently, the reaction temperature was lowered to room temperature by the joint use of both basic and acidic additives to improve the safety of the synthesis, as azides were to be handled as unstable reactants. Scale-up experiments were also performed, which led to the achievement of gram-scale production in a safe and straightforward way. The obtained 1,2,3-triazole-substituted β-aminocyclohexanecarboxylates can be regarded as interesting precursors for drugs with possible biological effects.

Introduction

In recent years, triazole-containing compounds have become potential targets for drug discovery [1,2]. A large number of 1,2,3-triazoles exhibit various biological effects [3], e.g., antiviral (**1**), antibacterial (**2**), antifungal (**3**) and anticancer (**4**) activities [4-7] (Figure 1). The 1,2,3-triazole skeleton is frequently used as a pharmacophore for the modification of known pharmaceuticals. Triazole analogues of several bioactive compounds have recently been reported. Examples are those of the well-known highly functionalized antiviral cyclic amino acid derivatives oseltamivir and zanamivir (**5** and **6** in Figure 1) [8,9]. The 1,2,3-triazole moiety is a constituent part of many modified nucleosides or carbanucleosides with antiviral, anti-HIV or cytostatic activities [10-12]. However, the scope of triazole chemistry is not confined to drug discovery. There are

an increasing number of applications in numerous other areas of modern chemical sciences, such as bioconjugation [13], supramolecular chemistry, [14] and polymer sciences [15].

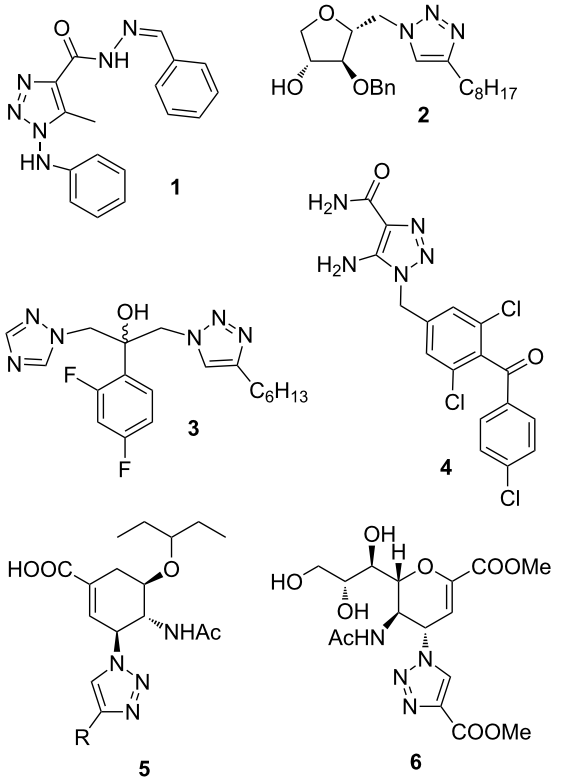

Figure 1: Examples of 1,2,3-triazoles with various biological activities.

Probably the most useful and powerful procedure for the synthesis of 1,2,3-triazoles is the Huisgen 1,3-dipolar cycloaddition of organic azides with acetylenes [16]. The classical Huisgen reaction, thermally induced, gives an approximate 1:1 mixture of 1,4- and 1,5-disubstituted 1,2,3-triazole isomers (Scheme 1) [17]. However, when Cu(I) catalysis is applied, the reaction becomes regioselective, exclusively yielding the 1,4-regioisomer within a relatively short reaction time [18-20]. Recently, Cu(I)-catalyzed azide–alkyne cycloaddition (CuAAC) has become the basis of the so-called click chemistry concept due to its wide applicability and efficiency.

Over the past twenty years, alicyclic β-amino acids have attracted great interest among synthetic chemists, thanks to their massive pharmacological potential [21,22]. For example, cispentacin ((1*R*,2*S*)-2-aminocyclopentanecarboxylic acid, **7**) is a widely investigated naturally occurring carbocyclic β-amino acid with strong antifungal properties against *Candida* species (Figure 2) [23]. Its synthetic 4-methylene derivative icofungipen (**8**), also an antifungal agent, is now proceeding

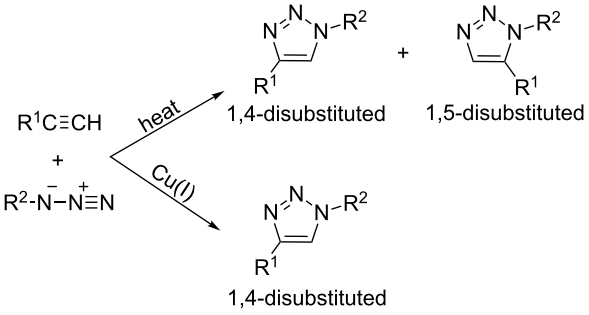

Scheme 1: 1,3-Dipolar azide–alkyne cycloadditions.

through clinical development for the oral treatment of yeast infections (Figure 2) [24]. Certain multi-substituted cyclohexane amino acid derivatives, such as oryzoxymycin (**9**) and tilidine (**10**), are also well-known bioactive agents with anticancer, antibacterial, antiviral or analgesic effects (Figure 2) [25,26]. The alicyclic β-amino acids are key intermediates for the synthesis of a series of pharmaceutically relevant products [27], such as amino esters, amino alcohols, azides and heterocycles. Moreover, they are frequently used as building blocks for the synthesis of new peptides and foldamers with possible biological effects [28].

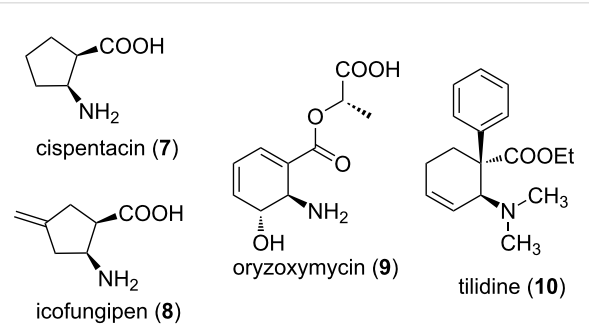

Figure 2: Selected bioactive alicyclic β-amino acids.

Modern continuous-flow (CF) technologies offer many advantages over classical batch-based procedures [29-32], including efficient mixing quality [33], excellent heat and mass transfer [34], shorter reaction times [35-37], reduced reagent consumption [38-40], improved safety [41,42], and operational simplicity [43]. Furthermore, CF methodologies provide opportunities for a simple and rapid scale-up [44,45] and automation [46,47] of chemical processes. They also tend to be environmentally benign technologies [48]. In consequence of these benefits, flow chemistry-based techniques have exerted a significant impact on modern synthetic chemistry, ranging from laboratory-based experiments to industrial-scale production.

Here, we describe a safe and efficient CF synthesis of a series of novel 1,2,3-triazole-modified β-aminocyclohexanecarboxylic acid derivatives as potential biologically active compounds. Gram-scale production is also reported, which predicts a possible usefulness for the pharmaceutical industry.

Results and Discussion

Several approaches are to be found in the literature for the Cu(I)-catalysed flow synthesis of triazoles. Heterogeneous Cu(I) sources are most popular, such as copper-in-charcoal (Cu/C) [49,50], solid supported Cu(I) species [51-54], and heated copper wirings [55-58], but a homogeneous technique has also recently emerged [59]. The main driving forces behind these CF methodologies are the safety aspects associated with the handling of azides and the inherent scalability of flow processing. Moreover, when organic azides are formed in situ, operational safety can be further improved [55,57]. We envisioned that it would be simplest to make use of copper powder as a catalytic source [60]. Similarly to cases when heated rings of copper wire are employed, a copper surface acts as a source of active copper species. Copper is constantly oxidized when exposed to air, and non-self-protecting layers of different oxides, including Cu_2O, are formed on its surface [61], which can promote CuAAC. Thus, we utilized copper powder in a stainless steel column, which served as a catalyst bed later on. The catalyst bed was placed into a stainless steel block with a Peltier heating system, which could heat the column up to 100 °C. A backpressure regulator was also integrated to ensure pressures up to 100 bar. The mixture of the reactants was pumped through the system continuously by means of an HPLC pump. This experimental setup is practical and cheap, as it does not require costly catalysts or special apparatus. At the same time this setup is safe, even with unstable reactants such as azides (Figure 3).

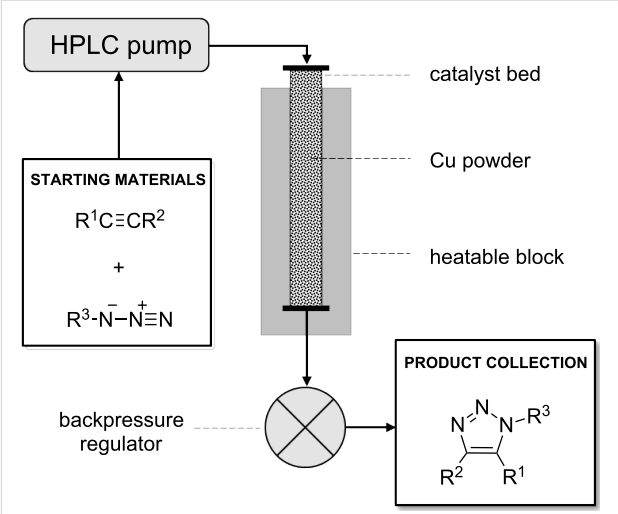

Figure 3: Experimental setup for the CF reactions.

To maximize the CF triazole synthesis reaction rates, it appeared easiest to use high-temperature conditions initially. The application of elevated pressure in CuAAC is also beneficial, as it can promote the product formation in accordance with Le Chatelier's principle [60] and also prevents the solvent from boiling over when high temperature is used. Thus, 100 °C and 100 bar were selected as conditions **A** for the CF synthesis. However, when azides are reacted, it is important to minimize the explosion hazard. Accordingly, we attempted to improve the rates of the reaction in the presence of additives, without the use of high temperature [60]. Amines are known to accelerate CuAAC, in particular by coordinating to catalytically active Cu(I) species and promoting their liberation from the copper matrix [62,63]. It was recently shown that the use of certain acids as additives is also beneficial, as this can further accelerate the formation of the triazole product [64-66] and also prevents the accumulation of unwanted byproducts, such as diacetylenes, bistriazoles, etc. [67]. At the same time, byproduct formation is catalysed by a base, and the joint utilization of a basic and an acidic additive is therefore favourable. This buffer system gives rise to a high reactivity in CuAAC, even at room temperature (rt), but without byproduct formation [60,67]. This system thus greatly improves the safety relative to the high-temperature conditions. The literature data led us to select *N*,*N*-diisopropylethylamine (DIEA) as a base and HOAc as an acid [67], which were used jointly as additives, each in 0.04 equivalents, at 100 bar and rt as conditions **B** [60].

As starting materials for the CF CuAAC reactions, azido-substituted β-aminocyclohexanecarboxylates **11**–**14** were prepared previously by a diastereoselective epoxidation of the corresponding 2-aminocyclohexenecarboxylates, followed by a regioselective oxirane ring opening with NaN_3 [68]. Three different alkynes (phenylacetylene, diethyl acetylenedicarboxylate and ethynyl ferrocene) were employed as dipolarophiles to yield a library of novel 1,2,3-triazole-modified cyclic β-amino acid derivatives. Compounds **11**–**14** were racemates, the structures in Table 1 show their relative stereochemistry. The CF syntheses were carried out under both conditions **A** and **B** in order to obtain a clear comparison between the performances of the two approaches. CH_2Cl_2 was used as a solvent, and the starting azides were used in a concentration of 0.085 M. A higher concentration of the starting azides led to the precipitation of the triazole product and a blockage in the CF reactor. Aliquots of 2.5 mL of a reaction mixture containing 1 equivalent of the azide and 1.5 equivalents of the acetylene were pumped through the reactor in each run with a a flow rate of 0.5 mL min^{-1}. At this flow rate the residence time on the catalyst bed was as low as 1.5 min and it took only 5 min of process

time to pump the 2.5 mL aliquots through the system. This resulted in around 100 mg of crude product, depending on the conversion and the molecular masses of the reactants.

In the Cu(I)-catalysed reactions between phenylacetylene and the azido-substituted β-amino acid derivatives **11**–**14**, 1,4-disubstituted 1,2,3-triazole isomers (**15**–**18**) were regioselectively formed. The high-pressure/high-temperature conditions **A** led to only medium yields (Table 1, entries 1–4), but under conditions **B** the yields of triazoles **15** and **16** were excellent, and those of triazoles **17** and **18** were high (76% and 89%, respectively; Table 1, entries 1–4). When the CF reactions of azides **13** and

Table 1: CF synthesis of 1,2,3-triazole-substituted alicyclic β-amino acid derivatives.

Entry	Azide[a] (1 equivalent)	Acetylene (1.5 equivalents)	Product	Yield[b] (%)	
				A[c]	**B**[d]
1	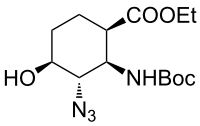 **11**	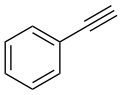	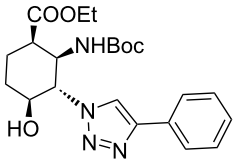 **15**	61	96
2	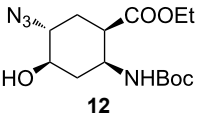 **12**	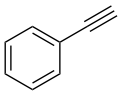	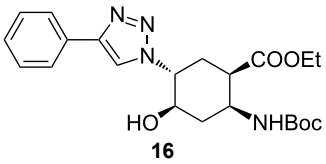 **16**	47	97
3	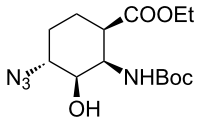 **13**	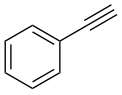	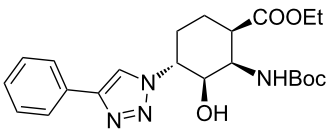 **17**	33	76 (98)[e]
4	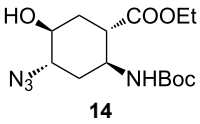 **14**	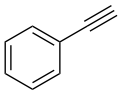	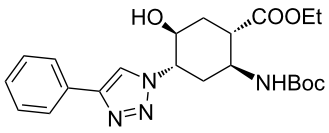 **18**	53	89 (98)[e]
5	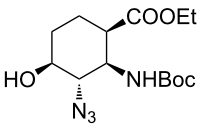 **11**	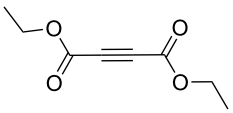	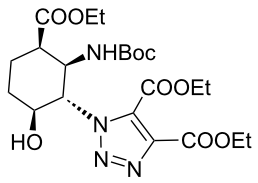 **19**	98	97
6	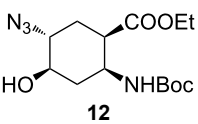 **12**	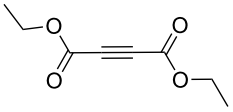	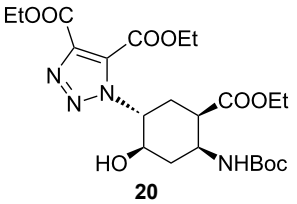 **20**	97	98
7	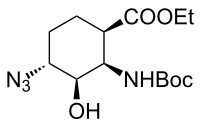 **13**	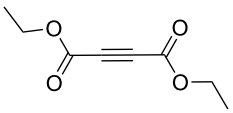	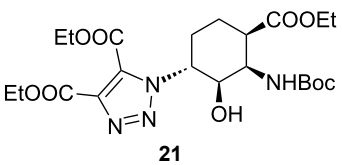 **21**	97	96

Table 1: CF synthesis of 1,2,3-triazole-substituted alicyclic β-amino acid derivatives. (continued)

8	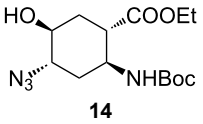 **14**	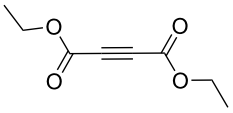	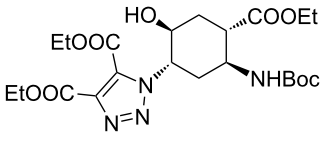 **22**	97	98
9	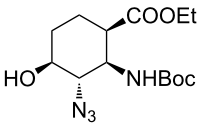 **11**	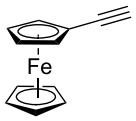	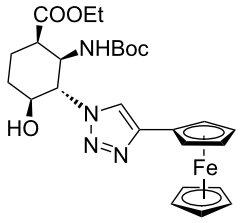 **23**	95	97
10	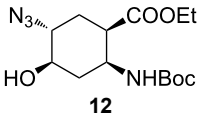 **12**	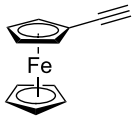	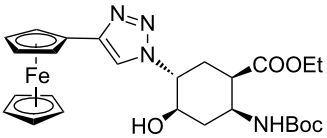 **24**	91	98
11	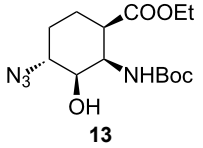 **13**	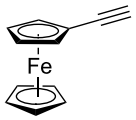	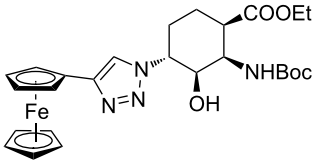 **25**	96	93
12	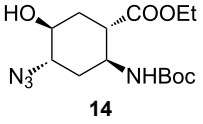 **14**	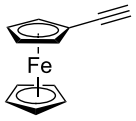	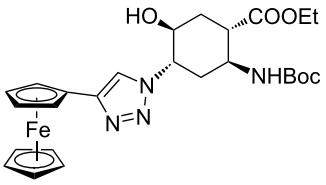 **26**	75	97

[a]c_{azide} = 0.085 M. [b]Yield of isolated product. [c]Conditions **A**: CH_2Cl_2 as solvent, 100 bar, 100 °C, flow rate 0.5 mL min^{-1}, without any additives. [d]Conditions **B**: CH_2Cl_2 as solvent, 100 bar, rt, flow rate 0.5 mL min^{-1}, with 0.04 equivalents of DIEA + 0.04 equivalents of HOAc. [e]Achieved under the following conditions: CH_2Cl_2 as solvent, 100 bar, 100 °C, flow rate 0.5 mL min^{-1}, with 0.04 equivalents of DIEA + 0.04 equivalents of HOAc.

14 with phenylacetylene were repeated under high-pressure/high-temperature conditions with the simultaneous use of additives (100 bar, 100 °C, 0.04 equivalents each of DIEA and HOAc; further conditions were not modified), triazoles **17** and **18** were obtained in very high yields (98% in both cases; Table 1, entries 3 and 4).

1,4,5-Trisubstituted 1,2,3-triazoles are of notable importance in drug discovery. For example, several 1,2,3-triazole-4,5-dicarboxylates display significant antituberculotic activity in vitro [69]. Thus, a nonterminal alkyne, diethyl acetylenedicarboxylate, was subjected to CF CuAAC with the azido-functionalized β-amino acid derivatives **11**–**14** as reaction partners. 1,4,5-Trisubstituted 1,2,3-triazole dicarboxylates **19**–**22** were obtained in excellent yields (>96%) under both conditions **A** and **B** (Table 1, entries 5–8). In this set of CF syntheses, no significant difference was observed between the performances of the two methods.

Ferrocene-triazole conjugates play a crucial role in the labelling and detection of various systems, such as biomolecules, polymers, nanomaterials and supramolecular assemblies [70]. They also have potential applications in medicinal chemistry and drug discovery as biosensing probes, in immunoassays and in host–guest chemistry [71]. Ferrocene-substituted amino acids have been of significant importance in the investigation of the secondary structures of different peptides and foldamers [72]. Thus, conjugates of the azido-functionalized β-amino acid

derivatives **11**–**14** were prepared with ethynylferrocene as a dipolarophile. Both conditions **A** and **B** afforded ferrocenyltriazoles **23**–**25** in excellent yields (>91%; Table 1, entries 9–11). However, in the case of ferrocenyltriazole **26** the high-pressure/high-temperature conditions **A** led to a yield of only 75%, whereas the use of additives at rt (conditions **B**) proved more efficient, with a yield of 97% (Table 1, entry 12). Triazoles **23**–**26** were obtained selectively as 1,4-disubstituted regioisomers.

To understand the differences between the results obtained with the three different dipholarophiles, it must be taken into account that the carboxylate groups of diethyl acetylenedicarboxylate and the aromatic system of the ferrocenyl group as ligands can probably coordinate copper from its matrix. Therefore, the concentration of the catalytically active Cu(I) species is increased as compared to the reactions with phenylacetylene [73-75]. Accordingly, the yields were usually higher in the reactions with diethyl acetylenedicarboxylate and ethynylferrocene than with phenylacetylene (Table 1, entries 5–12 versus entries 1–4). These differences can mainly be observed between the results obtained under conditions **A**. This is because the base, as an additive, evolves the same effect and improves the reactivity through the CuAAC, thus in the case of conditions **B** (the use of additives) the influence of the alkyne is practically masked.

The presence of trace amounts of copper in the chromatographically purified triazole products was determined by means of inductively coupled plasma mass spectrometry (ICP–MS). The analytical data in Table 2 show that the contents of copper impurities in the products were appropriately low, i.e., amounts of 3.9–9.1 μg g^{-1} were detected. It should be noted that the samples obtained with the joint use of DIEA + HOAc (conditions **B**) contained more copper than those obtained under conditions **A** (high-temperature/high-pressure without additives). The levels of copper contamination detected in our triazole products compare well with literature results relating to CF [50] and conventional batch experiments [76].

In conventional batch-based chemistry, the scale-up of chemical reactions can be a challenge because the output depends on the batch size. The situation becomes even more complicated when unstable reactants such as azides are handled on a large scale. However, the scalability of CF procedures is a straightforward function of time and the flow rate, and the risks associated with the accumulation of hazardous species are minimized, because the solution of the reactants is eluting continuously from the active zone of the reactor [33,34,44,45,60]. The CF CuAAC between azide **14** and diethyl acetylenedicarboxylate was scaled up in a simple, safe and efficient manner to achieve gram-scale production (Scheme 2). Methods **A** and **B** proved equally efficient in the small-scale CF syntheses of triazole **22** (Table 1, entry 8). However, we performed the large-scale experiment at 100 bar and rt in the presence of the additives (conditions **B**) so as to ensure maximum safety throughout the procedure. A CH_2Cl_2 solution of the reaction mixture containing 1 equivalent of the azide (c_{azide} = 0.085 M), 1.5 equivalents of the acetylene and 0.04 equivalents of each additive was pumped continuously through the system at a flow

Table 2: Copper contents in the triazole products after column chromatographic purification on silica gel.

Entry	Product	Copper content (μg g^{-1})[a]	
		A[b]	**B**[c]
1	**15**	4.6 (±0.5)	8.4 (±0.6)
2	**16**	4.2 (±0.3)	7.7 (±0.6)
3	**17**	3.9 (±0.5)	8.0 (±0.4)
4	**18**	4.7 (±0.6)	8.2 (±0.7)
5	**19**	5.2 (±0.4)	7.9 (±0.4)
6	**20**	5.1 (±0.3)	7.5 (±0.6)
7	**21**	4.8 (±0.6)	7.7 (±0.7)
8	**22**	5.3 (±0.3)	8.2 (±0.6)
9	**23**	6.1 (±0.5)	8.6 (±0.5)
10	**24**	4.8 (±0.4)	7.7 (±0.8)
11	**25**	5.4 (±0.3)	9.1 (±0.4)
12	**26**	4.9 (±0.6)	7.8 (±0.7)

[a]Determined by ICP–MS. [b]Conditions **A**: CH_2Cl_2 as solvent, 100 bar, 100 °C, flow rate 0.5 mL min^{-1}, without any additives. [c]Conditions **B**: CH_2Cl_2 as solvent, 100 bar, rt, flow rate 0.5 mL min^{-1}, with 0.04 equivalents of DIEA + 0.04 equivalents of HOAc.

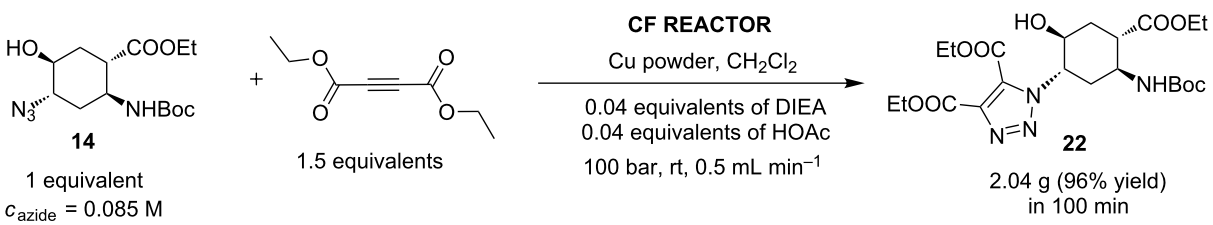

Scheme 2: Gramm-scale CF synthesis of triazole **22** under conditions **B**.

rate of 0.5 mL min^{-1}. During the whole scale-up procedure, the same portion of copper powder was used in the catalyst bed. The solution of the crude product was collected for 100 min, and after purification 2.06 g of triazole **22** was obtained, which is equivalent to a yield of 96%.

Conclusion

Twelve highly functionalized 1,2,3-triazole-substituted β-aminocyclohexanecarboxylic acid racemates were successfully prepared in CF mode as a small library of novel compounds with possible biological effects. The CF syntheses were first performed under high-pressure/high-temperature conditions with copper powder as a readily accessible Cu(I) source. Subsequently, to moderate the harsh reaction conditions, the reaction temperature could be lowered to rt in the presence of additives. The joint use of a base and an acid dramatically improved the reactivity in the CuAAC, while it completely eliminated unwanted byproduct formation. These conditions ensured enhanced safety and typically higher yields than those attained under the harsh reaction conditions. Simple, efficient and safe gram-scale production was also implemented in a short processing time, which can be important for potential industrial applications.

Experimental

General Information

The reagents and materials were of the highest commercially available purity grade and were used without any further purification. Flash column chromatography was performed on Merck silica gel 60, particle sizes ranged from 63 to 200 μm, and analytical thin-layer chromatography (TLC) on Merck silica gel 60 F254 plates. Compounds were visualized with UV light or $KMnO_4$. ^1H and ^{13}C NMR spectra were recorded on a Bruker Avance DRX 500 spectrometer, in $CDCl_3$ as a solvent, with TMS as internal standard, and at 500.1 and 125.0 MHz, respectively. Microanalyses were performed on a Perkin-Elmer 2400 elemental analyser.

Determination of the copper contents of the triazole products

Copper concentrations were determined by ICP–MS by using an Agilent 7700x instrument equipped with a collision cell. The determination was carried out on the isotope ^{63}Cu, with He as collision gas. The standard solutions for external calibration were prepared from a stock solution (Certipur, Merck) by dilution with doubly deionized water (Millipore MillQ, Merck). All glassware and plastic utensils used during the determination were precleaned by soaking in solutions of trace-metal-grade nitric acid and hydrochloric acid (Suprapur, Merck), followed by rinsing with copious amounts of doubly deionized water.

General procedure for the CF reactions

An H-Cube® system was used as a CF reactor in the "no H_2" mode. For the CF reactions, the catalyst bed (internal dimensions: 70 mm × 4 mm) was filled with ~900 mg of copper powder with an average particle size of 200 μm. 70 mg (0.21 mmol, 1 equivalent) of the corresponding azide and 0.32 mmol (1.5 equivalents) of the alkyne, and (only in method **B**) 1.5 μL (0.0084 mmol, 0.04 equivalents) of DIEA and 0.5 μL (0.0084 mmol, 0.04 equivalents) of HOAc were dissolved in 2.5 mL of CH_2Cl_2. The solution was homogenized by sonication, and then pumped through the CF reactor under the appropriate conditions. Between two reactions in the CF reactor, the catalyst bed was washed at rt for 5 min with CH_2Cl_2 at a flow rate of 1 mL min^{-1}. The crude product was checked by TLC with a mixture of *n*-hexane/EtOAc as an eluent, and the solvent was next evaporated off under vacuum. Column chromatographic purification was carried out on silica gel with a mixture of *n*-hexane/EtOAc as an eluent. The 1,2,3-triazole-modified compounds were characterized by elemental analysis and NMR experiments. For detailed analytical data see Supporting Information File 1.

Measurement of the residence time on the catalyst bed

To determine the residence time, a CH_2Cl_2 solution of a blue ink was pumped through the catalyst bed. The time that elapsed between the first contact of the ink with the bed and the moment when the blue colour appeared at the column outlet was measured.

Supporting Information

Supporting Information File 1

Detailed analytical data of the prepared compounds and a collection of NMR spectra.
[http://www.beilstein-journals.org/bjoc/content/supplementary/1860-5397-9-172-S1.pdf]

Acknowledgements

This research was partly realized within the scope of TÁMOP 4.2.4. A/2-11-1-2012-0001 „National Excellence Program – Elaborating and operating an inland student and researcher personal support system convergence program". The project was subsidized by the European Union and co-financed by the European Social Fund. We are grateful to the Hungarian Research Foundation (OTKA Nos. NK81371, PD103994 and K100530) and TÁMOP 4.2.2/B-10/1-2010-0012. IMM acknowledges the award of a János Bolyai scholarship from the Hungarian Academy of Sciences.

References

1. Moorhouse, A. D.; Moses, J. E. *ChemMedChem* **2008,** *3,* 715–723. doi:10.1002/cmdc.200700334
2. Hou, J. L.; Liu, X. F.; Shen, J.; Zhao, G. L.; Wang, P. G. *Expert. Opin. Drug Discov.* **2012,** *7,* 489–501. doi:10.1517/17460441.2012.682725
3. Agalave, S. G.; Maujan, S. R.; Pore, V. S. *Chem.–Asian J.* **2011,** *6,* 2696–2718. doi:10.1002/asia.201100432
4. Jordão, A. K.; Ferreira, V. F.; Lima, E. S.; de Souza, M. C. B. V.; Carlos, E. C. L.; Castro, H. C.; Geraldo, R. B.; Rodrigues, C. R.; Almeida, M. C. B.; Cunha, A. C. *Bioorg. Med. Chem.* **2009,** *17,* 3713–3719. doi:10.1016/j.bmc.2009.03.053
5. Vijaya Raghava Reddy, L.; Venkat Reddy, P.; Mishra, N. N.; Shukla, P. K.; Yadav, G.; Srivastava, R.; Shaw, A. K. *Carbohydr. Res.* **2010,** *345,* 1515–1521. doi:10.1016/j.carres.2010.03.031
6. Aher, N. G.; Pore, V. S.; Mishra, N. N.; Kumar, A.; Shukla, P. K.; Sharma, A.; Bhat, M. K. *Bioorg. Med. Chem. Lett.* **2009,** *19,* 759–763. doi:10.1016/j.bmcl.2008.12.026
7. Soltis, M. J.; Yeh, H. J.; Cole, K. A.; Whittaker, N.; Wersto, R. P.; Kohn, E. C. *Drug Metab. Dispos.* **1996,** *24,* 799–806.
8. Cho, J. H.; Bernard, D. L.; Sidwell, R. W.; Kern, E. R.; Chu, C. K. *J. Med. Chem.* **2006,** *49,* 1140–1148. doi:10.1021/jm0509750
9. Li, J.; Zheng, M.; Tang, W.; He, P.-L.; Zhu, W.; Li, T.; Zuo, J.-P.; Liu, H.; Jiang, H. *Bioorg. Med. Chem. Lett.* **2006,** *16,* 5009–5013. doi:10.1016/j.bmcl.2006.07.047
10. Xia, Y.; Liu, Y.; Wan, J.; Wang, M.; Rocchi, P.; Qu, F.; Iovanna, J. L.; Peng, L. *J. Med. Chem.* **2009,** *52,* 6083–6096. doi:10.1021/jm900960v
11. Pérez-Castro, I.; Caamaño, O.; Fernández, F.; García, M. D.; López, C.; De Clercq, E. *Org. Biomol. Chem.* **2007,** *5,* 3805–3813. doi:10.1039/b710348d
12. Kiss, L.; Forro, E.; Fulop, F. *Lett. Org. Chem.* **2011,** *8,* 220–228. doi:10.2174/157017811795038359
13. El-Sagheer, A. H.; Brown, T. *Chem. Soc. Rev.* **2010,** *39,* 1388–1405. doi:10.1039/b901971p
14. Fahrenbach, A. C.; Stoddart, J. F. *Chem.–Asian J.* **2011,** *6,* 2660–2669. doi:10.1002/asia.201100457
15. Kempe, K.; Krieg, A.; Becer, C. R.; Schubert, U. S. *Chem. Soc. Rev.* **2012,** *41,* 176–191. doi:10.1039/c1cs15107j
16. Huisgen, R. In *1,3-Dipolar Cycloadditional Chemistry;* Padwa, A., Ed.; Wiley: New York, 1984; pp 1–176.
17. Huisgen, R.; Szeimis, G.; Möbius, L. *Chem. Ber.* **1967,** *100,* 2494–2507. doi:10.1002/cber.19671000806
18. Rostovtsev, V. V.; Green, L. G.; Fokin, V. V.; Sharpless, K. B. *Angew. Chem., Int. Ed.* **2002,** *41,* 2596–2599. doi:10.1002/1521-3773(20020715)41:14<2596::AID-ANIE2596>3.0.CO;2-4
19. Wang, Q.; Chan, T. R.; Hilgraf, R.; Fokin, V. V.; Sharpless, K. B.; Finn, M. G. *J. Am. Chem. Soc.* **2003,** *125,* 3192–3193. doi:10.1021/ja021381e
20. Tornoe, C. W.; Christensen, C.; Meldal, M. *J. Org. Chem.* **2002,** *67,* 3057–3064. doi:10.1021/jo011148j
21. Kuhl, A.; Hahn, M. G.; Dumić, M.; Mittendorf, J. *Amino Acids* **2005,** *29,* 89–100. doi:10.1007/s00726-005-0212-y
22. Weiner, B.; Szymański, W.; Janssen, D. B.; Minnaard, A. J.; Feringa, B. L. *Chem. Soc. Rev.* **2010,** *39,* 1656–1691. doi:10.1039/b919599h
23. Konishi, M.; Nishio, M.; Saitoh, K.; Miyaki, T.; Oki, T.; Kawaguchi, H. *J. Antibiot.* **1989,** *42,* 1749–1755. doi:10.7164/antibiotics.42.1749
24. Mittendorf, J.; Kunisch, F.; Matzke, M.; Militzer, H.-C.; Schmidt, A.; Schönfeld, W. *Bioorg. Med. Chem. Lett.* **2003,** *13,* 433–436. doi:10.1016/S0960-894X(02)00958-7
25. Bunnage, M. E.; Ganesh, T.; Masesane, I. B.; Orton, D.; Steel, P. G. *Org. Lett.* **2003,** *5,* 239–242. doi:10.1021/ol0269704
26. Palko, M.; Kiss, L.; Fulop, F. *Curr. Med. Chem.* **2005,** *12,* 3063–3083. doi:10.2174/092986705774933443
27. Kiss, L.; Forro, E.; Fulop, F. In *Amino Acids, Peptides and Proteins in Organic Chemistry;* Hughes, A. B., Ed.; Wiley-VCH, 2009; pp 367–409.
28. Martinek, T. A.; Fülöp, F. *Chem. Soc. Rev.* **2012,** *41,* 687–702. doi:10.1039/c1cs15097a
29. Wegner, J.; Ceylan, S.; Kirschning, A. *Adv. Synth. Catal.* **2012,** *354,* 17–57. doi:10.1002/adsc.201100584
30. Yoshida, J.-i.; Kim, H.; Nagaki, A. *ChemSusChem* **2011,** *4,* 331–340. doi:10.1002/cssc.201000271
31. Geyer, K.; Gustafsson, T.; Seeberger, P. H. *Synlett* **2009,** 2382–2391. doi:10.1055/s-0029-1217828
32. Mak, X. Y.; Laurino, P.; Seeberger, P. H. *Beilstein J. Org. Chem.* **2009,** *5,* No. 19. doi:10.3762/bjoc.5.19
33. Nagy, K. D.; Shen, B.; Jamison, T. F.; Jensen, K. F. *Org. Process Res. Dev.* **2012,** *16,* 976–981. doi:10.1021/op200349f
34. Hartman, R. L.; McMullen, J. P.; Jensen, K. F. *Angew. Chem., Int. Ed.* **2011,** *50,* 7502–7519. doi:10.1002/anie.201004637
35. Ötvös, S. B.; Mándity, I. M.; Fülöp, F. *ChemSusChem* **2012,** *5,* 266–269. doi:10.1002/cssc.201100332
36. Ötvös, S. B.; Mándity, I. M.; Fülöp, F. *J. Catal.* **2012,** *295,* 179–185. doi:10.1016/j.jcat.2012.08.006
37. Yoshida, J.-i.; Nagaki, A.; Yamada, T. *Chem.–Eur. J.* **2008,** *14,* 7450–7459. doi:10.1002/chem.200800582
38. Ueno, M.; Suzuki, T.; Naito, T.; Oyamada, H.; Kobayashi, S. *Chem. Commun.* **2008,** 1647–1649. doi:10.1039/b715259k
39. Rasheed, M.; Wirth, T. *Angew. Chem., Int. Ed.* **2011,** *50,* 357–358. doi:10.1002/anie.201006107
40. Rueping, M.; Bootwicha, T.; Sugiono, E. *Beilstein J. Org. Chem.* **2012,** *8,* 300–307. doi:10.3762/bjoc.8.32
41. Ötvös, S. B.; Mándity, I. M.; Fülöp, F. *Mol. Diversity* **2011,** *15,* 605–611. doi:10.1007/s11030-010-9276-z
42. Brandt, J. C.; Wirth, T. *Beilstein J. Org. Chem.* **2009,** *5,* No. 30. doi:10.3762/bjoc.5.30
43. Bryan, M. C.; Wernick, D.; Hein, C. D.; Petersen, J. V.; Eschelbach, J. W.; Doherty, E. M. *Beilstein J. Org. Chem.* **2011,** *7,* 1141–1149. doi:10.3762/bjoc.7.132
44. He, P.; Haswell, S. J.; Fletcher, P. D. I.; Kelly, S. M.; Mansfield, A. *Beilstein J. Org. Chem.* **2011,** *7,* 1150–1157. doi:10.3762/bjoc.7.133
45. Kockmann, N.; Gottsponer, M.; Roberge, D. M. *Chem. Eng. J.* **2011,** *167,* 718–726. doi:10.1016/j.cej.2010.08.089
46. Smith, C. J.; Nikbin, N.; Ley, S. V.; Lange, H.; Baxendale, I. R. *Org. Biomol. Chem.* **2011,** *9,* 1938–1947. doi:10.1039/c0ob00815j
47. Baumann, M.; Baxendale, I. R.; Ley, S. V.; Smith, C. D.; Tranmer, G. K. *Org. Lett.* **2006,** *8,* 5231–5234. doi:10.1021/ol061975c
48. Wiles, C.; Watts, P. *Green Chem.* **2012,** *14,* 38–54. doi:10.1039/c1gc16022b
49. Lipshutz, B. H.; Taft, B. R. *Angew. Chem., Int. Ed.* **2006,** *45,* 8235–8238. doi:10.1002/anie.200603726
50. Fuchs, M.; Goessler, W.; Pilger, C.; Kappe, C. O. *Adv. Synth. Catal.* **2010,** *352,* 323–328. doi:10.1002/adsc.200900726
51. Girard, C.; Önen, E.; Aufort, M.; Beauvière, S.; Samson, E.; Herscovici, J. *Org. Lett.* **2006,** *8,* 1689–1692. doi:10.1021/ol060283l

52. Smith, C. D.; Baxendale, I. R.; Lanners, S.; Hayward, J. J.; Smith, S. C.; Ley, S. V. *Org. Biomol. Chem.* **2007,** *5,* 1559–1561. doi:10.1039/b702995k
53. Özçubukçu, S.; Ozkal, E.; Jimeno, C.; Pericàs, M. A. *Org. Lett.* **2009,** *11,* 4680–4683. doi:10.1021/ol9018776
54. Ozkal, E.; Özçubukçu, S.; Jimeno, C.; Pericàs, M. A. *Catal. Sci. Technol.* **2012,** *2,* 195–200. doi:10.1039/c1cy00297j
55. Bogdan, A. R.; Sach, N. W. *Adv. Synth. Catal.* **2009,** *351,* 849–854. doi:10.1002/adsc.200800758
56. Bogdan, A. R.; James, K. *Chem.–Eur. J.* **2010,** *16,* 14506–14512. doi:10.1002/chem.201002215
57. Ceylan, S.; Klande, T.; Vogt, C.; Friese, C.; Kirschning, A. *Synlett* **2010,** 2009–2013. doi:10.1055/s-0030-1258487
58. Kupracz, L.; Hartwig, J.; Wegner, J.; Ceylan, S.; Kirschning, A. *Beilstein J. Org. Chem.* **2011,** *7,* 1441–1448. doi:10.3762/bjoc.7.168
59. Varas, A. C.; Noël, T.; Wang, Q.; Hessel, V. *ChemSusChem* **2012,** *5,* 1703–1707. doi:10.1002/cssc.201200323
60. Ötvös, S. B.; Mándity, I. M.; Kiss, L.; Fülöp, F. *Chem.–Asian J.* **2013,** *8,* 800–808. doi:10.1002/asia.201201125
61. Boggio, J. E. *J. Chem. Phys.* **1979,** *70,* 5054–5058. doi:10.1063/1.437347
62. Meldal, M.; Tornøe, C. W. *Chem. Rev.* **2008,** *108,* 2952–3015. doi:10.1021/cr0783479
63. Rodionov, V. O.; Fokin, V. V.; Finn, M. G. *Angew. Chem., Int. Ed.* **2005,** *44,* 2210–2215. doi:10.1002/anie.200461496
64. Nolte, C.; Mayer, P.; Straub, B. F. *Angew. Chem., Int. Ed.* **2007,** *46,* 2101–2103. doi:10.1002/anie.200604444
65. Shao, C.; Cheng, G.; Su, D.; Xu, J.; Wang, X.; Hu, Y. *Adv. Synth. Catal.* **2010,** *352,* 1587–1592. doi:10.1002/adsc.200900768
66. Shao, C.; Wang, X.; Xu, J.; Zhao, J.; Zhang, Q.; Hu, Y. *J. Org. Chem.* **2010,** *75,* 7002–7005. doi:10.1021/jo101495k
67. Shao, C.; Wang, X.; Zhang, Q.; Luo, S.; Zhao, J.; Hu, Y. *J. Org. Chem.* **2011,** *76,* 6832–6836. doi:10.1021/jo200869a
68. Kiss, L.; Forró, E.; Fülöp, F. *Tetrahedron* **2012,** *68,* 4438–4443. doi:10.1016/j.tet.2011.12.065
69. Shanmugavelan, P.; Nagarajan, S.; Sathishkumar, M.; Ponnuswamy, A.; Yogeeswari, P.; Sriram, D. *Bioorg. Med. Chem. Lett.* **2011,** *21,* 7273–7276. doi:10.1016/j.bmcl.2011.10.048
70. Ganesh, V.; Sudhir, V. S.; Kundu, T.; Chandrasekaran, S. *Chem.–Asian J.* **2011,** *6,* 2670–2694. doi:10.1002/asia.201100408
71. Fouda, M. F. R.; Abd-Elzaher, M. M.; Abdelsamaia, R. A.; Labib, A. A. *Appl. Organomet. Chem.* **2007,** *21,* 613–625. doi:10.1002/aoc.1202
72. van Staveren, D. R.; Metzler-Nolte, N. *Chem. Rev.* **2004,** *104,* 5931–5986. doi:10.1021/cr0101510
73. Nakamura, E.; Mori, S. *Angew. Chem., Int. Ed.* **2000,** *39,* 3750–3771. doi:10.1002/1521-3773(20001103)39:21<3750::AID-ANIE3750>3.0.CO;2-L
74. Grodzicki, A.; Łakomska, I.; Piszczek, P.; Szymańska, I.; Szłyk, E. *Coord. Chem. Rev.* **2005,** *249,* 2232–2258. doi:10.1016/j.ccr.2005.05.026
75. Liang, L.; Astruc, D. *Coord. Chem. Rev.* **2011,** *255,* 2933–2945. doi:10.1016/j.ccr.2011.06.028
76. Kovács, S.; Zih-Perényi, K.; Révész, A.; Novák, Z. *Synthesis* **2012,** *44,* 3722–3730. doi:10.1055/s-0032-1317697

License and Terms

Beilstein Journal of Organic Chemistry

The rapid generation of isothiocyanates in flow

Marcus Baumann and Ian R. Baxendale*

Full Research Paper

Open Access

Address:
Department of Chemistry, University of Durham, South Road, Durham DH1 3LE, United Kingdom

Email:
Ian R. Baxendale* - i.r.baxendale@durham.ac.uk

* Corresponding author

Keywords:
chloroxime; dipolar cycloaddition; flow chemistry; flow synthesis; immobilised reagents; isothiocyanate; nitrile oxide

Beilstein J. Org. Chem. **2013,** *9,* 1613–1619.
doi:10.3762/bjoc.9.184

Received: 20 June 2013
Accepted: 23 July 2013
Published: 08 August 2013

This article is part of the Thematic Series "Chemistry in flow systems III".

Guest Editor: A. Kirschning

Abstract

Isothiocyanates are versatile starting materials for a wide range of chemical reactions. However, their high nucleophilic susceptibility means they are best prepared and used immediately. We report here on a flow platform for the fast and efficient formation of isothiocyanates by the direct conversion of easily prepared chloroximes. To expedite this chemistry a flow insert cartridge containing two immobilised reagents is used to affect the chemical transformation which typically eliminates the requirements for any conventional work-up or purification of the reaction stream.

Introduction

Flow based chemical synthesis is playing an increasingly pivotal role within the chemical sciences as it facilitates a more versatile and responsive workflow. It encompasses many aspects of synthesis from the rapid and on-demand preparation of important building blocks to the development of multi-step sequences leading to advanced chemical structures and more direct scaling of bulk producing reactions [1-10]. Consequently, the chemical literature is growing at a precipitous rate with numerous examples of key chemical transformations having been further optimised or improved upon when conducted within a pseudo-/continuous flow process [11,12]. From a synthesis perspective the majority of these endeavours have been directed at enhancing specific reaction safety profiles, identifying new reaction sequences or generating improvements to well-known yet cumbersome transformations [13-16]. Indeed, flow chemistry is moving from an academic curiosity to become a common tool in many synthesis laboratories paralleling the emergence and adoption of another enabling technology, the microwave reactor [17].

An area which has benefited significantly from the many recent developments in our understanding of flow chemistry is the synthesis of reactive precursors and handling of sensitive intermediates [18-23]. However, despite the breadth of chemistries already explored there are certain functional transformations notably absent, one particular class of important building blocks which has received less attention are isothiocyanates. These species are widely utilised as valuable starting materials for many thiourea-based organocatalysts [24-26], numerous heterocyclic entities [27-29] as well as important entry points towards

other key functional groups such as isocyanides [30,31], guanidines [32,33] and thiosemicarbazides [34]. Due to the limited commercial availability of diversely functionalised isothiocyanates chemists normally pursue a de novo synthesis, which most commonly involves the condensation of an amine with thiophosgene or carbon disulfide [35,36], both reagents causing safety concerns due to the formation of toxic, malodorous and/or extremely corrosive byproducts (Scheme 1a). An underutilised alternative sequence is the 1,3-dipolar cycloaddition reaction between a nitrile oxide and a thiourea compound which initially generates an unstable 1,4,2-oxathiazoline intermediate that readily rearranges into urea and eliminates the desired isothiocyanate product [37,38] (Scheme 1b).

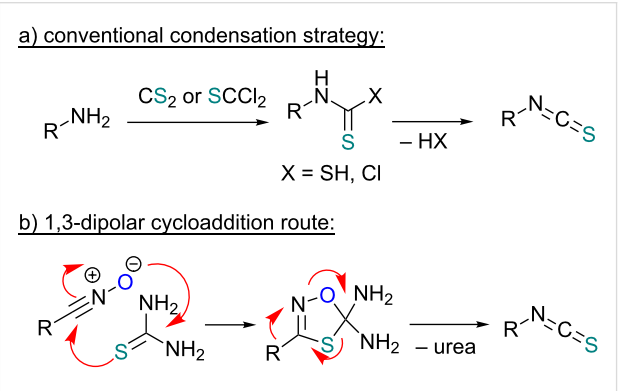

Scheme 1: Strategies towards isothiocyanates.

Whilst this approach appears on initial inspection to be very attractive it is somewhat hampered by the requirement to access the reactive nitrile oxide species, which once formed is prone to undergo fast dimerisation leading to furoxan byproducts (see Table 1) [39]. In fact this facile dimerisation reaction is regularly reported as troublesome in many reactions that progress through nitrile oxide intermediates. As a consequence a number of strategies to minimise this side reaction have been attempted. These include the use of highly diluted reaction mixtures, the use of large excesses of the corresponding dipolarophile partner, as well as the slow addition of reagents to create limiting concentrations of the active 1,3-dipole. Despite these efforts, the side reaction is still seen and there normally remains the requirement for time consuming purifications such as column chromatography in order to isolate pure products.

Immobilised reagents have shown great promise as enabling technologies when incorporated in flow reactors to aid in the processing, work-up and purification of reaction sequences [40-44]. In addition they have been successfully utilised in order to render dipolar cycloaddition reactions involving azomethine ylides [45,46] as well as nitrile oxides [47,48] more practical for generating important heterocyclic scaffolds such as pyrrolidines, isoxazolines and their derivatives [49-52]. We therefore considered that it should be possible to develop a mild and practical flow-based process to form isothiocyanates from the corresponding reactive nitrile oxide intermediates.

Our strategy makes use of two immobilised reagents (a weak base and a functionalised thiourea) placed as a 1:1-mixture within a single glass reactor cartridge (Scheme 2). The immobilised base affects the in situ formation of the reactive nitrile oxide from the chloroxime which is immediately captured by the local tethered thiocarbonyl dipolarophile. Consequently, this approach significantly minimises the formation of the furoxan byproduct by creating a scenario of pseudo high dilution of the nitrile oxide whilst allowing a concurrent high local concentration of the dipolarophile. Additionally the immobilised supports act as excellent sequestering agents for trapping even the small quantities of polar impurities within the matrix thus allowing for the isolation of the desired isothiocyanate product in high purity after only simple solvent removal.

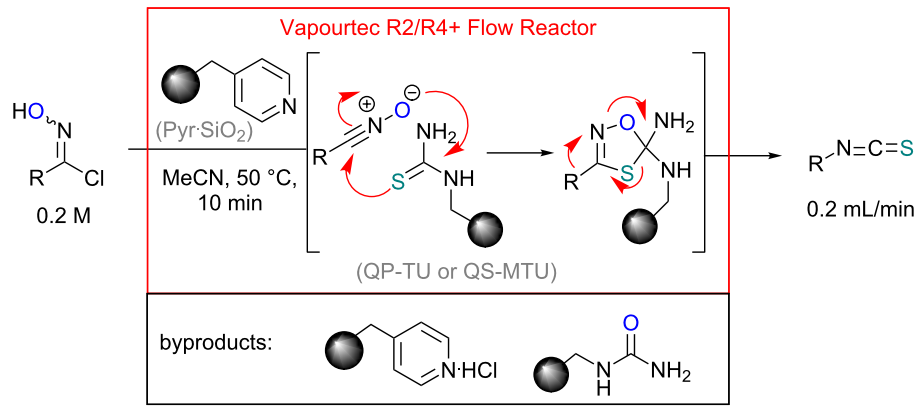

Scheme 2: Flow approach towards isothiocyanates.

Results and Discussion

Initially a set of batch experiments was performed using (4-bromophenyl)chloroxime **1a** as the substrate, which was efficiently prepared on gram scale from the corresponding benzaldehyde via oxime formation and subsequent NCS-mediated chlorination [53]. Screening different solvents (MeCN, acetone, EtOAc, MeOH and iPrOH) and immobilised thiourea species (QP-TU [54] and QS-MTU [55]) showed that the desired transformation can be effected with either immobilised thiourea source and furthermore tolerates a wide range of the solvents, with MeCN being identified as the best option. The choice of base was found to be of particular importance given that solution phase bases tested (NEt_3 or DBU even using slow addition) immediately generated substantial quantities of a white precipitate, which was later identified as the undesired furoxan byproduct (Table 1). In order to evaluate conditions to minimise this side reaction we studied several immobilised bases including QP-DMA (benzyldimethylamine resin) and SiO_2-pyr. The latter allowed for the isolation of the desired isothiocyanate in high yield and with very little contamination by the furoxan byproduct.

We translated the outcome of these preliminary results into a flow protocol using a commercially available Vapourtec R series flow reactor [56] which was operated with MeCN as the system solvent. Stock solutions of the chloroxime starting materials were prepared in the same solvent (0.25–0.5 M) and injected into a sample loop (2–10 mL size). Both the solid supported base (SiO_2-pyr) and immobilised thiourea species (QP-TU or QS-MTU) were blended (by shaking), filled into an glass column (10 cm length, 6.6 mm i.d., 1:1 ratio, 1.2 equiv each species) and the column inserted into a glass heating jacket which was maintained at 50 °C. The flow stream of the substrate was subsequently directed through the heated reactor column at a flow rate of 0.2 mL/min equating to an average residence time of 10 minutes. After passing a 100 psi backpressure regulator the typically colourless reaction mixture was collected yielding the product after evaporation of the solvent. ^{1}H NMR experiments were used to determine the product composition and purity and pleasingly revealed complete conversion of the substrates into the desired isothiocyanate product in high yield and purity as summarised in Table 2.

The reactions demonstrate a high tolerance for both electron poor and electron rich aromatic substrates (Table 2, entries 1–8) which all delivered the desired isothiocyanates reliably in high yield and purity. Furthermore, aliphatic chloroximes were found to work equally well, efficiently generating the corresponding isothiocyanate products again in high yields and purities (Table 2, entries 9–12). When using single diastereoisomers of α-chiral chloroximes the desired isothiocyanate product was correspondingly isolated as a single isomer (by ^{1}H NMR) suggesting a concerted reaction pathway to be in operation. Importantly, more complex substrates (i.e. *N*-chloropyrrolidines, Table 2, entries 13–15) can be subjected to the reaction conditions in order to not only install the desired isothiocyanate functionality but through concomitant elimination affect the formation of a cyclic imine, which is very attractive as it allows subsequent diversification of these polyfunctionalised heterocyclic building blocks. Overall, this exemplifies how the presented methodology can enable the rapid construction of scaffolds with unprecedented substitution patterns, which hold great interest due to their potential as highly decorated entities.

The most noteworthy feature of this flow protocol is its efficiency and simplicity allowing the desired product to be isolated following only solvent removal. The incomplete recovery

Table 1: Screening of different bases for the formation and conversion of nitrile oxides in batch:

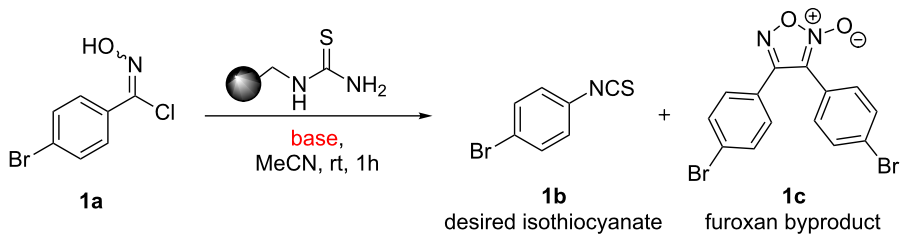

1a | **1b** desired isothiocyanate | **1c** furoxan byproduct

Entry	Base	Ratio isothiocyanate/furoxan	Comments
1	NEt_3 (0.2 M in MeCN)	1:1	dropwise addition of base
2	DBU (0.2 M in MeCN)	1:1	dropwise addition of base
3	QP-DMA	2.2:1	portionwise addition of base
4	SiO_2-pyr	>4:1	portionwise addition of base

Table 2: Isothiocyanates prepared in flow.

Entry	Starting material	Product	Isolated yield [%]	Scale [mmol]
1	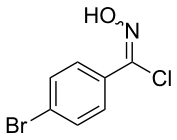	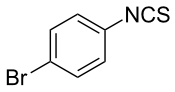 **1b**	93[a] 84[a]	1.0 5.0
2	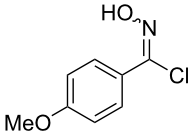	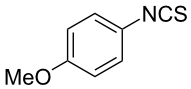 **2b**	89[a]	1.0
3	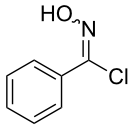	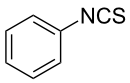 **3b**	91[a]	1.0
4	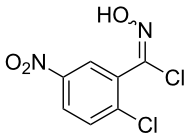	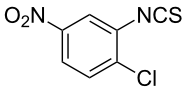 **4b**	78[a]	0.7
5	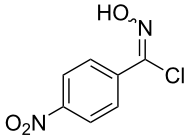	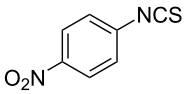 **5b**	76[a]	0.5
6	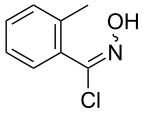	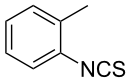 **6b**	94[a]	1.0
7	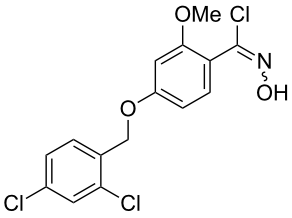	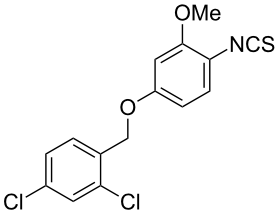 **7b**	91[a]	0.5
8	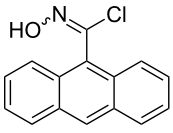	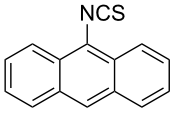 **8b**	85[a]	1.0
9	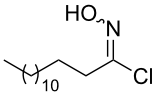	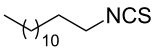 **9b**	89[a]	0.8
10	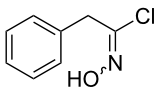	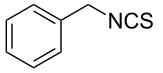 **10b**	84[a]	0.8
11	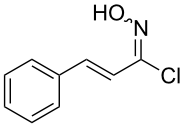	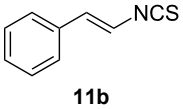 **11b**	81[a]	0.8

Table 2: Isothiocyanates prepared in flow. (continued)

12	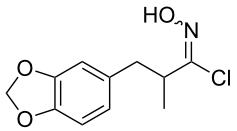	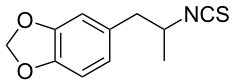 **12b**	87[a]	1.0
13	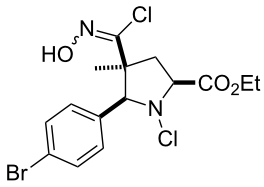	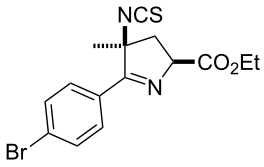 **13b**	73[b,c]	0.5
14	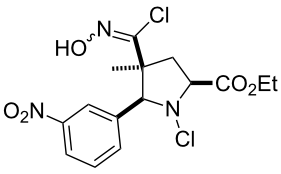	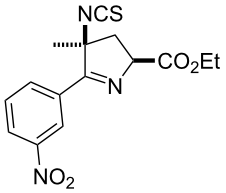 **14b**	71[b,c]	0.5
15	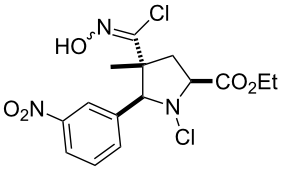	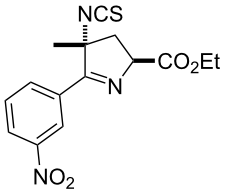 **15b**	76[b,c]	0.75

[a]Purity > 90% by ^{1}H NMR. [b]Purified by SiO_2 column chromatography. [c]2.5 equiv of SiO_2-pyridine used.

of material in these reactions can be accounted for by small amounts of the furoxan dimer which forms yet is trapped within the reactor column, thus evading its tedious removal via subsequent column chromatography. In addition our study demonstrates that thiourea – either immobilised on a polystyrene-type support (QP-TU) or on silica gel (QS-MTU) – serves as an efficient source of a sulfur atom. Given the higher loading of QP-TU (~5.5 mmol/g) compared to QS-MTU (~1.5 mmol/g) as well as its lower cost, QP-TU might be considered the more economical option, however, with the primary focus of this study being the small scale generation of valuable novel isothiocyanate products, this would only become relevant at larger scales (>100 g).

Conclusion

In conclusion, we have demonstrated an efficient and mild flow protocol for the synthesis of isothiocyanates from readily available chloroximes exploiting several immobilised reagents. This approach allows for the rapid access to various isothiocyanate building blocks avoiding time consuming purifications. Our study expands on the traditional use of immobilised thiourea species as simple metal scavengers and will likely lead to their further application as a convenient source of sulfur.

Supporting Information

Supporting Information File 1

Experimental part.
[http://www.beilstein-journals.org/bjoc/content/supplementary/1860-5397-9-184-S1.pdf]

Acknowledgements

We would like to express our gratitude to the Royal Society for funding to support this research.

References

1. Wegner, J.; Ceylan, S.; Kirschning, A. *Chem. Commun.* **2011,** *47,* 4583–4592. doi:10.1039/c0cc05060a
2. Baumann, M.; Baxendale, I. R.; Ley, S. V. *Mol. Diversity* **2011,** *15,* 613–630. doi:10.1007/s11030-010-9282-1
3. Baxendale, I. R. *J. Chem. Technol. Biotechnol.* **2013,** *88,* 519–552. doi:10.1002/jctb.4012
4. Baxendale, I. R.; Brocken, L.; Mallia, C. J. *Green Process Synth.* **2013,** *2,* 211–230. doi:10.1515/gps-2013-0029
5. Wiles, C.; Watts, P. *Green Chem.* **2012,** *14,* 38–54. doi:10.1039/c1gc16022b

6. Calabrese, G. S.; Pissavini, S. *AIChE J.* **2011,** *57,* 828–834. doi:10.1002/aic.12598
7. Hessel, V.; Cortese, B.; de Croon, M. H. J. M. *Chem. Eng. Sci.* **2011,** *66,* 1426–1428. doi:10.1016/j.ces.2010.08.018
8. Yoshida, J.-I.; Kim, H.; Nagaki, A. *ChemSusChem* **2011,** *4,* 331–340. doi:10.1002/cssc.201000271
9. Webster, A.; Greenman, J.; Haswell, S. J. *J. Chem. Technol. Biotechnol.* **2011,** *86,* 10–17. doi:10.1002/jctb.2482
10. Hartman, R. L.; McMullen, J. P.; Jensen, K. F. *Angew. Chem., Int. Ed.* **2011,** *50,* 7502–7519. doi:10.1002/anie.201004637
11. Yoshida, J. *Flash Chemistry: Fast Organic Synthesis in Microsystems;* John Wiley & Sons: Chichester, UK, 2008.
12. Baxendale, I. R.; Griffiths-Jones, C. M.; Ley, S. V.; Tranmer, G. K. *Chem.–Eur. J.* **2006,** *12,* 4407–4416. doi:10.1002/chem.200501400
13. Geyer, K.; Codée, J. D. C.; Seeberger, P. H. *Chem.–Eur. J.* **2006,** *12,* 8434–8442. doi:10.1002/chem.200600596
14. Baumann, M.; Baxendale, I. R.; Ley, S. V.; Smith, C. D.; Tranmer, G. K. *Org. Lett.* **2006,** *8,* 5231–5234. doi:10.1021/ol061975c
15. Kopach, M. E.; Roberts, D. J.; Johnson, M. D.; McClary Groh, J.; Adler, J. J.; Schafer, J. P.; Kobierski, M. E.; Trankle, W. G. *Green Chem.* **2012,** *14,* 1524–1536. doi:10.1039/c2gc35050e
16. Ruppert, J. F.; White, J. D. *J. Org. Chem.* **1974,** *39,* 269–270. doi:10.1021/jo00916a043
17. Tierney, J. P.; Lidström, P., Eds. *Microwave Assisted Organic Synthesis;* Blackwell CRC Press: Oxford, UK, 2005. doi:10.1002/9781444305548
18. Illg, T.; Löb, P.; Hessel, V. *Bioorg. Med. Chem.* **2010,** *18,* 3707–3719. doi:10.1016/j.bmc.2010.03.073
19. Breen, J. R.; Sandford, G.; Yufit, D. S.; Howard, J. A. K.; Fray, J.; Patel, B. *Beilstein J. Org. Chem.* **2011,** *7,* 1048–1054. doi:10.3762/bjoc.7.120
20. Watts, K.; Gattrell, W.; Wirth, T. *Beilstein J. Org. Chem.* **2011,** *7,* 1108–1114. doi:10.3762/bjoc.7.127
21. Maurya, R. A.; Park, C. P.; Kim, D.-P. *Beilstein J. Org. Chem.* **2011,** *7,* 1158–1163. doi:10.3762/bjoc.7.134
22. van den Broek, S. A. M. W.; Leliveld, J. R.; Becker, R.; Delville, M. M. E.; Nieuwland, P. J.; Koch, K.; Rutjes, F. P. J. T. *Org. Process Res. Dev.* **2012,** *16,* 934–938. doi:10.1021/op2003437
23. Smith, C. J.; Smith, C. D.; Nikbin, N.; Ley, S. V.; Baxendale, I. R. *Org. Biomol. Chem.* **2011,** *9,* 1927–1937. doi:10.1039/c0ob00813c
24. Sigman, M. S.; Jacobsen, E. N. *J. Am. Chem. Soc.* **1998,** *120,* 4901–4902. doi:10.1021/ja980139y
25. Vachal, P.; Jacobsen, E. N. *J. Am. Chem. Soc.* **2002,** *124,* 10012–10014. doi:10.1021/ja027246j
26. Doyle, A. G.; Jacobsen, E. N. *Chem. Rev.* **2007,** *107,* 5713–5743. doi:10.1021/cr068373r
27. Brandsma, L.; Nedolya, N. A.; Tarasova, O. A.; Trofimov, B. A. *Chem. Heterocycl. Compd.* **2000,** *36,* 1241–1260. doi:10.1023/A:1017582315266
28. Yella, R.; Patel, B. K. *J. Comb. Chem.* **2010,** *12,* 754–763. doi:10.1021/cc100124q
29. Baxendale, I. R.; Ley, S. V.; Smith, C. D.; Tamborini, L.; Voica, A.-F. *J. Comb. Chem.* **2008,** *10,* 851–857. doi:10.1021/cc800070a
30. Ley, S. V.; Taylor, S. J. *Bioorg. Med. Chem. Lett.* **2002,** *12,* 1813–1816. doi:10.1016/S0960-894X(02)00269-X
31. Bhat, V.; Allan, K. M.; Rawal, V. H. *J. Am. Chem. Soc.* **2011,** *133,* 5798–5801. doi:10.1021/ja201834u
32. Smith, C. D.; Baxendale, I. R.; Tranmer, G. K.; Baumann, M.; Smith, S. C.; Lewthwaite, R. A.; Ley, S. V. *Org. Biomol. Chem.* **2007,** *5,* 1562–1568. doi:10.1039/b703033a
33. Drewry, D. H.; Gerritz, S. W.; Linn, J. A. *Tetrahedron Lett.* **1997,** *38,* 3377–3380. doi:10.1016/S0040-4039(97)00653-9
34. Mustafa, S. M.; Nair, V. A.; Chittoor, J. P.; Krishnapillai, S. *Mini-Rev. Org. Chem.* **2004,** *1,* 375–385. doi:10.2174/1570193043403082
35. Mukerjee, A. K.; Ashare, R. *Chem. Rev.* **1991,** *91,* 1–24. doi:10.1021/cr00001a001
36. Wong, R.; Dolman, S. J. *J. Org. Chem.* **2007,** *72,* 3969–3971. doi:10.1021/jo070246n
37. Nyoung, K. J.; Ryu, E. K. *Tetrahedron Lett.* **1993,** *34,* 8283–8284. doi:10.1016/S0040-4039(00)61411-9
38. Kim, J. N.; Jung, K. S.; Lee, H. J.; Son, J. S. *Tetrahedron Lett.* **1997,** *38,* 1597–1598. doi:10.1016/S0040-4039(97)00121-4
39. Feuer, H., Ed. *Nitrile Oxides, Nitrones and Nitronates in Organic Synthesis,* 2nd ed.; John Wiley & Sons: Hoboken, New Jersey, USA, 2008.
40. Kirschning, A.; Solodenko, W.; Mennecke, K. *Chem.–Eur. J.* **2006,** *12,* 5972–5990. doi:10.1002/chem.200600236
41. Salimi, H.; Rahimi, A.; Pourjavadi, A. *Monatsh. Chem.* **2007,** *138,* 363–379. doi:10.1007/s00706-007-0616-3
42. Hodge, P. *Ind. Eng. Chem. Res.* **2005,** *44,* 8542–8553. doi:10.1021/ie040285e
43. Ley, S. V.; Baxendale, I. R. *Nat. Rev. Drug Discovery* **2002,** *1,* 573–586. doi:10.1038/nrd871
44. Ley, S. V.; Baxendale, I. R.; Bream, R. N.; Jackson, P. S.; Leach, A. G.; Longbottom, D. A.; Nesi, M.; Scott, J. S.; Storer, R. I.; Taylor, S. J. *J. Chem. Soc., Perkin Trans. 1* **2000,** 3815–4195. doi:10.1039/B006588I
45. Grafton, M.; Mansfield, A. C.; Fray, M. J. *Tetrahedron Lett.* **2010,** *51,* 1026–1029. doi:10.1016/j.tetlet.2009.12.071
46. Baumann, M.; Baxendale, I. R.; Ley, S. V. *Synlett* **2010,** 749–752. doi:10.1055/s-0029-1219344
47. Brasholz, M.; Saubern, S.; Savage, G. P. *Aust. J. Chem.* **2011,** *64,* 1397–1401. doi:10.1071/CH11079
48. Castellano, S.; Tamborini, L.; Viviano, M.; Pinto, A.; Sbardella, G.; Conti, P. *J. Org. Chem.* **2010,** *75,* 7439–7442. doi:10.1021/jo1014323
49. Tran, G.; Meier, R.; Harris, L.; Browne, D. L.; Ley, S. V. *J. Org. Chem.* **2012,** *77,* 11071–11078. doi:10.1021/jo302052m
50. Harding, S. L.; Marcuccio, S. M.; Savage, G. P. *Beilstein J. Org. Chem.* **2012,** *8,* 606–612. doi:10.3762/bjoc.8.67
51. Baumann, M.; Baxendale, I. R.; Kuratli, C.; Ley, S. V.; Martin, R. E.; Schneider, J. *ACS Comb. Sci.* **2011,** *13,* 405–413. doi:10.1021/co2000357
52. Baumann, M.; Baxendale, I. R.; Kirschning, A.; Ley, S. V.; Wegner, J. *Heterocycles* **2011,** *82,* 1297–1316. doi:10.3987/COM-10-S(E)77
53. Yu, G. J.; Yang, B.; Verkman, A. S.; Kurth, M. J. *Synlett* **2010,** 1063–1066. doi:10.1055/s-0029-1219781
54. QuadraPure™ Thiourea resin (QP-TU, loading ~5.5 mmol/g) is commercially available through Johnson-Matthey.
55. QuadraSil™ Methylthiourea (QS-MTU, loading ~1.5 mmol/g) is commercially available through Johnson-Matthey.
56. The Vapourtec R-series flow system is available from Vapourtec (http://www.vapourtec.co.uk/).

Beilstein Journal of Organic Chemistry

Gallium-containing polymer brush film as efficient supported Lewis acid catalyst in a glass microreactor

Rajesh Munirathinam[1], Roberto Ricciardi[1], Richard J. M. Egberink[1], Jurriaan Huskens[1], Michael Holtkamp[2], Herbert Wormeester[3], Uwe Karst[2] and Willem Verboom[*1]

Full Research Paper

Open Access

Address:
[1]Laboratory of Molecular Nanofabrication, MESA+ Institute for Nanotechnology, University of Twente, P.O. Box 217, 7500 AE Enschede, The Netherlands, [2]University of Münster, Institute of Inorganic and Analytical Chemistry, Corrensstr. 28/30, 48149 Münster, Germany, and [3]Laboratory of Physics of Interfaces and Nanomaterials, MESA+ Institute for Nanotechnology, University of Twente, P.O. Box 217, 7500 AE Enschede, The Netherlands

Email:
Willem Verboom[*] - w.verboom@utwente.nl

* Corresponding author

Keywords:
dehydration of oximes; flow chemistry; gallium; microreactors; Lewis acid catalysis; polymer brushes

Beilstein J. Org. Chem. **2013,** *9,* 1698–1704.
doi:10.3762/bjoc.9.194

Received: 05 June 2013
Accepted: 16 July 2013
Published: 16 August 2013

This article is part of the Thematic Series "Chemistry in flow systems III".

Guest Editor: A. Kirschning

Abstract

Polystyrene sulfonate polymer brushes, grown on the interior of the microchannels in a microreactor, have been used for the anchoring of gallium as a Lewis acid catalyst. Initially, gallium-containing polymer brushes were grown on a flat silicon oxide surface and were characterized by FTIR, ellipsometry, and X-ray photoelectron spectroscopy (XPS). XPS revealed the presence of one gallium per 2–3 styrene sulfonate groups of the polymer brushes. The catalytic activity of the Lewis acid-functionalized brushes in a microreactor was demonstrated for the dehydration of oximes, using cinnamaldehyde oxime as a model substrate, and for the formation of oxazoles by ring closure of *ortho*-hydroxy oximes. The catalytic activity of the microreactor could be maintained by periodic reactivation by treatment with $GaCl_3$.

Introduction

Heterogeneous catalysis plays a crucial role in organic synthesis both in industry and academia. In the present situation, microreactors offer a number of benefits over classical setups [1-3]. Especially, heterogeneous catalysis in a continuous-flow microreactor is gaining growing attention, owing to its advantages such as increased surface-to-volume ratio, faster heat and mass transfer, only small amounts of reagents are handled, when compared to conventional laboratory equipment [4].

Heterogeneous catalysis in microreactors is carried out using two approaches, viz. a) with a packed-bed microreactor, where the catalyst is attached to a polymeric material enclosed in the microchannel [5], and b) when the catalyst is covalently connected to the inner walls of a glass microreactor [6]. Although the former approach has advantages such as high catalyst loading and easy fabrication of the catalytic device by filling the channels with functional catalytic particles, however, heat transfer limitations and pressure drop developing along the microchannel are serious drawbacks [7].

The literature contains numerous examples of Lewis acid catalysis [8-11]. However, only a limited number of papers are known dealing with heterogeneous Lewis acid catalysis, where a Lewis acid is tethered onto a solid surface like silica or gold [12,13]. Furthermore, to the best of our knowledge, there are no examples of the immobilization of a Lewis acid to a microreactor channel wall.

Polymer brushes have proven to provide a unique platform in supported catalysis [14,15]. Previously, we have described the successful immobilization and evaluation of catalysts (e.g., basic organocatalyst [6], metallic nanoparticles [16], and enzymatic catalyst [17]) to the microchannel walls using polymer brushes. As a part of this program, herein, we report the anchoring of gallium as a Lewis acid catalyst making use of polystyrene sulfonate (PSS) polymer brushes. The choice for gallium was inspired by the successful application of solid supported gallium triflate to catalyze the Strecker reaction by Wiles and Watts [13]. The dehydration of cinnamaldehyde oxime [18] was used as a model reaction to study the catalytic activity of a microreactor with gallium immobilized onto its channel walls (Scheme 1).

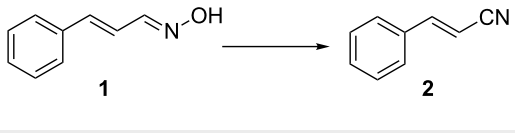

Scheme 1: Gallium-catalyzed dehydration of cinnamaldehyde oxime (**1**).

Results and Discussion

The catalytic polymer brush layer was first developed on a flat silicon oxide surface in order to optimize the reaction conditions before attempting the functionalization of a microreactor. Polystyrene sulfonate (PSS) polymer brushes [19] were synthesized according to the procedure summarized in Scheme 2. First, a monolayer of atom transfer radical polymerization (ATRP) initiator was covalently anchored on silicon oxide

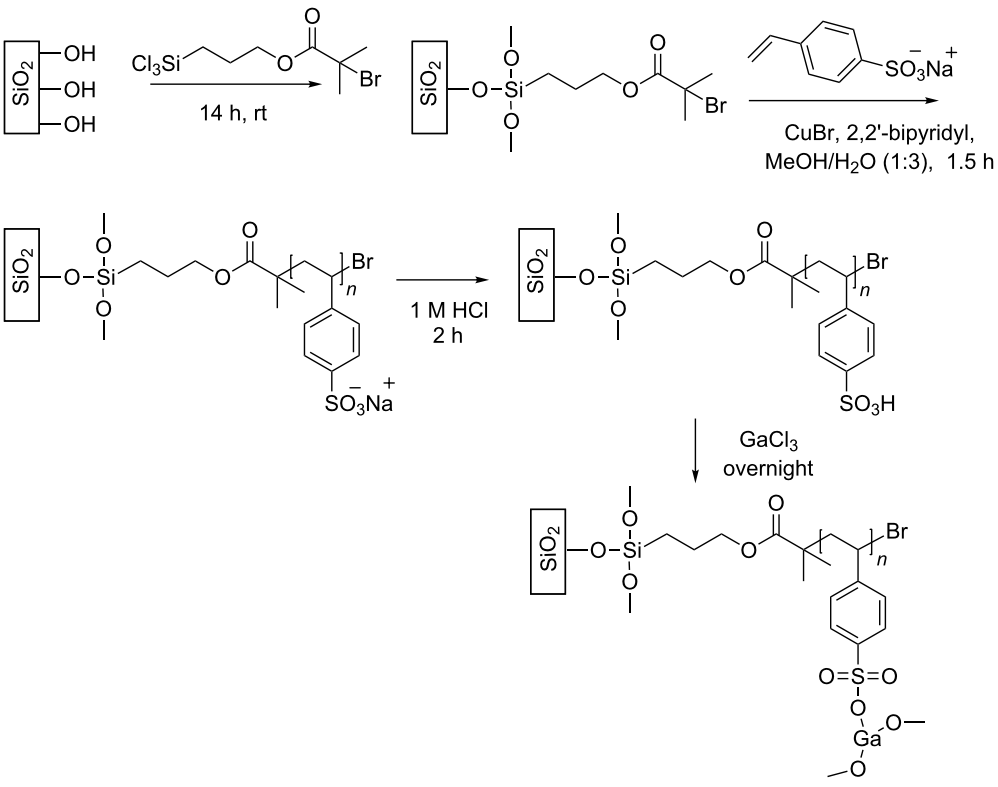

Scheme 2: General scheme for anchoring of initiator, ATRP of styrene sulfonate, activation, and reaction with gallium chloride.

substrates [20]. Then, a solution of styrene sulfonate in methanol/water (1:3) in the presence of 2-2'-bipyridyl and CuBr, was used to grow the PSS polymer brushes by means of ATRP. After activation of the polymer brushes with 1 M HCl, they were incubated with a 100 mM solution of $GaCl_3$ in acetonitrile.

Analysis of the surfaces by transmission FTIR spectroscopy after the polymerization step revealed the incorporation of sulfonic acid moieties, as it exhibited symmetric and asymmetric stretching vibrations at 1125 and 1011 cm^{-1}, respectively [21]. The intensity of these peaks remained the same, after activation with HCl and upon treatment with $GaCl_3$, indicating that the sulfonic acid moieties are still intact. Proof for the functionalization with gallium, however, was obtained by XPS spectroscopy. The atomic composition of the polymer brushes after anchoring of gallium was found to be C:O:S:Ga = 8:3.2:0.9:0.4, while no traces of chlorine were detected. From this, it was concluded that the polymer brushes contained on average one gallium per 2–3 styrene sulfonate groups. The thickness of the polymer brushes was determined by ellipsometry being about 77 nm in the dry state for a polymerization time of 1.5 h. Swelling studies on gallium-containing polymer brushes were performed in water, acetonitrile, and ethanol. Table 1 shows that the polymer brushes swell to the same extent in water as well as in organic solvents as acetonitrile and ethanol.

Table 1: Thickness of gallium-functionalized PSS polymer brushes on a flat silicon oxide surface.

	thickness (nm)
dry state	77 ± 2
water	91 ± 1
acetonitrile	95 ± 1
ethanol	96 ± 1

The same procedure used for the flat silicon oxide substrates was followed to immobilize gallium onto the interior of a glass microreactor with channel dimensions of 150 µm in width and depth, and having an internal volume of 13 µL. The PSS polymer brushes were grown and functionalized with gallium on the microchannel interior in the continuous flow-mode.

The dehydration of cinnamaldehyde oxime (**1**, 25 µM in acetonitrile) was used as a model reaction to study the catalytic activity of the gallium-functionalized microreactor, at 90 °C and 5 atm pressure, generated using a back pressure regulator in continuous flow. The conversion of the reagent was monitored online by in-line UV–vis detection, measuring the decrease in the extinction of the solution of oxime **1** at 286 nm. The reaction times were varied by changing the flow rates between 1 and 26 $\mu L \cdot min^{-1}$. The reaction showed nearly complete conversion at a residence time of 13 min. Under similar reaction conditions, after activating the PSS polymer brushes with 1 M HCl, no conversion was observed in the absence of gallium, proving that gallium is the catalytically active species. Under our conditions the reaction proceeded much faster when compared with the lab scale: the gallium(III) triflate (5 mol %) catalyzed dehydration of **1** in refluxing acetonitrile reported in literature [18] took 2 h to give **2** in 90% yield.

A kinetic analysis of the dehydration of oxime **1** was performed by carrying out the reaction at different concentrations of **1** (10–25 µM, Figure 1). The experimental data were fitted to a first-order rate equation, giving an observed rate constant, k_{obs}, of $(11 \pm 2) \times 10^{-3}$ s^{-1}. The values of the rate constants at different oxime concentrations were the same, within experimental error.

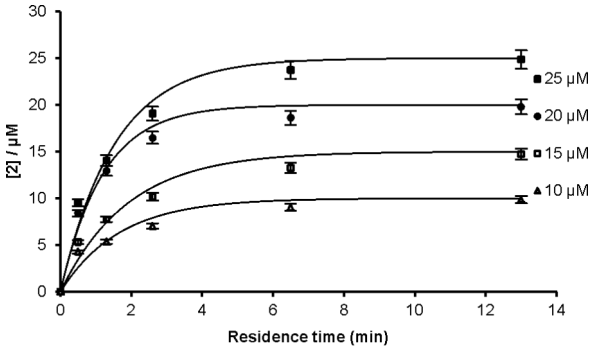

Figure 1: Gallium-catalyzed formation of nitrile **2** at 90 °C and 5 atm pressure.

The activation energy of the dehydration of oxime **1** was determined by calculating the k_{obs} values at different temperatures ranging from 70–90 °C (Supporting Information, Figure 1), with increments of five degrees. From the slope of the Arrhenius plot (Figure 2), the resulting activation energy was calculated to be 6.55 $kJ \cdot mol^{-1}$.

The substrate scope of the dehydration of oximes was extended using the same reaction conditions as above (Table 2). 4-Nitrobenzaldehyde oxime (**3**, Table 2, entry 1) resulted in a conversion of 62% within 13 min reaction time, while for the batch reaction, using gallium(III) triflate as a catalyst, 16 h at 120 °C was needed to give the nitrile **8** in 82% [18]. Anthracen-9-carbaldehyde oxime (**5**, Table 2, entry 3) showed a relatively poor conversion, which is ascribed to the steric hindrance of the molecule in reaching the catalytically active sites within the polymer brushes. In literature [18] this reaction, using

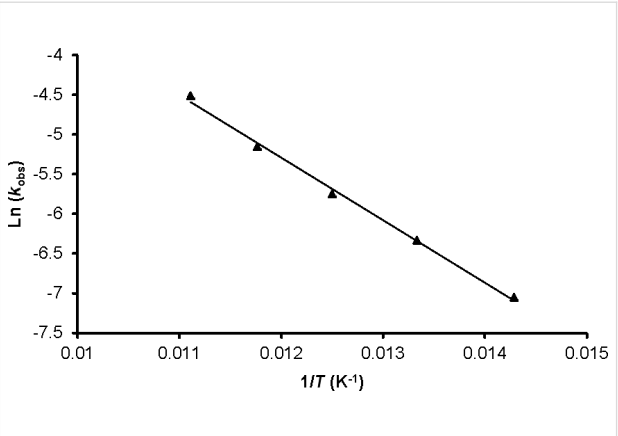

Figure 2: Arrhenius plot for the dehydration of cinnamaldehyde oxime (**1**).

gallium(III) triflate, required a reaction time of 8 h in refluxing acetonitrile to obtain the corresponding nitrile **10** in 87% yield. In case of 2-hydroxy-1-naphthaldehyde oxime (**6**) [22] (Table 2, entry 4) and salicylaldehyde oxime (**7**) [18] (Table 2, entry 5) dehydration happened between the *ortho*-hydroxy group and the oxime to give ring closure to the corresponding oxazoles **11** and **12**, respectively, in very good conversions.

The dehydration of **1** (25 μM in acetonitrile), under similar conditions as mentioned above, was used to test the stability of the catalytic layer in the microreactor. When the catalytic microreactor was continuously run for 50 h with a residence time of 13 min (flow rate of 1 μL·min^{-1}), the conversions remained nearly quantitative. However, with a shorter residence time of 78 s (flow rate of 10 μL·min^{-1}), the conversions (maximum about 55%) gradually decreased. Total reflection X-ray fluorescence (TXRF) analysis of one of the samples with residence times of 78 s and 13 min, showed the presence of 1.0 ppm and 0.2 ppm of gallium, respectively. Nevertheless, the catalytic activity could be easily reactivated to the original value (error 2–3%) by treating the microreactor with 100 mM $GaCl_3$ in acetonitrile overnight in the continuous flow mode (0.1 μL·min^{-1}) (Figure 3). This proves that, at a flow rate of 1 μL·min^{-1}, our catalytic system could be continuously used for at least two days without any noticeable decrease in the catalytic activity. If necessary, especially using higher flow rates, the catalytic system can be easily reactivated by treatment with $GaCl_3$. To estimate the amount of gallium present in the polymer brushes, the catalytically active microreactor was deactivated by flowing 1 M HCl with a flow rate of 1 μL·min^{-1} and subsequent, thorough rinsing with water and acetonitrile.

Table 2: Dehydration of oximes in the gallium-functionalized catalytic microreactor[a].

entry	substrate	product	conversion[b]
1 [18]	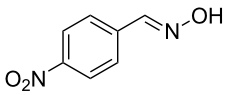 **3**	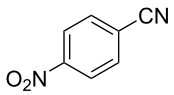 **8**	62
2 [23]	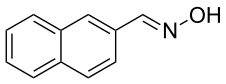 **4**	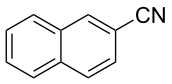 **9**	47
3 [18]	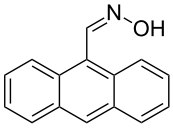 **5**	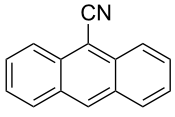 **10**	19
4 [22]	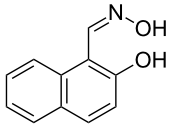 **6**	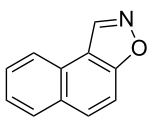 **11**	95
5 [18]	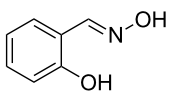 **7**	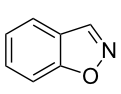 **12**	90

[a]All reactions were performed using 25 μM substrate in acetonitrile at 90 °C, 5 atm pressure, using a back pressure regulator, and a residence time of 13 min. [b]Conversions were determined using online UV–vis spectroscopy by following the change in the extinction of the substrate at a specific wavelength.

TXRF analysis of the solution showed the presence of 3.41 ± 0.01 µg of gallium. When the catalytic microreactor was activated and deactivated following the above mentioned protocol, the amount of gallium detected remained the same within the error limit.

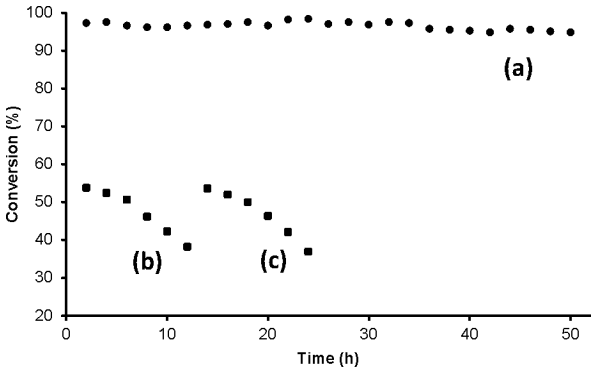

Figure 3: Conversion of cinnamaldehyde oxime (**1**, 25 µM in acetonitrile) by continuously running the catalytic microreactor: (a) for 50 h with 13 min residence time, (b) for 12 h with 78 s residence time, (c) also for 12 h with 78 s residence time but after reactivating the microreactor with $GaCl_3$.

Conclusion

In conclusion, to the best of our knowledge, we described the first example of the application of polystyrene sulfonate-based polymer brushes to anchor gallium as a Lewis acid catalyst onto the microchannel interior of a microreactor and proved its catalytic activity for the dehydration of oximes to the corresponding nitriles and the ring closure of *ortho*-hydroxy oximes to the corresponding oxazoles. In general, our catalytic system showed faster conversions for most substrates than using lab scale conditions. XPS data, obtained on a flat silicon oxide surface, showed that on average one gallium per 2–3 styrene sulfonate groups of the PSS polymer brushes was incorporated. Upon slow deactivation the catalytic activity of the microreactor can be easily reactivated to its initial value by flowing through a solution of $GaCl_3$. We believe that this approach has a wider scope and can be used to anchor other Lewis acids in a microreactor to study a range of Lewis acid-catalyzed reactions in an efficient way.

Experimental

Materials

The chemicals and solvents were purchased from Sigma-Aldrich unless otherwise stated and were used without purification unless specified. Single-side-polished silicon wafers were purchased from OKMETIC with (100) orientation. 3-(5'-Trichlorosilylpentyl) 2-bromo-2-methylpropionate was synthesized following a literature procedure [20]. CuBr was purified by washing with glacial acetic acid and, after filtration, by rinsing with ethanol and acetone, was stored in a vacuum desiccator. Methanol and ethanol (VWR, analytical reagent grade) were used without further purification, water was purified with the Milli-Q pulse (MILLIPORE, R = 18.2 MΩ cm) ultra-pure water system, dry toluene was from an encapsulated solvent purification system (MB-SPS-800), and acetonitrile (for analysis EMSURE® ACS, Reag. Ph Eur, Merck).

Methods

FTIR spectra were recorded using a Nicolet 6700 FTIR spectrometer. Ellipsometry measurements were performed with a Spectroscopic Ellipsometer M-2000X (J.A. Woolam Co., Inc.) with light reflected at 70° and a spot size of 2 mm diameter. Over a wavelength range of 340–1000 nm, with spectral resolution of about 2 nm both Psi and Delta were recorded as well as the intensity and amount of depolarization of the reflected light. The Complete EASE v.4.64 software package (J.A. Woolam Co., Inc.); was used to both control the instrument as well as for data analysis and modeling. For swelling experiments an in-situ homemade glass cell with an inner volume of about 70 mL was used. The 5 mm thick glass windows were positioned perpendicular to the light beam and were transparent in the employed wavelength range. For all measurements, the data were corrected for residual polarization by the windows. X-ray photoelectron spectroscopy (XPS) on the gallium-functionalized silicon oxide wafers were obtained on a Quantera Scanning X-ray Multiprobe instrument, equipped with a monochromatic Al Kα X-ray source producing approximately 25 W of X-ray power. XPS-data were collected from a surface area of 1000 µm × 300 µm with a pass energy of 224 eV and a step energy of 0.8 eV for survey scan and 0.4 for high resolution scans. For quantitative analysis, high resolution scans were used. Total reflection X-ray fluorescence analysis (TXRF) was carried out on a S2-PICOFOX instrument (Bruker AXS, Berlin, Germany) with an air-cooled molybdenum anode for X-ray generation. The excitation settings were 50 kV and 750 mA and quartz glass disks were used as sample carriers. The analysis was performed by signal integration over 500 seconds. For the determination, the signal of gallium ($K_{\alpha 1}$ = 9.251 keV) was quantified by using strontium ($K_{\alpha 1}$ = 9.251 keV) as internal standard ([Sr] = 10.0 µg/mL). Quantification was performed by the Bruker Spectra software (version 6.1.5.0) and based on the known concentration of the internal standard.

Set up of the flow microreactor

All microreactor experiments were performed in a setup as described in reference [16]. A back pressure regulator (Future Chemistry) was connected to the outlet of the microreactor. Glass microreactors with a residual volume of 13 µL and dimensions of 150 µm depth and 150 µm width were purchased from Micronit Microfluidics (Enschede, The Netherlands).

Synthesis of the catalytic polymer coating

Immobilization of the trichlorosilane initiator and the polymer brushes synthesis on the silicon oxide surface [19,20] and the microchannels [16] were carried out following literature procedures.

A solution of styrene sulfonate (1.25 g, 6.0 mmol) and 2,2'-bipyridyl (140 mg, 0.9 mmol) in a 3:1 mixture of methanol and water (12 mL) was degassed using the freeze-pump-thaw method (in a sealed Schlenk vessel). (The above-mentioned solution was frozen by immersion in liquid nitrogen. When the solvent was completely frozen the flask is kept under high vacuum for 5 min, with the flask still immersed in the liquid nitrogen. The flask was then closed and brought to room temperature until the solvent has completely melted. This process was repeated three times and after the last cycle the flask was filled with nitrogen.) CuBr (57 mg, 0.40 mmol) was added to this solution. To dissolve all solids, the mixture was stirred for 30 min under a continuous flow of nitrogen. Afterwards an initiator coated silicon wafer was placed in a Schlenk tube and the flask sealed with a septum. The tube was filled with argon and the monomer solution was syringed inside. For the polymerization in the device, the same solution was syringed through the microchannel till the device was completely filled. The solution was kept in contact with the silicon wafer and with the microchannel at a flow rate of 0.1 μL·min^{-1} for 1.5 h. After the polymerization, the silicon wafer and the microchannel were rinsed with water and methanol, and dried with a stream of nitrogen. In the next step the silicon wafers were soaked in a 1 M solution of HCl. The same solution was flowed with a flow rate of 0.1 μL·min^{-1} through the microreactor. After 2 h they were rinsed with water, acetone, and acetonitrile, and subsequently dried with a stream of nitrogen. For the preparation of the gallium-based Lewis acid bearing polymer brushes, all samples were first incubated overnight in a 100 mM solution of $GaCl_3$ in acetonitrile. The same solutions were flowed at a flow rate of 0.1 μL·min^{-1} through the microreactor. Subsequently, the silicon wafer and microchannel were rinsed with acetonitrile.

Kinetic study

The dehydration of cinnamaldehyde oxime (**1**, 10–25 μM) was carried out in acetonitrile at 90 °C under 5 atm pressure. Cinnamaldehyde oxime (**1**) and cinnamonitrile (**2**) exhibit the absorption maximum in acetonitrile at 286 nm and 271 nm, respectively. The conversion of cinnamaldehyde oxime (**1**) to cinnamonitrile (**2**) was calculated based on the decrease in the absorption at 286 nm using the formula: $[\mathbf{2}] = (\varepsilon_{286}(\mathbf{1}) \cdot [\mathbf{1}]_0 - A_{observed}) / (\varepsilon_{286}(\mathbf{1}) - \varepsilon_{286}(\mathbf{2}))$ ($A_{observed}$ = absorbance measured experimentally, while carrying out the reaction). The molar absorptivities (ε) of cinnamaldehyde oxime (**1**) and cinnamonitrile (**2**) in acetonitrile at 286 nm are 35640 and 17800 L·mol^{-1}·cm^{-1}, respectively. The k_{obs} values were calculated by fitting the experimental data with the following equation: $[\mathbf{2}] = [\mathbf{1}]_0 \cdot (1 - \exp(-k_{obs} \cdot t))$ using least-squares fit. The experimental errors in these measurements are ±4%.

Substrate scope

The dehydration reaction with different oxime substrates (Table 2, entries 1–5) was carried out in a catalytic microreactor at 90 °C, 5 atm pressure, with a residence time of 13 min. A substrate concentration of 25 μM was used for all the substrates. The conversions were determined using online UV–vis spectroscopy by following the change in the extinction of a substrate specific wavelength. In case of 2-hydroxy-1-naphthaldehyde oxime (**6**, Table 2, entry 4) and salicylaldehyde oxime (**7**, Table 2, entry 5), the conversions were determined by following the decrease in the absorbance at 353 nm (ε_{353} = 8360 L·mol^{-1}·cm^{-1}) and 310 nm (ε_{310} = 4820 L·mol^{-1}·cm^{-1}), respectively; the corresponding oxazoles **11** and **12** showed no absorbance in that region. With 4-nitrobenzaldehyde oxime (**3**, Table 2, entry 1) and 2-naphthaldehyde oxime (**4**, Table 2, entry 2), the conversions were determined by following the decrease in the absorbance at 303 nm (ε_{303} = 20560 L·mol^{-1}·cm^{-1}) and 283 nm (ε_{283} = 20360 L·mol^{-1}·cm^{-1}), respectively, using the formula that was applied for **1**, as the corresponding nitriles **8** and **9** showed molar absorptivities (ε) of 2200 and 7160 L·mol^{-1}·cm^{-1}, respectively, in that region. In case of anthracen-9-carbaldehyde oxime (**5**, Table 2, entry 3), the conversions were determined by following the increase in the absorbance at 403 nm (ε_{403} = 2600 L·mol^{-1}·cm^{-1}); the corresponding product **10** has a molar absorptivity (ε) of 13400 L·mol^{-1}·cm^{-1} in that region.

On-line UV–vis detection

The conversion of the oximes was followed using online UV–vis spectrometry as described in reference [16].

Supporting Information

Supporting Information File 1

Conversion of cinnamaldehyde oxime (**1**, 25 μM in acetonitrile) catalyzed by gallium in a microreactor at different temperatures.
[http://www.beilstein-journals.org/bjoc/content/supplementary/1860-5397-9-194-S1.pdf]

Acknowledgements

We acknowledge the financial support from NanoNext NL (RM) and the Netherlands Organisation for Scientific Research (NWO) (RR).

References

1. Watts, P.; Wiles, C. *Chem. Commun.* **2007,** 443–467. doi:10.1039/B609428G
2. Brivio, M.; Verboom, W.; Reinhoudt, D. N. *Lab Chip* **2006,** *6,* 329–344. doi:10.1039/B510856J
3. Hartman, R. L.; McMullen, J. P.; Jensen, K. F. *Angew. Chem., Int. Ed.* **2011,** *50,* 7502–7519. doi:10.1002/anie.201004637
4. Liu, X.; Ünal, B.; Jensen, K. F. *Catal. Sci. Technol.* **2012,** *2,* 2134–2138. doi:10.1039/C2CY20260C
5. Bogdan, A. R.; Mason, B. P.; Sylvester, K. T.; McQuade, D. T. *Angew. Chem., Int. Ed.* **2007,** *46,* 1698–1701. doi:10.1002/anie.200603854
6. Costantini, F.; Bula, W. P.; Salvio, R.; Huskens, J.; Gardeniers, H. J. G. E.; Reinhoudt, D. N. *J. Am. Chem. Soc.* **2009,** *131,* 1650–1651. doi:10.1021/ja807616z
7. Karim, A.; Bravo, J.; Gorm, D.; Conant, T.; Datye, A. *Catal. Today* **2005,** *110,* 86–91. doi:10.1016/j.cattod.2005.09.010
8. Engberts, J. B. F. N.; Feringa, B. L.; Keller, E.; Otto, S. *Recl. Trav. Chim. Pays-Bas* **1996,** *115,* 457–464. doi:10.1002/recl.19961151103
9. Sereda, O.; Tabassum, S.; Wilhelm, R. *Top. Curr. Chem.* **2010,** *291,* 349–393. doi:10.1007/978-3-642-02815-1_17
10. Fringuelli, F.; Piermatti, O.; Pizzo, F.; Vaccaro, L. *Eur. J. Org. Chem.* **2001,** 439–455. doi:10.1002/1099-0690(200102)2001:3<439::AID-EJOC439>3.0.CO;2-B
11. Prakash, G. K. S.; Mathew, T.; Olah, G. A. *Acc. Chem. Res.* **2012,** *45,* 565–577. doi:10.1021/ar2002039
12. Jyothi, T. M.; Kaliya, M. L.; Landau, M. V. *Angew. Chem., Int. Ed.* **2001,** *40,* 2881–2884. doi:10.1002/1521-3773(20010803)40:15<2881::AID-ANIE2881>3.0.CO;2-P
13. Wiles, C.; Watts, P. *ChemSusChem* **2012,** *5,* 332–338. doi:10.1002/cssc.201100370
14. Fernandes, A. E.; Dirani, A.; d'Haese, C.; Deumer, G.; Guo, W.; Hensenne, P.; Nahra, F.; Laloyaux, X.; Haufroid, V.; Nysten, B.; Riant, O.; Jonas, A. M. *Chem.–Eur. J.* **2012,** *18,* 16226–16233. doi:10.1002/chem.201202531
15. Long, W.; Jones, C. W. *ACS Catal.* **2011,** *1,* 674–681. doi:10.1021/cs2001175
16. Costantini, F.; Benetti, E. M.; Tiggelaar, R. M.; Gardeniers, H. J. G. E.; Reinhoudt, D. N.; Huskens, J.; Vancso, G. J.; Verboom, W. *Chem.–Eur. J.* **2010,** *16,* 12406–12411. doi:10.1002/chem.201000948
17. Costantini, F.; Benetti, E. M.; Reinhoudt, D. N.; Huskens, J.; Vancso, G. J.; Verboom, W. *Lab Chip* **2010,** *10,* 3407–3412. doi:10.1039/C0LC00187B
18. Yan, P.; Batamack, P.; Prakash, G. K. S.; Olah, G. A. *Catal. Lett.* **2005,** *101,* 141–143. doi:10.1007/s10562-005-4880-8
19. Martín, A.; Morales, G.; Martínez, F.; van Grieken, R.; Cao, L.; Kruk, M. *J. Mater. Chem.* **2010,** *20,* 8026–8035. doi:10.1039/C0JM01589J
20. Husseman, M.; Malmström, E. E.; McNamara, M.; Mate, M.; Mecerreyes, D.; Benoit, D. G.; Hedrick, J. L.; Mansky, P.; Huang, E.; Russell, T. P.; Hawker, C. J. *Macromolecules* **1999,** *32,* 1424–1431. doi:10.1021/ma981290v
21. Li, C.; Yang, J.; Wang, P.; Liu, J.; Yang, Q. *Microporous Mesoporous Mater.* **2009,** *123,* 228–233. doi:10.1016/j.micromeso.2009.04.005
22. Dale, T. J.; Sather, A. C.; Rebek, J., Jr. *Tetrahedron Lett.* **2009,** *50,* 6173–6175. doi:10.1016/j.tetlet.2009.08.086
23. Desai, D. G.; Swami, S. S.; Mahale, G. D. *Synth. Commun.* **2000,** *30,* 1623–1625. doi:10.1080/00397910008087199

License and Terms

Beilstein Journal of Organic Chemistry

[3 + 2]-Cycloadditions of nitrile ylides after photoactivation of vinyl azides under flow conditions

Stephan Cludius-Brandt, Lukas Kupracz and Andreas Kirschning*

Full Research Paper

Open Access

Address:
Institute of Organic Chemistry, Leibniz University Hannover, Schneiderberg 1b, 30167 Hannover, Germany

Email:
Andreas Kirschning* - andreas.kirschning@oci.uni-hannover.de

* Corresponding author

Keywords:
azirines; cycloaddition; flow chemistry; flow reactors; inductive heating; nitrile ylides; photochemistry; vinyl azides

Beilstein J. Org. Chem. **2013,** *9,* 1745–1750.
doi:10.3762/bjoc.9.201

Received: 23 June 2013
Accepted: 22 July 2013
Published: 26 August 2013

This article is part of the Thematic Series "Chemistry in flow systems III".

Associate Editor: M. Rueping

Abstract

The photodenitrogenation of vinyl azides to 2*H*-azirines by using a photoflow reactor is reported and compared with thermal formation of 2*H*-azirines. Photochemically, the ring of the 2*H*-azirines was opened to yield the nitrile ylides, which underwent a [3 + 2]-cycloaddition with 1,3-dipolarophiles. When diisopropyl azodicarboxylate serves as the dipolarophile, 1,3,4-triazoles become directly accessible starting from the corresponding vinyl azide.

Introduction

Recently, photochemistry has seen a renaissance despite the fact that under batch conditions specialized reaction vessels are required, in which the light source is placed in the centre of the reaction mixture: Technically this setup is difficult to control for large scale industrial applications because the issue of transferring a substantial amount of heat has to be addressed. On the other hand, photochemistry allows to perform many transformations that are hardly possible under thermal conditions. This includes photocatalytic reactions that have seen an immense interest lately [1].

Nitrile ylides **3** are 1,3-dipoles that have served for the preparation of different five-membered *N*-heterocycles in 1,3-dipolar cycloaddition reactions. They are commonly formed through three routes which are a) the addition of electrophilic carbenes to nitriles, b) the dehydrochlorination of imidoyl chlorides, and c) the photochemical ring opening of strained 2*H*-azirines **2** [2-5]. The latter route can be initiated by the photoinduced activation of vinyl azides **1**, which gives rise to 2*H*-azirines **2** via vinyl nitrenes after the loss of molecular nitrogen and subsequent ring-opening under photochemical conditions to provide the nitrile ylides **3** (Scheme 1). For recent examples for the use of azirines in organic syntheses please refer to [6-15]. Recently, the Seeberger group has published a flow protocol on the photochemical degradation of aryl azides and the subsequent formation of 3*H*-azepinones [16].

With the emergence of continuous processes involving miniaturized flow reactors in organic-chemistry laboratories, photochemistry has found a wider interest in the chemical commu-

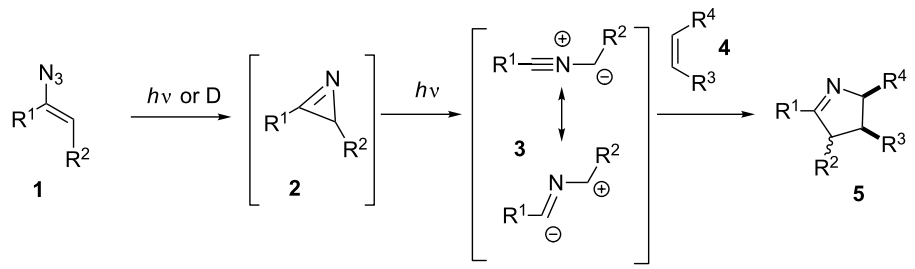

Scheme 1: Formation of azirines **2** from vinyl azides **1**, photoinduced ring-opening to the nitrile ylides **3,** and 1,3-dipolar cycloaddition to the pentacyclic *N*-heterocycles **5**.

nity [17,18]. Particularly large-scale photochemical syntheses can simply be achieved by numbering-up miniaturized flow reactors in a parallel set-up. Uniform irradiation can be guaranteed when the penetration depth of light is kept small (100–1000 μm). Furthermore, the production rate of a photochemical flow process can be controlled by varying the irradiation power, or by increasing or decreasing of the flow rate. Finally, miniaturized flow reactors have high heat-transfer coefficients so that the cooling of the photochemical process can efficiently be achieved.

These facts led us to initiate an investigation on the photochemical activation of vinyl azides and the trapping of the intermediate nitrile ylides **3** [19] by different dipolarophiles exploiting the advantages of photo flow-chemistry [20,21]. Here, we report on the first photochemical transformation of vinyl azides to pyrrole derivatives under continuous-flow conditions.

Only recently, we reported the two-step preparation of vinyl azides **1** in mircrostructured flow reactors starting from alkenes **6**, using the solid-phase bound iodine azide transfer-reagent **7** followed by HI elimination using immobilized DBU as fixed bed material (Scheme 2) [9,22,23]. All vinyl azides used in this report were prepared by azido-iodination of the corresponding alkenes followed by DBU-mediated HI elimination (for details see the Supporting Information File 1).

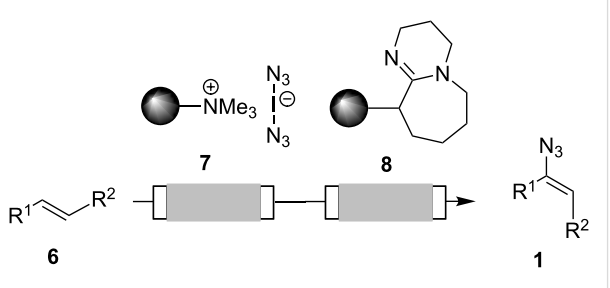

Scheme 2: Solid-phase assisted synthesis of vinyl azides **1** from alkenes **6** under flow conditions [9].

Results and Discussion

As the generation of azirines **2** can be conducted under thermal as well as under photochemical conditions, we first evaluated both processes with respect to their suitability under flow conditions (Scheme 3). The thermal reaction was studied in the presence of an external oscillating magnetic field of medium frequency (15–25 kHz). The best reactor set-up for inducing heat in a medium frequency field was found to be a steel capillary reactor (volume: 1.0 mL, inner diameter = 1.0 mm) with a steel core, which is encased by the inductor. An internal pressure of at least 250 psi allows transformations well above the boiling point of the solvent, and this was secured by placing a backpressure regulator behind the flow system. In contrast, the photochemical flow-reactor was composed of a Teflon (FEP) tubing (volume: 3.0 mL, inner diameter = 0.75 mm) and a Pyrex filter. These were placed onto the water-cooled quartz immersion well (type UV-RS-1, Heraeus) equipped with a medium-pressure mercury lamp (type TQ 150, λ = 190–600 nm). The reaction mixture was fed into the tubing by using a pump and collected in a flask after having passed through the reactor.

In essence 2*H*-azirines can be prepared continuously in good yields under thermal as well as under photochemical conditions in appropriate flow reactor devices (Table 1). Complete conversion was achieved at 190 °C after 1 min in dichloromethane. At higher temperatures as well as at reduced flow rates the amount of decomposition products increased. The photochemical transformation required longer reaction times, but the products were formed under thermally mild conditions in improved yields and with higher purity. Therefore, we decided to continue our studies with the photochemical flow-reactor and to extend these studies to the photoinduced nitrile ylide formation and the 1,3-dipolar cycloaddition. We initially chose to photolyze methyl 4-(1-azidovinyl)benzoate (**1a**) in the presence of acrylonitrile (**4a**) (Table 2). A solution of **1a** and **4a** in the respective solvent was passed through the photochemical flow-reactor with 5.5 mL volume and a pyrex filter.

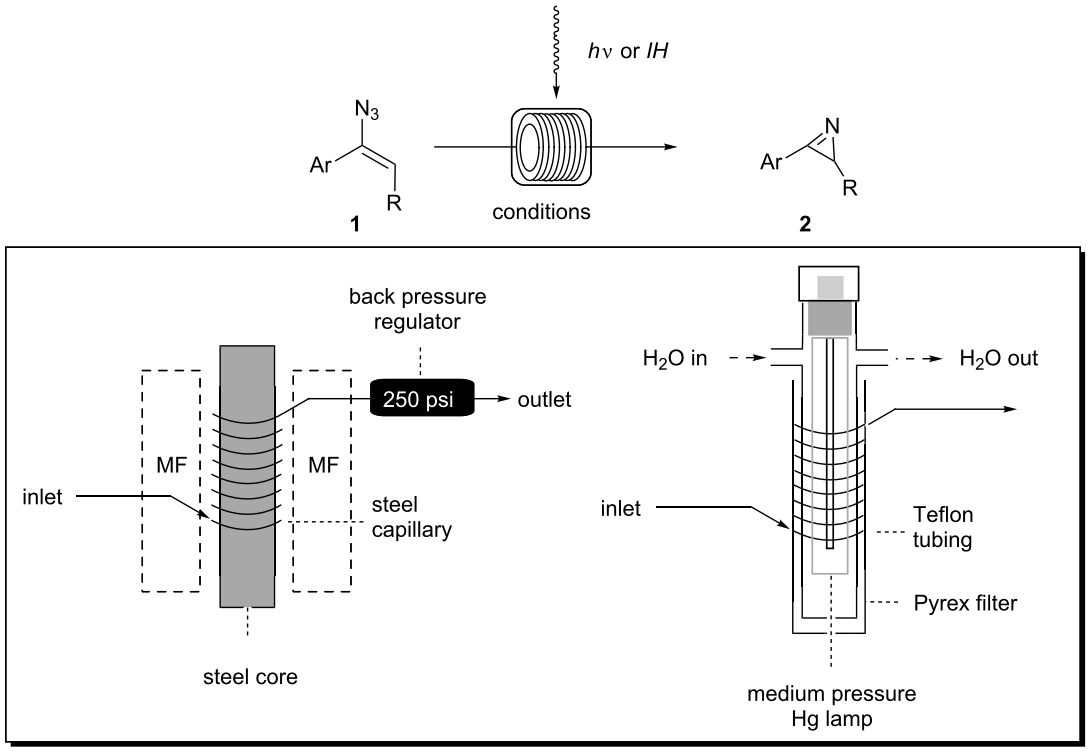

Scheme 3: Schematic presentation of the flow set-up for the synthesis of *2H*-azirines **2** under inductive heating (*IH*, left) and photochemical (*h*ν, right) conditions.

Table 1: Continuous synthesis of *2H*-azirines **2** under inductive heating and photochemical conditions. The experiments were conducted at a concentration of 0.05 M.

entry	product[a]	isolated yield (*h*ν) [%][b,c]	isolated yield (*IH*) [%][c,d]
1	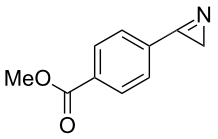 **2a**	97	82
2	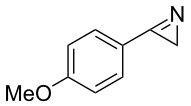 **2b**	90	79
3	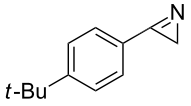 **2d**	92	72
4	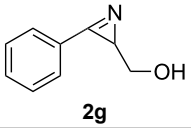 **2g**	95	42[e]

[a]Precursor vinyl azides and 2*H*-azirines are found in Scheme 4; [b]photo flow-conditions: toluene, 10 min (residence time), rt; [c]isolated yields are given; [d]inductive heating conditions: CH_2Cl_2, 1 min (residence time), 190 °C; [e]although the transformation was very rapid, we encountered substantial decomposition under thermal conditions.

Table 2: Optimization of the photolysis of vinyl azide **1a** and trapping of nitrile ylide with acrylonitrile **4a** under flow conditions.

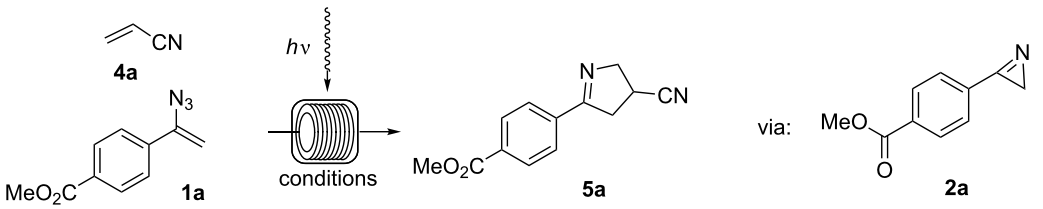

entry	concentration of **1a** [M]	ratio (**1a**:**4a**)	solvent	flow rate [mL/min]	isolated yield [%] of **5a**
1	0.025	1:10	toluene	0.05	-
2	0.025	1:10	benzene	0.05	-
3	0.025	1:10	CH_3CN	0.05	46
4	0.025	1:10	CH_3CN	0.1	53
5	0.012	1:10	CH_3CN	0.05	82
6	0.012	1:10	CH_3CN	0.1	74
7	0.012	1:10	CH_3CN	0.2	68
8	0.05	1:10	CH_3CN	0.05	96
9	0.05	1:5	CH_3CN	0.05	71
10	0.05	1:2	CH_3CN	0.05	65

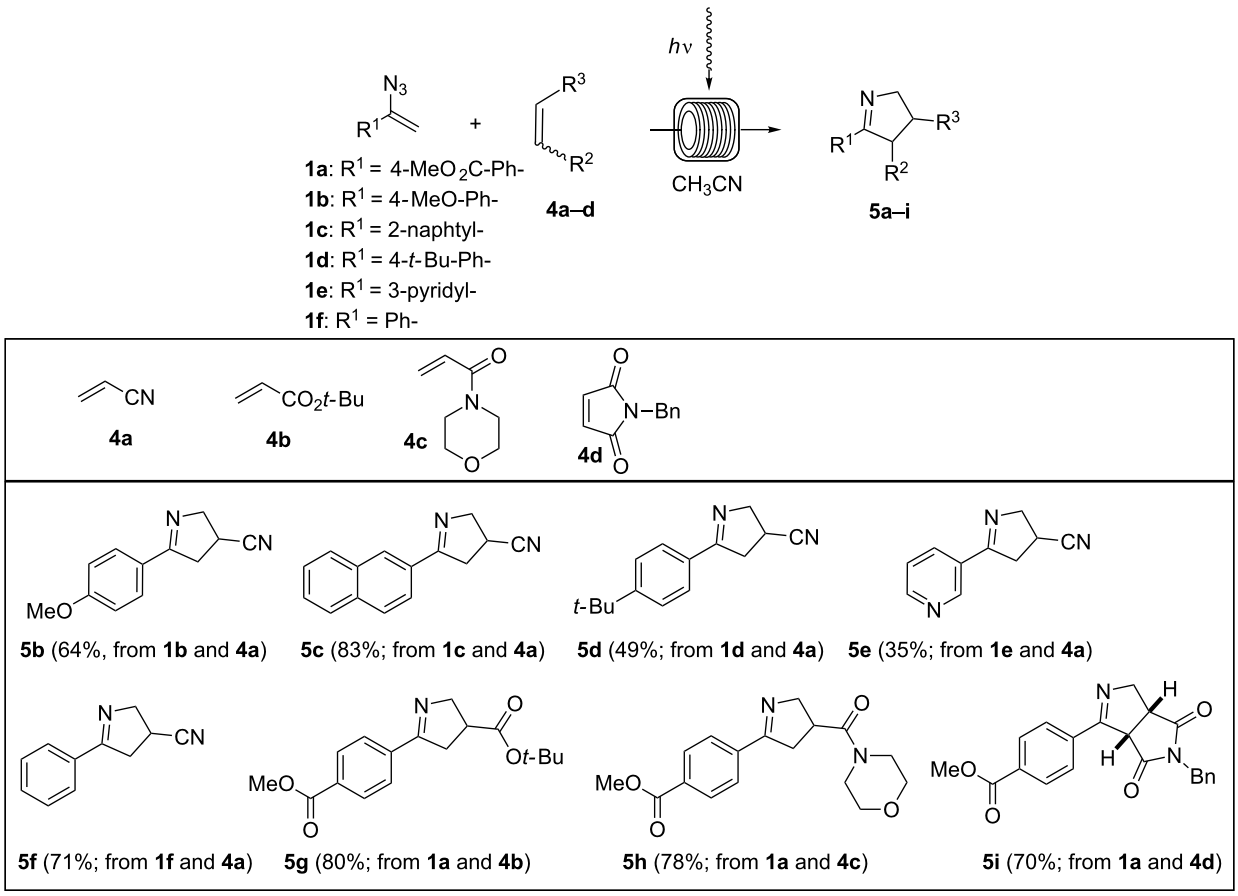

Scheme 4: Photoinduced cycloadditions of vinyl azides **1a**–**f** and electron-deficient alkenes **4a**–**d**. All experiments were conducted at room temperature in a photochemical flow-reactor (see above) using Teflon (FEP) tubing (volume: 5.5 mL, inner diameter = 0.75 mm) at a concentration of 0.05 M in CH_3CN; isolated yields are given.

Test reactions conducted either in benzene or in toluene resulted exclusively in the formation of the corresponding 2*H*-azirine **2a** in yields up to 95%, while no formation of the cycloaddition product was encountered (Table 2; entries 1 and 2). **2a** could easily be identified by the signal at 1.88 ppm in the ^{1}H NMR spectrum, which is characteristic for the methylene group of the newly formed 3-membered ring. This signal corresponds to the carbon signal at 20.2 ppm in the ^{13}C NMR spectrum. In contrast, acetonitrile turned out to be the solvent of choice and methyl 4-(4-cyano-4,5-dihydro-3*H*-pyrrol-2-yl)benzoate (**5a**) was isolated in 46% yield (Table 2, entry 3). By optimizing the reaction conditions with respect to concentration, flow rate, and ratio of starting materials (Table 2, entries 4–10), we found that a concentration of 0.05 mol/L for azide **1a** and a flow rate of 0.05 mL/min in the presence of a tenfold access of **4a** provided the cycloaddition product **5a** in 96% yield as a single regioisomer (Table 2, entry 8). Remarkably, after removal of the solvent under reduced pressure it was not necessary to further purify the product.

Next the scope of the photo-induced 1,3-dipolar cycloaddition was examined. With the optimized flow-protocol in hand we were able to synthesize a variety of dihydropyrroles (**5a**–**5i**) (Scheme 4). The electronic properties of the aromatic ring, which depend on the substituents have no prinicipal influence on the outcome of this cascade reaction. Only the pyridyl substituent in vinyl azide **1e** provided dihydropyrrole **5e** in unsatisfactory yield. The relative stereochemistry of **5i** was determined by comparison with literature data [24].

To our delight, this flow protocol also allowed us to prepare 2,3-dihydro-1*H*-1,2,4-triazole **5j** in good yield using diisopropyl azodicarboxylate (DIAD, **4e**) as the dipolarophile (Scheme 5).

Additionally, we found that even electron-deficient alkynes such as **4f** can serve as dipolarophiles in these reactions (Scheme 6). However, the resulting pyrrole **5k** could only be isolated in 26% yield.

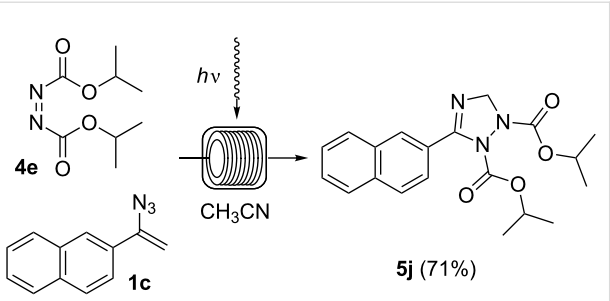

Scheme 5: Photoinduced cycloaddtion of vinyl azide **1c** and diisopropyl azodicarboxylate (**4e**). The experiment was conducted at room temperature in a photochemical flow-reactor (see above) using Teflon (FEP) tubing (volume: 5.5 mL, inner diameter = 0.75 mm) at a concentration of 0.05 M in CH_3CN.

Alternatively, the in-situ generated nitrile ylide can be trapped intramolecularly by a nucleophile such as a hydroxy group [25]. This is demonstrated by the photochemical degradation of vinyl azide **1g** which yielded 2,5-dihydrooxazole **9** in 76% yield (c = 0.01 M, flow rate = 0.02 mL/min) under flow conditions (Scheme 7). In this case, benzene turned out to be the solvent of choice.

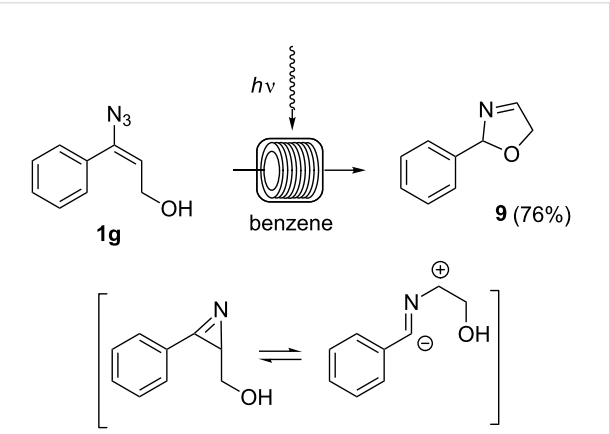

Scheme 7: Formation of 2,5-dihydrooxazole **9** starting from vinyl azide **1g** under flow conditions (c = 0.01 M, flow rate = 0.02 mL/min).

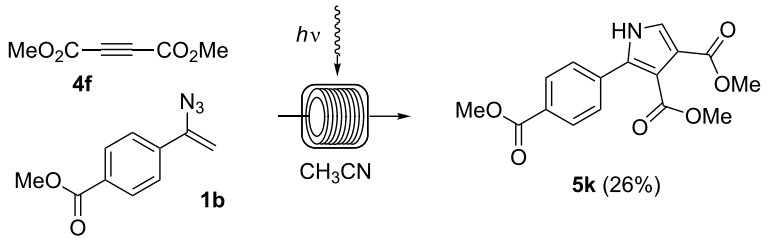

Scheme 6: Photoinduced cycloaddtion of vinyl azide **1b** and alkyne **4f**. The experiment was conducted at room temperature in a photochemical flow-reactor (see above) using Teflon (FEP) tubing (volume: 5.5 mL, inner diameter = 0.75 mm) at a concentration of 0.05 M in CH_3CN.

Conclusion

In summary, we developed a protocol for the one-step photochemical formation of dihydropyrroles under flow conditions starting from aromatic vinyl azides and activated alkenes. This transformation was achieved with a photochemical flow reactor and most likely proceeds via the respective 2*H*-azirines by photoinduced in-situ formation and subsequent heterolytic ring opening. The resulting 1,3-dipole is trapped directly with electron-deficient alkenes to form the [2 + 3] cycloaddition products. With this method, we were able to prepare a variety of dihydropyrroles. The electronic properties of the aromatic ring were of little importance for the principal outcome of the reaction. Notable, azodicarboxylates and electron deficient alkynes were employed for the first time which provided a 1,2,4-triazole and a pyrrole, respectively. Future work should cover a further generalization of this flow protocol along with telescoping it with vinyl azide formation.

Supporting Information

Supporting Information File 1

Descriptions on the synthesis and analyses of vinyl azides and as well as on cycloaddition products.
[http://www.beilstein-journals.org/bjoc/bjoc/content/supplementary/1860-5397-9-201-S1.pdf]

Acknowledgements

Financial support from a research fellowship from the German Research Foundation (DFG) for S. Cludius-Brandt is gratefully acknowledged.

References

1. Griesbeck, A. G.; Steinwäscher, J.; Reckenthäler, M.; Uhlig, J. *Res. Chem. Intermed.* **2013,** *39,* 33–42. doi:10.1007/s11164-012-0629-3
2. Padwa, A. *Adv. Heterocycl. Chem.* **2010,** *99,* 1–31. doi:10.1016/S0065-2725(10)09901-0
3. Palacios, F.; de Retana, A. M. O.; de Marigorta, E. M.; de los Santos, J. M. *Org. Prep. Proced. Int.* **2002,** *34,* 219–269. doi:10.1080/00304940209356770
4. Palacios, F.; de Retana, A. M. O.; de Marigorta, E. M.; de los Santos, J. M. *Eur. J. Org. Chem.* **2001,** 2401–2414. doi:10.1002/1099-0690(200107)2001:13<2401::AID-EJOC2401>3.0.CO;2-U
5. Heimgartner, H. *Angew. Chem., Int. Ed.* **1991,** *30,* 238–264. doi:10.1002/anie.199102381
6. Loy, N. S. Y.; Singh, A.; Xu, X.; Park, C.-M. *Angew. Chem., Int. Ed.* **2013,** *52,* 2212–2216. doi:10.1002/anie.201209301
7. Khlebnikov, A. F.; Novikov, M. S.; Pakalnis, V. V.; Yufit, D. S. *J. Org. Chem.* **2011,** *76,* 9344–9352. doi:10.1021/jo201563b
8. Palacios, F.; de Retana, A. M. O.; del Burgo, A. V. *J. Org. Chem.* **2011,** *76,* 9472–9477. doi:10.1021/jo201932m
9. Kupracz, L.; Hartwig, J.; Wegner, J.; Ceylan, S.; Kirschning, A. *Beilstein J. Org. Chem.* **2011,** *7,* 1441–1448. doi:10.3762/bjoc.7.168
10. Candito, D. A.; Lautens, M. *Org. Lett.* **2010,** *12,* 3312–3315. doi:10.1021/ol100975b
11. Novikov, M. S.; Amer, A. A.; Khlebnikov, A. F. *Tetrahedron Lett.* **2006,** *47,* 639–642. doi:10.1016/j.tetlet.2005.11.131
12. Alves, M. J.; Fortes, A. G.; Costa, F. T. *Tetrahedron* **2006,** *62,* 3095–3102. doi:10.1016/j.tet.2006.01.035
13. Palacios, F.; de Retana, A. M. O.; Gil, J. I.; Alonso, J. M. *Tetrahedron* **2004,** *60,* 8937–8947. doi:10.1016/j.tet.2004.07.013
14. Timén, A. S.; Somfai, P. *J. Org. Chem.* **2003,** *68,* 9958–9963. doi:10.1021/jo0352326
15. Pinho e Melo, T. M. V. D.; Cardoso, A. L.; Gomes, C. S. B.; Rocha Gonsalves, A. M. d'A. *Tetrahedron Lett.* **2003,** *44,* 6313–6315. doi:10.1016/S0040-4039(03)01534-X
16. Bou-Hamdan, F. R.; Lévesque, F.; O'Brien, A. G.; Seeberger, P. H. *Beilstein J. Org. Chem.* **2011,** *7,* 1124–1129. doi:10.3762/bjoc.7.129
17. Oelgemöller, M.; Shvydkiv, O. *Molecules* **2011,** *16,* 7522–7550. doi:10.3390/molecules16097522
18. Matsushita, Y.; Ichimura, T.; Ohba, N.; Kumada, S.; Sakeda, K.; Suzuki, T.; Tanibata, H.; Murata, T. *Pure Appl. Chem.* **2007,** *79,* 1959–1968. doi:10.1351/pac200779111959
19. Escolano, C.; Duque, M. D.; Vázquez, S. *Curr. Org. Chem.* **2007,** *11,* 741–772. doi:10.2174/138527207780831710
20. Knowles, J. P.; Elliott, L. D.; Booker-Milburn, K. I. *Beilstein J. Org. Chem.* **2012,** *8,* 2025–2052. doi:10.3762/bjoc.8.229
21. Hook, B. D. A.; Dohle, W.; Hirst, P. R.; Pickworth, M.; Berry, M. B.; Booker-Milburn, K. I. *J. Org. Chem.* **2005,** *70,* 7558–7564. doi:10.1021/jo050705p
22. Kirschning, A.; Hashem, Md. A.; Monenschein, H.; Rose, L.; Schöning, K.-U. *J. Org. Chem.* **1999,** *64,* 6522–6526. doi:10.1021/jo990478p
23. Kirschning, A.; Monenschein, H.; Schmeck, C. *Angew. Chem., Int. Ed.* **1999,** *38,* 2594–2596. doi:10.1002/(SICI)1521-3773(19990903)38:17<2594::AID-ANIE2594>3.0.CO;2-U
24. Tsuge, O.; Ueno, K.; Kanemasa, S.; Yorozu, K. *Bull. Chem. Soc. Jpn.* **1986,** *59,* 1809–1824. doi:10.1246/bcsj.59.1809
25. Padwa, A.; Rasmussen, J. K.; Tremper, A. *J. Am. Chem. Soc.* **1976,** *98,* 2605–2614. doi:10.1021/ja00425a033

License and Terms

Beilstein Journal of Organic Chemistry

The application of a monolithic triphenylphosphine reagent for conducting Ramirez *gem*-dibromoolefination reactions in flow

Kimberley A. Roper[1], Malcolm B. Berry[2] and Steven V. Ley[*1]

Full Research Paper

Open Access

Address:
[1]Innovative Technology Centre, Department of Chemistry, University of Cambridge, Lensfield Road, Cambridge, Cambridgeshire, CB2 1EW, U.K. and [2]GlaxoSmithKline, Gunnels Wood Road, Stevenage, Hertfordshire, SG1 2NY, U.K.

Email:
Steven V. Ley[*] - svl1000@cam.ac.uk

* Corresponding author

Keywords:
bromination; flow chemistry; Ramirez *gem*-dibromoolefination reaction; solid-supported reagent; triphenylphosphine monolith

Beilstein J. Org. Chem. **2013,** *9,* 1781–1790.
doi:10.3762/bjoc.9.207

Received: 30 June 2013
Accepted: 15 August 2013
Published: 02 September 2013

This article is part of the Thematic Series "Chemistry in flow systems III".

Guest Editor: A. Kirschning

Abstract

The application of a monolithic form of triphenylphosphine to the Ramirez *gem*-dibromoolefination reaction using flow chemistry techniques is reported. A variety of *gem*-dibromides were synthesised in high purity and excellent yield following only removal of solvent and no further off-line purification. It is also possible to perform the Appel reaction using the same monolith and the relationship between the mechanisms of the two reactions is discussed.

Introduction

The advantages of applying flow chemistry processing to organic synthesis have been extensively demonstrated in the literature, increasing the safety, efficiency and reproducibility of many organic chemistry reactions, causing this technology to be accepted as an important new tool to aid the modern research chemist [1-7]. Combining this enabling technology with solid-supported reagents and scavengers offers synergistic benefits over using the two technologies independently. Utilising polymer-supported reagents and scavengers to purify the flow stream permits telescoping of reaction sequences or facilitates direct isolation of pure compounds from flow reactors, removing the need for labour-intensive manual operations [8-13]. Reagents are typically supported on low-crosslinked gel-type or macroporous beads; however, these are characterised by poor mass transfer properties as well as presenting practical problems when used in packed beds in flow reactions due to changes in structure and morphology when subjected to solvents of varying polarity [14,15]. To avoid some of the problems associated with using resin beads, monolithic supports have been developed for use in continuous-flow chemistry systems. Monoliths are a single continuous piece of uniformly porous material, prepared by precipitation polymerisation of a functionalised monomer [16-20]. The monolith internal structure varies compared to bead-like supports, consisting of a

combination of large macropores for flow through passage, in combination with a network of smaller mesopores to allow diffusion towards the active sites. This combined geometry has been shown to result in superior chemical efficiency over traditional supports by providing a shorter diffusion pathway to active sites via convective flow-through the macropores, as well as providing lower void volumes [16]. Practically, their rigid structure is secure over a wide range of solvents and under reasonable pressures compared to beads due to a high degree of cross linking, making them advantageous when applied to flow processes [21,22].

Originally monoliths were developed to facilitate the isocratic separation of peptides [17,23]; however, our group and others have shown interest in using monolithic supports to facilitate key chemical transformations [24-35]. The above advantages of using monolithic supports over traditional beads in flow chemistry protocols can greatly facilitate the synthesis of fine chemicals using these enabling technologies [36]. We have recently reported on the development of a monolithic triphenylphosphine reagent and its application to the Staudinger aza-Wittig and Appel reactions in flow [37-40]. The immobilisation of triphenylphosphine in this manner allowed the facile production of a collection of pure compounds using flow chemistry technologies with no need for further offline purification. Following the successful application of this monolith to the Appel reaction (the transformation of alkyl alcohols to the corresponding bromides), we wished to investigate the application of this monolith to the closely related Ramirez *gem*-dibromoolefination reaction; the formation of *gem*-dibromoolefins from aldehydes or ketones.

In 1962 Ramirez, Desai and McKelvie reported the formation of dibromophosphorane **1** and (dibromomethylene)triphenylphosphorane (**2**) from the room temperature reaction of carbon tetrabromide with two equivalents of triphenylphosphine (Scheme 1) [41]. Addition of benzaldehyde then gave the desired *gem*-dibromoolefin, (2,2-dibromovinyl)benzene (**3**) in 84% yield. Triphenylphosphine oxide (**4**) was also isolated from the reaction as a byproduct. These *gem*-dibromoolefin products are particularly important intermediates in the one carbon homologation of an aldehyde into the corresponding terminal alkyne, known as the Corey–Fuchs reaction [42], and more recently stereospecific hydrogenolysis, Stille and Suzuki reactions have been used to further elaborate these useful products [43-45].

The triphenylphosphine oxide byproduct can often be difficult to remove from the reaction mixture, requiring extensive, time-consuming purification procedures to isolate the desired product in high purity. For Ramirez *gem*-dibromoolefination reactions, successful strategies have been developed to facilitate this separation through derivatising the triphenylphosphine (or its oxide) to achieve purification via filtration [46,47], as well as by immobilising the triphenylphosphine on a solid-support [48]. A polymer-supported equivalent of triphenylphosphine has also been successfully utilised by our group and by others in batch Wittig reactions [49,50], Mitsunobu and Staudinger aza-Wittig reactions [51,52], as well as many examples concerning the Appel reaction [51-57].

Following our success using a monolithic form of triphenylphosphine to facilitate the Appel reaction, we wanted to explore the use of this monolith for performing the Ramirez *gem*-dibromoolefination reaction in flow. The monolithic form of triphenylphosphine should have improved flow characteristics compared to bead-based equivalents circumventing the problems associated with using these solid-supported reagents in combination with flow techniques. Key intermediates for the Ramirez dibromoolefination reaction, **1** and **2** depicted in Scheme 1, are also known to be potential intermediates in the Appel reaction [58,59] and consequently we also wished to investigate the interplay between the two reaction mechanisms.

Results and Discussion

Formation of the triphenylphosphine monolith

The triphenylphosphine monoliths for the Ramirez reactions were formed using precipitation polymerisation of the phosphine monomer **5** (Scheme 2). A polymerisation mixture of the triphenylphosphine monomer **5**, cross-linking components divinylbenzene (**6**) and styrene (**7**) along with the porogen, 1-dodecanol (**8**), was heated to 50 °C until a homogeneous mixture was achieved. The initiator, dibenzoyl peroxide (**9**) was then added and the temperature maintained at 50 °C until this had completely dissolved. The mixture was then transferred to a glass column, the ends sealed with custom-made PTFE end

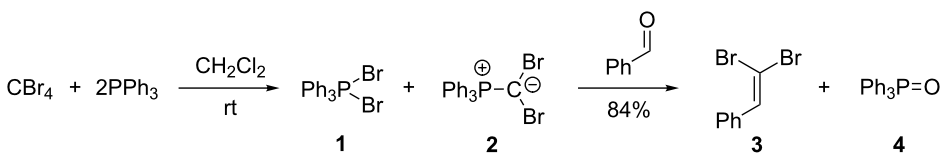

Scheme 1: Formation of *gem*-dibromoolefin **3** from the reaction of carbon tetrabromide and triphenylphosphine as reported by Ramirez et al. [41].

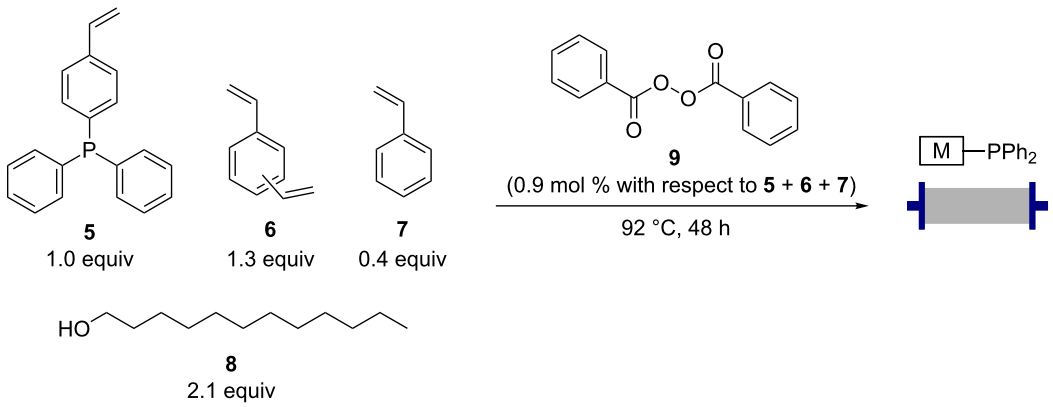

Scheme 2: Formation of the triphenylphosphine monoliths.

pieces and heated to 92 °C for 48 hours using a Vapourtec R4 heating unit. This protocol can be clearly viewed in a video previously released by our group [40], however the Ramirez monoliths employ a higher ratio of styrene to divinylbenzene. This results in a lower proportion of crosslinking within the monolith, allowing greater flexibility in the backbone of the polymer whilst still maintaining desirable monolithic characteristics during flow reactions. This greater flexibility has previously been shown to assist with the formation of active species **1** and **2** in solid-supported triphenylphosphine beads, by allowing neighbouring group interactions between the triphenylphosphine residues.

The resultant white polymer (see Figure 1, a) was cooled to room temperature and the end plugs exchanged with standard flow-through end pieces. The porogen and any unreacted starting materials were then eluted from the monolith using a stream of dichloromethane at elevated temperature (60 °C). This polymerisation protocol consistently gave a low pressure drop across the monoliths for use in flow reactions. The monoliths were calculated to have a phosphorus loading of 1.85 mmol of phosphorus per gram, resulting in approximately 4.63 mmol of phosphorus per monolith.

Loading the monolith to give the active Ramirez brominating species

Loading the monolith with carbon tetrabromide to give the active species for the Ramirez *gem*-dibroomolefination reactions was found to proceed in a facile manner using a single pass protocol with the monolith being cooled to 0 °C (Scheme 3). Cooling the monolith by submerging it in an ice-water bath was found to be necessary to prevent the formation

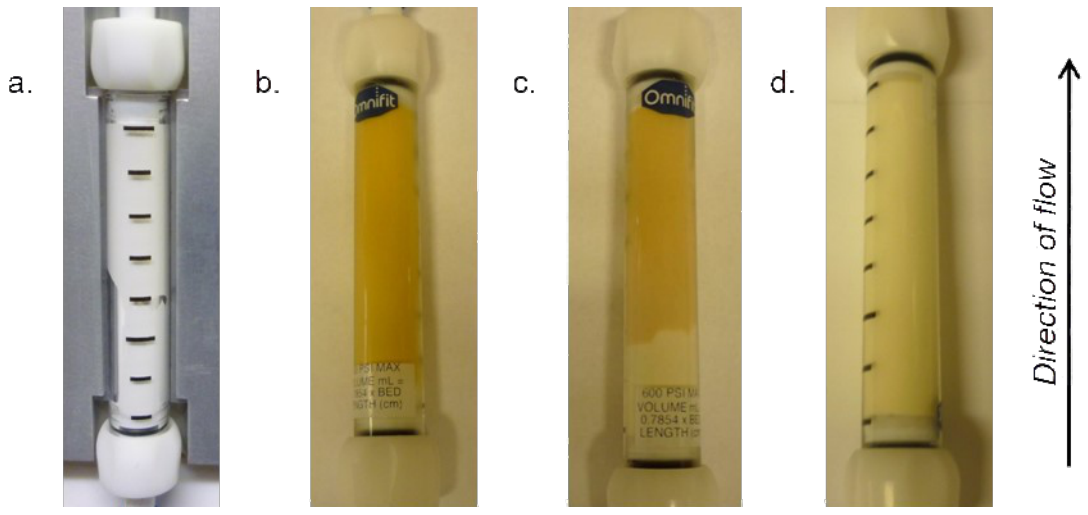

Figure 1: a. An unfunctionalised triphenylphosphine monolith; b. Monolith after functionalisation with carbon tetrabromide at 0 °C; c. Monolith after complete consumption of the active Ramirez *gem*-dibromoolefination species; d. Monolith after complete consumption of the active Ramirez *gem*-dibromoolefination species and the Appel brominating species.

of an inseparable side product, observed if reactions were performed at room temperature.

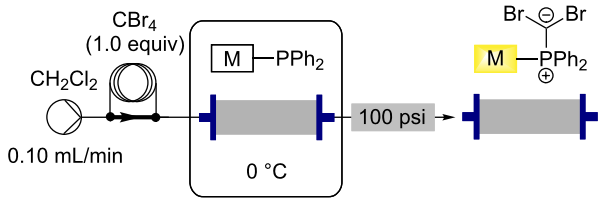

Scheme 3: Functionalising the triphenylphosphine monolith to give the active Ramirez monolith using carbon tetrabromide.

Interestingly, an external source of triphenylphosphine was not required to form the solid-supported equivalents of active species **1** and **2**, indicating that the polymer chains within the monolith have sufficient conformational freedom to allow neighbouring group interactions between triphenylphosphine sites. Any attempts to use a solution of triphenylphosphine to increase the active loading of the monolith was found to result in the formation of insoluble triphenylphosphine salts which crystallised and blocked the flow tubing downstream of the monolith.

The formation of the active species was accompanied by a colour change, resulting in a bright yellow polymer (Figure 1, b). Each monolith was shown to have an active loading towards the Ramirez transformation of approximately 0.8 mmol. Although this is a relatively low active loading, this is not unexpected as two equivalents of triphenylphosphine are required for the formation of one equivalent of the active Ramirez brominating species.

Ramirez *gem*-dibromoolefination reactions in flow

With the functionalised monolith in hand, it was then used to perform the Ramirez *gem*-dibromoolefination reaction in flow to transform aldehydes into their corresponding *gem*-dibromoolefins. A 0.1 M solution of the aldehyde in dichloromethane was prepared and introduced into the flow system via the use of a sample loop. This solution was passed through the loaded monolith at a rate of 0.5 mL/min while the monolith was maintained at 0 °C using a cooling bath (Scheme 4). The output was collected for 1 h 15 min and the solvent removed in vacuo to give complete conversion to the pure *gem*-dibromoolefin product without any further manipulation.

This procedure was applied to a wide variety of aldehydes, giving the *gem*-dibromoolefin products in high yields and purity following only removal of the solvent by evaporation (Table 1).

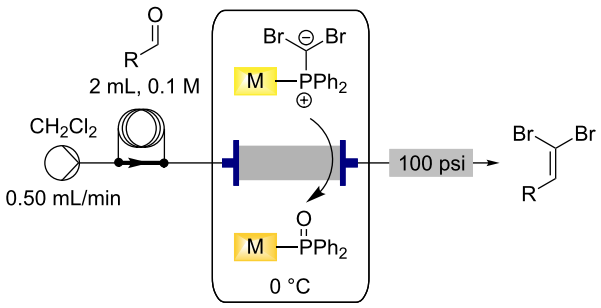

Scheme 4: Flow synthesis of *gem*-dibromoolefins using the functionalised triphenylphosphine monolith.

Benzylic aldehydes containing electron withdrawing and donating groups on the phenyl ring (Table 1, entries 1–4) were transformed in high yield, as well as alkyl aldehydes (Table 1, entries 5 and 6). Unsurprisingly, aldehydes containing a phenol moiety were found to give little or no mass return as the phenolic hydroxy group reacted with the triphenylphosphine sites within the monolith, leaving the product bound to the polymer. Interestingly the batch bromination of 3-phenylpropiolaldehyde (Table 1, entry 7) requires the addition of 2.5 equivalents of 2,6-lutidine [60], however pleasingly, this was not required when the substrate was brominated using the flow procedure. It was also possible to use the monolith on a series of heterocyclic substrates with high yields (Table 1, entries 8–10). However, nicotinaldehyde (Table 1, entry 11) was found to give a reduced yield and unusually contamination of subsequent products formed using the same monolith was observed. X-ray crystallography and mass spectrometry confirmed that the product isolated was the hydrobromide salt of the desired *gem*-dibromoolefin, presumably formed from an additional reaction with the monolith. The salt formed will coordinate to other ionic sites within the monolith, reducing the isolated yield and resulting in contamination of further products as it is slowly released from the column.

A colour change was associated with the reaction, with the monolith changing from a bright yellow to dull dark yellow colour (Figure 1, b and c). A single monolith could be used for multiple transformations with no cross contamination between substrates run in sequential reactions through a single monolith (with the exception of the nicotinaldehyde substrate explained above).

An important test of this methodology was the application to α-chiral aldehydes, to ensure that racemisation of the sensitive chiral centre is avoided in chiral structures (Table 2). A butane-2,3-diacetal derived aldehyde (Table 2, entry 1) and a diastereo-

Table 1: *Gem*-dibromides prepared from the corresponding aldehydes using the triphenylphosphine monolith in flow.

Entry	Starting material	Product	Isolated yield (%)[a]
1	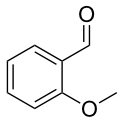		80
2	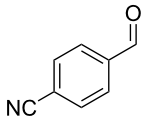	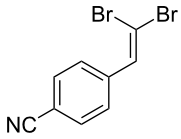	95
3	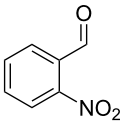		93
4	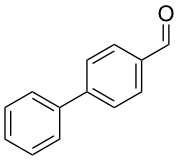	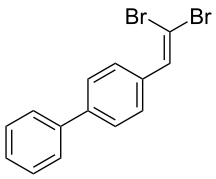	98
5	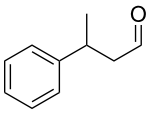	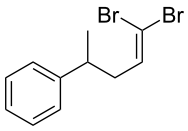	79
6		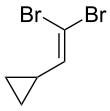	78[b]
7	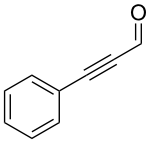	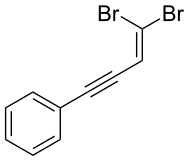	83
8	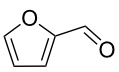	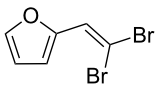	97
9	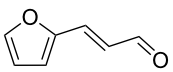	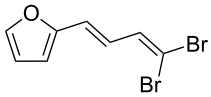	91
10	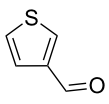	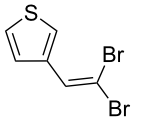	87
11	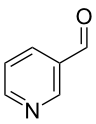	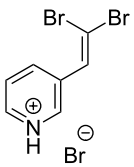	41[c]

[a]Reactions performed on a 0.2 mmol scale; [b]product volatile, [c]output collected for 2 hours rather than 1 h 15 min.

Table 2: α-Chiral aldehydes and ketones containing electron-withdrawing groups converted to the corresponding *gem*-dibromides using the triphenylphosphine monolith in flow.

Entry	Starting material	Product	Isolated yield (%)[a]
1	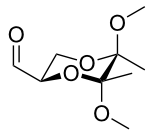	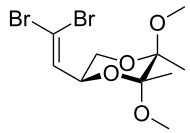	95
2	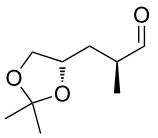	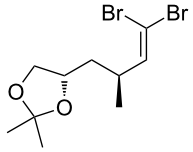	84
3	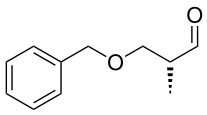	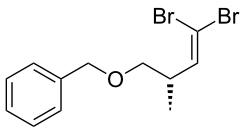	91
4	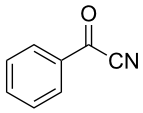	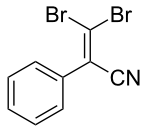	98
5	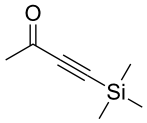	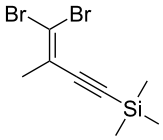	84[b]

[a]Reactions performed on a 0.2 mmol scale; [b]reaction run at 0.10 mL/min with a previously unused monolith.

meric aldehyde containing an acetonide (Table 2, entry 2) were successfully brominated using the flow protocol, being isolated in high yield with retention of stereochemistry as determined by ^{1}H NMR. The method was then applied to an enantiopure aldehyde (Table 2, entry 3) which could be transformed to the desired product in high yield [61].

There is also precedent for performing Ramirez *gem*-dibromoolefin reactions on carbonyl groups other than aldehydes, such as certain ketones activated using electron withdrawing groups [47]. A selection of these ketones were therefore subjected to the flow Ramirez reaction conditions (Table 2). Unsurprisingly, unactivated ketones such as cyclohexanone and benzophenone gave no conversion to the desired dibromide using the standard conditions. However, with some optimisation, an acyl cyanide (Table 2, entry 4) and a silyl protected ynone (Table 2, entry 5) could be converted to the desired *gem*-dibromoolefins respectively in high yields. Interestingly, it was found that full conversion could only be achieved for the silyl protected ynone using a low flow rate and a previously unused monolith, indicating some reduction in reactivity with each use of the monolith.

Utilising the loaded monolith for the Appel reaction in flow

The two active species formed during the Ramirez *gem*-dibromoolefination reaction (**1** and **2** in Scheme 1) are also known to be potential intermediates in the Appel reaction and we have previously shown that these monoliths can facilitate this formation using similar conditions [39]. We wished to investigate the relationship between the two reactions and hoped to establish conditions to perform both reactions using a single protocol. Using a similar configuration to the Ramirez reactions in flow, a selection of alcohols were directed through the monolith loaded with carbon tetrabromide at 0 °C (Scheme 5). Gratifyingly it was found that the monoliths prepared for the Ramirez *gem*-dibromoolefination reactions could be used directly for the Appel transformation, giving the bromide products in high yield and high purity following removal of the dichloromethane solvent (Table 3). Citronellol (Table 3, entry 1) and an indole derived alcohol (Table 3, entry 2), could be transformed in a facile manner using a single pass of the alcohol through the monolith at 0 °C, however the allyl alcohol (Table 3, entry 3) required recycling through the monolith to effect complete

Table 3: Alkyl bromides prepared from the corresponding alcohols using the triphenylphosphine monolith for the Appel reaction in flow.

Entry	Starting material	Product	Conversion after one pass (%)[a]	Time required for full conversion[b]	Isolated yield (%)[c]
1	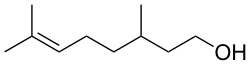	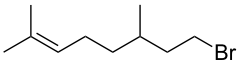	100	–	82
2	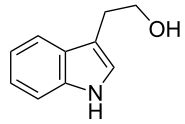	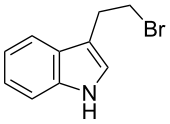	100	–	95
3	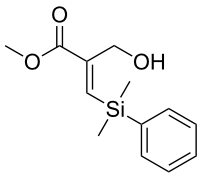	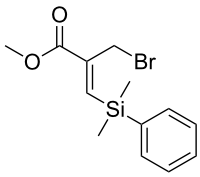	13	14 h 30 min	90

[a]One pass through the monolith at 0.5 mL/min, percentage conversion determined by ^{1}H NMR analysis; [b]substrate recirculated through the monolith at 0.5 mL/min until full consumption of starting material indicated by TLC; [c]reactions performed on a 0.2 mmol scale.

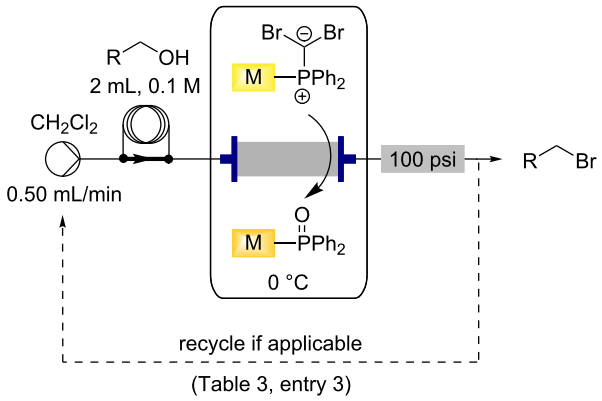

Scheme 5: Flow synthesis of bromides from the corresponding alcohols using the functionalised triphenylphosphine monolith in the Appel reaction at 0 °C.

conversion. In batch, this reaction required low temperature conditions (−78 °C) and the presence of base to give an isolated yield of 78% [62], however this could be improved to 90% by performing this reaction in flow at 0 °C. Loading the monolith using the protocol described above was found to give an approximate active loading of 0.6 mmol for the Appel reaction.

Utilising one monolith for both reactions potentially broadens the synthetic utility of the supported reagent and so performing both reactions sequentially using a single monolith was investigated. It was anticipated that these studies into the interplay between the reactions might also assist to elucidate the mechanism through which the Appel reaction proceeds on solid-support. It is known that the Appel reaction can proceed either through intermediates **1** and **2** which are common to both the Ramirez and Appel reactions, or via the alternative pathway (Scheme 6) which only requires one equivalent of triphenylphosphine per molecule of carbon tetrabromide to give intermediate **13** (Scheme 6) [59]. It has been previously noted that intermediate **2**, while not an active brominating agent in the Appel reaction, is known to assist in the formation of **10** by deprotonating the alcohol to form **11** [57]. However, it is thought that both possible pathways for the Appel reaction are utilised when using solid-supported triphenylphosphine due to the evidence for neighbouring-group interactions (the formation of **1** and **2**), along with site isolation effects ensuring the formation of **13**.

The reactions reported below were therefore performed sequentially using a single monolith. Pleasingly, it was found that after exhausting the monolith of the *gem*-dibromoolefination active species through multiple Ramirez reactions, the monolith could then be used to successfully perform the Appel reaction in flow. Approximately 0.55 mmol of alcohol could be transformed into the corresponding alkyl bromide following approximately 0.80 mmol of successful *gem*-dibromoolefination reactions. When the Appel reaction was performed after the Ramirez reaction, the monolith once again changed colour from dull dark yellow to off-white (depicted in Figure 1, c and d). However, when the loaded monolith was first used for the Appel reaction, there was no conversion observed for a subsequent Ramirez *gem*-dibromoolefination, with only the starting aldehyde being recovered from the output.

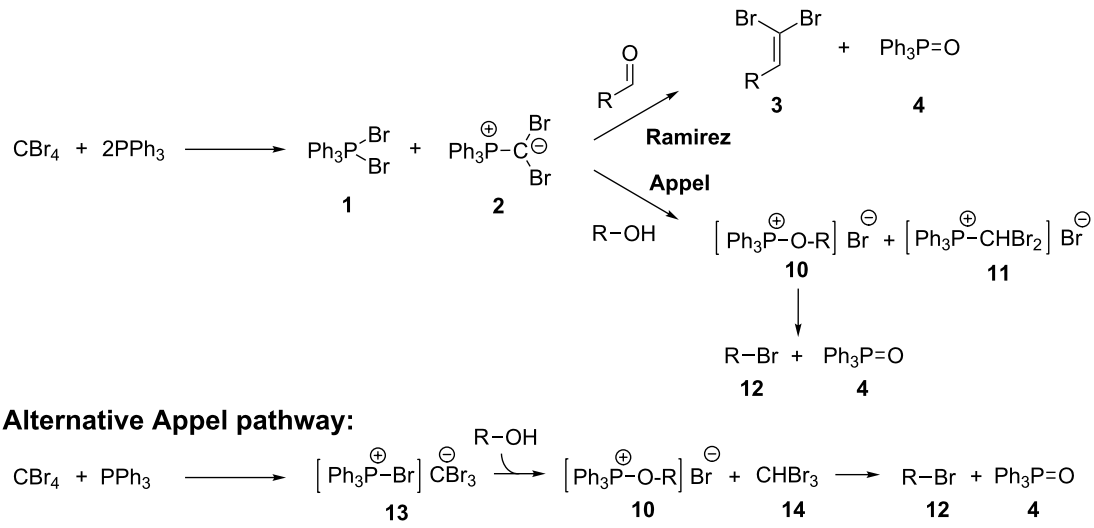

Scheme 6: Mechanisms for the Ramirez and Appel reactions [41,59].

These results indicate that the Appel reaction consumes all of the active Ramirez species **2** (Scheme 6), preventing the progress of the Ramirez dibromoolefination. However, if this species is consumed through multiple Ramirez *gem*-dibromoolefination reactions then an alternative brominating agent is utilised to perform the Appel reaction, or alternatively intermediate **2** is not required for the Appel mechanism using intermediate **1**. This is supported by previous observations in the literature that indicate that the predominant pathway for the Appel reaction on solid-support is through intermediates **1** and **2** although overall both pathways are utilised [59]. The possibility of performing the Appel reaction following the use of the same monolith for the Ramirez *gem*-dibromoolefination reaction gives wider synthetic applications for this flow methodology.

Conclusion

In summary, the monolithic form of triphenylphosphine recently described by our group [37-40] has been successfully applied to the Ramirez *gem*-dibromoolefination reaction in flow. The monolith was loaded with carbon tetrabromide at 0 °C using a single pass protocol to give the active brominating agent. This monolith was then utilised in the Ramirez reaction in flow, transforming a variety of different aldehydes to the corresponding *gem*-dibromoolefins in high yields and excellent purity following only removal of solvent. α-Chiral aldehydes were also successfully transformed, without racemisation of the stereocentre and two ketones bearing electron-withdrawing groups were converted into the desired dibromoolefins in high yield. It was further demonstrated that the same monoliths could be applied to the Appel reaction, giving a small selection of alkyl bromides in high yield and purity without further off-line purification protocols. It was also shown that a single monolith could be used sequentially for Ramirez reactions and then the Appel reaction, but not in reverse order. This indicates that the Appel reaction consumes the Ramirez active brominating agent during the reaction. An alternative mechanistic pathway can ensue if the Appel reaction is performed subsequent to the Ramirez reaction.

Supporting Information

Supporting Information File 1

Experimental part.
[http://www.beilstein-journals.org/bjoc/content/supplementary/1860-5397-9-207-S1.pdf]

Acknowledgements

We would like to thank the EPSRC and GlaxoSmithKline (Stevenage) for studentship support (KAR) and the BP 1702 Professorship (SVL) for financial support. We gratefully acknowledge Hokko Chemical Industry Co., Ltd. for their kind donation of diphenyl(4-vinylphenyl)phosphine.

References

1. Webb, D.; Jamison, T. F. *Chem. Sci.* **2010,** *1,* 675–680. doi:10.1039/c0sc00381f
2. Wegner, J.; Ceylan, S.; Kirschning, A. *Adv. Synth. Catal.* **2012,** *354,* 17–57. doi:10.1002/adsc.201100584
3. Wenger, J.; Ceylan, S.; Kirschning, A. *Chem. Commun.* **2011,** *47,* 4583–4592. doi:10.1039/C0CC05060A
4. Hartman, R. L.; McMullen, J. P.; Jensen, K. F. *Angew. Chem., Int. Ed.* **2011,** *50,* 7502–7519. doi:10.1002/anie.201004637

5. Mason, B. P.; Price, K. E.; Steinbacher, J. L.; Bogdan, A. R.; McQuade, D. T. *Chem. Rev.* **2007,** *107,* 2300–2318. doi:10.1021/cr050944c
6. Ahmed-Omer, B.; Brandta, J. C.; Wirth, T. *Org. Biomol. Chem.* **2007,** *5,* 733–740. doi:10.1039/b615072a
7. Baxendale, I. R.; Hayward, J. J.; Lanners, S.; Ley, S. V.; Smith, C. D. Heterogeneous Reactions. In *Microreactors in Organic Synthesis and Catalysis;* Wirth, T., Ed.; Wiley-VCH: Weinheim, Germany, 2008; pp 84–122.
8. Myers, R. M.; Roper, K. A.; Baxendale, I. R.; Ley, S. V. The Evolution of Immobilized Reagents and their Application in Flow Chemistry for the Synthesis of Natural Products and Pharmaceutical Compounds. In *Modern Tools for the Synthesis of Complex Bioactive Molecules;* Cossy, J.; Arseniyadis, S., Eds.; John Wiley & Sons: Hoboken, NJ, U.S.A., 2012; pp 359–394. doi:10.1002/9781118342886.ch11
9. García-Verdugo, E.; Luis, S. V. Flow Processes Using Polymer-supported Reagents, Scavengers and Catalysts. In *Chemical Reactions and Process under Flow Conditions;* Luis, S. V.; Garcia-Verdugo, E., Eds.; Royal Society of Chemistry: Cambridge, U.K., 2009; pp 44–85. doi:10.1039/9781847559739-00044
10. Baxendale, I. R.; Ley, S. V. Solid Supported Reagents in Multi-Step Flow Synthesis. In *New Avenues to Efficient Chemical Synthesis: Emerging Technologies;* Seeberger, P. H.; Blume, T., Eds.; Ernst Schering Foundation Symposium Proceedings, Vol. 2006/3; Springer-Verlag: Berlin, Germany, 2007; pp 151–185. doi:10.1007/2789_2007_033
11. Hodge, P. *Ind. Eng. Chem. Res.* **2005,** *44,* 8542–8553. doi:10.1021/ie040285e
12. Kirschning, A.; Solodenko, W.; Mennecke, K. *Chem.–Eur. J.* **2006,** *12,* 5972–5990. doi:10.1002/chem.200600236
13. Baxendale, I. R.; Deeley, J.; Griffiths-Jones, C. M.; Ley, S. V.; Saaby, S.; Tranmer, G. K. *Chem. Commun.* **2006,** 2566–2568. doi:10.1039/b600382f
14. Sherrington, D. C. *Chem. Commun.* **1998,** 2275–2286. doi:10.1039/a803757d
15. Svec, F.; Fréchet, J. M. J. *Science* **1996,** *273,* 205–211. doi:10.1126/science.273.5272.205
16. Peters, E. C.; Svec, F.; Fréchet, J. M. J. *Adv. Mater.* **1999,** *11,* 1169–1181. doi:10.1002/(SICI)1521-4095(199910)11:14<1169::AID-ADMA1169>3.0.CO;2-6
17. Svec, F.; Fréchet, J. M. J. *Anal. Chem.* **1992,** *64,* 820–822. doi:10.1021/ac00031a022
18. Švec, F.; Fréchet, J. M. J. Rigid Macroporous Organic Polymer Monoliths Prepared by Free Radical Polymerization. In *Monolithic Materials: Preparation, Properties and Applications;* Švec, F.; Tennikova, T. B.; Deyl, Z., Eds.; Journal of Chromatography Library, Vol. 67; Elsevier Science B. V.: Amsterdam, The Netherlands, 2003; pp 19–50.
19. Buchmeiser, M. R. *Polymer* **2007,** *48,* 2187–2198. doi:10.1016/j.polymer.2007.02.045
20. Švec, F.; Huber, C. G. *Anal. Chem.* **2006,** *78,* 2100–2107. doi:10.1021/ac069383v
21. Kunz, U.; Kirschning, A.; Wen, H.-L.; Solodenko, W.; Cecilia, R.; Kappe, C. O.; Turek, T. *Catal. Today* **2005,** *105,* 318–324. doi:10.1016/j.cattod.2005.06.046
22. Jas, G.; Kirschning, A. *Chem.–Eur. J.* **2003,** *9,* 5708–5723. doi:10.1002/chem.200305212
23. Švec, F.; Tennikova, T. B. Historical Review. In *Monolithic Materials: Preparation, Properties and Applications;* Švec, F.; Tennikova, T. B.; Deyl, Z., Eds.; Journal of Chromatography Library, Vol. 67; Elsevier Science B. V.: Amsterdam, The Netherlands, 2003; pp 1–15.
24. Nikbin, N.; Ladlow, M.; Ley, S. V. *Org. Process Res. Dev.* **2007,** *11,* 458–462. doi:10.1021/op7000436
25. Baumann, M.; Baxendale, I. R.; Ley, S. V.; Nikbin, N.; Smith, C. D. *Org. Biomol. Chem.* **2008,** *6,* 1587–1593. doi:10.1039/b801634h
26. Baumann, M.; Baxendale, I. R.; Martin, L. J.; Ley, S. V. *Tetrahedron* **2009,** *65,* 6611–6625. doi:10.1016/j.tet.2009.05.083
27. Lange, H.; Capener, M. J.; Jones, A. X.; Smith, C. J.; Nikbin, N.; Baxendale, I. R.; Ley, S. V. *Synlett* **2011,** 869–873. doi:10.1055/s-0030-1259923
28. Tripp, J. A.; Stein, J. A.; Svec, F.; Fréchet, J. M. J. *Org. Lett.* **2000,** *2,* 195–198. doi:10.1021/ol9912837
29. Kirschning, A.; Altwicker, C.; Dräger, G.; Harders, J.; Hoffmann, N.; Hoffmann, U.; Schönfeld, H.; Solodenko, W.; Kunz, U. *Angew. Chem., Int. Ed.* **2001,** *40,* 3995–3998. doi:10.1002/1521-3773(20011105)40:21<3995::AID-ANIE3995>3.0.CO;2-V
30. Kunz, U.; Schönfeld, H.; Kirschning, A.; Solodenko, W. *J. Chromatogr., A* **2003,** *1006,* 241–249. doi:10.1016/S0021-9673(03)00556-9
31. Solodenko, W.; Wen, H.; Leue, S.; Stuhlmann, F.; Sourkouni-Argirusi, G.; Jas, G.; Schönfeld, H.; Kunz, U.; Kirschning, A. *Eur. J. Org. Chem.* **2004,** 3601–3610. doi:10.1002/ejoc.200400194
32. Mennecke, K.; Kirschning, A. *Beilstein J. Org. Chem.* **2009,** *5,* No. 21. doi:10.3762/bjoc.5.21
33. Burguete, M. I.; García-Verdugo, E.; Vicent, M. J.; Luis, S. V.; Pennemann, H.; Graf von Keyserling, N.; Martens, J. *Org. Lett.* **2002,** *4,* 3947–3950. doi:10.1021/ol026805o
34. Altava, B.; Burguete, M. I.; García-Verdugo, E.; Luis, S. V.; Vicent, M. J. *Green Chem.* **2006,** *8,* 717–726. doi:10.1039/b603494b
35. Bou-Hamdan, F. R.; Krüger, K.; Tauer, K.; McQuade, D. T.; Seeberger, P. H. *Aust. J. Chem.* **2013,** *66,* 213–217. doi:10.1071/CH12405
36. Sachse, A.; Galarneau, A.; Coq, B.; Fajula, F. *New J. Chem.* **2011,** *35,* 259–264. doi:10.1039/c0nj00965b
37. Smith, C. J.; Smith, C. D.; Nikbin, N.; Ley, S. V.; Baxendale, I. R. *Org. Biomol. Chem.* **2011,** *9,* 1927–1937. doi:10.1039/c0ob00813c
38. Smith, C. J.; Nikbin, N.; Ley, S. V.; Lange, H.; Baxendale, I. R. *Org. Biomol. Chem.* **2011,** *9,* 1938–1947. doi:10.1039/c0ob00815j
39. Roper, K. A.; Lange, H.; Polyzos, A.; Berry, M. B.; Baxendale, I. R.; Ley, S. V. *Beilstein J. Org. Chem.* **2011,** *7,* 1648–1655. doi:10.3762/bjoc.7.194
40. Beilstein TV: "Conducting Appel reactions in flow using a triphenylphosphine monolith". http://www.beilstein.tv/tvpost/conducting-appel-reactions-in-flow-using-a-triphenylphosphine-monolith/ (accessed June 30, 2013).
41. Desai, N. B.; McKelvie, N.; Ramirez, F. *J. Am. Chem. Soc.* **1962,** *84,* 1745–1747. doi:10.1021/ja00868a057
42. Corey, E. J.; Fuchs, P. L. *Tetrahedron Lett.* **1972,** *13,* 3769–3772. doi:10.1016/S0040-4039(01)94157-7
43. Uenishi, J.; Kawahama, R.; Yonemitsu, O.; Tsuji, J. *J. Org. Chem.* **1996,** *61,* 5716–5717. doi:10.1021/jo961013r
44. Shen, W.; Wang, L. *J. Org. Chem.* **1999,** *64,* 8873–8879. doi:10.1021/jo991116k
45. Shen, W. *Synlett* **2000,** 737–739. doi:10.1055/s-2000-6626
46. Poupon, J.-C.; Boezio, A. A.; Charette, A. B. *Angew. Chem., Int. Ed.* **2006,** *45,* 1415–1420. doi:10.1002/anie.200503599

47. Fang, Y.-Q.; Lifchits, O.; Lautens, M. *Synlett* **2008,** 413–417. doi:10.1055/s-2008-1032045
48. Hodge, P.; Khoshdel, E. *React. Polym.* **1985,** *3,* 143–150.
49. Bolli, M. H.; Ley, S. V. *J. Chem. Soc., Perkin Trans. 1* **1998,** 2243–2246. doi:10.1039/A803612H
50. Bernard, M.; Ford, W. T. *J. Org. Chem.* **1983,** *48,* 326–332. doi:10.1021/jo00151a010
51. Choi, M. K. W.; He, H. S.; Toy, P. H. *J. Org. Chem.* **2003,** *68,* 9831–9834. doi:10.1021/jo035226+
52. Årstad, E.; Barrett, A. G. M.; Hopkins, B. T.; Köbberling, J. *Org. Lett.* **2002,** 1975–1977. doi:10.1021/ol026008q
53. Anilkumar, G.; Nambu, H.; Kita, Y. *Org. Process Res. Dev.* **2002,** *6,* 190–191. doi:10.1021/op010094c
54. Cainelli, G.; Contento, M.; Manescalchi, F.; Plessi, L. *Synthesis* **1983,** 306–308. doi:10.1055/s-1983-30314
55. Sherrington, D. C.; Craig, D. J.; Dagleish, J.; Domin, G.; Taylor, J.; Meehan, G. V. *Eur. Polym. J.* **1977,** *13,* 73–76. doi:10.1016/0014-3057(77)90140-9
56. Harrison, C. R.; Hodge, P. *J. Chem. Soc., Chem. Commun.* **1978,** 813–815. doi:10.1039/C39780000813
57. Hodge, P.; Khoshdel, E. *J. Chem. Soc., Perkin Trans. 1* **1984,** 195–198. doi:10.1039/P19840000195
58. Appel, R. *Angew. Chem., Int. Ed. Engl.* **1975,** *12,* 801–811. doi:10.1002/anie.197508011
59. Tömösközi, I.; Gruber, L.; Radics, L. *Tetrahedron Lett.* **1975,** *29,* 2473–2476. doi:10.1016/0040-4039(75)80041-4
60. Métay, E.; Hu, Q.; Negishi, E.-i. *Org. Lett.* **2006,** *8,* 5773–5776. doi:10.1021/ol0623825
61. Sneddon, H. F.; Gaunt, M. J.; Ley, S. V. *Org. Lett.* **2003,** *5,* 1147–1150. doi:10.1021/ol034248f
62. Harding, S. L. Azadirachtin: towards a second generation synthesis. Ph.D. Thesis, University of Cambridge, U.K., 2011.

License and Terms

Beilstein Journal of Organic Chemistry

Flow Giese reaction using cyanoborohydride as a radical mediator

Takahide Fukuyama, Takuji Kawamoto, Mikako Kobayashi and Ilhyong Ryu*

Letter

Open Access

Address:
Department of Chemistry, Graduate School of Science, Osaka Prefecture University, Sakai, Osaka 599-8531, Japan

Email:
Ilhyong Ryu* - ryu@c.s.osakafu-u.ac.jp

* Corresponding author

Keywords:
continuous flow system; cyanoborohydride; flow chemistry; iodoalkanes; microreactor; tin-free Giese reaction

Beilstein J. Org. Chem. **2013,** *9,* 1791–1796.
doi:10.3762/bjoc.9.208

Received: 02 July 2013
Accepted: 14 August 2013
Published: 03 September 2013

This article is part of the Thematic Series "Chemistry in flow systems III".

Guest Editor: A. Kirschning

Abstract

Tin-free Giese reactions, employing primary, secondary, and tertiary alkyl iodides as radical precursors, ethyl acrylate as a radical trap, and sodium cyanoborohydride as a radical mediator, were examined in a continuous flow system. With the use of an automated flow microreactor, flow reaction conditions for the Giese reaction were quickly optimized, and it was found that a reaction temperature of 70 °C in combination with a residence time of 10–15 minutes gave good yields of the desired addition products.

Introduction

Organo halides are among the most useful precursors to access carbon radical species, and they have found numerous applications in chemical synthesis [1-5]. Alkyl radicals are classified as nucleophilic radicals, and therefore they are able to add preferentially to alkenes possessing an electron-withdrawing substituent [6,7]. This type of reductive radical addition reaction, better known as the Giese reaction, was historically carried out most by using tributyltin hydride as the radical mediator [8,9]. Recently borane derivatives such as borohydride reagents [10-13] or NHC-boranes [14-18] can be used in simple radical C–C bond forming reactions or radical reduction as efficient substitutes for tin hydride reagents, whose toxicity is of great concern to organic chemists. Thus far we have demonstrated the borohydride-based tin-free Giese reactions [10] and the related radical carbonylation and hydroxymethylation reaction [11-13,18] employing this methodology. In Scheme 1, a general mechanism of a borohydride-based Giese reaction with the possible products is shown.

In recent years, microreaction technologies have made a significant impact on chemical synthesis and production in terms of their advantageous characteristics, which include efficient mixing, efficient mass and heat transfer, and high operational safety [19-23]. Radical reactions also benefit from these advantages, and we have reported both photo- [24-26] and thermally-induced [27-30] radical reactions that are facilitated by flow reaction technology [31]. In this study, we report that cyanoborohydride-based Giese reactions of primary, secondary,

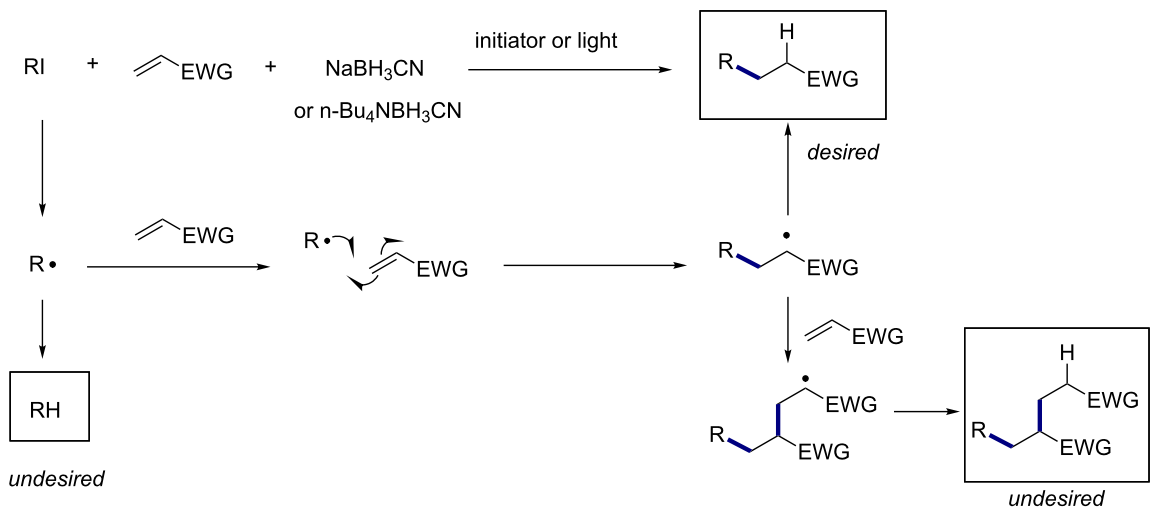

Scheme 1: Giese reaction using borohydride-based radical mediators.

and tertiary iodoalkanes with ethyl acrylate can be carried out efficiently using a microflow system. Optimal conditions for each substrate were quickly determined by the use of an automated microflow reactor [32], which revealed that running the continuous flow reactions at 70 °C for 10–15 min gave good yields of Giese addition products with effective suppression of the byproducts.

Results and Discussion

We employed an automated microflow reactor system, MiChS® System X-1 [33], equipped with a fraction collector, which allows screening of up to 20 reaction conditions in one operation through the programming of temperature and flow rates (Figure 1).

Initially, the reaction of 1-iodooctane (**1a**) with ethyl acrylate in the presence of $NaBH_3CN$ (2 equiv) and 10 mol % AIBN (2,2'-azobisisobutyronitrile) was investigated. A variety of different temperatures (90–110 °C) and residence times (2–10 min) were screened. The reaction of **1a** with ethyl acrylate was found to give the desired Giese reaction product **3a** together with two main byproducts, octane (**2a**) and the 1:2 addition adduct **4a**. As shown in Scheme 2, higher reaction temperatures tended to result in the formation of increased amounts of octane (**2a**).

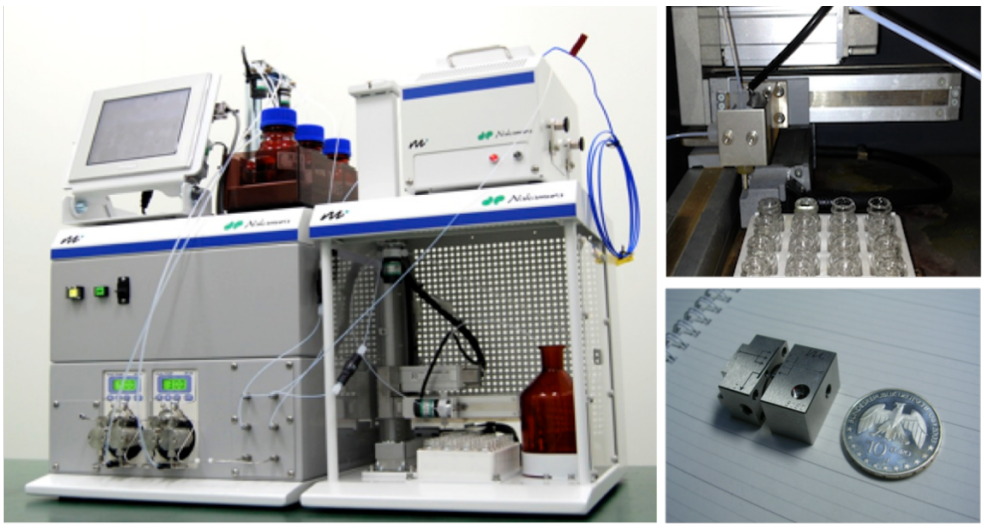

Figure 1: Pictures of the flow microreactor system (MiChS® System X-1), a micromixer (MiChS β-150, channel width: 150 μm), and a fraction collector used for this study.

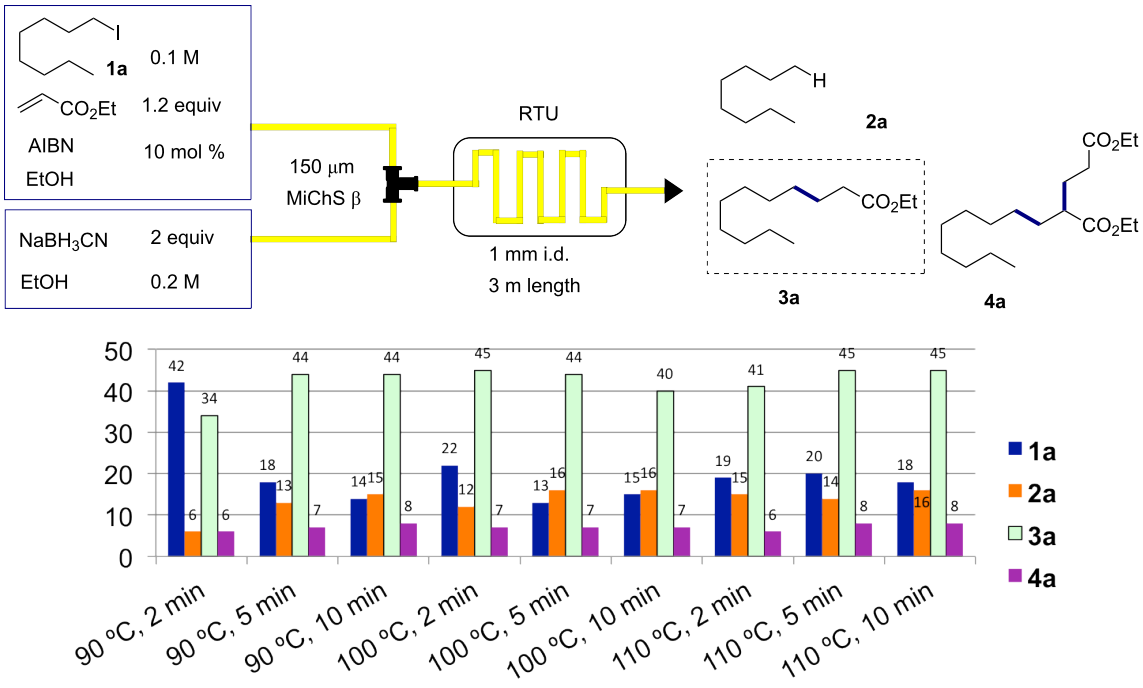

Scheme 2: First screening for the reaction of **1a** at different temperatures (90–110 °C) and residence times (2–10 min) in the presence of AIBN.

Under the same reaction conditions, the radical mediator Bu_4NBH_3CN gave similar results, whereas the reaction with Bu_4NBH_4 was found not to be suitable, since the competing reduction leading to **2a** became the dominant product from the reaction.

To check the background hydride reduction of **1a** with $NaBH_3CN$, we treated **1a** with 2 equiv of $NaBH_3CN$ at various temperatures (70–100 °C) for 10 min in the absence of a radical initiator and ethyl acrylate (Scheme 3). The reduction product **2a** was not formed in large amounts and we found that its for-

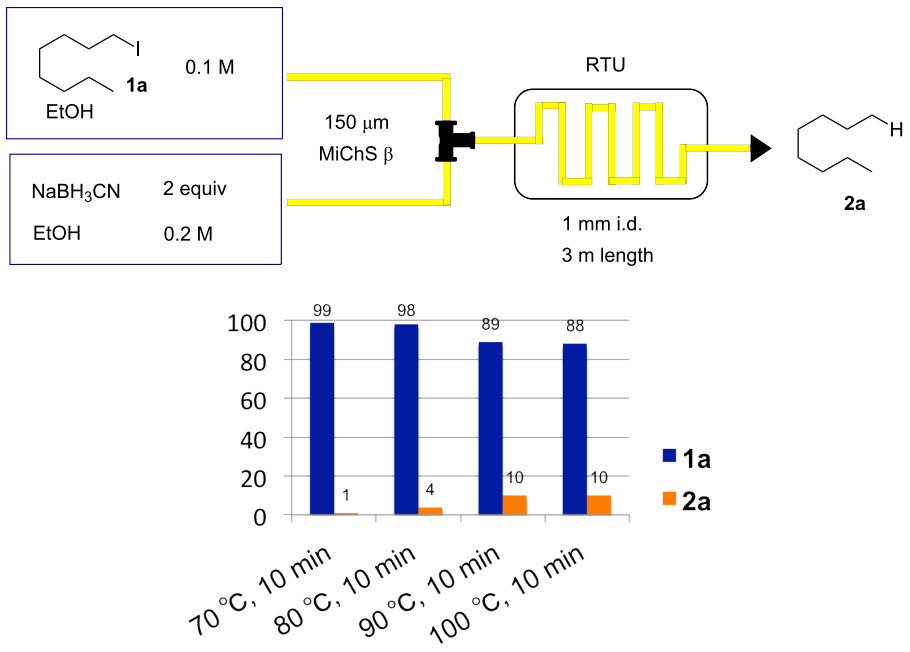

Scheme 3: Background reduction of **1a** with $NaBH_3CN$.

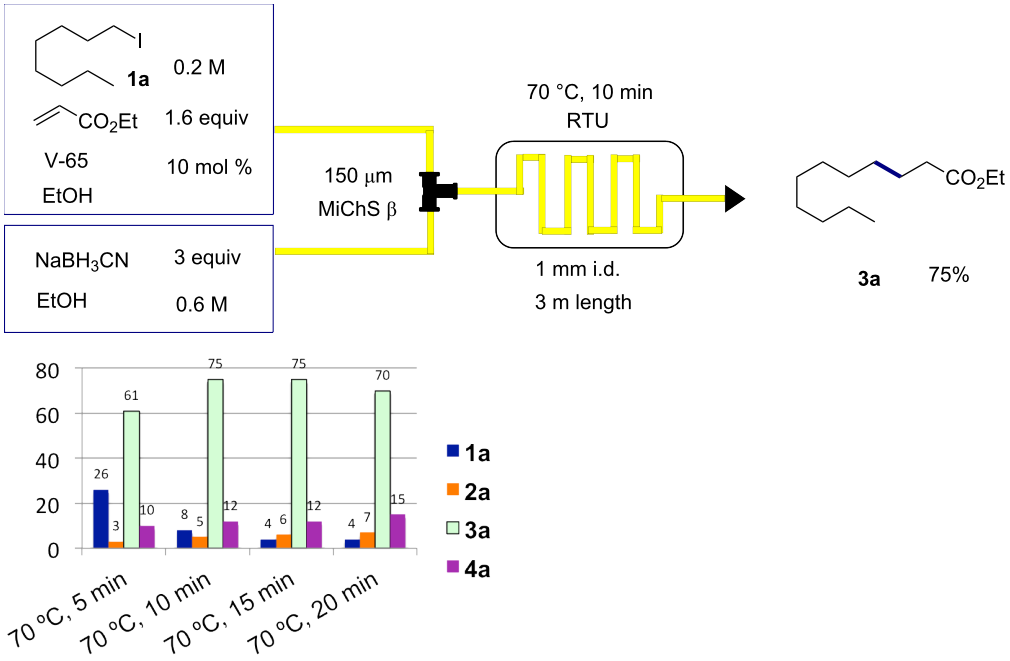

Scheme 4: Second screening at 70 °C and residence time (5–20 min) in the presence of V-65.

mation was effectively suppressed by lowering the temperature to 70 °C.

Setting the reaction temperature to 70 °C, we then further optimize the other reaction conditions. Consequently we found that the desired Giese product **3a** could be obtained in 75% yield (Scheme 4) when the reaction was carried out with 1.6 equiv of ethyl acrylate and 3 equiv of $NaBH_3CN$ and 10 min residence time in the presence of V-65 (2,2'-azobis(2,4-dimethylvaleronitrile)) as the radical initiator, which decomposes at a lower temperature than AIBN (Figure 2). For comparison, we also carried out a batch reaction using a 20 mL test tube on 0.5 mmol scale under similar reaction conditions (70 °C (bath temp.), 10 min), which gave only 34% yield of **3a** and a large amount of recovered **1a**. We assume that excellent thermal efficiency inherent to tiny reaction channels would ensure efficient reaction in the microreactors.

We then carried out the optimization of the reaction conditions for the secondary and tertiary alkyl iodides, 2-iodooctane (**1b**) and 1-iodoadamantane (**1c**), reacting with ethyl acrylate. We were pleased to find that under similar reaction conditions (70 °C, 10–15 min) these two flow Giese reactions worked well to give the corresponding addition products **3b** and **3c** in 88 and 81% yield, respectively (Scheme 5). It should be noted that for these secondary and tertiary substrates, simple reduction to give octane (**2b**) or adamantane (**2c**) was hardly observed.

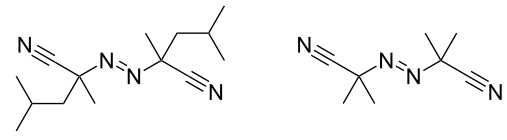

Figure 2: Structures of V-65 and AIBN and their ten hour half-life decomposition temperature.

Conclusion

The cyanoborohydride-mediated Giese reaction of alkyl iodides **1a**, **1b**, and **1c** with ethyl acrylate was studied in a continuous microflow reaction system. Optimized conditions with minimum formation of byproducts for the conversion of **1a** to **3a** were rapidly located by the use of an automated microflow system, MiChS® X-1, equipped with a static mixer having 150 µm width and an automated fraction collector. Using the optimized flow conditions (70 °C, 10–15 min), high yielding conversions of **1b** to **3b** and **1c** to **3c** were also obtained.

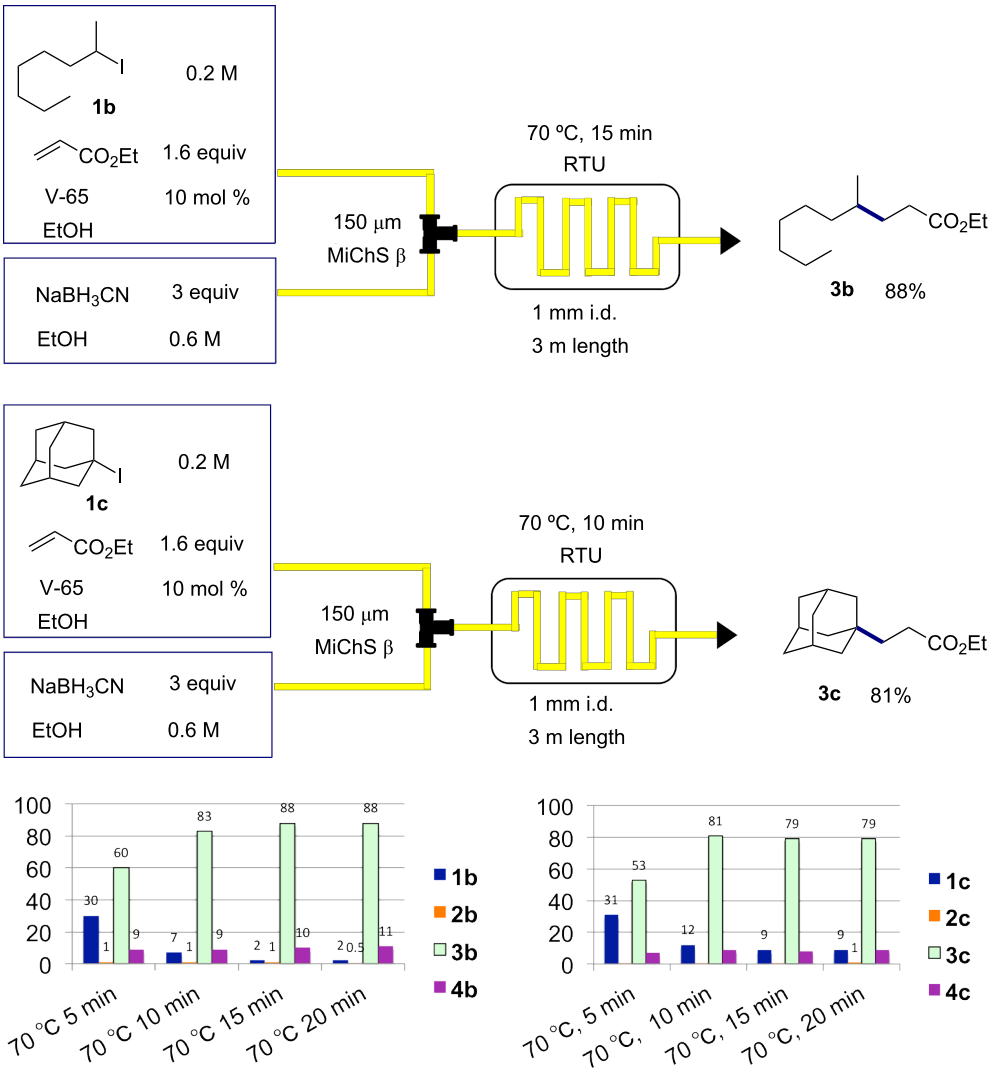

Scheme 5: Cyanoborohydride mediated Giese reaction of **1b** and **1c** with ethyl acrylate.

Supporting Information

Supporting Information File 1

Typical experimental procedure and supplementary experimental data.
[http://www.beilstein-journals.org/bjoc/content/supplementary/1860-5397-9-208-S1.pdf]

Acknowledgements

This work was supported by a Grant-in-Aid for Scientific Research from the Ministry of Education, Culture, Sports, and Technology (MEXT), Japan. T.K. acknowledges the Research Fellowship of the Japan Society for the Promotion of Science for Young Scientists (No. 249927).

References

1. Renaud, P.; Sibi, M. P., Eds. *Radicals in Organic Synthesis;* Wiley-VCH: Weinheim, 2001.
2. Togo, H., Ed. *Advanced Free Radical Reactions for Organic Synthesis;* Elsevier: Oxford, 2004.
3. Heinrich, M. R.; Gansäuer, A., Eds. *Radicals in Synthesis III; Topics Current Chemistry*, Vol. 230; Springer: Berlin, 2012.
4. Chatgilialoglu, C.; Studer, A., Eds. *Encyclopedia of Radicals in Chemistry, Biology and Materials;* Wiley: Chichester, U.K., 2012.
5. Rowlands, G. J. *Tetrahedron* **2009,** *65,* 8603. doi:10.1016/j.tet.2009.07.001
6. Giese, B. *Angew. Chem., Int. Ed.* **1983,** *22,* 753. doi:10.1002/anie.198307531
7. Fisher, H.; Radom, L. *Angew. Chem., Int. Ed.* **2001,** *40,* 1340. doi:10.1002/1521-3773(20010417)40:8<1340::AID-ANIE1340>3.0.CO;2-#
8. Giese, B.; González-Gómez, J. A.; Witzel, T. *Angew. Chem., Int. Ed.* **1984,** *23,* 69. doi:10.1002/anie.198400691

9. Gerth, D. B.; Giese, B. *J. Org. Chem.* **1986,** *51,* 3726. doi:10.1021/jo00369a039
10. Ryu, I.; Uehara, S.; Hirao, H.; Fukuyama, T. *Org. Lett.* **2008,** *10,* 1005. doi:10.1021/ol7031043
11. Kobayashi, S.; Kawamoto, T.; Uehara, S.; Fukuyama, T.; Ryu, I. *Org. Lett.* **2010,** *12,* 1548. doi:10.1021/ol1002847
12. Kawamoto, T.; Fukuyama, T.; Ryu, I. *J. Am. Chem. Soc.* **2012,** *134,* 875. doi:10.1021/ja210585n
13. Kawamoto, T.; Ryu, I. *Chimia* **2012,** *66,* 372.
14. Curran, D. P.; Solovyev, A.; Makhlouf Brahmi, M.; Fensterbank, L.; Malacria, M.; Lacote, E. *Angew. Chem., Int. Ed.* **2011,** *50,* 10294. doi:10.1002/anie.201102717
15. Ueng, S.-H.; Fensterbank, L.; Lacôte, E.; Malacria, M.; Curran, D. P. *Org. Lett.* **2010,** *12,* 3002. doi:10.1021/ol101015m
16. Ueng, S.-H.; Fensterbank, L.; Lacôte, E.; Malacria, M.; Curran, D. P. *Org. Biomol. Chem.* **2011,** *9,* 3415. doi:10.1039/c0ob01075h
17. Pan, X.; Lacôte, E.; Lalevée, J.; Curran, D. P. *J. Am. Chem. Soc.* **2012,** *134,* 5669. doi:10.1021/ja300416f
18. Kawamoto, T.; Okada, T.; Curran, D. P.; Ryu, I. *Org. Lett.* **2013,** *15,* 2144. doi:10.1021/ol4006294
19. Hessel, V.; Renken, A.; Schouten, J. C.; Yoshida, J., Eds. *Micro Process Engineering;* Wiley-VCH, 2009.
20. Wirth, T., Ed. *Microreactors in Organic Synthesis and Catalysis,* 2nd ed.; Wiley-VCH: Weinheim, 2013.
21. Jas, G.; Kirschning, A. *Chem.–Eur. J.* **2003,** *9,* 5708. doi:10.1002/chem.200305212
22. Fukuyama, T.; Rahman, M. T.; Sato, M.; Ryu, I. *Synlett* **2008,** 151. doi:10.1055/s-2007-1000884
23. Yoshida, J.; Saito, K.; Nokami, T.; Nagaki, A. *Synlett* **2011,** 1189. doi:10.1055/s-0030-1259946
24. Sugimoto, A.; Sumino, Y.; Takagi, M.; Fukuyama, T.; Ryu, I. *Tetrahedron Lett.* **2006,** *47,* 6197. doi:10.1016/j.tetlet.2006.06.153
25. Sugimoto, A.; Fukuyama, T.; Sumino, Y.; Takagi, M.; Ryu, I. *Tetrahedron* **2009,** *65,* 1593. doi:10.1016/j.tet.2008.12.063
26. Matsubara, H.; Hino, Y.; Tokizane, M.; Ryu, I. *Chem. Eng. J.* **2011,** *167,* 567. doi:10.1016/j.cej.2010.08.086
27. Fukuyama, T.; Kobayashi, M.; Rahman, M. T.; Kamata, N.; Ryu, I. *Org. Lett.* **2008,** *10,* 533. doi:10.1021/ol702718z
28. Wienhöfer, I. C.; Studer, A.; Rahman, M. T.; Fukuyama, T.; Ryu, I. *Org. Lett.* **2009,** *11,* 2457. doi:10.1021/ol900713d
29. Fukuyama, T.; Rahman, M. T.; Kamata, N.; Ryu, I. *Beilstein J. Org. Chem.* **2009,** *5,* No. 34. doi:10.3762/bjoc.5.34
30. Fukuyama, T.; Kajihara, Y.; Ryu, I.; Studer, A. *Synthesis* **2012,** 2555. doi:10.1055/s-0031-1290780
31. Fukuyama, T.; Ryu, I. Radical Chemistry by Using Flow Microreactor Technology. In *Encyclopedia of Radicals in Chemistry, Biology and Materials;* Chatgilialoglu, C.; Studer, A., Eds.; Wiley: Chichester, U.K., 2012; Vol. 21, pp 1243–1258. doi:10.1002/9781119953678.rad035
32. Sugimoto, A.; Fukuyama, T.; Rahman, M. T.; Ryu, I. *Tetrahedron Lett.* **2009,** *50,* 6364. doi:10.1016/j.tetlet.2009.08.089
33. http://www.michs.jp/index_en.html.

Beilstein Journal of Organic Chemistry

Ethyl diazoacetate synthesis in flow

Mariëlle M. E. Delville, Jan C. M. van Hest and Floris P. J. T. Rutjes*

Full Research Paper

Open Access

Address:
Radboud University Nijmegen, Institute for Molecules and Materials, Heyendaalseweg 135, 6525 AJ Nijmegen, the Netherlands

Email:
Floris P. J. T. Rutjes* - f.rutjes@science.ru.nl

* Corresponding author

Keywords:
diazo compounds; diazotization; ethyl diazoacetate (EDA); flow chemistry; microreactor technology

Beilstein J. Org. Chem. **2013,** *9,* 1813–1818.
doi:10.3762/bjoc.9.211

Received: 28 June 2013
Accepted: 15 August 2013
Published: 05 September 2013

This article is part of the Thematic Series "Chemistry in flow systems III".

Guest Editor: A. Kirschning

Abstract

Ethyl diazoacetate is a versatile compound in organic chemistry and frequently used on lab scale. Its highly explosive nature, however, severely limits its use in industrial processes. The in-line coupling of microreactor synthesis and separation technology enables the synthesis of this compound in an inherently safe manner, thereby making it available on demand in sufficient quantities. Ethyl diazoacetate was prepared in a biphasic mixture comprising an aqueous solution of glycine ethyl ester, sodium nitrite and dichloromethane. Optimization of the reaction was focused on decreasing the residence time with the smallest amount of sodium nitrite possible. With these boundary conditions, a production yield of 20 g EDA day^{-1} was achieved using a microreactor with an internal volume of 100 µL. Straightforward scale-up or scale-out of microreactor technology renders this method viable for industrial application.

Introduction

Diazo compounds are frequently used versatile building blocks in organic chemistry [1,2]. From this class of compounds diazomethane and ethyl diazoacetate (**1**, EDA) are arguably the synthetically most useful ones. Due to the potentially explosive nature of diazomethane and EDA [3-5], however, synthetic routes that involve large scale batchwise handling of such diazo compounds is generally avoided in industrial processes. With the advent of continuous processing over the past decade, new approaches have appeared to conceptually change the way chemical synthesis is performed. In particular continuous-flow microreactor technology offers multiple advantages over batch chemistry, including the inherently safe conducting of reactions due to the small reactor dimensions, efficient heat transport and excellent control over the reaction conditions [6-8]. While the synthesis of diazomethane has been extensively explored in batch [9] and in continuous-flow reactors [10,11], EDA is synthesized via different routes in batch [12,13], but relatively little is known about continuous-flow approaches [14]. Considering the importance of EDA in a wide variety of reactions e.g. cyclopropanation, X–H insertion, cycloaddition and ylide formation [13,15], and more recently, in the synthesis of valuable compound classes such as β-keto esters [16] and β-hydroxy-α-

diazocarbonyl compounds [17], we aimed to develop an inherently safe continuous-flow EDA process using microreactor and separation technology.

Ethyl diazoacetate (**1**) can be synthesized in flow via different pathways. Bartrum et al. [18] published a flow synthesis of numerous diazo esters starting from the corresponding arylsulfonylhydrazones, where the diazo moiety was installed through elimination of the sulfone substituent. Additionally, Ley et al. [19] recently prepared a range of α-hydroxy acids in flow starting from the corresponding amino acids, involving diazotization of the amine to the diazonium salt in a biphasic system. Inspired by Ley's approach, which is significantly more atom efficient than the sulfonylhydrazone pathway, we chose to synthesize EDA (**1**) from glycine ethyl ester (**2**) using readily available sodium nitrite [20] (Scheme 1). Although the diazotization step itself resembles the first step of Ley's hydroxy acid synthesis, we specifically aimed to produce and isolate the diazo product, which from there can be used for subsequent reactions.

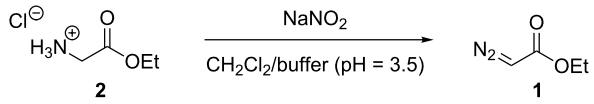

Scheme 1: Synthesis of ethyl diazoacetate (**1**).

We intended to optimize the process focusing on decreasing the residence time in order to reduce solvent use and gain in throughput. Reaction temperature was considered less of an issue since in an industrial setting energy can generally be efficiently regenerated. In-line phase separation was thought to greatly enhance the usefulness of the EDA flow synthesis. Therefore, the outlet of the microreactor was directly connected to membrane-based phase separator to obtain EDA in the organic phase, which in principle can then be immediately used for either batch [13,15] or continuous-flow [16,17] follow-up reactions. Straightforward scale-up or scale-out of microreactor technology renders this method viable for industrial application.

Results and Discussion

Flow synthesis

Ethyl diazoacetate (**1**) was synthesized from glycine ethyl ester (**2**) and sodium nitrite in a biphasic system of dichloromethane and an aqueous sodium acetate buffer. Dichloromethane was chosen as the organic phase to dissolve the water insoluble EDA, because of its low water uptake and low boiling point and its compatibility with potential follow-up reactions. In principle, however, any other organic solvent immiscible with water could be used. The pH of the buffer was set to 3.5 which had been identified by Clark et al. as the optimal pH for the reaction [12]. A schematic representation of the initial microreactor set-up is shown in Figure 1. The box with the dotted line indicates the single-glass microreactor containing two mixing units M of the folding flow type [21]. The reactor temperature was controlled by a Peltier element and sensed by a Pt1000 temperature sensor. At the outlet of the microreactor, a back-pressure regulator (BPR, 40 psi) was attached to guarantee a liquid phase even above boiling temperatures of the solvents. To ensure well-defined reaction times during optimization experiments, neat *N*,*N*-diisopropylethylamine (DIPEA) was added via syringe 4 to efficiently quench the reaction. The collected product (60 μmol) was analyzed by HPLC to establish the conversion of the reaction.

Univariate optimization

Determination of the optimal conditions for the reaction started off with investigating the important reaction parameters via a univariate optimization. Based on knowledge obtained from EDA synthesis in batch [12] and other flow reactions [22,23], residence time, temperature and $NaNO_2$ stoichiometry were chosen as relevant parameters. Temperature was expected to have a large influence on the rate of the reaction. Shortening the residence time to a minimum would minimize the risk of side reactions and reduce costs, and the reaction should be

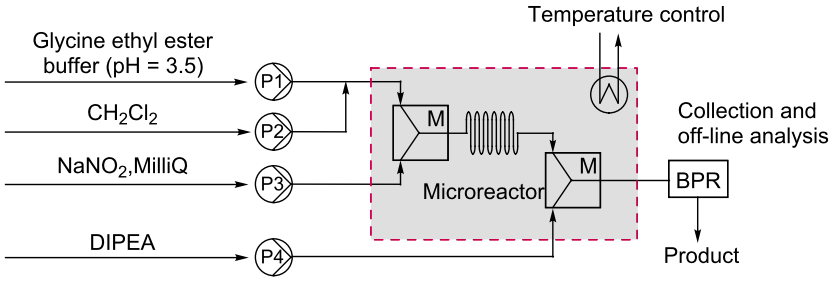

Figure 1: Schematic representation of the microreactor setup.

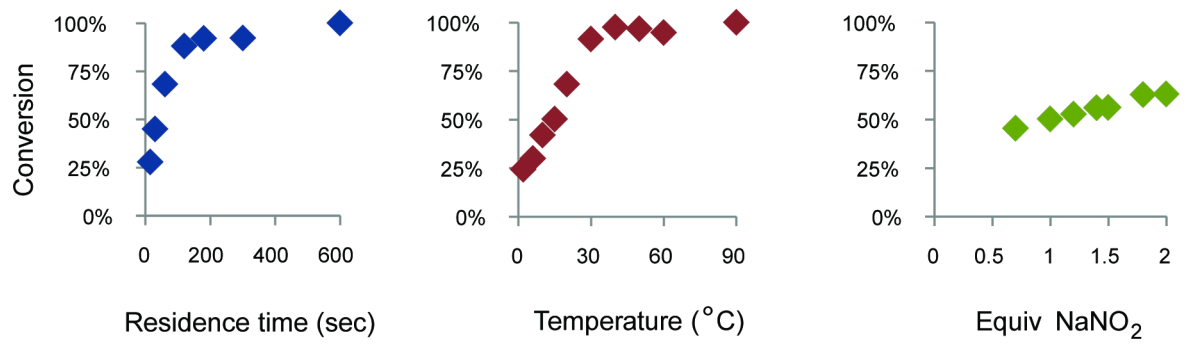

Figure 2: Univariate optimization using 30 s, 15 °C and 1.5 equiv $NaNO_2$ as standard.

performed with the smallest amount of $NaNO_2$ possible. The results of the univariate optimization are shown in Figure 2. EDA synthesis was shown to be fast, since within 200 seconds complete conversion was obtained at 15 °C. Additionally, the temperature shows a steep increase between 0–30 °C, indicating a large influence of both parameters on the reaction rate. The amount of $NaNO_2$ shows only a rather small influence. Based on these univariate optimizations the experimental ranges of the three parameters were determined to investigate the interrelationships via a multivariate optimization.

Multivariate optimization

An experimental design based on a D-optimal algorithm was created from the aforementioned three parameters within their respective ranges, namely 5–120 s, 0–60 °C and 0.7–1.5 equiv of $NaNO_2$. Using MATLAB (MathWorks, R2007a), fifty data points were selected of which the corresponding experiments were performed in random order. The resulting HPLC yields were normalized and fitted to a third order polynomial model. In-house-developed FlowFit software [24] was used to calculate the best possible model fit. The results are visualized in 2D-contour plots (Figure 3).

These plots show a rather broad optimum for the conversion of glycine ethyl ester (**2**) into EDA (**1**). The decrease in the upper left corner of the second contour plot can be explained by the high uncertainty of the model at the edge of the plots. As was expected, temperature has a large influence on the reaction rate. The conversion into EDA shows a steep increase with increasing temperature. High temperatures and increasing amounts of $NaNO_2$ decrease the residence time to a minimum of 20 seconds while still obtaining complete conversion. Not surprisingly, the minimal amount of $NaNO_2$ required is 1 equivalent. We aimed to reach complete conversion into EDA (**1**) maintaining a short residence time with a minimum amount of sodium nitrite, possibly using higher temperatures. Based on these boundary conditions, the optimal parameter settings were fixed at 20 seconds residence time, a temperature of 50 °C using 1.5 equivalents of $NaNO_2$. A triple-experiment was performed to prove that this set of optimal parameters indeed provided complete conversion into EDA. The experiment was performed in alternation with two other sets of parameters to rule out potential memory effects. HPLC yields of 95, 96 and 95% for the triple-experiment demonstrate the high reproducibility of the system.

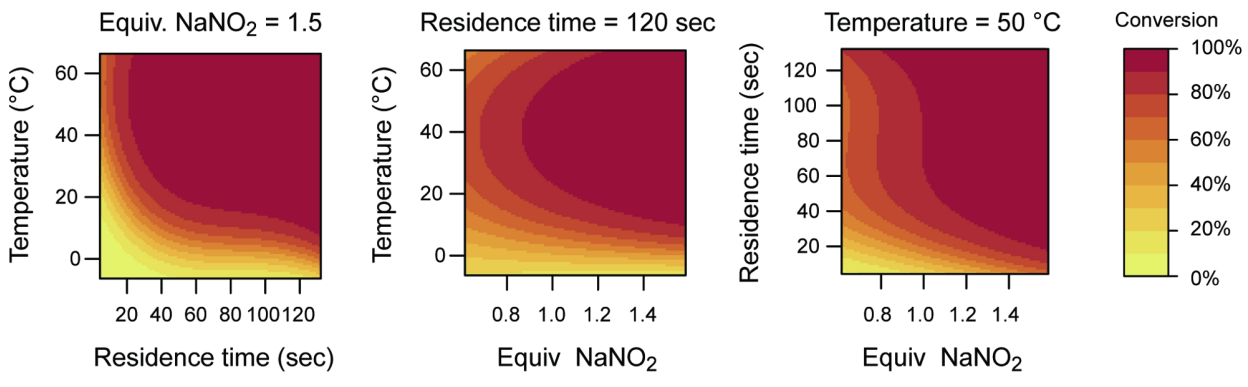

Figure 3: 2D-Contour plots of the multivariate optimization.

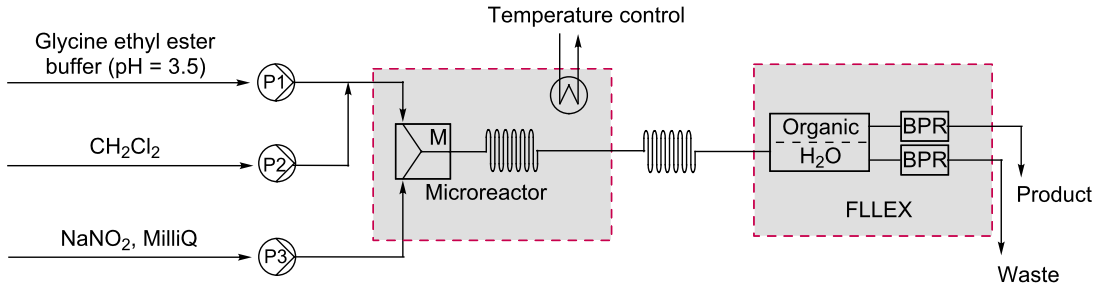

Figure 4: Phase separation using a Flow-Liquid–Liquid-Extraction module (FLLEX) directly coupled to the microreactor.

FLLEX module

Having established a microreactor protocol for the continuous-flow synthesis of EDA, the next issue was to separate the product from the biphasic system in which it was collected. In order to increase safety and decrease the hold-up of EDA, the phase separation ideally had to be performed in flow as well. Therefore, a Flow-Liquid–Liquid-Extraction module (FLLEX) [25] was connected to the system [26,27]. The module utilizes a hydrophobic Teflon membrane and two back-pressure regulators (BPRs) to create a pressure difference, which causes the organic layer, in this case dichloromethane, to pass through the membrane resulting in phase separation. A schematic representation of the whole setup is shown in Figure 4.

As the conversion into EDA was quantitative, quenching with DIPEA was no longer required. Between the microreactor and the FLLEX module some additional tubing was used to ensure complete partitioning of the compounds over the two phases. The back pressure of the FLLEX was set to 40 psi, similar to the BPR used previously, and a pressure difference of 0.14 bar. Direct full separation of phases resulted in a clean organic phase containing 409 mg EDA (11 wt % solution in CH_2Cl_2, after 30 min of collection) while all salts remain in the aqueous phase. This corresponds roughly to an EDA production of 20 g day^{-1} and a space time yield of 100 kg day^{-1} dm^{-3} as compared to a reported industrial scale batch process yielding EDA in 48 g day^{-1} dm^{-3} [12].

Conclusion

EDA can be safely synthesized utilizing microreactor and separation technology starting from cheap and readily available starting materials. Optimization of the reaction was aimed at reaching complete conversion into EDA within a minimized residence time using the smallest required amount of sodium nitrite, possibly applying higher temperatures. The optimal reaction conditions identified based on these criteria were a residence time of 20 seconds, a temperature of 50 °C and 1.5 equivalents of $NaNO_2$. Repeating the EDA synthesis in flow employing the optimal reaction parameters showed complete conversion and high reproducibility of the results. Additionally, we successfully combined a plug-and-play microreactor setup with a commercially available membrane-based phase separation module to perform a direct in-line extraction of the product. Even in our small set-up (internal volume 100 µL), we were able to generate approximately 20 g of pure EDA per day (11 wt % solution in CH_2Cl_2).

Experimental

Physical and spectroscopic measurements

NMR spectra were acquired at ambient temperature with a Bruker DMX 300 MHz spectrometer. ^{1}H NMR spectra were referenced to TMS or to the residual solvent peak. HPLC analysis was performed using an Agilent 1120 Compact LC, C-18 column, 10% acetonitrile in MilliQ, 254 nm. Pyridine (internal standard) has a retention time of 1.75 min, EDA of 9.67 min.

Chip dimensions

Three different microchips were used during the experiments.

1. Single borosilicate glass quench microreactor with an internal volume of 92 µL, a channel width of 600 µm and a channel depth of 500 µm.
2. Single borosilicate glass microreactor with an internal volume of 100 µL, a channel width of 600 µm and a channel depth of 500 µm.
3. Single borosilicate glass quench microreactor with an internal volume of 1 µL, a channel width of 120 µm and a channel depth of 50 µm.

Univariate optimization

Solution A: Glycine ethyl ester hydrochloride (40 mmol, 5.6 g) dissolved in 20 mL buffer 1. Solution B: CH_2Cl_2. Solution C: $NaNO_2$ (60 mmol, 4.1 g) dissolved in 30 mL degassed MilliQ.

Table 1: Conditions of the univariate experiments using 30 s, 15 °C and 1.5 equiv $NaNO_2$ as standard.

Time (s)	15	30	60	120	180	300	600	900		
Temperature (°C)	0	5	10	15	20	30	40	50	60	90
Amount of $NaNO_2$	0.7	1	1.2	1.4	1.5	1.8	2			

Solution Q: Neat DIPEA. Buffer 1: Sodium acetate trihydrate (132 mmol, 18.0 g) and pyridine (7.5 mL, internal standard) dissolved in 70 mL MilliQ. Concentrated hydrochloric acid (37%, 12 M) was added until a pH of 3.5 was reached (17 mL), resulting in a buffer with a total volume of 105 mL.

The flow rates and temperatures were set based on predetermined conditions of residence times and temperatures (Table 1). Experiments were performed in a glass microreactor with an internal volume of 92 µL. Solution Q was set at a flow rate 1/3 of the flow rate of solution A. Each experiment had a collection time equal to 30 µL of solution A. The product was collected in 1 mL of acetonitrile and analyzed by HPLC. Results are visualized in Figure 2.

Multivariate optimization

Solution A: Glycine ethyl ester hydrochloride (40 mmol, 5.6 g) dissolved in 20 mL buffer 1. Solution B: CH_2Cl_2. Solution C: $NaNO_2$ (60 mmol, 4.1 g) dissolved in 30 mL degassed MilliQ. Solution Q: Neat DIPEA.

The flow rates and temperatures were set based on predetermined conditions of residence times and temperatures (Table 2). Experiments with a residence time of 5 s were performed in a glass microreactor with an internal volume of 1 µL. For longer residence times, a microreactor with an internal volume of 92 µL was used. Solution Q was set at a flow rate 1/3 of the flow rate of solution A. Each experiment had a collection time equal to 30 µL of solution A. The product was collected in

Table 2: Experiments for the multivariate optimization deduced from a D-optimal experimental design algorithm.

Exp#	Molar ratio	Residence time (s)	Temperature (°C)	Exp#	Molar ratio	Residence time (s)	Temperature (°C)
1	1.5	5	0	26	1.1	120	0
2	1.5	120	60	27	1.5	120	60
3	1.5	45	0	28	0.7	5	0
4	0.7	5	60	29	1.1	15	60
5	1.5	45	60	30	1.1	120	60
6	1.5	120	40	31	1.1	45	60
7	1.5	45	0	32	1.5	5	20
8	0.7	45	0	33	1.5	120	20
9	1.5	15	20	34	0.7	15	0
10	1.1	5	20	35	0.7	5	20
11	0.7	45	20	36	1.1	5	60
12	1.5	120	0	37	1.5	15	60
13	1.1	15	0	38	0.7	45	60
14	0.7	5	60	39	1.1	120	60
15	0.7	120	40	40	1.1	120	40
16	0.7	45	60	41	1.1	5	40
17	1.5	120	0	42	0.7	5	40
18	1.5	5	60	43	1.1	5	0
19	1.5	45	40	44	0.7	120	60
20	0.7	120	60	45	1.1	120	0
21	1.5	5	0	46	0.7	15	40
22	1.5	5	60	47	0.7	5	0
23	1.1	45	0	48	0.7	120	0
24	1.1	120	20	49	0.7	120	20
25	1.5	5	40	50	0.7	120	0

1 mL of acetonitrile and analyzed by HPLC. Results are visualized in Figure 3 as 2D-contour plots.

FLLEX experiment

Solution A: Glycine ethyl ester hydrochloride (10 mmol, 1.4 g) dissolved in 5 mL buffer 2. Solution B: CH_2Cl_2. Solution C: $NaNO_2$ (15 mmol, 1.0 g) dissolved in 5 mL degassed MilliQ. Buffer 2: Sodium acetate trihydrate (100 mmol 13.6 g) dissolved in 80 mL MilliQ. Concentrated hydrochloric acid (37%, 12 M) was added until a pH of 3.5 was reached (7 mL). Additional MilliQ was added to obtain a total volume of 100 mL of buffer.

Solution A (86.25 μL/min) was combined in a stainless steel T-splitter with solution B (172.5 μL/min). The biphasic mixture immediately entered the glass microreactor (internal volume: 100 μL) where it was mixed with solution C (86.25 μL/min). The reaction was performed at 50 °C. After the reaction, the mixture was passed through 15 μL of FEP-tubing (ID = 254 μm) before entering the FLLEX module where phases were separated (40 psi, Δp = 0.14 bar). The set-up was stabilized for 2 min before collecting for 30 min. EDA was obtained as a solution in CH_2Cl_2 (1.52 g). According to ^{1}H NMR analysis, clean EDA was obtained. Based on the residual solvent peak in the ^{1}H NMR spectrum it was calculated to be a 27 wt % solution of EDA in CH_2Cl_2 meaning 409 mg of pure EDA.

Acknowledgements

We thank Dr. Pieter Nieuwland (FutureChemistry) for fruitful discussions. The NWO-ACTS Process-on-a-Chip (PoaC) program is kindly acknowledged for financial support.

References

1. Regitz, M. *Synthesis* **1972,** 351–373. doi:10.1055/s-1972-21883
2. Zhang, Z.; Wang, J. *Tetrahedron* **2008,** *64,* 6577–6605. doi:10.1016/j.tet.2008.04.074
3. Clark, J. D.; Shah, A. S.; Peterson, J. C.; Patelis, L.; Kersten, R. J. A.; Heemskerk, A. H.; Grogan, M.; Camden, S. *Thermochim. Acta* **2002,** *386,* 65–72. doi:10.1016/S0040-6031(01)00760-2
4. Clark, J. D.; Shah, A. S.; Peterson, J. C.; Patelis, L.; Kersten, R. J. A.; Heemskerk, A. H. *Thermochim. Acta* **2002,** *386,* 73–79. doi:10.1016/S0040-6031(01)00761-4
5. Hosmane, R. S.; Liebman, J. F. *Struct. Chem.* **2002,** *13,* 501–503. doi:10.1023/A:1020573723147
6. Wegner, J.; Ceylan, S.; Kirschning, A. *Adv. Synth. Catal.* **2012,** *354,* 17–57. doi:10.1002/adsc.201100584
7. Wiles, C.; Watts, P. *Chem. Commun.* **2011,** *47,* 6512–6535. doi:10.1039/c1cc00089f
8. Wirth, T., Ed. *Microreactors in Organic Synthesis and Catalysis;* Wiley-VCH: Weinheim, Germany, 2008. doi:10.1002/9783527622856
9. Cohen, J. D. *J. Chromatogr.* **1984,** *303,* 193–196. doi:10.1016/S0021-9673(01)96061-3
10. Ferstl, W. F.; Schwarzer, S.; Loebbecke, S. L. *Chem. Ing. Tech.* **2004,** *76,* 1326–1327. doi:10.1002/cite.200490233
11. Struempel, M.; Ondruschka, B.; Duate, R.; Stark, A. *Green Chem.* **2008,** *10,* 41–43. doi:10.1039/b710554a
12. Clark, J. D.; Heise, J. D.; Shah, A. S.; Peterson, J. C.; Chou, S. K.; Levine, J.; Karakas, A. M.; Ma, Y.; Ng, K.-Y.; Patelis, L.; Springer, J. R.; Stano, D. R.; Wettach, R. H.; Dutra, G. A. *Org. Process Res. Dev.* **2004,** *8,* 176–185. doi:10.1021/op034123q
13. Maas, G. *Angew. Chem., Int. Ed.* **2009,** *48,* 8186–8195. doi:10.1002/anie.200902785
14. Thathagar, M.; Poechlauer, P.; Braune, S. Process for the production of cyclopropane derivatives. WO2010055106, May 20, 2010.
15. Davies, H. M. L.; Beckwith, R. E. J. *Chem. Rev.* **2003,** *103,* 2861–2903. doi:10.1021/cr0200217
16. Bartum, H. E.; Blakemore, D. C.; Moody, C. J.; Hayes, C. J. *J. Org. Chem.* **2010,** *75,* 8674–8676. doi:10.1021/jo101783m
17. Krishna, P. R.; Prapurna, Y. L.; Alivelu, M. *Eur. J. Org. Chem.* **2011,** 5089–5095. doi:10.1002/ejoc.201100496
18. Bartrum, H. E.; Blakemore, D. C.; Moody, C. J.; Hayes, C. J. *Chem.–Eur. J.* **2011,** *17,* 9586–9589. doi:10.1002/chem.201101590
19. Hu, D. X.; O'Brien, M.; Ley, S. V. *Org. Lett.* **2012,** *14,* 4246–4249. doi:10.1021/ol301930h
20. Monbaliu, J. C.; Jorda, J.; Chevalier, B.; Stevens, C. V.; Morvan, B. *Chim. Oggi* **2011,** *29,* 50–52.
See for the use of sodium nitrite in flow chemistry for example.
21. MacInnes, J. M.; Vikhansky, A.; Allen, R. K. W. *Chem. Eng. Sci.* **2007,** *62,* 2718–2727. doi:10.1016/j.ces.2007.02.014
22. Delville, M. M. E.; Nieuwland, P. J.; Janssen, P.; Koch, K.; van Hest, J. C. M.; Rutjes, F. P. J. T. *Chem. Eng. J.* **2011,** *167,* 556–559. doi:10.1016/j.cej.2010.08.087
23. Delville, M. M. E.; van Gool, J. J. F.; van Wijk, I. M.; van Hest, J. C. M.; Rutjes, F. P. J. T. *J. Flow Chem.* **2012,** *4,* 124–128. doi:10.1556/JFC-D-12-00008
24. For more information about FlowFit software see: http://www.futurechemistry.com
25. http://www.syrris.com.
26. Tricotet, T.; O'Shea, D. F. *Chem.–Eur. J.* **2010,** *16,* 6678–6686. doi:10.1002/chem.200903284
27. Varas, A. C.; Noël, T.; Wang, Q.; Hessel, V. *ChemSusChem* **2012,** *5,* 1703–1707. doi:10.1002/cssc.201200323

License and Terms

Beilstein Journal of Organic Chemistry

Integrating reaction and analysis: investigation of higher-order reactions by cryogenic trapping

Skrollan Stockinger and Oliver Trapp*§

Letter

Open Access

Address:
Organisch-Chemisches Institut, Ruprecht-Karls-Universität Heidelberg, Im Neuenheimer Feld 270, 69120 Heidelberg, Germany

Email:
Oliver Trapp* - trapp@oci.uni-heidelberg.de

* Corresponding author
§ Fax: +49-6221-544904

Keywords:
benzyne; cryogenic CO_2 trap; cycloaddition; Diels–Alder reaction; flow chemistry; gas chromatography; on-column reaction gas chromatography

Beilstein J. Org. Chem. **2013,** *9,* 1837–1842.
doi:10.3762/bjoc.9.214

Received: 24 June 2013
Accepted: 14 August 2013
Published: 10 September 2013

This article is part of the Thematic Series "Chemistry in flow systems III".

Guest Editor: A. Kirschning

Abstract

A new approach for the investigation of a higher-order reaction by on-column reaction gas chromatography is presented. The reaction and the analytical separation are combined in a single experiment to investigate the Diels–Alder reaction of benzenediazonium-2-carboxylate as a benzyne precursor with various anthracene derivatives, i.e. anthracene, 9-bromoanthracene, 9-anthracenecarboxaldehyde and 9-anthracenemethanol. To overcome limitations of short reaction contact times at elevated temperatures a novel experimental setup was developed involving a cooling trap to achieve focusing and mixing of the reactants at a defined spot in a fused-silica capillary. This trap functions as a reactor within the separation column in the oven of a gas chromatograph. The reactants are sequentially injected to avoid undefined mixing in the injection port. An experimental protocol was developed with optimized injection intervals and cooling times to achieve sufficient conversions at short reaction times. Reaction products were rapidly identified by mass spectrometric detection. This new approach represents a practical procedure to investigate higher-order reactions at an analytical level and it simultaneously provides valuable information for the optimization of the reaction conditions.

Introduction

The combination of synthesis and analysis in a single experiment offers many advantages. Time-consuming steps, i.e. work-up and separation of the reaction products, can be minimized, and direct analytical information about a reaction is obtained, including the formation of by-products and eventually even the reaction kinetics [1-4]. This information is important to design efficient flow-through experiments and to scale-up a reaction in a continuous process [5-9], which is often the first step for large-scale production. We contributed to this research field by developing on-column reaction chromatography, a technique where a catalytically active separation phase is used to perform (catalyzed) reactions and separations at the same time [10-17]. Here, the catalyst is immobilized or dissolved in an inert stationary phase and coated on the inside of fused-silica capillaries, which are then installed in a gas chromatograph (Figure 1a), capillary electrophoresis (Figure 1b) or liquid sep-

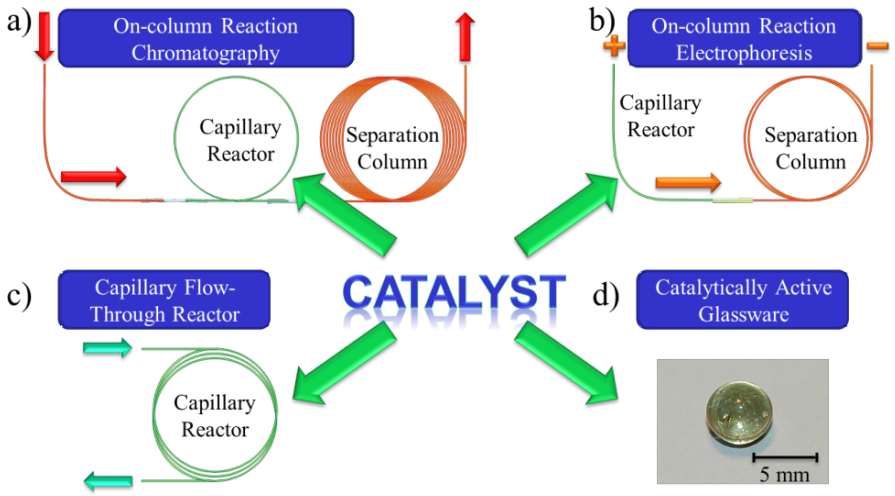

Figure 1: Overview of some capabilities of an immobilized or in an inert stationary phase dissolved catalyst. The use of reactive capillaries a) in on-column reaction GC, b) in on-column reaction capillary electrophoresis, c) as a capillary reactor to perform flow-through experiments, and d) to obtain catalytically active glassware.

aration instrument (Figure 1c). In addition, the catalyst can be applied to the surface modification of glassware to obtain catalytically active bulk reactors, i.e. coated glass stir bars (Figure 1d).

The use of catalytically active fused-silica capillaries in analytical separation devices is a very powerful approach, because several reactions can be simultaneously performed by injecting a whole library of reactants at the same time and – most importantly – under exactly the same reaction conditions. Because of the separation of the reactant mixture, occurring prior to reaching the catalytically active section of the capillary, we do not observe competing reactions, so that the reaction kinetics can be investigated under comparable reaction conditions. So far, we investigated only first-order or pseudo-first-order reactions, where, for example, one reactant is used as a carrier gas, i.e., hydrogen in hydrogenation reactions or hydrogen peroxide as oxidant [18]. However, there is a great demand for investigating higher-order reactions, where several reactants are mixed and converted into a single product. We are currently developing an approach characterized by injecting a pulse of a slower migrating reactant, followed by a pulse of a faster migrating reactant. At a defined point the faster migrating reactant will "catch up" with the slower migrating reactant, interact, and react to the product. To cope with the limitations of applicable temperature ranges necessary to transport and separate the reactants and products, we developed a novel approach, which is discussed in the present contribution.

Here, we use a focusing technique to concentrate and stop separating several substances in a single column section to study higher-order reactions and to increase the conversion in on-column reaction gas chromatography (ocRGC). The major challenge in investigating multi-ordered reactions by ocRGC is the necessary contact of all reactants and catalysts involved in the reaction under the desired reaction conditions for a sufficient amount of time.

There are various techniques available to focus a substance within a gas chromatographic (GC) run at a defined point on a separation column. In general, focusing results in a decreased band width causing a concentration of the sample. We can take advantage of this effect in ocRGC, because the conversion is directly proportional to the concentration. Focusing is used for several reasons, namely to improve peak shapes, to increase the signal-to-noise ratio, and simply expand the detection limit of an analyst. In practice, focusing is achieved by cooling a short section of the separation column and reheating it after a certain amount of time. Frequently, cryogenic cooling traps are used. In most cases the cryogenic cooling device is installed directly in the GC oven and connected to the column at the desired column section. Reheating is performed by turning off the cooling device. Commercially available cryogenic cooling devices use compressed gas or high pressure liquids, such as CO_2 or N_2, to cool the column section. An interesting application of a cryogenic cooling trap is the longitudinally modulated cryogenic sampler (LMCS) used by Marriott et al. [19]. It is used to focus and concentrate samples between columns in a multidimensional gas chromatographic setup (GC×GC) [20].

To experimentally test our novel ocRGC setup, we chose the cycloaddition of benzyne with anthracene derivatives in a typical Diels–Alder-reaction (Scheme 1) as a model reaction.

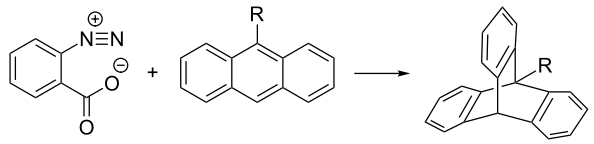

Scheme 1: Diels–Alder reaction of benzenediazonium-2-carboxylate with anthracene-9-derivatives toward triptycene-9-derivatives.

This reaction seemed suitable because of the volatility of all reactants and products and the required reaction temperature, which is in an adequate range for GC measurements. Besides, the Diels–Alder reaction is a commonly used reaction and of broad interest. The used dienophile, benzyne, is highly reactive and must be generated in situ [21-24]. This can be achieved by chemical decomposition initiated by fluoride [25], lithium [22,26], an oxidizing agent [27] or by physical decomposition by radiation [28] or heating [29-31] of a precursor system. Here, we used benzenediazonium-2-carboxylate as a benzyne precursor, which thermally decomposes by elimination of nitrogen and carbon dioxide.

Results and Discussion

Initially, we chose to inject the heat-labile benzenediazonium-2-carboxylate after the anthracene derivative, because we expected that the thermally formed benzyne would be surrounded by the anthracene derivative, and an optimal conversion should occur. Surprisingly, the inverse injection order leads to a significant increase in yield, which might be explained by a certain lag time in the formation of benzyne. Therefore, the benzenediazonium-2-carboxylate was injected first, followed by the anthracene derivative by using two syringes to avoid any product formation by contamination. It can be assumed that the thermal activation of the benzyne formation is already initiated in the injector at elevated temperature. During this period, benzyne is collected in the capillary section covered by the cooling trap, leading to an enhanced reactivity when the anthracene derivative is injected into the cooling trap. Morgen et al. [32] published a procedure in which the GC injector is used as a chemical reactor to convert several reactants into a product. In contrast, our approach limits the intended reaction to a defined column section in the cooling trap. Figure 2 visualizes the experimental setup. First, the reactants were injected into a short pre-column, which is used to transfer them to the cryogenic cooling trap. The separation column is connected with the cooling trap, and the cooling zone extends for about 4 mm at the very beginning of this capillary. The cryogenic cooling is realized by using a cryogenic CO_2 cold trap system directly installed in the GC oven. The cooling is started before the injection of the first reactant, so that all reactants are focused in this section. All reactants are collected in the cooling trap by this experimental setup. Thus, an unintended reaction occurring in the injector prior to the reaction taking place in the capillary section cooled by the cooling trap is avoided. After all reactants are injected, the GC run is started. It was found that the optimal cryogenic cooling time has to be extended by 1.0 min measured from the start of the measurements. The application of longer or shorter cooling times resulted in lower conversions, which might be explained by a spatial separation in case of cooling temperatures for longer cooling times and by the incomplete condensation of the reactants at the defined cooling section for too short cooling times, respectively. A fused silica column coated with chemically inert polydimethylsiloxane (GE-SE30) was used as a separation column to avoid any side reactions of the highly reactive benzyne with the stationary phase. It has to be pointed out that our approach is not limited to the use of neat polydimethylsiloxane, but other non-reactive stationary phases may be used, too. One of the advantages of the described experimental setup is the possibility to continuously tune the polarity and the properties of the stationary phase thereby optimizing the conditions for a particular reaction.

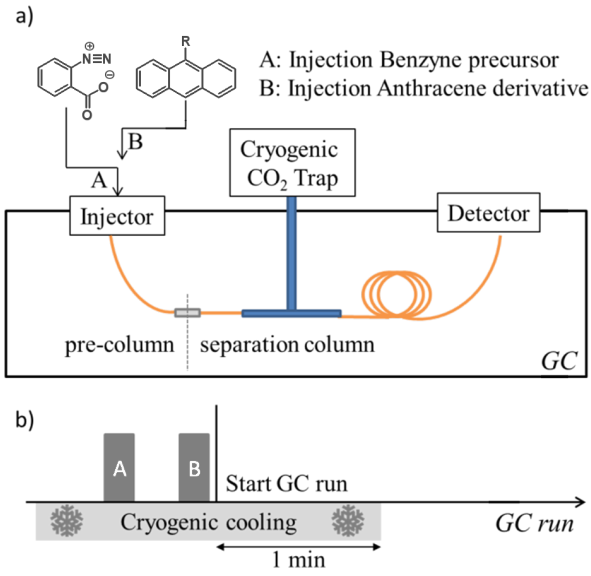

Figure 2: The experimental setup and a) the injection sequence protocol of the cryogenic ocRGC measurements b). Conditions: on-column cold injection, 60 °C for 5 min, then 6 °C/min to 180 °C, 120 kPa He; pre-column: fused silica, 10 cm, 250 nm film thickness, 250 µm i.d.; separation column: GE-SE30 (100% polydimethylsiloxane), 10 m, 500 nm film thickness, 250 µm i.d.

A typical chromatogram of the on-column Diels–Alder reaction with 9-anthracenemethanol is shown in Figure 3. Anthranilic acid was identified as the decomposition product of benzenediazonium-2-carboxylate in these ocRGC experiments. It is already formed by the sole injection of benzenediazonium-2-

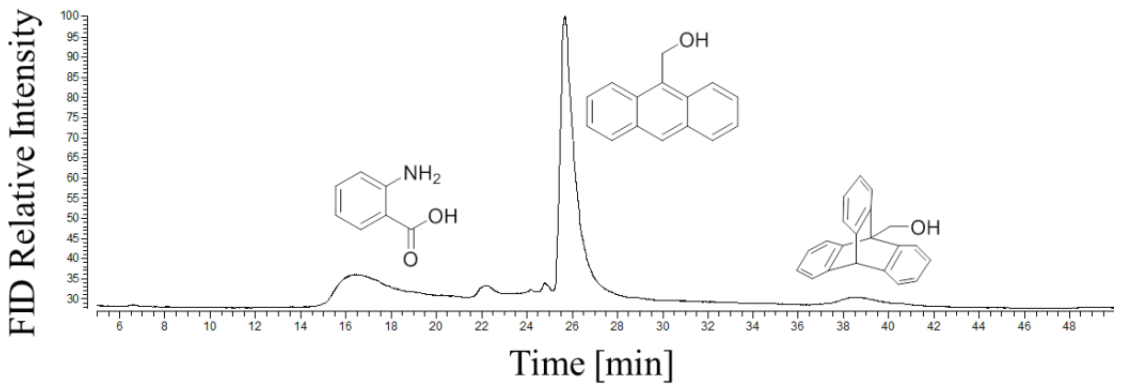

Figure 3: Experimental ocRGC chromatogram of 9-anthracenemethanol with benzenediazonium-2-carboxylate. Conditions: on-column cold injection, 60 °C for 5 min, then 6 °C/ min to 180 °C, 120 kPa He; pre-column: fused silica, 10 cm, 250 nm film thickness, 250 µm i.d.; separation column: GE-SE30 (100% polydimethylsiloxane), 10 m, 500 nm film thickness, 250 µm i.d.

carboxylate. An overview of the obtained yields of the formed triptycene-9-derivatives is given in Table 1. The yields are reproducible between 1.4 and 6% as expected for the very short reaction times during the heating step. All reactions were also performed by a regular synthesis in test tubes in order to compare the results with those of the ocRGC measurements (see Table 1).

The test tube system gives only moderate yields, even if the reaction temperature is raised to 80 °C. According to Stiles et al. the reaction of anthracene and benzenediazonium-2-carboxylate in refluxing benzene yields 30% triptycene with a reaction time of 64 hours [30]. Our measurements revealed that this yield could already be achieved after 3 hours. This could also be experimentally proven by the test-tube experiment. In both systems, test tube and ocRGC, the best yields were achieved with 9-anthracenemethanol as a diene component. For the test-tube system a yield of 16% after 24 hours at room temperature and 44% after 3 hours at 80 °C was found. The reaction time for the on-column reaction is considerably smaller, because an effective contact time of less than one second must be assumed. Consequently, the measured yield of 6% of 9-triptycenemethanol for the on-column measurement can be considered as an impressing result. Unfortunately, all other anthracene derivatives did not exceed a yield of 2% with the ocRGC method. For the test-tube experiments the yield of 9-anthracenemethanol is also higher than those of the other derivatives, but the differences are samller compared to the on-column system. Surprisingly, the substituents of the anthracene derivatives show a more pronounced effect on the conversion compared to the classical synthesis in a flask, which might be explained by differences in the relative migration velocities of the dienes. We calculated reaction rate constants from our experiments (k, Table 1), which clearly indicate that a large surface area substantially improves the rate of conversion. We observed an acceleration of a magnitude of approximately 1000 under these conditions. Nevertheless, both systems show the same tendency of an electronic influence of the substituents on the reactivity.

Table 1: Yield of triptycene-9-derivatives.[a]

R =	Synthesis in a flask				ocRGC[b]			
	t	T	Yield	k [s^{-1}]	t	T	Yield	k [s^{-1}]
H	24 h	rt	11%	1.4×10^{-6}	~1s	60 °C	[c]	
	3 h	80 °C	31%	3.4×10^{-5}				
Br	24 h	rt	7%	8.4×10^{-7}	~1s	60 °C	1.8%	1.8×10^{-2}
	3 h	80 °C	28%	3.0×10^{-5}				
CHO	24 h	rt	4%	4.7×10^{-7}	~1s	60 °C	1.4%	1.4×10^{-2}
	3 h	80 °C	13%	1.3×10^{-5}				
CH_2OH	24 h	rt	16%	2.2×10^{-6}	~1s	60 °C	6.0%	6.2×10^{-2}
	3 h	80 °C	44%	5.4×10^{-5}				

[a]100% coverage of the carbon-corrected FID area of anthracene-9-yl derivative and the associated triptycene-9-yl derivative. [b]Average values of at least three measurements are shown. The average standard deviation of the values does not exceed ±1%. [c]A detectable but infinitesimal small amount of transformation.

Thus, the reactivity order is not affected by our novel approach. In contrast to a classical reaction screening, our on-column gas chromatographic setup can be used to determine this reactivity order within a few hours, including the complete separation and characterization of all reactants, products and side-products and requiring only minute amounts of the reactants. Consequently, the method facilitates a complete screening of large substance libraries within a few days. Additionally, all detectable multi-order reactions may be investigated without any modification of the illustrated setup. Despite the advantage of an enrichment of the in-line sample concentration by the cryogenic CO_2 setup, reactions can be studied in greater detail. Individual reaction steps can be slowed down by cooling only locally at different positions of a catalytic column, and several substances can be pre-focused before the actual reaction occurs to allow for an easier investigation of the reaction process. In summary, the presented ocRGC setup with a cryogenic CO_2 cooling trap is a fast and accurate screening method for reactivity investigations of multi-order reactions.

Experimental

Benzenediazonium-2-carboxylate was synthesized according to a procedure described in [33,34]. Anthracene, 9-bromoanthracene, 9-anthracenecarboxaldehyde and 9-anthracenemethanol were purchased from Aldrich Chemical, Acros or ABCR and used without further purification. As GC–MS a Trace GC Ultra combined with an ISQ Single Quadrupole mass spectrometer, both from Thermo Scientific, were used. For cryofocusing a Cryogenic CO_2 Cold Trap System by SGE Analytical Science was installed, according to the experimental setup outlined in Figure 2. For cryofocusing CO_2 was used as a cooling liquid [35]. For the measurement of the reference substances 50 mg of benzenediazonium-2-carboxylate was mixed with 0.8 equiv anthracene or the anthracene derivative in 2 mL 1,2-dichloroethane or dichloromethane (DCM) and stirred under the conditions given in Table 1. After filtration and evaporation the reaction mixture was dissolved in pentane and washed with water. The diluted pentane solution was analyzed by GC–MS. For the ocRGC analysis separate DCM solutions of anthracene or anthracene derivative and benzenediazonium-2-carboxylate were prepared, both containing 1 mg per mL. The injection was performed by using two different on-column syringes from SGE (experimental setup is outlined in Figure 2) following the general on-column cold injection techniques with a secondary N_2-cooling time of 2 min. For analysis the FID signal was used and carbon-corrected.

Acknowledgements

We thank the Deutsche Forschungsgemeinschaft (DFG) for financial support of this research (SFB 623 'Molecular Catalysts: Structure and Functional Design'). O.T. was supported by the European Research Council under Grant Agreements No. StG 258740. We thank Chromasoft GmbH for the supply of the cryogenic CO_2 cold trap system.

References

1. Haswell, S. J. *Nature* **2006,** *441,* 705. doi:10.1038/441705a
2. Belder, D. *Angew. Chem.* **2010,** *122,* 6630–6632. doi:10.1002/ange.201002059
3. Belder, D. *Anal. Bioanal. Chem.* **2006,** *385,* 416–418. doi:10.1007/s00216-006-0428-z
4. Trapp, O. *Chim. Oggi* **2008,** *26,* 26–28.
5. Jas, G.; Kirschning, A. *Chem.–Eur. J.* **2003,** *9,* 5708–5723. doi:10.1002/chem.200305212
6. Kirschning, A.; Solodenko, W.; Mennecke, K. *Chem.–Eur. J.* **2006,** *12,* 5972–5990. doi:10.1002/chem.200600236
7. Baxendale, I. R.; Griffiths-Jones, C. M.; Ley, S. V.; Tranmer, G. K. *Chem.–Eur. J.* **2006,** *12,* 4407–4416. doi:10.1002/chem.200501400
8. Nikbin, N.; Ladlow, M.; Ley, S. V. *Org. Process Res. Dev.* **2007,** *11,* 458–462. doi:10.1021/op7000436
9. Bourne, S. L.; Koos, P.; O'Brien, M.; Martin, B.; Schenkel, B.; Baxendale, I. R.; Ley, S. V. *Synlett* **2011,** *18,* 2643–2647. doi:10.1055/s-0031-1289291
10. Trapp, O.; Weber, S. K.; Bauch, S.; Hofstadt, W. *Angew. Chem.* **2007,** *119,* 7447–7451. doi:10.1002/ange.200701326
11. Trapp, O. *J. Chromatogr., A* **2008,** *1184,* 160–190.
12. Trapp, O.; Weber, S. K.; Bauch, S.; Bäcker, T.; Hofstadt, W.; Spliethoff, B. *Chem.–Eur. J.* **2008,** *14,* 4657–4666. doi:10.1002/chem.200701780
13. Weber, S. K.; Bremer, S.; Trapp, O. *Chem. Eng. Sci.* **2010,** *65,* 2410–2416. doi:10.1016/j.ces.2009.09.006
14. Trapp, O.; Bremer, S.; Weber, S. K. *Anal. Bioanal. Chem.* **2009,** *395,* 1673–1679. doi:10.1007/s00216-009-2993-4
15. Trapp, O. *Electrophoresis* **2010,** *31,* 786–813. doi:10.1002/elps.200900599
16. Troendlin, J.; Rehbein, J.; Hiersemann, M.; Trapp, O. *J. Am. Chem. Soc.* **2011,** *133,* 16444–16450. doi:10.1021/ja207091x
17. Lang, C.; Gärtner, U.; Trapp, O. *Chem. Commun.* **2011,** *47,* 391–393. doi:10.1039/c0cc02306j
18. Fuessl, S.; Trapp, O. *Electrophoresis* **2012,** *33,* 1060–1067. doi:10.1002/elps.201100527
19. Chin, S.-T.; Maikhunthod, B.; Marriott, P. J. *J. Anal. Chem.* **2011,** *83,* 6485–6492. doi:10.1021/ac200973z
20. Seeley, J. V.; Seeley, S. K. *Anal. Chem.* **2013,** *85,* 557–578. doi:10.1021/ac303195u
21. Wittig, G.; Pohmer, L. *Angew. Chem.* **1955,** *67,* 348. doi:10.1002/ange.19550671306
22. Wittig, G.; Pohmer, L. *Chem. Ber.* **1956,** *89,* 1334–1351. doi:10.1002/cber.19560890539
23. Huisgen, R.; Rist, H. *Naturwissenschaften* **1954,** *41,* 358–359. doi:10.1007/BF00643284
24. Pellissier, H.; Santelli, M. *Tetrahedron* **2003,** *59,* 701–730. doi:10.1016/S0040-4020(02)01563-6
25. Wang, B.; Mu, B.; Chen, D.; Xu, S.; Zhou, X. *Organometallics* **2004,** *23,* 6225–6230. doi:10.1021/om049430e
26. Matsumoto, T.; Hosoya, T.; Katsuki, M.; Suzuki, K. *Tetrahedron Lett.* **1991,** *32,* 6735–6736. doi:10.1016/S0040-4039(00)93589-5
27. Birkett, M. A.; Knight, D. W.; Giles, R. G.; Mitchell, M. B. *J. Chem. Soc., Perkin Trans. 1* **1998,** 2301–2306. doi:10.1039/A803251C

28. Cho, H. Y.; Ajaz, A.; Himali, D.; Waske, P. A.; Johnson, R. P. *J. Org. Chem.* **2009,** *74,* 4137–4142. doi:10.1021/jo900245v
29. Stiles, M.; Miller, R. G. *J. Am. Chem. Soc.* **1960,** *82,* 3802. doi:10.1021/ja01499a094
30. Chen, Z.; Shou, W.; Wang, Y. *Synthesis* **2009,** *7,* 1075–1080. doi:10.1055/s-0028-1083356
31. Shou, W.-G.; Yang, Y.-Y.; Wang, Y.-G. *J. Org. Chem.* **2006,** *71,* 9241–9243. doi:10.1021/jo061648i
32. Attygalle, A. B.; Morgan, E. D. *Angew. Chem., Int. Ed. Engl.* **1988,** *27,* 460–478. doi:10.1002/anie.198804601
33. Friedman, L.; Logullo, F. M. *J. Org. Chem.* **1969,** *34,* 3089–3092. doi:10.1021/jo01262a065
34. Friedman, L.; Logullo, F. M. *J. Am. Chem. Soc.* **1963,** *85,* 1549. doi:10.1021/ja00893a045
35. Product Data Sheet: Cryogenic cold taps for GC Peak Focusing, by SGE Analytical Science.

License and Terms

Beilstein Journal of Organic Chemistry

Raman spectroscopy as a tool for monitoring mesoscale continuous-flow organic synthesis: Equipment interface and assessment in four medicinally-relevant reactions

Trevor A. Hamlin and Nicholas E. Leadbeater*

Full Research Paper

Open Access

Address:
Department of Chemistry, University of Connecticut, 55 North Eagleville Road, Storrs, CT 06269, USA

Email:
Nicholas E. Leadbeater* - nicholas.leadbeater@uconn.edu

* Corresponding author

Keywords:
flow processing; Raman spectroscopy; reaction monitoring; α,β-unsaturated carbonyl

Beilstein J. Org. Chem. **2013,** *9,* 1843–1852.
doi:10.3762/bjoc.9.215

Received: 24 May 2013
Accepted: 15 August 2013
Published: 11 September 2013

This article is part of the Thematic Series "Chemistry in flow systems III".

Guest Editor: A. Kirschning

Abstract

An apparatus is reported for real-time Raman monitoring of reactions performed using continuous-flow processing. Its capability is assessed by studying four reactions, all involving formation of products bearing α,β-unsaturated carbonyl moieties; synthesis of 3-acetylcoumarin, Knoevenagel and Claisen–Schmidt condensations, and a Biginelli reaction. In each case it is possible to monitor the reactions and also in one case, by means of a calibration curve, determine product conversion from Raman spectral data as corroborated by data obtained using NMR spectroscopy.

Introduction

Continuous-flow processing is used in the chemical industry on production scales. In a research and development setting, there has been increasing interest in using flow chemistry on smaller scales. To this end, a wide range of companies now produce equipment for both micro- and mesofluidic flow chemistry [1,2]. Some of the advantages of these devices are increased experimental safety, easy scale-up and thorough mixing of reagents [3-7]. It is not surprising, therefore, that a wide range of synthetic chemistry transformations have been reported using this equipment [8,9]. When it comes to evaluating the outcome of reactions performed using flow chemistry and optimizing reaction conditions, one option is to use inline product analysis. This opens the avenue for fast, reliable assay in comparison with the traditional approach in which performance is evaluated based on offline product analysis. When interfaced with microreactors, inline analysis has taken significant strides in recent years [7,10]. Spectroscopic tools such as infrared [11-15], UV–visible [16-18], NMR [19,20], Raman [21-25], and mass spectrometry [26,27] have all been interfaced with success. There have been less reports when it comes to

mesoflow systems. Perhaps most developed is the area of infrared monitoring. The now ubiquitous ReactIR equipment has been interfaced with commercially available flow equipment to allow for real-time analysis of reactions and on-the-fly optimization of conditions [28-30].

In our laboratory we have had success interfacing a Raman spectrometer with a scientific microwave unit [31]. This has allowed us to monitor reactions from both a qualitative [32-35] and quantitative [36,37] perspective. A recent report of the use of Raman spectroscopy for monitoring a continuous-flow palladium-catalyzed cross-coupling reaction [38] sparked our interest in interfacing our Raman spectrometer with one of our continuous-flow units and employing it for inline reaction monitoring of a number of key medicinally-relevant organic transformations. Our results are presented here.

Results and Discussion

Interfacing the spectrometer to the flow unit

In interfacing our Raman spectrometer with a continuous-flow reactor, our objective was to use a similar approach to that which proved successful when using microwave heating. Borosilicate glass is essentially "Raman transparent". Therefore reactions could be monitored by placing a Raman probe near the reaction vessel, without requirement to place any parts of the spectrometer inside the reaction vessel. The exposure of metallic components to the microwave field was avoided using a quartz light-pipe extending both the excitation laser and the acquisition fiber optic components of the spectrometer almost without any loss of light. The optimum distance of the light-pipe to the outside wall of the reaction vessel was found to be approximately 0.5 mm. Moving to our continuous-flow reactor, we decided to place the spectroscopic interface just after the back-pressure regulator assembly. This meant that we did not need to engineer a flow cell capable of holding significant pressure. Instead we used an off-the-shelf flow cell traditionally used in conjunction with other spectroscopic monitoring tools. The cell had screw-threaded inlet and outlet tubes of the same diameter as the tubing of the flow unit (i.d. 1 mm). The sample chamber had a width of 6.5 mm, height of 20 mm and a path length of 5 mm giving the cell a nominal internal volume of 0.210 mL (Figure 1a). We built an assembly to allow us to hold the cell in a fixed location and vary the distance of the quartz light-pipe so as to optimize the Raman signal intensity. The apparatus is shown in Figure 1b.

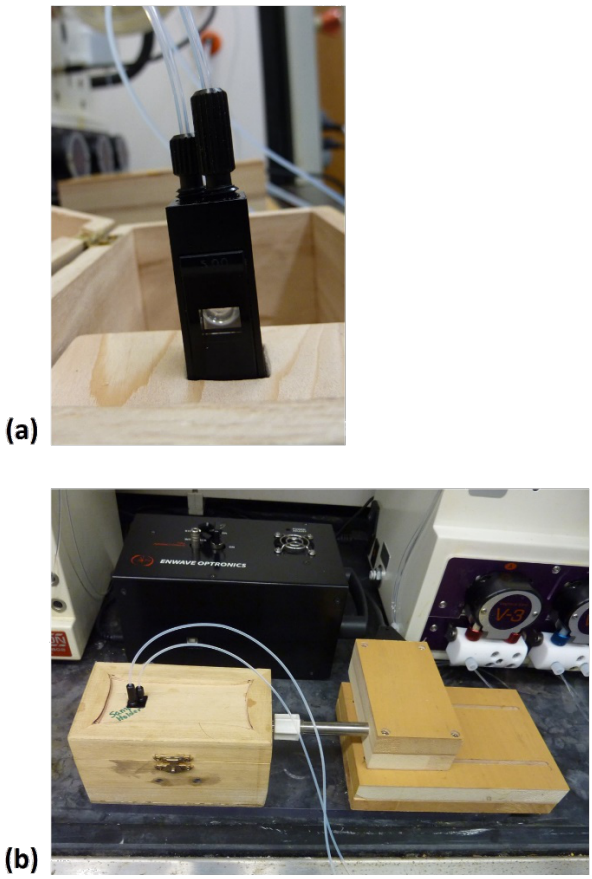

Figure 1: (a) Flow cell and (b) Raman interface used in the present study.

Testing the interface: The synthesis of 3-acetylcoumarin

As our first reaction for study, we selected the piperidine-catalyzed synthesis of 3-acetylcoumarin (**1**) from salicylaldehyde with ethyl acetoacetate (Scheme 1). We had extensive experience of monitoring this reaction both qualitatively [32] and quantitatively [36] when using microwave heating so believed it would be a good starting point for our present study. The reaction works well when using ethyl acetate as the solvent. However, **1** is not completely soluble at room temperature. To overcome potential clogging of the back-pressure regulator as well as mitigating the risk of having solid particles in the flow cell (which would perturb signal acquisition), we leveraged a technique we developed for this and other reactions previously [39]. Once the reaction stream has exited the heated zone, it is intercepted with a flow of a suitable organic solvent. This solubilizes the product and allows it to pass through the back-pres-

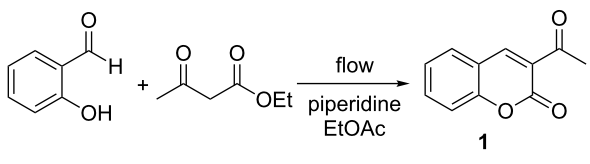

Scheme 1: The reaction between salicylaldehyde and ethyl acetoacetate to form 3-acetyl coumarin (**1**).

sure regulator unimpeded. In the case of **1**, we intercept the product stream with a flow of acetone.

Our first objective was to determine whether we could observe spectroscopically a slug of the coumarin passing through the flow cell. The Raman spectrum of **1** (Figure 2) exhibits strong Raman-active stretching modes at 1608 cm^{-1} and 1563 cm^{-1} while the salicylaldehyde and ethyl acetoacetate starting materials exhibit minimal Raman activity in this area. As a result, we chose to monitor the 1608 cm^{-1} signal. To mimic a product mixture, we pumped a solution of **1** in acetone through our flow reactor, intercepted it with an equal volume of ethyl acetate and passed this mixture through the flow cell. We recorded a Raman spectrum every 15 s in an automated fashion as the coumarin passed through the cell by using the "continuous-scan" function on our spectrometer. By subtracting the spectrum of the solvent mixture (1:1 ethyl acetate:acetone) from the spectra recorded, we were able to clearly see the growth of the signal due to **1** followed by a plateau as it passed through the cell and then a drop back to the baseline as the final aliquot exited (Figure 3).

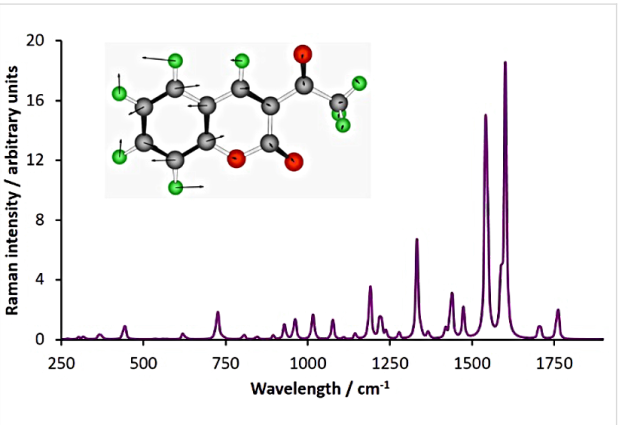

Figure 2: The Raman spectrum of 3-acetylcoumarin (**1**) generated using Gaussian 09 [40] at the B3LYP/6-31g(d) level of theory. The inset molecule illustrates the stretching mode responsible for the signal calculated at 1602 cm^{-1} (actual: 1608 cm^{-1}).

Knowing we could observe the product as it passed through the flow cell, we next performed the complete reaction. As a starting point, we chose as conditions a flow rate of 1 mL/min through a 10 mL PFA coil at room temperature. We were indeed able to monitor the reaction as shown in Figure 4. In an effort to optimize the reaction conditions, we varied both the temperature of the reactor coil and also the flow rate, monitoring each run and then compiling the data (Figure 4). While increasing the reaction temperature to 130 °C led to a marked increase in product conversion, reducing the flow rate from 1 mL/min to 0.5 mL/min at this temperature did not have a significant impact on the outcome of the reaction.

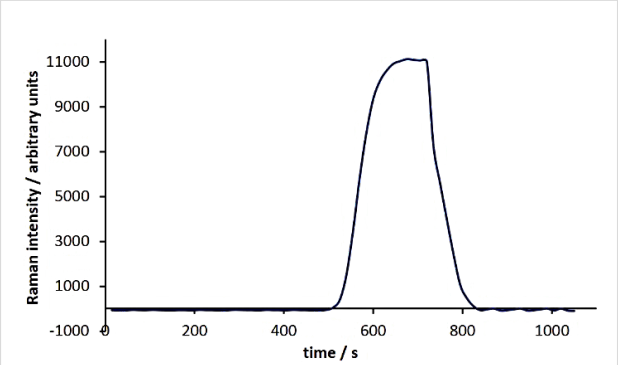

Figure 3: Monitoring an aliquot of 3-acetyl coumarin (**1**) as it passes through the flow cell (scan time = 15 s, integration = 10 s).

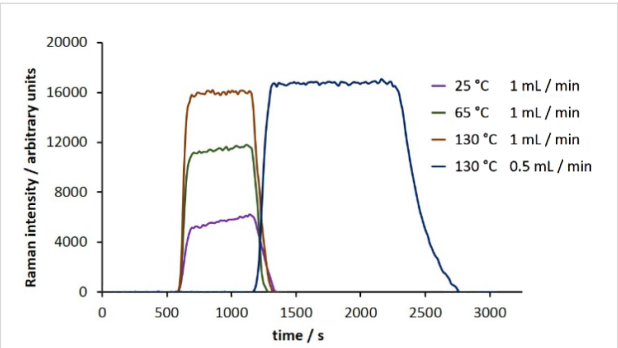

Figure 4: Monitoring the conversion of salicylaldehyde and ethyl acetoacetate to 3-acetylcoumarin (**1**) across a range of reaction conditions (scan time = 15 s, integration = 10 s).

In an attempt to quantify product conversion, we needed next to obtain a calibration curve to allow us to convert units of Raman intensity to units of concentration in standard terms. To achieve this, we passed solutions of various concentrations of 3-acetylcoumarin (**3**) in ethyl acetate/acetone through the flow cell and collected the Raman spectrum. When the signal intensity at 1608 cm^{-1} is plotted against concentration, after subtraction of signals due to the solvent, the result is a straight line (Figure 5).

The Stokes shift (which is being monitored) is inversely proportional to the temperature. Since the flow cell is situated after the product mixture exits the heated zone and because of the very efficient heat transfer observed using narrow-gauge tubing, the product mixture was essentially at room temperature by the time it passed through the flow cell. As a result, it was not deemed necessary to involve a scaling factor to account for temperature effects.

With the appropriate calibration curve in hand, we were able to obtain product conversion values for each set of reaction conditions screened, taking into account the fact that the product

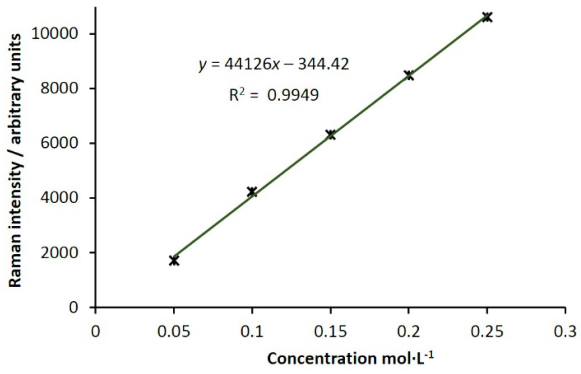

Figure 5: Plot of Raman intensity of the peak arising at 1608 cm^{-1} vs concentration of 3-acetyl coumarin (**1**), yielding a straight line, y = mx + b; m = Raman intensity·M^{-1} of **1**.

concentration is halved by the interception with acetone. To determine their accuracy, we also determined product conversion using NMR spectroscopy. Comparison of the values shows a good correlation (Table 1).

Expanding the technique to other reactions

The Knovenagel condensation

We turned our attention next to the Knoevenagel condensation of ethyl acetoacetate with a range of aromatic aldehydes (Scheme 2). Our objective was to optimize conditions using one aldehyde substrate spectroscopically from a qualitative standpoint and then screen other examples. We chose benzaldehyde as our initial substrate, ethyl acetate as the solvent and piperidine as a base catalyst. In order to determine the optimal spectral frequency at which to monitor we wanted to find a quick way to derive the Raman spectrum of the product **2a**. As was the case with **1**, this could be achieved computationally using Gaussian 09 at the B3LYP/6-31g(d) level of theory [40], and a signal at 1598 cm^{-1} selected for monitoring.

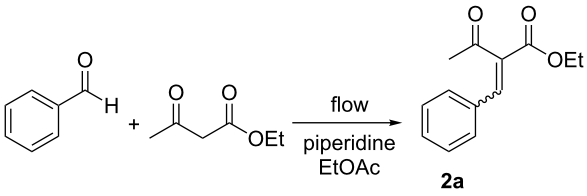

Scheme 2: The Knoevenagel condensation of benzaldehyde and ethyl acetoacetate to yield (*Z*)-ethyl 2-benzylidene-3-oxobutanoate (**2a**).

Performing the reaction across a range of conditions, flowing the reaction mixture at 1 mL/min through the 10 mL coil heated to 130 °C proved to be optimal (Figure 6). A 67% conversion to **2a** was obtained, as determined by GC analysis. Purification of the product mixture gave a 60% isolated yield of the *Z*-isomer of **2a**. Using these optimized reaction conditions, we screened

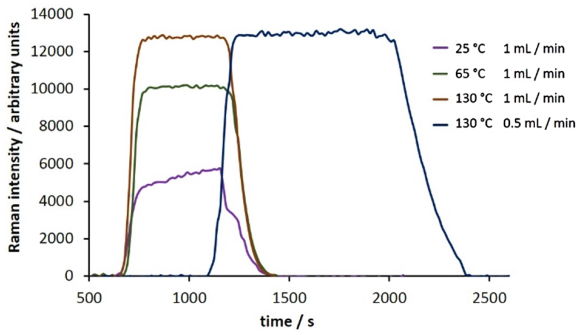

Conditions	Conversion to 2a (%)
25 °C, 1 mL/min	40
65 °C, 1 mL/min	63
130 °C, 1 mL/min	67
130 °C, 0.5 mL/min	68

Figure 6: Monitoring the conversion of benzaldehyde and ethyl acetoacetate to (*Z*)-ethyl 2-benzylidene-3-oxobutanoate (**2a**) across a range of reaction conditions (scan time = 15 s, integration = 10 s).

Table 1: Comparison of product conversion values obtained from Raman spectra with those obtained using NMR spectroscopy for the conversion of salicylaldehyde and ethyl acetoacetate to 3-acetylcoumarin (**1**).

Conditions	Raman monitoring			NMR
	Concentration of **1** when diluted with acetone (mol L^{-1})	Concentration of **1** after normalizing for dilution by acetone (mol L^{-1})	Conv. (%)	Conv. (%)
25 °C, 1 mL/min	0.125	0.25	25	22
65 °C, 1 mL/min	0.27	0.55	55	58
130 °C, 1 mL/min	0.37	0.74	74	79
130 °C, 0.5 mL/min	0.39	0.78	78	80

Table 2: Product conversion obtained for four aldehyde substrates in the Knoevenagel reaction with ethyl acetoacetate.

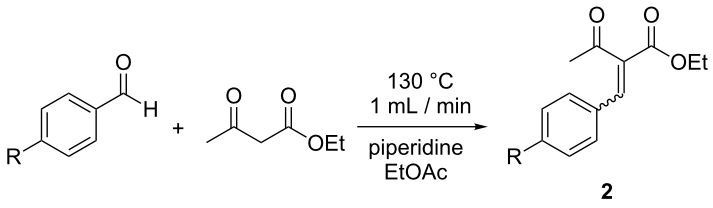

2

R	Product	Conv. (%)
H	**2a**	67 (60)[a]
OMe	**2b**	53
Me	**2c**	66
F	**2d**	63

[a]Isolated yield.

three para-substituted aldehyde substrates (Table 2). As expected, placing an electron-donating methoxy group on the aromatic ring led to lower product conversion as compared to benzaldehyde (Table 2, entry 2). A methyl- or fluoro-substituent has little effect on the outcome of the reaction (Table 2, entries 3 and 4).

The Claisen–Schmidt condensation

We moved next to study the Claisen–Schmidt condensation of benzaldehyde with acetophenone to yield chalcone (Scheme 3). Chalcones display interesting biological properties such as antioxidant, cytotoxic, anticancer, antimicrobial, antiprotozoal, antiulcer, antihistaminic, and anti-inflammatory activity [41]. They are also intermediates on the way to highly fluorescent cyanopyridine and deazalumazine dyes [42]. The calculated Raman spectrum of the product **3a** shows a very strong signal at 1604 cm^{-1} which was selected for monitoring. Using sodium hydroxide as the catalyst, the reaction was monitored under a range of reaction conditions (Figure 7). We fast discovered that at temperatures in excess of 65 °C we observed decomposition or else formation of a highly fluorescent byproduct, as evidenced by collapse of the Raman spectrum. We also observed a significant "tail" on the plot of signal intensity at 1604 cm^{-1} vs time. We attribute this to the fact that the chalcone product is very highly Raman active and even a trace in the flow cell can be readily detected. It does however highlight the fact that there may be both significant dispersion along the length of the reactor and the product is slow in clearing the flow cell. Dispersion is the consequence of laminar flow and some of the material takes longer to travel through the reactor than the rest. Thus, when a flow reactor is used to process a finite volume of reagents, the leading and trailing ends of the product emerging from the end of the reactor will have mixed to some extent with the solvent that preceded or followed it. This means that there are zones at the leading and trailing ends of the product stream in which the concentration of product is variable. Our optimal conditions for the reaction were heating at 65 °C with a flow

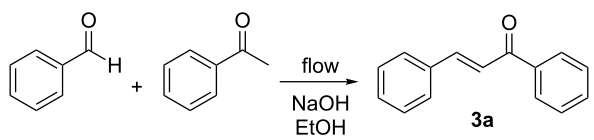

Scheme 3: Claisen-Schmidt condensation of benzaldehyde with acetophenone to yield chalcone, **3a**.

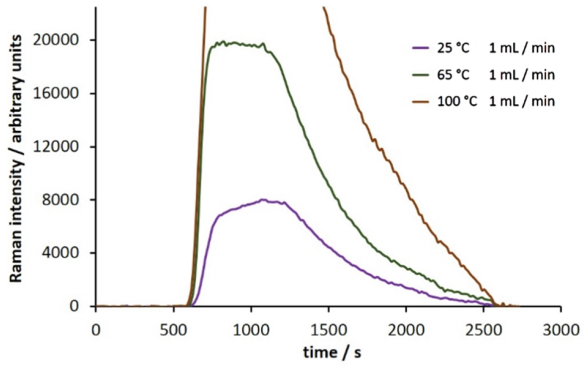

Conditions	Conversion to 3a (%)
25 °C, 1 mL/min	34
65 °C, 1 mL/min	90
100 °C, 1 mL/min	cannot monitor
65 °C, 0.5 mL/min	cannot monitor

Figure 7: Monitoring the conversion of benzaldehyde with acetophenone to chalcone, **3a**, across a range of reaction conditions (scan time = 15 s, integration = 10 s).

Table 3: Product conversion obtained for four aldehyde substrates in the Claisen-Schmidt reaction with acetophenone.

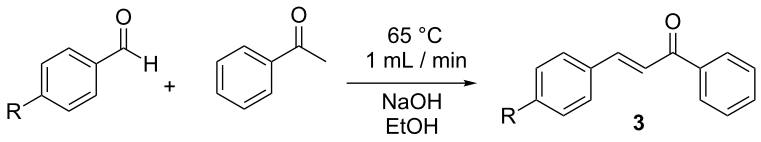

R	Product	Conv. (%)
H	**3a**	90
OMe	**3b**	66
Me	**3c**	84
F	**3d**	98 (90)[a]

[a]Isolated yield.

rate of 1 mL/min, this corresponding to a product conversion of 90%, as determined by GC analysis. Performing the reaction under these conditions using three substituted benzaldehydes as substrates, we obtained product conversions of 66−98% depending on how electron rich or deficient the aromatic ring of the aldehyde was (Table 3).

The Biginelli reaction

As our final reaction for study, we turned to the Biginelli reaction (Scheme 4) [43-48]. This acid-catalyzed cyclocondensation of urea, β-ketoesters and aromatic aldehydes to yield dihydropyrimidines has received significant attention, these products having pharmacological activity including calcium channel modulation, mitotic kinesin Eg5 inhibition, and antiviral and antibacterial activity [49,50]. The Biginelli reaction has been performed in flow previously as a route to densely functionalized heterocycles using HBr generated in a prior step as the catalyst for the reaction [51]. Copper catalysis has also been used in flow mode for preparing PEG-immobilized dihydropyrimidines [52]. We decided to screen a set of conditions for the reaction of benzaldehyde, ethyl acetoacetate and urea catalyzed by sulfuric acid (Figure 8).

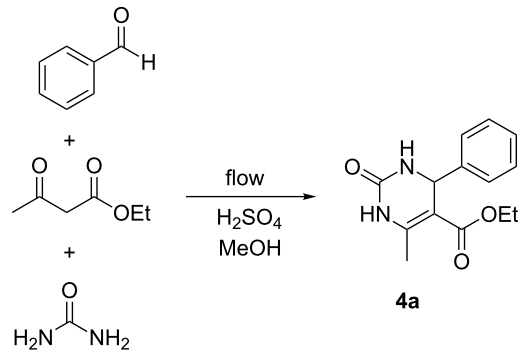

Scheme 4: The Biginelli cyclocondensation of benzaldehyde, ethyl acetoacetate, and urea to yield 5-ethoxycarbonyl-6-methyl-4-phenyl-3,4-dihydropyrimidin-2(1*H*)-one (**4a**).

The calculated Raman spectrum of the product, **4a**, shows a strong signal at 1598 cm^{-1} which was selected for monitoring. Using a catalyst loading of 10 mol % and a flow rate of 1 mL/min, we monitored the reaction over a temperature range from 25–120 °C. Seeing that the reaction did not reach completion within the 10 min in the heated zone, we then repeated the process at lower flow rates; first to 0.5 mL/min and then 0.25 mL/min. Our optimal conditions as determined by Raman monitoring were heating at 120 °C with a flow rate of 0.25 mL/min, this corresponding to a product conversion of

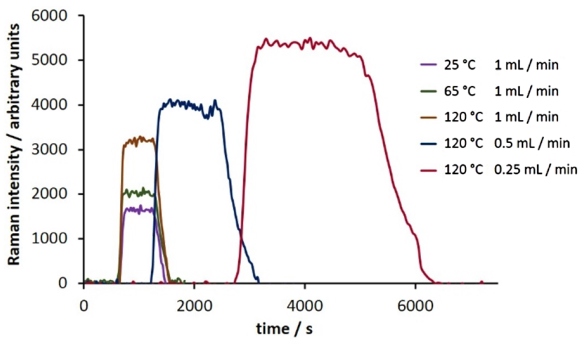

Conditions	Conversion to 4a (%)
25 °C, 1 mL/min	0
65 °C, 1 mL/min	5
130 °C, 1 mL/min	48
130 °C, 0.5 mL/min	62
130 °C, 0.25 mL/min	88

Figure 8: Monitoring the conversion of benzaldehyde, ethyl acetoacetate, and urea to 5-ethoxycarbonyl-6-methyl-4-phenyl-3,4-dihydropyrimidin-2(1*H*)-one (**4a**) across a range of reaction conditions (scan time = 15 s, integration = 10 s).

89%, as determined by GC analysis, and a product yield of 78% after purification. Performing the reaction using three other aldehyde substrates resulted in similar product conversions (Table 4).

Table 4: Product conversion obtained for four aldehyde substrates in the Biginelli reaction with ethyl acetoacetate and urea.

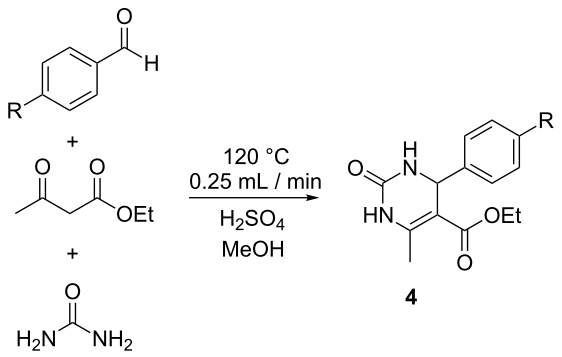

R	Product	Conv. (%)
H	**4a**	88 (78)[a]
OMe	**4b**	85
Me	**4c**	87
F	**4d**	91

[a]Isolated yield.

Conclusion

In conclusion, we describe here an apparatus for real-time Raman monitoring of reactions performed using continuous-flow processing. We assess its capability by studying four reactions. We find that it is possible to monitor reactions and also, by means of a calibration curve, determine product conversion from Raman spectral data as corroborated by data obtained using NMR spectroscopy. Work is now underway to expand the scope of the method to other classes of useful reactions.

Experimental

General experimental

All reagents are used as received from the various vendors without purification. Sodium sulfate, MeOH, EtOH, EtOAc, DMF and Et_2O (ACS Grade and reagent grade), were purchased from Sigma-Aldrich and used without further purification. Deuterated NMR solvents ($CDCl_3$) were purchased from Cambridge Isotope Laboratories. $CDCl_3$ stored over 4Å molecular sieves and K_2CO_3. NMR Spectra (^1H, ^{13}C, ^{19}F) were performed at 298 K on either a Bruker DRX-400 MHz NMR, or Bruker Avance 500 MHz NMR. ^1H NMR Spectra obtained in $CDCl_3$ were referenced to residual non-deuterated chloroform (7.26 ppm) in the deuterated solvent. ^{13}C NMR Spectra obtained in $CDCl_3$ were referenced to chloroform (77.3 ppm). ^{19}F NMR spectra were referenced to hexafluorobenzene (−164.9 ppm) [53]. Reactions were monitored by an Agilent Technologies 7820A Gas Chromatograph attached to a 5975 Mass Spectrometer or ^1H NMR. Flash chromatography and silica plugs utilized Dynamic Adsorbants Inc. Flash Silica Gel (60Å porosity, 32-63 μm).

Apparatus configuration

The Raman system used was an Enwave Optronics Spectrometer, Model EZRaman-L [32]. The continuous-flow unit used was a Vapourtec E-series. A Starna 583.65.65-Q-5/Z20 flow-cell (width: 6.5 mm, height: 20 mm, path length: 5 mm) was placed inline after the back-pressure regulator using 1 mm i.d. PFA tubing (the void volume between the flow reactor and the flow cell was 4.79 mL). The flow cell was secured in place in a custom-made box and the fiber-optic probe from the spectrometer inserted so it touched the wall of the flow cell. During a reaction, spectral data was recorded at pre-determined time intervals using the EZ Raman software provided with the instrument. The data was then exported to Excel for processing.

Typical procedure for monitoring the formation of 3-acetylcoumarin (1)

Performing the reaction: Into a 50 mL volumetric flask was added salicylaldehyde (6.106 g, 50 mmol, 1 equiv) and ethyl acetoacetate (6.507 g, 50 mmol, 1 equiv). Ethyl acetate was added to bring the total volume to 50 mL (1 M) and the reagents were thoroughly mixed. An aliquot of this solution (10 mL) was transferred to a 20 mL vial equipped with a Teflon-coated stir bar. The flow reactor was readied using the equipment manufacturer's suggested start-up sequence. Ethyl acetate was pumped at 1 mL/min to fill the reactor coil. The back-pressure regulator was adjusted to 7 bar and the reactor coil heated to 65 °C. After the heating coil, the product stream was intercepted with a stream of acetone (1 mL/min) by means of a T-piece to ensure complete solubility of the product. The Raman probe was inserted into the box containing the flow cell and was properly focused. A background scan of the ethyl acetate/acetone solvent system was taken. This background was then automatically subtracted from all subsequent scans, thereby removing any signals from the solvent. The Raman spectrometer was set to acquire a spectrum every 15 s throughout the run, with 10 s integration time, boxcar = 3, and average = 1. When the flow unit was ready, piperidine (0.099 mL, 0.1 mmol, 0.1 equiv.) was injected all at once into the vial containing the reagents and, after mixing for 15 s, the reaction mixture was loaded into the reactor at a flow rate of 1 mL/min. After the reaction mixture had been completely loaded into the reactor, ethyl acetate was again pumped through the coil at 1 mL/min. After the product had been fully discharged from the flow cell, the scans were halted. While the product mixture was

passing through the flow cell, a drop of the exit stream was removed and an NMR spectrum recorded to obtain product conversion for comparison with data obtained by Raman spectroscopy. NMR conversions were determined by comparing signals from the starting salicylaldehyde (9.84 ppm) and the coumarin product (8.45 ppm) [36].

Obtaining a relationship between signal strength and concentration: To obtain a calibration curve, spectra of 3-acetylcoumarin in 1:1 ethyl acetate/acetone were recorded at a range of concentrations by passing the solutions through the flow cell. A plot of signal strength due to the peak at 1608 cm^{-1} versus concentration of **1** was constructed (Figure 5). From this, units of Raman intensity could be converted to units of concentration in standard terms and hence product conversion determined.

Typical procedure for monitoring the Knoevenagel reaction

An analogous approach was used to prepare the Knoevenagel product as for the case of **1**, benzaldehyde (5.306 g, 50 mmol, 1 equiv) being used in place of salicylaldehyde and there being no need for acetone interception of the product mixture. The Raman spectrometer was programmed to take continuous scans using the same parameters as in the case of **1**. After the product had been fully discharged from the flow cell, the scans were halted. The resulting clear yellow solution was poured over aqueous 2 M HCl and extracted with ethyl acetate. The combined organic layers were washed with brine, dried over sodium sulfate, and the solvent was removed in vacuo by rotary evaporation affording the crude product. The crude product was loaded on a 15-cm silica gel column (55 g silica gel) and a gradient eluting system (99:1, 95:5, 90:10; Hex:EtOAc) was used to obtain (*Z*)-ethyl 2-benzylidene-3-oxobutanoate (**2a**, 1.3095 g, 60%) as a clear yellow oil. ^{1}H NMR ($CDCl_3$, 400 MHz) δ ppm 1.26 (t, J = 7.21 Hz, 3H), 2.41 (s, 3H), 4.32 (q, J = 7.09 Hz, 2H), 7.33–7.41 (m, 3H), 7.42–7.47 (m, 2H), 7.56 (s, 1H); ^{13}C NMR ($CDCl_3$, 100 MHz) δ ppm 14.08 (CH_3), 26.74 (CH_3), 61.92 (CH_2), 129.06 (CH), 129.74 (CH), 130.93 (CH), 133.17 (C), 134.88 (C), 141.48 (CH), 168.00 (C), 194.87 (C) [54].

Typical procedure for monitoring the Claisen–Schmidt reaction

Into a 50 mL volumetric flask was added 4-fluorobenzaldehyde (1.551 g, 12.5 mmol, 1 equiv) and acetophenone (1.637 g, 12.5 mmol, 1 equiv). Ethanol was added to bring the total volume to 50 mL (0.25 M) and the reagents were thoroughly mixed. An aliquot of this solution (10 mL) was transferred to a 20 mL vial equipped with a Teflon-coated stir bar. The flow reactor was readied using the equipment manufacturer's suggested start-up sequence. Ethanol was pumped at 0.5 mL/min to fill the reactor coil. The back-pressure regulator was adjusted to 7 bar and the reactor coil heated to 65 °C. After the heating coil, the product stream was intercepted with a stream of acetone (0.5 mL/min) by means of a T-piece to ensure complete solubility of the product. The Raman spectrometer was configured as in the case of monitoring formation of **1**. When the flow unit was ready, 2 M NaOH (0.125 mL, 0.25 mmol) was injected all at once and after mixing for 15 s the reaction mixture was loaded into the reactor coil at a flow rate of 0.5 mL/min. After the reaction mixture had been completely loaded into the reactor, ethanol was again pumped through the coil at 0.5 mL/min. After the product had been fully discharged from the flow cell, the scans were halted. The yellow product solution was poured into a beaker containing ice (100 g) causing an immediate precipitation of the product. To ensure complete precipitation, the solution was stirred at 0 °C. The solid product was collected via vacuum filtration and washed with cold ethanol. The material was dried in air to yield (*E*)-3-(4-fluorophenyl)-1-phenylprop-2-en-1-one, (**3d**, 0.5421 g, 91%) as a pale yellow solid. ^{1}H NMR ($CDCl_3$, 400 MHz) δ ppm 7.11 (t, J = 8.68 Hz, 2H), 7.46 (d, J = 15.89 Hz, 1H), 7.49–7.55 (m, 2H), 7.56–7.69 (m, 3H), 7.78 (d, J = 15.65 Hz, 1H), 8.02 (d, J = 7.34 Hz, 2H); ^{13}C NMR ($CDCl_3$, 100 MHz) δ ppm 116.42 (d, $J_{C\text{-}C\text{-}F}$ = 22.01 Hz, CH), 122.09 (d, $J_{C\text{-}C\text{-}C\text{-}C\text{-}F}$ = 2.20 Hz, C), 128.76 (s, 10C), 128.94 (s, 9C), 130.62 (d, $J_{C\text{-}C\text{-}C\text{-}F}$ = 8.80 Hz, CH), 131.45 (d, $J_{C\text{-}C\text{-}C\text{-}C\text{-}C\text{-}F}$ = 3.67 Hz, CH), 133.12 (C), 138.43 (C), 143.78 (CH), 164.35 (d, $J_{C\text{-}F}$ = 250.89 Hz, C), 190.59 (C); ^{19}F NMR ($CDCl_3$, 377 MHz) δ ppm −113.59, −111.32 (m) [55,56].

Typical procedure for monitoring the Biginelli reaction

In a 50 mL volumetric flask was dissolved urea (3.003 g, 50 mmol, 1 equiv.) in methanol (~30 mL). Into the flask was then added benzaldehyde (1.306 g, 50 mmol, 1 equiv) and ethyl acetoacetate (6.507 g, 50 mmol, 1 equiv). Methanol was added to bring the total volume to 50 (1 M) and the reagents were thoroughly mixed. An aliquot of this solution (10 mL) was transferred to a 20 mL vial equipped with a Teflon-coated stir bar. The flow reactor was readied using the equipment manufacturer's suggested start-up sequence. Methanol was pumped at 0.25 mL/min to fill the reactor coil. The back-pressure regulator was adjusted to 7 bar and the reactor coil heated to 120 °C. After the heating coil, the product stream was intercepted with a stream of *N*,*N*-dimethylformamide (0.25 mL/min) by means of a T-piece to ensure complete solubility of the product. The Raman spectrometer was set to acquire a spectrum every 25 s, with 20 s integration time, boxcar = 3, and average = 1. When the flow unit was ready, 6 M H_2SO_4 (0.2 mL, 0.1 equiv) was injected all at once and after mixing for 15 s the reaction mixture was loaded into the reactor coil at a flow rate of

0.25 mL/min. After the reaction mixture had been completely loaded into the reactor, methanol was again pumped through the coil at 0.25 mL/min. After the product had been fully discharged from the flow cell, the scans were halted. The reaction mixture was transferred to a separatory funnel, diluted with diethyl ether and quenched with satd. sodium bicarbonate (100 mL) and deionized water (100 mL). The layers were separated and the aqueous layer was extracted with diethyl ether (3 × 100 mL). The combined organic layers were washed with brine (2 × 100 mL) and dried over sodium sulfate. The solvent was removed in vacuo by rotary evaporation affording the crude product. The resulting solid was transferred to a filter funnel and was washed with cold methanol. The solid was isolated and air dried to afford 5-ethoxycarbonyl-6-methyl-4-phenyl-3,4-dihydropyrimidin-2(1*H*)-one, (**4a**, 2.030 g, 78%) as a fluffy white solid. ^{1}H NMR (DMSO-d_6, 500 MHz) δ ppm 1.18 (s., 3H), 2.34 (s., 3H), 3.67–4.60 (m, 2H), 5.24 (s., 1H), 7.34 (s., 5H), 7.80 (s., 1H), 7.74 (s, 1H), 9.26 (s, 1H); ^{13}C NMR (DMSO-d_6, 125 MHz) δ ppm 14.5 (CH_3), 18.2 (CH_3), 54.4 (CH), 59.6 (CH_2), 99.7 (C), 126.7 (CH), 127.7 (CH), 128.8 (CH), 145.3 (C), 148.8 (C), 152.6 (C), 165.8 (C) [57].

Supporting Information

Supporting Information File 1

NMR spectra of the isolated products (**1**, **2a**, **3d**, **4a**), further experimental information, and pictures of the Raman interface and Cartesian coordinates of the stationary points.
[http://www.beilstein-journals.org/bjoc/content/supplementary/1860-5397-9-215-S1.pdf]

Acknowledgements

Funding from the National Science Foundation (CAREER award CHE-0847262) is acknowledged. Vapourtec Ltd and Enwave Optronics are thanked for equipment support. Daniel Daleb of the University of Connecticut is thanked for his support in the construction of the flow cell apparatus.

References

1. Wiles, C.; Watts, P. *Micro Reaction Technology in Organic Synthesis;* CRC Press: Boca Raton, FL, USA, 2011.
2. Luis, S. V.; Garcia-Verdugo, E., Eds. *Chemical Reactions and Processes under Flow Conditions;* Royal Society of Chemistry: Cambridge, U.K, 2010.
3. Wiles, C.; Watts, P. *Chem. Commun.* **2011,** *47,* 6512–6535. doi:10.1039/c1cc00089f
4. Wegner, J.; Ceylan, S.; Kirschning, A. *Chem. Commun.* **2011,** *47,* 4583–4592. doi:10.1039/c0cc05060a
5. Razzaq, T.; Kappe, C. O. *Chem.–Asian J.* **2010,** *5,* 1274–1289. doi:10.1002/asia.201000010
6. Mark, D.; Haeberle, S.; Roth, G.; von Stetten, F.; Zengerle, R. *Chem. Soc. Rev.* **2010,** *39,* 1153–1182. doi:10.1039/b820557b
7. van den Broek, S. A. M. W.; Leliveld, J. R.; Delville, M. M. E.; Nieuwland, P. J.; Koch, K.; Rutjes, F. L. J. T. *Org. Process Res. Dev.* **2012,** *16,* 934–938. doi:10.1021/op2003437
8. Baxendale, I. R. *J. Chem. Technol. Biotechnol.* **2013,** *88,* 519–552. doi:10.1002/jctb.4012
9. Malet-Sanz, L.; Susanne, F. *J. Med. Chem.* **2012,** *55,* 4062–4098. doi:10.1021/jm2006029
10. McMullen, J. P.; Jensen, K. F. *Annu. Rev. Anal. Chem.* **2010,** *3,* 19–42. doi:10.1146/annurev.anchem.111808.073718
11. Moore, J. S.; Jensen, K. F. *Org. Process Res. Dev.* **2012,** *16,* 1409–1415. doi:10.1021/op300099x
12. Prim, D.; Crelier, S.; Segura, J.-M. *Chimia* **2011,** *65,* 815–816. doi:10.2533/chimia.2011.815
13. Greener, J.; Abbasi, B.; Kumacheva, E. *Lab Chip* **2010,** *10,* 1561–1566. doi:10.1039/c001889a
14. Steinfeldt, N.; Bentrup, U.; Jähnisch, K. *Ind. Eng. Chem. Res.* **2010,** *49,* 72–80. doi:10.1021/ie900726s
15. Floyd, T. M.; Schmidt, M. A.; Jensen, K. F. *Ind. Eng. Chem. Res.* **2005,** *44,* 2351–2358. doi:10.1021/ie049348j
16. Ferstl, W.; Klahn, T.; Schweikert, W.; Billeb, G.; Schwarzer, M.; Loebbecke, S. *Chem. Eng. Technol.* **2007,** *30,* 370–378. doi:10.1002/ceat.200600404
17. Benito-Lopez, F.; Verboom, W.; Kakuta, M.; Gardeniers, J. G. E.; Egberink, R. J. M.; Oosterbroek, E. R.; van den Berg, A.; Reinhoudt, D. N. *Chem. Commun.* **2005,** 2857–2859. doi:10.1039/b500429b
18. Lu, H.; Schmidt, M. A.; Jensen, K. F. *Lab Chip* **2001,** *1,* 22–28. doi:10.1039/b104037p
19. Gökay, O.; Albert, K. *Anal. Bioanal. Chem.* **2012,** *402,* 647–669. doi:10.1007/s00216-011-5419-z
20. Jones, C. J.; Larive, C. K. *Anal. Bioanal. Chem.* **2012,** *402,* 61–68. doi:10.1007/s00216-011-5330-7
21. Mozharov, S.; Nordon, A.; Littlejohn, D.; Wiles, C.; Watts, P.; Dallin, P.; Girkin, J. M. *J. Am. Chem. Soc.* **2011,** *133,* 3601–3608. doi:10.1021/ja1102234
22. Rinke, G.; Ewinger, A.; Kerschbaum, S.; Rinke, M. *Microfluid. Nanofluid.* **2011,** *10,* 145–153. doi:10.1007/s10404-010-0654-8
23. Leung, S. A.; Winkle, R. F.; Wootton, R. C. R.; deMello, A. J. *Analyst* **2005,** *130,* 46–51. doi:10.1039/b412069h
24. Lee, M.; Lee, J.-P.; Rhee, H.; Choo, J.; Chai, Y. G.; Lee, E. K. *J. Raman Spectrosc.* **2003,** *34,* 737–742. doi:10.1002/jrs.1038
25. Fletcher, P. D. I.; Haswell, S. J.; Zhang, X. *Electrophoresis* **2003,** *24,* 3239–3245. doi:10.1002/elps.200305532
26. Browne, D. L.; Wright, S.; Deadman, B. J.; Dunnage, S.; Baxendale, I. R.; Turner, R. M.; Ley, S. V. *Rapid Comm. Mass. Spectrosc.* **2012,** *26,* 1999–2010. doi:10.1002/rcm.6312
27. Koster, S.; Verpoorte, E. *Lab Chip* **2007,** *7,* 1394–1412. doi:10.1039/b709706a
28. Carter, C. F.; Lange, H.; Ley, S. V.; Baxendale, I. R.; Wittkamp, B.; Goode, J. G.; Gaunt, N. L. *Org. Process Res. Dev.* **2010,** *14,* 393–404. doi:10.1021/op900305v
29. Brodmann, T.; Koos, P.; Metzger, A.; Knochel, P.; Ley, S. V. *Org. Process Res. Dev.* **2012,** *16,* 1102–1113. doi:10.1021/op200275d
30. Rueping, M.; Bootwicha, T.; Sugiono, E. *Beilstein J. Org. Chem.* **2012,** *8,* 300–307. doi:10.3762/bjoc.8.32

31. Leadbeater, N. E.; Schmink, J. R.; Hamlin, T. A. In *Microwaves in Organic Synthesis,* 3rd ed.; de la Hoz, A.; Loupy, A., Eds.; Wiley-VCH: Weinheim, Germany, 2012.
32. Leadbeater, N. E.; Schmink, J. R. *Nat. Protoc.* **2008,** *3,* 1–7. doi:10.1038/nprot.2007.453
33. Leadbeater, N. E.; Smith, R. J.; Barnard, T. M. *Org. Biomol. Chem.* **2007,** *5,* 822–825. doi:10.1039/b615597a
34. Leadbeater, N. E.; Smith, R. J. *Org. Lett.* **2006,** *8,* 4589–4591. doi:10.1021/ol061803f
35. Leadbeater, N. E.; Smith, R. J. *Org. Biomol. Chem.* **2007,** *5,* 2770–2774. doi:10.1039/b707692d
36. Schmink, J. R.; Holcomb, J. L.; Leadbeater, N. E. *Chem.–Eur. J.* **2008,** *14,* 9943–9950. doi:10.1002/chem.200801158
37. Schmink, J. R.; Holcomb, J. L.; Leadbeater, N. E. *Org. Lett.* **2009,** *11,* 365–368. doi:10.1021/ol802594s
38. Chaplain, G.; Haswell, S. J.; Fletcher, P. D. I.; Kelly, S. M.; Mansfield, A. *Aust. J. Chem.* **2013,** *66,* 208–212. doi:10.1071/CH12379
39. Kelly, C. B.; Lee, C.; Leadbeater, N. E. *Tetrahedron Lett.* **2011,** *52,* 263–265. doi:10.1016/j.tetlet.2010.11.027
40. *Gaussian 09,* Revision A.02; Gaussian, Inc.: Wallingford CT, , 2009.
41. Batovska, D. I.; Todorova, I. T. *Curr. Clin. Pharmacol.* **2010,** *5,* 1–29. doi:10.2174/157488410790410579
42. Bowman, M. D.; Jacobson, M. M.; Blackwell, H. E. *Org. Lett.* **2006,** *8,* 1645–1648. doi:10.1021/ol0602708
43. Singh, K.; Singh, K. *Adv. Heterocycl. Chem.* **2012,** *105,* 223–308. doi:10.1016/B978-0-12-396530-1.00003-6
44. Panda, S. S.; Khanna, P.; Khanna, L. *Curr. Org. Chem.* **2012,** *16,* 507–520. doi:10.2174/138527212799499859
45. Kappe, C. O. *QSAR Comb. Sci.* **2003,** *22,* 630–645. doi:10.1002/qsar.200320001
46. Mukhopadhyay, C.; Datta, A.; Banik, B. K. *J. Heterocycl. Chem.* **2011,** *44,* 979–981. doi:10.1002/jhet.5570440439
47. Fang, Z.; Lam, Y. *Tetrahedron* **2011,** *67,* 1294–1297. doi:10.1016/j.tet.2010.11.075
48. Dallinger, D.; Kappe, C. O. *Nat. Protoc.* **2007,** *2,* 317–321. doi:10.1038/nprot.2006.436
49. Singh, K.; Arora, D.; Singh, K.; Singh, S. *Mini-Rev. Med. Chem.* **2009,** *9,* 95–106. doi:10.2174/138955709787001686
50. Kappe, C. O. *Eur. J. Med. Chem.* **2000,** *35,* 1043–1052. doi:10.1016/S0223-5234(00)01189-2
51. Pagano, N.; Herath, A.; Cosford, N. D. P. *J. Flow Chem.* **2011,** *1,* 28–31. doi:10.1556/jfchem.2011.00001
52. Prosa, N.; Turgis, R.; Piccardi, R.; Scherrmann, M.-C. *Eur. J. Org. Chem.* **2012,** 2188–2200. doi:10.1002/ejoc.201101726
53. Ravikumar, I.; Saha, S.; Ghosh, P. *Chem. Commun.* **2011,** *47,* 4721–4723. doi:10.1039/c0cc03469j
54. Li, Z.-N.; Chen, X.-L.; Fu, Y.-J.; Wang, W.; Luo, M. *Res. Chem. Intermed.* **2012,** *38,* 25–35. doi:10.1007/s11164-011-0322-y
55. Stroba, A.; Schaeffer, F.; Hindie, V.; Lopez-Garcia, L.; Adrian, I.; Froehner, W.; Hartmann, R. W.; Biondi, R. M.; Engel, M. *J. Med. Chem.* **2009,** *52,* 4683–4693. doi:10.1021/jm9001499
56. Wijnberg, H.; Vries, T. R.; Pouwer, K.; Nieuwenhuijzen, J. 3-Oxopropane-1-sulphonic acids and sulphonates. U.S. Patent 6,639,103, Oct 28, 2003.
57. Xu, D.-Z.; Li, H.; Wang, Y. *Tetrahedron* **2012,** *68,* 7867–7872. doi:10.1016/j.tet.2012.07.027

License and Terms

Beilstein Journal of Organic Chemistry

Continuous flow photocyclization of stilbenes – scalable synthesis of functionalized phenanthrenes and helicenes

Quentin Lefebvre, Marc Jentsch and Magnus Rueping*

Full Research Paper

Open Access

Address:
Institute of Organic Chemistry, RWTH Aachen University, Landoltweg 1, D-52074 Aachen, Germany

Email:
Magnus Rueping* - magnus.rueping@rwth-aachen.de

* Corresponding author

Keywords:
continuous-flow reactor; flow chemistry; helicenes; light-driven cyclization reaction; photocyclization; stilbenes

Beilstein J. Org. Chem. **2013,** *9,* 1883–1890.
doi:10.3762/bjoc.9.221

Received: 12 July 2013
Accepted: 14 August 2013
Published: 17 September 2013

This article is part of the Thematic Series "Chemistry in flow systems III".

Guest Editor: A. Kirschning

Abstract

A continuous flow oxidative photocyclization of stilbene derivatives has been developed which allows the scalable synthesis of backbone functionalized phenanthrenes and helicenes of various sizes in good yields.

Introduction

Phenanthrenes are versatile intermediates toward polycyclic aromatic hydrocarbons which are relevant for materials sciences, as well as toward helicenes, an intriguing class of molecules which show remarkable chiroptical properties due to their helical pitch. The rapidly expanding field of application of helicene-like molecules in materials sciences and optics demands the development of scalable and flexible syntheses [1-5].

Following the pioneering examples of Scholz [6] and Martin [7] in 1967, the photocyclization of stilbene derivatives under UV-light irradiation is now a classical method for the synthesis of phenanthrenes and helicene-like molecules [8]. However, the scalability of these reactions is limited by the required low concentration (~10^{-3} mol·L^{-1}) and usually long reaction times (>20 h). Therefore, most of the applications of this method are limited to small scale (<0.5 mmol), making it unsuitable for gram-scale synthesis of helicene-like molecules [9-12]. Much effort has devoted to the development of alternative pathways toward helicenes, but most approaches require lengthy syntheses of the precursors [13-15]. It should be noted that an elegant semi-one-pot procedure for the synthesis of phenanthrenes from styrenes and benzene was recently reported [16]. However, also in this case, the scale of the reaction is limited by the size of the photoreactor.

Reactions in flow are typically faster and cleaner compared to the corresponding reactions in batch. A flow setup is particu-

larly well-suited for photo-catalysed reactions as the efficiency of the transformation is no longer related to the scale [17-21]. Therefore, the development of an efficient protocol for the photocyclization of stilbene derivatives in flow would be of great interest. A recent contribution described the flow-synthesis of [5]helicene under visible light in the presence of a sensitizer [22], but, to the best of our knowledge, no reports on broadly applicable light-induced oxidative photocyclizations in flow are known. Herein, we report the first photocyclization of polysubstituted olefins using a continuous flow process and discuss advantages and limitations of this new protocol. Generally, the oxidative photodehydrogenation of *E*-stilbene results in the formation of phenanthrene (Scheme 1). In this reaction the *E*-olefin (or a *E*/*Z* mixture of the olefin) is photoisomerised to the reactive *Z*-olefin, which undergoes photocyclization. The corresponding dihydrophenanthene is subsequently oxidized with iodine to give the desired phenanthrene and HI, which can be quenched by propylene oxide or THF.

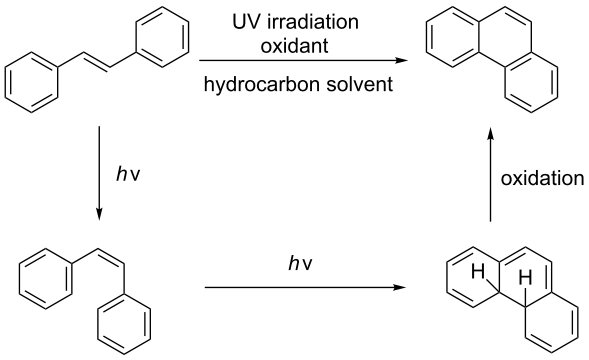

Scheme 1: Photocyclization of stilbene to phenanthrene.

Results and Discussion

In order to accomplish a first general photocyclization we started with the photocyclization of stilbene. Optimization of the reaction conditions in a small flow setup (5 mL FEP tubing, 150 W UV-lamp) is presented in Table 1. Although both THF and propylene oxide showed good ability to quench HI, we choose THF as additive due to its lower cost, volatility and toxicity [23,24]. Under the optimized conditions, *E*-stilbene (**1a**) could be converted to phenanthrene (**2a**) in 95% NMR yield with a retention time of 83 min (Table 1, entry 5).

The flow-reactor setup used for the optimization (Table 1) is shown in Figure 1. UV-transparent ethylene propylene copolymer capillary (FEP, outer/inner diameter 1/0.5 mm, total volume 5 mL) was tightly wrapped around the water-cooling unit (Duran glass) of a high-pressure mercury lamp (TQ 150, UV-Consulting Peschl). Further optimization and scope was performed with a similar setup using a bigger capillary (FEP, outer/inner diameter 4/2 mm, total volume 24 mL). For the sake of safety and to enhance the efficiency of irradiation by reflection, the setup was placed into a laboratory Dewar flask and the exposed parts of the setup were covered with aluminium foil (the temperature inside the Dewar was determined to be around 40 °C). The reaction mixture was injected into the system using a syringe pump and collected at the outlet of the tubing into a round bottom flask.

Table 1: Proof of principle and screening of reaction conditions.

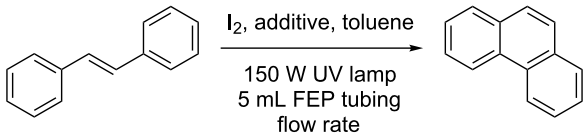

1a (concentration) **2a**

Entry[a]	Additive (20 equiv)	Concentration (mol/L)	Flow rate (mL/min)	Yield[b] (%)
1	propylene oxide	0.01	0.06	33
2	THF	0.01	0.04	37
3	THF	0.01	0.02	44
4	propylene oxide	0.001	0.06	99
5	THF	0.002	0.06	95
6	cyclohexene	0.002	0.06	–[c]
7	THF	0.002	0.08	68
8	THF	0.003	0.06	50

[a]1.1 equiv of iodine were used. The solvent was dry toluene. [b]Determined by ^{1}H NMR using mesitylene as internal standard. [c]Mainly *Z*-stilbene was observed.

Figure 1: Flow-reactor setup used in the optimization study.

Additionally, we developed a 5-fold bigger setup to enhance the throughput (Table 2). Slightly longer retention times were required, and degassed toluene provided better yields. Finally, phenanthrene (**2a**) was obtained in 94% yield when a flow rate of 0.2 mL/min (retention time of 120 min) was applied (Table 2, entry 4).

Table 2: Optimisation of the scale-up setup.

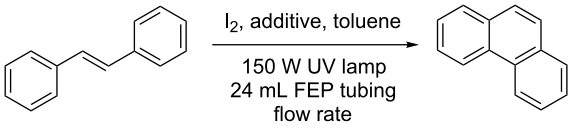

1a (c = 0.002 mol/L) **2a**

Entry[a]	Additive (20 equiv)	Flow rate (mL/min)	Yield[b] (%)
1	propylene oxide	0.2	66
2	THF	0.25	40
3	THF	0.2	85
4[c]	THF	0.2	94

[a]1.1 equiv of iodine were used. Dry toluene was used as solvent.
[b]Determined by ^{1}H NMR using mesitylene as internal standard.
[c]Degassed toluene was used.

With the optimised conditions in hand, we explored the scope of the reaction. Although photocyclization of disubstituted olefins in batch was well documented in the literature, only few cases of photocyclization of tri- and tetrasubstituted olefins were reported [16,25]. Therefore, we decided to demonstrate our methodology on both di- and trisubstituted olefins (Table 3). We disclose here the first photocyclization of trisubstituted olefins in flow, giving access to backbone-functionalised phenanthrene derivatives.

Table 3: Scope of the photocyclization of stilbene derivatives in continuous flow to give substituted phenanthrenes.

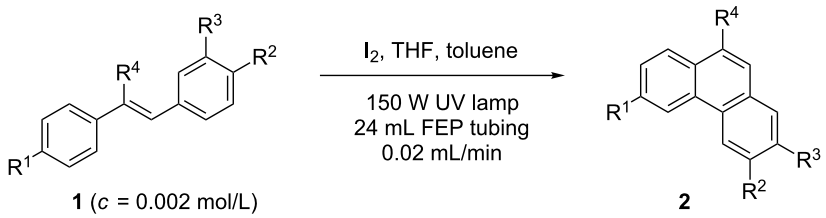

1 (*c* = 0.002 mol/L) **2**

Entry[a]	Substrate	Product (**2**)	Yield[b] (%)
1	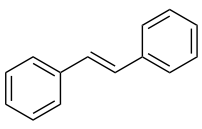	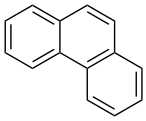 **2a**	64

Table 3: Scope of the photocyclization of stilbene derivatives in continuous flow to give substituted phenanthrenes. (continued)

2	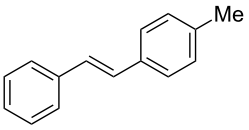	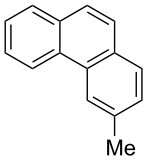 **2b**	64
3	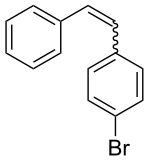	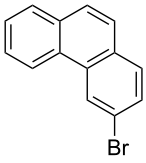 **2c**	61
4	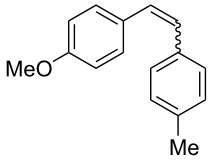	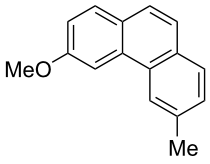 **2d**	77
5	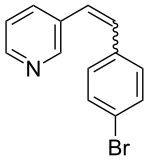	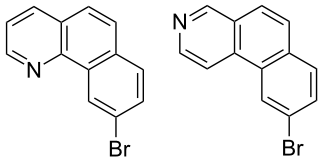 **2e** and **2e'**	31/34
6	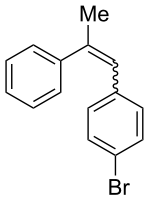	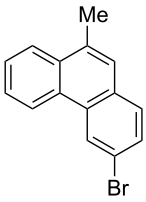 **2f**	77
7	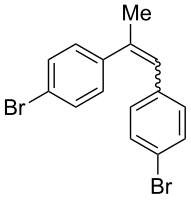	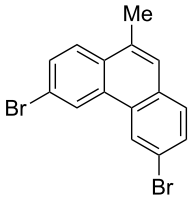 **2g**	89
8	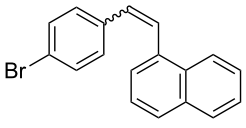	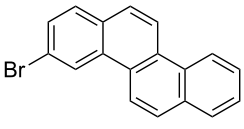 **2h**	64

[a]Reaction conditions: 1.1 equiv iodine, 20 equiv THF, UV-light, 2 h retention time. [b]Yield after chromatography.

We choose stilbenes with bromide and methyl substituents, as the latter can be used in subsequent oxidation, deprotonation, and radical addition reactions, whereas the former opens access to various functional groups via lithium-halogen exchange or cross-coupling chemistry. Methoxy groups were also tolerated, but nitro- and amino groups containing stilbenes showed low conversion or decomposition. Meta-substituted substrates gave inseparable regioisomers, and ortho-substitution led to low conversion. In the case of substrate **1e**, a separable 1:1 mixture of regioisomers **2e** and **2e'** was obtained (Table 3, entry 5).

However, generally a series of stilbenes reacted smoothly to the desired phenantrenes in good yields.

Recently, an unexpected synthesis of [4]helicenes was disclosed [26]. However, no 2-substituted [4]helicenes were synthesised using this method. Therefore, we investigated the photocyclization of the corresponding stilbene derivatives in our flow setup, for both di- and trisubstituted olefins (Table 4).

Again, various functional groups were tolerated in the flow photocyclization. Interestingly, if substrate **1k** was irradiated in toluene a single regioisomer **2k** was isolated (Table 4, entry 3), whereas the reaction in acetonitrile resulted in a separable 1:1 mixture of regioisomers **2k** and **2k'** (Table 4, entry 4).

Finally, we decided to apply our photo-flow methodology in the synthesis of functionalised [5]helicenes and [6]helicenes. We identified 3-acetyl-9,10-dimethoxyphenanthrene [27] as a powerful intermediate for the two-step synthesis of functionalisable helically chiral products. As shown in Scheme 2, Wittig or Horner–Wadsworth–Emmons reactions gave the corresponding olefins **1o–r** in good yields, which were subjected to photocy-

Table 4: Scope: synthesis of [4]helicenes by photocyclization in flow.

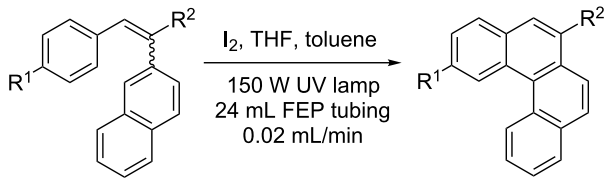

1 (*c* = 0.002 mol/L) **2**

Entry[a]	Substrate	Product (**2**)	Yield[b] (%)
1	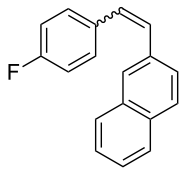	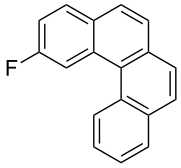 **2i**	85
2	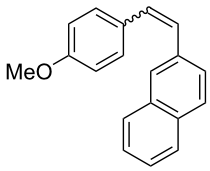	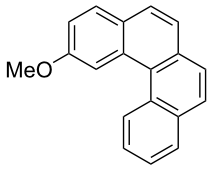 **2j**	75
3	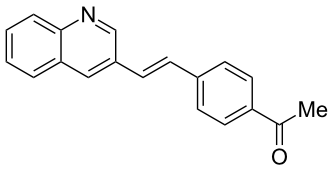	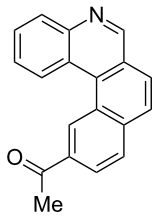 **2k**	74
4[c]	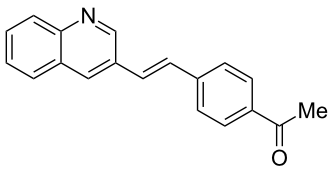	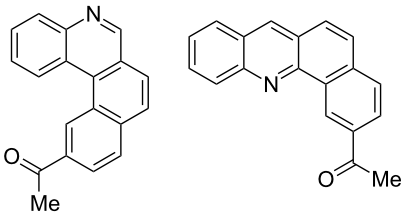 **2k** and **2k'**	40/41

Table 4: Scope: synthesis of [4]helicenes by photocyclization in flow. (continued)

5	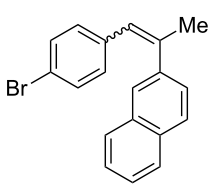	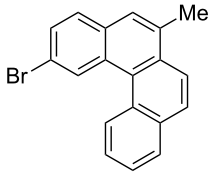 **2l**	75
6	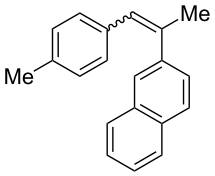	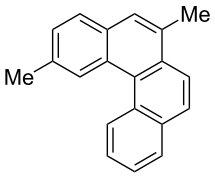 **2m**	73
7	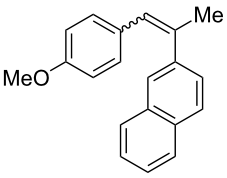	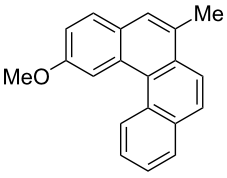 **2n**	99

[a]Reaction conditions: 1.1 equiv iodine, 20 equiv THF, UV-light, 2 h retention time. [b]Yield after chromatography. [c]Reaction was performed in dry, degassed acetonitrile.

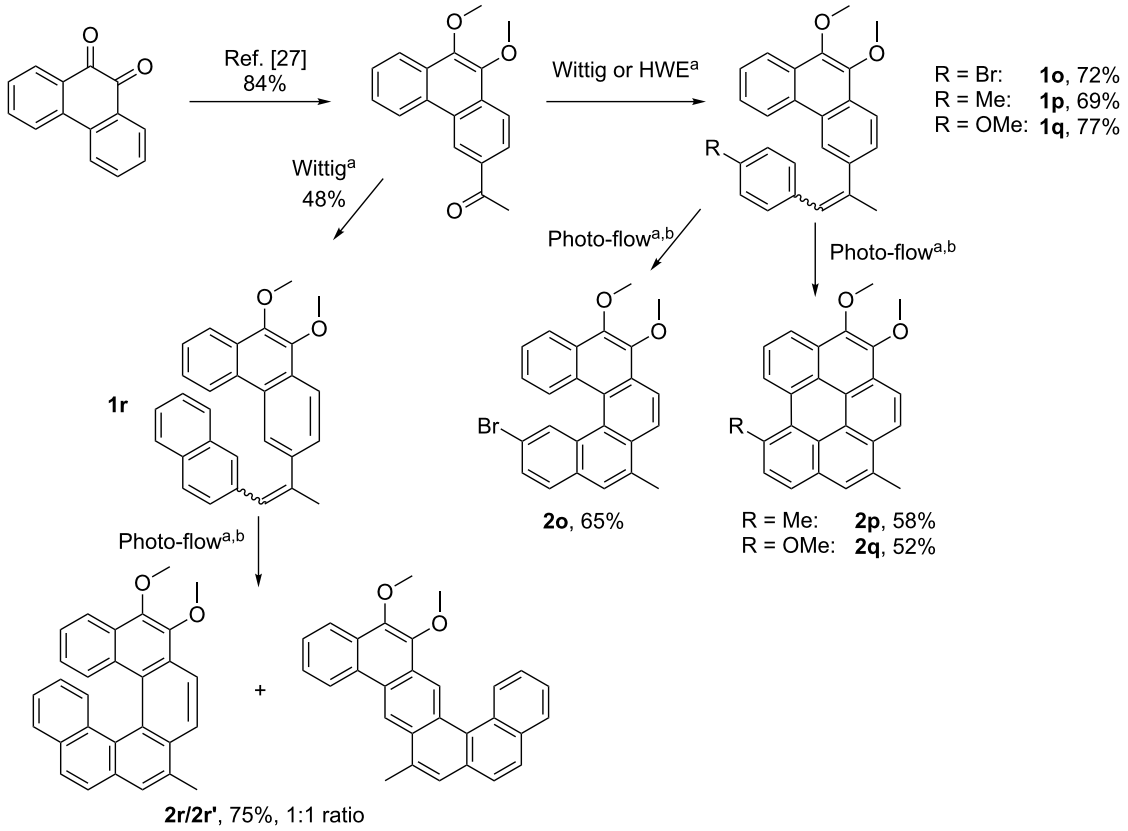

Scheme 2: Photo-flow synthesis of [5]- and [6]helicenes. [a]For experimental details see Supporting Information File 1. [b]Reaction conditions: 1.1 equiv iodine, 20 equiv THF, UV-light, 2 h retention time.

clization in flow using the optimised conditions for the simpler stilbenes. In the [5]helicene series, in each case only one product was isolated in moderate to good yield. The bromoolefin **1o** gave exclusively the desired helicene **2o**, but in the case of methyl- and methoxyolefins **1p** and **1q**, only the corresponding benzo[*ghi*]perylenes **2p** and **2q** were observed. Benzo[*ghi*]perylenes are typical byproducts observed in the photocyclization of [5]helicene-like molecules. Reactions to obtain selectively helicenes or benzo[*ghi*]perylenes, regardless of the substitution pattern, are still a challenging task. A functionalizable [6]helicene (**2r**) was obtained along with its ribbon-like regioisomer **2r'** in a 1:1 ratio and 75% combined yield.

In order to demonstrate the utility of the flow process we decided to scale up the synthesis of helical compound **2o**. To our delight, we observed that the [5]helicene precursor **1o** underwent photocyclization with considerably shorter retention times compared to the standard stilbene derivatives (Scheme 3). Thus, we prepared the [5]helicene derivative **2o** with up to 60 mg/h (for the full optimisation table, see Supporting Information File 1).

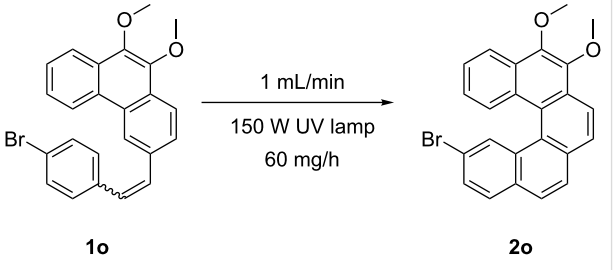

Scheme 3: Scale up synthesis of the [5]helicene derivative **2o**.

Conclusion

In summary, we have developed a new photo-flow methodology [28-32] for the synthesis of phenanthrenes and helicenes. Although photocyclization of stilbene derivatives was disclosed more than 40 years ago, this is the first report of UV-light-driven photocyclization in flow. In general phenantrenes as well as [4]-, [5]- and [6]helicenes with different substitution patterns are obtained in good to excellent yields. In addition our first attempts to scale up the flow photocyclization reactions were successful providing the opportunity for multi-gram syntheses.

Supporting Information

Supporting Information File 1

Experimental part.
[http://www.beilstein-journals.org/bjoc/content/supplementary/1860-5397-9-221-S1.pdf]

References

1. Shen, Y.; Chen, C.-F. *Chem. Rev.* **2012,** *112,* 1463–1535. doi:10.1021/cr200087r
2. Gingras, M. *Chem. Soc. Rev.* **2013,** *42,* 968–1006. doi:10.1039/c2cs35154d
3. Gingras, M.; Félix, G.; Peresutti, R. *Chem. Soc. Rev.* **2013,** *42,* 1007–1050. doi:10.1039/c2cs35111k
4. Gingras, M. *Chem. Soc. Rev.* **2013,** *42,* 1051–1095. doi:10.1039/c2cs35134j
5. Moorthy, J. N.; Mandal, S.; Mukhopadhyay, A.; Samanta, S. *J. Am. Chem. Soc.* **2013,** *135,* 6872–6884. doi:10.1021/ja312027c See for a recent example of application of a carbohelicene in optics.
6. Scholz, M.; Mühlstädt, M.; Dietz, F. *Tetrahedron Lett.* **1967,** *8,* 665–668. doi:10.1016/S0040-4039(00)90569-0
7. Flammang-Barbieux, M.; Nasielski, J.; Martin, R. H. *Tetrahedron Lett.* **1967,** *8,* 743–744. doi:10.1016/S0040-4039(00)90586-0
8. Liu, L.; Yang, B.; Katz, T. J.; Poindexter, M. K. *J. Org. Chem.* **1991,** *56,* 3769–3775. doi:10.1021/jo00012a005
9. Terfort, A.; Görls, H.; Brunner, H. *Synthesis* **1997,** 79–86. doi:10.1055/s-1997-1498
10. Reetz, M. T.; Sostmann, S. *J. Organomet. Chem.* **2000,** *603,* 105–109. doi:10.1016/S0022-328X(00)00173-X
11. El Abed, R.; Ben Hassine, B.; Genêt, J.-P.; Gorsane, M.; Marinetti, A. *Eur. J. Org. Chem.* **2004,** 1517–1522. doi:10.1002/ejoc.200300470
12. El Abed, R.; Aloui, F.; Genêt, J.-P.; Ben Hassine, B.; Marinetti, A. *J. Organomet. Chem.* **2007,** *692,* 1156–1160. doi:10.1016/j.jorganchem.2006.11.022
13. Stará, I. G.; Alexandrová, Z.; Teplý, F.; Sehnal, P.; Starý, I.; Šaman, D.; Buděšínský, M.; Cvaèka, J. *Org. Lett.* **2005,** *7,* 2547–2550. doi:10.1021/ol047311p
14. Míšek, J.; Teplý, F.; Stará, I. G.; Tichý, M.; Šaman, D.; Císařová, I.; Vojtíšek, P.; Starý, I. *Angew. Chem.* **2008,** *120,* 3232–3235. doi:10.1002/ange.200705463 *Angew. Chem., Int. Ed.* **2008,** *47,* 3188–3191. doi:10.1002/anie.200705463
15. Weimar, M.; Correa da Costa, R.; Lee, F.-H.; Fuchter, M. J. *Org. Lett.* **2013,** *15,* 1706–1709. doi:10.1021/ol400493x
16. Li, H.; He, K.-H.; Liu, J.; Wang, B.-Q.; Zhao, K.-Q.; Hu, P.; Shi, Z.-J. *Chem. Commun.* **2012,** *48,* 7028–7030. doi:10.1039/c2cc33100d
17. Matsushita, Y.; Ichimura, T.; Ohba, N.; Kumada, S.; Sakeda, K.; Suzuki, T.; Tanibata, H.; Murata, T. *Pure Appl. Chem.* **2007,** *79,* 1959–1968. doi:10.1351/pac200779111959
18. Oelgemöller, M.; Shvydkiv, O. *Molecules* **2011,** *16,* 7522–7550. doi:10.3390/molecules16097522
19. Knowles, J. P.; Elliott, L. D.; Booker-Milburn, K. I. *Beilstein J. Org. Chem.* **2012,** *8,* 2025–2052. doi:10.3762/bjoc.8.229
20. Oelgemöller, M. *Chem. Eng. Technol.* **2012,** *35,* 1144–1152. doi:10.1002/ceat.201200009
21. Shvydkiv, O.; Oelgemöller, M. Microphotochemistry: Photochemical Synthesis in Microstructed Flow Reactors. In *CRC Handbook of Organic Photochemistry and Photobiology;* Griesbeck, A.; Oelgemöller, M.; Ghetti, F., Eds.; CRC Press: Boca Raton, FL, USA, 2012; pp 125–178.
22. Hernandez-Perez, A. C.; Vlassova, A.; Collins, S. K. *Org. Lett.* **2012,** *14,* 2988–2991. doi:10.1021/ol300983b
23. Talele, H. R.; Gohil, M. J.; Bedekar, A. V. *Bull. Chem. Soc. Jpn.* **2009,** *82,* 1182–1186. doi:10.1246/bcsj.82.1182
24. Talele, H. R.; Chaudhary, A. R.; Patel, P. R.; Bedekar, A. V. *ARKIVOC* **2011,** No. ix, 15–37. doi:10.3998/ark.5550190.0012.902

25. Yavari, K.; Moussa, S.; Ben Hassine, B.; Retailleau, P.; Voituriez, A.; Marinetti, A. *Angew. Chem.* **2012,** *124,* 6852–6856. doi:10.1002/anie.201202024
Angew. Chem., Int. Ed. **2012**, *51*, 6748–6752 doi:10.1002/anie.201202024
26. Truong, T.; Daugulis, O. *Chem. Sci.* **2012,** *4,* 531–535. doi:10.1039/c2sc21288a
27. Wang, D. Z.; Katz, T. J. *J. Org. Chem.* **2005,** *70,* 8497–8502. doi:10.1021/jo0512913
28. Liao, H.-H.; Hsiao, C.-C.; Sugiono, E.; Rueping, M. *Chem. Commun.* **2013,** *49,* 7953–7955. doi:10.1039/c3cc43996h
See for recent applications of flow chemistry from our group.
29. Rueping, M.; Vila, C.; Bootwicha, T. *ACS Catal.* **2013,** *3,* 1676–1680. doi:10.1021/cs400350j
30. Rueping, M.; Bootwicha, T.; Sugiono, E. *Beilstein J. Org. Chem.* **2012,** *8,* 300–307. doi:10.3762/bjoc.8.32
31. Rueping, M.; Bootwicha, T.; Baars, H.; Sugiono, E. *Beilstein J. Org. Chem.* **2011,** *7,* 1680–1687. doi:10.3762/bjoc.7.198
32. Rueping, M.; Bootwicha, T.; Sugiono, E. *Adv. Synth. Catal.* **2010,** *352,* 2961–2965. doi:10.1002/adsc.201000538

License and Terms

Beilstein Journal of Organic Chemistry

One-step synthesis of pyridines and dihydropyridines in a continuous flow microwave reactor

Mark C. Bagley*[1], Vincenzo Fusillo[2], Robert L. Jenkins[2], M. Caterina Lubinu[2] and Christopher Mason[3]

Full Research Paper

Open Access

Address:
[1]Department of Chemistry, School of Life Sciences, University of Sussex, Falmer, Brighton, East Sussex, BN1 9QJ, UK, [2]School of Chemistry, Main Building, Cardiff University, Park Place, Cardiff, CF10 3AT, UK and [3]CEM Microwave Technology Ltd, 2 Middle Slade, Buckingham, MK18 1WA, UK

Email:
Mark C. Bagley* - m.c.bagley@sussex.ac.uk

* Corresponding author

Keywords:
Bohlmann–Rahtz; continuous flow processing; ethynyl ketones; flow chemistry; Hantzsch dihydropyridine synthesis; heterocycles; microwave synthesis; multicomponent reactions; pyridine synthesis

Beilstein J. Org. Chem. **2013,** *9,* 1957–1968.
doi:10.3762/bjoc.9.232

Received: 05 July 2013
Accepted: 11 September 2013
Published: 30 September 2013

This article is part of the Thematic Series "Chemistry in flow systems III".

Guest Editor: A. Kirschning

Abstract

The Bohlmann–Rahtz pyridine synthesis and the Hantzsch dihydropyridine synthesis can be carried out in a microwave flow reactor or using a conductive heating flow platform for the continuous processing of material. In the Bohlmann–Rahtz reaction, the use of a Brønsted acid catalyst allows Michael addition and cyclodehydration to be carried out in a single step without isolation of intermediates to give the corresponding trisubstituted pyridine as a single regioisomer in good yield. Furthermore, 3-substituted propargyl aldehydes undergo Hantzsch dihydropyridine synthesis in preference to Bohlmann–Rahtz reaction in a very high yielding process that is readily transferred to continuous flow processing.

Introduction

Microwave-assisted synthesis has revolutionized many processes in recent years as a valuable alternative to the use of conductive heating for accelerating transformations in synthetic organic chemistry [1], colloidal science [2], natural product chemistry [3], medicinal chemistry [4-6], solid-phase peptide synthesis [7] and in the biosciences [8]. Despite the many advantages of this heating method, and the introduction of a wide range of instrumentation [1], the scale up of microwave-mediated reactions still poses a number of challenges, in particular as a result of a lack of uniform heating [9]. Scale-up using batch methodologies in open reaction vessels can give excellent yields but might not be appropriate for certain volatile or toxic reagents whereas continuous flow processing, providing the reaction mixture is homogeneous, allows transfer

from small-scale sealed vessel conditions to mesoscale production often without any modification of reaction conditions or loss in product yield [10]. The transfer from microwave batch reaction to continuous flow processing can offer many advantages for scale up, certainly in terms of process intensification or in combination with reagent and scavenger cartridges for multi-step synthesis [11], and is possible using conventionally heated micro- or mesofluidic flow devices [12,13], but is also feasible under microwave dielectric heating. Strauss first demonstrated in 1994 that by combining microwave-heating technology with continuous flow processing, problems with the limited penetration depth of microwave irradiation and the physical restrictions of a standing wave cavity could be overcome [14]. A continuous flow reactor has the potential for rapid optimization using minimal quantities of reagents, and for 'scaling out' – the spatial resolution of reactants and products can, in principle, sustain indefinite production [15]. Following Strauss's original report, a variety of transformations have been described using this unique combination of microwave heating and continuous flow or stop-flow processing [16,17]. Continuous flow microwave reactors have been used in transition metal-mediated cross-coupling reactions by Organ et al. in a Pd-coated capillary [18-20], over a solid-supported Pd catalyst using a thin layer of gold as a selective heating element [21], or in a Pd-supported silica monolith flow reactor by Haswell et al. [22], using palladated Raschig rings in a PEEK [poly(ether ether ketone)] reactor by Kirschning et al. [23], in a de novo glass coiled flow cell by researchers at Boehringer Ingelheim [24] and with an encapsulated palladium catalyst by Baxendale and Ley, et al. [25], the latter to process multigram quantities in a microwave-assisted Suzuki–Miyaura coupling. A comparison on the use of palladium(0) nanoparticle catalysts on glass-polymer composite materials in batch and flow-through experiments by Kappe, Kunz and Kirschning revealed that continuous flow processing gave better conversions and improved catalyst recycling, with no loss of activity [26]. A range of other applications have been explored, from a continuous flow isothermal narrow channel microreactor for process intensification of benzyl alcohol oxidation [27], the esterification of benzoic acid in a microwave tubular flow reactor [28], a continuous flow recycle microwave reactor for homogeneous and heterogeneous processes [29], a mesoscale flow reactor utilizing Fe_3O_4 as a microwave absorbing packed reactor bed with internal fibre optic temperature measurement [30], to the continuous flow preparation of biodiesel on large scale [31], processing up to 7.2 L min^{-1}, and waxy ester production on pilot scale using a continuous microwave dry-media reactor [32]. The introduction of proprietary instruments capable of carrying out microwave-assisted transformations under flow processing have greatly expanded the range of chemistries scaled up and evaluated using this technology [1,9,16,33-42]. With all of these developments, it is becoming increasingly clear that flow chemistry, and to some degree microwave flow chemistry, is realizing its potential towards the next evolutionary step in synthetic chemistry [43].

In 2005 we described a new continuous flow reactor design for microwave-assisted synthesis that operates in the optimum standing-wave cavity of a proprietary instrument [44]. The principal features exhibited by this reactor, charged with sand to produce a series of microchannels, included improved performance over a Teflon coil reactor, heated using the same single-mode instrument, and direct measurement of the flow cell temperature using the instrument's in-built IR sensor. In a range of synthetic transformations (Scheme 1), including Bohlmann–Rahtz cyclodehydration of aminodienones **1** to the corresponding pyridines **2** [44,45], Fischer indole synthesis of tetrahydrocarbazole **5** from phenylhydrazine (**3**) and cyclohexanone (**4**) [44], and hydrolysis of 4-chloromethylthiazole (**6**) to give the corresponding alcohol **7** [44], the transfer from batch reactor operation to continuous flow processing was efficient and required little further optimization. Furthermore, we showed that methodology developed using different reaction platforms, including commercial microreactors and stainless steel continuous flow instruments, transfer well to our de novo microwave flow cell and from there can be scaled up using a commercial microwave flow reactor for mesoscale production [45]. The basic design of our microwave flow cell has been adapted by Kappe for the synthesis of dihydropyrimidinone **8** in a 3-component Biginelli reaction and for the preparation of N3-substituted dihydropyrimidinone **10** by Dimroth rearrangement of 1,3-thiazine **9** [46]. In these studies, the 10 mL flow cell was loaded with glass beads and irradiated at 120 or 200 °C, respectively, to give the target heterocycle in yields that compared very favourably with microwave-heated batch experiments. For dihydropyrimidinone **8**, a flow rate of 2 mL min^{-1} delivered a very respectable processing rate of 25 g h^{-1}.

Following the success of this reactor design in delivering pyridine and pyrimidine heterocycles, albeit from very different processes, and the recent advent of new technology for mesoscale microwave-assisted continuous flow reactions [30], we set out to establish if readily-available ethynyl carbonyl precursors were capable of delivering diverse heterocyclic targets under a continuous flow regime under microwave heating. Ley and Baxendale et al. [47] have demonstrated that ethynyl ketones can be generated in flow by the palladium-catalysed acylation of terminal alkynes and further transformed in a continuous process to pyrazoles by cyclocondensation with hydrazines using a commercially available conductive heating modular flow reactor. Given that this cyclocondensation proceeds in a similar fashion and high efficiency under

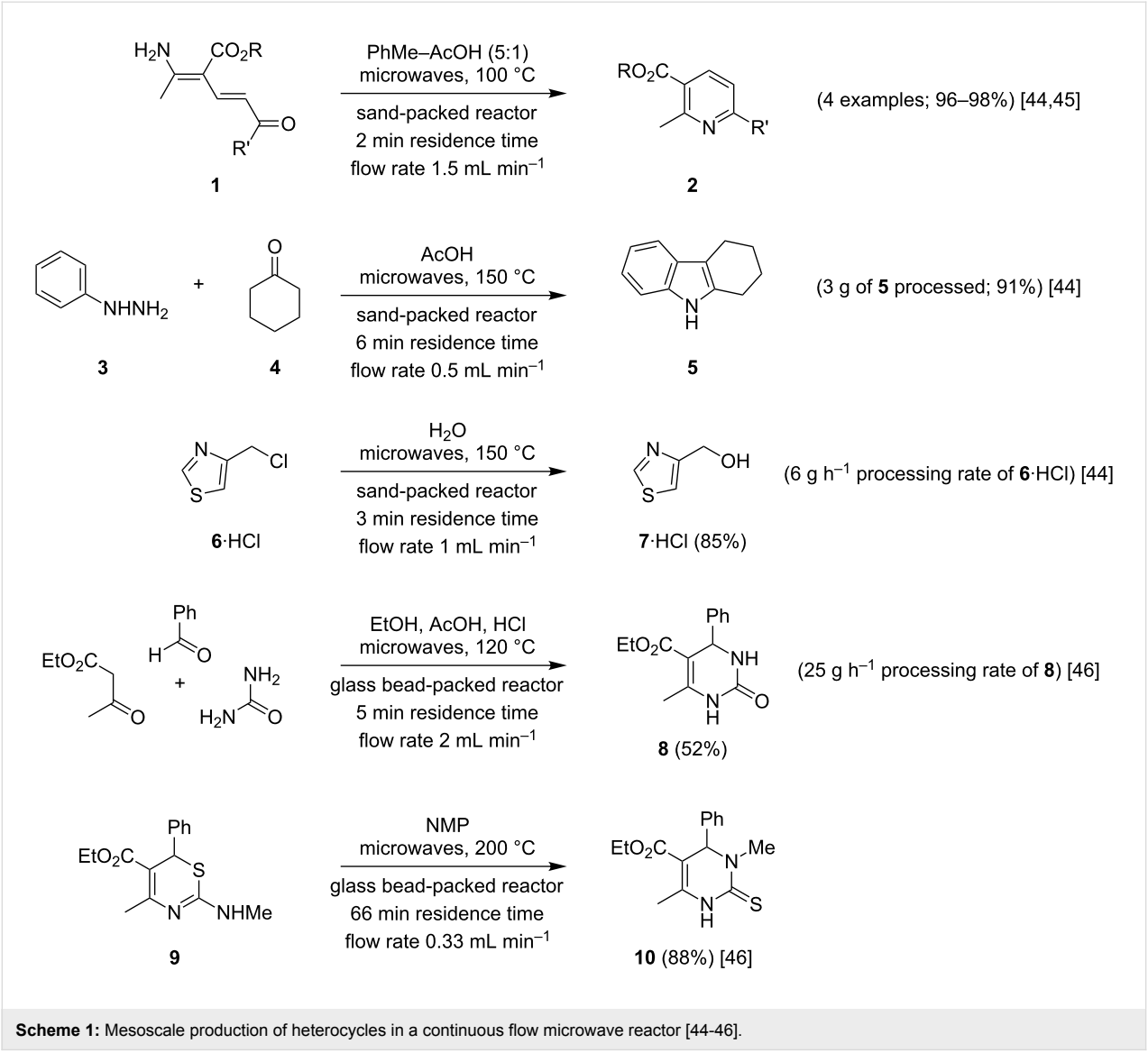

Scheme 1: Mesoscale production of heterocycles in a continuous flow microwave reactor [44-46].

microwave irradiation [48], and that we have previously demonstrated that pyridines and pyrimidines can both be formed rapidly and efficiently from ethynyl ketones using microwave dielectric heating, the transfer of synthetic procedures to a continuous flow processing regime in a microwave flow reactor seemed highly feasible to access pyridine derivatives in a single step.

Results and Discussion

Synthesis of pyridines in a continuous flow reactor

Many of our previous studies on the synthesis of pyridines in a continuous flow reactor examined the cyclodehydration of Bohlmann–Rahtz aminodienone intermediates in the presence of a Brønsted acid catalyst [44,45]. This relatively simple cyclization reaction was utilized previously as we had already established its facility under microwave irradiation and so it provided a good comparison of different technology platforms. If the cyclodehydration could be incorporated into a multi-step process and was spontaneous under the reaction conditions, following Michael addition to ethynyl ketones, then the continuous production of pyridines from readily-available materials could be realized.

Introduction to the Bohlmann–Rahtz pyridine synthesis

Bohlmann and Rahtz first reported the synthesis of trisubstituted pyridines from a stabilized enamine, such as ethyl β-aminocrotonate (**11**), and an ethynyl carbonyl compound, such as butynone (**12a**), in 1957 [49]. In its original form it was a two step procedure involving Michael addition, isolation of the corresponding aminodiene intermediate (e.g. **1a**) and subse-

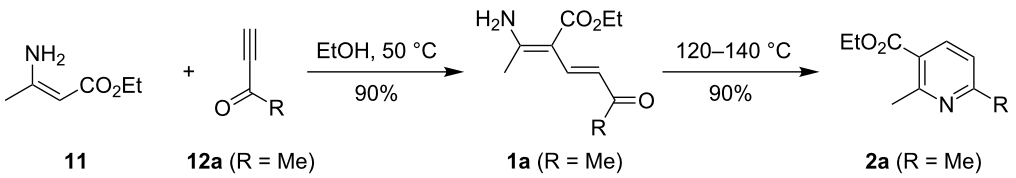

Scheme 2: The original Bohlmann–Rahtz synthesis of pyridines [49].

quent cyclodehydration under high temperature conditions neat under vacuum to give a 2,3,6-trisubstituted pyridine (**2a**: Scheme 2) with total regiocontrol. In recent years there has been renewed interest in this transformation for its application in target synthesis [50], in the development of one-pot procedures for pyridine synthesis [50-58], and for incorporation into domino processes [57-59]. Given our precedent that microwave irradiation can facilitate the one-pot Bohlmann–Rahtz synthesis of pyridines from ethynyl ketones [58-60], this reaction was an ideal starting point to investigate the synthesis of pyridines under a continuous flow regime, from which a comparison to other methods could be drawn.

Bohlmann–Rahtz pyridine synthesis in batch and flow

The reaction conditions, temperature and residence time were optimized in batch mode under microwave irradiation for the one pot synthesis of pyridine **2b** (Scheme 3) using ethyl β-aminocrotonate (**11**) and a readily available ethynyl ketone, phenylpropynone **12b** (R = Ph) [51], in the presence of acetic acid as a Brønsted acid catalyst for transfer to flow processing. A range of conditions were investigated (Table 1) and, in each case, ^{1}H NMR spectroscopic analysis of the crude reaction mixture revealed if unreacted starting materials were present. Microwave irradiation of a 1:1 ratio of starting materials **11** and **12b** at 100 °C for 15 min (hold time) in PhMe–AcOH (5:1 *v*/*v*) and spectroscopic analysis of the crude reaction mixture showed the two-step-in-one synthesis of pyridine **2b** was a success (Table 1, entry 1). Cyclodehydration was spontaneous under the reaction conditions as no aminodienone intermediate **1b**

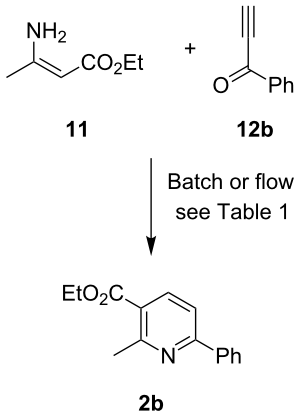

Scheme 3: Bohlmann–Rahtz synthesis of pyridine **2b**.

Table 1: Batch and flow experiments for Bohlmann–Rahtz synthesis of pyridine **2b**.

Entry	Process	Heating	Conditions[a]	Results[b]
1	Batch	Microwaves[c]	PhMe–AcOH, 100 °C, 15 min	**2b**:**12b** ~13:1[d]
2	Batch	Microwaves[c]	PhMe–AcOH, 100 °C, 20 min	**2b**:**12b** >95:5[d]
3	Batch	Microwaves[c]	PhMe–AcOH, 140 °C, 5 min	**2b** (74%)
4	Batch	Microwaves[c]	EtOH–AcOH, 120 °C, 5 min	**2b** (86%)
5	Flow	Microwaves[c]	EtOH–AcOH, 120 °C, 5 min	**2b** (76%)
6	Flow	Conductive[e]	EtOH–AcOH, 120 °C, 5 min	**2b** (86%)
7	Flow	Conductive[e]	EtOH–AcOH, 120 °C, 5 min	**2b** (71%)
8	Batch	Microwaves[f]	EtOH–AcOH, 120 °C, 5 min	**2b**[d] (32%)
9	Batch	Microwaves[f]	EtOH–AcOH, 100 °C, 2.5 min	**2b**[d] (28%)

[a]Reagents (0.3 mmol) were used in a molar ratio (**11**:**12b**) of 1:1 (entry 1) or 1.2:1 (entries 2–7) in PhMe–AcOH or EtOH–AcOH (5:1 *v*/*v*); temperature refers to vessel temperature, maintained by moderation of the initial microwave power (120 W for experiments in PhMe, 90 W for batch experiments in EtOH and 100 W using the flow cell), as measured by the in-built IR sensor (entries 1–5); [b]outcome determined by ^{1}H NMR spectroscopic analysis of the crude reaction mixture; numbers in parentheses refer to the isolated yield of pyridine **2b**; [c]carried out using a commercial CEM single-mode instrument; [d]unreacted starting materials were present; [e]carried out using a commercial Uniqsis FlowSyn stainless steel coil reactor at a flow rate of 1 mL min^{-1} (5 mL reactor; entry 6) [60] or 4 mL min^{-1} (20 mL reactor; entry 7); [f]the scaled up microwave-assisted reaction was carried out in a 60 mL Teflon vessel in batch mode using a commercial Milestone multi-mode instrument in a molar ratio (**1a**:**2b**) of 1.3:1 (15 mmol).

(R = Ph) was observed, although some unreacted propynone remained (**2b**:**12b** ~13:1). The use of a small excess of enamine **11** (1.3 equiv) and extending the reaction time to 20 min, improved the product ratio (Table 1, entry 2). At a higher reaction temperature, consumption of reactants was complete in 5 min on irradiation at 140 °C in PhMe–AcOH (5:1) (Table 1, entry 3) or at 120 °C in EtOH–AcOH (5:1) (Table 1, entry 4), to give pyridine **2b** in 74 or 86% isolated yield, respectively. The use of ethanol as a protic solvent appeared to improve the efficiency of the process, a phenomenon that has also been observed for two-step-in-one Bohlmann–Rahtz reactions [54], in the Michael addition of ethynyl ketones [51], both under conductive heating, and in the tandem oxidation Bohlmann–Rahtz synthesis of nicotinonitriles under microwave irradiation [59]. These batch experiments now established that microwave heating could establish efficient conversion to nicotinoate **2b** in 5 min using only a small excess of enamine **11** and so these parameters (Table 1, entry 4) were favoured for transfer to flow processing over previously reported procedures [58].

Following the success of the microwave batch reaction conditions, the most efficient parameters were transferred to the microwave flow reactor for continuous processing (Figure 1). The Pyrex tube was filled with sand, connected to a back-pressure regulator (100 psi) and primed with solvent at a flow rate of 0.6 mL min^{-1} (for 5 min residence time) using a HPLC pump. Microwave irradiation under continuous flow processing was initiated at an initial power of 100 W, which was modulated to maintain 120 °C vessel temperature as measured by the in-built IR sensor. Once the flow cell temperature stabilized, the solution of the reactants was introduced and the cell was irradiated at 120 °C for 5 min. Once all of the reactants were processed, the flow cell was washed with further batches of solvent and the outflow was quenched in a solution of aqueous $NaHCO_3$. After extraction and purification by column chromatography, pyridine **2b** was isolated as a single regioisomer in 76% yield (Table 1, entry 5) and comparable purity to the successful batch experiments. By carrying out both Michael addition and cyclodehydration in one continuous flow process, pyridine synthesis is possible in a single step from readily available materials, avoiding the need to isolate and purify Bohlmann-Rahtz intermediate **1b** and overcoming issues of its poor solubility, which in past reports have necessitated carrying out the flow process under high dilution conditions [44,45].

With successful transfer of parameters to the microwave flow reactor, flow experiments were investigated with a commercial conductive heating flow reactor (Table 1) using either a 5 mL [60] (Table 1, entry 6) or 20 mL (Table 1, entry 7) stainless steel coil reactor. Both processes gave efficient conversion to pyridine **2b** with small variations noted depending upon the size of the flow cell – the smaller reactor (5 mL) and slower flow rates delivering the highest efficiency (Table 1, entry 6). The isolated yield of the continuous flow process (86%) outperformed the traditional Bohlmann–Rahtz reaction [49] in terms of overall yield (81% over two steps) and step efficiency. Furthermore, the process was comparable in efficiency to previously reported two-step-in-one Bohlmann–Rahtz methods under conductive heating [51], such as heating at 50 °C for 6 h in PhMe–AcOH (85% yield) or heating at reflux in PhMe for 5.5 h in the presence of zinc(II) bromide (15 mol %) (86% yield), and provides improvements in reaction kinetics and processing rate.

Finally the improved performance of flow processing in this transformation was validated by a larger scale (15 mmol) microwave-assisted batch reaction in a 60 mL Teflon vessel using a commercial multi-mode instrument (Table 1, entries 8 and 9). Irradiation at 120 °C for 5 min (Table 1, entry 8), in this case as measured by thermocouple, gave multiple components by tlc analysis and provided pyridine **2b** in poor isolated yield

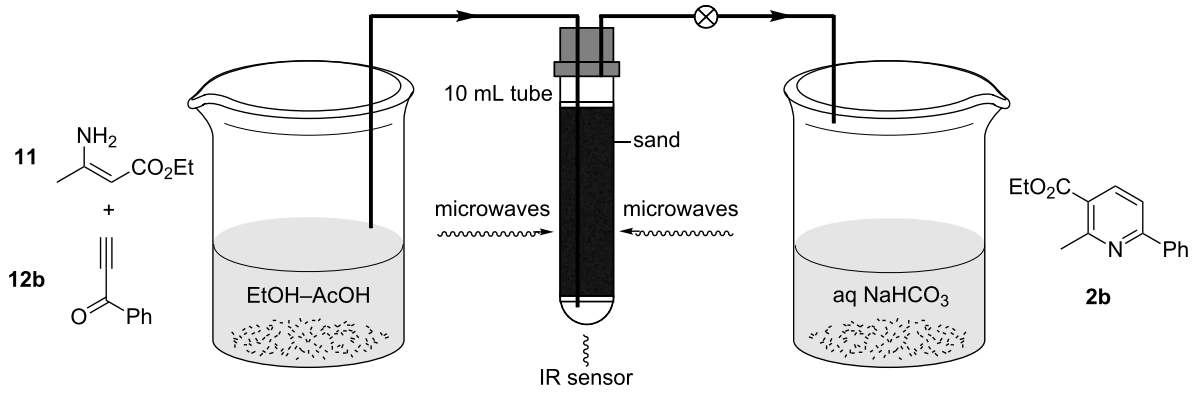

Figure 1: Microwave flow reactor for the Bohlmann–Rahtz synthesis of pyridine **2b**.

(32%) although did allow rapid access to gram quantities of material. In case a lack of homogeneity in heating had caused additional decomposition, the experiment was repeated over a shorter reaction time at a slightly lower temperature (Table 1, entry 9) but this caused no improvement in outcome (28% yield). Difficulties in scaling up a microwave-assisted batch reaction had been noted previously for the Bohlmann–Rahtz cyclodehydration [45]; in that case the use of a 60 mL vessel (1.9 mmol of **1b**) in a multi-mode instrument had proved highly efficient (96%) under similar conditions. However, transfer to a 100 mL vessel (7.7 mmol of **1b**) had caused a considerable decrease in efficiency (65%). For the two-step-in-one Bohlmann–Rahtz reaction these difficulties seemed to be even more pronounced: given the poor yield of the two processes (Table 1, entries 8 and 9), these difficulties were attributed to low efficiency in the initial Michael addition. For this multistep process, reaction parameters did not transfer well between single-mode 10 mL and multi-mode 60 mL reactors and this justified the use of continuous flow processing for efficient mesoscale production. It is evident that the reliability of scaling a microwave batch reaction is highly dependent upon the nature of the transformation and even small changes in the process in question can cause unexpected problems, which require further optimization of parameters to resolve. From these considerations, we conclude that the most reliable means to scale to gram production from mg scale in a microwave-assisted batch reaction using 10 mL sealed vessels is through continuous flow processing, using either microwave dielectric heating or conductive heating, which in this case gave comparable results.

Synthesis of dihydropyridines in a continuous flow reactor

Introduction to Hantzsch dihydropyridines

The Hantzsch dihydropyridine (DHP) synthesis, first discovered in 1881 [61,62], is a well-studied multicomponent reaction, that provides structures with well-catalogued clinical properties for the treatment of cardiovascular disease, thrombosis and atherogenesis [63-66]. The 4-component process has been carried out under high temperature conditions in an autoclave [67] and under microwave irradiation [10,68-72]. Furthermore, this reaction has been studied in a conductive heating Uniqsis FlowSyn reactor [71,73] and its comparison with microwave heating batch experiments showed that the energy efficiency of these technology platforms vary with scale, but broadly are comparable [73]. Furthermore, recently a bespoke microwave reactor with a glass containment cell has been used under continuous flow processing for 4-component Hantzsch DHP synthesis in good yield [74]. Given this precedent and our own previous studies on the use of microwave irradiation in a single-mode instrument to promote 4-component DHP synthesis [70], this reaction seemed ideal to expand the scope of the microwave flow cell. Mechanistically, there was evidence to support the hypothesis that the 4-component Hantzsch reaction [64] proceeds in a similar course to the Bohlmann–Rahtz pyridine synthesis [50], by Michael addition followed by cyclodehydration, and so it was reasonable to assume that similar conditions should enable the flow processing of material, provided that reactants and products were homogeneous in the solvent of choice, thus providing further comparative studies on the transfer of parameters between different platforms.

Hantzsch dihydropyridine synthesis in batch and flow

Previous methods for carrying out the microwave-assisted batch reaction were first consolidated by setting up a series of reactions that were purified in a consistent fashion. A solution containing an excess of ethyl acetoacetate (**13**), aqueous ammonia as the ammonia source, and either benzaldehyde (**14a**) or propionaldehyde (**14b**) (Scheme 4) was irradiated at 140 °C for 10 min in EtOH–H_2O (1:1 *v*/*v*) in a modification of the Leadbeater conditions [73] (Table 2, entries 1 and 2). The outcome was compared with a repeat of our previously established conditions [70], based upon Westman's report [68], in EtOH (Table 2, entries 3 and 4), in all cases purifying by flash chromatography on silica. For the synthesis of phenyl-**15a** (70% yield) and ethyl-DHP **15b** (87% yield) on 2.5 mmol scale these experiments indicated that the ideal solvent for this process was EtOH rather than EtOH–H_2O (1:1 *v*/*v*). Reducing the molar equivalents of acetoacetate **13** from 5 to 3.4 (the stoichiometry used by Leadbeater [73]) caused a significant reduction in the

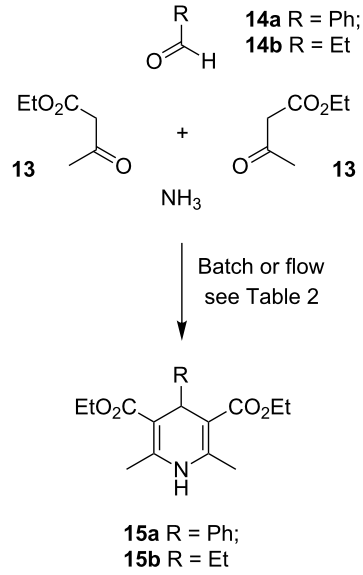

Scheme 4: Four-component synthesis of Hantzsch DHP **15a**,**b**.

Table 2: Batch and flow experiments for 4-component Hantzsch DHP **15** synthesis.

Entry	Process	Heating	Reagents and conditions[a]	**15**	Yield[b]
1	Batch	Microwaves[c]	**14a** (1 equiv), **13** (5 equiv), NH_4OH (4 equiv.), EtOH–H_2O, 140 °C, 10 min	**15a**	41%
2	Batch	Microwaves[c]	**14b** (1 equiv), **13** (5 equiv), NH_4OH (4 equiv.), EtOH–H_2O, 140 °C, 10 min	**15b**	67%
3	Batch	Microwaves[c]	**14a** (1 equiv), **13** (5 equiv), NH_4OH (4 equiv.), EtOH, 140 °C, 10 min	**15a**	70%
4	Batch	Microwaves[c]	**14b** (1 equiv), **13** (5 equiv), NH_4OH (4 equiv), EtOH, 140 °C, 10 min	**15b**	82%
5	Batch	Microwaves[c]	**14a** (1 equiv), **13** (3.4 equiv), NH_4OH (4 equiv), EtOH–H_2O, 140 °C, 10 min	**15a**	35%
6	Batch	Microwaves[c]	**14b** (1 equiv), **13** (3.4 equiv), NH_4OH (4 equiv), EtOH–H_2O, 140 °C, 10 min	**15b**	46%
7	Batch	Microwaves[c]	**14a** (1 equiv), **13** (2 equiv), NH_4OAc (3 equiv), EtOH–AcOH, 140 °C, 10 min	**15a**	43%
8	Batch	Microwaves[c]	**14b** (1 equiv), **13** (3.4 equiv), NH_4OAc (6 equiv), EtOH–AcOH, 140 °C, 10 min	**15b**	28%
9	Flow	Conductive[e]	**14a** (1 equiv), **13** (5 equiv), NH_4OH (4 equiv), EtOH, 140 °C, 10 min [71]	**15a**	43%
10	Flow	Conductive[e]	**14a** (1 equiv), **13** (5 equiv), NH_4OH (4 equiv), EtOH, 120 °C, 30 min	**15a**	35%
11	Flow	Conductive[e]	**14b** (1 equiv), **13** (5 equiv), NH_4OH (4 equiv), EtOH, 120 °C, 30 min	**15b**	34%
12	Flow	Conductive[e]	**14b** (1 equiv), **13** (5 equiv), NH_4OH (4 equiv), EtOH, 140 °C, 7.5 min	**15b**	39%
13	Flow	Conductive[e]	**14b** (1 equiv), **13** (5 equiv), NH_4OH (4 equiv), EtOH, 140 °C, 10 min	**15b**	68%

[a]Temperature refers to vessel temperature, maintained by moderation of the initial microwave power, as measured by the in-built IR sensor (entries 1–5); [b]isolated yield of DHP **15** after purification by column chromatography on silica, eluting with EtOAc–light petroleum; [c]carried out using a commercial CEM single-mode instrument at an initial power of 150 W; [d]unreacted starting materials were present; [e]carried out using a commercial Uniqsis FlowSyn stainless steel coil reactor (5 mL) at a flow rate of 0.5 mL min^{-1}.

yield for both reactions (Table 2, entries 5 and 6) and so did justify the use of such a considerable excess of this precursor. Similar observations on the ideal reagent stoichiometry have been made by Öhberg and Westman [68] in sealed tube microwave reactions and our yields were broadly comparable although higher than our previous report which included an additional purification step [70] (e.g. 70% (Table 2, entry 3) vs 84% [67] or 47% [70]). The use of NH_4OAc as ammonia source in EtOH–AcOH, under similar conditions to a 3-component Bohlmann–Rahtz reaction [54], failed to improve the efficiency of the process (Table 2, entries 7 and 8) and so, given the high yield and short reaction times of the Westman conditions (Table 2, entries 3 and 4), and the Leadbeater precedent [73], it was felt that this process was suitable for direct transfer to continuous flow processing under conductive heating to examine if this offered any improvement over Leadbeater's established flow chemistry protocol. Thus, a solution of NH_4OH, as the ammonia source, aldehyde **14a** and acetoacetate **13** (5 equiv) in EtOH was heated at 140 °C in a 5 mL stainless steel coil for a residence time of 10 min (Table 2, entry 9); the outflow was quenched in H_2O, extracted and purified using column chromatography [71]. Although the isolated yield of DHP **15a** was lower, in relation to the corresponding batch process, the continuous flow process was a success. Further optimization, by lowering the flow rate and decreasing the reaction time (Table 2, entries 10 and 11), caused a small reduction in the yield of both DHP **15a** and **15b**, which was improved little by increasing the flow rate and thus decreasing the residence time (Table 2, entry 12). However, returning to the original conditions (Table 2, entry 13) delivered a good yield of DHP **15b** (68%) under flow processing. Comparing the optimum conditions under continuous flow processing for this reaction, i.e. NH_4OH/EtOH/140 °C/10 min, with Leadbeater's process [73] for this transformation (43% yield vs 53% conversion), it was apparent that the small reduction in efficiency we had observed was reasonably well justified: the change in solvent had prevented problems with in-line precipitation and so greatly simplified the processing protocol. However, the transfer to a continuous flow regime had caused a significant reduction in yield with respect to our microwave batch reaction (Table 2, entry 3; 70% yield) and was considerably lower than the batch microwave process reported by Leadbeater on 0.5 mol scale under open vessel conditions, which delivered an outstanding yield of **15a** (96%) [10], so further experiments to improve the continuous flow processing of Hantzsch dihydropyridines were considered.

In an effort to improve the flow process further, a 3-component process was investigated. In this transformation, the use of an ammonia source was no longer necessary and instead acetoacetate **13** was replaced with ethyl β-aminocrotonate (**11**) (Scheme 5). Removing the need to generate the enamine in situ should improve the efficiency of the process and it was thought could lead to better transfer of reaction parameters between batch and flow platforms. The use of propynal **14c** would further expand the scope of this reaction and establish if 3-substituted propargyl aldehydes would undergo Hantzsch DHP **15c** synthesis or participate instead in a tandem Michael addition–cyclodehydration reaction, in accordance with the original Bohlmann–Rahtz report (which had used propynal), to

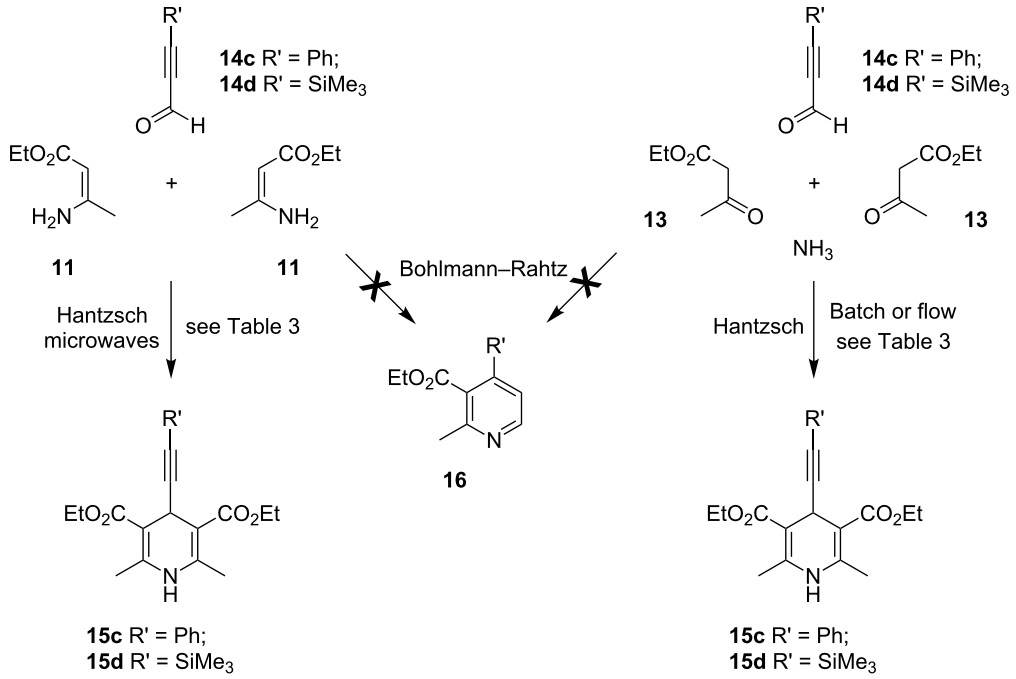

Scheme 5: Three- or four-component synthesis of Hantzsch DHP **15c,d**.

give trisubstituted pyridines **16** [49]. Returning to the microwave batch reactor, a solution of phenylpropargyl aldehyde (**14c**) and enamine **11** (2 equiv) in PhMe–AcOH (Table 3, entry 1) or EtOH–AcOH (5:1) was irradiated at 100 °C for 1 min, cooled and then extracted and purified as before to give DHP **15c** in a remarkable 98 or >98% yield, respectively. Clearly, using stoichiometry appropriate for Hantzsch DHP synthesis, this process was totally selective over Bohlmann–Rahtz pyridine synthesis and no 2,3,4-trisubstituted pyridine **16** was formed (Scheme 5). This supported earlier findings [49] by Bohlmann and Rahtz and highlights a reactivity trend of 3-substituted propargyl aldehydes in reaction with enamines. A comparable process in EtOH in the absence of AcOH failed to provide complete conversion (Table 3, entry 3), whereas the reagents were only poorly soluble in AcOH alone and so the effect of change in solvent was not pursued further. To try and

Table 3: Synthesis of Hantzsch DHP **15c,d** from propargyl aldehydes **14c,d** in batch and flow.

Entry	Process	Heating	Reagents and conditions[a]	15	Yield[b]
1	Batch	Microwaves[c]	**14c** (1 equiv), **11** (2 equiv), PhMe–AcOH, 100 °C, 1 min	**15c**	98%
2	Batch	Microwaves[c]	**14c** (1 equiv), **11** (2 equiv), EtOH–AcOH, 100 °C, 1 min	**15c**	>98%
3	Batch	Microwaves[c]	**14c** (1 equiv), **11** (2 equiv), EtOH, 120 °C, 15 min	**15c**	–[d]
4	Batch	Microwaves[c]	**14c** (1 equiv), **13** (2 equiv), NH_4OAc (3 equiv), EtOH–AcOH, 120 °C, 5 min	**15c**	96%
5	Batch	Microwaves[c]	**14d** (1 equiv), **11** (2 equiv), EtOH–AcOH, 100 °C, 1 min	**15d**	82%
6	Batch	Microwaves[c]	**14d** (1 equiv), **13** (2 equiv), NH_4OAc (3 equiv), EtOH–AcOH, 120 °C, 5 min	**15d**	84%
7	Flow[e]	Microwaves[c]	**14d** (1 equiv), **13** (2 equiv), NH_4OAc (3 equiv), PhMe–AcOH, 120 °C, 5 min	**15d**	–[f]
8	Flow[e]	Microwaves[c]	**14c** (1 equiv), **13** (2 equiv), NH_4OAc (3 equiv), EtOH–AcOH, 120 °C, 5 min	**15c**	70%
9	Flow[e]	Microwaves[c]	**14c** (1 equiv), **13** (2 equiv), NH_4OAc (3 equiv), EtOH–AcOH, 120 °C, 5 min	**15c**	85%[g]

[a]Temperature refers to vessel temperature, maintained by moderation of the initial microwave power, as measured by the in-built IR sensor; [b]isolated yield of DHP **15** after quenching in H_2O and extraction (entries 1–8); [c]carried out using a commercial CEM single-mode instrument at an initial power of 70 W (entries 1–3 and 5), 90 W (entries 4 and 6), 200 W (entry 7) or 100 W (entries 8 and 9); [d]unreacted starting materials were present; [e]carried out using the microwave flow reactor (10 mL) filled with sand at a flow rate of 0.6 mL min^{-1}; [f]heterogeneity in the solvent system caused pump failure; [g]isolated yield after quenching in aqueous $NaHCO_3$ solution and filtering the precipitated solid.

identify which component, aldehyde or acetoacetate, had been responsible for the dramatic improvement in yield, a 4-component Hantzsch reaction was also investigated (Table 3, entry 4). Irradiating a solution of propargyl aldehyde **14c**, acetoacetate **13** (2 equiv) and NH_4OAc (3 equiv) in EtOH–AcOH (5:1) at 120 °C for 5 min gave DHP **15c** in 96% isolated yield. Investigating an alternative propargyl aldehyde, the 3- or 4-component batch syntheses of DHP **15d** using 3-(trimethylsilyl)propynal (**14d**), similarly, gave excellent yields of the product under microwave irradiation (Table 3, entries 5 and 6). Thus, it was concluded that 3-substituted propargyl aldehydes are highly reactive and useful substrates for Hantzsch DHP synthesis and give little or no competing formation of the corresponding Bohlmann–Rahtz pyridine **16** under conditions that nominally can promote both processes.

With the batch methods established, a 4-component reaction using a propargyl aldehyde was transferred to the microwave flow reactor with minimal change in reaction parameters. The flow cell was primed with the solvent of choice and heated under microwave irradiation; once the temperature of the reactor stabilized, the reaction mixture was introduced. Using 3-(trimethylsilyl)propynal (**14d**) in PhMe–AcOH resulted in pump failure, due to the heterogeneity of the reagent flow in this reaction solvent (Table 3, entry 7). Switching to the use of phenylpropargyl aldehyde (**14c**) and changing the solvent system to EtOH–AcOH produced a homogeneous reagent flow and allowed the reaction mixture to be processed at 120 °C at a continuous flow rate of 0.5 mL min^{-1} through the microwave reactor. After passing through the back-pressure regulator, the outflow was quenched in H_2O and extracted (Table 3, entry 8) or quenched in aqueous $NaHCO_3$ solution and filtered (Table 3, entry 9) to give the 4-(phenylethynyl)-DHP **15c** in 70 or 85% yield, respectively. Although the yields of both flow reactions were slightly lower than their batch mode counterparts, (96% batch yield vs 85% yield under flow processing for the synthesis of **15c**) the continuous processing of Hantzsch DHPs had been realized.

Reviewing all of our methods for the microwave-assisted preparation of DHP derivatives, the isolated yield for the batch synthesis of Hantzsch DHP **15c** (96%) compares very favourably to other microwave-assisted 4-component Hantzsch reactions (cf. 81% yield of a DHP under flow processing [74], 51–92% yield [67] or 84–99% yield [72] of a range of derivatives in batch using a single-mode instrument, and 96% yield of **15a** under open vessel batch conditions on 0.5 mol scale [10]) and transfers well to flow processing giving 85% yield under microwave irradiation (cf. 81% [74]). Given the excellent performance of microwave dielectric heating in promoting the 4-component Hantzsch reaction with direct scalability under microwave irradiation [10] and under continuous flow processing, observed by ourselves and others [73,74], this technology stands out as the heating method of choice for the preparation of 1,4-DHP derivatives.

Conclusion

These studies have demonstrated that a microwave flow reactor can be used for the one-step preparation of pyridines and dihydropyridines using the Bohlmann–Rahtz reaction or Hantzsch multicomponent reaction, respectively. Bohlmann–Rahtz pyridine synthesis under continuous flow processing in the presence of a Brønsted acid catalyst allows Michael addition and cyclodehydration to be carried out in one step without the isolation of intermediates to give a trisubstituted pyridine as a single regioisomer. Furthermore, the use of microwave heating for facilitating this two-step-in-one transformation is well justified, compares favourably with the traditional two-step procedure and, using these protocols, delivers Bohlmann–Rahtz pyridines quickly and efficiently. In batch mode using a single-mode instrument this process is highly predictable and is most reliably scaled up using continuous flow processing, either on a conductive heating platform or using a microwave flow reactor in favour over a multimode batch reactor. On the other hand, the scale up of a microwave-assisted Hantzsch DHP synthesis under open-vessel conditions as described by Leadbeater [10] outperforms even the small-scale microwave-assisted batch reaction, but the use of continuous flow processing in a microwave reactor as shown by ourselves and others [74] can deliver the target heterocycle in excellent yield. For both Hantzsch and Bohlmann–Rahtz reactions, parameters transferred very well from high temperature batch conditions in a sealed vessel to continuous flow processing through a microwave flow cell in a single-mode cavity. In some cases, it was possible to further transfer parameters between conductive heating and microwave heated flow platforms, with only minor variations in yield. Furthermore, it has been affirmed that 3-substituted propargyl aldehydes are not suitable substrates for the Bohlmann–Rahtz reaction and instead undergo Hantzsch dihydropyridine synthesis in very high yield in a process that is readily transferred to continuous flow processing in a microwave flow cell. Although this sets a new challenge on how to access 2,3,4-trisubstituted pyridines using Bohlmann–Rahtz methods, a transformation which currently cannot be realized, it does provide a useful substrate for 3- or 4-component Hantzsch DHP synthesis that undergoes cyclocondensation with high efficiency. To conclude, continuous flow microwave-assisted reactions represent a reliable method to scale up the production of pyridine derivatives and, for the Bohlmann–Rahtz pyridine synthesis, give improved performance over a comparable large scale multimode batch experiment. This expands the growing set of heterocyclic targets that

have been accessed by the reactions of ethynyl ketones under continuous flow processing and sets the stage for their future incorporation into automated multistep processes.

Experimental

Diethyl 4-(trimethylsilylethynyl)-2,6-dimethyl-1,4-dihydropyridine-3,5-dicarboxylate (**15d**)

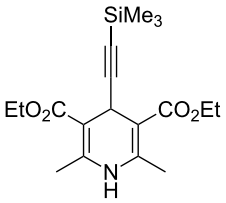

3-Component Hantzsch DHP synthesis in a single-mode microwave batch reactor (Table 3, entry 5). A mixture of 3-(trimethylsilyl)propynal (**14d**, 50 mg, 0.53 mmol) and ethyl β-aminocrotonate (**11**, 0.14 g, 1.1 mmol) in PhMe–glacial acetic acid (5:1, 2 mL) was irradiated at 100 °C for 1 min in a sealed tube using a CEM Discover microwave synthesizer at an initial power of 70 W. The reaction mixture was cooled in a stream of compressed air and partitioned between saturated aqueous $NaHCO_3$ solution (25 mL) and EtOAc (25 mL). The aqueous layer was further extracted with EtOAc (2 × 15 mL) and the combined organic extracts were washed with brine (15 mL), dried ($NaSO_4$) and evaporated in vacuo to give the title compound (0.15 g, 82%) as a yellow solid, mp 137–138 °C (aq EtOH); (Found: $[M + H]^+$, 350.1783. $C_{18}H_{27}NO_4Si$, $[M + H]$ requires 350.1782); R_f 0.47 (light petroleum–EtOAc, 1:1); IR (nujol)/cm^{-1}: 3302, 3244, 3107, 1699, 1661, 1636, 1503, 1328, 1301, 1208, 1120, 1095, 1026, 840; ^{1}H NMR (400 MHz, $CDCl_3$) δ 5.69 (br s, 1H, NH), 4.72 (s, 1H, 4-H), 4.11 (m, 2H, OC*H*HCH$_3$), 4.08 (m, 2H, OCH*H*CH$_3$), 2.20 (s, 6H, 2,6-CH$_3$), 1.21 (t, *J* 7.1, 6H, OCH$_2$C*H*$_3$), 0.00 (s, 9H, SiMe$_3$); ^{13}C NMR (100 MHz, $CDCl_3$) δ 167.0 (C), 144.9 (C), 109.8 (C), 100.2 (C), 82.5 (C), 59.8 (CH_2), 27.6 (CH), 19.5 (CH_3), 14.4 (CH_3), 0.22 (CH_3); MS (APcI) *m/z* (rel intensity): 350 (MH^+, 100%), 252 (15), 178 (15), 113 (10).

4-Component Hantzsch DHP synthesis in a single-mode microwave batch reactor (Table 3, entry 6). A solution of 3-(trimethylsilyl)propynal (**14d**) (50 mg, 0.53 mmol), ethyl acetoacetate (**11**) (0.14 g, 1.1 mmol) and ammonium acetate (0.12 g, 1.6 mmol) in EtOH–glacial acetic acid (5:1, 2 mL) was irradiated at 120 °C for 7 min in a sealed tube using a CEM Discover microwave synthesizer at an initial power of 90 W. The reaction mixture was cooled in a stream of compressed air and evaporated in vacuo. The residue was partitioned between saturated aqueous $NaHCO_3$ solution (25 mL) and CH_2Cl_2 (25 mL). The aqueous layer was further extracted with CH_2Cl_2 (2 × 15 mL) and the organic extracts were combined, washed with brine (15 mL), dried ($NaSO_4$) and evaporated in vacuo to give the title compound (0.16 g, 84%) as a pale yellow solid, with identical physical and spectroscopic properties.

Supporting Information

Supporting information contains experimental procedures for the synthesis of known compounds.

Supporting Information File 1

General experimental methods and detailed procedures for the synthesis of propynone **12b**, Bohlmann–Rahtz pyridine **2b** and Hantzsch dihydropyridines **15a**, **15b** and **15c**.
[http://www.beilstein-journals.org/bjoc/content/supplementary/1860-5397-9-232-S1.pdf]

Acknowledgements

We thank the EPSRC (GR/S41463 and GR/S25456; awards to MCB, MCL and VF), and the R M Phillips Trust (award to MCB) for support of our work, Otman Benali (Uniqsis), Laura Favretto (Milestone), Matthew Burwood (a1-envirotech) and Robin Wood (AstraZeneca) for valuable assistance, CEM (Microwave Technology) Ltd, Milestone S.r.I. and Uniqsis Ltd for permitting us to test their apparatus in our laboratories, and the EPSRC Mass Spectrometry Service at the University of Wales, Swansea UK for mass spectra.

References

1. Kappe, C. O.; Dallinger, D.; Murphree, S. S. *Practical Microwave Synthesis for Organic Chemists;* Wiley-VCH: Weinheim, Germany, 2009. doi:10.1002/9783527623907
2. Baghbanzadeh, M.; Carbone, L.; Cozzoli, P. D.; Kappe, C. O. *Angew. Chem., Int. Ed.* **2011,** *50,* 11312–11359. doi:10.1002/anie.201101274
3. Appukkuttan, P.; Van der Eycken, E. *Top. Curr. Chem.* **2006,** *266,* 1–47. doi:10.1007/128_051
4. Kappe, C. O.; Stadler, A. *Microwaves in Organic and Medicinal Chemistry;* Wiley-VCH: Weinheim, Germany, 2005. doi:10.1002/3527606556
5. Alcázar, J.; Oehlrich, D. *Future Med. Chem.* **2010,** *2,* 169–176. doi:10.4155/fmc.09.144
6. Kappe, C. O.; Dallinger, D. *Nat. Rev. Drug Discovery* **2006,** *5,* 51–63. doi:10.1038/nrd1926
7. Pedersen, S. L.; Tofteng, A. P.; Malik, L.; Jensen, K. J. *Chem. Soc. Rev.* **2012,** *41,* 1826–1844. doi:10.1039/c1cs15214a
8. Collins, J. M.; Leadbeater, N. E. *Org. Biomol. Chem.* **2007,** *5,* 1141–1150. doi:10.1039/b617084f
9. Moseley, J. D.; Woodman, E. K. *Energy Fuels* **2009,** *23,* 5438–5447. doi:10.1021/ef900598m
10. Bowman, M. D.; Holcomb, J. L.; Kormos, C. M.; Leadbeater, N. E.; Williams, V. A. *Org. Process Res. Dev.* **2008,** *12,* 41–57. doi:10.1021/op700187w

11. Ley, S. V. *Chem. Rec.* **2012,** *12,* 378–390. doi:10.1002/tcr.201100041
12. Glasnov, T. N.; Kappe, C. O. *Chem.–Eur. J.* **2011,** *17,* 11956–11968. doi:10.1002/chem.201102065
13. Wiles, C.; Watts, P. *Beilstein J. Org. Chem.* **2011,** *7,* 1360–1371. doi:10.3762/bjoc.7.160
14. Cablewski, T.; Faux, A. F.; Strauss, C. R. *J. Org. Chem.* **1994,** *59,* 3408–3412. doi:10.1021/jo00091a033
15. Ullah, F.; Samarakoon, T.; Rolfe, A.; Kurtz, R. D.; Hanson, P. R.; Organ, M. G. *Chem.–Eur. J.* **2010,** *16,* 10959–10962. doi:10.1002/chem.201001651
16. Glasnov, T. N.; Kappe, C. O. *Macromol. Rapid Commun.* **2007,** *28,* 395–410. doi:10.1002/marc.200600665
17. Gjuraj, E.; Kongoli, R.; Shore, G. *Chem. Biochem. Eng. Q.* **2012,** *26,* 285–307.
18. Comer, E.; Organ, M. G. *J. Am. Chem. Soc.* **2005,** *127,* 8160–8167. doi:10.1021/ja0512069
19. Comer, E.; Organ, M. G. *Chem.–Eur. J.* **2005,** *11,* 7223–7227. doi:10.1002/chem.200500820
20. Shore, G.; Morin, S.; Organ, M. G. *Angew. Chem., Int. Ed.* **2006,** *45,* 2761–2766. doi:10.1002/anie.200503600
21. He, P.; Haswell, S. J.; Fletcher, P. D. I. *Appl. Catal., A* **2004,** *274,* 111–114. doi:10.1016/j.apcata.2004.05.042
22. He, P.; Haswell, S. J.; Fletcher, P. D. I.; Kelly, S. M.; Mansfield, A. *Beilstein J. Org. Chem.* **2011,** *7,* 1150–1157. doi:10.3762/bjoc.7.133
23. Kunz, U.; Kirschning, A.; Wen, H.-L.; Solodenko, W.; Cecilia, R.; Kappe, C. O.; Turek, T. *Catal. Today* **2005,** *105,* 318–324. doi:10.1016/j.cattod.2005.06.046
24. Wilson, N. S.; Sarko, C. R.; Roth, G. P. *Org. Process Res. Dev.* **2004,** *8,* 535–538. doi:10.1021/op034181b
25. Baxendale, I. R.; Griffiths-Jones, C. M.; Ley, S. V.; Tranmer, G. K. *Chem.–Eur. J.* **2006,** *12,* 4407–4416. doi:10.1002/chem.200501400
26. Mennecke, K.; Cecilia, R.; Glasnov, T. N.; Gruhl, S.; Vogt, C.; Feldhoff, A.; Vargas, M. A. L.; Kappe, C. O.; Kunz, U.; Kirschning, A. *Adv. Synth. Catal.* **2008,** *350,* 717–730. doi:10.1002/adsc.200700510
27. Jachuck, R. J. J.; Selvaraj, D. K.; Varma, R. S. *Green Chem.* **2006,** *8,* 29–33. doi:10.1039/b512732g
28. Pipus, G.; Plazl, I.; Koloini, T. *Chem. Eng. J.* **2000,** *76,* 239–245. doi:10.1016/S1385-8947(99)00171-0
29. Chemat, F.; Poux, M.; de Martino, J.-L.; Berlan, J. *Chem. Eng. Technol.* **1996,** *19,* 420–424. doi:10.1002/ceat.270190506
30. Karney, M. J.; Porter, K. A.; Barnhardt, E. K.; Vanier, G. S. *RSC Adv.* **2013,** *3,* 7106–7111. doi:10.1039/c3ra40783g
31. Barnard, T. M.; Leadbeater, N. E.; Boucher, M. B.; Stencel, L. M.; Wilhite, B. A. *Energy Fuels* **2007,** *21,* 1777–1781. doi:10.1021/ef0606207
32. Esveld, E.; Chemat, F.; van Haveren, J. *Chem. Eng. Technol.* **2000,** *23,* 429–435. doi:10.1002/(SICI)1521-4125(200005)23:5<429::AID-CEAT429>3.0.CO;2-T
33. Shieh, W.-C.; Dell, S.; Repič, O. *Org. Lett.* **2001,** *3,* 4279–4281. doi:10.1021/ol016949n
34. Shieh, W.-C.; Dell, S.; Repič, O. *Tetrahedron Lett.* **2002,** *43,* 5607–5609. doi:10.1016/S0040-4039(02)01116-4
35. Shieh, W.-C.; Lozanov, M.; Repič, O. *Tetrahedron Lett.* **2003,** *44,* 6943–6945. doi:10.1016/S0040-4039(03)01711-8
36. Savin, K. A.; Robertson, M.; Gernert, D.; Green, S.; Hembre, E. J.; Bishop, J. *Mol. Diversity* **2003,** *7,* 171–174. doi:10.1023/B:MODI.0000006801.27748.3b
37. Bagley, M. C.; Davis, T.; Dix, M. C.; Fusillo, V.; Pigeaux, M.; Rokicki, M. J.; Kipling, D. *Future Med. Chem.* **2010,** *2,* 1417–1427. doi:10.4155/fmc.10.217
38. Arvela, R. K.; Leadbeater, N. E.; Collins, M. J., Jr. *Tetrahedron* **2005,** *61,* 9349–9355. doi:10.1016/j.tet.2005.07.063
39. Loones, K. T. J.; Maes, B. U. W.; Rombouts, G.; Hostyn, S.; Diels, G. *Tetrahedron* **2005,** *61,* 10338–10348. doi:10.1016/j.tet.2005.07.105
40. Pitts, M. R.; McCormack, P.; Whittall, J. *Tetrahedron* **2006,** *62,* 4705–4708. doi:10.1016/j.tet.2005.11.095
41. Bergamelli, F.; Iannelli, M.; Marafie, J. A.; Moseley, J. D. *Org. Process Res. Dev.* **2010,** *14,* 926–930. doi:10.1021/op100082w
42. Moseley, J. D.; Lenden, P.; Lockwood, M.; Ruda, K.; Sherlock, J.-P.; Thomson, A. D.; Gilday, J. P. *Org. Process Res. Dev.* **2008,** *12,* 30–40. doi:10.1021/op700186z
43. Baxendale, I. R.; Pitts, M. R. *Chim. Oggi* **2006,** *24* (3), 41–45.
44. Bagley, M. C.; Jenkins, R. L.; Lubinu, M. C.; Mason, C.; Wood, R. *J. Org. Chem.* **2005,** *70,* 7003–7006. doi:10.1021/jo0510235
45. Bagley, M. C.; Fusillo, V.; Jenkins, R. L.; Lubinu, M. C.; Mason, C. *Org. Biomol. Chem.* **2010,** *8,* 2245–2251. doi:10.1039/b926387j
46. Glasnov, T. N.; Vugts, D. J.; Koningstein, M. M.; Desai, B.; Fabian, W. M. F.; Orru, R. V. A.; Kappe, C. O. *QSAR Comb. Sci.* **2006,** *25,* 509–518. doi:10.1002/qsar.200540210
47. Baxendale, I. R.; Schou, S. C.; Sedelmeier, J.; Ley, S. V. *Chem.–Eur. J.* **2010,** *16,* 89–94. doi:10.1002/chem.200902906
48. Bagley, M. C.; Lubinu, M. C.; Mason, C. *Synlett* **2007,** 704–708. doi:10.1055/s-2007-970783
49. Bohlmann, F.; Rahtz, D. *Chem. Ber.* **1957,** *90,* 2265–2272. doi:10.1002/cber.19570901021
50. Bagley, M. C.; Glover, C.; Merritt, E. A. *Synlett* **2007,** 2459–2482. doi:10.1055/s-2007-986674
51. Bagley, M. C.; Brace, C.; Dale, J. W.; Ohnesorge, M.; Phillips, N. G.; Xiong, X.; Bower, J. *J. Chem. Soc., Perkin Trans. 1* **2002,** 1663–1671. doi:10.1039/B203397F
52. Bagley, M. C.; Dale, J. W.; Ohnesorge, M.; Xiong, X.; Bower, J. *J. Comb. Chem.* **2003,** *5,* 41–44. doi:10.1021/cc020067d
53. Bagley, M. C.; Xiong, X. *Org. Lett.* **2004,** *6,* 3401–3404. doi:10.1021/ol0485870
54. Xiong, X.; Bagley, M. C.; Chapaneri, K. *Tetrahedron Lett.* **2004,** *45,* 6121–6124. doi:10.1016/j.tetlet.2004.06.061
55. Aulakh, V. S.; Ciufolini, M. A. *J. Org. Chem.* **2009,** *74,* 5750–5753. doi:10.1021/jo900950x
56. Bagley, M. C.; Chapaneri, K.; Dale, J. W.; Xiong, X.; Bower, J. *J. Org. Chem.* **2005,** *70,* 1389–1399. doi:10.1021/jo048106q
57. Bagley, M. C.; Hughes, D. D.; Sabo, H. M.; Taylor, P. H.; Xiong, X. *Synlett* **2003,** 1443–1446. doi:10.1055/s-2003-40827
58. Bagley, M. C.; Lunn, R.; Xiong, X. *Tetrahedron Lett.* **2002,** *43,* 8331–8334. doi:10.1016/S0040-4039(02)01975-5
59. Bagley, M. C.; Lin, Z.; Pope, S. J. A. *Chem. Commun.* **2009,** 5165–5167. doi:10.1039/b910664b
60. Flow chemistry application note 15: Bohlmann–Rahtz pyridine synthesis, Uniqsis Ltd. http://www.uniqsis.com/fcApplications.aspx (accessed Aug 22, 2013).
61. Hantzsch, A. *Ber. Dtsch. Chem. Ges.* **1881,** *14,* 1637–1638. doi:10.1002/cber.18810140214
62. Hantzsch, A. *Justus Liebigs Ann. Chem.* **1882,** *215,* 1–82. doi:10.1002/jlac.18822150102
63. Vanden Eynde, J. J.; Mayence, A. *Molecules* **2003,** *8,* 381–391. doi:10.3390/80400381
64. Katritzky, A. R.; Ostercamp, D. L.; Yousaf, T. I. *Tetrahedron* **1987,** *43,* 5171–5186. doi:10.1016/S0040-4020(01)87693-6

65. Flaim, S. F.; Zelis, R. *Fed. Proc.* **1981,** *40,* 2877–2881.
66. Sunkel, C. E.; de Casa-Juana, M. F.; Cillero, F. J.; Priego, J. G.; Ortega, M. P. *J. Med. Chem.* **1988,** *31,* 1886–1890. doi:10.1021/jm00118a004
67. Watanabe, Y.; Shiota, K.; Hoshiko, T.; Ozaki, S. *Synthesis* **1983,** 761. doi:10.1055/s-1983-30505
68. Öhberg, L.; Westman, J. *Synlett* **2001,** 1296–1298. doi:10.1055/s-2001-16043
69. Stencel, L. M.; Kormos, C. M.; Avery, K. B.; Leadbeater, N. E. *Org. Biomol. Chem.* **2009,** *7,* 2452–2457. doi:10.1039/b902112d
70. Bagley, M. C.; Lubinu, M. C. *Synthesis* **2006,** 1283–1288. doi:10.1055/s-2006-926407
71. Flow chemistry application note 10: Hantzsch dihydropyridine synthesis, Uniqsis Ltd. http://www.uniqsis.com/fcApplications.aspx (accessed Aug 22, 2013).
72. Bandyopadhyay, D.; Maldonado, S.; Banik, B. K. *Molecules* **2012,** *17,* 2643–2662. doi:10.3390/molecules17032643
73. Devine, W. G.; Leadbeater, N. E. *ARKIVOC* **2011,** No. v, 127–143.
74. Baxendale, I. R.; Hornung, C.; Ley, S. V.; de Mata Muñoz Molina, J.; Wikström, A. *Aust. J. Chem.* **2013,** *66,* 131–144. doi:10.1071/CH12365

License and Terms

Beilstein Journal of Organic Chemistry

Microflow photochemistry: UVC-induced [2 + 2]-photoadditions to furanone in a microcapillary reactor

Sylvestre Bachollet[1], Kimitada Terao[2], Shin Aida[2], Yasuhiro Nishiyama[2], Kiyomi Kakiuchi[2] and Michael Oelgemöller[*1]

Letter

Open Access

Address:
[1]James Cook University, School of Pharmacy and Molecular Sciences, Townsville, QLD 4811, Australia and [2]Graduate School of Materials Science, Nara Institute of Science and Technology (NAIST), 8916-5, Takayama-cho, Ikoma, Nara 630-0101, Japan

Email:
Michael Oelgemöller[*] - michael.oelgemoeller@jcu.edu.au

* Corresponding author

Keywords:
cycloaddition; cyclobutane; flow chemistry; furanone; microflow chemistry; photochemistry

Beilstein J. Org. Chem. **2013,** *9,* 2015–2021.
doi:10.3762/bjoc.9.237

Received: 08 June 2013
Accepted: 10 September 2013
Published: 04 October 2013

This article is part of the Thematic Series "Chemistry in flow systems III".

Guest Editor: A. Kirschning

Abstract

[2 + 2]-Cycloadditions of cyclopentene and 2,3-dimethylbut-2-ene to furanone were investigated under continuous-flow conditions. Irradiations were conducted in a FEP-microcapillary module which was placed in a Rayonet chamber photoreactor equipped with low wattage UVC-lamps. Conversion rates and isolated yields were compared to analogue batch reactions in a quartz test tube. In all cases examined, the microcapillary reactor furnished faster conversions and improved product qualities.

Introduction

Continuous-flow chemistry has recently emerged as a new methodology in organic chemistry [1-4]. The combination of microstructured dimensions and flow operations has also proven advantageous for photochemical applications [5-9]. The narrow reaction channels guarantee efficient penetration of light and yield improved photonic efficiencies [10,11]. Likewise, the removal of the photoproducts from the irradiated area minimizes the risk of photodecompositions or secondary photoreactions [12,13]. Of the many photochemical reactions [14-16], [2 + 2]-photocycloadditions are especially interesting transformations since they allow for the construction of cyclobutanes under mild conditions [17-19]. A number of intra- as well as intermolecular [2 + 2]-photocycloadditions have consequently been described under continuous-flow conditions [20-22]. In an extension of our previous work on furanones [10,23], we have now studied intermolecular photoadditions of alkenes to these compounds [24,25]. Direct and sensitized protocols have both been described (Scheme 1). Sensitized additions allow for irradiations in the UVB range [26-28], whereas direct irradiations require UVC light instead [29-31].

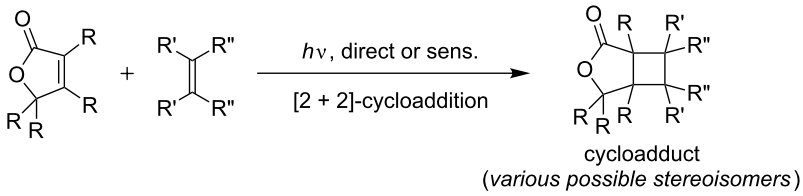

Scheme 1: General [2 + 2]-cycloaddition of furanones with alkenes.

Results and Discussion

Experimental setups

The reaction setup for batch irradiations is shown in Figure 1. A commercially available Rayonet chamber reactor (RMR-600; Southern New England) equipped with eight 4 W UVC lamps (λ = 254 nm; arc length: 7.6 cm) in a circular arrangement was chosen. The central chamber was manufactured from highly reflective aluminum and was approximately 23 cm deep and 18 cm in diameter. The reactor is cooled by an integrated fan and temperatures inside the chamber did not exceed 30 °C. Quartz test tubes (length: 12.7 cm; outer/inner diameter: 15/13 mm; filling volume: 10 mL; filling height: 7.6 cm), sealed with a precision seal septum, were used as reaction vessels and were hung into the centre of the chamber. After a preset irradiation time, the reaction mixture was concentrated to dryness and the crude product was analyzed by ^{1}H NMR spectroscopy. Conversions were determined by comparing the integration areas of selected signals from the starting furanone and the cycloaddition product. In selected cases, the pure products were isolated by column chromatography for characterization purposes and yield determination.

The microcapillary reactor setup is shown in Figure 2. UV-transparent fluorinated ethylene propylene copolymer capillary (FEP; outer/inner diameter: 1.6/0.8 mm) was tightly wrapped around a Pyrex glass cylinder (λ ≥ 300 nm; outer diameter: 8.5 cm). A total of 10 m of the capillary covered the cylinder body (windings: 38; coverage: 6 cm; internal volume: 5 mL). This microcapillary unit was placed in the centre of the Rayonet chamber reactor. The non-exposed ends of the capillary (approximately 50 cm each) were covered with black heat-shrink tubing. The inlet was connected to a shut-valve attached to a 10 mL syringe, whereas the outlet was inserted into an amber round-bottom flask outside the chamber reactor. The reaction mixture was loaded into the syringe, degassed with nitrogen, pumped through the microreactor at a given flow rate and collected in an amber flask.

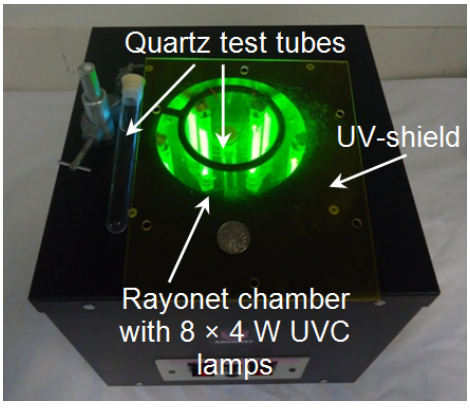

Figure 1: Rayonet chamber reactor (RMR-600; Southern New England) with quartz test tubes. A 10 AU-cent coin is shown for comparison.

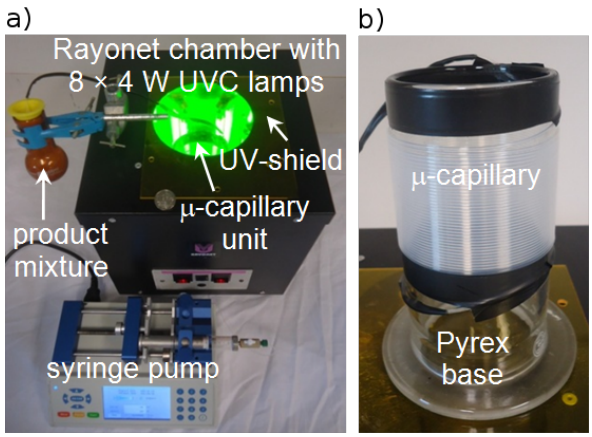

Figure 2: Microcapillary reactor. (a) Setup with inserted μ-capillary unit. A 10 AU-cent coin is shown for comparison. (b) μ-Capillary unit.

Irradiation conditions and light penetration

Model irradiations using furanone **1** and cyclopentene (**2**) in acetonitrile were performed under batch conditions to establish the most suitable reaction conditions (Scheme 1; R = R′ = H, R″ = –$(CH_2)_3$–). Upon direct irradiation with UVC light in a quartz tube for 5 h, almost complete conversion of **1** of 95% was achieved. Solely the *cis-anti-cis* isomer of **3** was obtained and was isolated in a yield of 67% after column chromatography, compared to 36% after distillation as reported in the literature [31]. In contrast, sensitized conditions (5 vol % of

acetone and irradiation with UVB light) gave an incomplete conversion of approximately 60%. A complex mixture of various stereoisomers of **3** and several unknown byproducts was obtained, which could not be separated satisfactory. Direct irradiation conditions were thus chosen for all further investigations. However, higher cycloalkenes (cyclohexene and *cis*-cyclooctene) gave stereoisomeric mixtures even under these direct irradiation conditions.

Microflow photochemical syntheses with UVC light are rare. Jamison and coworkers have recently used custom-made quartz coils [32,33], however, these are difficult to manufacture, restricted in length and fragile in handling. We have instead applied inexpensive and flexible FEP tubing that was wrapped tightly around a Pyrex glass base and placed this simple unit inside a common Rayonet chamber reactor ('outside-in' irradiation). A different immersion well type FEP-capillary setup ('inside-out' irradiation) was recently reported but required a custom-built quartz tube [34]. Capillary-based reactors were originally developed for post-column photochemical derivatizations to enhance detection in HPLC [35-37] but are now commonly used in flow photochemical studies [5-9]. FEP is transparent above 230 nm and shows a good UV-stability [37].

In acetonitrile, furanone **1** gave a simple UV-spectrum with the important n→π* absorption as a shoulder between 240 to 270 nm. It thus matches well with the dominant emission of the UVC lamp at 254 nm (Figure 3a). At this wavelength, **1** showed an extinction coefficient ($\varepsilon_{254\ nm}$) of 35 L mol^{-1} cm^{-1}. The light transmission for a 0.1 M solution of **1** was subsequently calculated from the Beer–Lambert law and was compared to the inner diameters of the reaction vessels (Figure 3b) [38]. Due to the circular arrangement of the fluorescent tubes in the chamber and hence irradiation from all directions, the effective pathlength of the test tube was reduced to 7.5 mm. Since the Pyrex base of the microcapillary module absorbed all UVC light, the microcapillary received light only from the outer direction. Due to its much smaller diameter, the light transmission in the microcapillary was still superior with 53%, compared to 0.3% in the test tube.

[2 + 2]-Cycloadditions with cyclopentene

The photoaddition of cyclopentene (**2**) to **1** was subsequently investigated in detail under batch and microflow conditions (Scheme 2, Table 1). Irradiation in a quartz test tube required exhaustive irradiation for 5 h to reach near completion (Table 1, entry 5) as confirmed by ^{1}H NMR spectroscopy. Product isolation was performed for two batches and gave similar yields based on conversion for the *cis-anti-cis* isomer of **3** of 75% and 71% (Table 1, entries 3 and 5), respectively. In $CDCl_3$, the CH_2O-group showed a pair of doublets of doublets at 4.32 and 4.40 ppm with a ^2J coupling constant of 9.5 Hz. Since the dihedral angles to the adjacent methine proton differ significantly, their ^3J coupling constants varied with 2.1 and 7.3 Hz, respectively. The cyclobutane methine protons emerged as clearly separated signals between 2.35 and 2.90 ppm. Their ^3J coupling constants were determined to be 2.9/3.6 and 6.7/7.5 Hz, thus confirming the *cis-anti-cis* geometry of **3**. Under continuous flow conditions, conversion rates increased more rapidly despite irradiation from just one direction. After 60 min of irradiation, 96% of furanone **1** was consumed and complete conversion was effectively achieved after 90 min (Table 1, entries 11–13). Repetition experiments were conducted with residence times of 7.5, 15 and 90 min and showed excellent reproducibility (Table 1, entries 6/7, 8/9 and 12/13). Product **3** was isolated from two experimental runs. Compared to their batch counter-

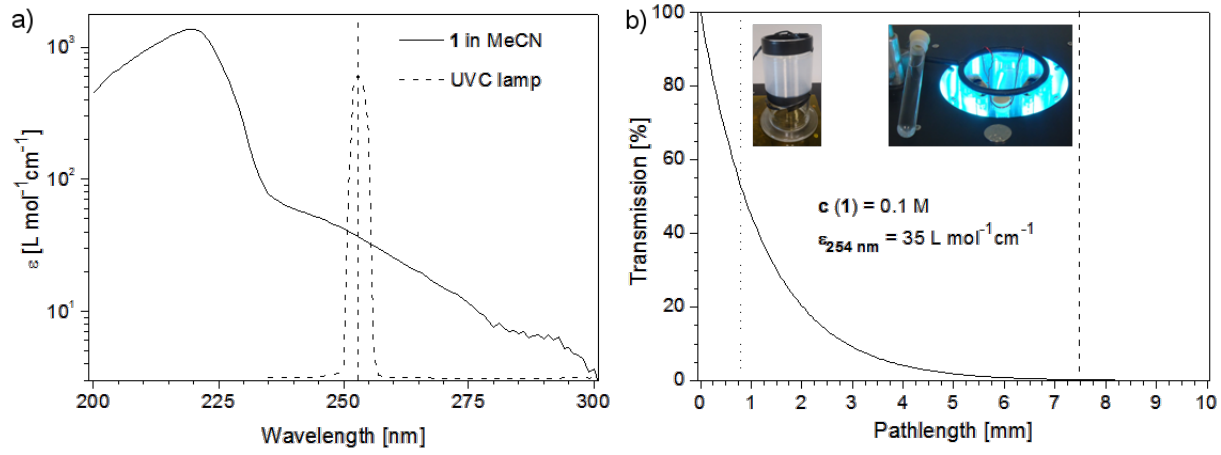

Figure 3: (a) UV-spectrum of **1** (in MeCN) vs emission spectrum of the UVC lamp. (b) Light-penetration profile for a 0.1 M solution of **1** at 254 nm. The vertical lines represent the effective pathlength in the test tube (---) vs the pathlength in the microcapillary (···).

parts, yields based on conversion of **1** were somewhat lower with 65% and 66% (Table 1, entries 10 and 12), which was attributed to the difficult handling of the syringe pump used. The isolation of product **3** by column chromatography was also challenging as fractions had to be analyzed by material-consuming NMR spectroscopy.

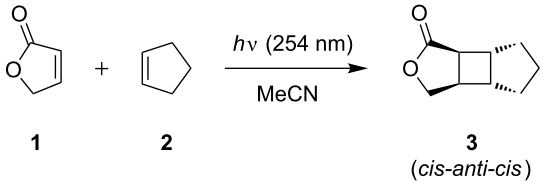

Scheme 2: [2 + 2]-Cycloadditions of furanone **1** with cyclopentene (**2**).

Table 1: Experimental results for the cycloaddition of **1** with **2**.

Entry	Reactor	Time [min]	Conversion [%][a]
1	Batch	60	28
2		90	53
3		180	71 (53[b]/75[c])
4		240	81
5		300	95 (67[b]/71[c])
6	μ-Reactor	7.5	38
7		7.5	40
8		15	50
9		15	53
10		30	85 (55[b]/65[c])
11		60	96
12		90	98 (65[b]/66[c])
13		90	98
14		120	100

[a]Determined by ^{1}H NMR analysis of the crude product (±2%). [b]Isolated yield after column chromatography. [c]Isolated yield based on conversion.

[2 + 2]-Cycloadditions with 2,3-dimethylbut-2-ene

Subsequent cycloadditions were performed using 2,3-dimethylbut-2-ene (**4**) as a reagent (Scheme 3, Table 2) [39]. In contrast to the reactions with cyclopentene, transformations were rather slow and gave more byproducts, possibly from competing ene-reactions [40]. Products arising from dimerization of **1**, however, could not be detected [41]. When conducted under batch conditions, conversions were determined as 17% after 90 min and 99% after 8 h of irradiation (Table 2, entries 1 and 2), respectively. From the latter experiment, cyclobutane **5** was isolated in a low yield of just 30%. In $CDCl_3$, the CH_3-groups in **5** gave four singlets between 1.02–1.21 ppm. Likewise, the CH_2O-bridge appeared at 4.25 and 4.40 ppm with a ^2J coupling constant of 10.1 Hz. The methine protons of the cyclobutane ring gave closely spaced signals at 2.69 and 2.73 ppm. The transformation was again more efficient under microflow conditions and conversions gradually improved with increasing retention time. Nearly complete consumption of **1** was achieved after 90 min (Table 2, entry 9). Good reproducibility was again demonstrated for reactions conducted for 30 and 60 min (Table 2, entries 5/6 and 7/8), respectively. Isolated yields based on conversion were moderate with around 45% (Table 2, entries 8 and 9).

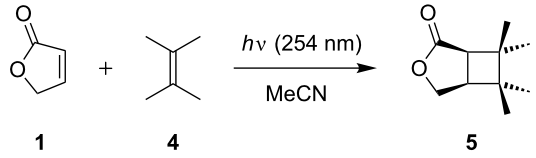

Scheme 3: [2 + 2]-Cycloadditions of furanone **1** with 2,3-dimethylbut-2-ene (**4**).

Table 2: Experimental results for the cycloaddition of **1** with **4**.

Entry	Reactor	Time [min]	Conversion [%][a]
1	Batch	90	17
2		480	99 (30[b])
3	μ-Reactor	7.5	16
4		15	25
5		30	50
6		30	53
7		60	88
8		60	90 (41[b]/46[c])
9		90	97 (43[b]/44[c])

[a]Determined by ^{1}H NMR analysis of the crude product (±2%). [b]Isolated yield after column chromatography. [c]Isolated yield based on conversion.

Reactor comparison

Judged by conversions achieved, the microcapillary reactor showed a better performance for both [2 + 2]-photoadditions studied. This outcome is primarily attributed to the higher light and photonic efficiencies in the microcapillary, in combination with its advantageous design features and dimensions. The key parameters for both setups are compiled in Table 3. Compared to the test tube, the irradiated area-to-volume (surface-to-volume) ratio of the microcapillary module was nine times larger with 3,260 m^2/m^3. The microcapillary module furthermore had a better coverage of the available reflective area of the irradiation chamber, thus maximizing light harvesting by the reaction mixture. At the end of this study, the FEP microcapillary was inspected for photobrittling, transparency losses or

polymeric deposits. Compared to an unused capillary, no visible or physical (e.g. flexibility) changes could be detected.

Table 3: Technical details of the two reactor types.

Parameter	Batch	μ-Capillary reactor
Aperture [cm^2]	60[a]	163[b]
Irradiated area [cm^2]	36[a]	163[b]
Irradiated volume [cm^3]	10	5
Irradiated area/volume ratio [m^2/m^3]	360	3,260
Reflective chamber area/aperture	21.7/1	8.0/1
Reflective chamber area/irradiated area	36.1/1	8.0/1

[a]Assuming a cylindrical geometry for the test tube. [b]Covered area by the microcapillary on the Pyrex base.

Conclusion

UVC-induced photoaddition can be successfully performed in flow using a flexible and inexpensive FEP-capillary unit inserted into a common chamber photoreactor. Model transformations conducted with cyclopentene and 2,3-dimethylbut-2-ene gave higher conversions compared to the conventional quartz test tube. The microcapillary unit had a 9-times larger surface-to-volume ratio, which resulted in a more efficient harvest of the available light. The results contribute to the growing field of 'microflow photochemistry' [5-9] and 'green flow chemistry' [42-45]. It is hoped that this technology will help to overcome the current reservations towards synthetic organic photochemistry [46] and that it will find future applications in chemical and pharmaceutical processes [47,48].

Experimental

General

All commercially available starting materials and reagents were purchased from Sigma-Aldrich or Alfa-Aesar and were used without further purification. Furanone **1** was synthesized from furfural following literature procedures [49]. NMR spectra were recorded on an Oxford 300 (^{1}H 300 MHz and ^{13}C 75 MHz) with the Varian Software VnmrJ Revision D. The residual solvent signal as used as an internal standard. Chemical shifts (δ) are given in ppm; coupling constants (*J*) in Hz. IR spectra were measured on a Nicolet 6700 FTIR spectrometer equipped with a Smart ITR diamond ATR accessory. High resolution mass spectra (HRMS) were obtained on a JEOL JMS-700 instrument. Analytical thin layer chromatography was performed on Merck TLC-Silica gel 60 F_{254} plates and ethyl acetate/*n*-hexane (1:9) as mobile phase and disappearance of furanone **1** was monitored. Preparative chromatography was carried out using Scharlau silica gel 60 and ethyl acetate/*n*-hexane (1:9). Fractions taken were analyzed by ^{1}H NMR spectroscopy. Irradiations were conducted in a Rayonet RPR-600 chamber reactor (Southern New England) equipped with 8 UVC lamps (4 W each). Microflow reactions were performed in a microcapillary reactor fabricated from FEP tubing (Bola, Germany; outer/inner diameter: 1.6/0.8 mm).

Irradiations

[2 + 2]-Cycloadditions under batch conditions: In a quartz test tube, a solution of **1** (1 mmol) and alkene (10 mmol) in acetonitrile (10 mL) was degassed with a gentle stream of nitrogen for 5 min. The test tube was sealed and placed in the centre of a Rayonet chamber reactor. The solution was irradiated with UVC light as indicated in Table 1 and Table 2. After evaporation of the solvent, the conversion was determined by ^{1}H NMR spectroscopy of the crude product. The signal integration for the olefinic C<u>H</u> protons of **1** was compared with the signal integration for the cyclobutane methine C<u>H</u> protons of **3** or **5**. In some cases, compounds **3** and **5** were isolated by column chromatography.

[2 + 2]-Cycloadditions under microflow conditions: A solution of **1** (1 mmol) and alkene (10 mmol) in acetonitrile (10 mL) was degassed carefully with nitrogen for 5 min and loaded into a syringe pump. The reaction mixture was pumped through the microcapillary reactor (residence times as indicated in Table 1 and Table 2) and was irradiated with UVC light. At the end of the reaction, the syringe was changed and the capillary was flushed with approx. 7.5 mL of pure acetonitrile. After evaporation of the solvent, the conversion rate was established by ^{1}H NMR analysis. In selected cases, the products **3** and **5** were isolated by column chromatography.

Octahydro-1*H*-cyclopenta[3,4]cyclobuta[1,2-*c*]furan-1-one (3) [31]: Colorless oil; ^{1}H NMR (300 MHz, $CDCl_3$) δ 1.43–1.92 (br. m, 6H), 2.42 (dddd, *J* = 7.5, 7.3, 3.6, 2.1 Hz, 1H), 2.53 (dd, *J* = 7.5, 2.9 Hz, 1H), 2.65 (ddd, *J* = 6.7, 6.5, 3.6 Hz, 1H), 2.85 (ddd, *J* = 6.8, 6.7, 2.9 Hz, 1H), 4.32 (dd, *J* = 9.5, 2.1 Hz, 1H, CH_2O), 4.40 (dd, *J* = 9.5, 7.3 Hz, 1H, CH_2O) ppm; ^{13}C NMR (75 MHz, $CDCl_3$) δ 24.5, 32.7, 32.8, 37.1, 41.1, 42.6, 44.1, 74.4, 180.7 ppm; IR (ATR) ν: 2939, 2856, 1756, 1372, 1179, 1150, 1009, 980 cm^{-1}; MS (EI^+) *m*/*z*: 153 [M + H], 152 $[M]^+$, 122, 93, 79, 68, 67, 53; MS (CI^+) *m*/*z*: 305 (dimer), 193, 153 $[M + H]^+$, 107, 57; HRMS (CI^+): $[M + H]^+$ calcd for $C_9H_{12}O_2$, 153.0916; found, 153.0918.

6,6,7,7-Tetramethyl-3-oxabicyclo[3.2.0]heptan-2-one (5): Colorless oil; ^{1}H NMR (300 MHz, $CDCl_3$) δ 1.02 (s, 3H, CH_3), 1.04 (s, 3H, CH_3), 1.06 (s, 3H, CH_3), 1.21 (s, 3H, CH_3), 2.69 (dd, *J* = 8.4, 1.6 Hz, 1H), 2.73 (ddd, *J* = 8.4, 5.6, 1.6 Hz, 1H), 4.25 (ddd, *J* = 10.1, 5.6, 1.6 Hz, 1H, CH_2O), 4.40 (dd, *J* = 10.1, 1.6 Hz, 1H, CH_2O) ppm; ^{13}C NMR (75 MHz, $CDCl_3$) δ 20.2,

20.7, 25.9, 27.0, 39.9, 41.0, 41.3, 45.8, 68.7, 178.7 ppm; IR (ATR) ν: 2958, 2870, 1748, 1456, 1368, 1214, 971 cm^{-1}; HRMS (CI^+): $[M + H]^+$ calcd for $C_{10}H_{15}O_2$, 169.1229; found, 169.1232.

Acknowledgements

This work was financially supported by the Australian Research Council (ARC, Discovery Project, DP130100794), the Global Initiatives Program and partially a Grant-in-Aid for Scientific Research (Ministry of Education, Culture, Sports, Science and Technology of the Japanese Government) and the Student Exchange Support Program from the Japan Student Service Organization (JASSO). The authors thank Dr. Norbert Hoffmann (University of Reims) for providing the UV-spectrum of **1**.

References

1. Protasova, L. N.; Bulut, M.; Ormerod, D.; Buekenhoudt, A.; Berton, J.; Stevens, C. V. *Org. Process Res. Dev.* **2013,** *17,* 760–791. doi:10.1021/op4000169
2. Baxendale, I. R. *J. Chem. Technol. Biotechnol.* **2013,** *88,* 519–552. doi:10.1002/jctb.4012
3. Watts, P.; Wiles, C. *J. Chem. Res.* **2012,** *36,* 181–193. doi:10.3184/174751912X13311365798808
4. Baraldi, P. T.; Hessel, V. *Green Process Synth.* **2012,** *1,* 149–167. doi:10.1515/gps-2012-0008
5. Oelgemöller, M. *Chem. Eng. Technol.* **2012,** *35,* 1144–1152. doi:10.1002/ceat.201200009
6. Knowles, J. P.; Elliott, L. D.; Booker-Milburn, K. I. *Beilstein J. Org. Chem.* **2012,** *8,* 2025–2052. doi:10.3762/bjoc.8.229
7. Oelgemöller, M.; Murata, A. *Med. Chem. News* **2012,** *4,* 30–40.
8. Oelgemöller, M.; Shvydkiv, O. *Molecules* **2011,** *16,* 7522–7550. doi:10.3390/molecules16097522
9. Coyle, E. E.; Oelgemöller, M. *Photochem. Photobiol. Sci.* **2008,** *7,* 1313–1322. doi:10.1039/b808778d
10. Shvydkiv, O.; Yavorskyy, A.; Tan, S. B.; Nolan, K.; Hoffmann, N.; Youssef, A.; Oelgemöller, M. *Photochem. Photobiol. Sci.* **2011,** *10,* 1399–1404. doi:10.1039/c1pp05024a
11. Aillet, T.; Loubiere, K.; Dechy-Cabaret, O.; Prat, L. *Chem. Eng. Process.* **2013,** *64,* 38–47. doi:10.1016/j.cep.2012.10.017
12. Maeda, H.; Nashihara, S.; Mukae, H.; Yoshimi, Y.; Mizuno, K. *Res. Chem. Intermed.* **2013,** *39,* 301–310. doi:10.1007/s11164-012-0650-6
13. Fuse, S.; Mifune, Y.; Tanabe, N.; Takahashi, T. *Org. Biomol. Chem.* **2012,** *10,* 5205–5211. doi:10.1039/c2ob25511a
14. Hoffmann, N. *Photochem. Photobiol. Sci.* **2012,** *11,* 1613–1641. doi:10.1039/c2pp25074h
15. Bach, T.; Hehn, J. P. *Angew. Chem., Int. Ed.* **2011,** *50,* 1000–1045. doi:10.1002/anie.201002845
16. Hoffmann, N. *Chem. Rev.* **2008,** *108,* 1052–1103. doi:10.1021/cr0680336
17. Lee-Ruff, E.; Mladenova, G. *Chem. Rev.* **2003,** *103,* 1449–1484. doi:10.1021/cr010013a
18. Bach, T. *Synthesis* **1998,** 683–703. doi:10.1055/s-1998-2054
19. Schuster, D. I.; Lem, G.; Kaprinidis, N. A. *Chem. Rev.* **1993,** *93,* 3–22. doi:10.1021/cr00017a001
20. Nettekoven, M.; Püllmann, B.; Martin, R. E.; Wechsler, D. *Tetrahedron Lett.* **2012,** *53,* 1363–1366. doi:10.1016/j.tetlet.2012.01.010
21. Vasudevan, A.; Villamil, C.; Trumball, J.; Olson, J.; Sutherland, D.; Pan, J.; Djuric, S. *Tetrahedron Lett.* **2010,** *51,* 4007–4009. doi:10.1016/j.tetlet.2010.05.119
22. Fukuyama, T.; Kajihara, Y.; Hino, Y.; Ryu, I. *J. Flow Chem.* **2011,** *1,* 40–45. doi:10.1556/jfchem.2011.00007
23. Shvydkiv, O.; Yavorskyy, A.; Nolan, K.; Youssef, A.; Riguet, E.; Hoffmann, N.; Oelgemöller, M. *Photochem. Photobiol. Sci.* **2010,** *9,* 1601–1603. doi:10.1039/c0pp00223b
24. Xue, F.; Li, J.; Mo, Y.; Wang, Z.; Chen, Q. *Chin. J. Org. Chem.* **2012,** *32,* 284–293. doi:10.6023/cjoc1104191
25. Hashem, A. I.; Senning, A.; Hamad, A.-S. S. *Org. Prep. Proced. Internat.* **1998,** *30,* 401–425. doi:10.1080/00304949809355303
26. Cucarull-González, J. R.; Hernando, J.; Alibés, R.; Figueredo, M.; Font, J.; Rodríguez-Santiago, L.; Sodupe, M. *J. Org. Chem.* **2010,** *75,* 4392–4401. doi:10.1021/jo100341a
27. Bertrand, S.; Hoffmann, N.; Pete, J.-P. *Tetrahedron* **1998,** *54,* 4873–4888. doi:10.1016/S0040-4020(98)00171-9
28. Hoffmann, N.; Buschmann, H.; Raabe, G.; Scharf, H.-D. *Tetrahedron* **1994,** *50,* 11167–11186. doi:10.1016/S0040-4020(01)89419-9
29. Rustullet, A.; Alibés, R.; de March, P.; Figueredo, M.; Font, J. *Org. Lett.* **2007,** *9,* 2827–2830. doi:10.1021/ol0710616
30. Tomioka, K.; Tanaka, M.; Koga, K. *Chem. Pharm. Bull.* **1989,** *37,* 1201–1207. doi:10.1248/cpb.37.1201
31. Tada, M.; Kokubo, T.; Sato, T. *Tetrahedron* **1972,** *28,* 2121–2125. doi:10.1016/0040-4020(72)88019-0
32. Zhang, Y.; Blackman, M. L.; Leduc, A. B.; Jamison, T. F. *Angew. Chem., Int. Ed.* **2013,** *52,* 4251–4255. doi:10.1002/anie.201300504
33. Shen, B.; Jamison, T. F. *Aust. J. Chem.* **2013,** *66,* 157–164. doi:10.1071/CH12426
34. Maskill, K. G.; Knowles, J. P.; Elliott, L. D.; Alder, R. W.; Booker-Milburn, K. I. *Angew. Chem., Int. Ed.* **2013,** *52,* 1499–1502. doi:10.1002/anie.201208892
35. Lores, M.; Cabaleiro, O.; Cela, R. *Trends Anal. Chem.* **1999,** *18,* 392–400. doi:10.1016/S0165-9936(98)00121-6
36. Di Pietra, A. M.; Gatti, R.; Andrisano, V.; Cavrini, V. *J. Chromatogr., A* **1996,** *729,* 355–361. doi:10.1016/0021-9673(95)01037-8
37. Poulsen, J. B.; Birks, K. S.; Gandelman, M. S.; Birks, J. W. *Chromatographia* **1986,** *22,* 231–234. doi:10.1007/BF02268764
38. Braun, A. M.; Maurette, M.-T.; Oliveros, E. *Photochemical Technology;* Wiley: Chichester, 1991.
39. Alibés, R.; Bourdelande, J. L.; Font, J. *Tetrahedron: Asymmetry* **1991,** *2,* 1391–1402. doi:10.1016/S0957-4166(00)80035-X
40. Hatsui, T.; Kitashirna, T.; Takeshita, H. *Bull. Chem. Soc. Jpn.* **1994,** *67,* 293–295. doi:10.1246/bcsj.67.293
41. Ohga, K.; Matsuo, T. *Bull. Chem. Soc. Jpn.* **1970,** *43,* 3505–3510. doi:10.1246/bcsj.43.3505
42. Newman, S. G.; Jensen, K. F. *Green Chem.* **2013,** *15,* 1456–1472. doi:10.1039/c3gc40374b
43. Melchert, W. R.; Reis, B. F.; Rocha, F. R. P. *Anal. Chim. Acta* **2012,** *714,* 8–19. doi:10.1016/j.aca.2011.11.044
44. Wiles, C.; Watts, P. *Green Chem.* **2012,** *14,* 38–54. doi:10.1039/c1gc16022b
45. Ley, S. V. *Chem. Rec.* **2012,** *12,* 378–390. doi:10.1002/tcr.201100041
46. Ciana, C.-L.; Bochet, C. G. *Chimia* **2007,** *61,* 650–654. doi:10.2533/chimia.2007.650

47. Malet-Sanz, L.; Susanne, F. *J. Med. Chem.* **2012,** *55,* 4062–4098. doi:10.1021/jm2006029
48. Chin, P.; Barney, W. S.; Pindzola, B. A. *Curr. Opin. Drug Discovery Dev.* **2009,** *12,* 848–861.
49. Näsman, J. H. *Org. Synth.* **1990,** *68,* 162–174.

License and Terms

Beilstein Journal of Organic Chemistry

Flow synthesis of a versatile fructosamine mimic and quenching studies of a fructose transport probe

Matthew B. Plutschack[1,2], D. Tyler McQuade*[1,2], Giulio Valenti[2] and Peter H. Seeberger[2]

Full Research Paper

Open Access

Address:
[1]Department of Chemistry and Biochemistry, Florida State University, Tallahassee, FL 32306, USA and [2]Max Planck Institute of Colloids and Interfaces, Am Mühlenberg 1, 14476 Potsdam, Germany

Email:
D. Tyler McQuade* - mcquade@chem.fsu.edu

* Corresponding author

Keywords:
flow chemistry; fructose mimic; gluts; NBDM

Beilstein J. Org. Chem. **2013,** *9,* 2022–2027.
doi:10.3762/bjoc.9.238

Received: 19 June 2013
Accepted: 03 September 2013
Published: 07 October 2013

This article is part of the Thematic Series "Chemistry in flow systems III".

Guest Editor: A. Kirschning

Abstract

We describe the synthesis of 1-amino-2,5-anhydro-D-mannose ("mannitolamine"), a key intermediate to the 7-nitro-1,2,3-benzadiazole conjugate (NBDM), using commercially available fluidic devices to increase the throughput. The approach is the first example of a flow-based Tiffeneau–Demjanov rearrangement. Performing this step in flow enables a ~64-fold throughput enhancement relative to batch. The flow process enables the synthesis to be accomplished three times faster than the comparable batch route. The high throughput enabled the production of larger quantities of the fluorescent fructose transport probe NBDM, enabling us to measure key photophysical properties that will facilitate future uptake studies.

Introduction

The impact of dietary fructose on human health is not well-understood. A growing body of work suggests that those eating diets high in fructose exhibit increased rates of metabolic disorders and aggressive cancers [1,2]. Since the landmark reports from Warburg [3], researchers have recognized that cancer cells/tissues consume more carbohydrates than normal tissues, fueling rapid growth and proliferation [4]. While cancer cells utilize multiple strategies to increase carbohydrate consumption, one mechanism is to increase passive glucose transporter (Glut) expression [2,5]. Uncharacteristic Glut expression is now implicated as a hallmark of not just cancer but also metabolic disorders [1]. Abnormal Glut expression is observed in the pancreatic islets and hepatic cells of people with diabetes, which may explain glucose insensitivity and the progression of non-alcoholic fatty liver disease [6,7].

Passive carbohydrate transporters are well-known targets for carbohydrate-based probes [8]. The positron emission tomography (PET) tracer 2-deoxy-2-[^{18}F]fluoro-D-glucose (FDG) primarily targets Glut1 [9]. Although FDG is an effective tumour probe [10], Glut1 is expressed in every type of tissue and this prevalence often results in false positive tests [11,12].

Unlike Glut1, the fructose-specific transporter Glut5 is expressed in fewer tissues [2]. We are developing probes that are selectively transported by Glut5. Using design principles gleaned from the Holman group [13-15] as well as other fructose analogue research [16], we synthesized NBDM [17] and demonstrated that this probe is transported into cancer cells known to overexpress Glut5 and poorly transported into cells known to express little Glut5 [2,5,18]. We demonstrated that the transport is inhibited by fructose but not by other dietary sugars (glucose, glucosamine) [17]. Furthering our understanding of fluorescent probes like NBDM will expedite the development of Glut5-specific PET compounds which could be non-invasive tools for determining Glut5 expression in vivo and provide a means for monitoring the onset and progression of metabolic syndrome and aggressive cancers.

The promising initial results obtained with NBDM prompted us to synthesize larger quantities of material. More NBDM is required to examine uptake across many cell lines and with access to amine **3**, we can prepare analogues with different fluorophores or other types of tags. Finally, access to more NBDM will enable assessment of probe photophysical properties as a function of concentration and in the presence of potential quenchers. This increased understanding will be critical when probing uptake into various biological systems where cell staining techniques or supplemental amino acids are used. Herein, we report an efficient flow synthesis of amine **3** that enabled an increase in scale as well as a reduction in the time needed to prepare NBDM. We also present fluorescent properties of NBDM under conditions relevant to future cellular studies.

Results and Discussion

Synthesis: The batch synthesis of 1-amino-2,5-anhydro-D-mannitol was reported by Claustre et al (Scheme 1). We used their basic approach, but improved throughput significantly [19]. The synthesis began with a Tiffeneau–Demjanov rearrangement of glucosamine·HCl using an acidic resin and $NaNO_2$ to make nitrous acid in situ (Scheme 2). The original conditions required neutralization by a basic resin. After rinsing both resins, a dilute aqueous solution of **1** resulted and overnight lyophilisation was required to isolate the product. Because the conditions are not easily integrated into a continuous process, we sought alternative approaches.

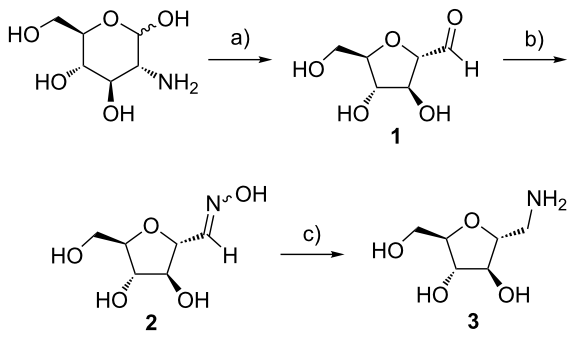

Scheme 1: Batch synthesis of NBDM. a) $NaNO_2$, Amberlite IR-120 H^+ (100 mL), 0 °C, water, 4 h. b) NH_2OH·HCl, NaOAc, MeOH, rt, 6 h. c) H_2, Pd/C (10%), 4.4% formic acid, MeOH, rt, 10 h.

Our initial approach was to continue using a resin (Amberlite IRA-900) supporting nitrite in flow. While the use of supported reagents in flow is now well-established, the use of supported nitrite has not been widely adopted [20]. Amberlite IRA-900 was exchanged by eluting the chloride ion from the resin using a 1 M solution of sodium nitrite until no more chloride was observed via an $AgNO_3$ test. Once the exchange was complete, the column was washed with deionized water. The column was first assessed by flowing a 0.2 M aqueous solution of D-(+)-glucosamine·HCl into a round bottom flask. Our initial experiment was performed at room temperature and took two days to reach completion. Heating the reaction to 40, 60 or 70 °C resulted in a clean acceleration in reaction rate.

Although the supported nitrite approach at elevated temperatures provided high yields of the desired product, the process was slow and throughput was restricted by the resin loading. In addition, attempts to increase concentration or use organic co-solvents further reduced the efficiency. Based on these problems, we turned our attention to Tiffeneau–Demjanov conditions using a catalytic amount of acid and sodium nitrite in water. Flow conditions enabled the use of high concentrations

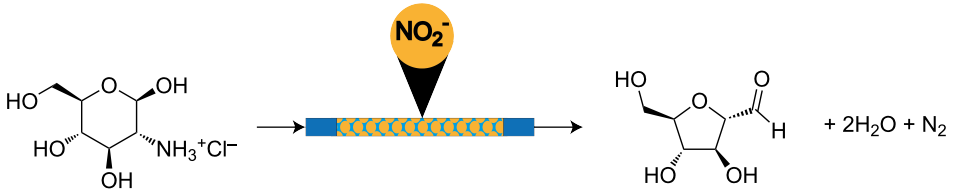

Scheme 2: The initial polymer-supported nitrite set up. A solution of glucosamine hydrochloride was passed over the resin into a round bottom flask and then stirred with heating.

(1.0 M) and temperatures (100 °C) even though the reaction evolves large quantities of nitrogen gas. At a flow rate of 5 mL/min at 100 °C using a 10 mL reactor (2 min residence time), we achieved a throughput of 800 mg/min (Scheme 3). Table 1 shows a comparison between previously reported batch conditions and our continuous flow conditions and illustrates that this first step has a throughput more than 63-fold higher than the batch Tiffeneau–Demjanov conditions.

Table 1: Batch versus flow comparison.

Time (h)	Compound	Batch yield (g)	Flow yield[a] (g)
4	**1**	3.06	194.4
6	**2**	2.63	63.8
10	**3**	2.21	4.8

[a]Flow yield is based off of throughput for the equivalent amount of time the batch conditions required. Throughput was estimated by the quantity of starting material pumped through the reactor. No percent yields were obtained because the crude mixtures could be used in the subsequent steps.

The concentrated Tiffeneau–Demjanov reaction not only increased the throughput but also enabled oxime formation without the removal of water. Using excess hydroxylamine hydrochloride (4 equiv) in methanol resulted in full conversion to compound **2**. At a total flow rate of 5 mL/min at 60 °C using a 20 mL reactor (4 minutes residence time), we achieved a throughput of 177 mg/min (24-fold improvement relative to batch).

The hydrogenolysis of the oxime illustrates a flow chemistry challenge. The output from the oxime step contains excess hydroxylamine and salts carried from the first step that poisoned the packed-bed catalyst we screened. In theory, continuous purification could remove these materials but existing strategies do not enable removal of water soluble byproducts from a water soluble product. Thus, we obtained crude **2** by simple work up: neutralization, concentration, precipitation of salts using tetrahydrofuran, filtration, concentration and dissolution in 10:1 ethanol/acetic acid. This solution was converted to amine **3** using an H-Cube (commercially available from Thales). With a flow rate of 1 mL/min at 100 bar and 70 °C using a 10% Pd/C CatCart, a throughput of 8 mg/min was achieved. The crude reaction solution was pure by NMR and was used without further purification. As shown in Table 1, the hydrogenolysis represents a bottleneck in the synthesis of compound **3** because the throughput drops down to only 2-fold enhancement relative to batch. We predict that this throughput could be significantly improved if the wider range of catalysts were screened.

The fructose analog probe NBDM was then produced by combining the concentrated output from the H-Cube in saturated sodium bicarbonate (0.4 M) with a 0.4 M solution of NBD-Cl. This step can be conducted in flow as well as in batch with no significant difference in yield or productivity. The low yield (20–30%) of NBDM may be the result of competitive reactivity between the NBD-Cl and the hydroxy groups present on **3**. When 1 M solutions of sodium bicarbonate are used

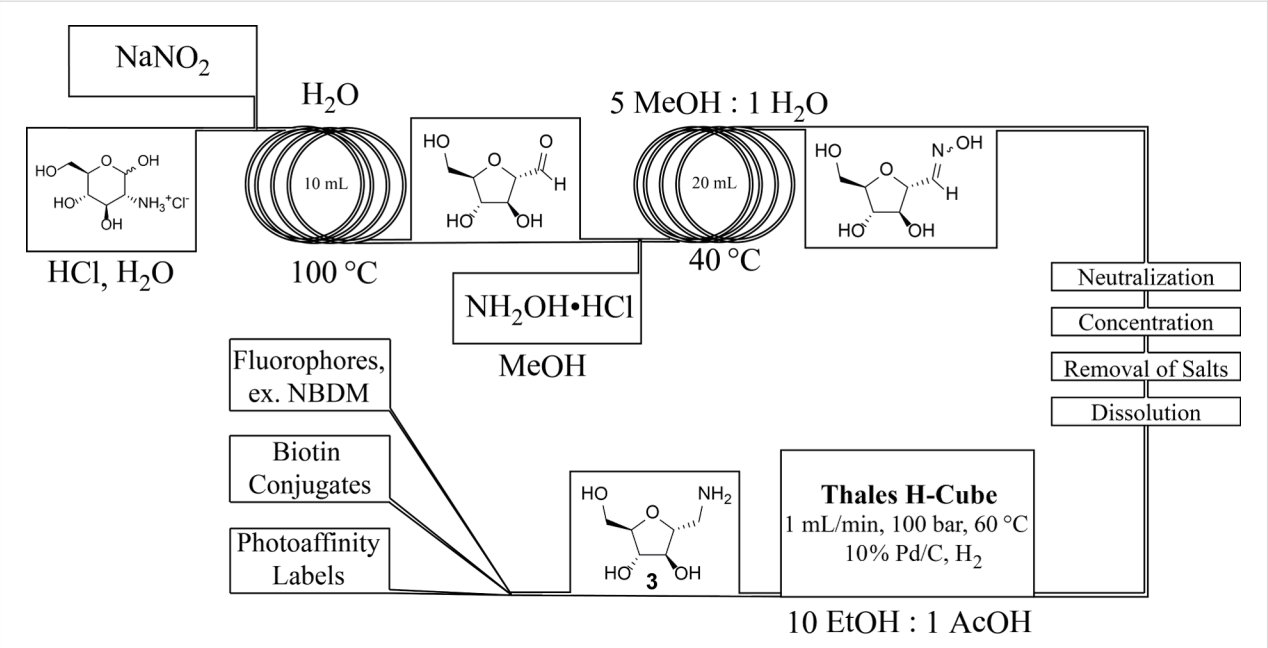

Scheme 3: Continuous flow synthesis of the key intermediate 1-amino-2,5-anhydro-D-mannose (**3**).

instead of saturated sodium bicarbonate, the resulting TLCs indicate the formation of more byproducts and the lower isolated yields of NBDM (<20%) also support this hypothesis. We are confident that a completely continuous high-throughput process to **3** could be realized with improvements in continuous extraction techniques. That being said, the semi-continuous approach we have defined here results in significant improvements compared to the original batch conditions.

Many fluorophores and biologically relevant tags have been developed for conjugation to amines. For this reason, amine **3** was of particular interest. Likely, **3** will be a key branch-point for the synthesis of numerous biologically active conjugates and our improved production of **3** will provide significantly greater quantities of conjugates. In particular, we can now produce NBDM using this system in a single day which is a 3-fold improvement relative to the original process. This rapid access to more material enabled us to begin to assess the fluorescent properties as a function of typical quenchers used in cell-staining as well as intrinsic quenchers found in cells. Without easy access to NBDM, the use of this compound in biological experiments would supersede the investigation of its fluorescent properties.

Fluorescence: Fluorescence in biological systems is often complicated by fluorophore quenching. Alexa fluorophores can be quenched by certain amino acids and NBD is known to self-quench at high concentrations [21,22]. Trypan blue is routinely used to quench autofluorescence in confocal fluorescence microscopy and fluorescence activated cell sorting (FACS) [23,24], and dyes like Bromophenol Blue, Brilliant Blue R, and Methylene Blue have been applied to colorimetric cytotoxicity assays as well as in vitro staining [25-28].

To better understand the behaviour of NBDM, we measured fluorescence at various concentrations and in the presence of various dyes, amino acids and sugars. The absorption and emission spectra are shown in Figure 1. The quenching experiments were carried out by measuring emission intensity at 546 nm (ex. 472 nm) as a function of NBDM concentration or quencher concentration. For each quenching experiment, 3–6 replicate fluorescence measurements were taken using a 96-well plate and a plate reader.

In our initial publication describing the uptake of NBDM into MCF-7 cells, we measured uptake as a function of concentration over a range of 1–40 μM (Figure 2) [17]. While we did not expect to observe significant self-quenching over this range, we measured the fluorescent intensity of NBDM from 1–40 μM (1X phosphate buffer solution). As expected, NBDM does not exhibit significant self-quenching over this range. The slight

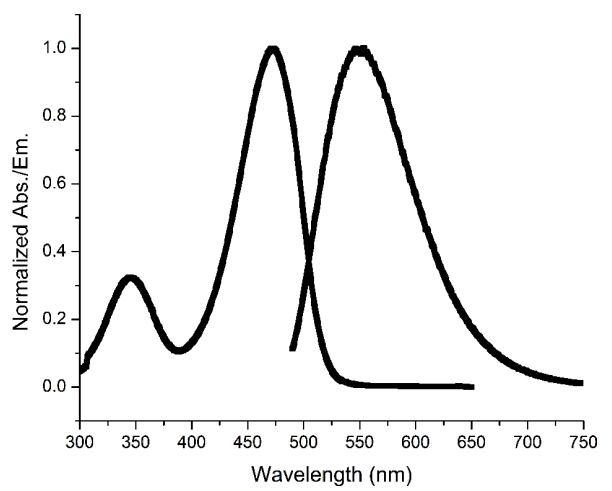

Figure 1: Normalized NBDM absorption and emission, 40 μM and 2 μM.

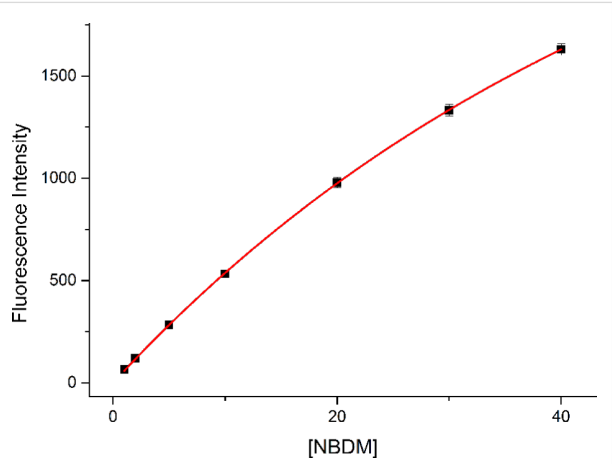

Figure 2: NBDM fluorescence from 1–40 μM (PBS buffer). The data set was plotted in OriginPro 8.6 and fitted using a self-quenching model, $I = \beta_f \left(1 - 10^{-\varepsilon_m [C]}\right) e^{k_{\text{life}}[C]}$ with direct weighting.

curvature that exists suggests that only modest self-quenching occurs (See Supporting Information File 1 for fitting data).

Often multiple dyes are used to locate or identify cells by selective staining. The fluorescence data for NBDM in the presence of four commonly used dyes is shown in Figure 3. These data do not fit a simple Stern–Volmer relationship (see Supporting Information File 1), which indicates that dynamic quenching is not the only mechanism. The data do, however, fit well to a composite Stern–Volmer model that accounts for both dynamic and static quenching.

Free amino acids at high concentrations can also quench fluorophores. To access the propensity for NBDM to be quenched by amino acids, we measured fluorescence in the presence of

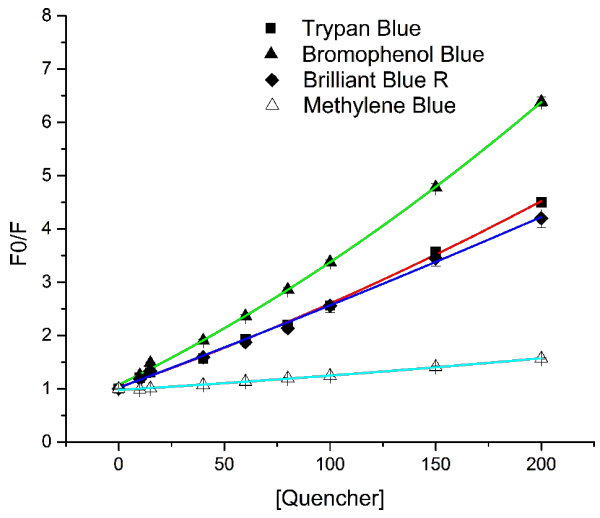

Figure 3: Comparison of quenching 2 μM NBDM, as measured by fluorescence intensity of Trypan Blue, Bromophenol Blue, Brilliant Blue R, and Methylene Blue. Each data set was plotted in OriginPro 8.6 and fitted using a polynomial fit (order = 2) with direct weighting.

varying concentrations of alanine, glutamine, lysine, tyrosine, methionine and histidine. As expected, the amino acids lacking functionality known to quench fluorophores (alanine, glutamine and lysine) did not quench NBDM at concentrations as high as 50 mM. Interestingly, tyrosine did not quench NBDM fluorescence even at concentrations as high as 2 mM (solubility limit for tyrosine). Methionine and histidine, however, did quench NBDM via a dynamic mechanism (Figure 4).

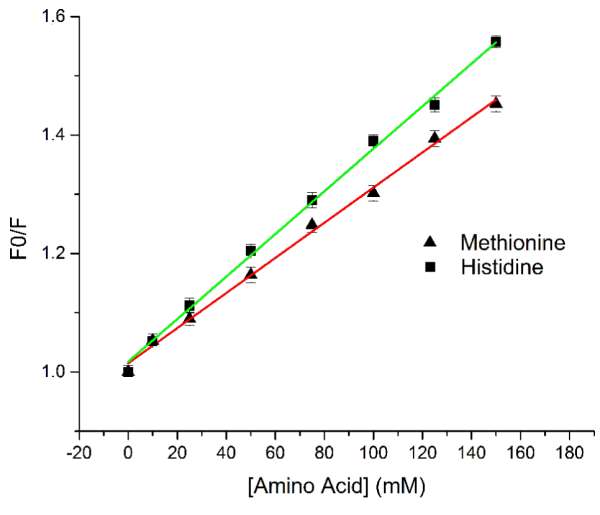

Figure 4: Comparison of quenching 2 μM NBDM, as measured by fluorescence intensity of methionine and histidine. Each data set was plotted in OriginPro 8.6 and fitted using a linear fit with direct weighting.

Carbohydrate–carbohydrate and carbohydrate–aromatic ring interactions are well-known [29,30]. Based on these interactions, we hypothesized that abnormal fluorescence behavior may be exhibited at high carbohydrate concentrations. This issue is significant because sugar uptake studies are often performed in the presences of added non-labeled sugars such as glucose, fructose or glucosamine. To assess our hypothesis, we measured the fluorescence of NBDM in the presence of glucose, fructose and glucosamine. No NBDM quenching was observed even at sugar concentrations as high as 100 mM.

Conclusion

In conclusion, we report the flow synthesis of the fluorescent fructose mimic NBDM. While we demonstrated for the first time that resin-supported nitrite ions can facilitate Tiffeneau–Demjanov rearrangements, we found that solution phase rearrangements were superior resulting in throughput gains >63-fold relative to batch conditions. We also demonstrated that the output of the Tiffeneau–Demjanov rearrangement reactor could be telescoped into the oxime reactions. The oxime reaction was very efficient exhibiting throughput gains as high as 24-fold over batch. In addition, we identified extraction and hydrogenation bottlenecks. Despite these limitations, the synthesis of NBDM can now be achieved in one day as opposed to three days in batch. The access to larger quantities to NBDM enabled us to assess the probe's quenching properties as a function of concentration and in the presence of various quenchers. These data are critical for future uptake studies that use confocal fluorescence microscopy or FACS strategies.

Supporting Information

Supporting Information File 1

Experimental part.
[http://www.beilstein-journals.org/bjoc/content/supplementary/1860-5397-9-238-S1.pdf]

Acknowledgements

Financial support from the Max Planck Society and the National Science Foundation (USA; CHE-1152020) is gratefully acknowledged.

References

1. Douard, V.; Ferraris, R. P. *J. Physiol.* **2013,** *591,* 401–414. doi:10.1113/jphysiol.2011.215731
2. Godoy, A.; Ulloa, V.; Rodríguez, F.; Reinicke, K.; Yañez, A. J.; de los Angeles Garcia, M.; Medina, R. A.; Carrasco, M.; Barberis, S.; Castro, T.; Martinez, F.; Koch, X.; Vera, J. C.; Poblete, M. T.; Figueroa, C. D.; Peruzzo, B.; Pérez, F.; Nualart, F. *J. Cell. Physiol.* **2006,** *207,* 614–627. doi:10.1002/jcp.20606

3. Warburg, O. *Science* **1956,** *123,* 309–314. doi:10.1126/science.123.3191.309
4. Liu, H. B.; Heaney, A. P. *Expert Opin. Ther. Targets* **2011,** *15,* 1049–1059. doi:10.1517/14728222.2011.588208
5. Zamora-León, S. P.; Golde, D. W.; Concha, R., II; Ivas, C. I.; Delgado-Lopez, F.; Baselga, J.; Nualart, F.; Vera, J. C. *Proc. Natl. Acad. Sci. U. S. A.* **1996,** *93,* 15522.
6. Orci, L.; Unger, R. H.; Ravazzola, M.; Ogawa, A.; Komiya, I.; Baetens, D.; Lodish, H. F.; Thorens, B. *J. Clin. Invest.* **1990,** *86,* 1615–1622. doi:10.1172/JCI114883
7. Regnell, S. E.; Lernmark, A. *Rev. Diabet. Stud.* **2011,** *8,* 454–467. doi:10.1900/RDS.2011.8.454
8. McQuade, D. T.; Plutschack, M. B.; Seeberger, P. H. *Org. Biomol. Chem.* **2013,** in press.
9. Chung, J.-H.; Cho, K.-J.; Lee, S.-S.; Baek, H. J.; Park, J.-H.; Cheon, G. J.; Choi, C.-W.; Lim, S. M. *J. Nucl. Med.* **2004,** *45,* 999–1003.
10. Hamanaka, R. B.; Chandel, N. S. *J. Exp. Med.* **2012,** *209,* 211–215. doi:10.1084/jem.20120162
11. Lawson, M. A. *West. J. Med.* **1994,** *161,* 411–412.
12. Lowe, V. J.; Naunheim, K. S. *Thorax* **1998,** *53,* 703–712. doi:10.1136/thx.53.8.703
13. Girniene, J.; Tatibouët, A.; Sackus, A.; Yang, J.; Holman, G. D.; Rollin, P. *Carbohydr. Res.* **2003,** *338,* 711–719. doi:10.1016/S0008-6215(03)00007-7
14. Tatibouët, A.; Lefoix, M.; Nadolny, J.; Martin, O. R.; Rollin, P.; Yang, J.; Holman, G. D. *Carbohydr. Res.* **2001,** *333,* 327–334. doi:10.1016/S0008-6215(01)00153-7
15. Yang, J.; Dowden, J.; Tatibouët, A.; Hatanaka, Y.; Holman, G. D. *Biochem. J.* **2002,** *367,* 533–539. doi:10.1042/BJ20020843
16. Levi, J.; Cheng, Z.; Gheysens, O.; Patel, M.; Chan, C. T.; Wang, Y.; Namavari, M.; Gambhir, S. S. *Bioconjugate Chem.* **2007,** *18,* 628–634. doi:10.1021/bc060184s
17. Tanasova, M.; Plutschack, M.; Muroski, M.; Sturla, S.; Strouse, G.; McQuade, D. T. *ChemBioChem* **2013,** in press.
18. Gowrishankar, G.; Zitzmann-Kolbe, S.; Junutula, A.; Reeves, R.; Levi, J.; Srinivasan, A.; Bruus-Jensen, K.; Cyr, J.; Dinkelborg, L.; Gambhir, S. S. *PLoS One* **2011,** *6,* e26902. doi:10.1371/journal.pone.0026902
19. Claustre, S.; Bringaud, F.; Azéma, L.; Baron, R.; Périé, J.; Willson, M. *Carbohydr. Res.* **1999,** *315,* 339–344. doi:10.1016/S0008-6215(99)00040-3
20. Caldarelli, M.; Baxendale, I. R.; Ley, S. V. *Green Chem.* **2000,** *2,* 43–46. doi:10.1039/b000816h
21. Brown, R. S.; Brennan, J. D.; Krull, U. J. *J. Chem. Phys.* **1994,** *100,* 6019–6027. doi:10.1063/1.467112
22. Chen, H.; Ahsan, S. S.; Santiago-Berrios, M. B.; Abruña, H. D.; Webb, W. W. *J. Am. Chem. Soc.* **2010,** *132,* 7244–7245. doi:10.1021/ja100500k
23. Mosiman, V. L.; Patterson, B. K.; Canterero, L.; Goolsby, C. L. *Cytometry* **1997,** *30,* 151–156. doi:10.1002/(SICI)1097-0320(19970615)30:3<151::AID-CYTO6>3.0.CO;2-O
24. Srivastava, G. K.; Reinoso, R.; Singh, A. K.; Fernandez-Bueno, I.; Hileeto, D.; Martino, M.; Garcia-Gutierrez, M. T.; Merino, J. M. P.; Alonso, N. F.; Corell, A.; Pastor, J. C. *Exp. Eye Res.* **2011,** *93,* 956–962. doi:10.1016/j.exer.2011.07.002
25. Ozawa, T.; Britz, G. W.; Kinder, D. H.; Spence, A. M.; VandenBerg, S.; Lamborn, K. R.; Deen, D. F.; Berger, M. S. *Neurosurgery* **2005,** *57,* 1041–1046. doi:10.1227/01.NEU.0000180036.42193.f6
26. Skehan, P.; Storeng, R.; Scudiero, D.; Monks, A.; McMahon, J.; Vistica, D.; Warren, J. T.; Bokesch, H.; Kenney, S.; Boyd, M. R. *J. Natl. Cancer Inst.* **1990,** *82,* 1107–1112. doi:10.1093/jnci/82.13.1107
27. Davies, J.; Burke, D.; Olliver, J. R.; Hardie, L. J.; Wild, C. P.; Routledge, M. N. *Gut* **2007,** *56,* 155–156. doi:10.1136/gut.2006.107300
28. Haritoglou, C.; Yu, A.; Freyer, W.; Priglinger, S. G.; Alge, C.; Eibl, K.; May, C. A.; Welge-Luessen, U.; Kampik, A. *Invest. Ophthalmol. Visual Sci.* **2005,** *46,* 3315–3322. doi:10.1167/iovs.04-1142
29. Seah, N.; Basu, A.; Begley, T. P. Carbohydrate–Carbohydrate Interactions. *Wiley Encyclopedia of Chemical Biology;* John Wiley & Sons, 2007.
30. Laughrey, Z. R.; Kiehna, S. E.; Riemen, A. J.; Waters, M. L. *J. Am. Chem. Soc.* **2008,** *130,* 14625–14633. doi:10.1021/ja803960x

License and Terms

Beilstein Journal of Organic Chemistry

Temperature measurements with two different IR sensors in a continuous-flow microwave heated system

Jonas Rydfjord[1], Fredrik Svensson[1], Magnus Fagrell[2], Jonas Sävmarker[1], Måns Thulin[3] and Mats Larhed[*1]

Full Research Paper

Open Access

Address:
[1]Department of Medicinal Chemistry, Uppsala University, Box 574, 751 23 Uppsala, Sweden, [2]Wavecraft AB, Bergsbrunnagatan 11, 753 23, Uppsala, Sweden and [3]Department of Mathematics, Uppsala University, Box 480, 751 06 Uppsala, Sweden

Email:
Mats Larhed[*] - mats.larhed@orgfarm.uu.se

* Corresponding author

Keywords:
continuous-flow; flow chemistry; heating; microwave; organic synthesis; temperature

Beilstein J. Org. Chem. **2013,** *9,* 2079–2087.
doi:10.3762/bjoc.9.244

Received: 10 July 2013
Accepted: 11 September 2013
Published: 10 October 2013

This article is part of the Thematic Series "Chemistry in flow systems III".

Guest Editor: A. Kirschning

Abstract

In a continuous-flow system equipped with a nonresonant microwave applicator we have investigated how to best assess the actual temperature of microwave heated organic solvents with different characteristics. This is non-trivial as the electromagnetic field will influence most traditional methods of temperature measurement. Thus, we used a microwave transparent fiber optic probe, capable of measuring the temperature inside the reactor, and investigated two different IR sensors as non-contact alternatives to the internal probe. IR sensor 1 measures the temperature on the outside of the reactor whilst IR sensor 2 is designed to measure the temperature of the fluid through the borosilicate glass that constitutes the reactor wall. We have also, in addition to the characterization of the before mentioned IR sensors, developed statistical models to correlate the IR sensor reading to a correct value of the inner temperature (as determined by the internal fiber optic probe), thereby providing a non-contact, indirect, temperature assessment of the heated solvent. The accuracy achieved with these models lie well within the range desired for most synthetic chemistry applications.

Introduction

In organic synthesis, being able to accurately determine the reaction temperature is often of utmost importance [1-3]. When using conventional heating the reaction mixture is typically heated from the outside, via the walls of the vessel. An internal temperature probe such as a thermometer or a thermocouple can in that case determine the temperature of the reaction mixture. In the last few decades the use of microwaves as a mode of heating has become increasingly popular in organic and medici-

nal chemistry [4-6], mostly owing to the development of computer-controlled dedicated reactors [7-10] that allow safe and rapid heating to high temperatures and elevated pressures. Microwave radiation directly heats the reaction mixture through two mechanisms; dipolar polarization and ionic conduction [11-13]. Compared to conventional heating this reverses the situation; in conventional heating the walls of the reaction vessel will be hotter than the reaction mixture whilst when using microwave heating the reaction mixture will have a higher temperature than the walls [8]. Unfortunately, under microwave radiation the usual methods to directly measure the internal liquid temperature of a reaction mixture such as thermocouples or mercury thermometers are affected by the electromagnetic field and will thus not be possible to use in the radiated zone [14-16]. In contrast, microwave transparent fiber optic probes can be used for correct temperature measurements. In a recent tutorial review Kappe highlighted the difficulties of temperature monitoring under microwave heating [16].

We recently described the concept of a nonresonant microwave applicator for continuous-flow organic chemistry [17,18]. The current setup is depicted in Figure 1 and features a HPLC pump, a generator, a reactor cavity, an applicator and a Ø (ID) 3 mm × 200 mm borosilicate glass tube reactor. Nonresonant mode applicators has the advantage of avoiding hot and cold spots by creating a uniform axial field, which in this setup surrounds a linear tubular borosilicate glass reactor [17]. The temperature in this setup was measured using an external Optris CT infrared (IR) sensor with a LT22 sensing head (Optris GmbH, Berlin, Germany) situated in the reactor cavity which measure the temperature of the outer wall of the reactor (IR sensor 1, see Figure 2a). Acknowledging the problem of determining the

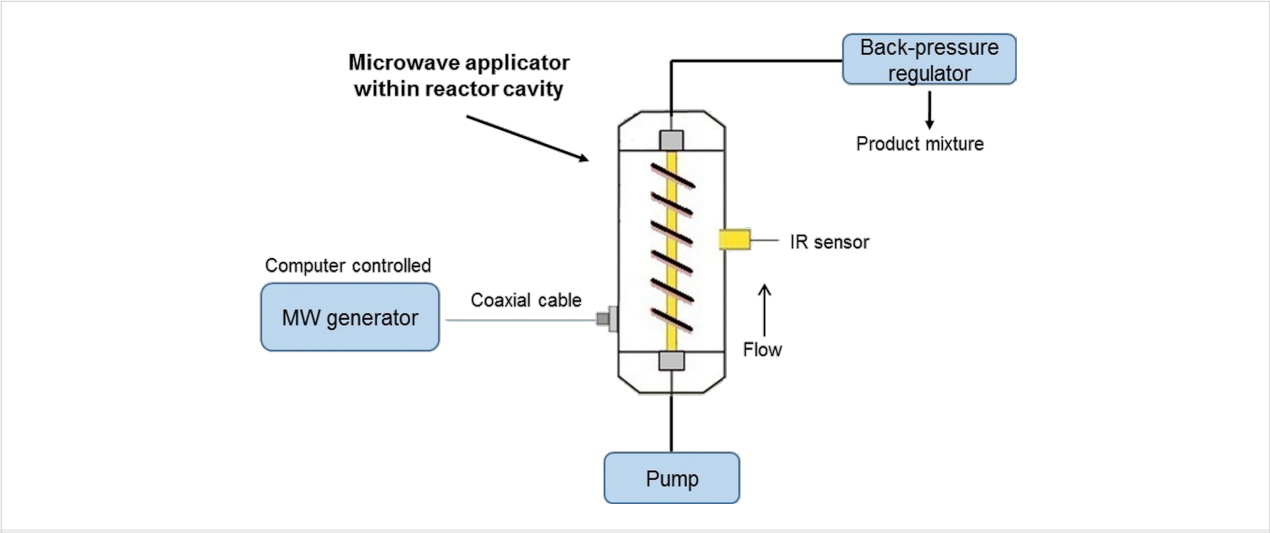

Figure 1: Instrument setup.

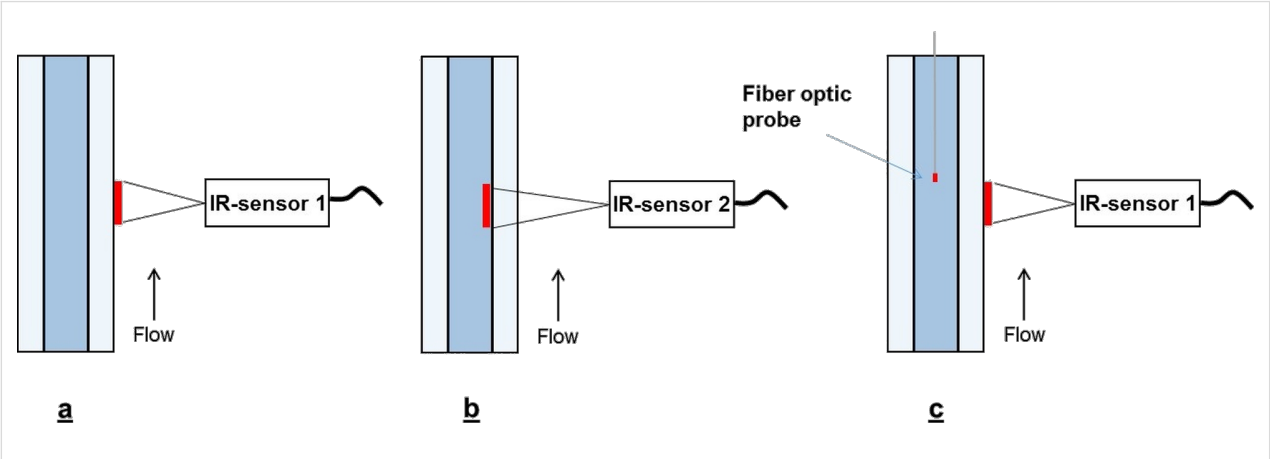

Figure 2: (a) Setup of system with temperature measurement by IR sensor 1. (b) Illustration of temperature measurement with IR sensor 2. (c) Simultaneous measurement of temperature by IR sensor 1 and an internal fiber optic probe.

temperature inside the reactor solely based on an IR sensor measuring the outer wall temperature, we decided to investigate the characteristics of this configuration with regards to what factors which affect the actual temperature of the flowing solvent in the reactor and, if possible, construct models to be able to relate the inside temperature to the outer temperature. Furthermore, we decided to include a second type of IR sensor with characteristics which could prove valuable in this and related applications (IR sensor 2, Optris CSmicro 3M, Optris GmbH, Berlin, Germany). IR sensor 2 has recently been introduced in the market and has a spectral response of 2.3 µm [19] which enable it to measure temperatures through borosilicate glass, effectively measuring on the actual fluid in the reactor (Figure 2b) [20].

Results and Discussion

Method

Measuring the internal temperature of the reactor

We opted for a fiber optic probe (Neoptix T1 Fiber Optic Temperature Probe, Neoptix Inc., Québec City) to be able to measure the temperature inside the glass reactor. The probe was positioned slightly above the measurement zone of the IR sensor (see Figure 2c, exemplified with IR sensor 1) to avoid possible problems with interference. IR sensor 1 or 2 was used to regulate the temperature and readings were then recorded using the fiber optic probe. This was done for five different temperatures (60, 80, 100, 120 and 140 °C) at four different flow rates (0.25, 0.5, 1, 2 mL/min) for nine different solvents categorized into groups depending on their tan δ value (High (tan δ > 0.5) [21]: isopropanol, methanol, DMSO; Medium (tan δ = 0.1–0.5) [21]: NMP, DMF, water; Low (tan δ < 0.1) [21]: Acetonitrile, THF, toluene). In total the full dataset with all measurements contains 173 data points for IR sensor 1 and 172 for IR sensor 2.

Data evaluation

The data collected were analyzed with regards to the influence of set temperature, flow rate and solvent to be able to distinguish between the two types of IR sensors and find the best way to correlate the "real" internal temperature of the reactor to the reading from the IR sensor in order to be able to apply a calibration to the IR sensor reading. We opted for linear multiple regression models using the full dataset, with all the measured data points. We also constructed several models with subsets of the data based on high, medium or low solvent absorption and one model where THF and toluene where excluded.

Results

Characterization of IR sensors

Examining the whole dataset for IR sensor 1 the average absolute error was 10.9 °C (Table 1). The average absolute errors were quite consistent for different flow rates, the extremes being 9.3 °C for 0.25 mL/min and 13.0 °C for 1.0 mL/min (Table 1). Examining the average absolute errors for different temperatures, an increase in average absolute error with temperatures were noted (also see Figure 3). The average absolute errors for the different solvents were also evaluated, which showed that THF and toluene have lower values (3.9 and 3.2 °C respectively) compared to the other solvents (all >10) (Table 1).

Table 1: Average absolute errors in measurements for the two IR sensors for all data and broken down by flow, set temperature and solvent.

Dataset	Average absolute error IR sensor 1 (°C)[a]	Average absolute error IR sensor 2 (°C)[a]
All data	10.9	5.4
Flow (mL/min)		
0.25	9.3	6.9
0.5	10.5	5.7
1	13.0	4.4
2	11.0	4.6
Set temperature (°C)		
60	6.0	5.0
80	9.1	4.0
100	11.3	5.4
120	13.7	6.2
140	15.2	6.6
Solvent		
isopropanol	11.0	4.2
methanol	12.9	5.7
DMSO	15.3	6.5
NMP	14.1	6.9
DMF	14.1	4.8
water	11.3	5.0
acetonitrile	10.5	4.4
THF	3.9	5.3
toluene	3.2	5.8

[a]Calculated as the average absolute difference between temperature measured by the IR sensor and the fiberoptic probe.

The average absolute error for the whole dataset for IR sensor 2 was lower than for IR sensor 1 (5.4 °C compared to 10.9 °C, Table 1). IR sensor 2 also gave substantially lower average absolute errors for most solvents, THF and toluene being the exceptions. The data indicate that higher flow rates produce a lower average absolute error for this sensor (Table 1 and Figure 3). However, no apparent correlation could be noticed for the average absolute error for different temperatures or solvents (Table 1).

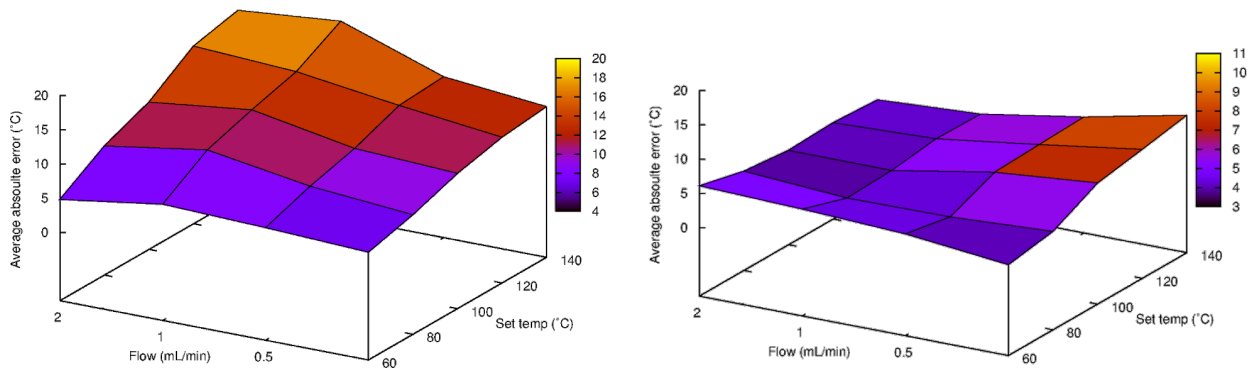

Figure 3: Average absolute errors in measurements for IR sensor 1 (left) and IR sensor 2 (right) plotted against flow and set temperature.

Model construction for IR sensor 1

A linear multiple regression model was constructed with the set temperature (corresponds to the IR sensor reading), flow rate and solvent properties (specific heat capacity, dipolar moment, dielectric constant and tan δ) as explanatory variables (Table 2, model 1). This full model provided an adjusted R^2 value of 0.985 (Table 2, model 1). Removing non-significant variables (99.9% level) from this model gave a new model (Table 2, model 2) with an adjusted R^2 value of 0.988.

As it was noted in the characterization of IR sensor 1 there was a large difference in errors between weakly microwave absorbing THF and toluene compared to the rest of the dataset. Removing toluene and THF from the full dataset and developing a new model using all variables before taking away non-significant (99.9% level) variables resulted in a model with only the set temperature as a variable, providing an adjusted R^2 value of 0.989 (Table 2, model 3).

Creating a less complicated model for the full dataset, disregarding solvent parameters and only taking into account set temperature and flow rate, shows that the flow rate is a non-significant variable (99.9% level), affording an adjusted R^2 value of 0.965 (Table 2, model 4). Removing flow rate as a variable and constructing a new model gives an adjusted R^2 value of 0.965 (Table 2, model 5). Creating models for high, medium and low absorbing solvents using only set temperature as a variable gives adjusted R^2 values of 0.986, 0.990 and 0.959 respectively (Table 2, models 6–8). A model created for only high and medium absorbing solvents gives an adjusted R^2 value of 0.988 (Table 2, model 9).

Model construction for IR sensor 2

In accordance with the results for IR sensor 1, a linear multiple regression model was constructed with the set temperature, flow rate and solvent properties (specific heat capacity, dipolar moment, dielectric constant and tan δ) as explanatory variables

Table 2: Linear multiple regression models for IR sensor 1.

Model	Adjusted R^2	RSE[a]	Variable	Coefficient	p value
Sensor 1, model 1 All data	0.985	3.96	Intercept	−13.30169	6.41×10^{-11}***
			set temperature	1.10228	$< 2\times10^{-16}$***
			flow rate	0.58598	0.2077
			tan δ	7.14174	6.69×10^{-12}***
			dielectric constant	0.05027	0.0536
			dipolar moment	2.09342	3.23×10^{-12}***
			specific heat capacity	1.45386	0.0364
Sensor 1, model 2 All data	0.988	3.999	Intercept	−14.51355	8.62×10^{-16}***
			set temperature	1.1011	$< 2\times10^{-16}$***
			tan δ	7.42205	1.30×10^{-12}***
			dipolar moment	2.40693	$< 2\times10^{-16}$***
			specific heat capacity	2.51959	1.14×10^{-8}***

Table 2: Linear multiple regression models for IR sensor 1. (continued)

Sensor 1, model 3 Excluded THF and toluene	0.989	3.467	Intercept	−0.1051	0.923
			set temperature	1.12938	$< 2\times10^{-16}$***
Sensor 1, model 4 All data	0.965	5.91	Intercept	−1.47943	0.411
			set temperature	1.11195	$< 2\times10^{-16}$***
			flow	1.02674	0.138
Sensor 1, model 5 All data	0.965	5.932	Intercept	−0.40469	0.807
			set temperature	1.11043	$< 2\times10^{-16}$***
Sensor 1, model 6 High tan δ	0.986	3.774	Intercept	2.01917	0.264
			set temperature	1.11088	$< 2\times10^{-16}$***
Sensor 1, model 7 Medium tan δ	0.990	3.191	Intercept	−1.05619	0.493
			set temperature	1.14437	$< 2\times10^{-16}$***
Sensor 1, model 8 Low tan δ	0.959	6.076	Intercept	−0.6141	0.838
			set temperature	1.05544	$< 2\times10^{-16}$***
Sensor 1, model 9 High and medium tan δ	0.988	3.505	Intercept	0.51549	0.664
			set temperature	1.12717	$< 2\times10^{-16}$***

[a]Residual standard error. *** Significant at 99.9%level.

(Table 3, model 1). This comprehensive model provided an adjusted R^2 value of 0.975 with all variables being significant (99.9% level) (Table 3, model 1). A refined model with set temperature and flow rate as variables shows that the flow rate is a significant variable (99.9% level) and generates an adjusted R^2 value of 0.963 (Table 3, model 2). Removing flow rate as a variable gives a model with an adjusted R^2 value of 0.946 (Table 3, model 3). Creating models for high, medium and low absorbing solvents using only set temperature and flow rate as variables furnish adjusted R^2 values of 0.983, 0.959 and 0.970, respectively (Table 3, models 4–6). A final model produced for only high and medium absorbing solvents gives an adjusted R^2 value of 0.970 (Table 3, model 7).

Discussion

Analyzing the collected data there seems to be a significant difference between the two IR sensors. Borosilicate-transparent IR sensor 2 has a lower mean absolute error before calibration

Table 3: Linear multiple regression models for IR sensor 2.

Model	Adjusted R^2	RSE[a]	Variable	Coefficient	P
Sensor 2, model 1 All data	0.975	4.127	Intercept	12.69142	1.93×10^{-9}***
			set temperature	0.90804	$< 2\times10^{-16}$***
			flow rate	5.4351	$< 2\times10^{-16}$***
			tan δ	−6.92092	1.28×10^{-10}***
			dielectric constant	0.12718	4.63×10^{-6}***
			dipolar moment	−1.73721	1.38×10^{-8}***
			specific heat capacity	−2.55026	5.17×10^{-4}***
Sensor 2, model 2 All data	0.963	*4.987*	Intercept	4.5697	0.00317
			set temperature	0.9026	$< 2\times10^{-16}$***
			flow rate	5.1261	1.65×10^{-15}***

Table 3: Linear multiple regression models for IR sensor 2. (continued)

Sensor 2, model 3 All data	0.946	6.002	Intercept	9.97626	1.62×10^{-8}***
			set temperature	0.89482	$< 2\times10^{-16}$***
Sensor 2, model 4 High tan δ	0.983	*3.3*	Intercept	3.52478	0.0398
			set temperature	0.8785	$< 2\times10^{-16}$***
			flow	6.29357	5.42×10^{-14}***
Sensor 2, model 5 Medium tan δ	0.959	*5.206*	Intercept	4.23114	0.135
			set temperature	0.89792	$< 2\times10^{-16}$***
			flow	5.70054	1.01×10^{-6}***
Sensor 2, model 6 Low tan δ	0.970	*4.656*	Intercept	4.55598	0.085468
			set temperature	0.94315	$< 2\times10^{-16}$***
			flow	3.929	0.000389***
Sensor 2, model 7 High and medium tan δ	0.970	*4.428*	Intercept	3.88411	0.0189
			set temperature	0.88809	$< 2\times10^{-16}$***
			flow	5.98535	$< 2\times10^{-16}$***

[a]Residual standard error. *** Significant at 99.9%level.

using the linear model. Interestingly, although a linear model taking only the temperature as a variable gives similar residual standard errors for both sensors, adding flow as a variable provides a better model for IR sensor 2, while not being a significant variable for IR sensor 1. This supports the notion that IR sensor 2 is able to measure the temperature of the actual fluid stream in the reactor, as the flow rate should affect the readings more for this sensor than IR sensor 1 measuring the outer temperature of the reactor. Adding solvent properties provides better models for both sensors, suggesting that inherent properties of the solvents highly influence their characteristics in this setup, affecting factors such as their ability to transfer heat to the reactor walls and how well they are heated. In organic synthesis applications it is unlikely that the chemist knows the characteristics of the reaction mixture to such an extent to be able to input values of such specific solvent variables, therefore less complicated models using known variables are preferred. On that note, a large difference in average absolute error was discovered for low absorbing solvents such as toluene and THF when compared to the rest of the dataset for IR sensor 1. As it is unlikely that such low absorbing reaction mixtures (without polar components such as starting materials, reagents, catalysts or additives) will be of interest for the synthetic community, we decided to develop a model with only the set temperature as a variable to describe medium and high absorbing fluid systems (cutoff: tan δ > 0.1). For these systems, the new model was an improvement compared to the corresponding model for the full dataset, and this also constitutes our suggested model for assessing the internal temperature by external measurement (outer reactor surface) with IR sensor 1.

The same conclusions regarding the size of the dataset can be made for IR sensor 2. Excluding solvent parameters from the dataset is beneficial to make a model for fluid systems with tan δ > 0.1, however, for this sensor both set temperature and flow rate is included as variables.

IR sensor 1 calibrated with model 9 (Table 2) provides more accurate measurements for medium and high absorbing fluid systems than does IR sensor 2 calibrated with model 7: the former has lower residual standard error (3.505 °C compared to 4.428 °C; p = 0.0068 using an F-test), although the average absolute error is not significantly lower (2.826 °C compared to 3.446 °C; p = 0.0868 using a Mann–Whitney test). With these calibrations, the absolute errors range from 0.024 to 8.28 °C for IR sensor 1 and from 0.00 to 13.30 °C for IR sensor 2.

When also including low absorbing fluid systems in the comparison, the situation is reversed, with IR sensor 2 providing more accurate measurements after calibration. Comparing IR sensor 1 calibrated with model 5 and IR sensor 2 calibrated with model 2, the former has a larger residual standard error (5.932 °C compared to 4.987 °C; p = 0.0107 using an F-test), but there is no significant difference between the average absolute errors (4.392 °C compared to 3.918 °C; p = 0.3076 using a Mann–Whitney test). With these calibrations, the

absolute errors range from 0.02 to 22.04 °C for IR sensor 1 and from 0.00 to 13.12 °C for IR sensor 2.

The practical aspects of the different methods of temperature measurements are also of great importance. An IR sensor does in that sense present a non-invasive measurement of temperature, be it external or internal. The fiber optic probe on the other hand will be invasive, and will disturb the flow in the reactor. Since it will also displace some of the reactor volume with its own body this might also to some extent affect the heating, as the power applied per volume unit will be higher where the fiber optic probe is located in the reactor. It is also quite sensitive to rough handling and may break, and, according to our experience, fiber optic probes are generally susceptible towards higher temperatures at elevated pressures in organic solvents.

Considering the above points the option of using the fiber optic probe as the standard tool for temperature measurements in continuous-flow synthesis appears less attractive. Although providing a direct measurement of the temperature in the reactor it is not robust enough for daily use and handling, especially under reaction conditions that may be relevant in organic synthesis applications [22,23].

There is also one practical aspect that was noted as a difference between the two IR sensors, and that is that IR sensor 2, the one measuring directly on the fluid in the reactor, provides a much faster response to changes in temperature (Figure 4). This means practically, that when the software control adjusts power to reach set temperature it does not have to compensate for the lag that is created for IR sensor 1 when the reactor walls need to be heated. This characteristic might prove in handy for processes where a change in properties of the contents of the reactor happens suddenly as the control software can respond more directly by adjusting the power accordingly to maintain set temperature. This rapid response and the ability to measure the temperature through the borosilicate glass also, in the authors' opinion, make an evaluation of IR sensor type 2 for use in batch instruments of prime importance.

For applications where such a setup as the one described is used for continuous production it is possible to, through a similar

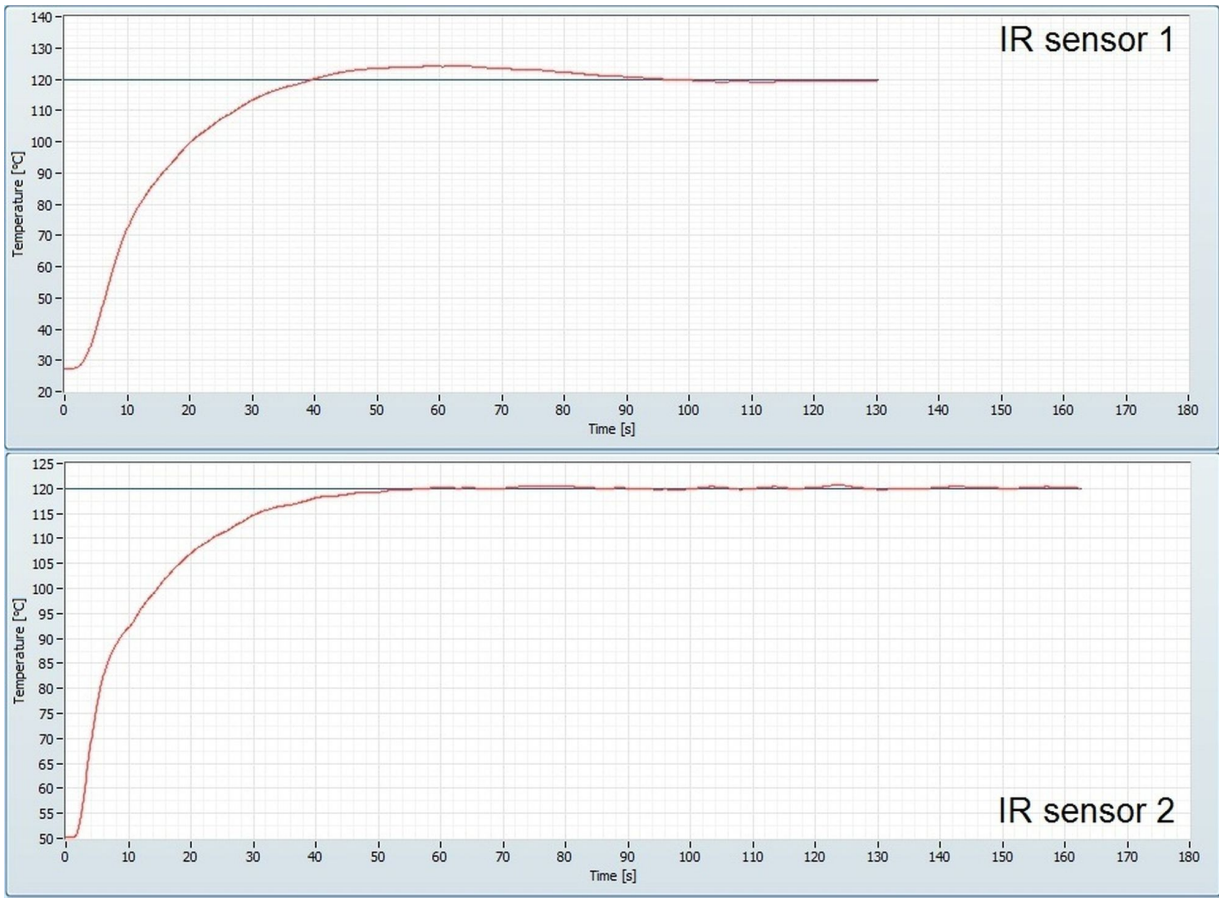

Figure 4: Heating profiles for IR sensor 1 (top) and IR sensor 2 (bottom) when heating isopropanol at a flow rate of 1 mL/min.

setup as the one we have used (Figure 1), simultaneously monitor the temperature with an IR sensor and a fiber optic probe. This way a temperature calibration based on the exact conditions can be performed, and the linearity within a specified set of conditions is in our experience very high (see for example, Figure 5). After the calibration has been performed the configuration can be changed again to only use an IR sensor for temperature measurement, applying the model found during the calibration to show the internal temperature. This is also our recommendation in general if knowledge of the exact temperature is of importance e.g for kinetic studies.

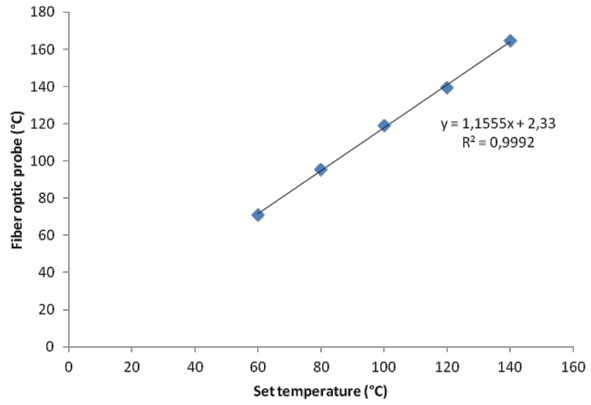

Figure 5: IR sensor 1, NMP, 1 mL/min.

Finally, recommending one type of IR sensor is not trivial, as both have their advantages and disadvantages; IR sensor 1 provides somewhat better accuracy when applying models to assess the internal temperature while IR sensor 2 is closer to the internal temperature uncorrected. IR sensor 2 also provides faster response to changes in internal temperature which might be advantageous, whilst IR sensor 1 on the other hand is less direct since the changes in internal temperature must propagate through the reactor wall before being registered.

Using linear multiple regression models offer improvements over the uncalibrated readings, for which the average absolute errors were 10.9 °C for IR sensor 1 and 5.4 °C for IR sensor 2 (Table 1). Although not able to reduce the error down to the level of the IR sensors themselves [20,24] the accuracy achieved with these models lie well within the range desired for most medicinal and organic chemistry applications. Thus, our recommendation must be that the choice should be based on the characteristics of the IR sensor, rather than its performance, as both types of IR sensor tested perform good. Currently efforts in our lab focus on improving temperature calibration by on-the-fly determination of tan δ.

Conclusion

It cannot be overstated that accurately measuring temperature under the influence of an electromagnetic field is not a trivial problem. In this evaluation we have used a fiber optic probe which allows the measurement of temperatures inside a reactor in a continuous-flow system using a nonresonant microwave heating device, and investigated two IR sensors as non-contact alternatives to this internal probe. Although differences were detected between the two IR sensors, in that IR sensor 2 provides a more direct measurement by being able to "see" through the borosilicate glass wall of the reactor, both sensors are, with a good degree of accuracy, able to assess the internal temperature after applying calibration by linear regression. Our study shows that temperature measurements using IR sensors in these systems can be improved using simple linear multiple regression models. In our case the models having the best balance between accuracy and simplicity used only one or two input variables. For IR sensor 1 the actual temperature was related only to the set temperature, and for IR sensor 2 the flow rate was also used as a variable. We also conclude that these models were improved when using only data for solvents with a tan δ > 0.1 (medium and high microwave absorbing solvents). In conclusion, we believe this investigation might be of interest for the future development and understanding of microwave heated continuous flow synthesis.

Supporting Information

Supporting Information File 1

Experimental data.
[http://www.beilstein-journals.org/bjoc/content/supplementary/1860-5397-9-244-S1.pdf]

Acknowledgements

We would like to thank the the Swedish Research Council (VR), Knut and Alice Wallenberg's foundation and Wavecraft for support.

References

1. Kappe, C. O.; Pieber, B.; Dallinger, D. *Angew. Chem., Int. Ed.* **2013,** *52,* 1088–1094. doi:10.1002/anie.201204103
2. Dudley, G. B.; Stiegman, A. E.; Rosana, M. R. *Angew. Chem., Int. Ed.* **2013,** *52,* 7918–7923. doi:10.1002/anie.201301539
3. Kappe, C. O. *Angew. Chem., Int. Ed.* **2013,** *52,* 7924–7928. doi:10.1002/anie.201304368
4. Caddick, S.; Fitzmaurice, R. *Tetrahedron* **2009,** *65,* 3325–3355. doi:10.1016/j.tet.2009.01.105
5. Kappe, C. O.; Stadler, A.; Dallinger, D. *Microwaves in Organic and Medicinal Chemistry;* Wiley-VCH Verlag GmbH & Co. KGaA: Weinheim, Germany, 2012.

6. Gising, J.; Odell, L. R.; Larhed, M. *Org. Biomol. Chem.* **2012,** *10,* 2713–2729. doi:10.1039/c2ob06833h
7. Stone-Elander, S. A.; Elander, N.; Thorell, J.-O.; Solås, G.; Svennebrink, J. *J. Labelled Compd. Radiopharm.* **1994,** *34,* 949–960. doi:10.1002/jlcr.2580341008
8. Strauss, C. R.; Trainor, R. W. *Aust. J. Chem.* **1995,** *48,* 1665–1692. doi:10.1071/CH9951665
9. Schanche, J.-S. *Mol. Diversity* **2003,** *7,* 291–298. doi:10.1023/B:MODI.0000006866.38392.f7
10. Kappe, C. O.; Stadler, A.; Dallinger, D. Equipment Review. *Microwaves in Organic and Medicinal Chemistry;* Wiley-VCH Verlag GmbH & Co. KGaA: Weinheim, Germany, 2012; pp 41–81.
11. Gedye, R. N.; Smith, F. E.; Westaway, K. C. *Can. J. Chem.* **1988,** *66,* 17–26. doi:10.1139/v88-003
12. Mingos, D. M. P.; Baghurst, D. R. *Chem. Soc. Rev.* **1991,** *20,* 1–47. doi:10.1039/cs9912000001
13. Gabriel, C.; Gabriel, S.; Grant, E. H.; Halstead, B. S. J.; Mingos, D. M. P. *Chem. Soc. Rev.* **1998,** *27,* 213–223. doi:10.1039/a827213z
14. Langa, F.; de la Cruz, P.; de la Hoz, A.; Díaz-Ortiz, A.; Díez-Barra, E. *Contemp. Org. Synth.* **1997,** *4,* 373–386. doi:10.1039/co9970400373
15. Mingos, D. M. P.; Whittaker, A. G. Microwave Dielectric Heating Effects in Chemical Synthesis. In *Chemistry Under Extreme and Non-Classical Conditions;* van Eldik, R.; Hubbard, C. D., Eds.; John Wiley and Sons, and Spectrum Akademischer Verlag: New York, Heidelberg, 1997; pp 479–514.
16. Kappe, C. O. *Chem. Soc. Rev.* **2013,** *42,* 4977–4990. doi:10.1039/c3cs00010a
17. Öhrngren, P.; Fardost, A.; Russo, F.; Schanche, J.-S.; Fagrell, M.; Larhed, M. *Org. Process Res. Dev.* **2012,** *16,* 1053–1063. doi:10.1021/op300003b
18. Fardost, A.; Russo, F.; Larhed, M. *Chim. Oggi* **2012,** *30* (4), 14–17.
19. OptrisGmbH optris® CSmicro 3M. http://www.optris.com/optris-csmicro-3m?file=tl_files/pdf/Downloads/Compact Series/Data Sheet optris CSmicro 3M.pdf.
20. OptrisGmbH Basic Principles of Non-Contact Temperature Measurement. http://www.optris.com/applications?file=tl_files/pdf/Downloads/Zubehoer/IR-Basics.pdf.
21. Kappe, C. O. *Angew. Chem., Int. Ed.* **2004,** *43,* 6250–6284. doi:10.1002/anie.200400655
22. Bremberg, U.; Lutsenko, S.; Kaiser, N.-F.; Larhed, M.; Hallberg, A.; Moberg, C. *Synthesis* **2000,** 1004–1008. doi:10.1055/s-2000-6298
23. Nilsson, P.; Gold, H.; Larhed, M.; Hallberg, A. *Synthesis* **2002,** 1611–1614. doi:10.1055/s-2002-33331
24. OptrisGmbH optris® CT LT. http://www.optris.com/optris-ct-lt?file=tl_files/pdf/Downloads/Compact Series/Data Sheet optris CT LT.pdf

License and Terms

Beilstein Journal of Organic Chemistry

Flow synthesis of phenylserine using threonine aldolase immobilized on Eupergit support

Jagdish D. Tibhe, Hui Fu, Timothy Noël, Qi Wang, Jan Meuldijk and Volker Hessel[*§]

Full Research Paper

Open Access

Address:
Micro Flow Chemistry and Process Technology, Department of Chemical Engineering and Chemistry, Eindhoven University of Technology, P.O. Box 513, 5600 MB Eindhoven, the Netherlands

Email:
Volker Hessel[*] - v.hessel@tue.nl

* Corresponding author
§ Tel.: +31(0)402472973

Keywords:
Eupergit; flow chemistry; immobilized enzyme; threonine aldolase

Beilstein J. Org. Chem. **2013,** *9,* 2168–2179.
doi:10.3762/bjoc.9.254

Received: 13 June 2013
Accepted: 24 September 2013
Published: 22 October 2013

This article is part of the Thematic Series "Chemistry in flow systems III".

Guest Editor: A. Kirschning

Abstract

Threonine aldolase (TA) from *Thermotoga maritima* was immobilized on an Eupergit support by both a direct and an indirect method. The incubation time for the direct immobilization method was optimized for the highest amount of enzyme on the support. By introducing the immobilized TA in a packed-bed microreactor, a flow synthesis of phenylserine was developed, and the effects of temperature and residence time were studied in particular. Calculations of the Damköhler number revealed that no mass transfer limitations are given in the micro-interstices of the packed bed. The yield does not exceed 40% and can be rationalized by the natural equilibrium as well as product inhibition which was experimentally proven. The flow synthesis with the immobilized enzyme was compared with the corresponding transformation conducted with the free enzyme. The product yield was further improved by operating under slug flow conditions which is related to the very short residence time distribution. In all cases 20% diastereomeric excess (de) and 99% enantiomeric excess (ee) were observed. A continuous run of the reactant solution was carried out for 10 hours in order to check enzyme stability at higher temperature. Stable operation was achieved at 20 minute residence time. Finally, the productivity of the reactor was calculated, extrapolated to parallel run units, and compared with data collected previously.

Introduction

Enzymes are bio-based catalysts having some distinct properties like high activity, high stereo-, regio- and chemoselectivity and high substrate specificity, which allow their use in a complex synthesis in a green and clean manner [1]. Recently, enzymes have received much attention for making processes more economically and ecologically beneficial, as they facili-

tate downstream processing requiring less separation steps, providing the best product quality with high purity at low energy consumption [2]. Still, the industrial applications of enzymes are hampered by many factors, like the lack of operational stability and the difficulty of enzyme recovery. Recently, Wang et al. have shown that the activity and recyclability of the CalB enzyme can be enhanced by the use of a polymersome Pickering emulsion. As such, a biphasic system could be used by loading the enzyme in the aqueous phase and organic reagents in the polymersome [3]. The above mentioned drawbacks may also be largely avoided by the use of an immobilized enzyme [4]. Immobilization has also been shown to enhance the stability of the enzyme [5]. A number of different immobilization methods were reviewed by Sheldon [6].

Despite the many advantages to use enzymes, their activity is often low, creating a demand for process intensification. In the last decade, different methods of process intensification have been proposed and tested for both fine-chemical and bulk-chemical processing [7-9]. It makes sense to test process intensification for biochemical processing as well. Microreactors, as a preferred process intensification tool, have gained considerable importance due to their many advantages over conventional batch reactors, including rapid heat and mass transfer, high surface area-to-volume ratios for dispersed media, and short processing times [10]. Indeed, there is indication that biocatalysis under flow conditions provided by a microreactor can result in better process control by external numbering-up in which each subunit of reaction can be examined separately with enhanced productivity [11].

Microreactors have been used in many fields of chemistry such as analytical systems [12], multiphase reaction systems [13-15], cross coupling reactions [16] and in chemical synthesis of pharmaceutical products [17]. Furthermore, the use of novel process windows to enhance the chemical production has also been reviewed [18-22]. From the industrial perspective, Hessel et al. have analyzed the patent situation in the field of microreaction technology [23]. In extension to such fine-chemical and pharmaceutical applications being investigated for almost 20 years, the quite recent introduction of microfluidic devices in bioprocess intensification and biocatalysis has been reviewed [24]. Asanomi et al. have also summarized the use of microfluidic devices in biocatalysis and compared them with conventional batch reactors [25]. The advantages of enzymatic microreactors have been demonstrated both in process development and for the production scale [26]. Similarly these reactors can provide high throughput opportunities, reduced reaction time with high conversion efficiency and high productivity per unit reaction volume for biocatalysis in fine chemistry [27]. These advantages have been demonstrated for reactions such as hydrolysis and esterification [27], oxidation and reduction [28], C–C bond formation [29], and polymerization [30].

Recent advancements in the field of enzymatic microreactors include the use of alginate/protamine/silica hybrid capsules with ultrathin membranes [31], monolithic enzyme microreactors [29,32], and biodegradable enzymatic microreactors based on surface-adhered physical hydrogels of PVA [33]. Babich et al. demonstrated the possibility of gram scale synthesis of phosphorylated compounds using phosphatase immobilized on Immobeads [34]. Buchegger et al. used a microfluidic mixer to study the pre-steady state development of an enzymatic bioreaction and found that the dynamics of a biochemical reaction can be studied in a few seconds [35].

Although many promising routes have been developed for the synthesis of chiral α-amino alcohols, these often depend on the use of toxic and expensive chiral ligands coupled to metal complexes [36]. Enzymes overcome these drawbacks as they are not toxic and they can be obtained easily from microorganisms. Threonine aldolases (TA) are a class of enzymes which is PLP (pyridoxal-5'-phosphate) dependent and can catalyze the aldol reaction between glycine and a variety of aromatic and aliphatic aldehydes [37-39]. The same enzyme can also catalyze the reverse reaction, i.e. the cleavage of threonine into glycine and acetaldehyde [40-42]. Fesko et al. conducted kinetic and thermodynamic studies using the phenylserine synthesis from glycine and benzaldehyde as a model reaction [43]. The same group also investigated the effect of ring-sided substituents of benzaldehyde on the product yield, revealing that TA accepts aromatic compounds having electron withdrawing groups as a substrate [44]. Aldolases are known to be hampered by thermodynamic and kinetic limitations, such as low diastereoselectivity and product yield. To overcome this drawback of aldolases, dynamic kinetic asymmetric transformation has been carried out in which a bi-enzymatic process was performed to achieve a high yield of the product by shifting the reaction equilibrium [45].

Eupergit oxirane acrylic beads provide a rapid and simple support for immobilization and have been used to immobilize various enzymes for a number of reactions [46]. Immobilization on Eupergit (a porous material) can be achieved without the need for any additional reagents, as the epoxy groups on Eupergit can react directly with the nucleophilic groups of the enzyme by forming strong covalent linkages like amino, hydroxy or mercapto functional groups. Eupergit has a high density of epoxy groups on the surface (oxirane density 300 μmol/g dry beads [47]), increasing the possibility of multipoint attachment of the enzyme. This multipoint attachment provides enhanced conformational stability, which translates to

long term operational stability. Fu et al. have already investigated the thermal stability of TA on different supports [48] and found that the enzyme stability increases after immobilization on Eupergit support.

In continuation of our previous work [48], this paper includes further investigation of the thermal stability of TA on Eupergit by a so-called direct and indirect method. Also, a flow synthesis of Eupergit-immobilized TA in a packed bed microreactor was established and compared to the use of free enzymes in the reaction of glycine and benzaldehyde. The reaction investigated is the synthesis of phenylserine starting from benzaldehyde and glycine (Scheme 1). The segmented flow experiments were carried out as an alternative to the free enzyme in a single phase flow to maximize the yield. A continuous activity check was performed for determining the stability of the immobilized enzyme over a longer period of time. The productivity of the flow systems reported here was also determined and compared with the performance published in previous literature.

Results and Discussion

Comparison of direct and indirect enzyme immobilization

For the direct immobilization method, 99% enzyme retention and 52% activity retention were observed, while in the indirect method the values were 78% and 89%, respectively (Table 1). In case of direct immobilization, the enzyme and support are both directly in contact with each other which resulted in higher values for enzyme retention. For the indirect method, however, the epoxy groups were converted into aldehyde groups. These groups can only react with nucleophiles such as amino groups. During treatment of Eupergit with ethylenediamine, a coupling of two adjacent epoxy groups on the support can occur which would result in a lower amount of enzyme retention. The multipoint attachment in case of direct immobilization may block the active site of the enzyme and, as a consequence, this would result in a lower degree of activity retention. In case of the indirect method the enzyme was separated from the support by a spacer element. This was formed by the reaction of ethylenediamine and glutaraldehyde. This reaction reduces the probability of blocking the active site of the enzyme which would provide higher activity retention. For the direct method, our results demonstrate a high activity to those reported in the literature. There, only 52.4% enzyme retention and activity retention of 20.7% were achieved while for the indirect method 37% enzyme loading with 31% of activity retention was observed [49].

Table 1: Comparison of direct and indirect method.

Method	Enzyme retention (%)	Activity retention (%)
Direct	99	52
Indirect	78	89

Comparison of thermal stability of TA immobilized by two different methods

For TA immobilized by using the direct method, the increase in stability of the enzyme is likely due to a multipoint attachment. Around 80% of activity retention was observed after 5 hours. The multipoint attachment may provide a rigid structure for the enzyme and increased stability. In case of the indirect method the enzyme almost behaves like a free enzyme, which is due to the introduction of spacer between the enzyme and the support. This enhances the conformational freedom of the enzyme. The behavior of the curve for the three cases free, indirect immobilized and direct immobilized TA is shown in Figure 1.

Optimization of immobilization time

The optimization of immobilization is discussed here only for the direct method. In order to make the process more feasible and cost effective for industrial applications, we reduced the time of immobilization of TA on Eupergit [50]. The amount of immobilized enzyme increases until it reaches a plateau after about 24 hours (Figure 2). At this point 99% of enzyme immobilization was achieved which is a substantial improvement with respect to 72 hours originally employed.

The phenylserine synthesis in batch using free enzyme

Batch reactions were carried out to estimate the yield of phenylserine formation and reaction time which can principally be

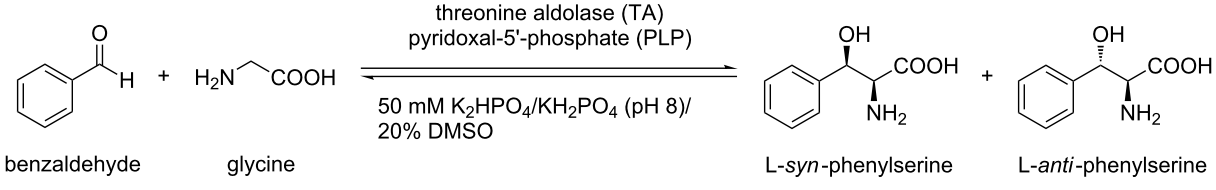

Scheme 1: Phenylserine synthesis.

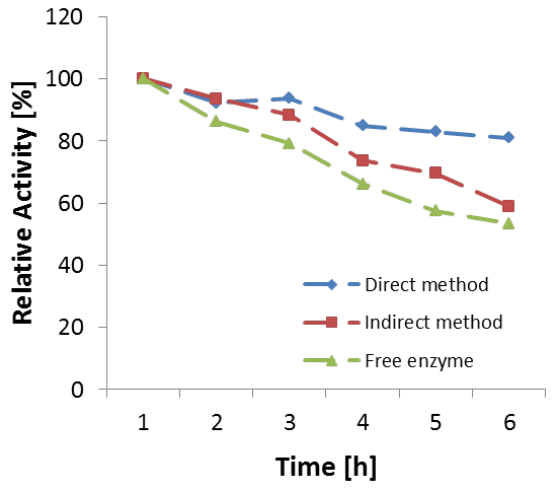

Figure 1: Activity loss of TA immobilized by two different methods and as a free enzyme at 80 °C. Reproduced with permission from Elsevier [48].

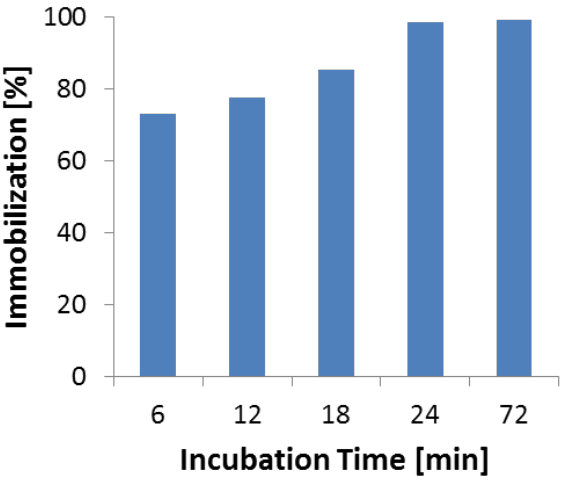

Figure 2: Degree of immobilization versus incubation time.

achieved. Flow processing, and in particular its productivity highly depends on achieving a complete transformation in a very short time, ideally within a few minutes or less. After 20 minutes, a 40% yield of phenylserine was achieved and no further yield increase was observed (Figure 3). TA-based reactions are known to be of equilibrium-type which limits the achievable yield to about 40% in the given case. Another reason could principally be deactivation of the enzyme. Yet, this is not so likely, since Figure 1 shows that even after 5 hours about 50% of the enzyme still shows activity. Thus, a self-inhibitory effect of the product on the TA at a given concentration can be made responsible or alternatively the reactant glycine which is present in high concentration could cause inhibition [51].

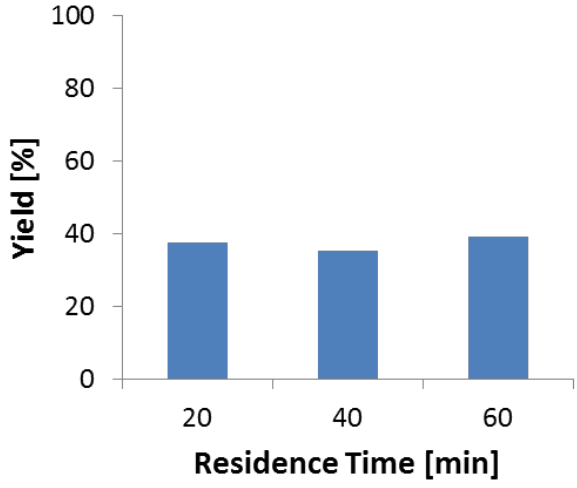

Figure 3: Batch reaction using free enzyme. Reaction conditions: Reaction volume (10 mL), TA (2.7 mg, specific activity – 0.135 U/mg), temperature (70 °C).

Product inhibition study

The product inhibition study was carried out in order to understand whether there is an effect of product formed during the reaction which might block the active site of the enzyme. To achieve this we carried out three reactions for 40 minutes at 70 °C. The amount of product which was added before the reaction is 20, 40 and 60 mol % (Figure 4). It has been observed that when the amount of product increases the yield starts to decrease which indicates that the product inhibition effect does exist. This is due to the very high concentration of product as compared to the amount of enzyme used for the reaction.

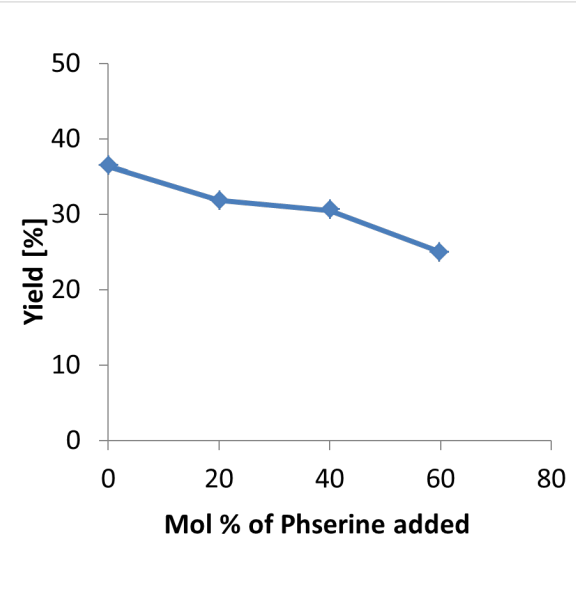

Figure 4: Product inhibition study.

Synthesis of phenylserine by using immobilized TA in a microreactor

Effect of temperature

The effect of the reaction temperature on the yield of phenylserine was investigated at a residence time of 10 minutes (flow rate = 25 µL/min). As shown in Figure 5, the yield increased up to a temperature of 70 °C reaching a value of maximal 25% which is in line with the limitations based on the equilibrium discussed before. Above 70 °C, a decrease in yield was observed (Figure 5). It can be assumed that above 70 °C the reaction rate is even higher, however enzyme deactivation becomes more substantial. Therefore, we chose 70 °C as the optimum temperature for the following experiments.

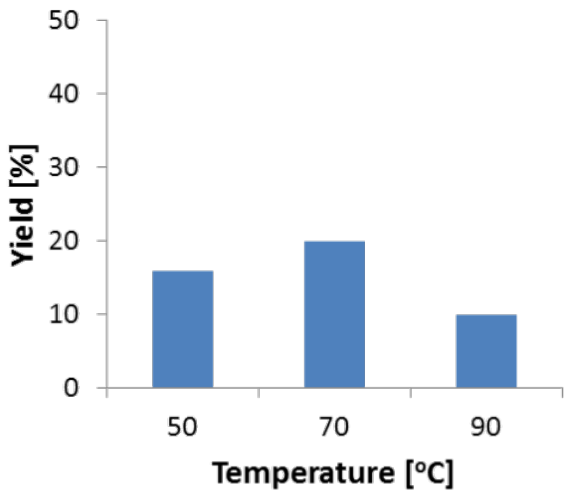

Figure 5: Effect of temperature on product yield. Reaction conditions: Reaction volume (0.250 mL), TA (1.1 mg, specific activity – 0.052 U/mg), flow rate (25 µL/min). Samples were taken after 30 minutes at the indicated temperature.

Effect of flow rates

When operating the packed bed microreactor with immobilized TA at 70 °C, the yield of phenylserine can be further increased to 30% at longer residence times (Figure 6). This result resembles the batch performance reported above. The reason can be the already supposed product inhibition of the enzyme or a specific flow effect. At higher flow rates and shorter residence times the product yield decreases. In order to check whether mass transfer limitations are involved, we estimated the mass transfer coefficient for transport of the substrate to the particles.

Mass transfer calculations

The calculation of the Damköhler number was carried out for the reaction with immobilized TA under the same conditions discussed before in the section above. The following values were used to calculate the mass transfer coefficient, porosity

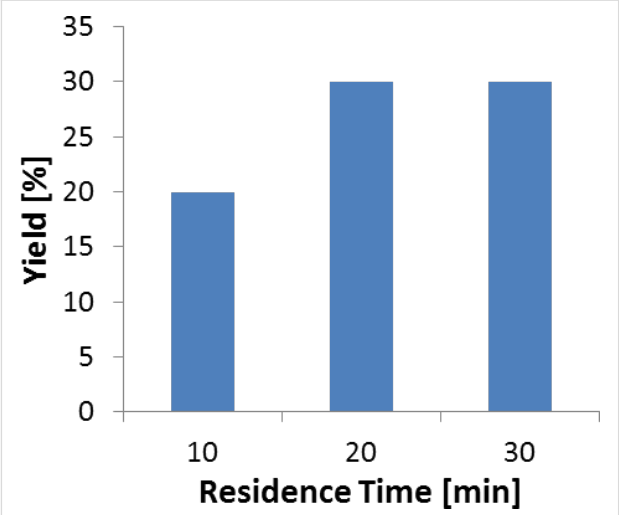

Figure 6: Effect of flow rates on yield for immobilized enzymes in a packed bed microreactor (70 °C). Reaction conditions: Reaction volume (0.250 mL), TA (1.1 mg, specific activity – 0.052 U/mg), temperature (70 °C).

(ε) = 0.5 estimated, density (ρ) = 1024 kg/m^3, viscosity of fluid (µ) = 0.00134 kg/ms and thermal conductivity (K) = 0.58 (W/m·K).

The Reynolds number (Re) for a fluid flow through a bed of approximately spherical particles of diameter D can be calculated, according to Equation 1 in which the void fraction is ε and the superficial velocity is V.

$$\mathrm{Re} = \frac{\rho V D}{\mu(1-\varepsilon)} \tag{1}$$

The Reynolds number was 0.1 and the Schmidt (Sc) number was calculated to be 1.309. Next, the Sherwood number (Sh) was calculated using the following equation,

$$\mathrm{Sh} = \mathrm{Re}^{0.5} \cdot \mathrm{Sc}^{\frac{1}{3}} \tag{2}$$

The Sherwood number was found to be 1.093 which provided a mass transfer coefficient (k) of 17 × 10^{-6}. The reaction rate v_{max} was calculated using experimental data and the value was 1.67 × 10^{-6} mol/m^{2}s. This allowed us to determine the Damköhler number (Da) using following equation,

$$\mathrm{Da} = \frac{\text{Rate of reaction}}{\text{Rate of mass transfer}} \tag{3}$$

The Damköhler number turned out to be 0.98 × 10^{-3}, which is much smaller than the threshold criterion 1. Therefore, no mass transfer limitation can be encountered in the present case.

Free enzymes in flow using a capillary microreactor

Some flow experiments were performed in Teflon tubing at 70 °C with the free enzyme and unraveled an almost linear increase of product yield with increasing residence times. Under these homogeneous conditions, very short diffusion distance between the reactants and the enzyme is guaranteed. Yet, the yield does not increase above 15% for a residence time of 20 minutes which is about half compared to heterogeneous conditions. This could point towards a higher enzyme activity and/or to higher enzyme loadings in the immobilized state.

For a residence time of 60 min (Figure 7) a yield of 32% was achieved, which is not substantially higher than found for the best yield using the immobilized enzyme under microreactor operation conditions. Studies under even longer residence times could not be conducted, since the corresponding flow rates could not be accommodated with the pumps used.

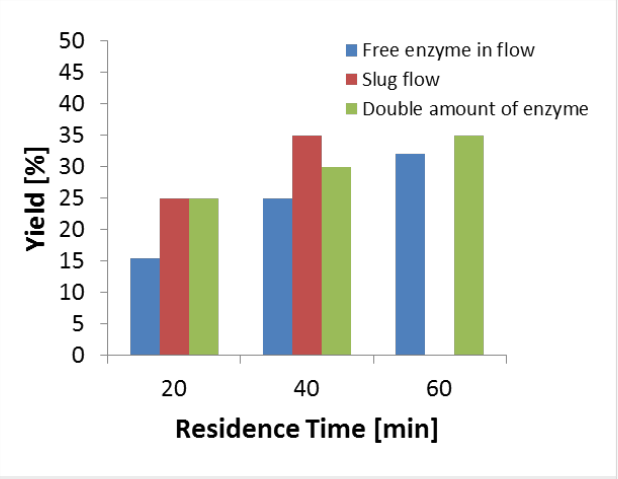

Figure 7: Effect of residence time on yield for free enzymes in a Teflon tube microreactor at 70 °C. Reaction conditions: For free enzyme in flow: Reaction volume (0.500 mL), TA (0.135 mg, specific activity – 0.135 U/mg). Slug flow: Reaction volume (0.500 mL), TA (0.135 mg, specific activity – 0.135 U/mg). Double amount single phase: Reaction volume (0.500 mL), TA (0.27 mg, specific activity – 0.135 U/mg).

Next, segmented flow experiments were carried out by injecting argon in the tube microreactor which generated a slug flow with a flow rate of 12.5 µL/min and 6 µL/min, respectively, which corresponded to residence times of 20 and 40 minutes. We aimed to achieve a much narrower residence time distribution under slug flow conditions as opposed to the laminar parabolic flow profile of the single-phase flow system. The latter can lead to a considerable share of reactants experiencing a (much) shorter residence time than the given (averaged) residence time based on the nominal flow rates. Under slug flow conditions, all reactants will see almost the same residence time due to reduced axial dispersion allowing the reactor to operate as an ideal plug flow reactor. Additionally, slug flow is known to create profound transversal recirculation patterns within the liquid slugs which constitute a permanent highly mixed fluid system. Single-phase flow operations do not show similarly strong passive mixing. However, as no mass transfer limitations exist for the immobilized enzyme which also should apply here, the mixing issue can be regarded of less relevance than the residence time control issue.

Indeed, the slug flow derived yields are higher compared to the single-phase flow process. The product yield for the slug flow process with a residence time of 20 min, is lower compared to the flow operation with the immobilized enzyme. For a residence time of 40 min the product yield is 34%. Thus, it is slightly higher than the best yield obtained for a flow reactor using the immobilized enzyme as packed bed. When comparing this result with the free enzyme reaction using a capillary microreactor, the yield increases from 16 to 25% (20 min residence time) and only a 5% increase of the yield for 40 min residence time. Obviously, slug flow operation does have a slight effect on yields. When the amount of enzyme was doubled for a single-phase flow experiment using a Teflon tube microreactor, the product yield improved from 16% to 25% (20 min residence time). A longer residence time of 40 min further increases the yield to 30% which did not change when employing a residence time of 60 min. Again, either deactivation of TA or product inhibition can be made responsible as discussed above.

Long term enzyme stability

A continuous experiment was performed to study the long term stability of immobilized enzyme at 70 °C. The stability of Eupergit-bound TA (direct method) has already been discussed. The studies revealed that at 80 °C there is 20% loss of enzyme activity within 4 hours. It was anticipated that at lower temperatures the lifetime of the immobilized enzyme would be extended and would allow long term operation of the flow system. Indeed, the product yield was almost constant at around 30–35% even after 10 hours of continuous operation (Figure 8). Here, the inhibitory effect by the product might be reduced due to the large amount of enzyme (1.1 mg) and the small reactor volume of about 250 µL. The continuous removal of the product from the reaction system may reduce this effect. This signifies the stable operation of the immobilized enzyme over a longer period of time which is useful to reduce the cost of the process by reusing the catalyst.

Conclusion

To the best of our knowledge, we report the first use of immobilized threonine aldolase in a microreactor for the flow synthesis of phenylserine. So far, we achieved a maximum of about 30% yield under the typical flow rates using TA bound to Eupergit.

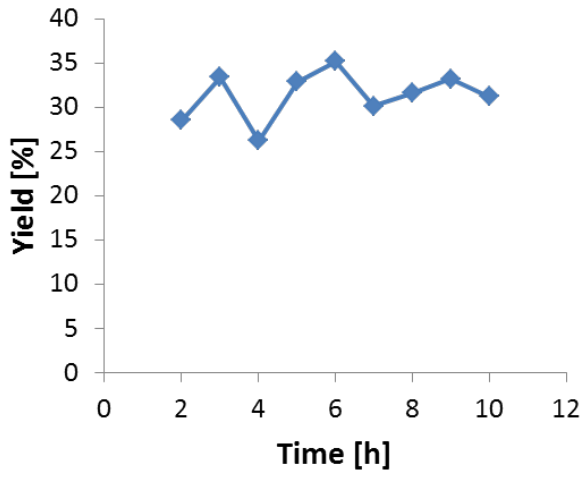

Figure 8: Long term enzyme stability at 70 °C. Reaction conditions: Reaction volume (0.250 mL), TA (1.1 mg, specific activity – 0.052 U/mg), flow rate (12.5 µL/min), temperature (70 °C).

The yield was about 35% for the free enzyme using a tubular microreactor. Here slug flow performed slightly better than single-phase flow operation. Several explanations have been provided which rationalizes the findings reported above. These include the residence time distribution present for the single-phase flow operation, different degrees of enzyme deactivation, and different degrees of enzyme activity – each being different for the three flow operations investigated. This gives room for future optimization. Above all, however, the existence of an equilibrium between starting materials and products is the major factor of being restricted to a maximum of 40% yield. Here, removal of the product from the enzyme thereby readjusting the equilibrium is the method of choice. One opportunity to achieve this could be the decarboxylation of phenylserine as depicted in Scheme 2 which is currently been investigated in our laboratories.

Taking into account the experimentally derived flow performance mentioned above, the calculated TA-enzyme based microreactor productivity was found to be 5.4 mg/h. From an industrial perspective on microreactors, it is reasonable to assume that an external numbering-up of 10 (respectively, 54 mg/h) along with scaling-out of those reactors the production of 200 mg/h in total can be achieved. This value is not too far away from the production need for commercial high-value products in pharmacy at a price of 500 €/g and higher. The comparison between theoretical and experimental values for productivity has been shown in Table 2.

Both the theoretical and experimental productivities are based on a quite low (experimentally used) amount of active enzymes; simply for reasons of availability. In [48] we calculated also productivities of other enzymatic microreactors (with other enzymes, having no availability limitation) and this result in much higher productivities.

In this paper, we made a first step towards a critical view on the commercial potential for high-priced pharmaceutical products using enzymatic microreactor technology.

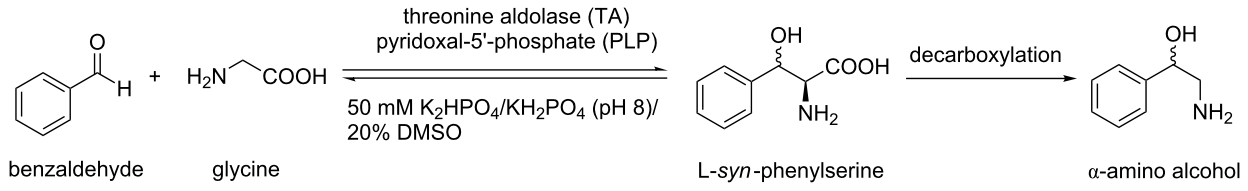

Scheme 2: Synthesis of chiral α-aminoalcohol by telescoping aldolase reaction with decarboxylation.

Table 2: Comparison of productivity between the theoretical calculations and experimental observations.

Calculations	Specific activity of enzyme (U/mg)	Amount of Eupergit inside reactor (mg)	Productivity values (g/h)
Theoretical[a]	0.188	133	0.280
Experimental	0.135	125	0.0054

[a]see [48].

Experimental

Materials

The enzyme L-*allo*-threonine aldolase (L-low-TA) (EC 4.1.2.48) having concentration of 3 mg/mL and activity of 0.135 U/mg has a strong preference for L-*allo*-threonine from *Thermotoga maritima* and was kindly donated by the Junior Research Group ‘‘Industrial Biotechnology’’ (University of Leipzig, Germany). L-threonine, β-nicotinamide adenine dinucleotide disodium salt (NADH) were purchased from AppliChem GmbH (Darmstadt, Germany). Glycine, benzaldehyde, pyridoxal-5’-phosphate (PLP), Eupergit CM, 2-mercaptoethanol, 25% glutaraldehyde solution in water, ethylenediamine and other reagents were all purchased from Sigma Aldrich (Zwijndrecht, NL) and used as received. For immobilization of TA on Eupergit 1 M phosphate buffer solution was used, while for the phenylserine synthesis a 50 mM solution was used.

TA immobilization

The immobilization was carried out by a direct and an indirect method. For the direct method, the enzyme was bonded directly to the surface of the support, while the indirect method a spacer is used to provide enhanced enzyme mobility. The experimental procedure for direct immobilization (Figure 9) and indirect immobilization (Figure 10) as well as enzyme retention, activity retention and determination of enzyme concentration are well explained in [48].

Immobilization at different incubation times

At first the immobilization was carried out using the procedure given in literature [51]. 500 mg of Eupergit was treated with 2.5 mL of the TA enzyme solution (4.365 mg of TA) in a test tube at room temperature. The test tube was then kept in an orbital shaker for a predetermined time. Five different contact times were determined (6, 12, 18, 24 and 72 h).

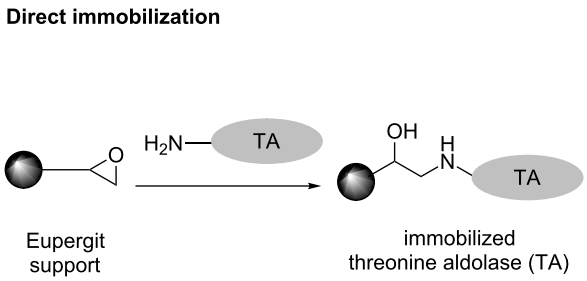

Figure 9: Direct immobilization.

Enzyme reactions

Batch reactions

Batch reactions were carried out in 20 mL test tubes at 70 °C, while stirring. The test tube was charged with 750 mg glycine (1 M), 106 mg benzaldehyde (0.1 M), 100 μL 5 mM PLP solution, 2 mL DMSO, 0.9 mL (2.7 mg) TA solution (activity = 0.407 U/mL) and 7 mL of a 50 mM phosphate buffer solution. The samples were collected at three different reaction times (20, 40 and 60 min). In each case 1 mL of sample was collected and the reaction was terminated by adding a 30% trichloroacetic acid solution. Then, all samples were extracted with 2 mL of internal standard solution (1,3-dimethoxybenzene in ethyl

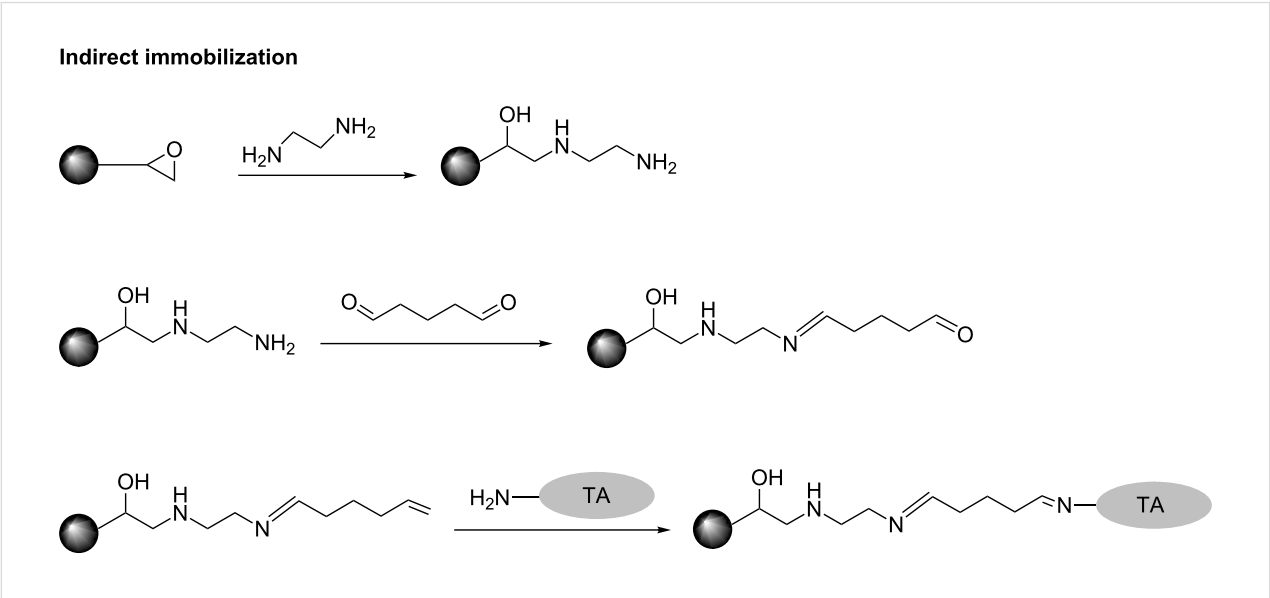

Figure 10: Indirect immobilization.

acetate). The enantiomeric excess (ee) and the diasteriomeric excess (de) of phenylserine were determined by HPLC analysis of the aqueous phase, while conversion of benzaldehyde was determined from analysis of the organic layer using gas chromatography. Since no byproducts could be detected, the degree of conversion reflected the yield of phenylserine formation.

Flow reactions

A Teflon tubing with an inner diameter of 500 μm and a volume of 500 μL was used to perform the flow experiments. The tubing was completely immersed into the thermostat bath at 70 °C. Amounts of reactants employed were kept similar as for the batch experiments. The solution was taken up in a single syringe and pumped at different flow rates (25 μL/min, 12.5 μL/min, 6 μL/min). The samples were collected at the outlet and immediately hydrolyzed by adding a 30% solution of trichloroacetic acid. For each reaction three samples were collected. Then a sample was taken from the syringe after 12 hours and conversion was determined to be 7%. The setup for the reaction is shown in Figure 11.

Immobilized enzyme reaction using micro flow

A simple glass tube with an inner diameter of 3.5 mm and a length of 5 cm was used as housing for the TA immobilized Eupergit support. A neck was constructed at the outlet for holding the glass wool which prevented wash out of the immobilized support from the reactor. In each experiment the same amount of Eupergit (125 mg corresponding to dry wet of Eupergit) was used as fixed-bed material. The length of the Eupergit bed was determined to be 4.7 cm +/− 0.2 cm, while the volume of the filled reactor was around 250 μL. The reactor was kept in a vertical position during all experiments (Figure 12a and b). During operation the reactor was incased in a thermostat. The reaction mixture contained 750 mg (1 M) of glycine, 106 mg (0.1 M) of benzaldehyde, 100 μL of 5 mM PLP solution, 2 mL of DMSO, and 7.9 mL of 50 mM phosphate buffer solution. For each experiment a fresh batch of immobilized TA was used. For each reaction three samples were collected and the average was calculated.

Analysis of the reaction

Determination of conversion (yield)

The conversion of benzaldehyde was determined by GC–FID (Varian 430-GC) having a CP-Sil 5 CB column of 30 meters (0.25 mm ID with film thickness of 1 micron), and a flame ionization detector. The carrier gas was helium (1 mL/min, split ratio 100). The oven temperature was maintained at 100 °C for 1 minute and then increased to 250 °C at a rate of 25 °C/min. The injector temperature was fixed at 250 °C and the detector temperature at 250 °C.

Determination of enantiomeric excess (ee) and diastereomeric excess (de)

Determination of the enantiomeric excess (ee) and the diastereomeric excess (de) was achieved by HPLC using a chiral column (Chirex 3126 (D)-penicillamine Column 250 × 4.6 mm) under the following conditions: 75% 2 mM $CuSO_4$ solution + 25% methanol at a flow rate of 1 mL/min. Detection of products was achieved at a wavelength of 254 nm. The column temperature was kept at 40 °C throughout the analysis. The separation of all the four isomers is depicted in Figure 13. The correct elution of the different stereoisomers was elucidated by injecting pure sample of each compound and comparison with literature [43-45].

In all experiments, 20% of diastereomeric excess of phenylserine was observed and a >99% enantiomeric excess was obtained for both diastereomers.

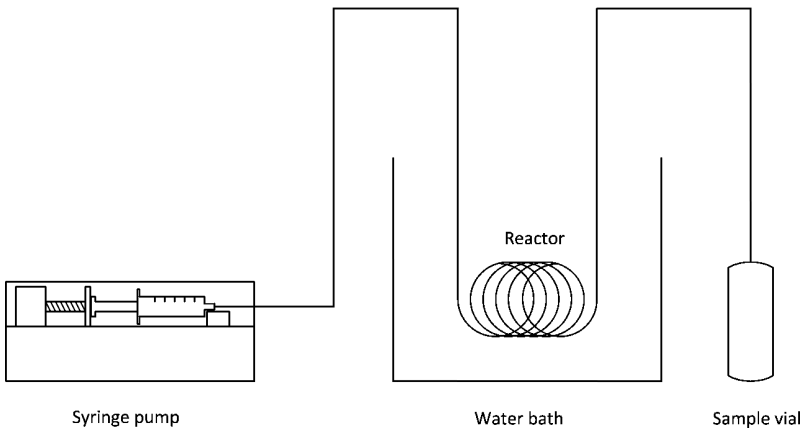

Figure 11: Flow reaction set-up using free enzyme.

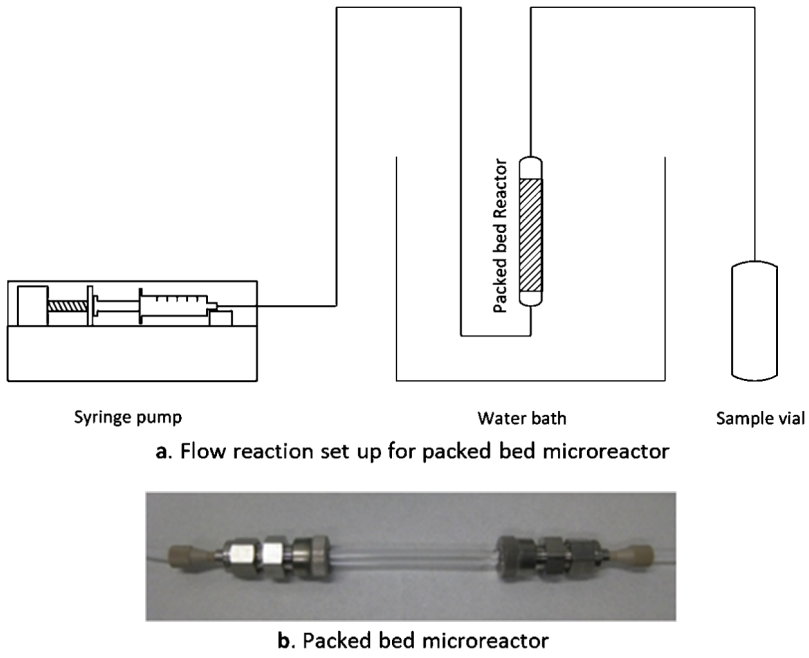

Figure 12: Experimental setup for packed be microreactor.

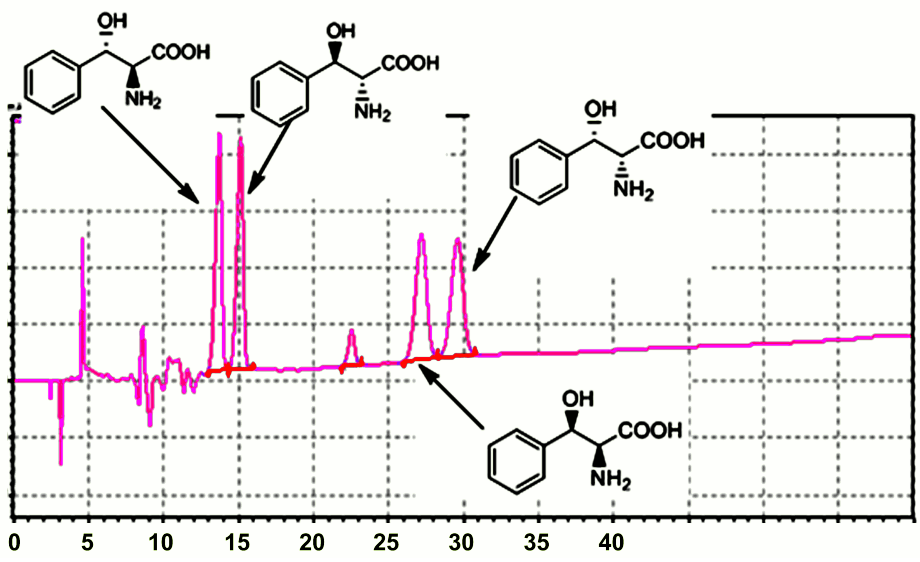

Figure 13: Analysis of the four isomers of phenylserine on a chiral column.

Acknowledgements

The authors are thankful to the ProAChim project in the frame of ERA-NET Industrial Biotechnology (ERA IB, No. 035581) for providing funding and would also like to thank Dr. Nicole Weizenmann from Junior Research Group ‘‘Industrial Biotechnology’’, Institute of Biochemistry, University of Leipzig, Perlickstraße 5, D-04103 Leipzig, Germany for detailed discussions on experiments.

References

1. Koeller, K. M.; Wong, C. H. *Nature* **2001,** *409,* 232–240. doi:10.1038/35051706
2. Hilterhaus, L.; Thum, O.; Liese, A. *Org. Process Res. Dev.* **2008,** *12,* 618–625. doi:10.1021/op800070q
3. Wang, Z.; van Oers, M. C. M.; Rutjes, F. P. J. T.; van Hest, J. C. M. *Angew. Chem., Int. Ed.* **2012,** *51,* 10746–10750. doi:10.1002/anie.201206555

4. Krajewska, B. *Enzyme Microb. Technol.* **2004,** *35,* 126–139. doi:10.1016/j.enzmictec.2003.12.013
5. Cabral, J. M. S.; Kennedy, J. F. Immobilization techniques for altering thermal stability of enzymes. In *Thermostability of enzymes;* Gupta, M. N., Ed.; Springer Verlag: Berlin, 1993; pp 163–179.
6. Sheldon, R. A. *Adv. Synth. Catal.* **2007,** *349,* 1289–1307. doi:10.1002/adsc.200700082
7. Stankiewicz, A.; Moulijn, J. *Chem. Eng. Prog.* **2000,** *96,* 22–34.
8. Lutze, P.; Gani, R.; Woodley, J. M. *Chem. Eng. Process.* **2010,** *49,* 547–558. doi:10.1016/j.cep.2010.05.002
9. Freund, H.; Sundmacher, K. *Chem. Eng. Process.* **2008,** *47,* 2051–2060. doi:10.1016/j.cep.2008.07.011
10. Ehrfeld, W.; Hessel, V.; Loewe, H. *Microreactors;* Wiley-VCH: Weinheim , 2000.
11. Urban, P. L.; Goodall, D. M.; Bruce, N. C. *Biotechnol. Adv.* **2006,** *24,* 42–57. doi:10.1016/j.biotechadv.2005.06.001
12. Peterson, D. S. *Lab Chip* **2005,** *5,* 132–139. doi:10.1039/B405311G
13. Doku, G. N.; Verboom, W.; Reinhoudt, D. N.; van den Berg, A. *Tetrahedron* **2005,** *61,* 2733–2742. doi:10.1016/j.tet.2005.01.028
14. Shang, M.; Noël, T.; Wang, Q.; Hessel, V. *Chem. Eng. Technol.* **2013,** *36,* 1001–1009. doi:10.1002/ceat.201200703
15. Stouten, S. C.; Wang, Q.; Noël, T.; Hessel, V. *Tetrahedron Lett.* **2013,** *54,* 2194–2198. doi:10.1016/j.tetlet.2013.02.064
16. Noël, T.; Buchwald, S. L. *Chem. Soc. Rev.* **2011,** *40,* 5010–5029. doi:10.1039/C1CS15075H
17. Watts, P.; Haswell, S. J. Chemical Synthesis in Microreactors. In *Microengineering in Biotechnology;* Hughes, M. P.; Hoettges, K. F., Eds.; Methods in Molecular Biology, Vol. 583; Springer Verlag, 2008; pp 109–120. doi:10.1007/978-1-60327-106-6_4
18. Stouten, S. C.; Noël, T.; Wang, Q.; Hessel, V. *Aust. J. Chem.* **2013,** *66,* 121–130. doi:10.1071/CH12465
19. Hessel, V.; Kralisch, D.; Kockmann, N.; Noël, T.; Wang, Q. *ChemSusChem* **2013,** *6,* 746–789. doi:10.1002/cssc.201200766
20. Hessel, V.; Vural-Gürsel, I.; Wang, Q.; Noël, T.; Lang, J. *Chem. Eng. Technol.* **2012,** *35,* 1184–1204. doi:10.1002/ceat.201200038
21. Hessel, V.; Wang, Q. *Chim. Oggi* **2011,** *29* (3), 81–84.
22. Hessel, V.; Wang, Q. *Chim. Oggi* **2011,** *29* (5), 70–74.
23. Dencic, I.; Hessel, V.; de Croon, M. H. J. M.; Meuldijk, J.; van der Doelen, C. W. J.; Koch, K. *ChemSusChem* **2012,** *5,* 232–245. doi:10.1002/cssc.201100389
24. Marques, M. P. C.; Fernandes, P. *Molecules* **2011,** *16,* 8368–8401. doi:10.3390/molecules16108368
25. Asanomi, Y.; Yamaguchi, H.; Miyazaki, M.; Maeda, H. *Molecules* **2011,** *16,* 6041–6059. doi:10.3390/molecules16076041
26. Bolivar, J. M.; Wiesbauer, J.; Nidetzky, B. *Trends Biotechnol.* **2011,** *29,* 333–342. doi:10.1016/j.tibtech.2011.03.005
27. Matsuura, S.-i.; Ishii, R.; Itoh, T.; Hamakawa, S.; Tsunoda, T.; Hanaoka, T.; Mizukami, F. *Chem. Eng. J.* **2011,** *167,* 744–749. doi:10.1016/j.cej.2010.10.042
28. Tudorache, M.; Mahalu, D.; Teodorescu, C.; Stan, R.; Bala, C.; Parvulescu, V. I. *J. Mol. Catal. B: Enzym.* **2011,** *69,* 133–139. doi:10.1016/j.molcatb.2011.01.007
29. Dräger, G.; Kiss, C.; Kunz, U.; Kirschning, A. *Org. Biomol. Chem.* **2007,** *5,* 3657–3664. doi:10.1039/B712804E
30. Kundu, S.; Bhangale, A. S.; Wallace, W. E.; Flynn, K. M.; Guttman, C. M.; Gross, R. A.; Beers, K. L. *J. Am. Chem. Soc.* **2011,** *133,* 6006–6011. doi:10.1021/ja111346c
31. Wang, J.-Y.; Yu, H.-R.; Xie, R.; Ju, X.-J.; Yu, Y.-L.; Chu, L.-Y.; Zhang, Z. *AIChE J.* **2012,** *59,* 380–389. doi:10.1002/aic.13834
32. Szymańska, K.; Pudło, W.; Mrowiec-Białoń, J.; Czardybon, A.; Kocurek, J.; Jarzębski, A. B. *Microporous Mesoporous Mater.* **2013,** *170,* 75–82. doi:10.1016/j.micromeso.2012.11.037
33. Fejerskov, B.; Smith, A. A. A.; Jensen, B. E. B.; Hussmann, T.; Zelikin, A. N. *Langmuir* **2013,** *29,* 344–354. doi:10.1021/la3040903
34. Babich, L.; Hartog, A. F.; van der Horst, M. A.; Wever, R. *Chem.–Eur. J.* **2012,** *18,* 6604–6609. doi:10.1002/chem.201200101
35. Buchegger, W.; Haller, A.; van den Driesche, S.; Kraft, M.; Lendl, B.; Vellekoop, M. *Biomicrofluidics* **2012,** *6,* 012803. doi:10.1063/1.3665717
36. Bodkin, J. A.; McLeod, M. D. *J. Chem. Soc., Perkin Trans. 1* **2002,** 2733–2746. doi:10.1039/B111276G
37. Kimura, T.; Vassilev, V. P.; Shen, G.-J.; Wong, C. H. *J. Am. Chem. Soc.* **1997,** *119,* 11734–11742. doi:10.1021/ja9720422
38. Miura, T.; Kajimoto, T. *Chirality* **2001,** *13,* 577–580. doi:10.1002/chir.1180
39. Vassilev, V. P.; Uchiyama, T.; Kajimoto, T.; Wong, C.-H. *Tetrahedron Lett.* **1995,** *36,* 4081–4084. doi:10.1016/0040-4039(95)00720-W
40. Bell, S. C.; Turner, J. M. *Biochem. Soc. Trans.* **1973,** *1,* 678–681. doi:10.1042/bst0010678
41. Dainty, R. H. *Biochem. J.* **1970,** *117,* 585–592.
42. John, R. A. *Biochim. Biophys. Acta* **1995,** *1248,* 81–96.
43. Fesko, K.; Reisinger, C.; Steinreiber, J.; Weber, H.; Schürmann, M.; Griengl, H. *J. Mol. Catal. B: Enzym.* **2008,** *52–53,* 19–26. doi:10.1016/j.molcatb.2007.10.010
44. Steinreiber, J.; Fesko, K.; Reisinger, C.; Schürmann, M.; van Assema, F.; Wolberg, M.; Mink, D.; Griengl, H. *Tetrahedron* **2007,** *63,* 918–926. doi:10.1016/j.tet.2006.11.035
45. Steinreiber, J.; Schurmann, M.; Wolberg, M.; van Assema, F.; Reisinger, C.; Fesko, K.; Mink, D.; Griengl, H. *Angew. Chem., Int. Ed.* **2007,** *46,* 1624–1626. doi:10.1002/anie.200604142
46. Boller, T.; Meier, C.; Menzler, S. *Org. Process Res. Dev.* **2002,** *6,* 509–519. doi:10.1021/op015506w
47. Sukyai, P.; Rezić, T.; Lorenz, C.; Mueangtoom, K.; Lorenz, W.; Haltrich, D.; Ludwig, R. *J. Biotechnol.* **2008,** *135,* 281–290. doi:10.1016/j.jbiotec.2008.04.002
48. Fu, H.; Dencic, I.; Tibhe, J.; Sanchez Pedraza, C. A.; Wang, Q.; Noël, T.; Meuldijk, J.; de Croon, M.; Hessel, V.; Weizenmann, N.; Oeser, T.; Kinkeade, T.; Hyatt, D.; Van Roy, S.; Dejonghe, W.; Diels, L. *Chem. Eng. J.* **2012,** *207–208,* 564–576. doi:10.1016/j.cej.2012.07.017
49. Knezevic, Z.; Milosavic, N.; Bezbradica, D.; Jakovljevic, Z.; Prodanovic, R. *Biochem. Eng. J.* **2006,** *30,* 269–278. doi:10.1016/j.bej.2006.05.009
50. Dencic, I.; Meuldijk, J.; de Croon, M.; Hessel, V. J. *Flow Chem.* **2011,** *1,* 13–23. doi:10.1556/jfchem.2011.00005
51. Janssen, M.; van Langen, L. M.; Pereira, S. R. M.; van Rantwijk, F.; Sheldon, R. A. *Biotechnol. Bioeng.* **2002,** *78,* 425–432. doi:10.1002/bit.10208

License and Terms

Beilstein Journal of Organic Chemistry

Micro-flow synthesis and structural analysis of sterically crowded diimine ligands with five aryl rings

Shinichiro Fuse*[1], Nobutake Tanabe[1], Akio Tannna[2], Yohei Konishi[2] and Takashi Takahashi[1]

Full Research Paper

Open Access

Address:
[1]Department of Applied Chemistry, Tokyo Institute of Technology, 2-12-1, Ookayama, Meguro-ku, Tokyo, 152-8552, Japan and [2]Mitsubishi Chemical Croup, Science and Technology Research Center, Inc., 1000 Kamoshida-cho, Aoba-ku, Yokohama 227-8502, Japan

Email:
Shinichiro Fuse* - sfuse@apc.titech.ac.jp

* Corresponding author

Keywords:
amidine formation; diimine; flow chemistry; polymerization

Beilstein J. Org. Chem. **2013,** *9,* 2336–2343.
doi:10.3762/bjoc.9.268

Received: 17 July 2013
Accepted: 07 October 2013
Published: 01 November 2013

This article is part of the Thematic Series "Chemistry in flow systems III".

Guest Editor: A. Kirschning

Abstract

Sterically crowded diimine ligands with five aryl rings were prepared in one step in good yields using a micro-flow technique. X-ray crystallographic analysis revealed the detailed structure of the bulky ligands. The nickel complexes prepared from the ligands exerted high polymerization activity in the ethylene homopolymerization and copolymerization of ethylene with polar monomers.

Introduction

The design of a ligand is a key step in the development of new catalysts because the ligand framework influences the reactivity of the metal center. That is why sterically crowded and neutral-chelating diimine ligands have garnered a great deal of attention [1-17]. In recent years, *N*-aryl 1,3,5-triazapenta-1,4-dienes **1** and **2** have been reported, and they are useful with late transition metal olefin-polymerization catalysts [18,19], and for the stabilization and isolation of reactive metal species [20,21]. In 1997, Murillo and coworkers reported the synthesis of a neutral, and bulky chelating ligand **1**, and its use in the formation of a Co complex (Figure 1) [22]. Stephan and coworkers reported the synthesis of a bulkier chelating ligand **2a**, and its use in the formation of various metal complexes [20,21]. Rojas and coworkers reported the synthesis of a series of bulky chelating ligands **2b–g**, and detailed their use in the preparation of ethylene polymerization catalysts [18,19]. We became curious about the structure and function of 1,2,3,4,5-pentaaryl-1,3,5-triazapenta-1,4-diene ligand **3**, which is sterically more hindered, because there are as many as five aryl rings that can provide further opportunities to change and tune the steric and

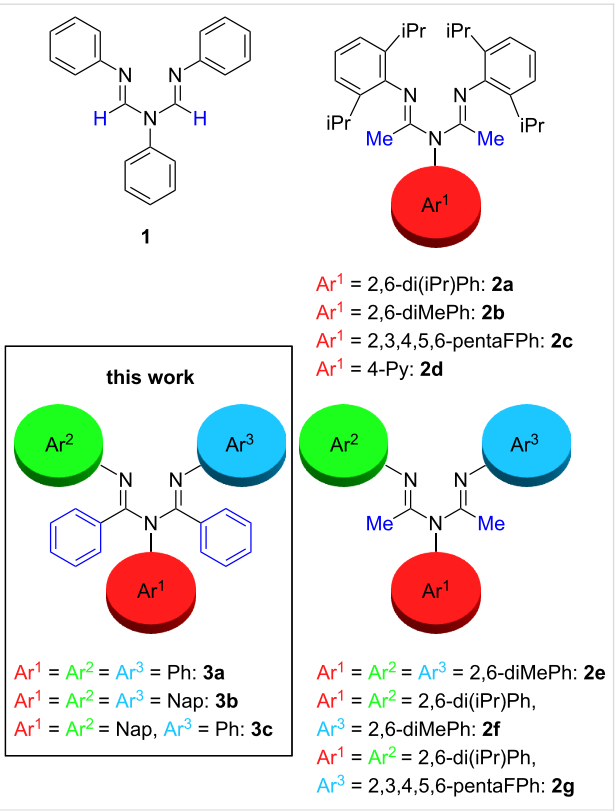

Figure 1: Sterically crowded, and neutral chelating diimine ligands.

electrical environments of the ligands [23,24]. However, as far as we could ascertain, this has been reported only once [25]. In this pioneering work, 1,2,3,4,5-pentaphenyl-1,3,5-triazapenta-1,4-diene ligand **3a** was prepared, but the report included neither the complexation nor a detailed structural study.

Herein, we report an efficient micro-flow synthesis and structural analysis of sterically crowded 1,2,3,4,5-pentaaryl-1,3,5-triazapenta-1,4-diene ligands **3b** and **3c**, and their use in the co-polymerization of ethylene and polar monomers. According to the previous report, 1,2,3,4,5-pentaphenyl-1,3,5-triazapenta-1,4-diene ligand **3a** was prepared by the reaction of *N,N′*-diphenyl benzamidine and *N*-phenylbenzimidochloride in benzene in 13 days [25]. In the present study, we intended to prepare these ligands from readily available materials in only one step [18,21].

Results and Discussion

Two equivalents of *N*-naphthylbenzimidochloride (**4**) was reacted with one equivalent of naphthylamine (**5**) in CH_2Cl_2 in the presence of DIEA (*N,N*-diisopropylethylamine) at room temperature (Scheme 1). The reaction proceeded smoothly, and consumption of naphthylamine was confirmed by TLC analysis within 10 min. After an aqueous workup, the desired product **3b** was obtained in a moderate yield (44%) with the concomitant generation of naphthylamine (**5**) and amide **8**. Reportedly, **3a** can form an HCl adduct, and the adduct decomposes to the corresponding amidine and imidochloride [25]. It is conceivable that **3b** overreacted with DIEA·HCl to afford **6**, or **4** and **7** in the reaction mixture and that **5** and **8** were generated from the hydrolysis of these compounds under aqueous workup conditions. We decided to use a micro-flow reactor in order to suppress the overreaction [26,27] because the micro-flow technique [28-35] enables the precise control of reaction time and temperature. The micro-flow system was made from simple and inexpensive laboratory instruments (syringes, syringe pumps, water bath, T-shape mixer, standard tubing and fittings), as shown in Figure 2. The T-shape mixer was made of stainless steel and immersed in a water bath (20 °C). A solution of **4** (0.1 M) in CH_2Cl_2, a solution of aryl amine **5** or **9** (0.1 M), and DIEA (0.7 M) in CH_2Cl_2 were introduced using syringe pumps at the indicated flow rates. The reaction was quenched by pouring the mixture into a saturated aqueous solution of NH_4Cl in CH_2Cl_2. After an aqueous workup, the products **3b** and **3c** were purified by silica gel chromatography. Reaction time was controlled by changing the flow rates.

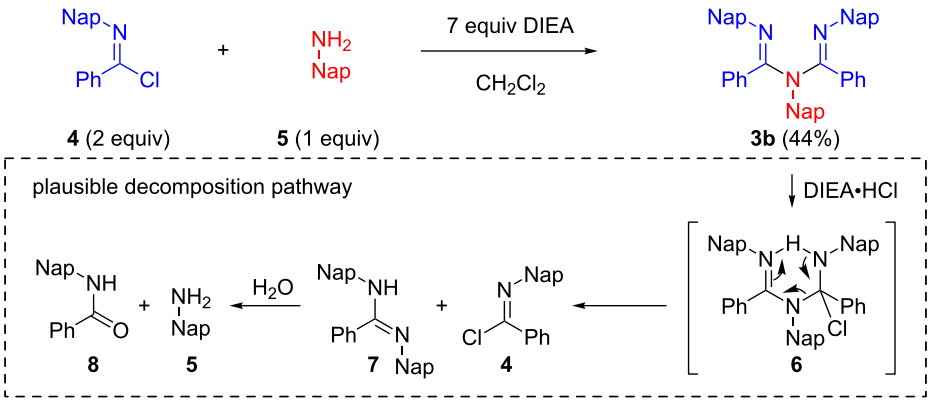

Scheme 1: One-step synthesis of the ligand **3b**, and a plausible decomposition pathway for **3b** to naphthylamine (**5**) and amide **8**.

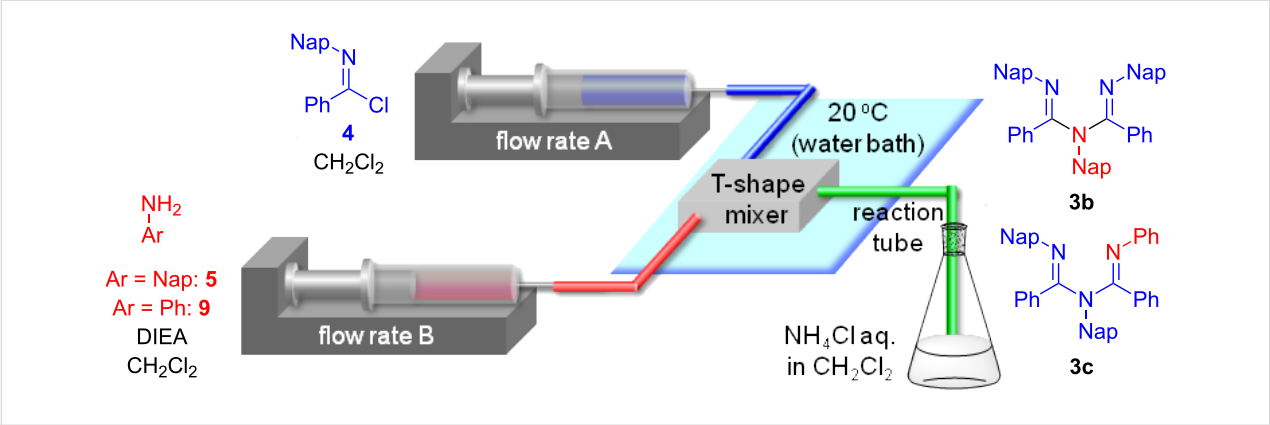

Figure 2: Micro-flow synthesis of the ligands **3b** and **3c**.

As expected, the yield of **3b** was improved by reducing the reaction time (Table 1, entries 1–4). The highest yield was observed for a reaction time of 38 s (Table 1, entry 4). A further shortening of the reaction time resulted in a reduction in the yield because of substrate recovery (Table 1, entry 5).

Table 1: Micro-flow synthesis of ligands **3b** and **3c**.

entry	flow rate A [μL/min]	flow rate B [μL/min]	time [s]	Ar–NH_2	yield[a] [%]
1[b]	54	27	300	**5**	65
2[b]	106	53	150	**5**	72
3[b]	214	107	75	**5**	75
4[b]	426	213	38	**5**	84
5[b]	854	427	19	**5**	66
6[c]	214	107	50	**9**	55
7[c]	426	213	25	**9**	69
8[c]	854	427	13	**9**	66

[a]Isolated yield. [b]Reaction tube volume is 400 μL. [c]Reaction tube volume is 266 μL.

The structure of the ligand **3b** was unambiguously determined by ^{1}H NMR, ^{13}C NMR, IR, HRMS and X-ray crystallographic analysis [36] (Figure 3). The ORTEP structure of **3b** showed that in the solid state the ligand adopts a non-planar arrangement similar to the previously reported ligands **2a–c**, and **2e–g** [18,19,21]. In ligand **3b**, N(1) and N(2) nearly occupied a common plane with C(1) and C(2), while N(3) was twisted out of this plane and was nearly perpendicular. The bond lengths for imines C(1)–N(1) and C(2)–N(3) were 1.273(4) and 1.278(4) Å, respectively, while the bond lengths for amines C(1)–N(2) and C(2)–N(2) were 1.420(4) and 1.421(4) Å, respectively. Reportedly, the two amine bond lengths were different in the case of ligands, **2a**, **2b**, **2e**, **2f**, and **2g** for which N=C–N–C=N was not in a common plane. On the other hand, the two amine bond lengths were nearly identical in the case of ligand **2c** where N=C–N–C=N was in a common plane. Interestingly, in the case of ligand **3b**, the bond lengths of the two amines, C(1)–N(2) and C(2)–N(2) were nearly identical, although N=C–N–C=N was not in a common plane.

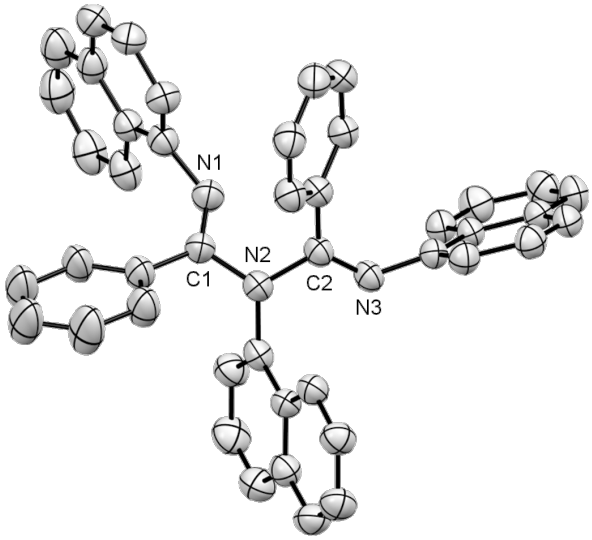

Figure 3: ORTEP drawing of **3b**. Thermal ellipsoids are set at 35% probability level. Hydrogen atoms are omitted for clarity. Selected bond lengths [Å] and angles [°] are as follows: C(1)–N(1) 1.273(4), C(1)–N(2) 1.420(4), C(2)–N(2) 1.421(4), C(2)–N(3) 1.278(4), N(1)–C(1)–N(2) 115.3(3), C(1)–N(2)–C(2) 117.0(3), N(2)–C(2)–N(3) 117.8(3).

The asymmetric ligand **3c** was obtained by the coupling of *N*-naphthylbenzimidochloride (**4**) with aniline (**9**). The product was obtained in a satisfactory yield (69%) under the conditions of entry 7 (25 s), as shown in Table 1. We speculated that the slightly lower yield of **3c** compared to **3b** came from the instability of **3c** during purification process. The compound **3c** was less stable than **3b**. Rojas et al. reported that the regioselectivity in the nucleophilic addition of an amidine to an

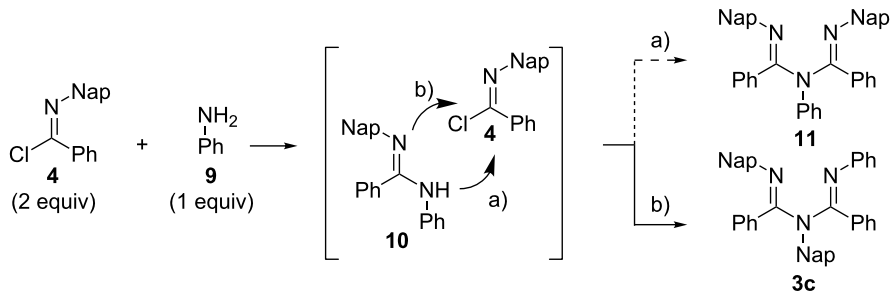

Scheme 2: Synthesis of the ligand **3c** through the coupling of **4** and **9**.

imidochloride depends on the employed reaction conditions, – in particular, the order of addition and the base selection [37] – and the symmetric ligands were obtained through the coupling of *N*-2,6-di(iPr)-phenylbenzimidochloride with aryl amines in the presence of Et_3N in toluene [18,19]. Interestingly, in our case, only the asymmetric ligand **3c** was obtained, although similar reaction conditions were employed (Scheme 2). The result showed that the nucleophilic addition of amidine **10** occurred from the sterically more hindered nitrogen atom (path b).

The structure of the asymmetric ligand **3c** was unambiguously determined by ^{1}H NMR, IR, HRMS and X-ray crystallographic analysis (Figure 4). The ORTEP structure of **3c** showed that in the solid state, the ligand adopted a non-planar arrangement similar to that of **3b**. In the ligand **3c**, N(1) and N(2) occupied a plane that was near that of C(1) and C(2), while N(3) was twisted out of this plane and was almost perpendicular. The bond lengths for imines C(1)–N(1) and C(2)–N(3) were 1.269(3) and 1.274(3) Å, respectively, while the bond lengths for amines C(1)–N(2) and C(2)–N(2) were 1.413(3) and 1.411(3) Å, respectively. The bond lengths for amines C(1)–N(2) and C(2)–N(2) were nearly identical, although N=C–N–C=N was not in a common plane. These features were similar to that of **3b**.

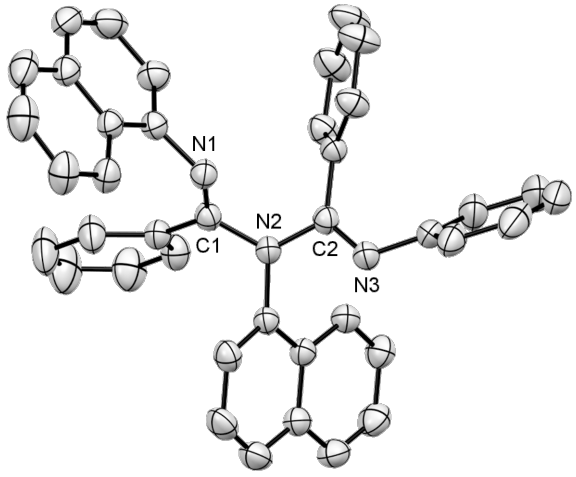

Figure 4: ORTEP drawing of **3c**. Thermal ellipsoids are set at 35% probability level. Hydrogen atoms are omitted for clarity. Selected bond lengths [Å] and angles [°] are as follows: C(1)–N(1) 1.269(3), C(1)–N(2) 1.413(3), C(2)–N(2) 1.411(3), C(2)–N(3) 1.274(3), N(1)–C(1)–N(2) 116.5(2), C(1)–N(2)–C(2) 119.1(2), N(2)–C(2)–N(3) 117.4(2).

A complexation of the synthesized ligands **3b** and **3c** with nickel(II) was performed (Scheme 3) in accordance with a reported procedure [38]. An equimolar amount of $NiBr_2$(dme) (dme = 1,2-dimethoxyethane) and the synthesized ligands were mixed in CH_2Cl_2 and stirred for 4 h at room temperature. Free ligands **3b** or **3c** were not observed by ^{1}H NMR analysis of the obtained crude mixtures. NMR characterization of the complexes **12** and **13** was poor due to the paramagnetic nature of the pseudo-tetrahedral nickel centers. In the case of **12**, green needle-like crystals suitable for X-ray crystallographic analysis were obtained (Figure 5). The molecular structure confirmed the formation of a six-membered chelate ring by the ligand in a *N,N* binding mode to the nickel dibromide. All the aryl rings were almost perpendicular to the chelate plane probably due to the strong steric repulsions among the aryl rings. The tetrahedral geometry around nickel was distorted similar to the previously reported nickel complexes of **2b**, **2f** and **2g** [18,19]. For example, Br(1) was almost perpendicular to the plane of the metal-containing ring. This can be observed in the corresponding angle N(1)–Ni(1)–Br(1) 102.2(3)°, while the angle of N(1)–Ni(1)–Br(2) was 120.9(3)°. The C(1)–N(1), C(2)–N(3),

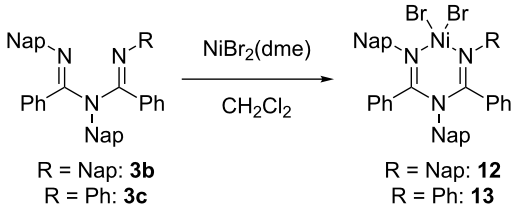

Scheme 3: Complexation of the ligands **3b** and **3c** with $NiBr_2$(dme).

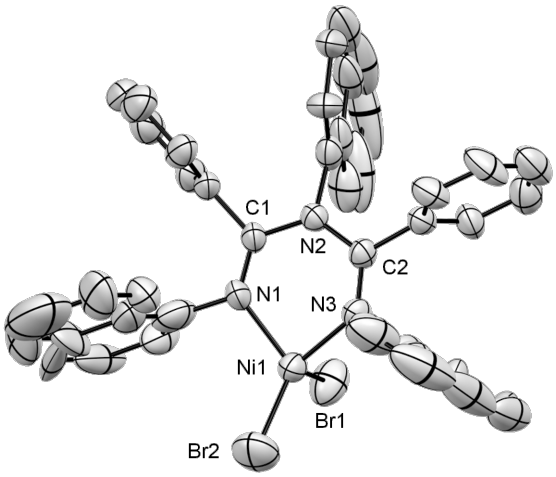

Figure 5: ORTEP drawing of **12**. Thermal ellipsoids are set at 35% probability level. Hydrogen atoms and cocrystallized CH_2Cl_2 are omitted for clarity. Selected bond lengths [Å] and angles [°] are as follows: C(1)–N(1) 1.277(11), C(1)–N(2) 1.393(11), C(2)–N(2) 1.396(11), C(2)–N(3) 1.305(11), Ni(1)–N(1) 1.947(8), Ni(1)–N(3) 1.943(8), N(1)–C(1)–N(2) 122.8(8), C(1)–N(2)–C(2) 126.2(7), N(2)–C(2)–N(3) 121.2(8), C(2)–N(3)–Ni(1) 127.5(6), N(1)–Ni(1)–N(3) 89.3(3), C(1)–N(1)–Ni(1), 127.7(6), N(1)–Ni(1)–Br(1) 102.2(3), N(1)–Ni(1)–Br(2) 120.9(3).

C(1)–N(2) and C(2)–N(2) bond lengths were 1.277(11) Å, 1.305(11) Å, 1.393(11) Å and 1.396(11) Å respectively, indicating the double and single bond character around the imines and amine nitrogen, respectively.

A series of olefin polymerizations were briefly tested as shown in Table 2. Both catalysts **12** and **13** exerted high activity for the ethylene homopolymerization (Table 2, entries 1 and 2). As far as we could ascertain, neither propene homopolymerization nor copolymerization of ethylene with polar monomers by using the catalysts derived from *N*-aryl-1,3,5-triazapenta-1,4-dienes **1–3** have been reported [18,19]. Thus, we tested the polymerization activity of the catalyst **12** in the copolymerization of ethylene with 5-norbornen-2-ol (NBO) and ethyl acrylate (EtA) (Table 2, entries 3 and 4) and propene homopolymerization (Table 2, entry 5). Although the propene homopolymerization activity of catalyst **12** was moderate, catalyst **12** exerted a high activity in the copolymerization of ethylene with both polar monomers.

Conclusion

In summary, sterically crowded diimine ligands **3b** and **3c** were prepared in one step in good yields using a micro-flow technique. One of the advantages of using microreactors is the ease of scale-up. It should be possible to scale-up our developed process by either continuous running or by increasing the number of the microreactors. X-ray crystallographic analysis revealed the detailed structure of ligands **3b** and **3c**. Interestingly, **3c** retained an asymmetric structure which ran contrary to a previous report. Unexpectedly, both bond lengths of the two amines C(1)–N(2) and C(2)–N(2) in both ligands were nearly identical, although N=C–N–C=N was not in a common plane. The complexation of **3b** and **3c** with nickel afforded **12** and **13**. X-ray crystallographic analysis of **12** revealed that all the aryl rings are nearly perpendicular to the chelate plane. The nickel complex **12** exerted a high polymerization activity in both ethylene homopolymerization and the copolymerization of ethylene with polar monomers. The synthesized ligands **3b** and **3c** retained as many as five aryl rings, which offered another opportunity to change the steric and electric environment. The developed process should be valuable for the preparation of various 1,2,3,4,5-pentaaryl-1,3,5-triazapenta-1,4-diene ligands and for the creation of novel and useful catalysts.

Experimental

General

NMR spectra were recorded on a JEOL Model ECP-400 (400 MHz for ^{1}H, 100 MHz for ^{13}C) instrument in the indicated solvent. Chemical shifts are reported in units of parts per

Table 2: Evaluation of polymerization activities of nickel complexes **12** and **13**.[a]

entry	catalyst[b]	monomer[c]	temperature, time [°C, h]	V_p [kg/mol·h]
1	**12**	ethylene	60, 0.5	140
2	**13**	ethylene	60, 0.5	110
3	**12**	ethylene/NBO	60, 1	25
4	**12**	ethylene/EtA	60, 1	35
5	**12**	propene	60, 1	5

[a]Entries 1–4 were carried out in a 2 L autoclave reactor in 1 L toluene in the presence of 500 equiv of modified methyl aluminoxane (MMAO)[39] as cocatalyst and 400 psig of ethylene. Entry 5 was carried out in a 2 L autoclave reactor in 750 mL propene in the presence of 500 equiv of MMAO as the cocatalyst. [b]Entries 1, 4 and 5 were carried out using 0.11 mmol of the catalyst. Entries 2 and 3 were carried out using 0.10 and 0.09 mmol of the catalysts, respectively. [c]Entries 3 and 4 were carried out using 500 equiv of NBO or EtA.

million (ppm) relative to the signal (0.00 ppm) for internal tetramethylsilane for solutions in $CDCl_3$ (7.26 ppm for ^1H, 77.0 ppm for ^{13}C). Multiplicities are reported by using the following abbreviations: s, singlet; d, doublet; t, triplet; q, quartet; m, multiplet; br, broad; and, *J*, coupling constants in Hertz. IR spectra were recorded on a Perkin-Elmer Spectrum One FTIR spectrometer. HRMS (ESI–TOF) was measured with a Waters LCT Premier^{TM} XE. All reactions were monitored by thin-layer chromatography carried out on 0.25 mm E. Merck silica gel plates (60F-254) with UV light, visualized by ceric sulfate solution. Flash column chromatography was performed on Silica Gel 60 N, purchased from Kanto Chemical Co. The T-shape mixer (Flom Co. Ltd., #9513, 19 mm × 28 mm × 8 mm, diameter 0.6 mm) was made of stainless steel and had a T-shape channel. The reaction tube (diameter 0.5 mm) was made of Teflon®. A Harvard Pump 11 Plus Single Syringe (HARVARD apparatus), a KDS 100 syringe pump, and a KDS 200 syringe pump (KD Scientific) were used to inject compounds into the T-shape mixers. The workup process included quenching of the reactions, liquid–liquid extraction, washing and drying, and was performed using a Zodiac CCX-1200 (Tokyo Rikakikai Co., Ltd.). Chromatographic separation was performed using a Purif®-α2 (Shoko Scientific Co., Ltd.).

Experimental details

General procedure for the preparation of imidochlorides: The mixture of *N*-(1-naphthyl)benzamide and $SOCl_2$ (2 mL/mmol amide) was stirred at 65 °C for 4 h. The reaction mixture was concentrated in vacuo. The residue was used for the next reaction without further purification.

General procedure for micro-flow synthesis of 1,2,3,4,5-pentaaryl-1,3,5-triazapenta-1,4-dienes 3b and 3c: A T-shape mixer and reaction tube were immersed in a water bath (20 °C). Syringe pumps and a mixer were connected using a Teflon® tube (diameter 0.25 mm). Imidochloride **4** was dried azeotropically with toluene. Aryl amine **5** or **9** (0.1 M), DIEA (0.7 M) and imidochloride **4** (0.1 M) were dissolved in CH_2Cl_2 under an argon atmosphere and were stored in syringes. Each solution was introduced to a T-shape mixer using the syringe pump. The mixed solution went through the reaction tube, and the resultant solution was poured into vigorously stirred saturated aqueous NH_4Cl (1.5 mL) in CH_2Cl_2 (2 mL). After being stirred for several minutes, Et_2O (30 mL) was added to the reaction mixture under vigorous stirring for 30 s. The aqueous layer was separated and added to saturated aqueous $NaHCO_3$ (2 mL) after being vigorously stirred for 30 s. The aqueous layer was separated and brine (2 mL) was added followed by vigorous stirring for 30 s. After removing the aqueous layer, the organic layers were dried over Na_2SO_4 (10 g) and concentrated in vacuo. The residue was purified by column chromatography on silica gel (0% to 10% Et_2O in hexane with 1% Et_3N) to give 1,2,3,4,5-pentaaryl-1,3,5-triazapenta-1,4-diene **3b** or **3c**.

1,3,5-Trinaphthyl-2,4-diphenyl-triazapenta-1,4-diene (3b): ^1H NMR (400 MHz, $CDCl_3$) δ 8.22 (brd, *J* = 5.8 Hz, 1H), 8.15 (brs, 1H), 7.89 (brd, *J* = 5.4 Hz, 1H), 7.74–7.90 (m, 2H), 7.73 (brd, *J* = 6.8 Hz, 2H), 7.58 (brd, *J* = 7.8 Hz, 1H), 7.10–7.58 (m, 20H), 7.07 (t, *J* = 7.8 Hz, 1H), 7.39 (brd, *J* = 7.8, 1H), 6.64 (brs, 1H); ^{13}C NMR (67.8 MHz, $CDCl_3$) δ 156.2, 145.6, 136.1, 135.2, 134.7, 134.0, 130.1, 129.5, 128.8, 128.3, 128.2, 127.2, 126.3, 125.9, 125.8, 125.6, 125.2, 125.0, 123.6, 123.5, 123.0, 122.5, 121.6, 118.0, 115.7; FTIR (neat) 3055, 1624, 1572, 1529, 1495, 1393, 791, 771 cm^{-1}; HRMS (ESI–TOF, *m*/*z*): $[M + H]^+$ calcd. for $C_{44}H_{32}N_3$, 602.2596; found, 602.2613.

1,3-Dinaphthyl-2,4,5-triphenyl-triazapenta-1,4-diene (3c): ^1H NMR (400 MHz, $CDCl_3$) δ 8.29 (d, *J* = 6.4 Hz, 2H), 8.25 (d, *J* = 8.3 Hz, 2H), 7.78 (brd, *J* = 7.8 Hz, 1H), 7.73 (d, *J* = 7.8 Hz, 2H), 7.61 (d, *J* = 7.8 Hz, 1H), 7.36–7.60 (m, 9H), 7.40–7.20 (m, 2H), 7.16 (t, *J* = 7.8 Hz, 1H), 7.05–6.60 (m, 7H), 6.54 (brs, 1H), 5.71 (brd, *J* = 6.8, 1H); FTIR (neat) 3056, 1631, 1595, 1524, 1497, 1438, 1323, 775, 698 cm^{-1}; HRMS (ESI–TOF, *m*/*z*): $[M + H]^+$ calcd. for $C_{40}H_{30}N_3$, 552.2440; found, 552.2435.

General procedure for the preparation of nickel complexes 12 and 13

The following manipulations were performed under an inert atmosphere using standard glove box techniques. A solution of the prepared ligand **3b** or **3c** (1 equiv) and $NiBr_2$(dme) (1 equiv) in dry CH_2Cl_2 (50 mL/mmol) was stirred for 4 h at room temperature. The obtained crude mixture was used for the polymerization without purification.

Procedure for the preparation of nickel complex 12 crystals

The following manipulations were performed under an inert atmosphere using standard glove box techniques. A solution of the prepared ligand **3b** (66 mg, 0.11 mmol) in 40 mL of dry CH_2Cl_2 was slowly added to $NiBr_2$(dme) (34 mg, 0.11 mmol). The resultant mixture was stirred for 1 h at room temperature. Then, the stirring was stopped and the mixture was allowed to stand overnight at room temperature. Green colored needle-like crystals of **12**, suitable for X-ray analysis were obtained.

Procedure for the homopolymerization of ethylene

To a 2 L autoclave reactor, 1,000 mL of dry toluene and MMAO (500 equiv, 6.5 wt % in toluene) were added. The resultant mixture was heated to 60 °C, then the crude nickel complex (1 equiv) was injected under an ethylene pressure of 400 psig, which was fed continuously at that pressure over the course of the reaction. After being stirred for 0.5 h, ethanol was

added to quench the polymerization, and ethylene was vented. The resultant mixture was collected, and concentrated in vacuo to afford a crude polymer. Polymerization activities were calculated from the mass of the crude polymer that was obtained.

Procedure for the copolymerization of ethylene with polar monomers

To a 2 L autoclave reactor, 1,000 mL of dry toluene and comonomers (500 equiv) along with MMAO (500 equiv, 6.5 wt % in toluene) were added. The resultant mixture was heated to 60 °C, then the crude nickel complex (1 equiv) was injected under an ethylene pressure of 400 psig, which was fed continuously at that pressure over the course of the reaction. After being stirred for 1 h, ethanol was added to quench the polymerization, and ethylene was vented. The resultant mixture was collected, and concentrated in vacuo to afford the crude polymer. Polymerization activities were calculated from the mass of the crude polymer that was obtained.

Procedure for the homopolymerization of propene

To a 2 L autoclave reactor, MMAO (500 equiv, 6.5 wt % in toluene) and 750 mL of propene were added. Then the crude nickel complex (1 equiv) was injected with nitrogen. The resultant mixture was heated to 60 °C. After being stirred for 1 h, ethanol was added to quench the polymerization, and propene was vented. The resultant mixture was collected, and concentrated in vacuo to afford a crude polymer**.** Polymerization activities were calculated from the mass of the crude polymer that was obtained.

Supporting Information

Supporting Information File 1

^{1}H and ^{13}C NMR spectra.
[http://www.beilstein-journals.org/bjoc/content/supplementary/1860-5397-9-268-S1.pdf]

Acknowledgements

The authors thank Dr. Hidehiro Uekusa, Tokyo Institute of Technology for X-ray crystallographic analysis of intermediates and Dr. Shigekazu Ito, Tokyo Institute of Technology for fruitful discussion, and Global COE Program “Education and Research Center for Emergence of New Molecular Chemistry,” MEXT, Japan, for financial support.

References

1. Ittel, S. D.; Johnson, L. K.; Brookhart, M. *Chem. Rev.* **2000,** *100,* 1169. doi:10.1021/cr9804644
2. Lersch, M.; Tilset, M. *Chem. Rev.* **2005,** *105,* 2471. doi:10.1021/cr030710y
3. Dagorne, S.; Atwood, D. A. *Chem. Rev.* **2008,** *108,* 4037. doi:10.1021/cr078351k
4. Nakamura, A.; Ito, S.; Nozaki, K. *Chem. Rev.* **2009,** *109,* 5215. doi:10.1021/cr900079r
5. Chen, E. Y.-X. *Chem. Rev.* **2009,** *109,* 5157. doi:10.1021/cr9000258
6. Mkhalid, I. A. I.; Barnard, J. H.; Marder, T. B.; Murphy, J. M.; Hartwig, J. F. *Chem. Rev.* **2009,** *110,* 890. doi:10.1021/cr900206p
7. Driver, T. G. *Org. Biomol. Chem.* **2010,** *8,* 3831. doi:10.1039/c005219c
8. Xu, L.-M.; Li, B.-J.; Yang, Z.; Shi, Z.-J. *Chem. Soc. Rev.* **2010,** *39,* 712. doi:10.1039/B809912J
9. Asay, M.; Jones, C.; Driess, M. *Chem. Rev.* **2010,** *111,* 354. doi:10.1021/cr100216y
10. Nomura, K.; Zhang, S. *Chem. Rev.* **2010,** *111,* 2342. doi:10.1021/cr100207h
11. Sehnal, P.; Taylor, R. J. K.; Fairlamb, I. J. S. *Chem. Rev.* **2010,** *110,* 824. doi:10.1021/cr9003242
12. Delferro, M.; Marks, T. J. *Chem. Rev.* **2011,** *111,* 2450. doi:10.1021/cr1003634
13. Partyka, D. V. *Chem. Rev.* **2011,** *111,* 1529. doi:10.1021/cr1002276
14. Takeuchi, D. *Macromol. Chem. Phys.* **2011,** *212,* 1545. doi:10.1002/macp.201100182
15. Gephart, R. T., III; Warren, T. H. *Organometallics* **2012,** *31,* 7728. doi:10.1021/om300840z
16. Lang, H.; Jakob, A.; Milde, B. *Organometallics* **2012,** *31,* 7661. doi:10.1021/om300628g
17. Li, T.; Schulz, S.; Roesky, P. W. *Chem. Soc. Rev.* **2012,** *41,* 3759. doi:10.1039/c2cs15343b
18. Valdebenito, C.; Garland, M. T.; Quijada, R.; Rojas, R. *J. Organomet. Chem.* **2009,** *694,* 717. doi:10.1016/j.jorganchem.2008.11.066
19. Peoples, B. C.; De la Vega, G.; Valdebenito, C.; Quijada, R.; Ibañez, A.; Valderrama, M.; Rojas, R. *J. Organomet. Chem.* **2012,** *700,* 147. doi:10.1016/j.jorganchem.2011.11.035
20. Masuda, J. D.; Stephan, D. W. *Can. J. Chem.* **2005,** *83,* 477. doi:10.1139/v05-057
21. Masuda, J. D.; Stephan, D. W. *Dalton Trans.* **2006,** 2089. doi:10.1039/B513531A
22. Cotton, F. A.; Daniels, L. M.; Matonic, J. H.; Wang, X. P.; Murillo, C. A. *Polyhedron* **1997,** *16,* 1177. doi:10.1016/s0277-5387(96)00366-x
23. Fuse, S.; Masui, H.; Tannna, A.; Shimizu, F.; Takahashi, T. *ACS Comb. Sci.* **2012,** *14,* 17. doi:10.1021/co200081j
24. Masui, H.; Fuse, S.; Takahashi, T. *Org. Lett.* **2012,** *14,* 4090. doi:10.1021/ol3017337
25. Cooper, F. C.; Partridge, M. W.; Short, W. F. *J. Chem. Soc.* **1951,** 391. doi:10.1039/jr9510000391
26. Tanaka, K.; Motomatsu, S.; Koyama, K.; Tanaka, S.-i.; Fukase, K. *Org. Lett.* **2006,** *9,* 299. doi:10.1021/ol062777o
27. Nagaki, A.; Togai, M.; Suga, S.; Aoki, N.; Mae, K.; Yoshida, J.-i. *J. Am. Chem. Soc.* **2005,** *127,* 11666. doi:10.1021/ja0527424
28. Luis, S. V.; Carcia-Verdugo, E., Eds. *Chemical Reactions and Processes under Flow Conditions;* Royal Society of Chemistry: Cambridge, 2010. doi:10.1039/9781847559739
29. McMullen, J. P.; Jensen, K. F. *Annu. Rev. Anal. Chem.* **2010,** *3,* 19. doi:10.1146/annurev.anchem.111808.073718
30. Fuse, S.; Tanabe, N.; Yoshida, M.; Yoshida, H.; Doi, T.; Takahashi, T. *Chem. Commun.* **2010,** *46,* 8722. doi:10.1039/c0cc02239j
31. Suga, S.; Yamada, D.; Yoshida, J. *Chem. Lett.* **2010,** *39,* 404. doi:10.1246/cl.2010.404
32. Baumann, M.; Baxendale, I. R.; Ley, S. V. *Mol. Diversity* **2011,** *15,* 613. doi:10.1007/s11030-010-9282-1

33. Yoshida, J.-i.; Kim, H.; Nagaki, A. *ChemSusChem* **2011,** *4,* 331. doi:10.1002/cssc.201000271
34. Fuse, S.; Tanabe, N.; Takahashi, T. *Chem. Commun.* **2011,** *47,* 12661. doi:10.1039/c1cc15662d
35. Fuse, S.; Mifune, Y.; Tanabe, N.; Takahashi, T. *Org. Biomol. Chem.* **2012,** *10,* 5205. doi:10.1039/c2ob25511a
36. CCDC 934692 (**3b**), CCDC 934694 (**3c**), and 934693 (**12**) contain the supplementary crystallographic data for this paper. These data can be obtained free of charge from The Cambridge Crystallographic Data Centre via http://www.ccdc.cam.ac.uk/data_request/cif.
37. Caris, R.; Peoples, B. C.; Valderrama, M.; Wu, G.; Rojas, R. *J. Organomet. Chem.* **2009,** *694,* 1795. doi:10.1016/j.jorganchem.2009.01.005
38. Azoulay, J. D.; Rojas, R. S.; Serrano, A. V.; Ohtaki, H.; Galland, G. B.; Wu, G.; Bazan, G. C. *Angew. Chem., Int. Ed.* **2009,** *48,* 1089. doi:10.1002/anie.200804661
39. MMAO is a modified methylaluminoxane activator containing 25% isobutyl aluminoxane prepared by the controlled hydrolysis of Me_3Al and $(iBu)_3Al$.

License and Terms

Beilstein Journal of Organic Chemistry

Synthesis of homo- and heteromultivalent carbohydrate-functionalized oligo(amidoamines) using novel glyco-building blocks

Felix Wojcik, Sinaida Lel, Alexander G. O'Brien, Peter H. Seeberger* and Laura Hartmann*

Full Research Paper

Open Access

Address:
Department of Biomolecular Systems, Max Planck Institute of Colloids and Interfaces, Research Campus Golm, 14424 Potsdam, Germany, and Institute for Chemistry and Biochemistry, Freie Universität Berlin, Arnimallee 22, 14195 Berlin, Germany

Email:
Peter H. Seeberger* - Peter.Seeberger@mpikg.mpg.de;
Laura Hartmann* - Laura.Hartmann@mpikg.mpg.de

* Corresponding author

Keywords:
continuous flow; flow chemistry: flow synthesis; glycoligands; multivalency; photochemistry; solid-phase synthesis; thiol–ene; thioglycosides

Beilstein J. Org. Chem. **2013,** *9,* 2395–2403.
doi:10.3762/bjoc.9.276

Received: 28 June 2013
Accepted: 10 October 2013
Published: 07 November 2013

This article is part of the Thematic Series "Chemistry in flow systems III".

Guest Editor: A. Kirschning

Abstract

We present the solid phase synthesis of carbohydrate-functionalized oligo(amidoamines) with different functionalization patterns utilizing a novel alphabet of six differently glycosylated building blocks. Highly efficient in flow conjugation of thioglycosides to a double-bond presenting diethylentriamine precursor is the key step to prepare these building blocks suitable for fully automated solid-phase synthesis. Introduction of the sugar ligands via functionalized building blocks rather than postfunctionalization of the oligomeric backbone allows for the straightforward synthesis of multivalent glycoligands with full control over monomer sequence and functionalization pattern. We demonstrate the potential of this building-block approach by synthesizing oligomers with different numbers and spacing of carbohydrates and also show the feasibility of heteromultivalent glycosylation patterns by combining building blocks presenting different mono- and disaccharides.

Introduction

Multivalent carbohydrate ligand–protein receptor interactions play a key role for many events in glycobiology such as cell–cell or pathogen recognition [1]. Therefore, carbohydrate functionalization of non-natural materials such as polymers or dendrimers allows for bioactive materials that are used to modulate cellular behavior [1-3]. Since single carbohydrate ligand–protein interactions are usually weak [4], several sugar ligands have to be introduced in order to achieve the desired biological effect [4]. This multivalent presentation of ligands then results in an increased binding affinity to the targeted

protein receptors [4]. It is well understood that the number and spacing of ligands have a tremendous influence on the resulting binding and thus biological properties [5-7]. Therefore, in order to understand and explore these interactions and their potential for biomedical applications, a more detailed look at the binding mechanisms as well as structure–activity relationship studies of multivalent glycomaterials is required.

Multivalent sugar presentation has been realized on a variety of different scaffolds such as polymers [8,9], dendrimers [10] or naturally-occurring scaffolds such as peptides [11-13] or oligonucleotides [14]. Such constructs have contributed to our current understanding of multivalent interactions [5]. Nevertheless, binding studies on multivalent compounds with different scaffold architectures or combinations of different sugar ligands are limited due to the often undefined chemical composition, limited variations in architecture and functionalization as well as unspecific biological activity of the scaffolds. Precision oligo/polymers are a novel class of defined artificial scaffolds having the potential to bridge this current gap of artificial carbohydrate presenting scaffolds and to be an important platform for structure–activity relationship studies [15-17]. Precision macromolecules combine the advantages of synthetic scaffolds such as polymers with the advantages of naturally-occurring scaffolds such as peptides as they are highly defined, versatile in their structure (linear or branched) [18] and biocompatible with a decreased risk of inherent immunogenicity [19].

Recently, we showed that monodisperse, sequence-defined glycooligomers obtained by sequential addition of building blocks on solid support are valuable tools for tuning and understanding carbohydrate–lectin interactions [20]. Carbohydrate conjugation was achieved by copper-catalyzed azide alkyne cycloaddtion (CuAAC) of carbohydrate ligands on alkyne presenting oligomers [21]. As an alternative conjugation approach to CuAAc, a very efficient thiol–ene coupling (TEC) [22-25] protocol in a continuous flow photoreactor was developed involving post functionalization of alkene presenting oligomers by thioglycosides [26]. The flow system allows for precise control over the reaction conditions, is easy to scale up and provides efficient irradiation of the samples by virtue of a sub-millimeter path length. Continuous removal of the desired product minimizes unwanted secondary reaction pathways [27-39]. We also introduced the so-called building block approach in the context of thiol–ene coupling via the continuous-flow technique. A first example involved conjugating a glucose ligand to a building block and subsequent solid phase assembly of a glycooligomer [26].

When compared to postfunctionalization, the building-block approach allows not only control of the ligand positioning, but also enables well-defined sequences with different types of ligands: Simply by choosing from an alphabet of building blocks, applying them for solid-phase synthesis and final cleavage from the resin, the desired multivalent structures can be obtained. Heteromultivalent glycooligomers presenting different sugars at different positions along the scaffold should be accessible by combining different carbohydrate functionalized building blocks and without the requirement of complex protecting group or sequential functionalization strategies [40]. In order to explore the feasibility of the building-block approach for the synthesis of precision glycooligo/polymers, in this work we report on the reaction of several thioglycosides and the double bond presenting diethylenetriamine succinic acid building block (DDS) **1**, giving access to a small alphabet of carbohydrate-functionalized building blocks. TEC in flow enabled determining the reactivity of each thioglycoside at >275 nm, leading to optimized reaction conditions for the production of six glycosylated building blocks (Figure 1). These building blocks can then be used for the assembly of monodisperse, sequence-defined glycooligomers via fully automated standard amide coupling. Straightforward variations in the scaffold architecture, number and distance of sugar ligands as well as the sequence-defined introduction of different sugars are demonstrated by choosing different building block combinations during solid-phase synthesis.

Results and Discussion

For the preparation of the desired sugar building blocks double-bond presenting building block DDS **1** and thioglycosides **2**–**7** are required. The large scale synthesis of DDS **1** was achieved according to a published procedure [26]. The required β-thioglycosides **2**–**7** were prepared via their corresponding glycosyl bromides followed by S_N2 displacement of the anomeric bromide with thiourea [41] or Na_2S/CS_2 [42].

DDS **1** and thioglycosides **2**–**7** were subjected to TEC in flow at >275 nm (Scheme 1). A FEP flow photoreactor equipped with a Pyrex-filtered medium pressure Hg lamp (400 Watt, λ_{max} = 366 nm) cooled to room temperature was employed [43]. Continuous reagent delivery was ensured by a standard commercially available syringe pump (for details see Supporting Information File 1). Reactivity evaluation studies were performed utilizing a 2 mL FEP loop, for the gram-scale production of glycosylated building blocks a 5 mL FEP loop was used. This particular photochemical set up (Figure 2a) allows for several reaction parameters to be studied for later high scale synthesis of the glycosylated building blocks **8**–**13** while using only small amounts of reagents for optimization. As thiol–ene addition is strongly concentration dependent [26], similar concentrations for thioglycosides **2**–**7** during TEC are required for a valid comparison. Due to reagent solubility, a concentra-

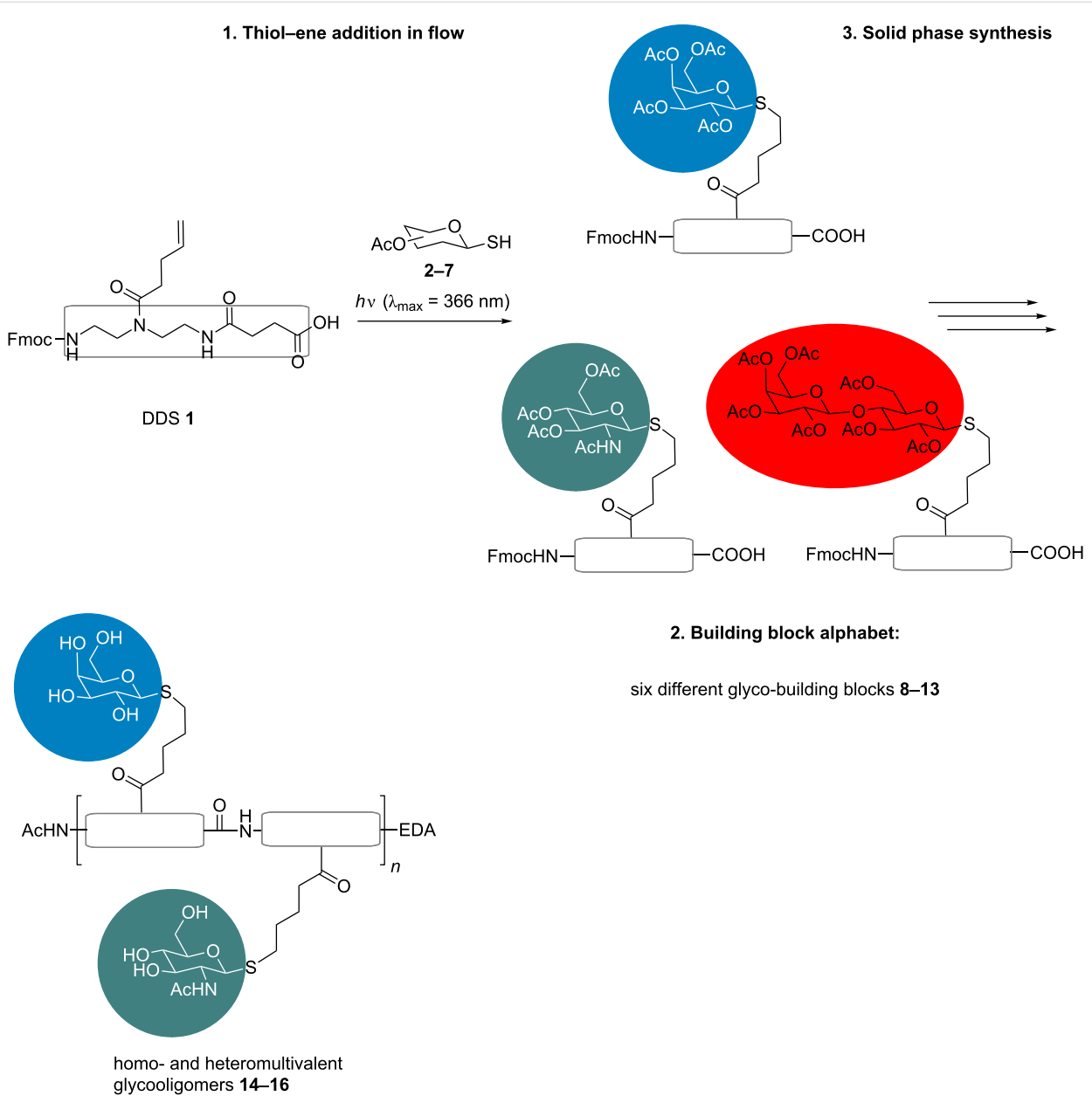

Figure 1: Versatile synthetic strategy for access to multivalent glycoligands: First, the building block DDS **1** is functionalized with different acetyl-protected thioglycosides **2**–**7** via thiol–ene addition in flow at >275 nm, resulting in a building block alphabet of six different glyco-building blocks **8**–**13**. These building blocks are then applied for the solid-phase synthesis of sequence-defined glycooligomers **14**–**16**.

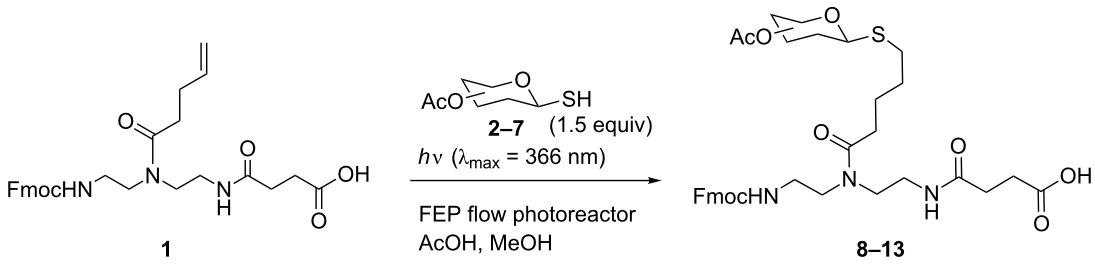

Scheme 1: Carbohydrate functionalization of DDS.

tion of 0.1 M could be only realized by premixing all reagents before injection. In this case it is important to notice that no background reactivity could be measured when performing the reaction without irradiation under similar flow conditions.

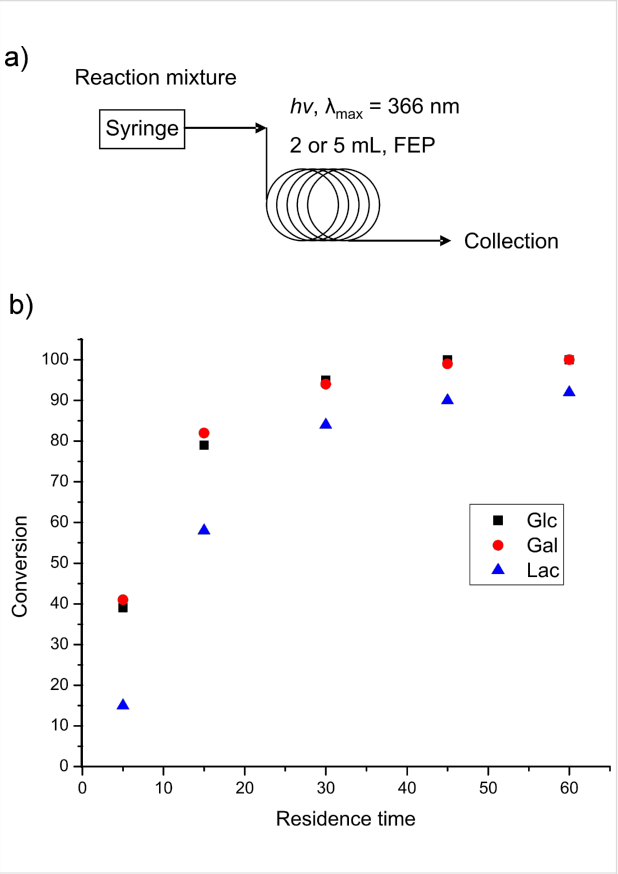

Figure 2: a) Schematic diagram of the TEC photoflow reactor. b) Plot of residence time versus conversion for the addition of the β-Glc(OAc)$_4$-SH **2**, β-Gal(OAc)$_4$-SH **3** and β-Lac(OAc)$_7$-SH **7** to the DDS building block **1**.

Integration of the HPLC UV-signals at 254 nm was used to establish residence time versus conversion plots (Figure 2). The plots showed close to complete conversion within 30 min residence time and 1.5 equiv of thioglycoside β-Glc(OAc)$_4$-SH **2** (95%) or β-Gal(OAc)$_4$-SH **3** (94%) (Figure 2; Glc and Gal). Similar reactivities were also observed for monosaccharides **4**–**6**, supporting the substrate scope of this approach and its suitability to access a library of differently glycosylated building blocks. Referring to larger thio-substrate β-Lac(OAc)$_7$-SH **7** a diminished reactivity with the same previously mentioned reaction conditions was determined (Figure 2b; Lac).

With optimized reaction conditions in place, large amounts of glycosylated building blocks are required to support solid phase oligomer synthesis. Large scale production of glycosylated building blocks **8**, **9**, **10** and **13** relied on the previously established conditions (30 min; 1.5 equiv thioglycoside; 0.1 M). Although the reactivity of aminoglycosides **5** and **6** is in the same range as that of glycosides **2**–**4**, we chose a higher excess of thiol component (2 equiv) for the production of glycosylated building blocks **11** and **12**, resulting in >95% conversion and an easy purification of the reaction mixture. Using this process, gram quantities of glycosylated building blocks **8**–**13** were obtained in 70–89% isolated yield after purification (Table 1).

With the isolated and characterized glyco-building blocks **8**–**13** obtained via TEC in flow, we then assembled three different glycooligomers **14**–**16** (Figure 3) to show the potential of the building block approach for the straightforward synthesis of a variety of differently glycosylated structures. The oligomer synthesis is based on standard peptide synthesis protocols and amide formation via activation of the building blocks' free carboxy group, coupling to the solid support followed by deprotection of the amino group (Figure 3). This allows us to synthesize chemically defined oligomers with full control over the monomer sequence [15,16,18,26] using differently functionalized and spacer building blocks. Due to the use of fully functionalized building blocks the desired product can be obtained directly after cleavage from the resin and after overall deprotection.

In order to be suitable for solid-phase synthesis, the building blocks have to be soluble in DMF or NMP, permanent protective groups have to be stable towards piperidine exposure and the activated species should selectively react with primary amines without prior decomposition. Indeed, all glyco-building blocks described here, fulfil these criteria and can be applied for

Table 1: Overview of the preparation of glycosylated building block and used upscale conditions.

Building block	Thiol component	Equiv	Residence time	Conversion	Yield
β-GlcS_DDS **8**	β-Glc(OAc)$_4$-SH **2**	1.5	30 min	95%	84%
β-GalS_DDS **9**	β-Gal(OAc)$_4$-SH **3**	1.5	30 min	94%	81%
β-RhaS_DDS **10**	β-Rha(OAc)$_3$-SH **4**	1.5	30 min	95%	89%
β-GlcNAcS_DDS **11**	β-GlcNAc(OAc)$_3$-SH **5**	2	30 min	>95%	81%
β-GalNAcS_DDS **12**	β-GalNAc(OAc)$_3$-SH **6**	2	30 min	>95%	85%
β-LacS_DDS **13**	β-Lac(OAc)$_7$-SH **7**	1.5	30 min	84%	70%

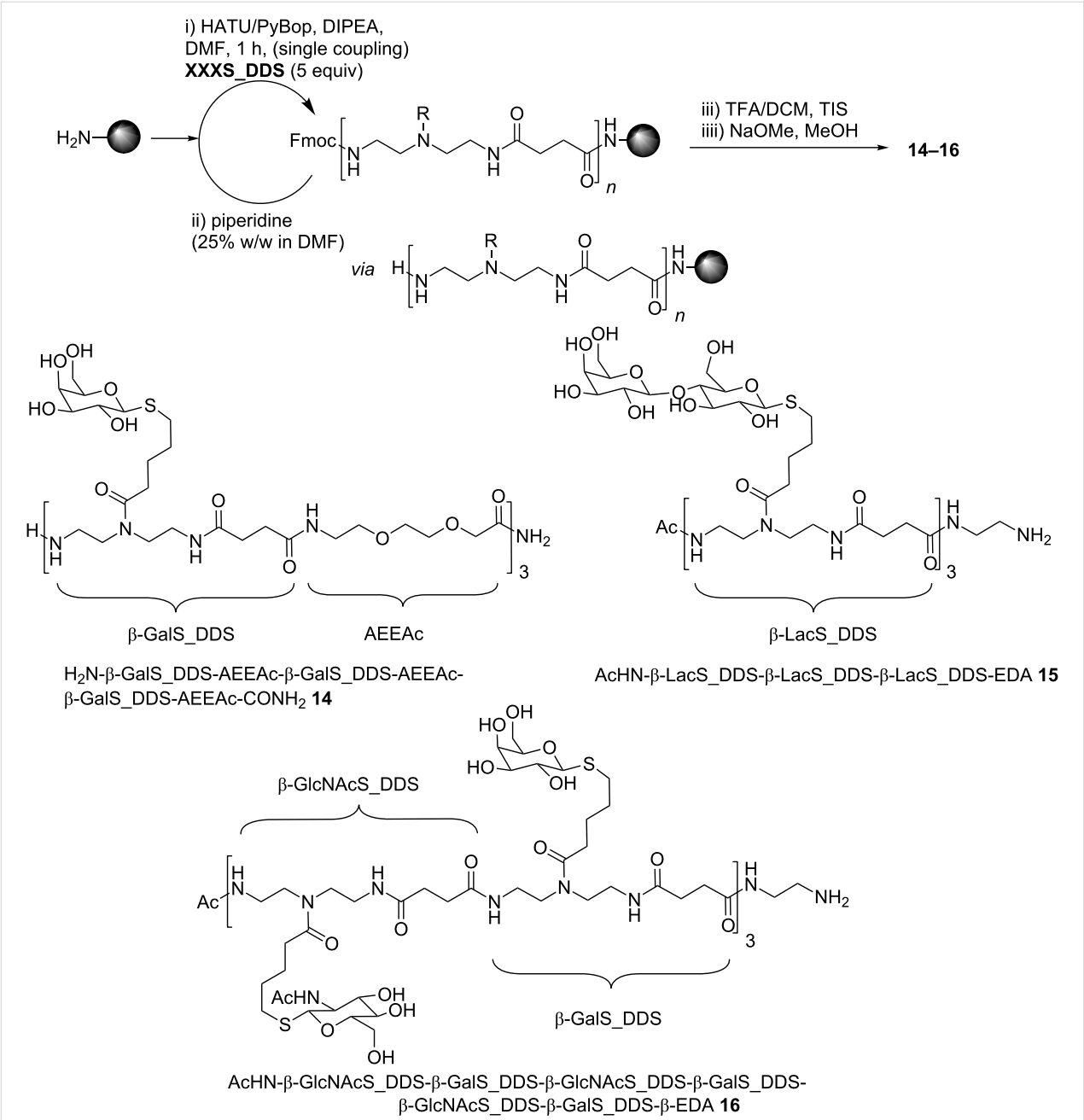

Figure 3: Solid phase coupling procedure and the obtained homo- and heteromultivalent glycoligands **14**–**16**.

sequential coupling under PyBop or HATU activation and Fmoc deprotection with 25% piperidine in DMF on solid support (Figure 3). Final deprotection from the resin was performed with TFA/DCM mixtures, followed by acetyl deprotection in solution under Zemplén conditions [44]. Although the glycosylated building blocks **9**–**13** suffer from steric hindrance and have a relatively high molecular weight in comparison to amino acids, they show remarkably good coupling efficiency during amide bond formation on solid support. Glycooligomer **14**, combining three ß-GalS_DDS and three amino-diethoxy-acetic acid (AEEAc) building blocks in alternating sequence, was accessible in high yields (81%) and purity (94% determined via integration of the HPLC signal at 214 nm) by referring only to single coupling (5 equiv) for one hour using PyBop activation (see Supporting Information File 1). After diethyl ether precipitation no further purification of compound **14** was necessary. This structure represents an example for a combination of glycosylated and non-glycosylated building blocks that allows for the variation of the density, number and spacing of sugar ligands along the scaffold. In order to test whether the

building block approach is also suitable for the direct introduction of larger sugar ligands such as the Lac disaccharide, we synthesized structure **15** presenting three Lac ligands placed right next to each other in a short oligomer chain. Indeed, depending on the building blocks applied and oligomer structures targeted, different activating reagents are required. Glycooligomer **15** introducing Lac groups was obtained as highly pure material after solid-phase synthesis using HATU activation instead of PyBop followed by HPLC purification. Another important advantage of the presented building block approach is the straightforward access to so-called heteromultivalent glycooligomers. Here different sugar ligands are presented at different positions along the oligomer chain. To date, such heteromultivalent systems are mainly obtained by functionalization with mixtures of sugar ligands that do not allow for a precise positioning of the different sugar ligands [9,45]. Alternatively, a polymer-analogue strategy is required where different functional groups are placed along a polymer chain that allow for orthogonal conjugation strategies introducing the different sugars sequentially [37,46]. Our approach simply relies on choosing from our differently glycosylated building blocks that are introduced in the desired pattern by automated solid-phase synthesis. As a proof of principle we synthesized glycoligand **16** as a multivalent scaffold that presents two different monosaccharides. β-GlcNAc and β-Gal are exposed in alternating fashion with an overall oligomer length of six building blocks and a molecular weight of 3000 Da. Similar to glycooligomer **15** this structure was obtained as highly pure material after solid-phase synthesis using HATU activation and HPLC purification.

Conclusion

In this article we reported on the synthesis of glycosylated building blocks via photochemical thiol–ene chemistry in a continuous-flow reactor using five different monosaccharides and one disaccharide. We showed that this flow set up provides excellent conversion rates with several substrates. All monosaccharides were shown to react under the same conditions with equivalent conversion rates, whereas the peracetylated β-thiolactose as a disaccharide showed slightly diminished reactivity. Additionally, these small scale reactions were transferred into the gram-scale production of six different glycosylated building blocks.

These carbohydrate presenting building blocks were then applied for solid-phase synthesis resulting in three monodisperse, sequence-defined glycooligomers with different glycosylation patterns. The building-block approach for the synthesis of glycooligomers thus allows for the control of the ligand positioning as well as the straightforward introduction of defined sequences of different types of ligands. Ongoing studies focus on the synthesis of a larger set of different glycooligo/polymers and the evaluation of their binding properties as sugar mimetics. For example, homomultivalent oligomer **14** and analogues are characterized for their interactions with asialoglycoprotein receptors, while heteromultivalent oligomer **16** represents a potential mimic of poly(lacNAc), which is known to be an important naturally-occurring galectin binder.

Experimental

General TEC procedure. A photoreactor was set up using 5 mL (for optimization reactions 2 mL) loop of FEP tubing around a Pyrex and a medium pressure Hg lamp [26,43]. A recirculating chiller (Huber Unistat 360, filled with spectroscopically pure water as coolant) was used to maintain the reactor at a temperature of 25–30 °C (for further details see Supporting Information File 1). Using a syringe pump (Harvard PHD2000), a solution of DDS **1** (1.0 equiv), acetyl-protected thioglycosidesglycoside **2**–**7** (1.5–2.0 equiv) and acetic acid (3 equiv) in degassed methanol was injected into the photoreactor. The entire reactor output was collected and evaporated under reduced pressure to afford the crude material.

β-GlcS_DDS (8): A solution of acetyl protected β-thioglucose **2** (1.35 g; 3.69 mmol, 1.5 equiv) and DDS **1** (1.25 g; 2.46 mmol, 1.0 equiv) in MeOH (24 mL) and AcOH (0.42 mL) (residence time, 30 min; flow rate 167 μL min^{-1}) was reacted under photochemical conditions according to the general TEC procedure. The reactor outcome was concentrated and purified via silica chromatography (DCM/MeOH + 1% AcOH 15:1) giving compound **8** (1.8 g; 84%). The analytical data is in accordance with published data [26].

β-GalS_DDS (9): A solution of acetyl protected β-thiogalactose **3** (1.35 g; 3.69 mmol, 1.5 equiv) and DDS **1** (1.25 g; 2.46 mmol, 1.0 equiv) in MeOH (24 mL) and AcOH (0.42 mL) (residence time, 30 min; flow rate 167 μL min^{-1}) was reacted under photochemical conditions according to the general TEC procedure. The reactor outcome was concentrated and purified via silica chromatography (DCM/MeOH + 1% AcOH 15:1) giving compound **9** (1.74 g; 81%). IR (film) ν: 2945, 1748, 1225 cm^{-1}; $[\alpha]_D^{20}$ −32.19 (*c* 1, MeOH); ^{1}H NMR (400 MHz, $CDCl_3$) 7.76 (d, *J* = 7.5, 2H), 7.58 (d, *J* = 7.4, 2H), 7.39 (t, *J* = 7.4, 2H), 7.30 (t, *J* = 7.4, 2H), 7.07–6.83 (m, 1H), 5.86–5.64 (m, 1H), 5.47–5.35 (m, 1H), 5.19 (t, *J* = 9.8, 1H), 5.10–4.97 (m, 1H), 4.65–4.27 (m, 3H), 4.25–3.80 (m, 4H), 3.62–3.18 (m, 8H), 2.73–2.53 (m, 4H), 2.52–2.29 (m, 4H), 2.12 (s, 3H), 2.05–1.99 (m, 6H), 1.97 (s, 3H), 1.76–1.50 (m, 4H); ^{13}C NMR (100 MHz, $CDCl_3$) (mixture of rotamers) 175.0, 173.1, 172.9, 170.7, 170.4, 170.2, 169.9, 156.9, 143.9, 143.9, 141.4, 141.4, 127.9, 127.2, 125.2, 125.1, 120.2, 120.2, 84.1, 74.5, 72.0, 67.5, 67.5, 67.0, 61.5, 48.5, 48.3, 47.3, 45.9, 40.1, 39.9, 39.3, 38.6, 32.6, 32.4,

30.9, 29.8, 29.4, 29.4, 29.3, 24.5, 24.5, 20.9, 20.8, 20.8, 20.7; HRMS (ESI) *m/z*: $[M + Na]^+$ calcd for $C_{42}H_{53}N_3O_{15}SNa$, 894.3095; found, 894.3096; RP-HPLC analysis, 5% to 95% MeCN in 10 min, retention time = 8.1 min.

β-RhaS_DDS (10): A solution of acetyl protected L-β-thiorhamnose **4** (1.13 g; 3.69 mmol, 1.5 equiv) and DDS **1** (1.25 g; 2.46 mmol, 1.0 equiv) in MeOH (24 mL) and AcOH (0.42 mL) (residence time, 30 min; flow rate 167 μL min^{-1}) was reacted under photochemical conditions according to the general TEC procedure. The reactor outcome was concentrated and purified via silica chromatography (DCM/MeOH + 1% AcOH 17:1) giving compound **10** (1.78 g; 89%). IR (film) ν: 2940, 1745, 1630, 1224 cm^{-1}; $[\alpha]_D^{20}$ −5.83 (*c* 1, MeOH); ^1H NMR (400 MHz, $CDCl_3$) 7.74 (d, *J* = 7.5, 2H), 7.57 (d, *J* = 7.4, 2H), 7.38 (t, *J* = 7.3, 2H), 7.29 (t, *J* = 7.6, 2H), 6.96 (br s, 1H), 5.86–5.65 (m, 1H), 5.30 (dd, *J* = 3.3, 1.5, 1H), 5.22–5.16 (m, 1H), 5.14 (s, 1H), 5.07 (t, *J* = 9.8, 1H), 4.46–4.26 (m, 2H), 4.24–4.12 (m, 2H), 3.67–3.09 (m, 8H), 2.82–2.23 (m, 8H), 2.17–2.09 (m, 3H), 2.04 (s, 3H), 1.97 (s, 3H), 1.73–1.56 (m, 4H), 1.19 (d, *J* 6.2, 3H); ^{13}C NMR (100 MHz, $CDCl_3$) (mixture of rotamers) 175.3, 175.2, 174.9, 174.8, 173.1, 172.9, 170.4, 170.1, 170.1, 157.3, 156.9, 143.9, 143.9, 141.4, 141.4, 127.9, 127.2, 125.2, 125.1, 120.1, 120.1, 82.3, 71.8, 71.3, 69.7, 67.3, 67.0, 48.5, 48.2, 47.3, 46.2, 45.9, 40.1, 39.8, 39.2, 38.6, 32.6, 32.4, 31.1, 30.8, 30.8, 29.7, 29.4, 29.2, 29.1, 24.5, 24.4, 21.1, 20.9, 20.8, 17.5, 17.5;; HRMS (ESI) *m/z*: $[M + Na]^+$ calcd for $C_{40}H_{51}N_3O_{13}SNa$, 836.3040; found, 836.3056; RP-HPLC analysis, 5% to 95% MeCN in 10 min, retention time = 7.8 min.

β-GlcNAcS_DDS (11): A solution of acetyl protected β-thioglucosamine **5** (0.72 g; 1.97 mmol, 2.0 equiv) and DDS **1** (0.5 g; 0.99 mmol, 1.0 equiv) in MeOH (10 mL) and AcOH (0.17 mL) (residence time, 30 min; flow rate 167 μL min^{-1}) was reacted under photochemical conditions according to the general TEC procedure. The reactor outcome was concentrated and purified via silica chromatography (DCM/MeOH + 1% AcOH 10:1) giving compound **11** (0.70 g; 81%). IR (film) ν: 2940, 1744, 1654, 1229 cm^{-1}; $[\alpha]_D^{20}$ +25.65 (*c* 2, MeOH); ^1H NMR (400 MHz, $CDCl_3$) 7.77–7.71 (m, 2H), 7.57 (d, *J* = 7.3, 2H), 7.37 (t, *J* = 7.4, 2H), 7.33–7.25 (m, 2H), 5.21–4.99 (m, 2H), 4.64–4.50 (m, 1H), 4.41–3.99 (m, 6H), 3.72–3.56 (m, 1H), 3.51–3.17 (m, 8H), 2.76–2.52 (m, 4H), 2.50–2.28 (m, 4H), 2.02 (s, 3H), 2.00–1.95 (m, 6H), 1.89 (d, *J* = 9.1 Hz, 2H), 1.75–1.42 (m, 2H); ^{13}C NMR (100 MHz, $CDCl_3$) (mixture of rotamers) 174.8, 174.7, 173.2, 171.2, 171.2, 171.1, 170.1, 169.5, 169.5, 157.2, 157.0, 143.8, 141.3, 127.9, 127.2, 125.1, 120.1, 83.7, 83.7, 75.7, 74.1, 68.6, 68.6, 67.0, 66.9, 62.4, 53.0, 53.0, 48.2, 47.9, 47.2, 46.1, 45.8, 39.7, 38.5, 38.3, 32.3, 32.1, 30.9, 29.8, 29.3, 29.3, 28.3, 23.9, 23.8, 23.1, 20.9, 20.8, 20.7; HRMS (ESI) *m/z*: $[M + Na]^+$ calcd for $C_{42}H_{54}N_4O_{14}SNa$, 893.3255; found, 893.3263; RP-HPLC analysis, 5% to 95% MeCN in 10 min, retention time = 7.1 min.

β-GalNAcS_DDS (12): A solution of acetyl protected β-thiogalactosamine **6** (0.72 g; 1.97 mmol, 2.0 equiv) and DDS **1** (0.5 g; 0.99 mmol, 1.0 equiv) in MeOH (10 mL) and AcOH (0.17 mL) (residence time, 30 min; flow rate 167 μL min^{-1}) was reacted under photochemical conditions according to the general TEC procedure. The reactor outcome was concentrated and purified via silica chromatography (DCM/MeOH + 1% AcOH 10:1) giving compound **12** (0.73 g; 85%). IR (film) ν: 1746, 1655, 1236 cm^{-1}; $[\alpha]_D^{20}$ +145.42 (*c* 2, MeOH); ^1H NMR (400 MHz, $CDCl_3$) 7.77–7.69 (m, 2H), 7.56 (d, *J* = 7.3, 2H), 7.36 (t, *J* = 7.4, 2H), 7.32–7.23 (m, 2H), 5.39–5.25 (m, 1H), 5.14–5.01 (m, 1H), 4.57 (t, *J* = 10.5, 1H), 4.41–3.94 (m, 6H), 3.90–3.77 (m, 1H), 3.54–3.04 (m, 8H), 2.78–2.52 (m, 4H), 2.51–2.27 (m, 4H), 2.10 (s, 3H), 2.05–1.84 (m, 9H), 1.79–1.45 (m, 4H); ^{13}C NMR (100 MHz, $CDCl_3$) (mixture of rotamers) 175.2, 174.8, 174.7, 173.1, 173.0, 171.5, 171.3, 170.8, 170.7, 170.5, 170.5, 157.2, 143.8, 143.8, 141.3, 128.0, 127.2, 125.2, 125.1, 120.1, 84.2, 84.0, 74.3, 71.7, 71.6, 67.0, 66.9, 61.8, 61.8, 49.2, 48.2, 47.8, 47.3, 46.2, 45.8, 39.7, 38.5, 38.4, 32.3, 32.1, 30.7, 30.6, 29.7, 29.6, 29.4, 28.4, 28.3, 23.9, 23.8, 23.2, 23.2, 20.8, 20.7; HRMS (ESI) *m/z*: $[M + Na]^+$ calcd for $C_{42}H_{54}N_4O_{14}SNa$, 893.3255; found, 893.3247; RP-HPLC analysis, 5% to 95% MeCN in 10 min, retention time = 7.1 min.

β-LacS_DDS (13): A solution of acetyl protected β-thiolactose **7** (0.79 g; 1.18 mmol, 1.5 equiv) and DDS **1** (0.4 g; 0.79 mmol, 1.0 equiv) in MeOH (7.9 mL) and AcOH (0.17 mL) (residence time, 30 min; flow rate 167 μL min^{-1}) was reacted under photochemical conditions according to the general TEC procedure. The reactor outcome was concentrated and purified *via* silica chromatography (DCM/MeOH + 1% AcOH 15:1) giving compound **13** (0.65 g; 70%). IR (film) ν: 1750, 1230, 1051 cm^{-1}; $[\alpha]_D^{20}$ −35.00 (*c* 2, MeOH); ^1H NMR (400 MHz, $CDCl_3$) 7.72 (d, *J* = 7.5, 2H), 7.55 (d, *J* = 7.5, 2H), 7.37 (t, *J* = 7.3, 2H), 7.29–7.25 (m, 2H), 5.31 (s, 1H), 5.16 (dt, *J* = 9.2, 3.1, 1H), 5.06 (t, *J* = 7.9, 1H), 4.96–4.85 (m, 2H), 4.47–4.04 (m, 9H), 3.87–3.71 (m, 2H), 3.55 (br s, 1H), 3.45–3.29 (m, 8H), 2.63–2.54 (m, 4H), 2.44–2.29 (m, 2H), 2.34–2.27 (m, 2H); 2.11 (s, 3H), 2.06–2.05 (m, 3H), 2.02–1.98 (m, 12H), 1.93 (s, 3H), 1.67–1.52 (m, 4H); ^{13}C NMR (100 MHz, $CDCl_3$) (mixture of rotamers) 174.9, 174.7, 172.8, 172.7, 170.6, 170.5, 170.3, 170.3, 170.1, 170.0, 169.8, 169.8, 169.7, 169.7, 169.6, 169.1, 169.1, 157.0, 156.7, 143.8, 143.7, 141.3, 141.2, 127.8, 127.7, 127.1, 125.0, 125.0, 120.0, 120.0, 101.0, 83.2, 76.1, 73.8, 70.9, 70.6, 70.3, 69.1, 66.9, 66.8, 66.6, 62.2, 62.1, 60.8, 60.8, 48.3, 47.9, 47.1, 46.00, 45.6, 39.9, 38.9, 38.4, 32.4, 32.2, 30.7, 29.7, 29.6, 29.5, 29.2, 29.1, 24.2, 20.8, 20.7, 20.7, 20.6, 20.4; HRMS (ESI) *m/z*: $[M + Na]^+$ calcd for $C_{54}H_{69}N_3O_{23}SNa$, 1182.3940;

found, 1182.3956; RP-HPLC analysis, 5% to 95% MeCN in 10 min, retention time = 9.3 min.

H_2N-β-GalS_DDS-AEEAc- β-GalS_DDS-AEEAc-β-GalS_DDS-AEEAc-$CONH_2$ (14): Compound **14** (30 mg, 16.2 μmol) was obtained as white hygroscopic powder after cleavage from the resin, precipitation into diethyl ether and deactylation with a yield of 81%. MALDI–TOF–MS: $[M + Na]^+$ calcd for $C_{75}H_{135}N_{13}O_{33}S_3Na$, 1864.83 (monoisotopic); found, 1864.63; RP-HPLC analysis 5% to 95% MeCN in 10 min, retention time = 3.9 min.

AcHN-β-LacS_DDS-β-LacS_DDS-β-LacS_DDS-EDA (15): Acetyl protected compound **15** was cleaved from the resin and precipitated into diethyl ether. The crude material was purified via preparative RP-HPLC (5 to 95% MeCN in 30 min) and freezed-dried. After final deactylation compound **15** (11 mg, 5.6 μmol) was obtained as white hygroscopic powder with 28% yield. MALDI–TOF–MS: $[M + H]^+$ calcd for $C_{79}H_{140}N_{11}O_40S_3$, 1978.84 (monoisotopic); found, 1979.06; $[M + Na]^+$ calcd for $C_{79}H_{139}N_{11}O_40S_3Na$, 2000.82 (monoisotopic); found, 2000.88; $[M + K]^+$ calcd for $C_{79}H_{139}N_{11}O_40S_3K$, 2016.80 (monoisotopic); found, 2017.01; RP-HPLC analysis 5% to 50% MeCN in 30 min, retention time = 5.9 min.

AcHN-β-GlcNAcS_DDS-β-GalS_DDS-β-GlcNAcS_DDS-β-GalS_DDS-β-GlcNAcS_DDS-β-GalS_DDS-β-EDA (16) Acetyl protected compound **16** was cleaved from the resin and precipitated into diethyl ether. After deactylation in solution, the crude material was purified via preparative RP-HPLC (5 to 50% MeCN in 30 min) and freezed-dried. Compound **16** (12.6 mg, 4.2 μmol) was obtained as white hygroscopic powder with 21% yield. MALDI–TOF–MS: $[M + Na]^+$ calcd for $C_{124}H_{217}N_{23}O_{49}S_6Na$, 3027.34 (monoisotopic); found, 3027.71; RP-HPLC analysis 5% to 50% MeCN in 30 min, retention time = 7.8 min.

Supporting Information

Supporting Information File 1

Further experimental procedures, characterization data and spectra.
[http://www.beilstein-journals.org/bjoc/content/supplementary/1860-5397-9-276-S1.pdf]

Acknowledgements

The authors thank the Max Planck Society as well as the German Research Foundation (DFG, Emmy Noether program HA5950/1-1) for financial support and Prof. Tyler McQuade and Dr. Kerry Gilmore for helpful discussions.

References

1. Bertozzi, C. R.; Kiessling, L. L. *Science* **2001,** *291,* 2357–2364. doi:10.1126/science.1059820
2. Kiessling, L. L.; Gestwicki, J. E.; Strong, L. E. *Angew. Chem., Int. Ed.* **2006,** *45,* 2348–2368. doi:10.1002/anie.200502794
3. Krannig, K.-S.; Schlaad, H. *J. Am. Chem. Soc.* **2012,** *134,* 18542–18545. doi:10.1021/ja308772d
4. Fasting, C.; Schalley, C. A.; Weber, M.; Seitz, O.; Hecht, S.; Koksch, B.; Dernedde, J.; Graf, C.; Knapp, E. W.; Haag, R. *Angew. Chem., Int. Ed.* **2012,** *51,* 10472–10498. doi:10.1002/anie.201201114
5. Jayaraman, N. *Chem. Soc. Rev.* **2009,** *38,* 3463–3483. doi:10.1039/b815961k
6. Pieters, R. J. *Org. Biomol. Chem.* **2009,** *7,* 2013–2025. doi:10.1039/b901828j
7. Lindhorst, T. K. *Top. Curr. Chem.* **2002,** *218,* 201–235. doi:10.1007/3-540-45010-6_7
8. Kiessling, L. L.; Gestwicki, J. E.; Strong, L. E. *Curr. Opin. Chem. Biol.* **2000,** *4,* 696–703. doi:10.1016/S1367-5931(00)00153-8
9. Becer, C. R.; Gibson, M. I.; Geng, J.; Ilyas, R.; Wallis, R.; Mitchell, D. A.; Haddleton, D. M. *J. Am. Chem. Soc.* **2010,** *132,* 15130–15132. doi:10.1021/ja1056714
10. Cloninger, M. J. *Curr. Opin. Chem. Biol.* **2002,** *6,* 742–748. doi:10.1016/S1367-5931(02)00400-3
11. Wittmann, V.; Seeberger, S. *Angew. Chem., Int. Ed.* **2000,** *39,* 4348–4352. doi:10.1002/1521-3773(20001201)39:23<4348::AID-ANIE4348>3.0.CO;2-X
12. Galan, M. C.; Dumy, P.; Renaudet, O. *Chem. Soc. Rev.* **2013,** *42,* 4599–4612. doi:10.1039/c2cs35413f
13. Jeon, I.; Lee, D.; Krauss, I. J.; Danishefsky, S. J. *J. Am. Chem. Soc.* **2009,** *131,* 14337–14344. doi:10.1021/ja9052625
14. Schlegel, M. K.; Hutter, J.; Eriksson, M.; Lepenies, B.; Seeberger, P. H. *ChemBioChem* **2011,** *12,* 2791–2800. doi:10.1002/cbic.201100511
15. Hartmann, L. *Macromol. Chem. Phys.* **2011,** *212,* 8–13. doi:10.1002/macp.201000479
16. Hartmann, L.; Borner, H. G. *Adv. Mater.* **2009,** *21,* 3425–3431. doi:10.1002/adma.200801884
17. Mosca, S.; Wojcik, F.; Hartmann, L. *Macromol. Rapid Commun.* **2011,** *32,* 197–202. doi:10.1002/marc.201000593
18. Wojcik, F.; Mosca, S.; Hartmann, L. *J. Org. Chem.* **2012,** *77,* 4226–4234. doi:10.1021/jo202561k
19. Chabre, Y. M.; Roy, R. *Curr. Top. Med. Chem.* **2008,** *8,* 1237–1285. doi:10.2174/156802608785848987
20. Ponader, D.; Wojcik, F.; Beceren-Braun, F.; Dernedde, J.; Hartmann, L. *Biomacromolecules* **2012,** *13,* 1845–1852. doi:10.1021/bm300331z
21. Hoyle, C. E.; Bowman, C. N. *Angew. Chem., Int. Ed.* **2010,** *49,* 1540–1573. doi:10.1002/anie.200903924
22. Dondoni, A.; Marra, A. *Chem. Soc. Rev.* **2012,** *41,* 573–586. doi:10.1039/c1cs15157f
23. Griesbaum, K. *Angew. Chem., Int. Ed. Engl.* **1970,** *9,* 273–287. doi:10.1002/anie.197002731
24. Dondoni, A. *Angew. Chem., Int. Ed.* **2008,** *47,* 8995–8997. doi:10.1002/anie.200802516
25. Northrop, B. H.; Coffey, R. N. *J. Am. Chem. Soc.* **2012,** *134,* 13804–13817. doi:10.1021/ja305441d
26. Wojcik, F.; O'Brien, A. G.; Götze, S.; Seeberger, P. H.; Hartmann, L. *Chem.–Eur. J.* **2013,** *19,* 3090–3098. doi:10.1002/chem.201203927

27. Suzuki, Y.; Laurino, P.; McQuade, D. T.; Seeberger, P. H. *Helv. Chim. Acta* **2012,** *95,* 2578–2588. doi:10.1002/hlca.201200487
28. Bou-Hamdan, F. R.; Levesque, F.; O'Brien, A. G.; Seeberger, P. H. *Beilstein J. Org. Chem.* **2011,** *7,* 1124–1129. doi:10.3762/bjoc.7.129
29. O'Brien, A. G.; Horváth, Z.; Lévesque, F.; Lee, J. W.; Seidel-Morgenstern, A.; Seeberger, P. H. *Angew. Chem., Int. Ed.* **2012,** *51,* 7028–7030. doi:10.1002/anie.201202795
30. Bogdan, A. R.; Poe, S. L.; Kubis, D. C.; Broadwater, S. J.; McQuade, D. T. *Angew. Chem., Int. Ed.* **2009,** *48,* 8547–8550. doi:10.1002/anie.200903055
31. Lévesque, F.; Seeberger, P. H. *Angew. Chem., Int. Ed.* **2012,** *51,* 1706–1709. doi:10.1002/anie.201107446
32. Mason, B. P.; Price, K. E.; Steinbacher, J. L.; Bogdan, A. R.; McQuade, D. T. *Chem. Rev.* **2007,** *107,* 2300–2318. doi:10.1021/cr050944c
33. Andrews, R. S.; Becker, J. J.; Gagné, M. R. *Angew. Chem., Int. Ed.* **2012,** *51,* 4140–4143. doi:10.1002/anie.201200593
34. Bou-Hamdan, F. R.; Seeberger, P. H. *Chem. Sci.* **2012,** *3,* 1612–1616. doi:10.1039/c2sc01016j
35. Knowles, J. P.; Elliott, L. D.; Booker-Milburn, K. I. *Beilstein J. Org. Chem.* **2012,** *8,* 2025–2052. doi:10.3762/bjoc.8.229
36. Noël, T.; Buchwald, S. L. *Chem. Soc. Rev.* **2011,** *40,* 5010. doi:10.1039/c1cs15075h
37. Booker-Milburn, K. *Nat. Chem.* **2012,** *4,* 433–435. doi:10.1038/nchem.1356
38. Gutierrez, A. C.; Jamison, T. F. *Org. Lett.* **2011,** *13,* 6414–6417. doi:10.1021/ol2027015
39. Wegner, J.; Ceylan, S.; Kirschning, A. *Adv. Synth. Catal.* **2012,** *354,* 17–57. doi:10.1002/adsc.201100584
40. Baradel, N.; Fort, S.; Halila, S.; Badi, N.; Lutz, J. F. *Angew. Chem., Int. Ed.* **2013,** *52,* 2335–2339. doi:10.1002/anie.201209052
41. Floyd, N.; Vijayakrishnan, B.; Koeppe, A. R.; Davis, B. G. *Angew. Chem., Int. Ed.* **2009,** *48,* 7798–7802. doi:10.1002/anie.200903135
42. Jana, M.; Misra, A. K. *J. Org. Chem.* **2013,** *78,* 2680–2686. doi:10.1021/jo302115k
43. Hook, B. D. A.; Dohle, W.; Hirst, P. R.; Pickworth, M.; Berry, M. B.; Booker-Milburn, K. I. *J. Org. Chem.* **2005,** *70,* 7558–7564. doi:10.1021/jo050705p
44. Wang, Z. In *Comprehensive Organic Name Reactions and Reagents*; John Wiley & Sons, Inc.: 2009, p 3123–3128. doi:10.1002/9780470638859
45. Gestwicki, J. E.; Cairo, C. W.; Strong, L. E.; Oetjen, K. A.; Kiessling, L. L. *J. Am. Chem. Soc.* **2002,** *124,* 14922–14933. doi:10.1021/ja027184x
46. Lutz, J. F. *Angew. Chem., Int. Ed.* **2007,** *46,* 1018–1025. doi:10.1002/anie.200604050

License and Terms

Beilstein Journal of Organic Chemistry

A combined continuous microflow photochemistry and asymmetric organocatalysis approach for the enantioselective synthesis of tetrahydroquinolines

Erli Sugiono* and Magnus Rueping*

Full Research Paper

Open Access

Address:
Institute of Organic Chemistry, RWTH Aachen University, Landoltweg 1, D-52074 Aachen, Germany

Email:
Erli Sugiono* - erli.sugiono@rwth-aachen.de; Magnus Rueping* - magnus.rueping@rwth-aachen.de

* Corresponding author

Keywords:
asymmetric transfer hydrogenation; binolphosphate; continuous-flow reactors; flow chemistry; microreactors; organocatalysis; photochemistry

Beilstein J. Org. Chem. **2013,** *9,* 2457–2462.
doi:10.3762/bjoc.9.284

Received: 25 July 2013
Accepted: 18 October 2013
Published: 13 November 2013

This article is part of the Thematic Series "Chemistry in flow systems III".

Guest Editor: A. Kirschning

Abstract

A continuous-flow asymmetric organocatalytic photocyclization–transfer hydrogenation cascade reaction has been developed. The new protocol allows the synthesis of tetrahydroquinolines from readily available 2-aminochalcones using a combination of photochemistry and asymmetric Brønsted acid catalysis. The photocylization and subsequent reduction was performed with catalytic amount of chiral BINOL derived phosphoric acid diester and Hantzsch dihydropyridine as hydrogen source providing the desired products in good yields and with excellent enantioselectivities.

Introduction

Tetrahydroquinolines [1-4] represent a well-known structural motif found in a large number of biologically active natural products. Optically active tetrahydroquinolines are important building blocks for the pharmaceutical and agrochemical industries. Due to their importance, new and efficient procedures for their synthesis have been developed. Among the synthetic protocols developed for the preparation of optically active tetrahydroquinolines, the asymmetric hydrogenation of substituted quinolines represents the most widely used and efficient method to prepare this class of N-heterocyclic compound [5-17].

In the past years, continuous-flow chemistry has received considerable attention and microstructured continuous-flow devices have emerged as useful devices for different chemical reactions [18-22]. Microreactor technology offers numerous

practical advantages such as better reaction yield due to enhanced mixing quality, better control of reaction variables, reduced safety hazards, reduced reagent consumption, enhanced heat and mass transfer due to the high surface-to-volume ratio and rapid experimentation and optimization.

Recently, microreactor devices have been adopted for photochemical applications and microflow photochemistry has emerged as efficient synthesis tool [23-31]. The narrow inner dimensions of microfabricated reactors is advantageous for photochemical synthesis since it allows better light penetration and uniform irradiation through the entire reactor and the complete reaction medium, in comparison with reactions performed in conventional batch systems.

Here we report the development of continuous-flow photochemical reaction in combination with asymmetric Brønsted acid catalysis for the synthesis of optically active tetrahydroquinolines. Readily available substituted 2-aminochalcones were envisioned to undergo photocyclization to the corresponding quinolines which in the presence of a chiral BINOL-derived phosphoric acid diester and Hantzsch dihydropyridine as hydride donor [32-37] could provide the desired enantioenriched tetrahydroquinolines (Scheme 1) [38].

Results and Discussion

The continuous-flow microreactor system for the experiment was set up according to Scheme 2. The flow device was set up with multiple commercially available glass reactors connected

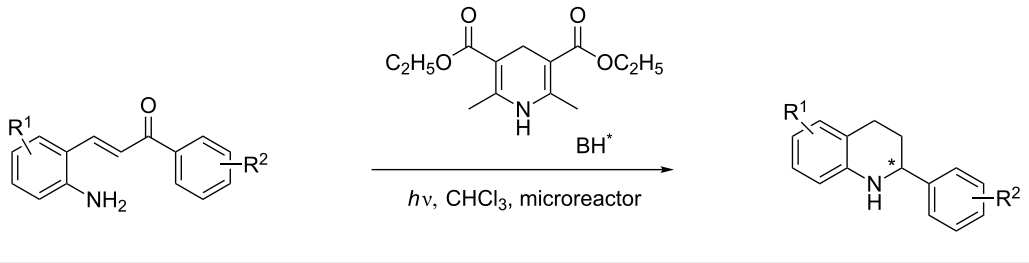

Scheme 1: Photocyclization–reduction of 2-aminochalcone.

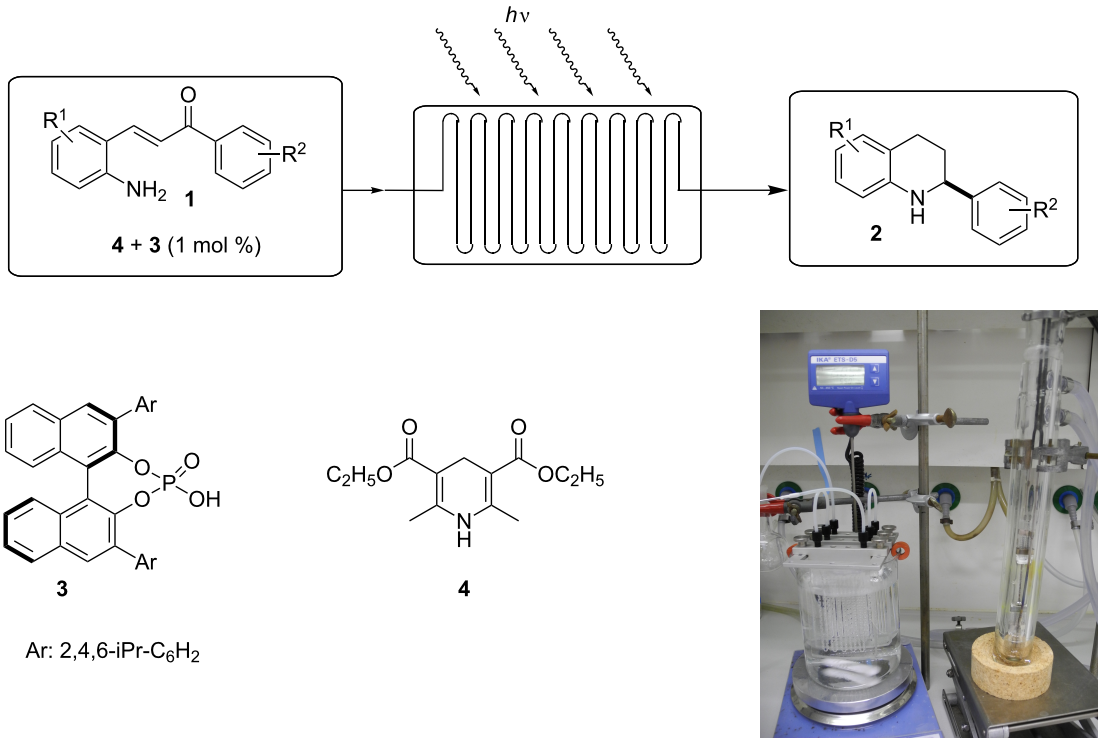

Scheme 2: Experimental setup of continuous-flow photocyclization–reduction cascade.

in parallel and placed in a water bath [39]. The light required to perform the reaction is supplied from a high-pressure mercury lamp located outside of the reactor. The lamp consists of a double-jacketed water-cooled pyrex immersion well. The reagents were degassed and introduced into the microreactor using a programmable syringe pump. The product solution was collected in a flask wrapped with aluminium foil to prevent further irradiation.

Our initial investigation of reaction conditions involved the photocyclization–reduction cascade of 2-aminochalcone **1a** in the presence of Hantzsch dihydropyridine **4** as hydrogen source and catalytic amount of chiral Brønsted acid **3**. The effect of temperature, flow rate and concentration on the reaction yield and enantioselectivity are summarized in Table 1. As shown in Table 1, performing the reaction in a pyrex test tube (i.d.: 12 mm; λ > 300 nm) with 1 mol % of Brønsted acid **3** at 40 °C for 60 min afforded the product in 7% isolated yield and 95% enantioselectivity (Table 1, entry 2). Conducting the reaction using the same light source and under the same reaction conditions in a single pass flow reaction showed a noticeable impact on the yield as the product **2a** could be isolated in 59% yield and 93% enantiomeric excess (Table 1, entry 1 vs entry 2). Improvement of the reaction yield shows the superior performance of the microflow reactor since the light penetration through the microchannels was significantly increased. A slight improvement of yield was achieved when the reaction was carried out at 55 °C (Table 1, entry 3).

Noticeable improvement on the chemical yield was observed when the reaction was conducted at a lower concentration providing the product in 74% isolated yield and 94% enantiomeric excess (Table 1, entry 4 vs entry 3). Further decrease of the concentration to 0.03 M gave the best result affording the product in 82% yield (Table 1, entry 6). It is worth mentioning that decreasing the flow rate had only a minimum effect on the yield but resulted in significant loss of enantioselectivity (Table 1, entry 5 vs 4). This result indicates that the residence time plays a crucial role in this photocyclization–reduction cascade. Due to prolonged irradiation of the reaction mixture, an undesired background reaction initiated by photoexcited dihydropyridine occurred leading to the loss of enantioselectivity [40,41].

With the optimized reaction conditions in hand, the substrate scope of this new photocyclization–asymmetric transfer hydrogenation sequence was examined. The results are summarized in Table 2. In general, different 2-aminochalcones bearing substituted aromatic residues on both ketone and enone moieties underwent the desired photocyclization and subsequent asymmetric reduction to afford the corresponding tetrahydroquinolines in good yields and high enantioselectivities.

Conclusion

In conclusion, we have demonstrated the great potential of a new continuous-flow microreactor system for the photocyclization–reduction cascade of 2-aminochalcones. Under the contin-

Table 1: Optimization of the Brønsted acid catalyzed transfer hydrogenation of quinolines.[a]

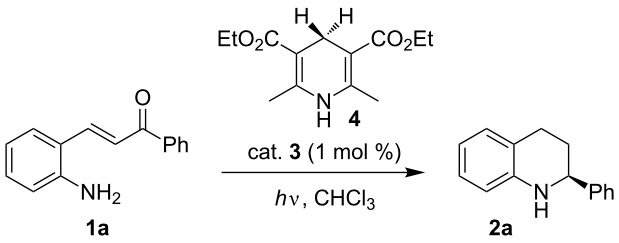

1a 2a

Entry	Conc. [mol/L]	Temp. [°C]	Time [min]	Flow rate [mL min^{-1}]	Yield [%][b]	ee [%][c]
1	0.1	40	60	0.1	59	93
2[d]	0.1	40	60	batch	7	95
3	0.1	55	60	0.1	64	96
4	0.05	55	60	0.1	74	94
5	0.05	55	120	0.05	79	88
6	0.03	55	60	0.1	82	94
7[d]	0.03	55	60	batch	29	96
8	0.03	55	120	0.05	88	83

[a]Reaction conditions: **1a**, **4** (2.4 equiv), **3** (1 mol %) in $CHCl_3$, irradiation with a TQ 150 high pressure mercury lamp. [b]Isolated yields after column chromatography. [c]Determined by chiral HPLC analysis. [d]Performed under batch condition.

Table 2: Scope of the continuous-flow photocyclization–asymmetric reduction domino sequence.[a]

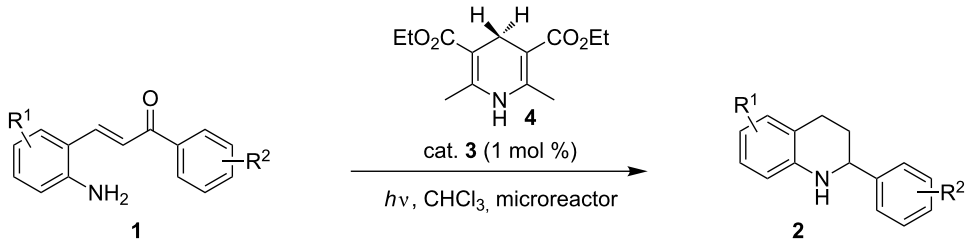

Entry[a]	Substrate **1**	Product **2**	Yield [%][b]	ee [%][c]
1	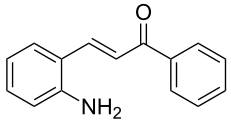 **1a**	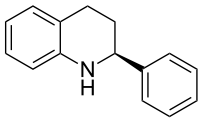 **2a**	82	94
2	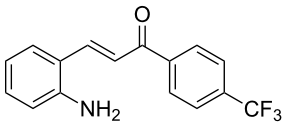 **1b**	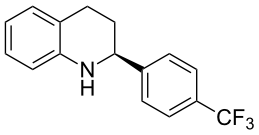 **2b**	88	96
3	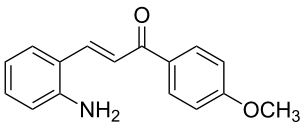 **1c**	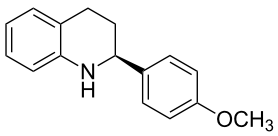 **2c**	73	91
4	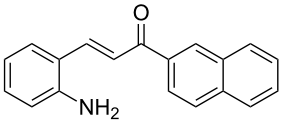 **1d**	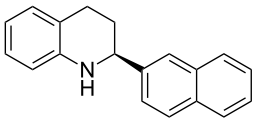 **2d**	71	91
5	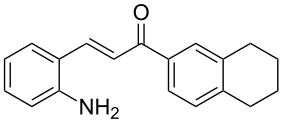 **1e**	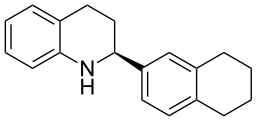 **2e**	63	89
6	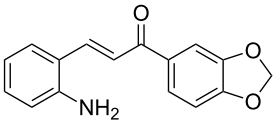 **1f**	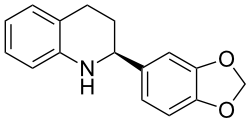 **2f**	73	90
7	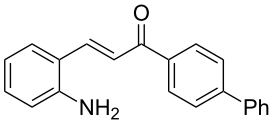 **1g**	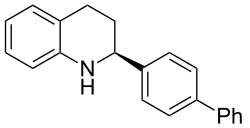 **2g**	75	88
8	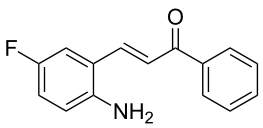 **1h**	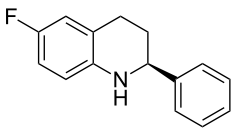 **2h**	64	90

Table 2: Scope of the continuous-flow photocyclization–asymmetric reduction domino sequence.[a] (continued)

9	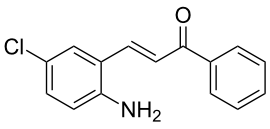 **1i**	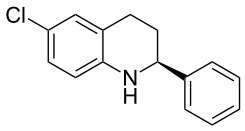 **2i**	57	91

[a]Reaction conditions: **1**, **4** (2.4 equiv), **3** (1 mol %) in $CHCl_3$ (0.03 M) at 55 °C, flow rate 0.1 mL/min, residence time = 60 min, irradiation with a TQ 150 high pressure mercury lamp. [b]Isolated yields after column chromatography. [c]Determined by chiral HPLC analysis.

uous-flow condition a variety of substituted 2-aminochalcones underwent the photocyclization and the subsequent transfer hydrogenation to afford a series of differently substituted tetrahydroquinolines in good yields and with excellent enantioselectivities. This efficient protocol for the synthesis of tetrahydroquinoline from readily available 2-aminochalcone provides an attractive alternative to the existing procedures and serves as a basis for further exploration of this new concept.

References

1. Keay, J. G. In *Comprehensive Organic Synthesis;* Trost, B. M.; Fleming, I., Eds.; Pergamon: Oxford, U.K., 1991; Vol. 8, p 579. doi:10.1016/B978-0-08-052349-1.00239-0
2. Katritzky, A. R.; Rachwal, S.; Rachwal, B. *Tetrahedron* **1996,** *52,* 15031–15070. doi:10.1016/S0040-4020(96)00911-8
3. Barton, D. H.; Nakanishi, K.; Cohn, O. M. *Comprehensive Natural Products Chemistry;* Elsevier: Oxford, U.K., 1999; Vol. 1–9.
4. Sridharan, V.; Suryavanshi, P. A.; Menéndez, J. C. *Chem. Rev.* **2011,** *111,* 7157–7259. doi:10.1021/cr100307m
5. Rueping, M.; Antonchick, A. P.; Theissmann, T. *Angew. Chem., Int. Ed.* **2006,** *45,* 3683–3686. doi:10.1002/anie.200600191
6. Rueping, M.; Theissmann, T.; Raja, S.; Bats, J. W. *Adv. Synth. Catal.* **2008,** *350,* 1001–1006. doi:10.1002/adsc.200800020
7. Rueping, M.; Sugiono, E.; Steck, A.; Theissmann, T. *Adv. Synth. Catal.* **2010,** *352,* 281–287. doi:10.1002/adsc.200900746
8. Rueping, M.; Theissmann, T. *Chem. Sci.* **2010,** *1,* 473–476. doi:10.1039/C0SC00206B
9. Rueping, M.; Stoeckel, M.; Sugiono, E.; Theissmann, T. *Tetrahedron* **2010,** *66,* 6565–6568. doi:10.1016/j.tet.2010.04.091
10. Rueping, M.; Theissmann, T.; Stoeckel, M.; Antonchick, A. P. *Org. Biomol. Chem.* **2011,** *9,* 6844–6850. doi:10.1039/c1ob05870c
11. Rueping, M.; Bootwicha, T.; Sugiono, E. *Beilstein J. Org. Chem.* **2012,** *8,* 300–307. doi:10.3762/bjoc.8.32
12. Guo, Q.-S.; Du, D.-M.; Xu, J. *Angew. Chem., Int. Ed.* **2008,** *47,* 759–762. doi:10.1002/anie.200703925
13. Han, Z.-Y.; Xiao, H.; Chen, X.-H.; Gong, L.-Z. *J. Am. Chem. Soc.* **2009,** *131,* 9182–9183. doi:10.1021/ja903547q
14. Ren, L.; Lei, T.; Ye, J.-X.; Gong, L.-Z. *Angew. Chem., Int. Ed.* **2012,** *51,* 771–774. doi:10.1002/anie.201106808
15. Tu, X.-F.; Gong, L.-Z. *Angew. Chem., Int. Ed.* **2012,** *51,* 11346–11349. doi:10.1002/anie.201204179
16. Patil, N. T.; Raut, V. S.; Tella, R. B. *Chem. Commun.* **2013,** *49,* 570–572. doi:10.1039/c2cc37623g
17. Wang, D.-S.; Chen, Q.-A.; Lu, S.-M.; Zhou, Y.-G. *Chem. Rev.* **2012,** *112,* 2557–2590. doi:10.1021/cr200328h
18. Ehrfeld, W.; Hessel, V.; Löwe, H. *Microreactors: New Technology for Modern Chemistry;* Wiley-VCH: Weinheim, Germany, 2000. doi:10.1002/3527601953
19. Wirth, T., Ed. *Microreactors in Organic Synthesis and Catalysis;* Wiley-VCH: Weinheim, Germany, 2008. doi:10.1002/9783527622856
20. Yoshida, J.-i. *Flash Chemistry – Fast Organic Synthesis in Microsystems;* Wiley-VCH: Weinheim, Germany, 2008.
21. Hessel, V.; Schouten, J. C.; Renken, A.; Wang, Y.; Yoshida, J.-i., Eds. *Handbook of Micro Reactors;* Wiley-VCH: Weinheim, Germany, 2009.
22. Luis, S. V.; Garcia-Verdugo, E., Eds. *Chemical Reactions and Processes under Flow Conditions;* Royal Society of Chemistry: Cambridge, U.K., 2010.
23. Matsushita, Y.; Ichimura, T.; Ohba, N.; Kumada, S.; Sakeda, K.; Suzuki, T.; Tanibata, H.; Murata, T. *Pure Appl. Chem.* **2007,** *79,* 1959–1968. doi:10.1351/pac200779111959
24. Coyle, E. E.; Oelgemöller, M. *Photochem. Photobiol. Sci.* **2008,** *7,* 1313–1322. doi:10.1039/b808778d
25. Oelgemöller, M.; Shvydkiv, O. *Molecules* **2011,** *16,* 7522–7550. doi:10.3390/molecules16097522
26. Aida, S.; Terao, K.; Nishiyama, Y.; Kakiuchi, K.; Oelgemöller, M. *Tetrahedron Lett.* **2012,** *53,* 5578–5581. doi:10.1016/j.tetlet.2012.07.143
27. Oelgemoeller, M. *Chem. Eng. Technol.* **2012,** *35,* 1144–1152. doi:10.1002/ceat.201200009
28. Knowles, J. P.; Elliott, L. D.; Booker-Milburn, K. I. *Beilstein J. Org. Chem.* **2012,** *8,* 2025–2052. doi:10.3762/bjoc.8.229
29. Oelgemöller, M.; Shvydkiv, O. Microphotochemistry: Photochemical Synthesis in Microstructured Flow Reactors. *CRC Handbook of Organic Photochemistry and Photobiology;* CRC Press, 2012; pp 125–178.
30. Neumann, M.; Zeitler, K. *Org. Lett.* **2012,** *14,* 2658–2661. doi:10.1021/ol3005529
31. Sakeda, K.; Wakabayashi, K.; Matsushita, Y.; Ichimura, T.; Suzuki, T.; Wada, T.; Inoue, Y. *J. Photochem. Photobiol., A* **2007,** *192,* 166–171. doi:10.1016/j.jphotochem.2007.05.019
32. You, S.-L. *Chem.–Asian J.* **2007,** *2,* 820–827. doi:10.1002/asia.200700081
33. Rueping, M.; Sugiono, E.; Schoepke, F. R. *Synlett* **2010,** 852–865. doi:10.1055/s-0029-1219528
34. Rueping, M.; Dufour, J.; Schoepke, F. R. *Green Chem.* **2011,** *13,* 1084–1105. doi:10.1039/c1gc15027h
35. Zheng, C.; You, S.-L. *Chem. Soc. Rev.* **2012,** *41,* 2498–2518. doi:10.1039/c1cs15268h

36. Richter, D.; Mayr, H. *Angew. Chem., Int. Ed.* **2009,** *48,* 1958–1961. doi:10.1002/anie.200804263
37. Zhu, X.-Q.; Liu, Y.-C.; Cheng, J.-P. *J. Org. Chem.* **1999,** *64,* 8980–8981. doi:10.1021/jo9905571
38. Liao, H.-H.; Hsiao, C.-C.; Sugiono, E.; Rueping, M. *Chem. Commun.* **2013,** *49,* 7953–7955. doi:10.1039/c3cc43996h
39. The glass microreactors (Type: LTF-V and LTF-VS) were purchased from Little Things Factory (http://www.LTF-GmbH.de). All glasswares used for this study are borosilica glass.
40. Ohnishi, Y.; Kagami, M.; Ohno, A. *Chem. Lett.* **1975,** *4,* 125–128. doi:10.1246/cl.1975.125
41. Inoue, Y.; Imaizumi, S.; Itoh, H.; Shinya, T.; Hashimoto, H.; Miyano, S. *Bull. Chem. Soc. Jpn.* **1988,** *61,* 3020–3022. doi:10.1246/bcsj.61.3020

Beilstein Journal of Organic Chemistry

Investigating the continuous synthesis of a nicotinonitrile precursor to nevirapine

Ashley R. Longstreet[1], Suzanne M. Opalka[1], Brian S. Campbell[1], B. Frank Gupton[2] and D. Tyler McQuade[*1]

Full Research Paper

Open Access

Address:
[1]Department of Chemistry and Biochemistry, Florida State University, 95 Chieftan Way, Tallahassee, FL 32306, United States and [2]Department of Chemistry, Virginia Commonwealth University, 1001 West Main Street, P.O. Box 842006 Richmond, Virginia 23284, United States

Email:
D. Tyler McQuade[*] - mcquade@chem.fsu.edu

* Corresponding author

Keywords:
continuous; flow chemistry; HIV; Knoevenagel; nevirapine; nicotinonitriles

Beilstein J. Org. Chem. **2013,** *9,* 2570–2578.
doi:10.3762/bjoc.9.292

Received: 14 July 2013
Accepted: 14 October 2013
Published: 20 November 2013

This article is part of the Thematic Series "Chemistry in flow systems III".

Guest Editor: A. Kirschning

Abstract

2-Chloro-3-amino-4-picoline (CAPIC) is a strategic building block for the preparation of nevirapine, a widely-prescribed non-nucleosidic reverse transcriptase inhibitor for the treatment of HIV-infected patients. A continuous synthesis to the bromo derivative of a CAPIC intermediate, 2-bromo-4-methylnicotinonitrile, that terminates in a dead-end crystallization is described. The route uses inexpensive, acyclic commodity-based raw materials and has the potential to enable lower cost production of nevirapine as well as other value added structures that contain complex pyridines. The route terminates in a batch crystallization yielding high purity CAPIC. This outcome is expected to facilitate regulatory implementation of the overall process.

Introduction

Nevirapine (**3**) was the first commercially available non-nucleoside reverse transcriptase inhibitor (NNRTI), and has remained an important medicine in the management of human immunodeficiency virus (HIV) [1,2]. Nevirapine combined with lamivudine (3TC) and azidothymidine (AZT) or tenofovir (TDF) is one of the preferred first-line combination drug therapies recommended by the World Health Organization (WHO) [3-5]. WHO initiatives are expected to increase the demand for nevirapine over the next 10 years (Figure 1) [6]. Although several viable NNRT substitutes for nevirapine are available, nevirapine manufacturing requirements will remain high because clinicians are reluctant to change treatment once a successful combination therapy is identified and many remain healthy with the nevirapine based combinations. Furthermore, the recent development of an extended release dosage form of nevirapine that enables once a day administration is expected to further increase market demand [6-8]. The high demand coupled with the financial burden associated with long-term HIV treatments

has resulted in shortages and patients opting to reduce dosing which increases development of resistant strains [9-12]. This confluence of increased demand and cost provides an opportunity to reevaluate both the chemistry as well as the manufacturing platforms by which this drug can be produced.

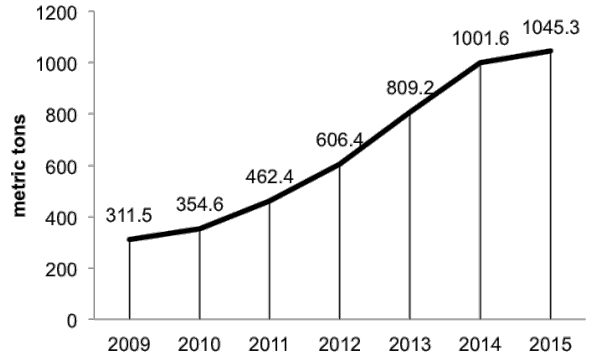

Figure 1: The estimated demand of for nevirapine until 2015 [6].

The two key Food and Drug Administration (FDA) registered starting materials in the commercial nevirapine process are 2-chloro-3-amino-4-picoline (CAPIC) (**1a**) and 2-cyclopropylaminonicotinic acid (2-CAN) (**2**) (Scheme 1) [13]. The CAPIC process comprises approximately 64% of the total production cost. Based on our previous experience with the development of the current commercial batch processes for nevirapine [13] and its pyridine precursors [14], we have started a program to define lower costs nevirapine processes. After a cost of goods analysis, we have come to the conclusion that the most promising cost saving path forward is through the use of acyclic, commodity-based starting materials in the assembly of the active pharmaceutical ingredient (API) (analysis will be included on future publications). We hypothesized that by both reducing the cost of goods via chemistry changes and reducing the unit operations the most significant cost reduction could be achieved. Herein, we demonstrate a proof of concept flow synthesis of the key intermediate used to produce the bromo derivative of the CAPIC precursor, 2-bromo-4-methylnicotinonitrile (**6b**). The

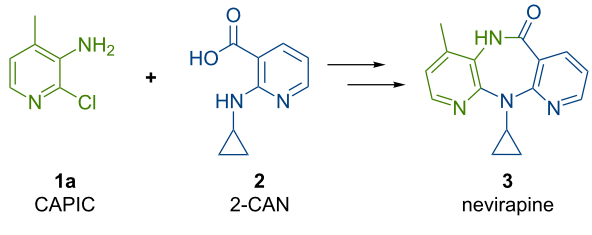

Scheme 1: Commercial building blocks to nevirapine.

synthesis telescopes three steps using substantially less expensive starting materials.

Flow or continuous chemistry is alternative to batch chemistry where reactions are performed by passing reagents through devices containing small-dimensional channels as opposed to using batch reactors [15-17]. Flow reactors are particularly advantageous in multistep syntheses where telescoping steps avoids isolation of dangerous and/or unstable intermediates and reduces solvent usage and waste production incurred through intermediate purifications [18-27]. The large surface to volume ratios found in the small channels allow for more efficient mixing and heat transfer often resulting in shorter contact times [28,29]. Consequently, flow chemistry allows chemists to expand their window of process operability by working at elevated temperatures and pressures to increase reaction rates and decrease catalyst loadings [30-33]. Unlike scaling-up batch reactions, which requires additional optimization, scaling-up flow processes only requires implementing multiple reactors to work in parallel [29].

We have recently developed a method to synthesize polysubstituted 2-halonicotinonitriles in high yields via enamine intermediates **5** by reacting alkylidene malononitriles in the presence of acetic anhydride with *N*,*N*-dimethylformamide dimethyl acetal (DMF-DMA) [34]. Previous attempts to synthesize the nicotinonitriles via enamines resulted in poor yields due to dimerization of the starting alkylidene malononitrile [35-37]. A high yield enamine approach allows us to begin the synthesis from the commodity chemicals (acetone and malononitrile) and bypass the pyridone intermediate used in the original CAPIC synthesis (Scheme 2a) by effecting the ring closure under Pinner reaction conditions (Scheme 2b) [14].

We set out to investigate the possibility of performing a continuous synthesis of 2-bromo-4-methylnicotinonitrile starting from acetone and malononitrile (Scheme 3) using the Vapourtec R series reactor system [38]. The batch synthesis commences with a Knoevenagel reaction condensing malononitrile and acetone catalyzed by aluminum oxide producing isopropylidenemalononitrile (**4**) [39,40]. The penultimate enamine **5** results by treating **4** with DMF-DMA in the presence of acetic anhydride, and ultimately 2-bromo-4-methylnicotinonitrile (**6b**) is produced after **5** is treated with HBr in acetic acid. Transferring the batch synthesis into a semi-continuous process requires one to consider solvent exchanges and byproducts that might complicate downstream operations.

We immediately recognized the water formed in the Knoevenagel condensation would quench the DMF-DMA in the second step. In addition, our batch Knoevenagel condensation was base

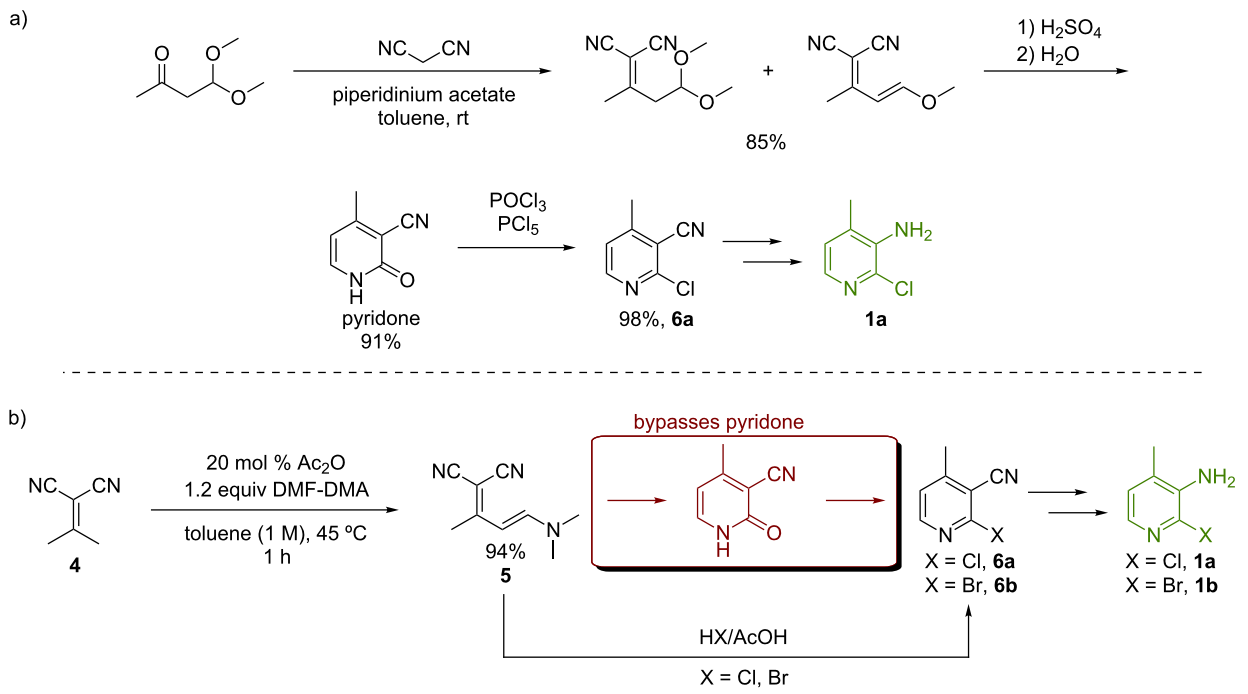

Scheme 2: a) Current commercial process to CAPIC and b) newly developed batch synthesis to CAPIC and its bromo derivative.

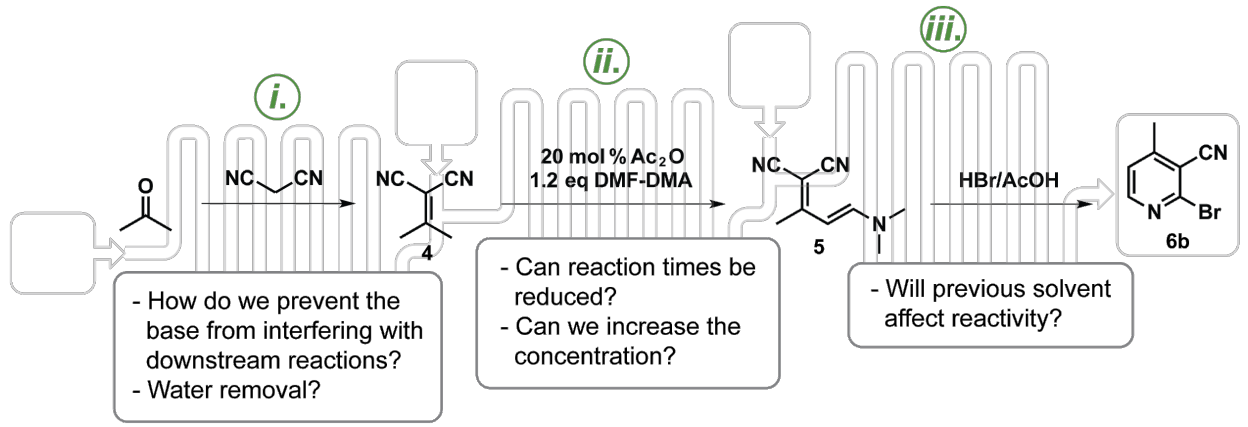

Scheme 3: Proposed synthesis to 2-bromo-4-methylnicotinonitrile using a continuous approach with the considerations for each reaction. i. Knoevenagel condensation to produce the isopropylidenemalononitrile (**4**). ii. Reaction of the isopropylidenemalononitrile with DMF-DMA to produce an enamine (**5**). iii. Dead end cyclization to the desired 2-bromo-4-methylnicotinonitrile (**6b**) using HBr.

catalyzed and we discovered that base increased dimer byproducts in the enamine step. Therefore, we chose to employ a solid basic reagent that would simultaneously catalyze the Knoevenagel reaction and confine the reagent to the first step, as well as a solid desiccant to remove the water. Previously we have used solid catalysts and/or solid reagents in a number of continuous processes [41-44]. Another challenge was the need to increase the rate of enamine **5** formation. Under some conditions, the enamine step required up to 24 hours [34]. Factoring these and other considerations, we designed the process shown in Scheme 3 with a summary of considerations for each step.

Results and Discussion

We began our investigation by optimizing the enamine formation (**5**, Figure 2) because we predicted that success with this central step would help define the flanking reactions. Initial batch studies revealed that the reaction occurred rapidly (1 h) in toluene (1.0 M) heated to 45 °C to produce **4** in 94% yield [34],

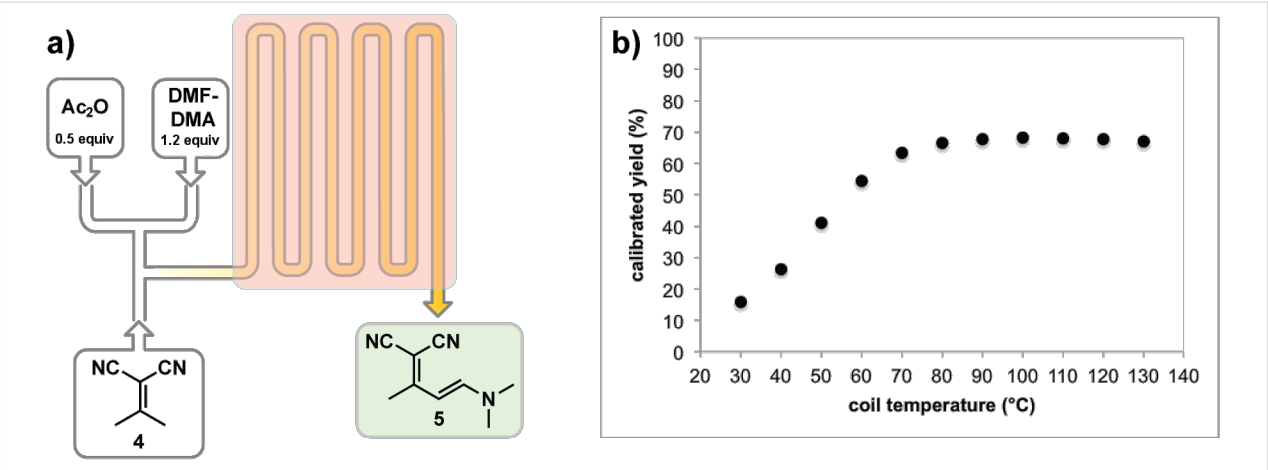

Figure 2: a) Flow scheme to produce the enamine intermediate **5** from isopropylidenemalononitrile (**4**) (see Supporting Information File 1 for details). b) Coil temperature effect on yield at a 0.10 M reaction concentration with a 2 min residence time.

but the product precipitated and these conditions were rejected to avoid reactor clogging. Based on literature precedent and our own screening, we discovered that DCM solubilized **4**, **5**, and **6b** (Scheme 3). In batch, use of DCM would require non-traditional glassware because temperatures exceeding the standard boiling point at atmospheric pressure were required to avoid unwanted dimer formation unless low reaction concentrations (0.10 M) were used. A flow reactor is ideal for performing reactions well outside of normal operating conditions and we pushed forward seeking high temperature conditions using DCM [45].

When screening conditions, we initially investigated the effect temperature had on the reaction at a 0.10 M concentration (Figure 2b). Placing backpressure regulators after the heated coil allowed the temperature of the reactor coil to be raised far above the boiling point of DCM. As shown in Figure 2b, increasing the temperature to 80 °C provided 67% yield with a 2 min residence time. We then examined reaction concentrations to reduce the volume of DCM (Table 1). We were not only able to increase the concentration to 1.0 M by heating to 95 °C, but were also able to increase yields to >93% with a 2 min residence time. In comparison, our batch method with similar concentration conditions in toluene was complete in 1 h with 94% yield [34]. These flow conditions were high yielding in one thirtieth of the reaction time. This example underscores the benefit of operating outside of normal process windows [45]. Attempts to increase the reaction concentration beyond 1.0 M led to reactor clogging due to the limited of solubility of **5**.

We proceeded to develop a continuous process by coupling the enamine step with the Knoevenagel condensation (Scheme 4). To achieve this, we included two columns: a packed-bed of Al_2O_3 to catalyze the reaction and a packed bed of 3 Å molecular sieves to absorb water before the addition of DMF-DMA (Scheme 4). The mass of each solid used (2.00 g of Al_2O_3 and 1.50 g molecular sieves) was chosen based on the size of the available columns. Assuming that the Knoevenagel condensation occurred primarily in the Al_2O_3 column, we only varied the temperature of the Al_2O_3 column. The Al_2O_3 column temperature was initially set to 25 °C which yielded 91% of **5** from acetone and malononitrile (Table 2, entry 2). We observed that the Al_2O_3 column reactor temperature increased during the

Table 1: Concentration screen for enamine formation.

Entry	Reaction concentration (M)	Residence time (min)	Coil temperature (°C)	Yield (%)[a]
1	0.10	2	100	68
2	0.20	2	95	93
3	0.40	2	95	96
4	0.60	2	95	98
5	0.80	2	95	97
6	0.98	2	95	97

[a]Determined by GC analysis using mesitylene as an internal standard. See Figure 2a for flow scheme.

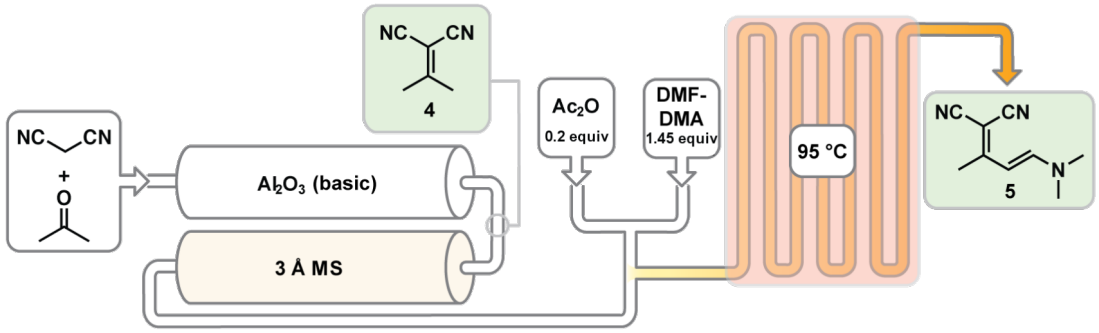

Scheme 4: Flow scheme to produce the enamine **5** starting from acetone and malononitrile (See Supporting Information File 1 for details).

Table 2: Screened conditions for formation of **5** starting from acetone and malononitrile.

Entry	Al_2O_3 column temperature (°C)	3 Å MS column temperature (°C)	Residence time of coil (min)[a]	Yield (%)[b]
1	25	20	2	NA[c]
2	25	20	4	91
3	20	25	4	91
4	10	25	4	92
5	35	20	4	88
6	50	20	4	88
7	75	20	4	84
8	95	20	4	81
9	95	20	6	81

[a]Coil temperature was 95 °C. [b]Determined by GC analysis using mesitylene as an internal standard. [c]The fast flow rates needed for this residence time caused the pressure of the system to exceed the maximum limit. See Scheme 4 for flow scheme.

reaction and thus examined the use of temperatures below 25 °C. Cooling the column did not provide any observable improvement (Table 2, entries 3 and 4) prompting us to examine higher temperatures. Heating the column past 25 °C increased the byproduct formation which lowered the yield (Table 2, entries 5–8). Increasing the residence time through the alumina column had no positive impact on yield (Table 2, entry 9).

The successful combination of the Knoevenagel/enamine steps prompted us to evaluate the stability of this two-step system. We often find that when multisteps are combined the system stability can become an issue. To measure the stability, we ran the reaction under the optimized conditions and monitored the product distribution. When the aforementioned optimized column temperatures were used (20 °C Al_2O_3 column, 25 °C 3 Å MS column), the alumina column begins to fail (Figure 3). At a collection time of 12 min (Table 2, entry 3), the yield is at its maximum at 91%. However, by ~17 min, the yield drops to 48%. We speculate that at high reactant concentrations the water produced fouls the Al_2O_3 column. This conjecture is supported by the increased production of **7** when excess malononitrile reacts with DMF-DMA (Scheme 5). Heating the column to 95 °C allowed the Al_2O_3 column to remain activated longer. Despite the fact that higher alumina column temperatures result in less than optimal yields of the enamine, we examined the system stability at 95 °C. As can be seen in Figure 3, increasing the alumina column temperature provides improved stability compared to 25 °C; however, the column performance exhibits shallow decline over the first 37 min and then fails rapidly beyond 37 min. The fact that we can resurrect the column performance somewhat suggests that this stability issue can be addressed when and if this process is implemented on scale. To demonstrate that further gains in stability are possible, we examined the impact of reaction concentration on column stability.

Process chemists often seek the highest operating concentrations to reduce solvent costs. Recognizing this aspiration, we performed the aforementioned Knoevenagel reaction at 2.0 M. Considering that many process reactions run at 0.20 M, this starting concentration was high. The high starting concentra-

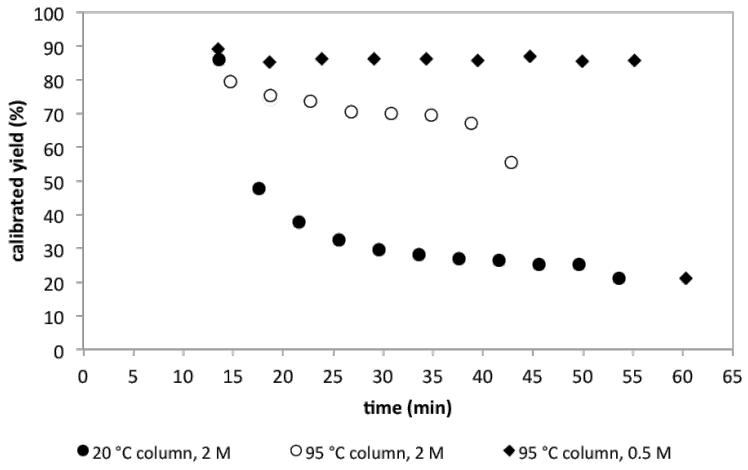

Figure 3: Comparing the long-term stability of the Al_2O_3 and 3 Å MS columns when the Al_2O_3 column temperature (20 °C and 95 °C) and Knoevenagel reaction concentration (2.0 M and 0.50 M) are varied. The time between 0 and 13 min was the equilibration period.

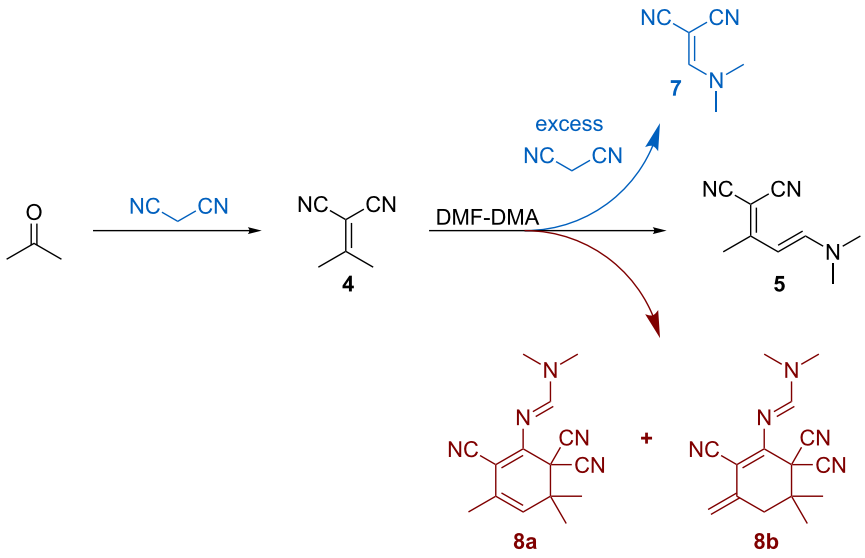

Scheme 5: Several byproducts were observed when producing **5** starting from acetone and malononitrile. **7** is formed from excess malononitrile when the Knoevenagel reaction does not go to completion. The formation of dimers **8a** and **8b** can begin at any point during the reaction.

tion also allowed us to realize a 1.0 M reaction concentration once addition of the acetic anhydride and DMF-DMA (Scheme 4). While the higher the concentration the better, our prior efforts have revealed that packed-bed catalyst stability can rapidly decline at high concentrations while at lower concentrations can run for an extended length of time [44]. With this in mind, we lowered the Knoevenagel concentration to 0.50 M. This setup also resulted in the residence time in the Al_2O_3 column and 3 Å MS to reduce from 2.88 min and 2.72 min to 0.90 min and 0.85 min respectively. The faster residence time could account for less water absorption in the Al_2O_3 column. Because we can still hold the acetic anhydride/DMF-DMA concentrations high lowering the Knoevenagel concentration only results in the enamine concentration decreasing by factor of 1.25 (0.40 M). As shown in Figure 3, reducing the Knoevenagel to 0.50 M and heating the alumina column to 95 °C results in a dramatic improvement in system stability. The output of the enamine, however, remains similar. The reaction at a 1 M concentration would produce approximately 7 g of enamine product within the 24 min window and at a 0.4 M concentration approximately 5.8 g in the 42 min window. While we are bolstered by these improvements, we suggest that a commercial version of this process must address how to achieve long-term stability at the higher concentrations.

Creating a chemical process for an active pharmaceutical ingredient is a careful integration of chemical and regulatory challenges. While from an academic standpoint a completely continuous process provides the opportunity to advance process chemistry/technology, a new process can often require significant investment for regulatory validation. We wish to implement our technology as quickly as feasible and to do so we want to avoid potential regulatory problems. Therefore, we have opted to carry out the Pinner cyclization as terminal cyclization/crystallization step where the already validated material could be collected. To optimize the cyclization step, we combined only the enamine/cyclization steps to reduce system complexity. When we subjected 25 mL of the enamine **5** output to a solution of HBr in AcOH for 45 min (55 °C) the desired nicotinonitrile **6b** crystallized out of solution in 81% overall yield (2-steps, Scheme 6). While our intent was not to create a completely continuous process at this time, commercially available reactors that can handle strong acid are available and this step could easily be achieved in flow (for an example of an strong acid resistant reactor, see reference [38]).

We completed the process by integrating all three steps together using the lower concentration Knoevenagel condensation (0.50 M) with the heated Al_2O_3 column at 95 °C due to its long-term stability (Scheme 7). We ran 100 mL of material through the process and after simple trituration with water 69% (5.4 g for 100 mL) of the desired 2-bromo-4-methylnicotinonitrile (**6b**) was obtained and was analytically pure as determined by

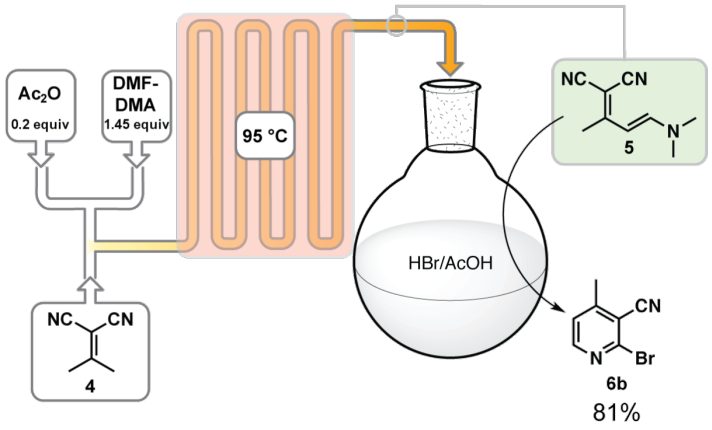

Scheme 6: Flow scheme to produce 2-bromo-4-methylnicotinonitrile (**6b**) in 81% yield from **4** with a 1 M concentration and 2 min residence time in the coil (See Supporting Information File 1 for further details).

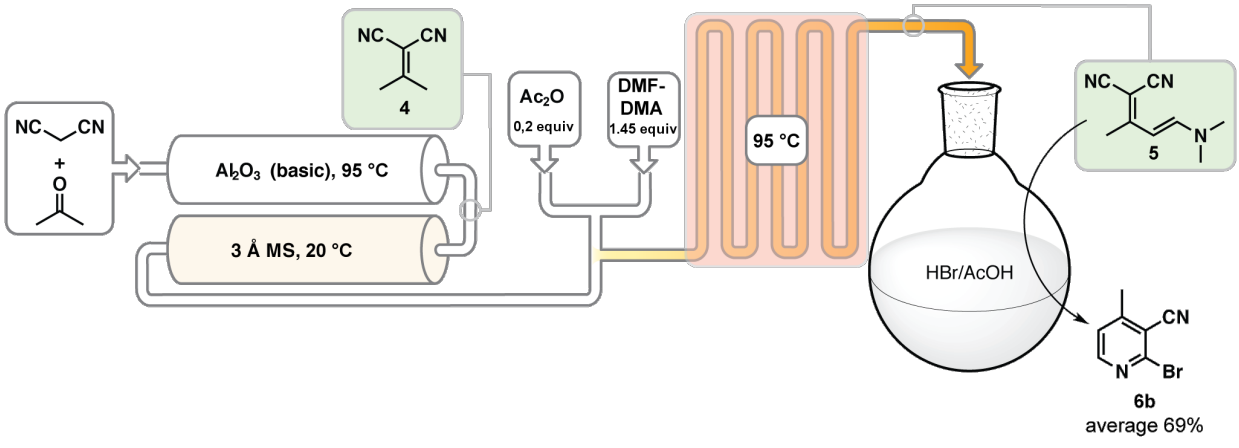

Scheme 7: Reactor scheme for the continuous synthesis of 2-bromo-4-methylnicotinonitrile (**6b**) with an average of 69% yield. The reaction concentration within the columns was 0.50 M, while the reaction concentration in the coil was 0.40 M. The residence time in the Al_2O_3 column was 0.90 min, in the 3 Å MS column 0.85 min, in the coil 4 min, and the reaction time for the cyclization to occur to produce **6b** was 45 min (See Supporting Information File 1 for further details).

elemental analysis. We have also performed the enamine cyclization using HCl instead of HBr and have produced the registered chloride in 81% yield [34].

Conclusion

Here, we have demonstrated the semi-continuous synthesis of 2-bromo-4-methylnicotinonitrile starting from acetone and malononitrile by utilizing solid Al_2O_3 and 3 Å MS columns and decreasing the reaction time of the enamine formation to a matter of minutes using DCM conditions outside of normal process windows. The cyclization under Pinner conditions using the crude output from the Knoevenagel/enamine steps provides an overall yield of 69% (>88% yield per step). While the Al_2O_3 column is stable for a limited time (between 24 and 42 min depending on the reaction concentration used), the current solution would be to simply replace the columns throughout the production process or implement larger columns. At the current state, the amount of Al_2O_3 and molecular sieves needed for every one gram of 2-bromo-4-methylnicotinonitrile is 0.37 g and 0.28 g respectively. Despite the limited stability, the amount of Al_2O_3 used in flow to produce 5.4 g of 2-bromo-4-methylnicotinonitrile is less than the amount of Al_2O_3 required for the batch process (about 0.98 g is needed per 1 g of product [34]). We also predict that by replacing the alumina columns with a soluble base and a water/base separation a stable, higher concentration process can be easily achieved from our preliminary results [22,46]. Finally, we have demonstrated that from a simple acyclic precursor, 2-bromo-4-methylnicotinonitrile can be achieved in a three-unit operation process yielding high purity crystalline materials. The chloride product is already registered and suggests that this strategy could be implemented in existing nevirapine processes.

Supporting Information

The Supporting Information describes synthesis and characterization data of all substances given in this article, reactor setup, operational details and screening conditions.

Supporting Information File 1

Experimantal section.
[http://www.beilstein-journals.org/bjoc/content/supplementary/1860-5397-9-292-S1.pdf]

Acknowledgements

The authors thank the Clinton Health Access Initiative and Corning Glass, Inc. for support. DTM and ARL, in addition, thank the NSF (CHE – 1152020), FSU and Vapourtec, Ltd. for support.

References

1. De Clercq, E. *J. Clin. Virol.* **2004,** *30,* 115–133. doi:10.1016/j.jcv.2004.02.009
2. De Clercq, E. *Antiviral Res.* **1998,** *38,* 153–179. doi:10.1016/S0166-3542(98)00025-4
3. World Health Organization. Antiretroviral therapy for HIV infection in adults and adolescents: Recommendations for a public health approach. 2010 revision. http://www.who.int/hiv/pub/arv/adult2010/en/index.html (accessed Oct 31, 2012).
4. Doherty, T.; Sanders, D.; Goga, A.; Jackson, D. Implications of the new WHO guidelines on HIV and infant feeding for child survival in South Africa. http://www.who.int/bulletin/volumes/89/1/10-079798/en/index.html (accessed Oct 31, 2012).
5. van Leth, F.; Phanuphak, P.; Ruxrungtham, K.; Baraldi, E.; Miller, S.; Gazzard, B.; Cahn, P.; Lalloo, U. G.; van der Westhuizen, I. P.; Malan, D. R.; Johnson, M. A.; Santos, B. R.; Mulcahy, F.; Wood, R.; Levi, G. C.; Reboredo, G.; Squires, K.; Cassetti, I.; Petit, D.; Raffi, F.; Katlama, C.; Murphy, R. L.; Horban, A.; Dam, J. P.; Hassink, E.; van Leeuwen, R.; Robinson, P.; Wit, F. W.; Lange, J. M. A. *Lancet* **2004,** *363,* 1253–1263. doi:10.1016/S0140-6736(04)15997-7
6. Proceedings of "Joint WHO/UNAIDS annual consultation with pharmaceutical companies: Global forecasts of antiretroviral demand 2012-2015". November 5-6, 2012, Geneva, Switzerland. http://www.who.int/hiv/amds/forecasting_meeting2012/en/ (accessed June 6, 2013).
7. Renaud-Théry, F.; Avila-Figueroa, C.; Stover, J.; Thierry, S.; Vitoria, M.; Habiyambere, V.; Souteyrand, Y. *AIDS Res. Treat.* **2011,** No. 749041. doi:10.1155/2011/749041
8. Arribas, J. R.; Eron, J. *Curr. Opin. HIV AIDS* **2013,** *8,* 341–349.
9. Pasquet, A.; Messou, E.; Gabillard, D.; Minga, A.; Depoulosky, A.; Deuffic-Burban, S.; Losina, E.; Freedberg, K. A.; Danel, C.; Anglaret, X.; Yazdanpanah, Y. *PLoS One* **2010,** *5,* e13414. doi:10.1371/journal.pone.0013414
10. Paredes, R.; Marconi, V. C.; Lockman, S.; Abrams, E. J.; Kuhn, L. *J. Infect. Dis.* **2013,** *207* (Suppl. 2), S93–S100. doi:10.1093/infdis/jit110
11. WHO Progress Report 2011: Global HIV/AIDS Response. http://www.who.int/hiv/pub/progress_report2011/en/index.html (accessed June 19, 2013).
12. Hirsch, M. S.; Günthard, H. F.; Schapiro, J. M.; Vézinet, F. B.; Clotet, B.; Hammer, S. M.; Johnson, V. A.; Kuritzkes, D. R.; Mellors, J. W.; Pillay, D.; Yeni, P. G.; Jacobsen, D. M.; Richman, D. D. *Clin. Infect. Dis.* **2008,** *47,* 266–285. doi:10.1086/589297
13. Boswell, R. F.; Gupton, B. F.; Lo, Y. S. Method for Making Nevirapine. U.S. Patent 6,680,383, Jan 20, 2004.
14. Gupton, B. F. Process for making 3-amino-2-chloro-4-methylpyridine. U.S. Patent 6,399,781, June 4, 2002.
15. Wegner, J.; Ceylan, S.; Kirschning, A. *Chem. Commun.* **2011,** *47,* 4583–4592. doi:10.1039/C0CC05060A
16. Wiles, C.; Watts, P. *Chem. Commun.* **2011,** *47,* 6512–6535. doi:10.1039/C1CC00089F
17. Yoshida, J.-I. *Chem. Rec.* **2010,** *10,* 332–341. doi:10.1002/tcr.201000020
18. Bogdan, A. R.; Poe, S. L.; Kubis, D. C.; Broadwater, S. J.; McQuade, D. T. *Angew. Chem., Int. Ed.* **2009,** *48,* 8547–8550. doi:10.1002/anie.200903055
19. Lévesque, F.; Seeberger, P. H. *Angew. Chem., Int. Ed.* **2012,** *51,* 1706–1709. doi:10.1002/anie.201107446

20. Booker-Milburn, K. *Nat. Chem.* **2012,** *4,* 433–435. doi:10.1038/nchem.1356
21. Smith, C. J.; Smith, C. D.; Nikbin, N.; Ley, S. V.; Baxendale, I. R. *Org. Biomol. Chem.* **2011,** *9,* 1927–1937. doi:10.1039/c0ob00813c
22. Sahoo, H. R.; Kralj, J. G.; Jensen, K. F. *Angew. Chem., Int. Ed.* **2007,** *46,* 5704–5708. doi:10.1002/anie.200701434
23. Baxendale, I. R. *J. Chem. Technol. Biotechnol.* **2013,** *88,* 519–552. doi:10.1002/jctb.4012
24. Hopkin, M. D.; Baxendale, I. R.; Ley, S. V. *Org. Biomol. Chem.* **2013,** *11,* 1822–1839. doi:10.1039/c2ob27002a
25. Polyzos, A.; O'Brien, M.; Petersen, T. P.; Baxendale, I. R.; Ley, S. V. *Angew. Chem., Int. Ed.* **2011,** *50,* 1190–1193. doi:10.1002/anie.201006618
26. Baxendale, I. R.; Ley, S. V.; Mansfield, A. C.; Smith, C. D. *Angew. Chem., Int. Ed.* **2009,** *48,* 4017–4021. doi:10.1002/anie.200900970
27. Kupracz, L.; Hartwig, J.; Wegner, J.; Ceylan, S.; Kirschning, A. *Beilstein J. Org. Chem.* **2011,** *7,* 1441–1448. doi:10.3762/bjoc.7.168
28. Hartman, R. L.; McMullen, J. P.; Jensen, K. F. *Angew. Chem., Int. Ed.* **2011,** *50,* 7502–7519. doi:10.1002/anie.201004637
29. Mason, B. P.; Price, K. E.; Steinbacher, J. L.; Bogdan, A. R.; McQuade, D. T. *Chem. Rev.* **2007,** *107,* 2300–2318. doi:10.1021/cr050944c
30. Hessel, V. *Chem. Eng. Technol.* **2009,** *32,* 1655–1681. doi:10.1002/ceat.200900474
31. Pieber, B.; Cantillo, D.; Kappe, C. O. *Chem.–Eur. J.* **2012,** *18,* 5047–5055. doi:10.1002/chem.201103748
32. Reichart, B.; Tekautz, G.; Kappe, C. O. *Org. Process Res. Dev.* **2013,** *17,* 152–157. doi:10.1021/op300273u
33. Reichart, B.; Kappe, C. O. *Tetrahedron Lett.* **2012,** *53,* 952–955. doi:10.1016/j.tetlet.2011.12.043
34. Longstreet, A. R.; Campbell, B. S.; Gupton, B. F.; McQuade, D. T. *Org. Lett.* **2013,** *15,* 5298–5301. doi:10.1021/ol4025265
35. Baldwin, J. J.; Raab, A. W.; Ponticello, G. S. *J. Org. Chem.* **1978,** *43,* 2529–2535. doi:10.1021/jo00406a052
36. Cope, A. C.; Hoyle, K. E. *J. Am. Chem. Soc.* **1941,** *63,* 733–736. doi:10.1021/ja01848a025
37. Williams, J. K. *J. Org. Chem.* **1963,** *28,* 1054–1059. doi:10.1021/jo01039a045
38. Vapourtec Flow Chemistry Equipment, UK. http://www.vapourtec.co.uk (accessed June 21, 2013).
39. Texier-Boullet, F.; Foucaud, A. *Tetrahedron Lett.* **1982,** *23,* 4927–4928. doi:10.1016/S0040-4039(00)85749-4
40. Broman, S. L.; Petersen, A. U.; Tortzen, C. G.; Vibenholt, J.; Bond, A. D.; Nielsen, M. B. *Org. Lett.* **2012,** *14,* 318–321. doi:10.1021/ol2030586
41. Bogdan, A. R.; Mason, B. P.; Sylvester, K. T.; McQuade, D. T. *Angew. Chem., Int. Ed.* **2007,** *46,* 1698–1701. doi:10.1002/anie.200603854
42. Bogdan, A.; McQuade, D. T. *Beilstein J. Org. Chem.* **2009,** *5,* No. 17. doi:10.3762/bjoc.5.17
43. Opalka, S. M.; Longstreet, A. R.; McQuade, D. T. *Beilstein J. Org. Chem.* **2011,** *7,* 1671–1679. doi:10.3762/bjoc.7.197
44. Opalka, S. M.; Park, J. K.; Longstreet, A. R.; McQuade, D. T. *Org. Lett.* **2013,** *15,* 996–999. doi:10.1021/ol303442m
45. Razzaq, T.; Kappe, C. O. *Chem.–Asian J.* **2010,** *5,* 1274–1289. doi:10.1002/asia.201000010
46. Noël, T.; Kuhn, S.; Musacchio, A. J.; Jensen, K. F.; Buchwald, S. L. *Angew. Chem., Int. Ed.* **2011,** *50,* 5943–5946. doi:10.1002/anie.201101480

License and Terms

Beilstein Journal of Organic Chemistry

Continuous-flow Heck synthesis of 4-methoxybiphenyl and methyl 4-methoxycinnamate in supercritical carbon dioxide expanded solvent solutions

Phei Li Lau[1,2], Ray W. K. Allen[1] and Peter Styring[*1]

Full Research Paper

Open Access

Address:
[1]Department of Chemical & Biological Engineering, Sir Robert Hadfield Building, The University of Sheffield, Sheffield S7 2GA, United Kingdom and [2]Department of Chemical and Environmental Engineering, The University of Nottingham, Malaysia Campus, Jalan Broga, 43500 Semenyih, Selangor Darul Shsan, Malaysia

Email:
Peter Styring[*] - p.styring@sheffield.ac.uk

* Corresponding author

Keywords:
continuous flow; flow chemistry; Heck; palladium; supercritical carbon dioxide

Beilstein J. Org. Chem. **2013,** *9,* 2886–2897.
doi:10.3762/bjoc.9.325

Received: 22 August 2013
Accepted: 20 November 2013
Published: 17 December 2013

This article is part of the Thematic Series "Chemistry in flow systems III".

Guest Editor: A. Kirschning

Abstract

The palladium metal catalysed Heck reaction of 4-iodoanisole with styrene or methyl acrylate has been studied in a continuous plug flow reactor (PFR) using supercritical carbon dioxide ($scCO_2$) as the solvent, with THF and methanol as modifiers. The catalyst was 2% palladium on silica and the base was diisopropylethylamine due to its solubility in the reaction solvent. No phosphine co-catalysts were used so the work-up procedure was simplified and the green credentials of the reaction were enhanced. The reactions were studied as a function of temperature, pressure and flow rate and in the case of the reaction with styrene compared against a standard, stirred autoclave reaction. Conversion was determined and, in the case of the reaction with styrene, the isomeric product distribution was monitored by GC. In the case of the reaction with methyl acrylate the reactor was scaled from a 1.0 mm to 3.9 mm internal diameter and the conversion and turnover frequency determined. The results show that the Heck reaction can be effectively performed in $scCO_2$ under continuous flow conditions with a palladium metal, phosphine-free catalyst, but care must be taken when selecting the reaction temperature in order to ensure the appropriate isomer distribution is achieved. Higher reaction temperatures were found to enhance formation of the branched terminal alkene isomer as opposed to the linear *trans*-isomer.

Introduction

The use of cross-coupling reactions between organometallic reagents and organic halides as a straightforward method of carbon–carbon bond formation has gained much popularity over the past three decades. The development of these cross-coupling methods has undoubtedly revolutionalised the protocols for the construction of natural products, building blocks for supra-

molecular chemistry, self-assembly of organic materials and polymers, and lead compounds in medicinal chemistry from simpler entities [1]. These include the Suzuki, Kumada, and Heck reactions. Among these, the palladium-catalysed Heck reaction [2] is one of the most explored families of such reactions. In the Heck reactions, a vinylic hydrogen is replaced by a vinyl, aryl or benzyl group through reaction with a halide compound. This reaction has been recognised as an indispensably simple yet effective method for molecular structure elaboration. The Heck reaction is a useful component of the chemist's toolkit as it allows carbon chain extension, with the addition of an alkene motif, using catalytic C–C bond formation chemistry. Traditionally, Heck reactions have been performed using homogeneous palladium catalysts with added phosphines, either as free reagents, coordinated discrete ligands or built into the ligand system itself. In recent years there has been a drive to develop phosphine-free catalysts and systems to ease separation and reduce both cost and product contamination [3]. Further efforts have focused on the development of heterogeneous catalysts or immobilised homogeneous catalysts, particularly for use in continuous flow reactor systems [3-6].

The yield and selectivity of Heck reactions are profoundly influenced by a number of variables, such as the nature of the base, solvent, catalyst and operating conditions. The addition of base is necessary to neutralise the halide acid formed in the reaction, which would otherwise become detrimental to the reaction system. A wide array of bases, organic and inorganic, has been investigated. Among them, tertiary amines such as triethylamine (Et_3N), tributylamine (Bu_3N) and alkali salts like carbonates, acetates or phosphates play crucial roles [7]. Solubility of the base and its basicity in the appropriate solvents are criteria that need to be considered.

Traditionally, most Heck reactions are carried out in polar aprotic solvents, such as *N,N*-dimethylformamide (DMF), 1-methyl-2-pyrrolidone (NMP) and *N,N*-dimethylacetamide (DMA), though other organic solvents, such as toluene, hexane, methanol and ethanol have been utilised [6]. In addition, the reactions have been carried out in biphasic mode using a mixture of solvents, such as ethylene glycol and toluene [8]. The drive to carry out reactions in environmentally benign media also led to studies being carried out in "green" (environmentally friendly) solvents, such as aqueous media, some supercritical fluids (SCFs), ionic liquids and even "solventless" systems [9-12]. Pioneering work using SCFs as reaction media was carried out independently in the late 1990s [13,14] using a palladium complex with fluorinated phosphine ligands. Most of the published results utilising supercritical fluid media have been based on homogeneously-catalysed stirred reactions, using custom-built constant volume high pressure autoclaves. Naturally this triggers the question about the possibility of using continuous reactions, an issue which this paper addresses. For continuous flow systems the catalyst stability is important as it must be used over numerous runs without catalysts degradation, metal leaching or reduction in activity through impurity deposition [12,15]. Virtually all forms of palladium have been used as catalysts for the Heck reaction. A wide array of combinations depending on the components of the catalytic system is possible, for example the catalyst can present as nanoparticles, ligand-less, unsupported or supported among other forms [16].

Practically speaking, heterogeneous catalysts provide benefits such as ease of separation and recovery from the reaction mixture. In general, heterogeneous catalysts tend to be more robust and stable under harsh reaction conditions, such as elevated temperatures and can be easily stored over longer periods, which in turn provides the possibility of by-passing the use of expensive, sensitive ligands and inert atmospheres [17]. The catalysts can be reused and recycled either as they are or after some form of regeneration [17]. The types of heterogeneous catalyst can be further categorised by their support, with examples including polymers, dendrimers, mesoporous materials, zeolites, metal oxides, and carbon.

Reactions using palladium supported on mesoporous materials have been reported by numerous authors. Among them, Zhao et al. [18] studied the coupling of non-activated aryl iodides with different alkenes using Pd-MCM-41-NH_2. Other examples include Pd-FSM 16 (functionalised with pyridine-carboimine or quinoline-carboimine) [19], oxime carbapalladacycle anchored on several mesoporous materials [20], and a palladium bipiyridyl complex anchored on nanosized MCM-41 [21]. Furthermore, a myriad of zeolites have been applied in Heck reactions, with examples including: modernite, HY or beta [22,23], montmorillonite [24], layered double hydroxides (LDH) [25]. Heterogeneous catalysts also lend themselves particularly well to continuous processing. One such example is reported by Karbass et al. [26], who carried out continuous flow reaction using Pd(0) derived from [$Pd_3(OAc)_6$] supported on polymeric monoliths containing methylimidazole, an ionic-liquid (IL) moiety in near-critical ethanol. It is thought that the resins act as catalysts to release active palladium-species into solution. It also appeared that the IL-like unit was capable of capturing and stabilising the catalytically active soluble palladium species that are generated during the reaction. The reaction system eliminated the requirement of an inert atmosphere. Reactions between iodobenzene and methyl acrylate achieved 85% yield and 100% selectivity to *trans*-methyl cinnamate at 200 °C and 80 bar. The reaction system was then extended to acrylonitrile as the olefinic substituent, and achieved a yield of 66% and 70% *trans*-selectivity under similar conditions [26].

Other examples of carbon–carbon cross-coupling reactions utilising continuous flow systems were also reported. However, conventional organic solvents were required either during the reaction or for the extraction progress [3,4,26-31].

The majority of the examples of catalysts discussed employ phosphines as electron-donating ligands but this is undesirable as they are toxic, air-sensitive, and moisture-sensitive [32]. An excess amount of phosphine and palladium are normally required under the Heck reaction conditions as they are susceptible to decomposition. Unfortunately, an excess of phosphine reduces the reaction rate, while higher quantities of palladium result in potentially significant increased production costs [33]. Palladium on a magnesium–lanthanum mixed oxide support (Pd/MgLaO) was reported to be an efficient, thermally stable and highly active heterogeneous catalyst in the Heck reactions of styrene and halides, including iodides, chlorine substituents, and both activated and non-activated bromine [32]. It has been rationalised that the MgLaO support itself appears to act as a base, which in turn acted as an electron-donating group relative to Pd, thereby eliminating the requirement of the phosphine ligand. The catalyst can also aid the reaction without requiring an inert atmosphere.

In this paper we report the Heck reaction between 4-iodoanisole and either styrene or methyl acrylate in a continuous flow reactor. The solvent system used was a mixture of $scCO_2$ and THF/methanol which contained the alkene and the organic base, DIPEA. In order to reduce the complexity of the system, palladium metal supported on silica was used as catalyst and no phosphines were added. While this was likely to reduce the activity of the system over homogeneously catalysed reactions using complexes with elaborate ligand design, it would also make purification simpler.

Results and Discussion

Two reactions were studied using continuous flow chemistry as shown in Scheme 1. In both cases 4-iodoanisole was used as the aryl halide. The alkene used was either styrene to yield the stilbenes **1** or methyl acrylate to yield the cinnamate ester **2**. For each reaction there are three possible regioisomers. The thermodynamically favoured *trans*- (**t**) isomer is most common in standard organic solvents although under certain conditions the *cis*- (**c**) isomer can be formed under kinetic control. The third possibility is the *geminal* or branched (**b**) isomer which is usually formed where a cationic intermediate forms that facilitates migration of the σ-Pd–C bond from the terminal alkenic 1-position to the 2-position. In the majority of publications, the formation of the branched isomer is either not observed or not reported. Certainly for activated alkenes the branched isomer rarely forms [12], however we have reported previously that it can be observed in both homogeneous and heterogeneously catalysed reactions and also under conditions of continuous flow [5].

Synthesis stilbenes under stirred tank and continuous flow conditions

The synthesis of 4-methoxystilbene (**1**) was carried out under continuous flow conditions and also in a stirred autoclave reactor to compare the processes. In the autoclave reaction (Figure 1) a single composition was investigated corresponding to the concentrations in the continuous flow reaction set for a $scCO_2$/organic solution ratio of 5:1. The pressure of the autoclave was set as close to 200 bar as possible, however because no back pressure regulator was present this was achieved by setting the applied pressure at 167 bar then increasing the temperature to 145 °C to attain reaction temperature and a pressure close to 200 bar. Because the autoclave is a sealed system it was difficult to take samples on a regular basis. Therefore, the

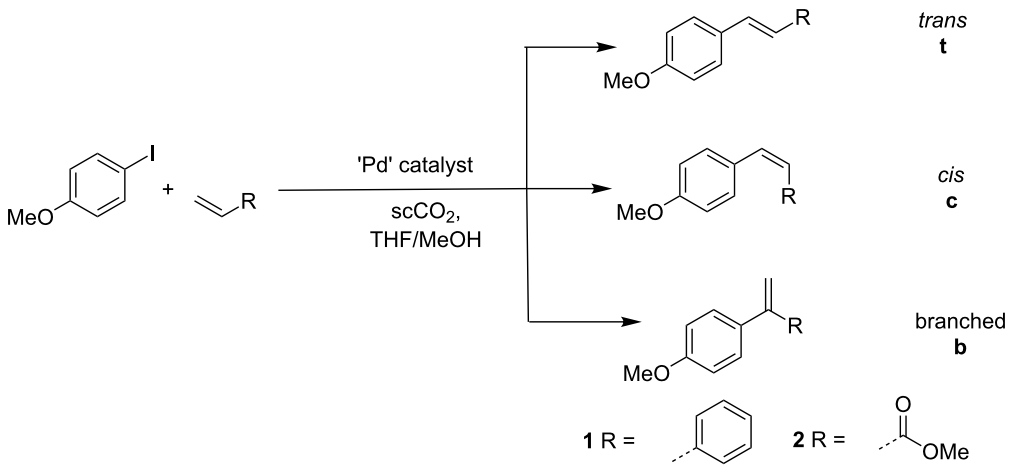

Scheme 1: General Heck reaction showing the possible isomers that can be produced.

reactor was run for 24 hours and the sample then analysed after de-pressurising the system. A total conversion of 94% was obtained (GC analysis relative to the limiting reagent 4-iodoanisole), with 77% conversion to the **t** isomer and 17% to the **b** isomer. No **c** isomer was detected. This gave a **t**/**g** ratio of 4.5 to 1. The remaining analysis corresponded to unreacted 4-iodoanisole.

Continuous flow reactions

All reactions were performed in 300 or 100 cm stainless steel tubular plug flow reactors (PFRs) of 1 mm internal diameter. A larger diameter (3.9 mm) PFR was also used as a comparison in one example (Figure 2). Initial studies used flow rates commensurate with the concentration used in the autoclave reactor.

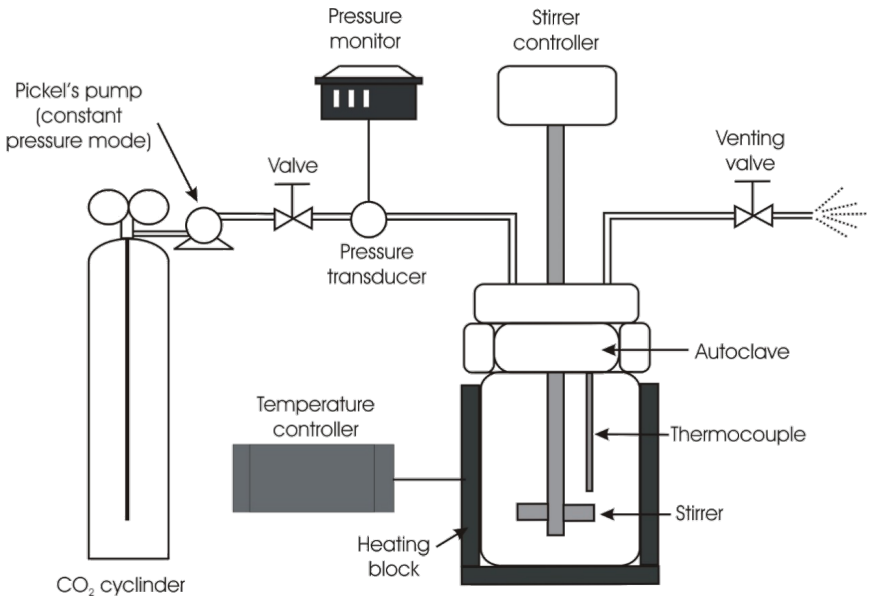

Figure 1: Schematic diagram of the stirred autoclave reactor. Pickel's pump NWA PM101 was used to achieve supercritical pressure.

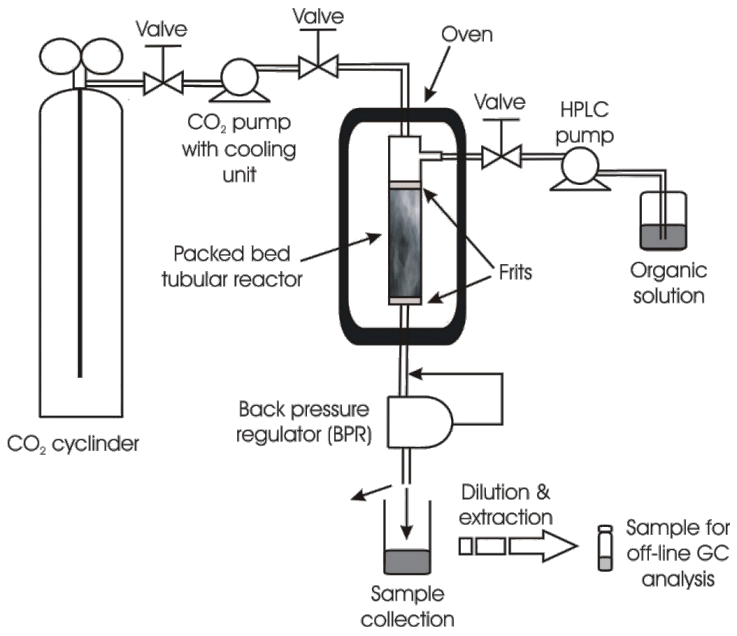

Figure 2: Schematic diagram of the continuous flow system. The reactor shown is the 3.9 mm i.d. PFR. For the 1 mm i.d. reactor this was a coil of the 300 cm or 100 cm tube according to the specific reaction.

Residence time in the continuous flow reactors

The volume of the unpacked 1 mm diameter reactors in the styrene and methyl acrylate reactions were 2.36 and 0.79 mL respectively. The reactors containing catalyst with packing were found to have a porosity of 0.80, so neglecting packing swelling, the total volumes available for flow for the 300 cm and 100 cm length reactors were 1.89 and 0.63 mL respectively. Unless otherwise stated, the $scCO_2$ flow rate was 0.1 mL min^{-1} while the organic flow rate was precisely varied over the range shown in Table 1 to give the total flow rates shown. The range of possible residence times on each reactor are also given in Table 1, based on the total flow rates and effective reactor volumes.

Table 1: Correlation of reaction flow rates to reactor residence times.

Flow rates, mL/min			Residence times, min	
$scCO_2$	Organic	Total	300 cm reactor	100 cm reactor
0.1	0.033	0.133	14.2	4.7
0.1	0.025	0.125	15.1	5.0
0.1	0.02	0.12	15.7	5.2
0.1	0.017	0.117	16.1	5.4
0.1	0.014	0.114	16.5	5.5
0.1	0.013	0.113	16.7	5.6
0.1	0.011	0.111	17.0	5.7

Because of the piping pre- and post-reactor there was a volume through which flow was possible but without reaction. Therefore, after the commencement of organic solution flow, samples were not collected over the initial 2 hour period to allow transit of the fluids through the reactor system. The reactor was operated over an eight hour period taking the first sample at 3 hours unless otherwise shown and then at regular intervals.

In the initial flow studies, the $scCO_2$ flow rate was set at 0.1 mL min^{-1} and the organic solution flow rate at 0.02 mL min^{-1}. The temperature was controlled to ±0.1 °C using a Memmert oven. Three reaction temperatures were chosen: 145, 155 and 165 °C. The first samples were analysed 3 hours after the organic flow was started to allow complete flushing of the complete reactor system with reagents. Samples were then taken at regular intervals over an eight hour period. Figure 3 shows the total conversions obtained for combined **t** and **b** isomers. No **c** isomer was observed in any of the reactions carried out.

The first feature of note is that the initial conversion at all temperatures is low. The system takes time to reach equilibrium as the catalyst becomes conditioned so therefore requires a start-up procedure before reaching full conversion capacity.

At 145 °C, conversion of 47% is achieved with a **t**/**b** ratio of 6:1 although the system is far from running at equilibrium conversion. Curve fitting shows that after 24 hours approximately 60% conversion would be achieved. Therefore on comparable timescale the continuous flow reactor gives a lower conversion but with a slightly improved selectivity for the conversion to the **t** isomer. Increasing the temperature to 155 °C resulted in 75% conversion after 8 hours with a **t**/**b** ratio of 4:1. At 165 °C the conversion was 86% after 8 hours although the **t**/**b** ratio has decreased to 3:1.

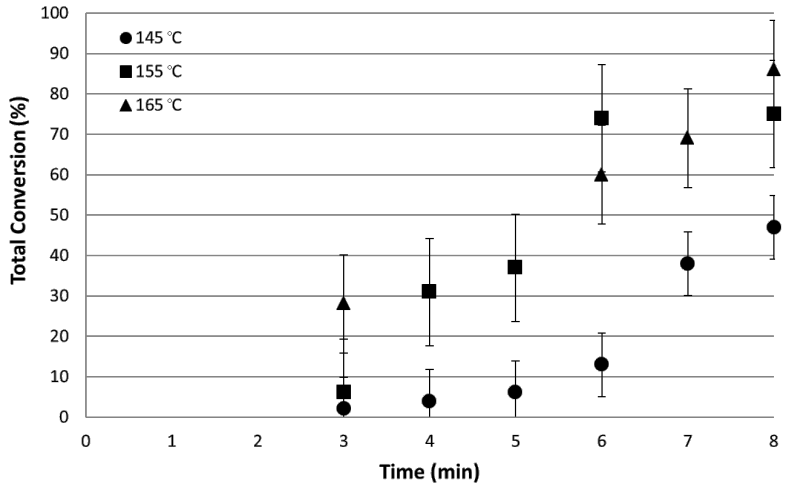

Figure 3: Total conversion of 4-iodoanisole as a function of reactor run time for three reaction temperatures.

The effect of overall flowrate through the reactor was determined by changing the organic flow rate while keeping that of the $scCO_2$ constant at 0.1 mL min^{-1}. Therefore, the concentration of the organic reagents increased with increased flow. The temperature was maintained at 155 °C and the pressure at 200 bar throughout. Figure 4 shows the reaction profile for the rates studied. Optimum conversion of 76% was observed at 0.12 mL min^{-1}. At faster flows the conversion decreased with the lowest conversion (1%) was observed for the fastest flow rate of 0.133 mL min^{-1}. At slower flow rates the conversion decreased away from the optimum value showing the process to be a compromise between flow rate and reaction rate.

Increasing the pressure from 200 to 250 bar had a dramatic effect on conversion. The continuous flow reaction was repeated at 145 °C and flow rate of 0.12 mL min^{-1} but at 250 bar $scCO_2$ pressure. The results are shown in Figure 5. While the conversion increased to 48% at 200 bar with continued use until the reaction was stopped, there was less than 5% conversion in all cases when the pressure was increased to 250 bar. At this time we cannot account for this almost complete inhibition of the reaction at increased pressure so we are carrying out further studies to elucidate the precise mechanism. We are also investigating the effect of pressure over an extended range to consider solutions at sub- and near-critical

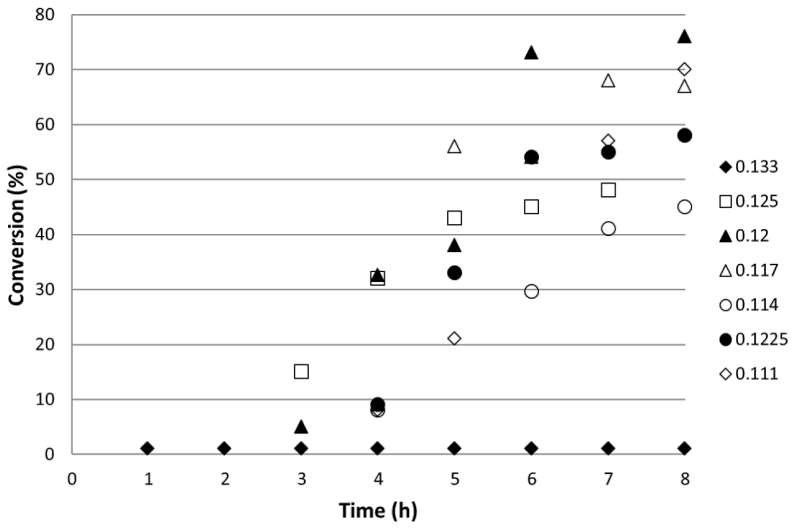

Figure 4: Total conversion of 4-iodoanisole at 155 °C and 200 bar as a function of reactor run time for different combined flow rates and therefore residence times. The values of the total flow rates given in the legend are mL min^{-1}.

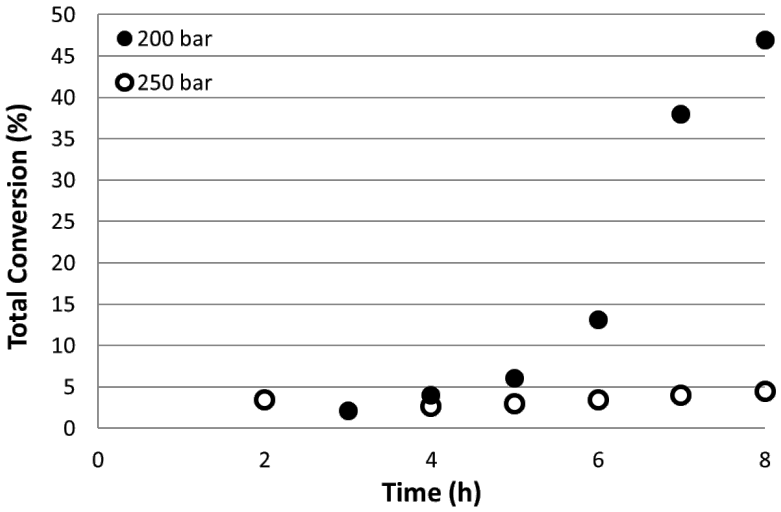

Figure 5: Total conversion of 4-iodoanisole as a function of reactor run time at 145 °C and at 200 (•) and 250 (o) bar CO_2 pressure.

pressures to determine the optimum conditions for conversion and selectivity in continuous flow systems. Furthermore, it was noted that while there was a dramatic change in conversion, the **t**/**b** ratio remained unchanged at 6:1.

Synthesis of methyl 4-methoxycinnamate under continuous flow conditions

An activated alkene, methyl acrylate was reacted with 4-iodoanisole under catalytic PFR conditions and the conversion and product distribution monitored. A column containing the 2% Pd/SiO_2 catalyst with Chromosorb packing (1:3) was constructed with dimensions 100 cm × 1 mm by cutting fresh sections of the 300 cm tubes used for the reactions previously described using styrene. Each reactor therefore contained 15.7 μmol Pd dispersed throughout the volume. The pressure was maintained at 200 bar and 155 °C throughout and the total flow rate was set to be 0.12 mL min^{-1} using a $scCO_2$ flow rate of 0.1 mL min^{-1}. The residence time on the reactor was calculated as 5.2 minutes. Including flow in the upstream and downstream pipework then the total time on the system was 84 minutes so the first sample was taken after 90 minutes.

Figure 6 shows that reaction between 4-iodoanisole and methyl acrylate proceeded more rapidly than the reaction with styrene under the same operational conditions. The conversion reached equilibrium after only 3.5 hours with a conversion of 4-iodoanisole of 90 ± 3%. Comparisons between methyl acrylate and styrene also shows that the latter requires a reaction run time of about 6 hours to achieve comparable yields and conversion. The increased reactivity of methyl acrylate over styrene can be explained in terms of the increased resonance stabilisation of the intermediate through electron delocalisation over the ester carbonyl motif.

Another aspect of interest is the product selectivity in the reactions involving 4-iodoanisole and methyl acrylate. The terminal product, methyl *trans*-methoxycinnamate (**2t**) was obtained exclusively, whereas in the system using styrene, a mixture of the trans-linear (**1t**) and terminal-branched (**1b**) isomers were observed with the composition dependent on the system temperature. This may be explained due to a steric effect [34]. In the case of methyl acrylate, proper alignment of the double bond for migratory insertion is hindered by the presence of the methyl group, thereby favouring the formation of the terminal arylation product. The presence of the methyl group on methyl acrylate might have a more profound impact on steric limitation than the phenyl group of styrene. The results shown here are consistent to published literature utilising 4-iodoanisole and

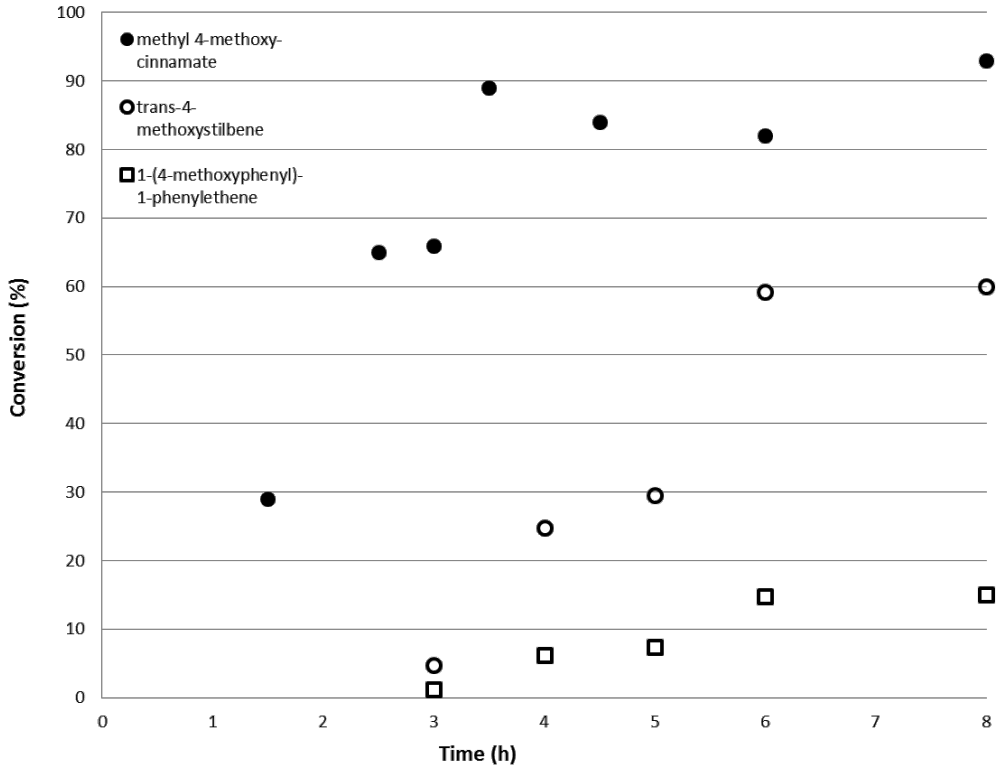

Figure 6: Conversion of 4-iodoanisole to methyl 4-methoxycinnamate (●) at 155 °C and 200 bar as a function of reactor run time. The open symbols are the conversions to the different isomeric products for the reaction of 4-iodoanisole with styrene for comparison.

methyl acrylate in the presence of ruthenium- and platinum-complex catalysts, in which complete regioselectivity towards the *trans*-isomer was achieved [19].

Having obtained encouraging conversions in the 1 mm diameter reactor, it was decided to scale the reaction out to a 3.9 mm internal diameter PFR. The 9 cm long reactor was packed with the catalyst and packing material and the reaction carried out under identical reaction conditions to those used in the 1 mm reactor. Accounting for the 0.80 porosity of the reactor filled with the packed catalyst, the total available volume for fluid flow in the 3.9 mm reactor was 0.88 mL with a residence time at a combined flow rate of 0.12 mL min^{-1} of 7.3 minutes.

Figure 7 shows that the yields obtained in the 1 mm PFR are slightly lower than those achieved in the 3.9 mm reactor, however the mass of catalyst was also lower. Furthermore, the 3.9 mm PFR gave complete conversion of the starting material after only 4 hours flow and this conversion was maintained while flow continued. In order to study the effects of the cata-

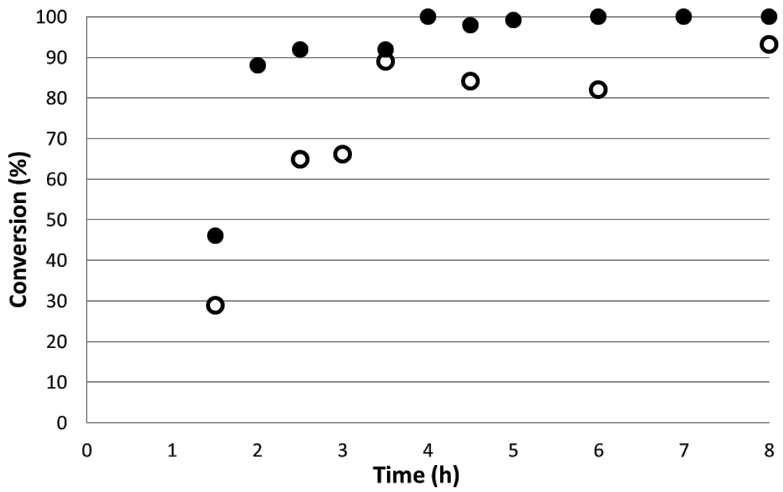

Figure 7: Comparison of conversion as a function of reactor run time for the reaction of methyl acrylate in the 1 mm × 300 cm (o) and 3.9 mm × 9 cm (●) plug flow reactors over the Pd-SiO_2 catalyst.

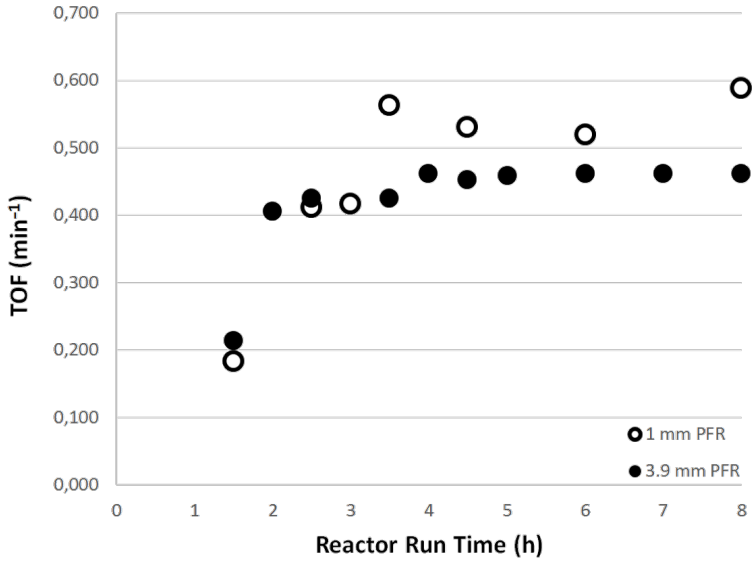

Figure 8: TOF values for the 1 mm (o) and 3.9 mm (●) PFRs at a total flow rate of 0.12 mL min^{-1}, 155 °C and 200 bar for the reaction of 4-iodoanisole with methyl acrylate.

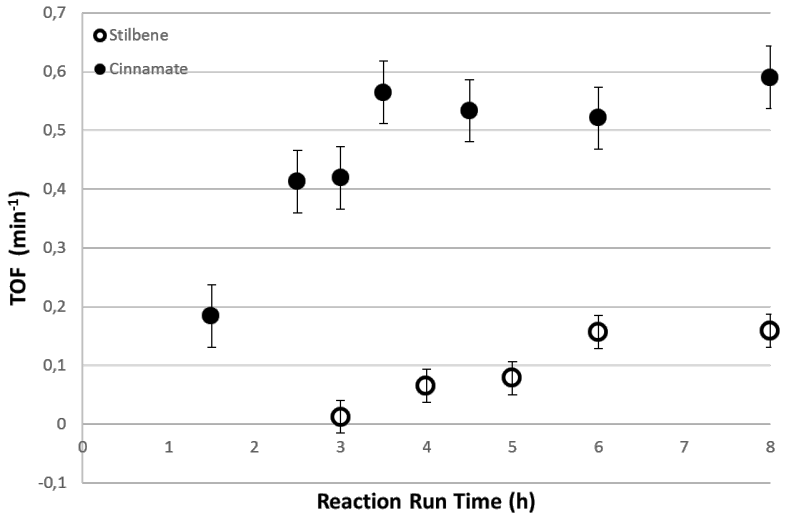

Figure 9: Turnover frequencies of the Heck reactions at 155 °C using styrene (o) as combined isomeric products, and methyl acrylate (●) as a function of reactor run time for the 1 mm internal diameter plug flow reactors.

lyst amount, the turnover frequency (TOF) was also calculated and this is shown in Figure 8. It is clear that within experimental error that the TOFs in the two reactor configurations are essentially identical which is encouraging in terms of the ability to both scale up and scale out the reactions. The TOF is defined as the number of moles of substrate converted per mol of catalyst per unit time. For a continuous flow system this can be defined in terms of the molar or volumetric flow rates (u_M or u_V), the conversion as a mol fraction (x) and the number of mol of substrate at the start of the reaction (n_S) and the number of mol of catalyst (n_{CAT}) as shown in Equation 1.

$$\text{TOF} = \frac{x u_V n_S}{n_{CAT}} \quad (1)$$

The TOFs were also calculated for the reactions of styrene and methyl acrylate with 4-iodoanisole in the 1 mm PFRs in order to normalise with respect to catalyst concentration as the lengths of the reactor and therefore residence times for the same flow rate differed three-fold. The results are shown in Figure 9 and emphasise the more reactive nature of the methyl acrylate as a substrate. Indeed the methyl acrylate is almost four times more reactive than styrene under identical conditions of temperature and pressure.

Conclusion

Supercritical carbon dioxide ($scCO_2$) can be effectively used as a reaction solvent for the palladium metal-catalysed Heck reaction between an aryl halide and an alkene under continuous flow conditions in a plug flow reactor (PFR). The efficiency of the reaction depends on the nature of the alkene used, the temperature and pressure of the reaction and the flow rate of the reagents over the fixed bed catalyst. It was found that increasing the temperature of the reaction between 4-iodoanisole and styrene resulted in an increased conversion but that the distribution of isomers was affected with more of the branched, germinal addition isomer being produced at higher temperatures. In the case of reaction with methyl acrylate as the alkene, only the single *trans*-substituted isomer was produced. Increasing the pressure from 200 to 250 bar in the PFR had the dramatic effect of almost completely inhibiting the reaction. The turnover frequency is, as expected, considerably higher when methyl acrylate is used instead of styrene. However, there is very little change in the TOF for methyl acrylate when the internal diameter of the PFR was increased from 1.0 to 3.9 mm. This is encouraging for the design of continuous flow reactor systems as the TOF is essentially insensitive to diameter scaling over the length scales studied and hence there are good prospects for scaling the flow to handle bigger substrate inventories.

Experimental

Reagents and instruments

All reagents were purchased from Sigma-Aldrich unless otherwise stated and were used as received without further purification. The supported catalyst, 2% palladium on silica was purchased from Johnson Matthey.

Gas chromatography–mass spectra GC–MS analyses (EI and CI modes) were performed using a PerkinElmer GC–MS with a 30 m × 0.25 mm × 0.25 μm Phenomenex-ZB5 column by Jane Stanbra and Simon Thorpe in the Department of Chemistry, The

University of Sheffield. The oven temperature programme was 60–260 °C at 10 °C/min with a final temperature isothermal hold for 10 minutes, corresponding to a total run time of 30 minutes. The MS mass limit was set at between 50 and 450 Da. GC analyses were carried out using a Varian 3900 GC fitted with an autosampler (AS 8400) and a flame ionisation detector (FID) on a 15 m × 0.25 mm × 0.25 μm CP-Sil 5CB Chrompak Capillary Column. The oven temperature programme was set to ramp from an initial temperature of 50 °C (held for 1 minute) to 250 °C (held for 0.5 minutes) at a rate of 20 °C/minute, totalling to a run time of 11.5 minutes. The temperatures of the injector and the FID were set at 200 and 250 °C respectively.

Inductively coupled plasma-atomic emission (ICP-AE) analyses were performed on a Spectro Ciros CDD instrument (Spectro-Analytical, UK) by Alan Cox and Neil Bramall, Department of Chemistry, The University of Sheffield. The catalyst particles were rinsed with organic solvents (diethyl ether, THF and methanol, 2 × 5 mL each), followed by distilled water (2 × 5 mL) and dried under vacuum prior to analysis. During the sample preparation step, the catalyst sample was quantitatively transferred to a clean (acid-washed) tube and 6 mL of concentrated hydrochloric acid and 2 mL of concentrated nitric acid were added. The sample was placed in a dri-block which was thermostatically controlled with the temperature gradually raised to 150 °C. The sample was then maintained at this temperature for 1 hour. After this digestion period, the sample was left to cool and quantitatively transferred to a 50 mL tube and topped up to 50 mL with 1% nitric acid. The element of interest (palladium) was measured against a calibrated sample prepared from known standards. The sample was introduced to the instrument using a flow regulated pump. On reaching the nebuliser, the liquid sample met argon gas, generating a spray of droplets. The heavy droplets were captured by the spray chamber walls and were pumped to a waste container. The fine droplets (ca. 2% of the sample) passed through the spray chamber and into the argon plasma (ca. 7000 °C) via the torch. The resulting atoms and ions were excited and emitted light of characteristic wavelengths (Pd measured at 340.458 nm). The light was detected by charged coupled devices (CCD chips) mounted on the spectrometer. The concentration of Pd was then calculated using the instrument software. ICP–AE analysis gave the concentration of palladium metal on the silica gel support as 0.02 g or 0.189 mmol Pd/g. This was later diluted with Chromopac for use in the flow reactors at a ratio of 1:3 catalyst/packing.

Stirred autoclave reactions

The autoclave reaction set-up is shown schematically in Figure 1. A standard reaction solution made from 4-iodoanisole (1 equivalent, 3.5105 g, 15 mmol), styrene (2 equivalents, 3.1245 g, 30 mmol), *N*,*N*-diisopropylethylamine (DIPEA, 2 equivalents, 5.23 mL, 30 mmol) and dissolved in THF (15 mL) and methanol (15 mL each) was prepared and stirred thoroughly until completely mixed. The ratio of organic to $scCO_2$ used in the autoclave corresponded to the 5:1 volumetric ratio used in the continuous flow reactions. The tetrahydrofuran and methanol were used to dissolve the organo iodide and act as a miscible, polar modifier to enhance the solvating properties of the $scCO_2$. The 60 mL autoclave was charged with 2.4 mL of the reaction solution, corresponding to 4% of the autoclave volume. 2% Palladium on a silica support catalyst (20.4 mg, 2.463 mmol) was then added and the autoclave sealed and inserted into a pre-heated aluminium heating block (external temperature 145 °C, internal temperature 120 °C). After a period of 30 minutes the remaining reactor volume (57.6 mL) was pressurised with $scCO_2$ at 167 bar using a Pickel's pump NWA PM-101 operating in constant pressure mode. The reaction was stirred for 24 hours at a rate of 145 rpm. To work-up the reaction mixture, the autoclave was allowed to cool to room temperature and then slowly depressurised by venting the CO_2. The reaction mixture remaining in the autoclave was then dissolved in additional tetrahydrofuran, before extracting into diethyl ether and washing with water. The resulting organic mixture (top layer) was then withdrawn and dried over magnesium sulfate then analysed by gas chromatography using a Varian 3900 GC with reference to standard solutions of *trans*-4-methoxystilbene.

Continuous flow reactions

Particles of the catalyst, 2% Pd on silica, (250 mg) thoroughly mixed with the packing material (Chromosorb 750; 100–120 mesh; 750 mg) were packed into standard HPLC columns (length 300 cm, internal diameter 1 mm). The columns were laid out straight and a small pressure (1 bar) was applied to fill the material into the column. No vacuum was used. The catalysts were dispersed in a uniform manner through the whole length of the column, and finally the ends plugged with 25 μm stainless steel frits. For the reaction with methyl acrylate, the column was cut into 100 cm sections. The unpacked volume of the 300 cm long reactor was 2.36 mL and the 100 cm long reactor 0.79 mL. In all cases the columns were then coiled a small volume within the cavity of a Memmert oven. The setup for the continuous flows is shown schematically in Figure 2.

The reactor was connected to the fluid delivery system using standard Swagelok fittings, and housed in a Memmert oven with custom fitted inlet and outlet ports. Supercritical carbon dioxide was generated by passing the feed from a CO_2 cylinder (BOC, liquefied at 15 °C, 50 bar pressure) through a Jasco PU-1580-CO2 supercritical pump. The system was first satu-

rated with CO_2 at high flowrates (1 to 2 mL) until the desired pressure was reached, followed by gradual reduction of the CO_2 flowrate to the target value. The system was heated up when the reactor was saturated with CO_2 at 200 bar. When the desired temperature was reached, the system was left to equilibrate for a further period of 15 minutes. Pumping the organic reaction mixture (4-iodoanisole, 15 mmol; styrene, 30 mmol; *N,N*-diisopropylethylamine, 30 mmol; tetrahydrofuran, 15 mL; methanol, 15 mL) was achieved using a Jasco PU-1580 HPLC pump set at constant flow mode. The organic reaction mixture was pumped at a variety of flowrates while maintaining constant scCO_2 flowrate of 0.1 mL/min for all runs. The entire system pressure was controlled by a Jasco PU-1580-81 back pressure regulator (BPR). Samples were collected at regular intervals using vials placed underneath the BPR outlet port. The CO_2 evaporated immediately on de-pressurisation leaving a solid residue containing the mixture of products. The samples were then analysed by gas chromatography (GC) and GC-mass spectrometry (GC–MS) against known calibration standards of the starting material and products. At the end of reaction, the system tubing and reactor were flushed with CO_2 and the organic solvent mixture (THF and methanol) for a further period of 6 hours to remove any products, byproducts and unreacted organic reagent.

A larger continuous flow reactor with 3.9 mm internal diameter of length 9 cm was also used as a comparison to assess the effects of scaling up the flow reactor. This was constructed from stainless steel tubing with 25 μm steel frits at each end, connected to the solvent delivery system using standard ¼ inch Swagelok fittings. The reactor body was filled with the 1:3 (w/w) mixture of the 2% palladium on silica catalyst and Chromosorb packing material. The unpacked volume of the reactor was 1.075 mL.

Sample analysis

To work up the reaction, the raw sample was diluted with diethyl ether (2 × 3 mL), then washed with an equivalent volume of distilled water to dissolve the halide salt formed. Diethyl ether (2 mL) was added to a GC vial and 5 drops of solution from the organic top layer of the extraction mixture was withdrawn using a Pasteur pipette and added into the GC vial. The solution was thoroughly mixed and analysed by GC and/or GC–MS.

Acknowledgements

We are grateful to the Engineering and Physical Sciences Research Council (GR/R41668/01) and the University of Sheffield (Fees) for the funding of a Ph.D. studentship to P.L.L. We also thank the University of Nottingham School of Chemistry for hosting P.L.L. as part of the Ph.D. programme and in particular Professor Martyn Poliakoff, FRS, Dr Jason Hydes and Dr Ben Walsh for her supervision on site.

References

1. de Meijere, A.; Bräse, S. *J. Organomet. Chem.* **1999,** *576,* 88–110. doi:10.1016/S0022-328X(98)01087-0
2. Heck, R. F.; Nolley, J. P., Jr. *J. Org. Chem.* **1972,** *37,* 2320–2322. doi:10.1021/jo00979a024
3. Phan, N. T. S.; Brown, D. H.; Adams, H.; Spey, S. E.; Styring, P. *Dalton Trans.* **2004,** 1348–1357. doi:10.1039/b316553c
4. Phan, N. T. S.; Brown, D. H.; Styring, P. *Tetrahedron Lett.* **2004,** *45,* 7915–7919. doi:10.1016/j.tetlet.2004.08.153
5. Phan, N. T. S.; Brown, D. H.; Styring, P. *Green Chem.* **2004,** *10,* 526–532. doi:10.1039/b405203j
6. Diederich, F.; Stang, P. J., Eds. *Metal-Catalysed Cross-Coupling Reactions;* Wiley-VCH: Weinheim, 1998. doi:10.1002/9783527612222
7. Köhler, K.; Heidenreich, R. G.; Krauter, J. G. E.; Pietsch, M. *Chem.–Eur. J.* **2002,** *8,* 622–631. doi:10.1002/1521-3765(20020201)8:3<622::AID-CHEM622>3.0.CO;2-0
8. Bhanage, B. M.; Zhao, F.-G.; Shirai, M.; Arai, M. *Tetrahedron Lett.* **1998,** *39,* 9509–9512. doi:10.1016/S0040-4039(98)02225-4
9. Mikami, K. *Green Reaction Media in Organic Synthesis;* Blackwell Publishing: Oxford, 2005. doi:10.1002/9780470988770
10. Jessop, P. G.; Leitner, W., Eds. *Chemical Synthesis Using Supercritical Fluids;* Wiley-VCH: Weinheim, 1999. doi:10.1002/9783527613687
11. Leitner, W. *Acc. Chem. Res.* **2002,** *35,* 746–756. doi:10.1021/ar010070q
12. Raynor, C. M. *Org. Process Res. Dev.* **2007,** *11,* 121–132. doi:10.1021/op060165d
13. Carroll, M. A.; Holmes, A. B. *Chem. Commun.* **1998,** 1395–1396. doi:10.1039/a802235f
14. Morita, D. K.; Pesiri, D. R.; David, S. A.; Glaze, W. H.; Tumas, W. *Chem. Commun.* **1998,** 1397–1398. doi:10.1039/a802621a
15. Styring, P.; Grindon, C.; Fisher, C. M. *Catal. Lett.* **2001,** *77,* 219–225. doi:10.1023/A:1013209202418
16. Alonso, F.; Beletskaya, I. P.; Yus, M. *Tetrahedron* **2005,** *61,* 11771–11835. doi:10.1016/j.tet.2005.08.054
17. Kohler, K.; Prockl, S. S.; Kleist, W. *Curr. Org. Chem.* **2006,** *10,* 1585–1601. doi:10.2174/138527206778249630
18. Zhao, F.; Shirai, M.; Ikushima, Y.; Arai, M. *J. Mol. Catal. A: Chem.* **2002,** *180,* 211–219. doi:10.1016/S1381-1169(01)00436-8
19. Horniakova, J.; Raja, T.; Kubota, Y.; Sugi, Y. *J. Mol. Catal. A: Chem.* **2004,** *217,* 73–80. doi:10.1016/j.molcata.2004.02.019
20. Corma, A.; García, H.; Leyva, A. *Tetrahedron* **2004,** *60,* 8553–8560. doi:10.1016/j.tet.2004.06.121
21. Tsai, F.-Y.; Wu, C.-L.; Mou, C.-Y.; Chao, M.-C.; Lin, H.-P.; Liu, S.-T. *Tetrahedron Lett.* **2004,** *45,* 7503–7506. doi:10.1016/j.tetlet.2004.08.065
22. Dams, M.; Drijkoningen, L.; De Vos, D.; Jacobs, P. *Chem. Commun.* **2002,** 1062–1063. doi:10.1039/b201180h
23. Corma, A.; García, H.; Leyva, A.; Primo, A. *Appl. Catal., A* **2003,** *247,* 41–49. doi:10.1016/S0926-860X(03)00060-7
24. Poyatos, M.; Márquez, F.; Peris, E.; Claver, C.; Fernandez, E. *New J. Chem.* **2003,** *27,* 425–431. doi:10.1039/b204911b
25. Choudary, B. M.; Madhi, S.; Chowdari, N. S.; Kantam, M. L.; Sreedhar, B. *J. Am. Chem. Soc.* **2002,** *124,* 14127–14136. doi:10.1021/ja026975w

26. Karbass, N.; Sans, V.; Garcia-Verdugo, E.; Burguete, M. I.; Luis, S. V. *Chem. Commun.* **2006,** 3095–3097. doi:10.1039/b603224a
27. Phan, N. T. S.; Khan, J.; Styring, P. *Tetrahedron* **2005,** *61,* 12065–12073. doi:10.1016/j.tet.2005.07.109
28. Phan, N. T. S. Polymer-Supported Catalysts for Greener Synthesis. Ph.D. Thesis, The University of Sheffield, 2005.
29. Lee, C. K. Y.; Holmes, A. B.; Ley, S. V.; McConvey, I. F.; Al-Duri, B.; Leeke, G. A.; Santos, R. C. D.; Seville, J. P. K. *Chem. Commun.* **2005,** 2175–2177. doi:10.1039/b418669a
30. Liu, S.; Fukuyama, T.; Sato, M.; Ryu, I. *Org. Process Res. Dev.* **2004,** *8,* 477–481. doi:10.1021/op034200h
31. Solodenko, W.; Wen, H.; Leue, S.; Stuhlmann, F.; Sourkouni-Argirusi, G.; Jas, G.; Schönfeld, H.; Kunz, U.; Kirschning, A. *Eur. J. Org. Chem.* **2004,** 3601–3610. doi:10.1002/ejoc.200400194
32. Cwik, A.; Hell, Z.; Figueras, F. *Adv. Synth. Catal.* **2006,** *348,* 523–530. doi:10.1002/adsc.200505225
33. Hillier, A. C.; Grasa, G. A.; Viciu, M. S.; Lee, H. M.; Yang, C.; Nolan, S. P. *J. Organomet. Chem.* **2002,** *653,* 69–82. doi:10.1016/S0022-328X(02)01154-3
34. Beletskaya, I. P.; Cheprakov, A. V. *Chem. Rev.* **2000,** *100,* 3009–3066. doi:10.1021/cr9903048

License and Terms

Beilstein Journal of Organic Chemistry

Continuous flow nitration in miniaturized devices

Amol A. Kulkarni

Review

Open Access

Address:
Chem. Eng. & Proc. Dev. Division, CSIR-National Chemical Laboratory, Pune – 411 008, India, phone: +91-20-25902153

Email:
Amol A. Kulkarni - aa.kulkarni@ncl.res.in

Keywords:
continuous flow; flow chemistry; nitration; nitric acid; microreactors; tubular reactor

Beilstein J. Org. Chem. **2014,** *10,* 405–424.
doi:10.3762/bjoc.10.38

Received: 08 August 2013
Accepted: 14 January 2014
Published: 14 February 2014

This article is part of the Thematic Series "Chemistry in flow systems III".

Guest Editor: A. Kirschning

Abstract

This review highlights the state of the art in the field of continuous flow nitration with miniaturized devices. Although nitration has been one of the oldest and most important unit reactions, the advent of miniaturized devices has paved the way for new opportunities to reconsider the conventional approach for exothermic and selectivity sensitive nitration reactions. Four different approaches to flow nitration with microreactors are presented herein and discussed in view of their advantages, limitations and applicability of the information towards scale-up. Selected recent patents that disclose scale-up methodologies for continuous flow nitration are also briefly reviewed.

Review

1 Introduction

Nitration of aromatics is one of the oldest and industrially most important reactions. A reaction between an organic compound and a nitrating agent leads to the introduction of a nitro group onto a carbon, nitrogen or oxygen atom of that organic compound [1]. Among the earliest reports are those of Faraday nitrating benzene, the synthesis of nitrobenzene by Mitscherlich [2] using benzene and fuming nitric acid, and the use of mixed acids (nitric acid and sulfuric acid) for aromatic nitration by Mansfield [3]. In general, nitration reactions are fast and highly exothermic. Typically, the nitration of aromatic compounds is acid-catalyzed and it involves an electrophilic substitution where the nitronium ion (NO_2^+) acts as the reactive species [4-6].

Based on estimations of 2007 and the proposed world production capacity, the overall world production of nitric acid in 2012 is assumed to be close to 78 Mi TPA, of which 85% is used for the production of ammonium nitrate as fertilizer and 6% for production of nylon. The remaining 9% – that is about 8 Mi TPA – are used for the nitration of aromatics [7]. Nitro derivatives of aromatic compounds are used in variety of basic chemicals, specialty chemicals, and knowledge chemicals. They are also employed in dyes, perfumes, pharmaceuticals, explosives [8], intermediates, colorants, and pesticides. In general, the annual demand for nitric acid grows in the range of 3 to 6%. A large proportion of nitric acid consumed during aromatic nitration is directed towards the synthesis of aniline derivatives,

which are produced by nitration followed by reduction. These aniline derivatives find applications in insecticides, pigments, dyes, resins, textiles, elastomers, plant growth regulators, pharmaceuticals, fuel additives, antioxidants, and rubber accelerators. In the leather industry *m*-nitrophenol is used as a fungicide and *p*-nitrophenol as a chemical intermediate for leather preservatives. 2,4-Dinitrophenol is useful for the manufacturing of photographic developers and serves as a wood preservative and also as an insecticide. 4-Amino-2-nitrophenol and 2-nitro-*p*-phenylenediamine are components of permanent hair dye products and fur dye. Several aniline derivatives are also used for the synthesis of various dyes [9], the first one being the aniline Yellow [10] reported in 1880. The history of the relevance of nitration for the dye and colorant industry covers more than a century. Nitro derivatives of the toluene diisocynate are employed in the manufacturing of flexible polyurethane foams, which are used in transformation, furniture, and carpet underlay. 2,4,6-Trinitrotoluene is a military and industrial explosive. Nitro derivatives of glycerine, urea and naphthalene also exhibit explosive properties. Some of the aniline based dyes were used for medical applications, too. The extension of the aniline based medicines led to hundreds of drugs [11], which were used for medication during and after World War II (1939–45). Several nitro derivatives are applied to the synthesis of the respective amino groups, which form important building blocks in the synthesis of active pharmaceutical ingredients (APIs). Almost 65% of APIs requires at least one nitration step in the whole process. Among the other basic chemicals that are used in significantly large quantities are a large number of organic molecules, e.g., nitrobenzenes, nitrophenols, nitrotoluenes, nitroxylenes, nitronaphthalenes, nitrohaloaromatics, nitroanilines, nitrotoluidines, imidazole derivatives, nitroketones, pyridine and quinoline derivatives, and nitro alcohols. Thus, part of the human life and life style is dependent of nitration as a unit reaction.

In general, several types of nitrating agents are used for nitration. A literature search covering the last 50 years is presented in Figure 1. One third reports on nitrations of organic substrates with sulfuric acid and nitric acid as the nitrating agents.

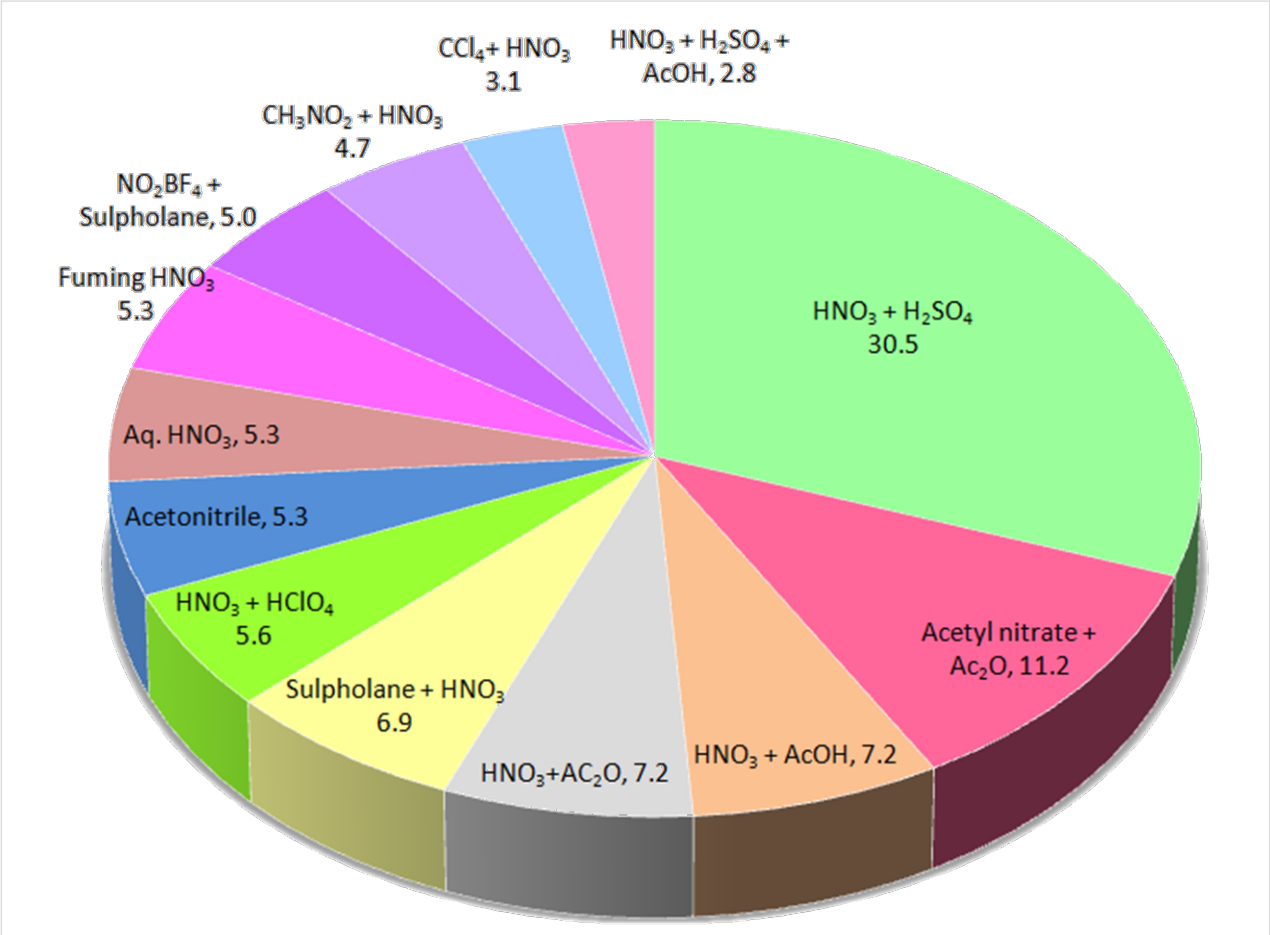

Figure 1: Analysis of the literature on aromatic nitration over the last 50 years. Numbers next to each nitrating agent correspond to the percentage of literature in which the respective agent is used for nitration.

However, the use of other activating agents (e.g., acetic anhydride) is not uncommon. Typically, nitrations with undiluted nitric acid generate water that leads to the dilution of the nitric acid, so that the concentration of the nitronium ions and thus the reaction rates are reduced. It also gives a lower selectivity due to the oxidation of the aromatic substrate. The isolation of the product from the organic phase is problematic, even after complete conversion is achieved. Nitric acid is commonly used in excess and it can form a complex with the organic products, so that only after reaction, significant dilution with water allows separating the organic phase from the diluted nitric acid. The sulfuric acid in so-called "mixed acid", i.e., a mixture of HNO_3 and H_2SO_4, catalyzes the generation of nitronium ions and extracts water, which is generated from the dissociated nitric acid. Usually, the sulfuric acid is used in excess in the preparation of the mixed acid. Therefore, in the presence of sulfuric acid nitrations are usually faster and selective. A variety of other acids including solid acids can be used in place of sulfuric acid to enhance the rates of nitration. This review focuses on continuous nitration under flow conditions, while the mechanisms of nitration will not be discussed in detail, as they are well understood [12]. In the absence of any other acid, nitric acid alone can act as a self-protonating agent or self-catalyst in which one molecule of nitric acid protonates a second one leading to the formation of a nitronium ion [13]. The electrophilic nitration is the most common reaction. It proceeds through the nitronium ion NO_2^+ as an electrophilic species. One of the most widely accepted mechanism for the electrophilic nitration involves the sequence of reactions depicted below [12]:

$$HNO_3 + HA \leftrightarrow H_2NO_3^+ + A^- \quad (1)$$

$$H_2NO_3^+ \leftrightarrow NO_2^+ + H_2O \quad (2)$$

$$Ar-H + NO_2^+ \leftrightarrow ArHNO_2^+ \quad (3)$$

$$ArHNO_2^+ + A^- \leftrightarrow ArNO_2 + HA \quad (4)$$

In the first step, the presence of a strong acid catalyst HA protonates HNO_3 thereby releasing the reactive species NO_2^+ and water in the second step. Both of these steps are rapid and reversible. The third step is much slower – and hence rate-controlling – than the reverse of the second step due of the presence of water and the poor solubility of the aromatic species in the mineral acid medium. In the rate-controlling step the nitronium ion attacks the aromatic ring to give an intermediate carbocation, which deprotonates rapidly to afford the nitroaromatic product in the final step. Therefore, nitration in mineral acid exhibits a second-order kinetic behavior, first-order in HNO_3 as well as in the aromatic substrate. However, the reaction rates strongly depend upon the strengths of the cumulative acid [14]. The strength of the nitric acid and the quantity of the sulfuric acid necessary for a given nitration depend on the substrate and the desired extent of nitration. The weight ratio of consumed sulfuric acid to the weight of water in the final acid (spent acid) after the nitration is complete is termed the dehydrating value of sulfuric acid (D.V.S.). The D.V.S. value is estimated by multiplying the mol ratio of sulfuric acid to water with 5.444. This is one of the most common parameters for exploring the nature of a substrate that undergoes nitration [15]. However, the nature of nitration and the corresponding heat effects largely depend upon the nitrating agent, the conditions of the nitration, and the reactivity of the aromatic substrate [16].

Generally, the economics of a nitration process largely depends on the procedure used to remove the water from the system and the regeneration of the dehydrating agent [17]. Theoretically, the application of undiluted nitric acid – usually used in excess – is expected to avoid the use of water. In practice, however, the separation of nitroarenes is facilitated in the diluted nitric acid. Nitration with diluted nitric acid generates the nitronium ion in the following manner:

$$2NHO_3 \leftrightarrow NO_2^+ + NO_3^- + H_2O \quad (5)$$

In general, this approach is not considered economically feasible, so that most nitrations are carried out with the next cheapest nitrating agent i.e., a mixture of nitric and sulfuric acids. If they are used in excess, both of them are usually treated by neutralization, by feeding the weak nitric acid to an absorption tower, or recovered from the spent acid. Generally, the latter two options are not viable unless the quantity is very large. A simple neutralization is unacceptable given stringent environmental regulations. Adherence to regulations and requirements adds to the process costs [17].

2 Nitration: modes and systems

Conventional aromatic nitration usually follows a batch or a semi-batch approach, where the mixing of reactants and the reaction itself are carried out very slowly [18,19]. Some of the most important concerns, which do not allow for an easy scale-up include: (i) an inadequate heat transfer area (20–100 m^2/m^3), (ii) an inhomogeneous system, mainly due to immiscible substrates and inefficient mixing, leading to mass transfer limitations, (iii) batch to batch variation in the degree of conversion, yield and selectivity, (iv) prolonged reaction times, (v) reactions at very low temperatures to reduce the rate of heat generation, (vi) the use of excess nitrating agent, mainly the spent acid, which occupies significant volume, has to be neutralized

thereby needing large quantity of water, and generates inorganic salts. As one or more of these limitations are experienced in every batch operation it is necessary to check their feasibility for continuous flow processing. Such transformations from batch to flow have been carried out for a lot of reactions and many continuous nitration plants of commercial scale exist. However, the real challenge is in taking-up such an exercise for products where these transformations will not only help to overcome safety issues, but also significantly enhance the yield of the desired isomer. Having the importance of nitration in mind and considering the challenges industrial nitration is faced with in terms of the sustainability of individual processes a few large scale consortia have focused on continuous flow nitration using miniaturized devices [20,21].

An analysis of the literature shows that as many as 45% of the nitrations are for liquid phase systems both homogeneous (miscible) and heterogeneous (immiscible) with only 24% for homogeneous systems. Most of the remaining examples involve the substrate in solid phase. Only very rarely is the nitration of gases reported in the literature. Thus, suitable devices and equipment for nitrations are determined by the phases involved and their activity. The presence of multiple phases clearly indicates the choice of substrates explored in the nitrations reported so far and the use of solvents for specific substrates, mainly to maintain the system in liquid phase (although immiscible). More details on the selection of the experimental setup will be elaborated in section 3.

In this review, we analyze recent studies on continuous flow nitration using miniaturized flow reactors. We provide a guideline that helps to quickly decide under which conditions it is worthwhile to conduct continuous flow nitration from a practical point of view. Key features of this report are: (a) a thorough overview on continuous flow nitrations, (b) a discussion on general issues that have to be considered when conducting continuous nitrations, (c) how data from individual reactions are collected and analyzed in order to devise scale-up or numbering-up processes or extend the approach for the continuous preparation of other derivatives and (d) guidelines supporting to identify the best setup for continuous flow nitrations using microreactors.

3 Continuous flow nitration

During World War II, both batch and continuous flow nitration were conducted for the production of different nitroarenes (e.g. nitroglycerin, ethylene glycol dinitrate, diethylene glycol dinitrate, cyclotrimethylenetrinitramine, pentaerythritol tetranitrate, nitrocellulose, etc.). Continuous processes were enforced as they allowed to retain the same scale of operation while keeping the plant size limited [17]. Continuous apparatus for the nitration of solid materials and the production of solid nitrated compounds were commercially used in several European countries. Yet, as of today, a large number of nitrations are still conducted in batch mode across the world. The primary reasons for the batch mode approach are the small scale and infrequent production owing to multipurpose facilities. However, even these small production centers leave a large chemical footprint. Therefore, many examples of efficient continuous flow nitrations have been established in the last few years.

The initial development and demonstration of the continuous flow synthesis using miniaturized devices or microreactors took place in academia and research institutions. The benefits of the approach are particularly evident for highly exothermic reactions and for reactions involving unstable intermediates. Later, this approach was adopted by the industry and feasibility studies on microreactors provided concepts for pilot plant development and commercial scale manufacturing. Early explorations included the nitration of aromatic substrates. Selected references on continuous flow nitration are given in Table 1. In the following, we analyze and discuss important points collected from the literature, which are relevant for the experimental setup, the scale of operation, the reproducibility, the lack of data etc. This examination may be helpful to decide whether the current level of knowledge is sufficient to extend the approach of continuous flow nitration to other aromatic substrates and whether the available data are sufficient to for a scale-up.

3.1 Analysis of the literature

The literature that covers continuous flow nitration can be coarsely classified on the basis of (a) the nitrating agent, (b) the type of reaction device, (c) the property of the system being homogeneous or multiphase, and (d) the exothermic extent of individual reactions. A typical experimental setup for continuous flow nitration includes pumps for the dosing of reactants, a micromixer for the rapid and efficient mixing of these reactants, and a residence time unit, which may be either a microfluidic device with channels or a tube.The residence time unit is either immersed in a constant temperature bath or has built-in cooling/heating systems to maintain a specific temperature. A schematic of such a setup is shown in Figure 2. In Table 1 specific parameters are shown to provide a firsthand overview of the typical conditions and setups. In general, the heat of reaction for all of them ranges from −73 to −253 kJ/mol, and almost all substrates are in liquid phase, propane being the sole exception. Typical residence times are between 5 s to 15 min corresponding to an average heat release rate of −10 to −50 kJ/s/mol. These numbers require a heat transfer area per unit volume between 300 and 2540 m^2/m^3, which corresponds to channel diameters in the range of 0.0016 to 0.013 m. These dimensions are actually close

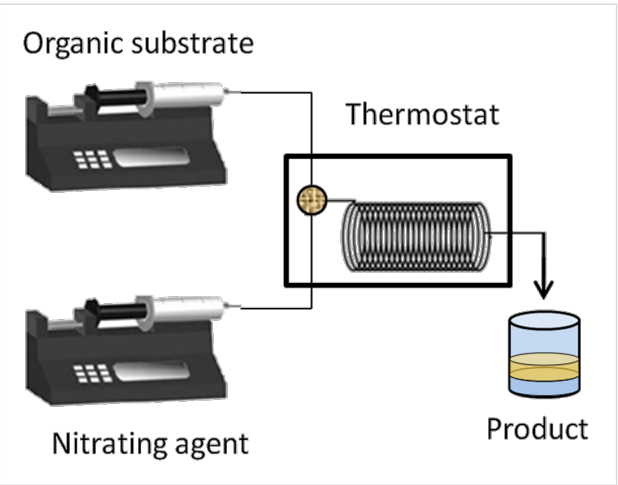

Figure 2: Schematic of a typical experimental setup for aromatic nitration. The circular segment shown inside the thermostat is usually a micromixer.

to the channel diameters used in most of the experiments. In this review, we have classified the literature on the basis of the nitrating agent, so that the comments on hydrolytic termination, isolation and other work-up aspects can be separately applied for each class.

3.1.1 Nitration with mixed acids. As mentioned above 30% of reported nitrations utilize mixed acids as a nitrating agent. The nature of mixed acids varies from system to system. In one of the first feasibility studies under continuous flow conditions Burns and Ramshaw [42] used a simple T-junction with three intersecting channels followed by a coiled capillary (length ~30 cm and 180 cm, i.d. ~0.127 mm to 0.3 mm), which served as a microreactor system. The reactor coil was placed on a hot plate that was insulated with layers of polyurethane foam to ensure a minimum heat loss. The experimental setup resembles the schematic shown in Figure 2. It was observed that the concentration of nitrobenzene increases with reactor length at different concentrations of the sulfuric acid in nitric acid. The initial nitration rates were governed by the kinetics and by mass transfer limitations. Both of these regimes strongly depend on the concentration of sulfuric acid given at a fixed wt % of nitric acid. In case of toluene nitration, at a given fixed composition of the nitrating agent the initial rate doubles with an increase in the reactor temperature from 25 °C to 60 °C over a wider range of inlet flow ratio of the two phases. Interestingly, the initial reaction rates are reported to be higher when the inlet velocity of the reacting mixture is increased, a fact later elaborated in detail by Dummann et al. [43].

Table 1: Summarized literature survey on continuous flow nitration using microreactors (NA: nitric acid, Org: organic substrate).

No.	Author (year)	Substrate	Experimental conditions			% Conversion [% selectivity] (% yield)
			Temp. (°C)	τ (min)	Nitrating agent	
1	Denton et al. [22]	2-nitropropane	204–232	10	70% HNO_3 (NA/Org = 1)	50
2	Veretennikov et al. [23]	chlorobenzene	65	10	97% HNO_3 (NA/Org = 3)	99
3	Anderson [24]	2-amino-6-chloro-4-hydroxy-1,3-diazine	45	2.5	90% HNO_3 (Org + H_2SO_4)	85
4	De Jong et al. [25]	2-amino-4-chloro-6-hydroxy-pyrimidine (+ H_2SO_4)	45	7 h	90% HNO_3 (NA:Org = 3.09:1)	81.60
5	Dagade et al. [26]	toluene	120	–	NA:Org = 0.59:1	55 [73]
6	Panke et al. [27]	pyrazole-5-carboxylic acid (+ H_2SO_4)	90	35	HNO_3 + H_2SO_4	(73)
		2-methylindole (+ H_2SO_4)	3	0.8	$NaNO_3$ + H_2SO_4	(70)
		pyridine *N*-oxide (+ H_2SO_4)	120	78	Nitrating mixture	(78)
		toluene (+ Ac_2O + H_2SO_4)	30	70	neat HNO_3	–
7	Antes et al. [28]	toluene	−10	3 s	NA:Org = 2.56:1	89–92
8	Ducry and Roberge [29]	phenol	45		NA:Org = 1.8:1 (Org:AcOH = 1:6)	75 [79.4] (o:m ~ 1.1)
			20	15	NA:Org = 1.4:1	77 [74.6] (o:m ~ 1)

Table 1: Summarized literature survey on continuous flow nitration using microreactors (NA: nitric acid, Org: organic substrate). (continued)

9	Kulkarni et al. [30]	salicylic acid	50	7	HNO_3 + AcOH (AcOH:Org = 10)	100
10	Pelleter & Renaud [31]	3-methylpyrazole (+ H_2SO_4)	65	90	69% HNO_3 (NA:Org = 13)	[88]
		3-ethyl-1*H*-pyrazole (+ H_2SO_4)	65	25	69% HNO_3 (NA:Org = 33)	[55]
11	Yang et al. [32]	benzene	75	72 s	NA:Org = 3.1:1	44.70 [99.9]
12	Kockmann & Roberge [33]	phenol	20		65% HNO_3 (NA:Org = 1.4:1)	77 [74.6]
13	Shen et al. [34]	isooctanol	35	7.2 s	Nitrating mixture (NA:Org = 1.5:1)	98.20
14	Kulkarni et al. [35]	benzaldehyde	5		Nitrating mixture (NA:Org = 3.5:1)	100
15	Brocklehurts et al. [36]	8-bromo-1*H*-quinolin-2-one	90	3	100 % HNO_3 (NA:Org = 20:1)	100
		1-benzosuberone	10	5	(NA:Org = 10:1)	79
16	Knapkiewicz et al. [37]	2-isopropoxybenzaldehyde	10	5.4 s	red fuming HNO_3 (NA:Org = 6.47:1) (Org + dichloromethane)	65
17	Löwe et al. [38]	propane	385–455	1 s	(NA/Org = 1)	2
18	Gage et al. [39]	*N*-(5-bromo-4-methylpyridine-2-yl)acetamide	0–5	11 h	Fuming HNO_3 + H_2SO_4 (NA/Org = 1.1) (Org+SA)	50 [99]
19	Yu et al. [40]	*p*-difluorobenzene	30–70	0.3–1	Nitrating mixture (SA/NA = 1.8)	98 [99]
20	Chen et al. [41]	*N*-(1-ethylpropyl)-3,4-xylidine	60–90	0.8–9 s	HNO_3 65–98% (NA/Org = 4.3)	100 [92–99]
21	Burns and Ramshaw [42]	benzene and toluene	25 to 60			

Continuous flow nitration of a few important arenes using the standard nitrating mixture in a CYTOS microreactor was carried out by Panke et al. [27]. The nitration product of 1-methyl-3-propyl-1*H*-pyrazole-5-carboxylic acid is an intermediate for the "life-style drug" Sildenafil® (Scheme 1). Similarly, nitration of 2-methylindole, pyridine *N*-oxide and toluene (also with an acetyl nitrate Ac_2O/HNO_3 mixture) were conducted. The conventional procedure for the conversion of 2-methylindole (**4**) into 2-methyl-5-nitroindole (**5**) relies on the addition of $NaNO_3$ in H_2SO_4 to the starting material (Scheme 2) over a period of 1.5 hours. This helps to maintain the internal temperature at 0 °C and gives 80% yield. The continuous laboratory scale process required only 0.8 minutes at 3 °C to obtain 70% yield of the desired nitro derivative. For the nitration of pyridine *N*-oxide (**6**), which requires a higher temperature (~120 °C), the approach using a microreactor resulted in a yield of 78%, an improvement compared to the

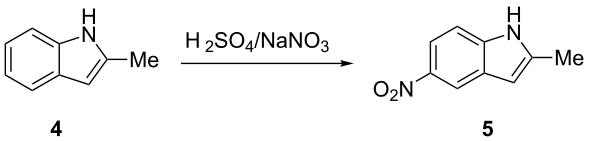

4 **5**

Scheme 2: Nitration of 2-methylindole (**4**). *T* = 3 °C, residence time = 48 s, yield: 70%. [27].

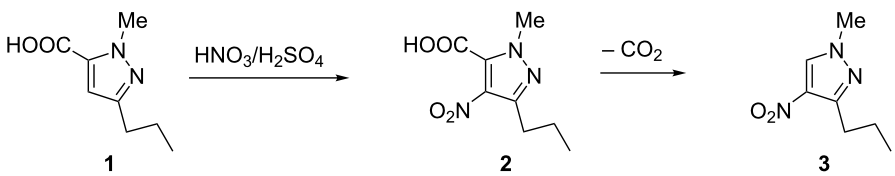

1 **2** **3**

Scheme 1: Nitration of substituted pyrazole-5-carboxylic acid **1**. *T* = 90 °C, residence time = 35 min, yield: 73% [27].

conventional approach (72% yield, Scheme 3). The authors carried out the continuous nitration of toluene (**8**) with the nitrating mixture H_2SO_4/HNO_3 and with acetyl nitrate generated in situ from HNO_3 and Ac_2O (Scheme 4). The first method resulted in >98% conversion and 48%, 36% and 8.2% yields, respectively, for *ortho*-, *meta*- and *para*-mono-nitro isomers. The second method led to a complete conversion with 54%, 39% and 2.7% yields, respectively. The yield of the secondary nitration products was smaller in the presence of acetic anhydride. This observation is important as nitrations that involve acetic anhydride are inherently unsafe, yet the range of conversion and the yields that are achieved will be different depending upon the mechanism.

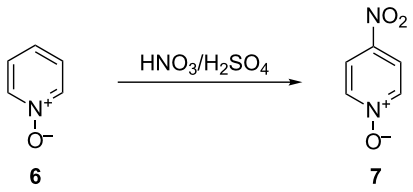

6 7

Scheme 3: Nitration of pyridine-*N*-oxide (**6**), *T* = 120 °C, residence time = 80 min, yield: 78% (72% in the flask experiment) [27].

In general, the dinitroaniline derivatives are produced by nitration of anilines. Chen et al. [41] studied the one-step dinitration that yields *N*-(1-ethylpropyl)-3,4-dimethyl-2,6-dinitroaniline. Under conventional conditions of nitration, oxidation or over-nitration of aniline derivatives is unavoidable, as the reaction rates are strongly limited by interfacial mass transfer due to biphasic conditions. The selectivity of the isomer of interest can be increased by avoiding any pre-protection of the amino groups of aniline derivatives. All the experiments have been carried out in a microreactor (0.2 mL volume) with very high heat and mass transfer coefficient allowing excellent temperature control (<±2 °C) (Figure 3). In the conventional two-step approach the aniline solution (30 wt %) is treated with diluted nitric acid as the first step [44], and after isolation the intermediate is again treated with additional concentrated nitric acid as the second step. The reaction time is 4 hours and the reaction gives 89% yield of pendimethalin (*N*-(1-ethylpropyl)-3,4-dimethyl-2,6-dinitroaniline) and *N*-nitrosopendimethalin with a molar ratio of 7:3. Higher concentrations of nitric acid gave higher degrees of conversion. When carried out in a microreactor the same reaction gives 100% conversion and 97% yield with 3 mol equivalents of nitric acid at 60 °C. The process could be scaled-up up to 432 tons per year and the protocol has been adapted for other aniline derivatives.

Continuous flow nitration of 2-amino-6-chloro-4-pyrimidinol (**14**) for the synthesis of 2-amino-6-chloro-5-nitro-4-pyrimidinol (**15**) and its stable diisopropylamine salt using 90% nitric acid in sulfuric acid are reported by De Jong et al. [25] (Scheme 5). The substrate is dissolved in sulfuric acid and the

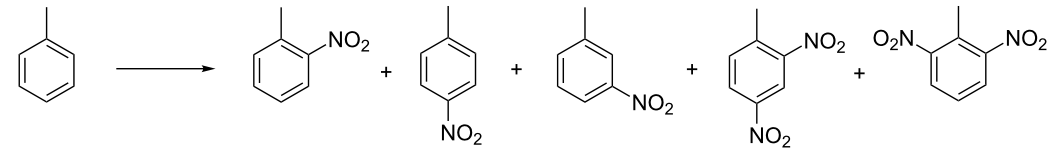

8 9 10 11 12 13

Scheme 4: Nitration of toluene (**8**). Method 1: H_2SO_4/HNO_3, *T* = 65 °C, residence time = 15 min. Method 2: $Ac_2O/H_2SO_4/HNO_3$, *T* = 30 °C, residence time = 70 min (higher selectivity and major products 2-nitrotoluene (**9**) and 4-nitrotoluene (**10**) were obtained in 54% and 39%, respectively) [27].

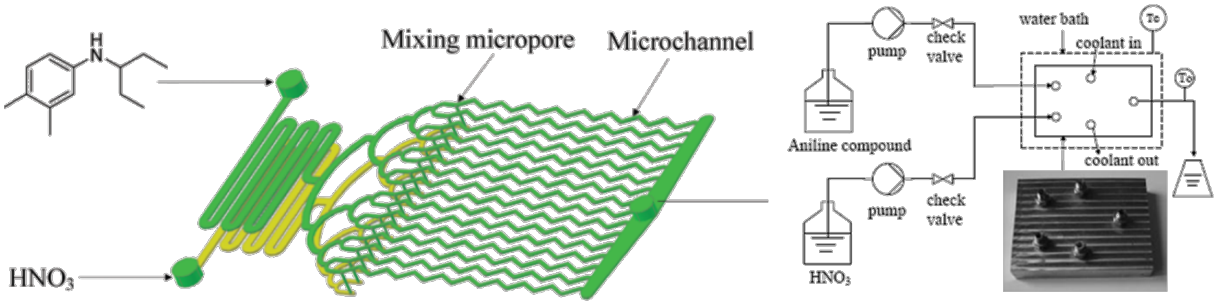

Figure 3: Graphical presentation of a microreactor used for double nitration and the schematic of the experimental setup. The microreactor includes a built-in facility for heat transfer. Reproduced with permission from [41]. Copyright 2013 The Royal Society of Chemistry.

reaction is carried out in a translucent Teflon tube immersed in a constant-temperature bath. Typical residence time of the reaction mixture in the tube was approximately 2.5 min and the outlet mixture was quenched in a tank containing cold water.

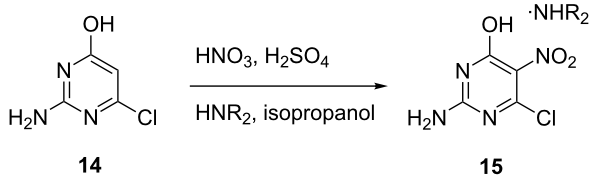

14 15

Scheme 5: Nitration of 2-amino-6-chloro-4-pyrimidinol (**14**) [25].

In another study, Kulkarni et al. [35] showed that the nitration of benzaldehyde (**16**) can be carried out in a safe manner in a continuous mode using a microreactor system (Scheme 6). The performance of this two phase reaction critically depended on the choice of a micromixer. The availability of high heat transfer area helped to increase the reaction temperature to reduce the reaction time to 2 min. Efficient mixing, which can be achieved by using structured micromixers, i.e., caterpillar micromixer, was favored over the simple T-micromixer. The experimental setup consisted of two syringe pumps, which pump the reactants – a nitrating mixture and benzaldehyde – through 20 mL glass syringes connected to SS316 tubes by a glass-to-metal PTFE connector. After the micromixer a hastelloy tube (1.38 mm i.d. and 6 m long) acted as a residence time unit immersed in a thermostat maintained at 5 °C. The contact angles of the aqueous phase on the SS316 ensured that it remained in the continuous phase, while benzaldehyde was present in the form of discontinuous slugs. The authors observed that the rate constant of the reaction leading to the formation of the *meta*-isomer was higher and the rate of change in the ratio of isomers increased with increasing amounts of nitric acid. The greatest mol fraction of the *meta*-isomer **17** was obtained when the HNO_3 was employed in 3.5 equivalents of **16**. The same reaction was conducted with a nitrate mixture composed of sulfuric acid, nitric acid and acetic anhydride, which led to a homogeneous system. However, an over-oxidation of **16** was encountered due to the presence of acetic anhydride, so that benzoic acid was formed. The poor solubility of benzoic acid in the aqueous phase led to an immediate clogging of the tubular reactor. This undesired clogging occurred under a wide range of temperature and residence time conditions thereby preventing a successful nitration. This example illustrates that a homogeneous reaction mixture is not a sufficient condition to successfully transform a known nitration into continuous mode, the handling of the solubility of the undesired solid has to be considered as well. This issue was finally dealt with by dissolving the benzoic acid in a suitable solvent (*n*-hexane), which also reduced the reaction time to a few seconds. However, even though the conversion of benzaldehyde was complete, the presence of acetic anhydride resulted in a significant change in the isomeric ratio and yielded many undesired products. In another example, continuous flow nitration of salicylic acid (**19**) with HNO_3/AcOH was performed by Kulkarni et al. [30] in a SS316 tubular microreactor. Compound **19** was completely converted to mono-nitro derivatives in less than 7 min, and afforded 5-nitrosalicylic acid (**20**) as the major product (Scheme 7). A large excess of acetic acid in the reaction mixture was necessary to avoid precipitation of the desired product **20**. The authors reported the formation of byproducts when the reaction was conducted at higher temperatures. Continuous operation for 2 hours consistently yielded the same composition at the outlet. In a more detailed work, these authors showed the importance of heat transfer for the continuous flow nitration of salicylic acid, as poor heat transfer can give a higher conversion rate but lower selectivity for the desired product. Contrary to a patent description [45], glass is less suited than metal SS316 or Hastelloy due to lower thermal conductivity. Thus, the choice of material of the reactor plays a significant role in controlling the yield and selectivity of the desired product.

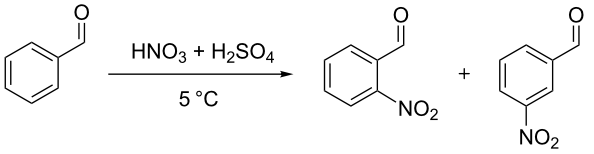

16 17 18

Scheme 6: Nitration of benzaldehyde (**16**) [35].

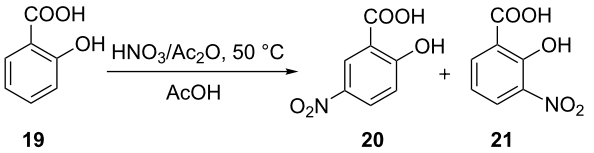

19 20 21

Scheme 7: Nitration of salicylic acid (**19**) [30].

Ducry and Roberge [29] used a glass microreactor with <0.5 mm channel width and 2.0 mL internal volume for the continuous flow nitration of phenol (Scheme 8). The nitration was investigated with a wide range of phenol concentrations as well as different equivalents of HNO_3. Acetic acid was used as a solvent. Experiments were also carried out with 10% water instead of an organic solvent. In the absence of a solvent the results from the continuous flow experiment turned out to be superior to batch experiments with a significant increase in the formation of mono-nitro products. The authors reported that

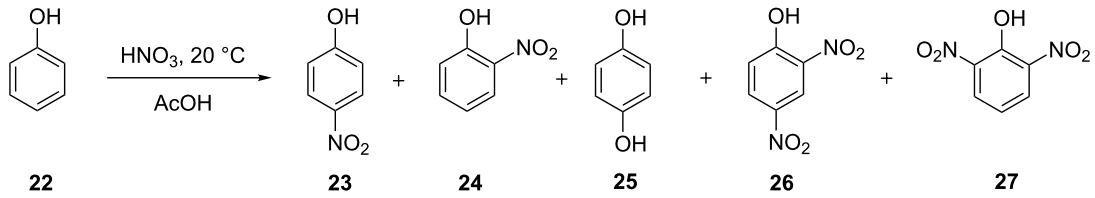

Scheme 8: Nitration of phenol (**22**) yielding mono-nitro isomers **23** and **24** as main products, hydroquinone (**25**), dinitrophenols (**26** and **27**), and polymeric side products.

with 1.4 equivalents of nitric acid at 20 °C a yield of 77% of mono nitrophenols can be achieved.

An important example of continuous flow nitration leading to alkyl nitropyrazoles was reported by Pelleter and Renaud [31]. The nitration products 3-methyl-4-nitropyrazole (**29**), 3,5-dimethyl-4-nitropyrazole (**31**) and 3-ethyl-4-nitropyrazole (**32**) were obtained with nitrating mixture and were expected to show detonating properties under severe confinement (Scheme 9). This flow synthesis did not allow the pressure inside the reactor to undergo rapid variations in a short time, thereby increasing the safety of this synthesis approach. The experimental setup for this nitration is shown in Figure 4. The set-up is similar to the systems used in the literature except that a back pressure regulator was used to ensure that any pressure variations during synthesis are suppressed to avoid any critical situation. It is important to note that the pyrazole was nitrated after dissolving it in the sulfuric acid. For a reactor of 10 mL volume, the temperature was maintained at 65 °C, and the hydrolysis was carried out by dropping the reaction mixture into a cold aqueous solution saturated with potassium carbonate. The residence time for the synthesis of compounds **29** and **31** was 90 minutes, while it was 25 minutes for compound **32**. The formation of dinitro derivatives can be prevented by a strict temperature control. While the authors indicate that a higher amount of products may be synthesized by increasing the number of micromixers and extending operating hours, specific calculations on the economic viability are not given. A longer residence time leads to lower flow rates and thus to laminar flow conditions. In spite of a higher heat transfer area, such conditions do not offer high heat transfer rates and result in axial dispersion. Consequently, restricting the temperature below 65 °C can avoid the dinitro products, ensuring that the reaction mixture is locally homogeneous. One of the ways to reduce the axial dispersion is a segmented flow, which is implemented by using an inert gas or immiscible inert liquid. However, under such conditions it is essential to ensure a continuous mixing along the length of reactor. In this report, the authors used excess acid. While it may be required for a reaction to keep the entire mixture homogeneous, the overall process suffers from a neutralization step to isolate the product. However, since the large-scale synthesis of nitropyrazoles is not a safe reaction under batch conditions, the continuous flow synthesis is the process of choice.

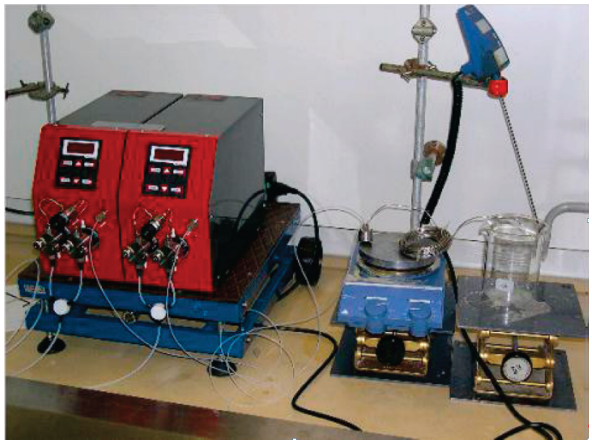

Figure 4: Photograph of the experimental setup for the synthesis of alkyl-nitropyrazoles. IMM's SIMM-V2 micromixer was used to ensure better mixing at the cost of pressure drop. Reproduced with permission from [31]. Copyright 2009 The American Chemical Society.

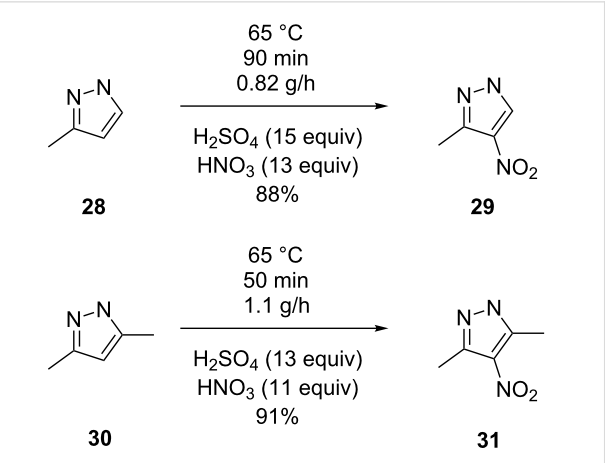

Scheme 9: Synthesis of 3-methyl-4-nitropyrazole (**29**) and 3,5-dimethyl-4-nitropyrazole (**31**) [31].

Henke and Winterbauer [46] reported a corrosion resistant microreactor built up of PTFE and tantalum for the simulation

of different nitration reactions. The microreactor proposed for this adiabatic nitration included components made in tantalum and PTFE connected in series. In the reactor, the dimensions of the components vary along the length and thus they induce mixing, initially of sulfuric acid with nitric acid and later with benzene. Orifices with different diameters induce different flow regimes in the reactor. The authors claim this microreactor has infinite scalability, as it is based on the addition of different components in sequence. In one of the first reports on the continuous flow nitration of benzene without the use of sulfuric acid Othmer et al. [47] used a column (1 inch diameter and 1.22 m long) that was attached to a reflux condenser, which led into a decanter. It was reported that the continuous nitration plant is advantageous over the batch process in terms of greater production capacity per man-hour and per square foot of floor space. Furthermore, the mixed acid can be avoided. The raw material costs are also lower due to a virtually quantitative conversion. However, the major disadvantages of the continuous process are associated with the comparatively higher costs of the reactor and additional equipment materials, which are required to be composed of stainless steel or other resistant material.

Dummann et al. [43] used a capillary-microreactor for studying the nitration of a single aromatic ring. The authors did not provide details about the specific aromatic substrate. Nevertheless, the observations are useful in giving a fair idea on what to expect and what to consider from a nitration reaction in general. In their approach they restricted their analysis to the nitration of monocyclic aromatic substrates with mono and dinitro derivatives as products and a phenolic byproduct. The experimental setup consisted of a Y-piece followed by a capillary-microreactor (PTFE capillary ~ i.d. = 0.5 to 1.0 mm) immersed in a thermostated jacket. This jacket was maintained at a constant temperature between 60 to 120 °C by using a countercurrent flow of silicone oil at high flow rates. This setup is similar to the one shown in Figure 2, but adds a quenching line to quench the reaction inline by rapidly reducing the temperature to 20 °C for a specific section of the reaction tube. The reaction is carried out under pressure (~4 bar) to avoid any degassing from the reaction mixture. From various experiments under different conditions the authors observed that increasing the flow velocity actually increases the degree of conversion along with an increase of the byproduct due to parallel reaction and reduces the byproduct due to sequential reaction. Consequently, controlling the residence time distribution and the heat transfer rates allows for a restricted formation of byproducts from the sequential reaction. With an increase of the fluid velocity the overall mass transfer coefficient was found to increase. It seems that a higher fluid velocity facilitates the rapid mixing of the two reagents and thereby enhances the heat generation rate in the system. Given a constant heat transfer area, although the heat transfer coefficient increases with an increasing velocity, a higher rate of heat generation causes a rise in the local temperature thereby enhancing the rates for parallel reactions. A control of the residence time supports the avoidance of byproducts from sequential reactions. This observation is common for all systems and thus it is necessary to optimize the energy balance in the system depending on the heat transfer rates, the heat of the reaction and the inlet flow rates.

Veretennikov et al. [23] reported on the continuous flow nitration of chlorobenzene (**33**) for the production of mono-nitrochlorobenzene (**34**, **35**) by using 75–97% nitric acid in a series of continuous stirred reactors (Scheme 10, Figure 5). The reactors were made from 1Cr18Ni10Ti steel and the reactor volume was 60 mL. The experiments were carried out over a range of 65–85 °C at a molar ratio of nitric acid to chlorobenzene in the range of 1.5 to 3. The authors have reported the highest yield of mono-nitrochlorobenzene (98.2%) at a molar ratio of 3 with 90% nitric acid, 75 °C and 45 minutes residence time. The third reactor is used for hydrolysis by water addition. The authors have quantitatively measured the role of hydrolysis on the basis of the precipitated products and suggested a method for the selective separation of nitrobenzene **34** by exploiting the principle of preferred solubility domain.

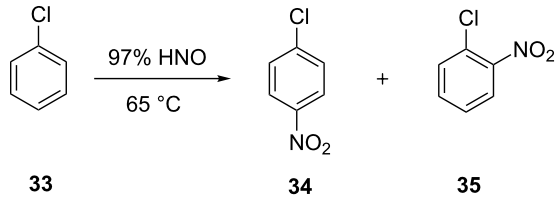

Scheme 10: Nitration of chlorobenzene (**33**) [23].

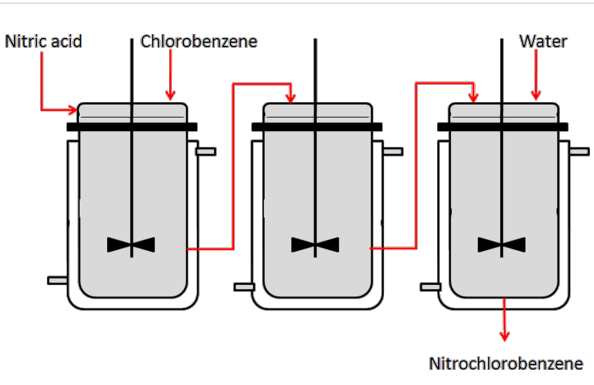

Figure 5: Continuous flow nitration of chlorobenzene (**33**) with nitric acid in a sequence of continuously stirred reactors [23].

In a similar approach, a single continuous glass/Teflon stirred tank (CSTR) with a volume of 1.06 L (d = 9.5 cm, h = 15.1 cm) was used by Quadros et al. [48] for the adiabatic nitration of benzene witth mixed acids. The pilot-scale continuous stirred reactor was operated at a temperature range of 80–135 °C with 4.9–5.6 wt % HNO_3. At fixed residence time and fixed concentration of sulfuric acid, adiabatic rise in the local temperature was observed. The fraction of mono-nitrobenzene in the reaction mixture increased with increasing impeller speed, which clearly indicated that the reaction was mass transfer limited. The authors showed that the kinetic parameters are a function of the sulfuric acid concentration, which acts as a catalyst. While the adiabatic operation was shown to work in this case, the set of optimal conditions or the effect of various parameters on the yield of the product was not reported.

3.1.2 Nitration with fuming nitric acid. The use of sulfuric acid or any other acid in combination with nitric acid leads to the rapid generation of nitronium ions in their ionic form stabilized by water. However, the application of these nitration conditions under continuous flow conditions in a pilot plant setup or commercial large-scale process, results in economic as well as environmental problems as the sulfuric acid has to be neutralized and substantial amounts have to be separated, which entails additional process equipment of the plant. Fuming nitric acid allows for the avoidance of sulfuric acid and also reduces the chemical footprint of the nitration systems. We discuss here the flow nitration with fuming nitric acid without reviewing the mechanism in detail.

The continuous flow nitration of 2-isopropoxybenzaldehyde (**36**) with red fuming HNO_3 has been reported for the first time by Knapkiewicz et al. [37] (Scheme 11). The product 2-isopropoxy-5-nitrobenzaldehyde (**37**) is an intermediate to obtain a nitro-substituted Hoveyda–Grubbs catalyst. Scale-up based on the conventional batch approach yielded a higher extent of the undesired regioisomer **38** (37% rise than the laboratory scale batch). The selectivity of the desired product **37** was improved under flow conditions. A continuous flow silicon-glass microreactor equipped with multiple functionalities such as multistream micromixer, reaction channel, large-area cooling chamber, and five integrated miniature temperature sensors was used (Figure 6). At the reactor outlet compound **37** was collected in ice water for 120 min followed by separation and isolation of the organic layer. While the batch experiment yielded only 30% of the desired nitro derivative **37**,

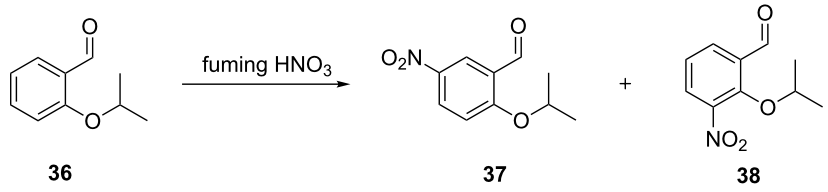

Scheme 11: Nitration of 2-isopropoxybenzaldehyde (**36**) by using red fuming nitric acid [37].

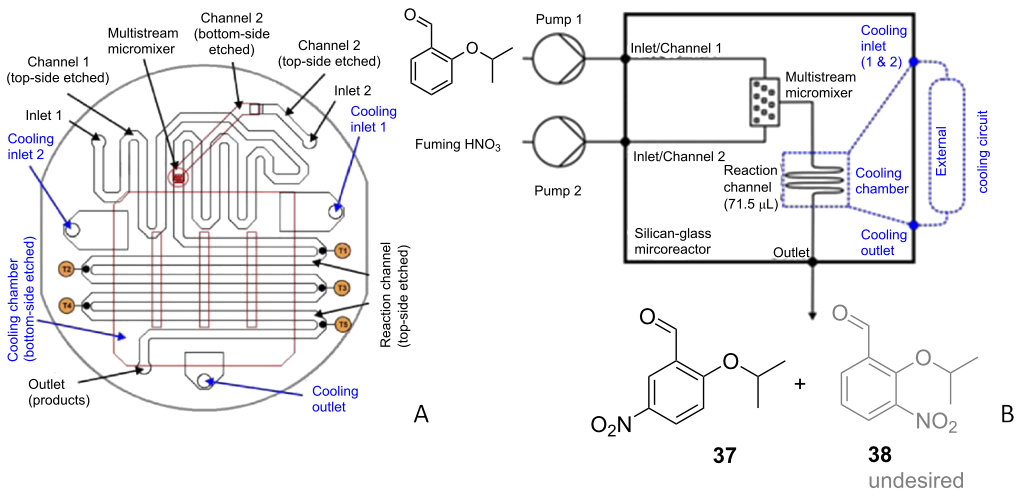

Figure 6: Silicon-glass microreactor by Knapkiewicz et al. [37]. (A) Layout of the microreactor with a built-in micromixer, (B) schematic of the experimental setup. Reproduced with permission from [37] Copyright 2012 The American Chemical Society.

the continuous flow process yielded close to 67% yield at a comparable scale.

Gage et al. [39] developed a simple and practical flow reactor to produce nitropyridine in an exothermic nitration reaction (ΔH ~ −167 kJ/mol). Their approach is suitable for large-scale productions of up to hundreds or thousands of kilograms of nitroaromatics, Typically nitropyridine is prepared in batch mode by dissolving 5-bromo-2-amino-4-methylpyridine (**39**) in concentrated sulfuric acid, to which fuming nitric acid is added at 25−33 °C. The reported yield of the desired product is 52−55% (Scheme 12).

The experimental setup included the feed vessels, the mixer, the residence time loop, and a collecting vessel, all of which are connected by stainless steel tubing and ports (Figure 7). The reactant **39** was dissolved in H_2SO_4 (1/3 wt/wt) and HNO_3/H_2SO_4 (~1/12 wt/wt). 97% conversion is achieved in 20 minutes residence time at 50–55 °C reactor temperature.

Scale-up was possible by using a larger apparatus consisting of a 45 m long reactor tube (15 mm i.d.) with a total volume of 7.95 L. The flow of reactants was achieved by applying nitrogen pressure on the feed tanks (Figure 7). The authors demonstrated their concept for larger flow rates (70 mL/min)

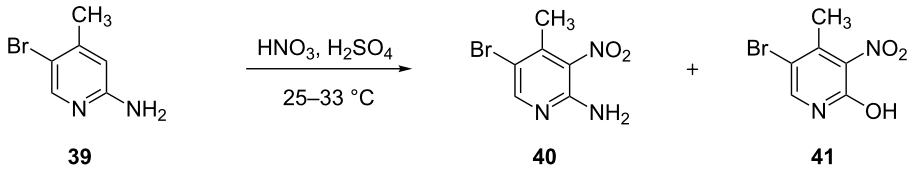

39 **40** **41**

Scheme 12: Synthesis of nitropyridine (**40**) [39].

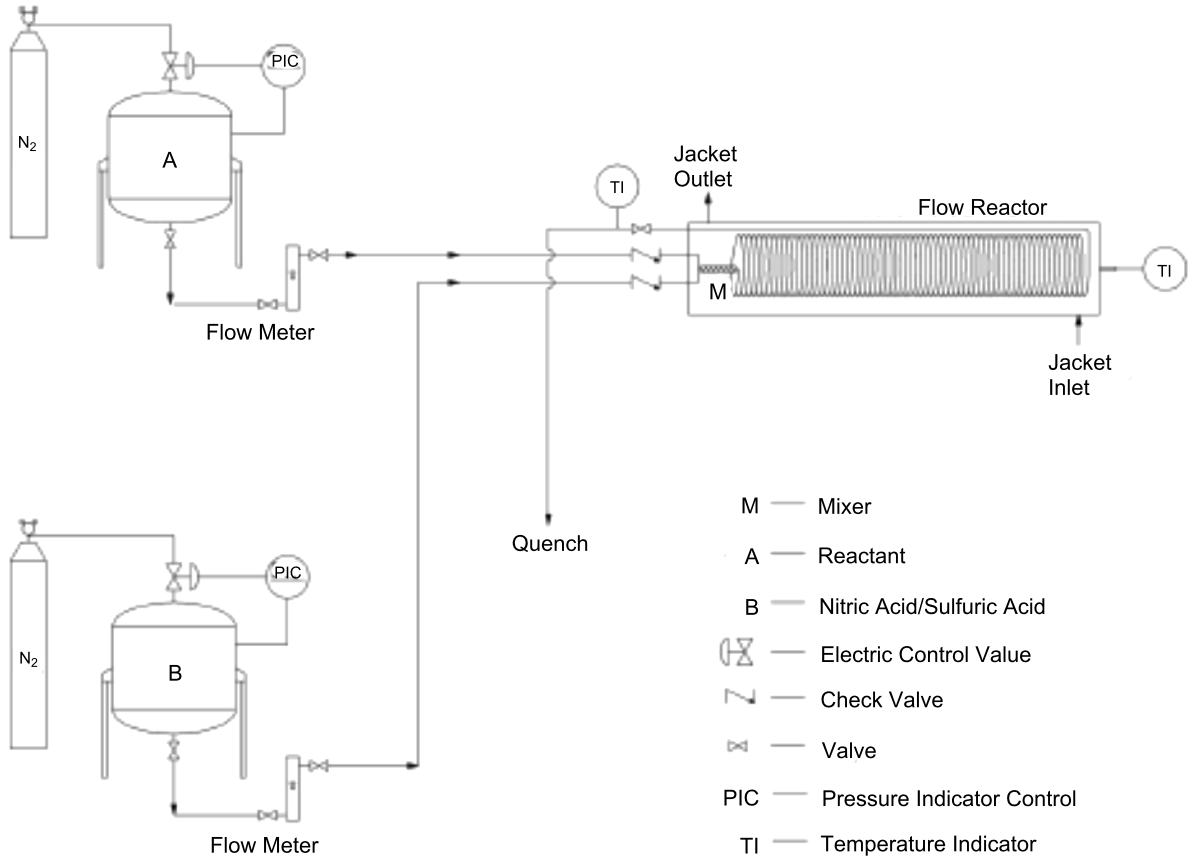

Figure 7: Schematic of the experimental setup involving a pressure based charging system [39]. Reproduced with permission from [39]. Copyright 2012 The American Chemical Society.

with an isolated yield of 59% for nitropyridine **40**. However, the approach requires a pre-calibration of the flow meters depending upon the density of the fluids. Although the reported variation in the flow rates was 4%, this results in a variation of the local concentration, so that an inhomogeneous conversion pattern is obtained. Obviously, the scale-up experiments gave much lower yields than the theoretical value, which indicates that temperature control is an important issue to ensure the desired heat transfer. Furthermore, uniform distribution of residence time and continuous product monitoring is necessary to avoid a runaway reaction in the flow reactor.

Yu et al. [40] reported on the continuous flow process for the synthesis of 2,5-difluoronitrobenzene (**43**) via nitration of *p*-difluorobenzene (**42**) with a nitrating mixture composed of 2.0 equiv concentrated sulfuric acid and 1.1 equiv fuming nitric acid (Scheme 13). Two different approaches were tested. In the first approach, the reactants were continuously mixed by using a T-mixer followed by a tubular reactor maintained at a constant temperature (10–15 °C). Hydrolysis was carried out with ice water (~20 mol per mol of the reactant). The usage of a single tube facilitated a higher isolated yield of isomers **43** and **44** with increasing residence times. However, the conversion was only 76% and an increase of the temperature entails a higher amount of byproducts. Although the authors regard the phase separation accountable, usually it remains in the slug flow unless the aromatic substrate is soluble in the nitrating agent. Typically the slug flow gives excellent interfacial mass transfer rates due to continuous surface renewal as the slugs travel through the tubular reactor. Thus, the phase separation actually may not be the reason for the lower conversion. An increased conversion could be possible by further increasing the residence time or by providing the necessary concentration of nitric acid to achieve the desired D.V.S. value for this system. The mass transfer rates can be enhanced by increasing the flow rates. However, for a given tubular reactor at a constant flow rate the reaction rates can be enhanced by increasing the temperature. Furthermore, a smaller concentration of nitronium ions also affects the reaction rates, provided the nitric acid is used in significant excess [16]. The residence time was varied by using tubes of different lengths at identical flow rates. This approach is particularly important because a change of flow rates to vary the residence time usually entails different implications, such as influencing the mixing and heat transfer during mixing of the reagents. At a fixed tube length smaller residence times are achieved by increasing the flow rates leading to a better mixing and a better convective heat transfer. However, high flow rates lead to an increased overall heat generation rate for a fixed heat transfer area, which can enhance the reaction rates. On the other hand, a variation of the tube lengths for fixed flow rates gives more consistent data as the inlet conditions are fixed and the flow pattern or the velocity profiles in the reactor remains unchanged due to constant flow rates.

In order to achieve complete conversion the experimental setup (Figure 8) involved three sections. The first two sections were run at a residence time of 1 min while the third one was run with a residence time of 20 s. Each section was maintained at a different temperature, more specifically 30–35 °C, 65–70 °C and −5 to 0 °C, respectively. The role of the last segment was to quench the reaction. This setup is reported to achieve 98% yield for the desired product at a rate of 6.25 kg/h. Lower reaction rates due to the continuously reducing concentration of nitric acid along with the reactor length was compensated by an increase of the temperature and also by keeping an optimal residence time. The observations indicated that the smaller diameter reactor tubes yielded more side products. On the other hand, a larger diameter reactor led to lower conversion rates. Although the authors have recycled and reused the nitrating mixture by adding make-up nitric acid for some of the experiments, further optimizations are necessary to achieve an economical process.

In a novel approach, Antes et al. [28] disclosed (i) online monitoring of nitrations in microreactors by using FTIR microscopy as well as thermographic methods and (ii) the continuous separation and detection of the nitration products by using HPLC. In order to avoid a post treatment of the mixed acids in the conventional approach, the authors used fuming nitric acid. The experimental setup comprised three independent pumps for toluene, fuming nitric acid, and ice-water. The reaction took place in a silicon microreactor consisting of nine reaction chan-

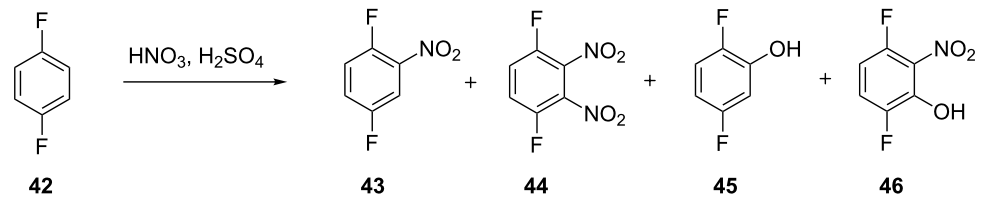

Scheme 13: Nitration of *p*-difluorobenzene (**42**) [40].

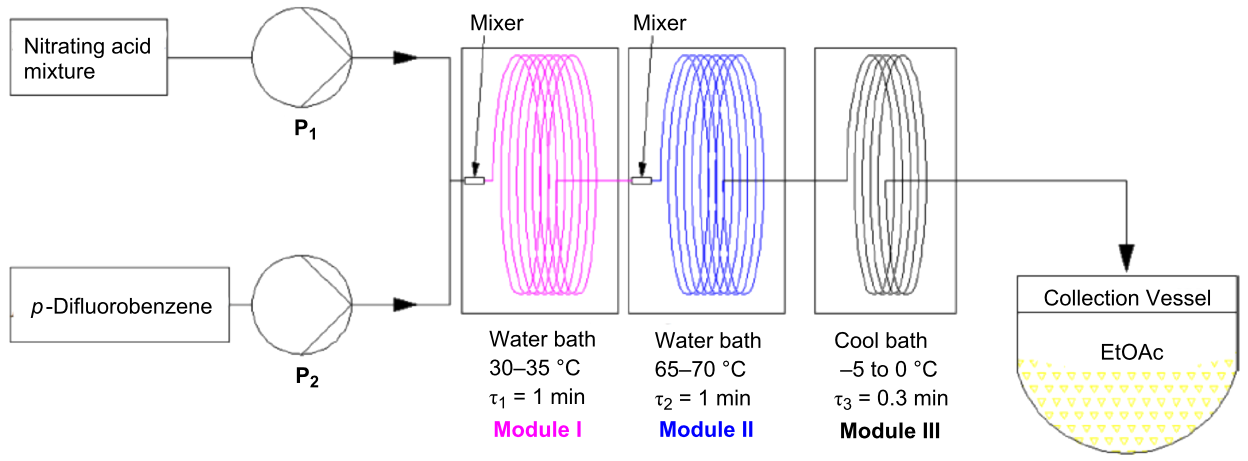

Figure 8: Schematic of the flow reactor arrangement. Reproduced with permission from [40]. Copyright 2013 The American Chemical Society.

nels in parallel (0.25 mm channel width) with a G-shaped micromixer. The design has G-shapes in alternate directions, which cause a continuous change in the flow direction, splitting and recombining. The highest yields for mono-nitrotoluenes (89–92%) were obtained at −10 °C and in a residence time of 3 s by using 2.56 equivalents of nitric acid per mol of toluene. The experiments using the microreactor yielded a 10% rise in the *para*-isomer compared with the industrial batch process. A similar approach was used for the nitration of thioureas, and the authors showed by online FTIR spectroscopy that the mechanism of the nitration of thioureas is based on subsequent nitrosation and nitration steps.

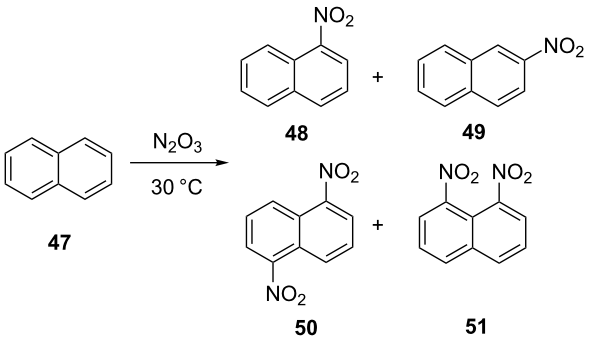

Scheme 14: Nitration of naphthalene (**47**) [34].

The same group also analyzed continuous processes to perform the strongly exothermic nitration of naphthalene (**47**) (Scheme 14) with N_2O_5, both in the gas phase and in the liquid phase [49,50]. The authors reported that the nitration with the conventional batch method requires a cooling to temperatures between −50 to −20 °C, while the same reactions can be carried out in a microstructured flow reactor at 30 °C with a residence time of just 3 s. The outlet product composition contains both, the mononitro derivatives as well as the dinitro compounds. In macroscopic batch reactors the isomer ratio of **50** and **51** is always ca. 1:3.6, while the flow synthesis yielded more 1,5-dinitro compound **50** (**50**:**51** ~1:2.8). The isomer ratio of mononitronaphthalene products **48**:**49** could also be changed to 32:1 in a microreactor, while the typical isomer ratio in industrial processes is 20:1.

In another example of producing energetic materials using microreactors, Shen et al. [34] reported the two phase nitration of isooctanol and a mixed acid to produce 2-ethylhexyl nitrate. A SS316 microreactor was used, in which the mixing of the reagents occurred after the distribution of the first reactant (Figure 9), and the reaction took place in 78 mm long parallel microchannels (0.5 mm × 0.5 mm) connected to a common outlet. The hydrolysis and instantaneous termination of the nitration reaction occurred outside the microreactor by rapid dilution of the reaction mixture with an ice-water mixture at 0 °C. The experimental observations showed that for an identical residence time and in the presence of 2% H_2O (by mass), the conversion of isooctanol was unaffected by changing the sulfuric acid concentration from 67% to 86% (by mass). The amount of sulfuric acid and the residence time corroborated the expected trends in this two phase nitration reaction. However, the authors have justified their observations on the basis of the interfacial mass transfer rates. For this system, the range of flow rates covers different flow regimes, namely, the parallel flow with a smooth interface, the parallel flow with a wavy interface, and the chaotic thin striations flow. Since the overall reaction rates are controlled by interfacial mass transfer, an increase in the linear velocity results in higher average reaction rates. An excellent mixing and control on mass transfer rates allows carrying out this reaction safely and stably in the specially

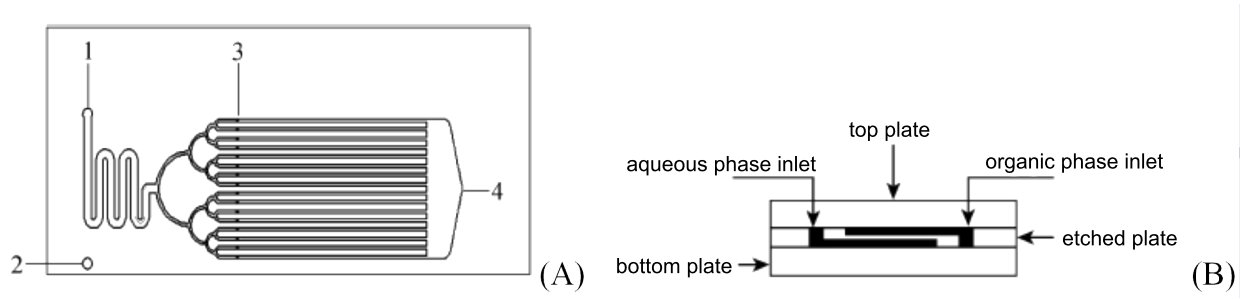

Figure 9: Structure of the microreactor. (A) Top view (1, 2 – inlets, 3 – mixing points, 4 – outlet). (B) Lateral view of the inlets for the microreactor. Reproduced with permission from [34]. Copyright 2009 Elsevier.

designed microreactor at 25-40 °C with 98.2% conversion of isooctanol an no byproducts.

3.1.3 Vapour phase nitration. In an early study on the continuous flow nitration of 2-nitropropane (**52**), Denton et al. [22] demonstrated that high pressure and high temperature conditions, i.e., 900 to 1200 psi and 203–232 °C, using an equimolar nitric acid (70%) gives about 50% yields per pass (Scheme 15). Their reaction assembly consists of a stainless steel preheater tube (outer diameter of 6.24 mm) passed through a 40 inch long 20 mm outer diameter. The reactor was packed with glass beads to increase the contact surface and mixing [51]. A water condenser was used for quenching the reaction by cooling, followed by a pressure reduction to atmospheric pressure by using a needle valve, which was further cooled by means of an ice condenser followed by a gas–liquid separator.

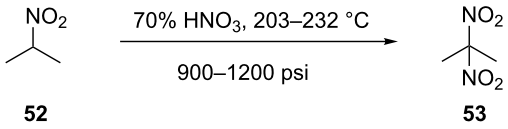

Scheme 15: Nitration of 2-nitropropane (**52**) [38].

Similar to the aforementioned study, Löwe et al. [38] reported the vapor phase nitration of propane in a multistep microreactor in a highly sophisticated and safe system. Different steps in the process are integrated in a single reactor. While the reaction occurs at high temperature (380–450 °C), the quenching was performed by hydrolysis as well as by rapid cooling of the diluted reaction mixture. The term per-pass conversion is used when the unreacted reactant is recycled back to the inlet. If no such recycling is carried out, the per-pass conversion is estimated on the basis of the total reactant used in the reaction. The per-pass conversion was maintained at 2% at the cost of selectivity for 2-nitropropane (**52**), which gets significantly affected by the residence time. The authors employed an integrated single flow reactor composed of a special stainless steel alloy (1.4361, X1CrNiSi18154). Electrical heaters and two integrated water coolers were used for heat transfer in different sections of the integrated reactor. The integration of these functions in one setup facilitates the handling of hazardous chemicals at higher temperatures and avoids any release of toxic gases into the environment.

A corrosion resistant glass syringe pump was used for pumping the nitric acid to the evaporator section, which upon mixing with pre-heated propane proceeded to the heated reaction section, whose temperature was maintained between 380 and 455 °C. At the outlet of the reaction section, the reaction mixture was diluted with water by an integrated caterpillar micro mixer and subsequently sparged through an ice-water filled flask to condense volatile nitric compounds outside the integrated microreactor. Reaction optimization was conducted over a wider range of mol ratio of the reactants (propane:HNO_3 ~ 0.5 to 6), different residence times (0.4 to 2.5 s), and gas flow velocities between 5 and 0.9 m/s. An analysis of the exit stream revealed the formation of 2-nitropropane, 1-nitropropane and nitroethane. At a residence time of 1 s, the yield of 2-nitropropane was independent of the temperature. However, an increase in temperature entailed a decrease in the yield of 1-nitropropane and vice versa for nitroethane. At a constant temperature the mol fraction of 2-nitropropane was (i) independent of the residence time at a constant inlet mol ratio and (ii) decreased with an increasing inlet mol ratio of propane to nitric acid. The authors concluded that the microstructured reactors are not advantageous for this case, because the rapid quenching of the radical chain mechanism causes a lower conversion. The important consequences of this work are (i) the development of an integrated microreactor concept, (ii) issues related to safety and operation are improved significantly to ensure that the toxic chemicals do not escape throughout the process, (ii) the authors conclude by saying that a holistic process design approach should not be overlooked without focusing entirely on using the “micro reactor” concept.

3.1.4 Nitration with solid acid catalysts. The continuous flow vapour phase nitration using a solid acid catalyst has also been explored [26]. It is known that the solid acid catalysts, i.e., ZSM and other zeolite catalysts, can improve the selectivity of *p*-nitrotoluene in a conventional reactor using a mixed acid as the nitrating agent [52,53]. Continuous flow nitration of toluene in a packed bed microreactor using concentrated nitric acid as the nitrating agent was reported by Halder et al. [54]. Different 'solid acid' catalysts were studied to identify the right catalyst that would yield better isomer distribution. In such cases, self-protonation of nitric acid drives the reaction rapidly, and the isomer ratio of nitrotoluenes remains similar to the standard nitrating mixture and without byproducts. However, in the microreactor, concentrated nitric acid reacted very rapidly in the absence of any sulfuric acid or a solid acid catalyst. Nitric acid and toluene were brought into contact by using a SS316L T-mixer (1.58 mm inner diameter) at room temperature. The immiscible reactants were passed through a tubular microreactor (SS316L, i.d. = 0.775 mm, l = 8.5 cm) packed with different solid acid catalysts (Stevens catalysts A and B, ZSM-5-280). In the fixed bed microreactor, 13 mg of catalyst (d_p = 75–150 μm) was packed over 6.0 cm distance, after which the remaining reactor length was filled with smaller inert glass beads (20 mg, d_p = 63–75 μm) to prevent the carryover of any fine catalyst particles and subsequent clogging of the filter placed at the end of the reactor. The nitration was terminated by collecting the product in a sodium carbonate solution. Most of the conversion took place outside the solid acid catalyst bed. Moreover, the nitration of toluene with 90 wt % nitric acid using a microreactor was found almost entirely preceded under kinetic control. However, with only nitric acid as the nitrating agent, the nitrotoluenes were generated in a low yield. The formation of water adversely affected the availability of nitronium ions. This can be overcome by using sulfuric acid which reacts with the formed water. Thus, the optimal conditions can be achieved by increasing the temperature to a limit that does not lead to runaway conditions.

Recently, Yang et al. [32] studied the nitration of benzene in a continuous flow microreactor loaded with a microfiber structured Nafion/SiO_2 solid acid catalyst. The catalyst was prepared by using the solgel technology that leads to coating on the surface of the microchannel reactor (thickness ~200–400 nm particles). Consequently, a slightly porous surface is formed that is able to improve the mass transfer rates in close proximity to the reactor wall. At 75 °C and a 36% (w/w) loading of the microstructured solid acid catalyst, the authors have reported 44.7% conversion of benzene with a 99.9% selectivity of nitrobenzene. At an equivalent conversion level, the microstructured Nafion/SiO_2 catalyst was 600 times more effective in terms of activity per acid site compared to the liquid sulfuric acid. However, in order to practice this approach, the following information may be useful: (i) the longevity of the catalyst (turn over number) under different situations, (ii) the stability of the catalyst and the support under different aqueous and organic compositions, and (iii) the method of catalyst deposition.

3.2 Analysis of recent patents

The continuous flow nitration of naphthalene-2,7-disulfonic acid leading to 1,8-dinitronaphthalene-3,6-disulfonic acid has been disclosed in CN102320995A [55] using mixed acids (Figure 10). The inventors have studied the performance by varying the reaction temperature between 35 and 120 °C and the reaction time up to 120 minutes. Examples were reported for the nitration at 50 °C for a residence time of 60 minutes that allowed an adiabatic temperature of less than 160 °C. Additional examples with a tubular reactor equipped with packing Raschig rings and SV static mixers are also mentioned.

In a very interesting method disclosed in CN103044261A [56], continuous centrifugal extractors were used for nitrations. The simultaneous addition of the mixed acid solution as a heavy-phase and the raw material (substrate) as a light-phase to different centrifugal extraction separation devices facilitates the

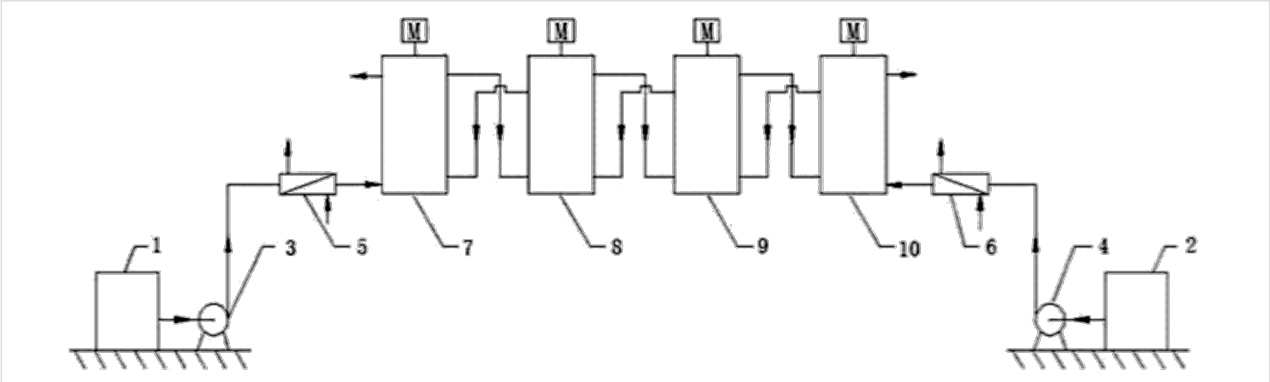

Figure 10: Schematic of the continuous nitration system reported in CN103044261A [56].

reaction and extraction to be achieved simultaneously. The system works in a counter current mode. The reaction temperature and the rotating speed of the centrifuge were varied between 10 to 160 °C and 800–2000 r/min, respectively. The invention claims to achieve a continuous compact automated device that can be used for the large-scale production and isolation of the organic and aqueous streams. The inventors reported the nitration of aromatic hydrocarbons, namely benzene, toluene or chlorobenzene and polyhydric alcohols such as glycerol or 1,2,4-butanetriol. The flow reactor size is claimed to be reduced to 0.6 to 1% of the conventional batch reactor for identical production capacity.

In a novel approach, US20130197268A1 [57] discloses an invention for the continuous nitration of benzene with a mixture of nitric acid and sulfuric acid under adiabatic conditions for producing nitrobenzene. The sulfuric acid was recovered and recycled by evaporating water, unreacted benzene and nitrobenzene by low pressure distillation. The heat integration was achieved by using the adiabatic heat for benzene recovery, and the pre-purification of nitrobenzene by distillation.

4 Nitration: from laboratory synthesis to process

Continuous flow nitration using miniaturized devices is an excellent approach to avoid issues related to heat transfer, mass transfer, homogeneity inside the reactor, and mixing. Large-scale continuous flow nitration was implemented in selected cases, mainly for basic organic substrates. At this stage, aromatic nitrations, whose process economics are significantly affected by the selectivity of specific isomers, are considered for the continuous flow approach. In addition to a few important issues, two parameters that help to tune the isomeric ratio of products will be discussed with the objective to illustrate the development from a synthesis procedure to an actual process.

4.1 Nitrating agents used under continuous flow conditions

For industrially important aromatic nitrations the conventional nitrating mixture (40:60) and the mixture of sulfuric acid with fuming nitric acid are the nitrating agents of choice. The advantages of using the nitrating mixture as nitrating agent are known and the use of sulfuric acid in large quantity, which promotes the generation of nitronium ions and the absorption of the generated water is ideally suited for many cases. In Figure 1 an overview of the industrial relevance of nitrating agents is presented. About 30.5% of these nitrations specifically rely on the classical nitrating mixture as preferred nitrating agent. The trapping of water is crucial to avoid dilution and the crunch of nitronium ion. The neutralization of acids and the removal of salts formed during neutralization are costly and unavoidable steps if nitrations are carried out in large scale. The presence of sulfuric acid in large quantity reduces the actual production capacity from a given reactor. On the other hand, fuming nitric acid as nitrating agent allows circumventing the use of sulfuric acid and thereby simplifies neutralization and salt separation steps. However, it needs to be noted that the handling and the storage of fuming nitric acid is not safe. There are great future prospects for conducting aromatic nitration under continuous flow conditions. To foster nitration under continuous flow conditions, it is necessary to develop continuous (i) dilution, neutralization, extraction and salt separation steps while using the nitrating mixture and (ii) dilution, extraction and possibly enrichment of acid by evaporation and its recycling while using the fuming nitric acid. The amount of sulfuric acid and/or nitric acid strongly depends on the activity of the organic substrate. It is always useful to prepare the nitrating mixture with different compositions of HNO_3 (fuming or concentrated) and H_2SO_4 inline before the mixture comes in contact with the organic substrate. Similarly, the use of different mol ratios of the nitrating agent with respect to the organic substrate can also be explored at laboratory-scale development. Such practices will save a significant amount of time for a given study and for exploring the parametric effect.

4.2 Heat management in nitration

With respect to the heat management in continuous flow nitration, the approaches, which are found in the literature can be classified in two categories. The first approach uses the microreactors or flow reactors with built-in channels as depicted in Figures 3, 6, 9 or zones for heat transfer. i.e., integrated microreactors [38], where the heat transfer occurs from one or two faces of the microchannel with most of the channels having a square or rectangular cross-section. In the second approach the flow reactor is immersed inside a constant temperature bath as depicted in Figures 2, 4, 7 and 8. In this case, the constant temperature is guaranteed by the constantly circulated heat transfer fluid with an external temperature control. In general, the rate of heat removal strongly depends on the heat transfer area, the thermal conductivity of the device material, the superficial velocity of the heat transfer fluid, the superficial velocity of the reacting fluid, and the specific heat capacity of the reacting fluid. Thus, for the devices with build-in heat management system the actual area available for heat transfer is only half of the total reacting fluid wetting area. On the other hand, the immersed systems provide a complete exposure to the heat transfer fluid. Thus, identical heat transfer rates can be achieved with either a lower heat transfer fluid temperature or a lower flow rate of heat transfer fluid for the immersed microfluidic systems compared to the built-in channels. Generally, the immersed systems with external temperature control are less sophisticated and are therefore cheaper. The advantage of the

integrated microreactors is in their compactness. Immersed microreactors are advantageous due to their simplicity and smaller number of connections. In practice, the nature of heat transfer remains more or less the same. The modularity of the entire system and the utility costs are essential factors for choosing which heating mode to choose for scale-up.

4.3 Interfacial reactions: real and apparent kinetics

The nitration of organic substrates using different nitrating agents can be classified based on whether the reaction is homogeneous or heterogeneous (multiphase). Taking into account the liquid phase substrates alone, almost 78% of the reactions reported in the literature, are two-phase reactions based on an analysis similar to the one depicted in Figure 1. In such systems the reaction takes place only after one of the reactants diffuses into the other. Thus, the rate of mass transfer controls the reaction rates. As a result, the actual reaction kinetics reported in the literature does not always explicitly indicate whether the mass transfer limitation was overcome. While this limitation actually renders much of the data from the literature on conversion and selectivity from experiments using round bottom flask or stirred systems useful only in terms of the products, it cannot be directly utilized for the estimation of kinetic parameters of experiments under different conditions. The Taylor flow or dispersion achieved in miniaturized systems significantly reduces the mass transfer limitations. To achieve reliable data, the flow rates should be adjusted in a way that avoids very long slugs. Although most of the regime maps in the literature are subject to the physical properties of the fluids as well as the channel dimensions and shape, an approximate analysis of flow regimes may be useful to ensure that the mass transfer limitations are overcome.

4.4 Handling of solids

A large proportion of either the organic substrates or their nitro derivatives reported in the literature are solids. In the conventional method the nitration of solid substrates is facilitated by using either a solvent in large excess – typically a weak acid, which does not get nitrated such as acetic acid – or sulfuric acid. The latter is mainly used for deactivated substrates to not only facilitate the dissolution of the substrate, but also form a complex, which increases the activity of the substrate for getting nitrated. On the other hand, a solid product precipitating during the reaction, results in a significant increase in the viscosity of the solution. While the use of techniques like reactions under sonication to prevent wall adhesion or particle agglomeration, inducing mechanical vibrations to the system to keep the solids in suspension, and the usage of high flow rates to ensure that the superficial flow velocity is higher than the settling velocity of solids is feasible, an optimal combination of using solvents in adequate quantity and maintaining a high superficial velocity are best suited to prevent precipiation. However, given a complex geometry of a microreactor the low pressure zones inherently enhance the possibility of particle accumulation in these zones even at high velocities. In laboratory equipment the simplest concept to avoid clogging relies on dilution.

4.5 Reliability of the analysis and establishing mass balance

For most nitrations, the products and the reactants are very poorly soluble in the aqueous phase, which comprises diluted nitric acid or diluted spent acid. In most of the cases, although the outlet product mixture is extracted by using a common organic solvent such as toluene, ethylene dichloride, hexane, ether, a certain fraction of the mono and dinitro derivatives and the reactant remain the aqueous phase. Consequently, an analysis based on the organic phase alone may not result in conclusive information about the extent of the reaction. Furthermore, ignoring the composition of the aqueous phase leads to an inaccurate measurement of the extent of byproducts. These points become important when the reactant has certain, even very small impurities, which may get nitrated rapidly and remain dissolved in the highly polar acidic medium. In most cases, publications about continuous flow nitration do not indicate whether the aqueous phase was also analyzed. Moreover, it is essential to establish the exact mass balance for a given reaction, so that the efficacy of the process can be evaluated.

5 Conclusion

The analysis of the literature clearly indicates that it is feasible for anyone to setup a flow reaction system for the nitration of aromatic substrates. Flow setups allow for the rapid screening and optimization of parameters to achieve optimal conditions for the nitration of arenes. In most cases, the reaction needs to be terminated by inline hydrolysis. Semi-batch hydrolysis should be avoided, as the dilution of excess acid does not occur uniformly. This can pose a problem at a later stage because of the high concentration of the nitrated product in the presence of an excess of the nitrating agent. It is quite common that either the reactant or the nitro derivative may have limited solubility in the reaction mixture, which poses a significant challenge in ensuring that the flow synthesis can operate continuously.

Depending upon its density the precipitate generated during the reaction may respond differently to the flow conditions and the geometry of the channels. One of the ways to overcome the situation is by using a solvent [58] with a good solubility for the organic substrates/products at the cost of increasing the volume of the reactor. Furthermore, an additional purification step, typically distillation, is required. While these procedures are routine on a laboratory scale they may not be suitable for large-scale

manufacturing. In such cases, it is possible to avoid the need of an additional reagent or dilution with a substrate (if in liquid phase) that serves as the solvent.

In practice, nitrations are followed by a reduction step to end up with an amino group. Commonly, nitrations yield several products as discussed in Schemes 4, 6, 8 and 14, which impedes direct hydrogenation. Thus, the separation of isomers after the nitration is an essential step. It will always remain a challenge to develop a liquid phase nitration that selectively yields only one nitro isomer or to achieve a separation protocol for the mixtures of reduction products, namely for different amines. Due to safety issues fuming nitric acid was only rarely used under batch conditions. However, fuming nitric acid becomes an option with the continuous flow approach, as safety issues can be better handled. This approach will also help to estimate the kinetic parameters for nitration in a more accurate manner, so that it is possible to have a good control on the temperature inside the reactor.

Now that the continuous flow nitration has emerged as an established technique that helps to control the yield of the desired isomer to some extent, it is necessary for the chemists and chemical engineers to work together for optimizing single protocols based on detailed mathematical analysis. The key is to understand the rate-controlling step, which can be interfacial mass transfer, kinetics or even thermodynamics as in the case of a solubility limited reaction.

Acknowledgements

The author wishes to thank the IndusMagic program of CSIR for supporting the work on continuous flow nitration. The help of Ms. Yachita Sharma in providing the Schemes in a suitable format is acknowledged. This review article is dedicated to Dr. Ramesh A. Joshi of the Organic Chemistry Division of the CSIR-National Chemical laboratory, Pune on his 61st birthday.

References

1. Panja, C. New Synthetic Methods Based on Electrophilic (Superelectrophilic) and Nucleophilic Reactions. Ph.D. Thesis, University of Southern California, Los Angeles, 2006.
2. Mitscherlich, E. *Pogg. Ann.* **1834,** *31,* 625.
3. Olah, G. A.; Malhorta, R.; Narang, S. C. *Nitration Methods and Mechanisms;* Wiley-VCH: New York, 1989.
4. Hughes, E. D.; Ingold, C. K.; Reed, R. I. *Nature* **1946,** *158,* 448.
5. Halberstadt, E. S.; Hughes, E. D.; Ingold, C. K. *Nature* **1946,** *158,* 514. doi:10.1038/158514b0
6. Halberstadt, E. S.; Hughes, E. D.; Ingold, C. K. *J. Chem. Soc.* **1950,** 2441–2452. doi:10.1039/jr9500002441
7. Maxwell, G. R. *Synthetic Nitrogen Products: A Practical Guide to the Products and Processes;* Kluwer: New York, 2005; pp 213–250.
8. Urbanski, T. *Chemistry and Technology of Explosives;* Pergamon Press, PWN-Polish Scientific Publishers: Warszawa, 1964; Vol. 1.
9. Venkataraman, K. *The Chemistry of Synthetic Dyes;* Academic Press: New York, 1952; Vol. 1.
10. Auerbach, G. *Text. Color.* **1880,** *2,* 137–139.
11. Wagener, D. J. T. *The History of Oncology;* Springer, 2009; pp 150–151.
12. Ingold, C. K. *Structure and Mechanism in Organic Chemistry,* 2nd ed.; Cornell University Press: New York, 1969.
13. Kanhere, J. M.; Chandalia, S. B. *Ind. J. Tech.* **1981,** *19,* 5.
14. Deno, N. C.; Peterson, H. J.; Sacher, E. *J. Phys. Chem.* **1961,** *65,* 199–201. doi:10.1021/j100820a002
15. Groggins, P. H. *Unit Processes in Organic Synthesis,* 3rd ed.; McGraw-Hill Book Co.: New York, 1947.
16. Hoggett, J. G.; Moodie, R. B.; Penton, J. R.; Schofield, K. *Nitration and aromatic reactivity;* Cambridge University Press: Cambridge, 1971.
17. deC Crater, W. *Ind. Eng. Chem.* **1948,** *40,* 1627–1635. doi:10.1021/ie50465a014
18. Albright, L. F.; Carr, R. V. C.; Schmitt, R. J. *Nitration* **1996,** *623,* 1–9. doi:10.1021/bk-1996-0623.ch001
19. Zaldívar, J. M.; Molga, E.; Alós, M. A.; Hernández, H.; Westerterp, K. R. *Chem. Eng. Process.* **1996,** *35,* 91–105. doi:10.1016/0255-2701(95)04119-2
20. New-Eco-efficient Industrial Process Using Microstructured Unit Components. http://www.nepumuc.info/project_summery.htm (accessed Jan 10, 2014).
21. Indus Magic. http://www.indusmagic.org (accessed Jan 10, 2014).
22. Denton, W. I.; Bishop, R. B.; Nygaard, E. M.; Noland, T. T. *Ind. Eng. Chem.* **1948,** *40,* 381–384. doi:10.1021/ie50459a004
23. Veretennikov, E. A.; Lebedev, B. A.; Tselinskii, I. V. *Russ. J. Appl. Chem.* **2001,** *74,* 1872–1876. doi:10.1023/A:1014840627266
24. Anderson, N. G. *Org. Process Res. Dev.* **2001,** *5,* 613–621. doi:10.1021/op0100605
25. De Jong, R. L.; Davidson, J. G.; Dozeman, G. J.; Fiore, P. J.; Giri, P.; Kelly, M. E.; Puls, T. P.; Seamans, R. E. *Org. Process Res. Dev.* **2001,** *5,* 216–225. doi:10.1021/op000298d
26. Dagade, S. P.; Waghmode, S. B.; Kadam, V. S.; Dongare, M. K. *Appl. Catal., A* **2002,** *226,* 49–61. doi:10.1016/S0926-860X(01)00882-1
27. Panke, G.; Schwalbe, T.; Stirner, W.; Taghavi-Moghadam, S.; Wille, G. *Synthesis* **2003,** 2827–2830. doi:10.1055/s-2003-42491
28. Antes, J.; Boskovic, D.; Krause, H.; Loebbecke, S.; Lutz, N.; Tuercke, T.; Schweikert, W. *Chem. Eng. Res. Des.* **2003,** *81,* 760–765. doi:10.1205/026387603322302931
29. Ducry, L. A.; Roberge, D. M. *Angew. Chem.* **2005,** *117,* 8186–8189. doi:10.1002/ange.200502387
30. Kulkarni, A. A.; Nivangune, N. T.; Kalyani, V. S.; Joshi, R. A.; Joshi, R. R. *Org. Process Res. Dev.* **2008,** *12,* 995–1000. doi:10.1021/op800112u
31. Pelleter, J.; Renaud, F. *Org. Process Res. Dev.* **2009,** *13,* 698–705. doi:10.1021/op8002695
32. Yang, J.-L.; Li, J.-F.; Lu, Y. *Acta Phys.–Chim. Sin.* **2009,** *25,* 2045–2049. doi:10.3866/PKU.WHXB20090926
33. Kockmann, N.; Roberge, D. M. *Chem. Eng. Technol.* **2009,** *32,* 1682–1694. doi:10.1002/ceat.200900355
34. Shen, J.; Zhao, Y.; Chen, G.; Yuan, Q. *Chin. J. Chem. Eng.* **2009,** *17,* 412–418. doi:10.1016/S1004-9541(08)60225-6
35. Kulkarni, A. A.; Kalyani, V. S.; Joshi, R. A.; Joshi, R. R. *Org. Process Res. Dev.* **2009,** *13,* 999–1002. doi:10.1021/op900129w
36. Brocklehurst, C. E.; Lehmann, H.; La Vecchia, L. *Org. Process Res. Dev.* **2011,** *15,* 1447–1453. doi:10.1021/op200055r

37. Knapkiewicz, P.; Skowerski, K.; Jaskólska, D. E.; Barbasiewicz, M.; Olszewski, T. K. *Org. Process Res. Dev.* **2012,** *16,* 1430–1435. doi:10.1021/op300116j
38. Löwe, W.; Wei, G.; Jiang, M.; Hofmann, C.; Kost, H.-J.; Schütt, C. *Green Process. Syn.* **2012,** *1,* 439–448. doi:10.1515/gps-2012-0054
39. Gage, J. R.; Guo, X.; Tao, J.; Zheng, C. *Org. Process Res. Dev.* **2012,** *16,* 930–933. doi:10.1021/op2003425
40. Yu, Z.; Lv, Y.; Yu, C.; Su, W. *Org. Process Res. Dev.* **2013,** *17,* 438–442. doi:10.1021/op300350v
41. Chen, Y.; Zhao, Y.; Han, M.; Ye, C.; Dang, M.; Chen, G. *Green Chem.* **2013,** *15,* 91–94. doi:10.1039/c2gc36652e
42. Burns, J. R.; Ramshaw, C. *Chem. Eng. Commun.* **2002,** *189,* 1611–1628. doi:10.1080/00986440214585
43. Dummann, G.; Quittmann, U.; Gröschel, L.; Agar, D. W.; Wörz, O.; Morgenschweis, K. *Catal. Today* **2003,** *79–80,* 433–439. doi:10.1016/S0920-5861(03)00056-7
44. McDaniel, L. A. Nitration processes. U.S. Patent US4621157, Nov 4, 1986.
45. Roberge, D.; Ducry, L. Nitration of activated aromatics in microreactors. WO-Patent WO2007/087816 A1, Aug 9, 2007.
46. Henke, L.; Winterbauer, H. *Chem. Eng. Techol.* **2005,** *28,* 749–752. doi:10.1002/ceat.200500096
47. Othmer, D. F.; Jacobs, J. J., Jr.; Levy, J. F. *Ind. Eng. Chem.* **1942,** *34,* 286–291. doi:10.1021/ie50387a007
48. Quadros, P. A.; Oliveira, N. M. C.; Baptista, C. M. S. G. *Chem. Eng. J.* **2005,** *108,* 1–11. doi:10.1016/j.cej.2004.12.022
49. Antes, J. T.; Marioth, E.; Schmid, K.; Krause, H.; Loebbecke, S. In *Int. Microreactor Tech. Symp. (IMRET4),* Atlanta, USA; 2000; p 194.
50. Loebbecke, S.; Tuercke, T.; Marioth, E.; Schmid, K.; Krause, H. 31th Int. Annu. Conf. ICT Karlsruhe, Karlsruhe; 2000.
51. Su, Y.; Chen, G.; Yuan, Q. *Chem. Eng. Sci.* **2011,** *66,* 2912–2919. doi:10.1016/j.ces.2011.03.024
52. Kwok, T. J.; Jayasuriya, K.; Damavarapu, R.; Brodman, B. W. *J. Org. Chem.* **1994,** *59,* 4939–4942. doi:10.1021/jo00096a042
53. Bernasconi, S.; Pirngruber, G. D.; Kogelbauer, A.; Prins, R. *J. Catal.* **2003,** *219,* 231–241. doi:10.1016/S0021-9517(03)00201-X
54. Halder, R.; Lawal, A.; Damavarapu, R. *Catal. Today* **2007,** *125,* 74–80. doi:10.1016/j.cattod.2007.04.002
55. Jianhua, W. Method for performing tubular continuous nitrification on naphthalene-2,7-disulfonic acid during production of H acid. Chinese Patent CN102320995A, Jan 12, 2012.
56. Liang, X. H. M. Safe production method of nitro-compound. Chinese Patent CN103044261A, April 17, 2013.
57. Knauf, T.; Racoes, A.; Rausch, A. K.; Wulf, D. Method for producing nitrobenzene by adiabatic nitriding. U.S. Patent US20130197268 A1, Aug 1, 2013.
58. Henderson, R. K.; Jiménez-González, C.; Constable, D. J. C.; Alston, S. R.; Inglis, G. G. A.; Fisher, G.; Sherwood, J.; Binks, S. P.; Curzons, A. D. *Green Chem.* **2011,** *13,* 854–862. doi:10.1039/c0gc00918k

License and Terms